Effect of Land Surface Heterogeneity on Satellite Near-Surface Soil Moisture Observations

by

Rocco Panciera

Submitted in total fulfilment of the requirements of the degree of

Doctor of Philosophy

October 2009

Department of Civil and Environmental Engineering,

The University of Melbourne, Australia

Abstract

Soil moisture in the top few meters of the Earth's surface has an important role in regulating the energy and water balance at the soil surface and it is therefore a crucial variable for many environmental disciplines which are concerned with atmospheric and land surface processes such as meteorology, hydrology and climatology. Consequently, there is a pressing need for soil moisture observations at a wide range of spatial scales, global coverage and sufficient temporal repetition to serve the environmental applications mentioned above. In recent decades, remote sensing technology has matured the potential to estimate near-surface soil moisture (approximately the top 5cm) from space. However, a space mission with optimal configuration for remote sensing of near-surface soil moisture has not been flown to date. The first satellite mission with an optimal observing frequency for remote sensing of near-surface soil moisture will be the Soil Moisture and Ocean Salinity Mission (SMOS), due to be launched in September 2009. SMOS will carry an L-band (1.4GHz) microwave radiometer and will provide near-surface soil moisture estimates with global coverage, three-days revisit time and spatial resolution of approximately 40km. Due to this coarse spatial resolution**,** significant spatial heterogeneity in land surface conditions will exist within SMOS footprints. The soil moisture retrieval algorithm adopted for SMOS partially accounts for the land surface heterogeneity by modeling the microwave emission of different fractions of the footprint having different vegetation types. Nevertheless, to date the soil moisture retrieval algorithm adopted for SMOS and its main assumptions have not been tested at the spatial resolution of future SMOS footprints and over highly heterogeneous land surface conditions.

The principal objectives of this research are to (i) test the soil moisture retrieval algorithm adopted for SMOS at SMOS spatial resolution (40km), and (ii) develop a soil moisture retrieval approach applicable to the SMOS algorithm which properly accounts for the land surface heterogeneity. Given that SMOS data are not yet available, the approach developed in this thesis

is based on aircraft L-band data collected in this study over a well monitored catchment, which are used to simulate the data soon to be available from SMOS.

The aircraft and ground data used in this study were collected during the National Airborne Field Experiment 2005 (NAFE'05), conducted in November 2005 in south-eastern Australia as part of this study. The NAFE'05 field campaign has provided an unprecedented data set for investigation of passive microwave soil moisture remote sensing techniques, which puts this study in the forefront of international research on this topic.

Before testing the SMOS algorithm at the SMOS footprint scale, in this study the core radiative transfer model of the algorithm is evaluated for the Australian conditions using high-resolution (62.5m and 1km) airborne data. The linear scaling of L-band observations is also verified using concurrent multi-resolution (62.5m, 250m, 500m and 1km) aircraft observations of the same area. The SMOS algorithm and the retrieval approach currently proposed is then tested using SMOS footprints simulated by aggregating the aircraft data (1km) to SMOS spatial resolutions (40km). The error in near-surface soil moisture retrieval due to the impact of land surface heterogeneity is assessed, and the weaknesses of retrieval approach currently proposed for SMOS identified based on detailed ground data on near-surface soil moisture and land surface conditions at the SMOS footprint scale.

A new retrieval approach, applicable to the SMOS algorithm is finally proposed to overcome the weaknesses identified in the approach currently proposed for SMOS. The new approach accounts for the heterogeneity within the SMOS footprint of vegetation density, the land surface factor which is shown in this thesis to have the more significant impact on retrieval of near-surface soil moisture. Upon testing of the new approach using the simulated SMOS footprints, this thesis shows that the new approach significantly reduces the error in SMOS soil moisture retrieval obtained with the approach currently proposed for SMOS.

This is to certify that

(i) this thesis comprises only my original work towards the PhD,except where indicated,

(ii) due acknowledgnen has been made in the text to all other material used,

(iii) this thesis is less than 100,000 words in length, exclusive of tables, maps, bibliographies and appendices.

Rocco Panciera

empty page

To my mother Elisabetta,

for being with me,

and to my father Piergiorgio,

who went back to the stars.

'Don't Panic'

- Douglas Adams -

The Hitchiker's Guide to the Galaxy

empty page

Acknowledgment

This PhD thesis involved over four years of my life, in which I matured not only as a scientist, but most importantly as a person. I would therefore like to thank everyone that, in a way or the other, shared this incredible experience with me.

My biggest thanks goes to my mother, Elisabetta, and my father, Piergiorgio, for making the early years of my life wonderful and serene, and for unconditionally supporting my dreams, even when they meant being many many miles away from home. I feel that, despite not being with us anymore, my father is able to see what I achieved thanks to his love and support.

The person which had by far the strongest influence on my path as a scientist is certainly my main supervisor, Jeff Walker. I thank him for teaching me to always seek riguor, accuracy and consistency, this way harnessing the disorder that otherwise seems to dominate every other aspect of my life. Thanks have to be extended also to my two other supervisors, Edward Kim and NASA Goddard Space Flight Center for giving me the opportunity to study in the US, and Jetse Kalma, for the insightful reviews of my chapters.

A special thank goes to everyone who participated to the NAFE'05 field campaign, which was an intense campaign but it was also a lot of fun Thanks in particular to Cristina Martinez for doing the initial surveys with me, and then sharing the burden of logistic organization and helping me keeping centered when things got stressful. I should also thank her for the providing the soil texture data for the Goulburn catchment. A big thanks goes also to all the NAFE'05 participants: G. Boulet, C. Dever, J. Fenollar, J. Grant, G. Hancock, L. Holz, J. Johanson, P. Jones, S. Jones, V. Maggioni, V. Paruscio, R. Pipunic, M. Rinaldi, P. de Rosnay, C. Rüdiger, P. Saco, K. Saleh, M. Thyer, T. Wells, and R. Young.

Last but not least, thanks to all the dear friends who coloured my life in Melbourne during these four years. Thanks to Carmen, for showing me around Brazil, to Nela, for being such an incredible person, to Nawal, for our serene time together, to Nadia, for giving it a try. I should also thank the long distance friends in Italy, in particular Elisa “carotina”, Viviana, Massimo, Beata, Michele “Nano” and Alina, for the great times together back in the days. I should also thank all those random backpackers which I met in remote places around the world, whose smile helped creating incredible memories.

Table of Contents

Chapter Three

Chapter Four

List of Figures

List of Tables

List of Symbols

Symbol	Units	Definition
a	[-]	Areal pixel fraction
b	[-]	Vegetation parameter for calculation of optical depth from vegetation water content
b_0	[-]	Microwave effective temperature exponent
C	$J.m^{-3}\cdot K^{-1}$	Soil heat capacity
C	[-]	Clay fraction
C_{LM}	[-]	Laser Mastersizer clay fraction
C_{pol}	[-]	Vegetation optical depth polarisation correction factor
C_t	[-]	Temperature attenuation coefficient
COV	[-]	Brightness temperatures variance/covariance matrix
CTI	[-]	Compound Topographic Index
e	[-]	Bare soil emissivity
H_R	[-]	Microwave roughness parameter
h	m	Distrance of semivariogram sample points
l	cm	Thickness of the vegetation layer
L_C	mm	Surface heights correlation length
K	$W.m^{-1}\cdot K^{-1}$	Soil thermal conductivity
N_R	[-]	Microwave roughness exponent
N_p	[-]	Number of semivariogram sample points at distance *h*
p	[-]	Generic surface physical parameter
Q_R	[-]	Polarisation mixing parameter
R_{tt}	[-]	Ratio between vegetation structure parameter *tt* at V and H polarization
T_B	K	Brightness temperature
$T_{B\text{-}ATM\text{-}DOWN}$	K	Downward atmospheric microwave emission
$T_{B\text{-}ATM\text{-}UP}$	K	Upward atmospheric microwave emission
T_{BPM}	K	SMOS measured brightness temperatures
$T_{B\text{-}SKY}$	K	Sky background microwave emission
$T_{B\text{-}TOA}$	K	Top of the atmosphere microwave emission

T_{DEPTH}	K	Deep soil temperature (50cm)
T_{EFF}	K	Microwave effective soil temperature
T_S	K	Soil temperature
T_{SURF}	K	Surface soil temperature (2.5cm)
tt	[-]	Vegetation structure parameter
T_V	K	Vegetation temperature
w_0	v/v	Microwave effective temperature parameter
α	m^{-1}	Vertical soil temperature attenuation coefficient
α	m^{-1}	Vegetation absorptivity
α	m^2	Uupstream area that contributes flow
β	rad	Local topographic slope
γ	[-]	Vegetation transmissivity
γ	$(v/v)^2$	Semivariance
Γ	[-]	Rough soil reflectivity
Γ^*	[-]	Smooth soil reflectivity
δ	[-]	Soil moisture mean relative difference
$\overline{\delta}$	[-]	Soil moisture mean relative difference
ε_G	F/m	Complex soil dielectric constant
ε_{veg}	F/m	Complex vegetation dielectric constant
θ	%v/v v/v	Volumetric soil moisture
θ_{veg}	kg/m^2	Vegetation water content
ϑ	rad	Radiation incidence angle
λ	cm	Radiation wavelength
η_m	deg	SMOS half-swath angle
τ	[-]	Vegetation optical depth
τ_{ATM}	[-]	Atmospheric optical thickness
τ_{FNAD}	[-]	Forest nadir equivalent optical depth
τ_{NAD}	[-]	Nadir equivalent vegetation optical depth
σ^o	dB	Backscattering coefficients
σ_P	[-]	Standard deviation of the estimate of surface physical parameter *p*
σ_S	mm	Standard deviation of surface heights

ω	[-]	Vegetation single scattering albedo

Glossary

Key Acronyms

AMSR-E	Advanced Microwave Scanning Radiometer
ATBD	Algorithm Theoretical Based Document
ARA	Airborne Research Australia
CESBIO	Centre d’Etudes Spatiales de la BIOsphère
CF	Cost Function
CoSMOS	Campaign for validating the Operation of SMOS
DEM	Digital Elevation Model
HDAS	Hydraprobe Data Acquisition System
ENVISAT	Environmental Satellite
ESTAR	Electronically Scanned Thinned Array Radiometer
ERS	European Remote Sensing Satellites
ESA	European Space Agency
FOV	sensor Field Of View
JERS	Japanese Earth Resources Satellite
LAI	Leaf Area Index
L-MEB	L-band Microwave Emission of the Biosphere (model)
MIRAS	Microwave Interferometric Radiometer with Aperture Synthesis
MODIS	MODerate resolution Imaging Spectroradiometer
NAFE	National Airborne Field Experiment
NASA	Natioanl Aeronautics and Space Administration
NDVI	Normalised Difference Vegetation Index
NDWI	Normalised Difference Water Index
PLMR	Polarimetric L-band Multibeam Radiometer
RADARSAT	Canadian RAdar SATellite
RFI	Radio Frequency Interference
SAR	Synthetic Aperture Radar
SERA	Small Environmental Research Aircraft
SGP	Southern Great Plains
SMAP	Soil Moisture Active Passive
SMEX	Soil Moisture Experiment
SMMR	Scanning Multichannel Microwave Radiometer

SMOS	Soil Moisture and Ocean Salinity Mission
SMOS L2	SMOS Level 2 soil moisture algorithm
SMOSREX	Surface Monitoring Of the Soil Reservoir EXperiment
VWC	Vegetation Water Content
WEF	SMOS L2 synthetic antenna pattern weighting function

empty page

Prologue

The National Airborne Field Experiment 2005 (NAFE'05) undertaken during this study has provided an unprecedented data set for investigation of passive microwave soil moisture remote sensing techniques. While the NAFE'05 experiment was an international effort of several institutions with more than 40 participants, the author of this thesis played a central role in all aspects of the field campaign, including conceptualisation and planning of the airborne monitoring and ground sampling strategies, management of the ground sampling activities, and the post-processing, documentation and archiving of all collected data. Additionally, in the context of this study the author conceived and developed a novel portable near-surface soil moisture monitoring system, the Hydraprobe Spatial Data Acquisition System (HDAS), which allowed the collection of the ground near-surface soil moisture data of unprecedented detail and extent for use in this thesis.

empty page

Chapter One

1 Introduction

This thesis develops a technique to reduce the error in near-surface soil moisture estimates from spaceborne passive microwave sensors, by accounting for the heterogeneity of land surface conditions within the sensor field of view. Using experimental data collected in the course of this research, it is demonstrated that this technique will significantly reduce the error in satellite near-surface soil moisture retrieval. The technique has been developed specifically for the first dedicated passive microwave soil moisture satellite, the European Soil Moisture and Ocean Salinity Mission (SMOS), which will use L-band (1.4GHz) measurements to map near-surface soil moisture globally at a near-daily time scale.

The main steps taken to develop these techniques are the first evaluation of the core radiative transfer model of the SMOS soil moisture retrieval algorithm for the Australian conditions using airborne data, and an analysis of the land surface controls on near-surface soil moisture distribution at the satellite footprint scale. These initial steps provided the tools in order to test the accuracy of the soil moisture retrieval approach proposed for SMOS at the satellite footprint scale in the presence of spatial variability of the land surface, and to develop a new retrieval approach for SMOS which overcomes the shortfalls identified in the SMOS proposed approach.

1.1 Importance of Soil Moisture

Soil moisture of the top few meters of the Earth's surface plays an important role in regulating the energy and water balance at the soil surface (Betts et al., 1996; Entekhabi et al., 1996). It is therefore a crucial variable for many environmental disciplines which are concerned with atmospheric and land surface processes such as meteorology, hydrology and climatology (Koster and Suarez, 2003a; Western et al., 2004; Conil et al., 2007). Moreover, information on the soil moisture is crucial to humans due to its impact on activities such as agriculture and trafficability (Jackson et al., 1987). More specifically, there is evidence that reliable observations of soil moisture at regional, continental and global scales will benefit:

- flood forecasting through better prediction of the partitioning of precipitation between runoff and infiltration (Entekhabi et al., 1993; Su et al., 1995; Western et al., 2004);
- land management through improved modeling of erosion producing zones (Fitzjohn et al., 1998; Castillo et al., 2003; Shinoda and Yamaguchi, 2003);
- weather and climate forecasting through improved modeling of the interaction of land surface processes (Engman, 1992; Betts et al., 1994; Koster et al., 2003b; Conil et al., 2007) and better land surface initialisation in weather prediction models (Beljaars et al., 1996);
- agricultural applications by assisting irrigation scheduling, which will lead to water conservation benefits and better crop yield prediction (Jackson et al., 1987; Saha, 1995);
- early drought prediction through better prediction of plant stress (Engman, 1990; Vijaya Kumar et al., 2005) and the ability to quantitatively monitor drought in both space and time (Jackson et al., 1987; Sridhar et al., 2008);
- modeling of nitrogen and CO2 biogeochemical cycling (D'Odorico et al., 2003; Porporato et al., 2003; Turcu et al., 2005), and estimation of surface emission of CO2 (Jin et al., 2008); and
- management of agricultural practices, including trafficability in the fields (Wigneron et al., 1998).

Changes to soil moisture patterns are also expected to be an important indicator of global warming, particularly during the vegetation growing period (Huszár et al., 1999; Li et al., 2007). Therefore, climate model simulations of future soil moisture should be compared with soil moisture observations, in order to further verify climate model simulations (Koster et al., 2003a; Li et al., 2007). Consequently, there is a pressing need for soil moisture observations at a wide range of spatial scales, with sufficient temporal repetition to serve the hydrological, agricultural, meteorological and climatological applications mentioned above.

1.2 Statement of Problem

In recent decades, remote sensing technology has matured to the point that near-surface soil moisture can be estimated at global scale from space, (e.g., Wigneron et al., 2003; Wagner et al., 2006). Near-surface soil moisture is relative to approximately the top 5cm of the Earth’s surface. For simplicity, in this thesis it will be generally referred to as “soil moisture”. Several studies have shown that the soil moisture information provided by remote sensing technology for the near-surface layer can be used to retrieve the soil moisture content at much greater depth (e.g., Houser et al., 1998; Walker et al., 2001). Although such studies rely on data assimilation of the remotely sensed information into land surface models, rather than on the identification of a physical coupling between surface and deep layer, they made a strong case to support the potential of global soil moisture remote sensing systems for environmental applications. In spite of the importance of soil moisture observations, there is not yet a dedicated soil moisture mission in space. However, there are a number of soil moisture products becoming available from sensors with non-ideal configurations for soil moisture monitoring, such as the Advanced Microwave Scanning Radiometer (AMSR-E)(Njoku et al., 2003) and the Advanced Synthetic Aperture Radar (ASAR)(Wagner et al., 2003), and there are two soil moisture dedicated satellites in various stages of design and construction.

While the Soil Moisture Active Passive (SMAP)(NASA, 2007) mission of the National Aeronautics and Space Administration (NASA) is still in its design phase with an anticipated 2013 launch, the Soil Moisture and Ocean Salinity (SMOS)(Kerr et al., 2001) mission of the European Space Agency (ESA) has completed its ground testing and launch is imminent. Both of these missions will use passive microwave technology at low frequencies

(~1-6GHz), as this has demonstrated the best soil moisture response under a variety of topographic and vegetation cover conditions (Ulaby et al., 1986; Engman and Chauhan, 1995; Jackson et al., 1999; Uitdewilligen et al., 2003. However, the use of this optimal frequency imposes a limit on the spatial resolution at which the land surface can be resolved; even the introduction in SMOS of synthetic aperture radiometry technology (Le Vine, 1999) will not reduce spatial resolutions below 30km (Kerr et al., 2000).

At such scales, significant spatial heterogeneity in soil moisture exists, due to topography, spatial variability of soil and vegetation properties, and the highly intermittent nature of precipitation fields (Entekhabi and Rodrigueziturbe, 1994; Rodriguez-Iturbe et al., 1995). Current soil moisture products do not explicitly account for this spatial variability, as the land surface is assumed to be uniform within each land surface unit (pixel) where soil moisture is retrieved. Since the relationship between soil moisture and the microwave emission is non-linear, the sub-pixel heterogeneity of soil moisture and land surface conditions introduces uncertainty in the retrieval of soil moisture from space over large, heterogeneous areas such as satellite pixels.

For example, the simple synthetic situation shown in Figure 1.1 demonstrates that errors as large as 4%v/v, the total error budget for a satellite soil moisture mission, can result solely from typical sub-pixel heterogeneity in soil moisture. Here, a land surface is assumed to comprise fractions with 10%v/v and 50%v/v respectively, and otherwise uniform land surface conditions. Whilst in reality there will be intermixed patches of varying soil moisture together with heterogeneity of other land surface parameters, this simple example allows simple demonstration of the problem while avoiding the complicating non-linear response that exists in truly heterogeneous pixels. Therefore the problem of the heterogeneity in land surface conditions at the scale of current generation passive microwave remote sensing is an unresolved and pressing issue for the scientific community in view of the imminent launch of SMOS and in preparation for SMAP.

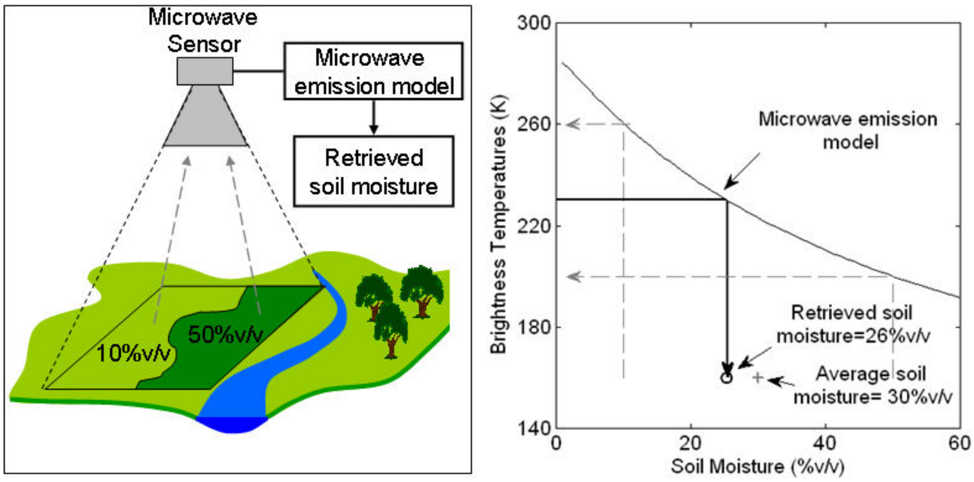

Figure 1.1. Synthetic example of the effect of sub-pixel heterogeneity of soil moisture on the soil moisture retrieval. The example is for a pixel split in two halves at respectively 10%v/v and 50%v/v soil moisture content. All other characteristics are uniform: clay soil, 25ºCelsius soil temperature and 1Kg/m^2 of water content in the vegetation canopy. The model used to produce the curve is the L-band Microwave Emission of the Biosphere Model (SMOS mission).

This thesis is focused on the soil moisture retrieval approach currently proposed for the SMOS mission and implemented in the so-called "SMOS L2" soil moisture retrieval algorithm. In contrast to what is done in current soil moisture products, which treat the pixel as a uniform surface, the SMOS approach seeks to account for the sub-pixel heterogeneity of land surface conditions by dividing the pixel into fractions determined using high-resolution maps of land use, and then simulating the microwave emission for each of these sub-pixel fractions separately. Thus, this method explicitly assumes that land use variability is the most important factor in terms of soil moisture retrieval. Additionally, in the case where the canopy density of all the pixel fractions is moderate, the assumption is made that soil moisture and vegetation optical depth are uniform amongst the pixel fractions. Both these assumptions need to be rigorously evaluated and the importance of the sub-pixel heterogeneity of other land surface factors needs to be tested with real data.

This thesis addresses this urgent and important question by testing the soil moisture retrieval approach proposed for SMOS and its assumptions with real L-band observations at the size of a SMOS footprint, by aggregating aircraft observations made at L-band. This is done over a well monitored catchment occupied by a mix of native grasslands, crops and moderately dense Eucalypt forest, with a wealth of ground and remotely sensed ancillary data to monitor the variability of soil moisture, vegetation and land surface conditions.

1.3 Objectives and Scope

This research focuses on the soil moisture retrieval over areas with a strong contrast of vegetation density between forested areas and areas of moderately vegetated soil such as crops and grasslands The principal objectives are to develop a soil moisture retrieval approach for SMOS which accounts for the sub-pixel heterogeneity of land surface conditions between those land cover types, and to test this approach with real data. In particular, Additional aims which have to be addressed in order to achieve these principal objectives include:

- development of a novel soil moisture monitoring system, the Hydraprobe Data Acquisition System (HDAS), which integrated a soil moisture probe (Hydraprobe) with a GPS positioning system and GIS using a handheld computer in a portable format;
- collection of an airborne and ground-based field data set suitable for the application of soil moisture retrieval approaches to be evaluated at the SMOS footprint scale;
- evaluation of the L-band Microwave Emission of the Biosphere (L-MEB) radiative transfer model, which is the basis of the SMOS L2 soil moisture retrieval algorithm, with airborne data from local (62.5m) to satellite (40km) scale;
- verification of the soil roughness parameterisation for passive microwave soil moisture retrieval at airborne resolutions (62.5m-1km);

- assessment of the scaling properties of microwave emission fields as detected at different resolutions;
- understanding the link between land surface characteristics (e.g., soil type, topography, land cover) and spatio-temporal variability of soil moisture in the study area;
- assessing the error in retrieved soil moisture at SMOS resolution due to the sub-pixel heterogeneity of land surface conditions, under the assumption of pixel uniformity upon which the current soil moisture products are based on; and
- testing of the soil moisture retrieval approach proposed for SMOS and its assumption of uniformity of soil moisture and vegetation optical depth in the pixel in the case of pixels composed of a mix of moderately vegetated soil (crops and grasslands) and moderately dense Eucalypt forest, typical of the Australian environment. This is the first time that the SMOS soil moisture retrieval approach adopted by ESA is tested at the satellite footprint scale using field observations.

These seemingly separate objectives are instead closely inter-linked. They will provide an experimental framework with observations as close as possible to those expected from SMOS, and will allow testing of the soil moisture retrieval approach proposed for SMOS and of the new approach to be developed in this thesis, coupled with an unprecedented knowledge of the land surface conditions at the scale of a SMOS footprint.

1.4 Outline of Approach

This study involves three parts: (i) Collection and processing of airborne and ground-based field data; (ii) Testing of the soil moisture retrieval approach proposed for SMOS and its assumptions with real data, and (iii) Development and testing of new techniques to better account for the sub-pixel heterogeneity of land surface conditions in the soil moisture retrieval from SMOS. Each part of this study is hereby outlined individually.

Part 1: Since no actual SMOS data were available to develop the techniques proposed in this thesis, the extensive airborne and ground-based NAFE'05 data set collected at the beginning of this study is processed in order to closely simulate the data expected from SMOS, and to provide knowledge of the spatial distribution of soil moisture and other relevant land surface factors in the study area. The data collection campaign involved airborne ground-based monitoring of an area of the size of a SMOS footprint (approximately 40km x 40km) over one month in November 2005. In order to create observations as close as possible to those expected from SMOS, multi-resolution airborne observations of the study area are compared to verify the linear scaling of microwave emission fields. This supports the aggregation of high-resolution aircraft data to SMOS resolution done in part 2.

Part 2: Here the soil moisture retrieval approach proposed for SMOS and its main assumptions are tested with the NAFE'05 data. The first step of the analysis is that of evaluating the L-MEB model, which is the basis of the SMOS L2 soil moisture retrieval algorithm, and its parameters for the land surface conditions of the study area using high-resolution airborne data. The model is then used to produce high-resolution soil moisture maps across the entire study area to be later used for testing the various retrieval approaches. The ground data on the spatial distribution of soil moisture and land surface factors are then analysed in order to assess the land surface heterogeneity in the study area and the links between the spatial distribution of different land surface factors and that of soil moisture in the study area. The impact of such land surface heterogeneity on the soil moisture retrieval using the SMOS algorithm is then assessed through a preliminary synthetic study and subsequently using the real data. This phase results in the identification of the land surface factors whose heterogeneity at the SMOS footprint scale most strongly affects the soil moisture retrieval, and in an assessment of the weaknesses of the soil moisture retrieval approach proposed for SMOS which will be addressed in part 3.

Part 3: A novel retrieval approach is finally proposed for SMOS and its accuracy with respect to the current SMOS approach tested with real data. This approach, which can be easily implemented within the SMOS L2 algorithm, relaxes one of the main assumptions on which the SMOS L2 algorithm is based on, thereby allowing the SMOS L2 algorithm to meet the SMOS target accuracy of 4%v/v; The next section describes in details how the three parts of this study are laid out in the manuscript.

1.5 Organisation of Thesis

This thesis is organised into nine Chapters which can be loosely grouped into 6 sections:

Section 1 – background and proposed approach (Chapters 1 and 2);

Section 2 – model and field data description(Chapters 3 and 4);

Section 3 – model testing and data exploration (Chapters 5 and 6);

Section 4 – evaluation of current techniques (Chapter 7);

Section 5 – development and testing of novel techniques (Chapter 8);

Section 6 – conclusions and recommendation for future work (Chapter 9).

Chapter 2 presents an overview of the existing techniques to estimate soil moisture and its spatial and temporal distribution through remote sensing. Previous investigations that dealt with the problem of soil moisture retrieval error induced by land surface heterogeneity are then reviewed and the shortcomings in the current techniques to reduce that error are identified.

The SMOS mission and the SMOS L2 soil moisture retrieval algorithm are described in detail in Chapter 3, together with the radiative transfer equations of the L-MEB model, which is the basis of the SMOS L2 algorithm. Chapter 4 describes the NAFE'05 field campaign, which provided all the airborne and ground data used in this study, presents the data collection strategy, and the details about any ancillary data relevant to this thesis.

In Chapter 5, after evaluation of the L-MEB model using the airborne and ground data collected during the NAFE’05 field campaign, high-resolution soil moisture maps of the entire study area are produced. These will be subsequently used in Chapters 7 and 8 for testing the soil moisture retrieval approach proposed for SMOS. In Chapter 6, the heterogeneity of the land surface conditions in the NAFE’05 study area is investigated using spatial ground measurements of soil moisture and ancillary data on topography, vegetation density, and soil texture. This leads to an understanding of the relationship between land surface factors and soil moisture distribution that will be used in Chapters 7 and 8 to identify the weaknesses of the current retrieval techniques.

Chapter 7 makes an assessment of the L-MEB model at satellite scale. This provides an assessment of the soil moisture retrieval error expected at the SMOS footprint scale under the assumption of pixel uniformity, as made by current methods. Using both a synthetic study and analysis with real data, the error is interpreted in terms of the heterogeneity of soil moisture and land surface factors analysed in Chapter 6.

The soil moisture retrieval approach proposed for SMOS is tested in Chapter 8 with real data. The weaknesses of the approach and its main assumptions to account for the land surface heterogeneity are identified. Moreover, a novel alternative approach for SMOS is proposed, and shown to take better account of the land surface heterogeneity.

A discussion of results, conclusions and recommendations for future research is given in Chapter 9.

Chapter Two

2 Literature Review and Proposed Approach

This Chapter presents an overview of the existing techniques to estimate soil moisture and its spatial and temporal distribution through remote sensing, with focus on the problem of the error in coarse-scale soil moisture retrieval induced by land surface heterogeneity. First, the nature and sources of spatial variability of soil moisture and its link to land surface factors are discussed to introduce the problem. Next, a review of the techniques developed to monitor that variability through remote sensing is presented and the advantages of the passive microwave technique adopted by SMOS for global soil moisture remote sensing are discussed. Finally, the impact of land surface heterogeneity on the retrieval of accurate soil moisture estimates from passive microwave observations is discussed, and a new approach is proposed, applicable to SMOS, to reduce the error in soil moisture estimation due to land surface heterogeneity.

2.1 Soil Moisture Spatial Variability

At a particular point in time soil moisture is influenced by: (i) the precipitation history, (ii) the texture of the soil, which determines the drainage rate and the water holding capacity, (iii) the local topography, which affects runoff and infiltration, (iv) the soil depth, which determines lateral drainage and saturation by excess of lateral flow and (v) the land cover (vegetation), which influences evapotranspiration and deep percolation (Mohanty and Skaggs, 2001). Understanding how these different factors interact with each other in determining the spatio-temporal dynamics of soil moisture and whether the relative importance of each factor changes with the spatial scale considered has been a major research interest for decades. The typical spatial scale of footprints from present passive microwave sensors is 40km, and that expected for the foreseeable future through advances in the technology of building new orbiting antennas will not be smaller than 10km (NASA, 2007). From the point of view of remote sensing, the variability of soil moisture within these large areas is of major interest as "remote sensing techniques provide a means of directly obtaining spatial information over wide areas. These data are known to be averaged over the sensor's footprint on the ground, and much concern is still focused on relevant issues like the […] inherent variability of hydrological variables at scales that are finer than the footprint scale" (Lanza et al., 1997).

Traditionally, soil moisture spatial variability studies using ground-based point-scale measurements were limited to small fields ($<1km^2$) with fairly uniform soil properties, topography and vegetative conditions. Several studies in the early 1970s focused on small catchments and observed that soil moisture at any location could be fairly well predicted from a combination of topography and soil hydraulic properties information (Dunne and Black, 1970a; Dunne and Black, 1970b; Beven and Kirkby, 1979; O'Loughlin, 1981). Based on these findings, several "physically-based" methods were developed to predict the spatial distribution of soil moisture within catchments, like the widely used TOPMODEL (Beven et al., 1979). These methods captured the fundamental mechanisms of water redistributions across the landscape, essentially the relative intensity of lateral drainage in the soil and vertical infiltration determined by topographic slope, distance from the outlet and hydraulic conductivity. However, these methods were soon found to be too simple and restrictive in their assumptions to be able to explain the complex interactions between land surface characteristics and spatial variability of soil moisture across many landscapes with various soil types, topography, land cover and climatic conditions (Barling et al., 1994; Ambroise et al., 1996; Blazkova et al., 2002).

Certain time invariant association between soil moisture patterns and soil texture (time stability) were observed by Vachoud et al. (1985) in a small catchment of small relief using time stability analysis. Time stability indicates the persistency of spatial patterns of soil moisture associated to spatial patterns of some other land surface characteristic, like for example soil texture. The analysis was extended by Grayson and Western (1998) to a catchment with significant relief in order to find locations that exhibited catchment average behaviour for remote sensing validation purposes. These authors showed that overall the soil moisture patterns were not time stable and therefore could not conclude on the predominance of any land surface controls on the soil moisture distribution.

More recently, the availability of extensive data sets of point measurement in monitored catchments has shed some light on the complex interaction between land surface factors and soil moisture distribution, as well as on the seasonal variation of land surface control on soil moisture variability. The geostatistical analysis of soil moisture patterns in various small humid and sub-humid catchments in Australia and New Zealand showed that controls on soil moisture spatial patterns could change between places and over time with catchment moisture status (Grayson et al., 1997a; Western et al., 1998; Grayson et al., 1999; Western et al., 2004). At more humid sites topography was shown to play an important role in controlling the soil moisture variation in space, while at drier sites variations in soil texture played a more important role. Even at the same site controls on soil moisture were found to be quite different with the transition from wet to dry seasons. During summer, mean and spatial variability of soil moisture across the catchment was typically low, as a consequence of the low lateral redistribution due to low hydraulic conductivity for low soil moisture values. Also, because any available soil moisture would evaporate quickly, evapotranspiration was moisture-limited and soil moisture was generally close to the wilting point. Since the wilting point is uniform across the catchment, soil moisture was also uniform. During winter, soil moisture states were instead dominated by lateral water movement through both surface and sub-surface paths, with topography leading to organisation of soil moisture along drainage lines. The seasonal switch between land surface controls was also observed by Teuling and Troch (2004), who showed that both soil texture and vegetation controls could act to either increase or decrease spatial variability of soil moisture, and that this effects varied with the overall moisture conditions.

In more recent years, the use of airborne active and passive microwave remote sensors has enhanced the capability to monitor soil moisture over large land areas with spatial extents that are more representative of satellite footprints and encompass various soil types, topography, land cover and climatic conditions. Differences in land cover as well as land use practices (affecting soil texture, surface roughness and vegetation dynamics through harvesting) are likely to occur in larger areas. Rainfall and geology also become more variable at a large scale. Because the scale of variability of these controls tends to be large, the scale of variability of soil moisture is expected to be larger as well (Western et al., 1998). Moreover, as argued by Kachanoski and de Jong (1988), since hydrological processes operate at different spatial scales, the time stability of soil moisture spatial patterns should also be a function of scale, i.e. some process could alter the persistence of soil moisture patterns at small scale (like that of a small watershed), while the change is insignificant at larger scales (like that of a satellite footprint).

Analysis of the spatial structure of soil moisture and its link to land surface factors at a range of scales, from 1km^2 up to 10,000km^2 was made possible through the remotely sensed soil moisture data obtained from airborne passive microwave observations during the Washita'92 and Southern Great Plains'97 (SGP'97) field experiments. At the field scale (1km^2), ground-based soil moisture measurements from these campaigns were analysed to investigate soil moisture time stability within the aircraft footprint for validation of the airborne data. The impact of topography and characteristics related to land use (vegetation and surface roughness) on soil moisture patterns was clearly observed at fields when all other land surface factors were uniform across the field (Famiglietti et al., 1999; Mohanty et al., 2000a; Mohanty et al., 2000b). On fields with more variable conditions, the role of topography in soil moisture distribution was stronger during periods of rainfall, at the end of which the relative importance of soil texture and land use factors increased (Yoo and Kim, 2004).

At larger scales (up to 10,000km^2), analysis of the relationship between soil moisture and regional soil and land cover characteristics using airborne passive microwave observations was undertaken using SGP'97 data (Kim and Barros, 2002a, b; Jacobs et al., 2004; Jawson and Niemann, 2007) and Washita'92 data (Cosh and Brutsaert, 1999). Results indicated that at these scales soil moisture variability was most strongly connected to soil texture, specifically sand and clay content. In drier conditions, soil moisture variability approached the spatial correlation structure of sand content, followed by that of clay content and finally vegetation water content (VWC). The impact of soil texture on soil moisture was observed to weaken during and immediately after rainfall events, when the spatial structure of soil moisture appears to be dominated by rainfall spatial gradients and topography (Yoo et al., 1998; Kim et al., 2002a; Jawson et al., 2007). Jawson et al. (2007) also observed that when increasing the scale at which soil moisture patterns are analysed, characteristics related to land use (vegetation and surface roughness) became increasingly correlated with soil moisture pattern, although the importance of soil texture was still significant

An important investigation at a variety of scales was also undertaken using extensive data sets of traditional ground-based point measurements at a variety of scales by Choi et al. (2007). This study showed the predominance of soil texture, in particular sand content, in explaining the soil moisture variability from small (<1km^2) to large scales (1000km^2) over several areas in the US, Belgium and Spain having a variety of topographic and land cover conditions.

It should be noted that SGP'97 and Washita'92 study areas, where most of the above studies were based, were characterised by relatively smooth topography and moderate vegetation variability. Consequently these findings need further verification in other regions of the world with more variable land surface conditions and different climatic regimes.

At even larger scales (more than 100,000km^2), data sets from ground-based point measurements at agricultural sites in the Former Soviet Union, Mongolia, China, and the USA suggested that the soil moisture variance has two components; (i) the very small scale, determined by soils, topography and land cover, and (ii) the large scale (500km), determined by precipitation and evaporation patterns (Vinnikov et al., 1996; Entin et al., 2000). At these larger scales, heterogeneity in rainfall disrupts temporal stability of fields by introducing random spatial variability (Kachanoski et al., 1988).

The preceding discussion of soil moisture spatial variability and its link to land surface factors highlighted that, although there is a widespread tendency in hydrology to assume that at the small catchment scale (<1km^2) topography plays a dominant role (Grayson and Western, 2001), the generality of this hypothesis is poorly supported in the literature. Indeed there are clear examples where other controls, soil texture or land cover, are more important (Vachaud et al., 1985; Grayson et al., 1997a; Western et al., 1998; Teuling et al., 2004; Western et al., 2004; Choi et al., 2007). Despite the relatively small body of literature which investigated soil moisture variability at scales more similar to that of satellite footprints, there is good evidence that other controls, soil texture in particular, but also land use related characteristics and the rainfall gradients, may play a crucial role in determining spatial soil moisture distribution. Moreover, it was noted in several studies that that within the same area the relative importance of each land surface factor might change significantly through time (Yoo et al., 1998; Kim et al., 2002a, b; Jacobs et al., 2004; Choi et al., 2007; Jawson et al., 2007).

These observations imply that the interpretation of the spatially averaged information provided by remote sensors will not be straightforward. This is because due the high variability of soil moisture fields and the temporally and spatially variable correlation between sub-pixel variability of soil moisture and land surface characteristics, it is extremely difficult to monitor soil moisture on the ground in a way that represents the footprint average soil moisture conditions.

The variability in land surface characteristics affects the interpretation of the spatially averaged information provided by remote sensors in yet another way: it affects the relationship between the mean soil moisture conditions within the footprint and the spatially averaged microwave emission measured by the sensor, resulting from the heterogeneous soil moisture and land surface conditions. This effect is different from that discussed above. The former is associated with physical land surface processes of lateral water distribution, vertical infiltration, evaporation, root water uptake, whereas the latter is controlled by the radiative transfer properties of the soil-vegetation layer.

This thesis deals specifically with this second problem. Before discussing in detail the effect of land surface heterogeneity on the microwave emission measured by the remote sensors, it is necessary to give an overview of remote sensing methods available for soil moisture monitoring and to describe the physical basis of microwave remote sensing.

2.2 Remote Sensing Techniques for Monitoring Soil Moisture

Global remote sensing of soil moisture has been a major research goal for nearly three decades. Several studies have shown that soil moisture can be measured by a variety of techniques, which differ essentially in the parts of the electromagnetic spectrum sensed and in the source of the electromagnetic radiation. Investigations have been undertaken using sensors that measure the radiation emitted by the earth surface in the microwave domain ("passive microwave") using both tower-mounted sensors (Wang, 1983; Wang et al., 1983; De Rosnay et al., 2006a; Saleh et al., 2006a; Saleh et al., 2006b; Della Vecchia et al., 2007; Saleh et al., 2007; Wigneron et al., 2007), and airborne sensors (Jackson et al., 1982; Jackson et al., 1984; Wood et al., 1993; Jackson et al., 1995a; Drusch et al., 1999a; Jackson et al., 1999; Jackson, 2001; Bindlish and Barros, 2002; Kim et al., 2002b; Njoku et al., 2002; Uitdewilligen et al., 2003; Lakshmi et al., 2004; Jackson et al., 2005; Merlin et al., 2008; Panciera et al., 2008a). Other investigation used sensors that measured the radiation reflected by the surface given a microwave pulse sent by the sensor ("active microwave") (Wood et al., 1993; Giacomelli et al., 1995; Bindlish et al., 2002; Njoku et al., 2002) or the radiation in the visible/infra-red domain (Carlson et al., 1994; Moran et al., 1994; Gillies et al., 1997). Moreover, techniques for global soil moisture estimation were tested using space sensors in the microwave domain (Shi et al., 1997; Chauhan et al., 2003; Njoku et al., 2003; Zribi et al., 2003; McCabe et al., 2004; Wan et al., 2004; McCabe et al., 2005; Zribi et al., 2005; Verstraeten et al., 2006; Yang et al., 2006; Chand and Badarinath, 2007; Narayan and Lakshmi, 2008; Rahman et al., 2008) and combined microwave/visible/infra-red domains (Chauhan et al., 2003; Verstraeten et al., 2006).

Remote sensing has the advantage with respect to other traditional techniques for soil moisture monitoring (essentially those based on continuous measurements at fixed locations and land surface models) to (i) provide an integrated measurement over a large area, (ii) provide a frequent coverage of the entire (or a vast part of) globe and (iii) to rely as less as possible on complex modelling of land-surface-atmosphere physical processes, which at global scale would imply excessive computational burden.

Although there is now a wide consensus in the scientific community that remote sensing using microwave sensors is the most promising technology for global soil moisture monitoring (Engman et al., 1995; Jackson et al., 1996b; Wigneron et al., 2003; Prigent et al., 2005; Wagner et al., 2006; Wagner et al., 2007), each of the techniques mentioned above holds certain advantages associated with the resolution at which the land surface can be resolved from space sensors (which depends directly on the frequency), the sensitivity to soil moisture changes or the sources of noise to the soil moisture signal. Therefore in the following sections a brief review of the physical basis upon which each technique is based is given. Based on this review, section 2.2.4 presents a discussion of the advantages and limitations of each technique in light of their application for global monitoring of soil moisture.

2.2.1 Visible Radiation

The ratio of reflected to incoming solar radiation at the earth surface (known as "albedo") in the visible region of the spectrum (0.4 - 0.8μm) has been long recognised as having a dependence upon the moisture status of the soil surface (Ångström, 1925). The effect of increasing soil moisture content is to reduce the albedo by a factor of about 2 for a bare soil (Jackson et al., 1976), although this effect is somewhat less detectable for sand.

Remote sensing of soil moisture using the visible region of the electromagnetic spectrum is therefore based on the measurement of the albedo, and can provide good spatial resolution from space sensors (e.g. ~30m for Landsat visible bands). However, the measurement of the albedo provides only a poor indication of soil moisture content. It has been shown that albedo is also greatly influenced by many other factors such as organic matter, soil texture, surface roughness, angle of incidence, plant cover and colour causing a wide variation in albedo of different soil types even when dry (Engman, 1991; Troch et al., 1996).

Apart from these confounding factors, important limitations of soil moisture remote sensing in the visible spectrum are that (i) reflected solar energy responds to only the top few millimeters of the soil profile (Idso et al., 1975), therefore providing soil wetness information for a very shallow layer of the soil which is difficult to link with deeper layers, (ii) it requires solar illumination, therefore limiting the observations to day time overpasses and (iii) it is limited to areas with no cloud cover. These complicating factors limit the utility of solar reflectance measurements for soil moisture content determination, which have been so far mainly utilised in conjunction with techniques based on thermal infra-red radiation.

2.2.2 Thermal Radiation

Thermal infra-red remote sensing operates in a slightly longer wavelength region of the electromagnetic spectrum (3 -14μm) than visible remote sensing, and measures the thermal emission of the earth. Methods for inferring soil moisturecontent using thermal infra-red remote measurements are based on the effect of water on the thermal properties of the soil (heat capacity, thermal conductivity), which in turn affect the surface radiant temperature as well as the soil resistance to diurnal changes in temperatures due to external meteorological forcings (Ellyett and Pratt, 1975; Schmugge et al., 1980; Van de Griend and Engman, 1985). The amplitude of the diurnal range of soil surface temperature has been found to have a good correlation with the soil moisture content in the 0 to 2 and 0 to 4cm layers of a bare soil (Schmugge et al., 1980).

Thermal infra-red sensing can provide good spatial resolution from space sensors (~250m for infra-red and 1km for thermal bands). However, the effectiveness of these measurements is limited by cloud cover, vegetation and meteorological factors (Engman, 1990; de Troch et al., 1996), with measurements being severely hampered by the presence of even slight amounts of vegetation (Sadeghi et al., 1984), as the resulting image produced by the remote sensor may have no relation to the radiative temperature of the earth's surface below. However, in this case thermal infra-red observations may still be used to give an indication of plant moisture stress through rising leaf temperatures (McVicar and Jupp, 1998), which is an indication of the soil moisture status. Therefore, inference of soil moisture content from thermal infra-red imagery is usually performed in conjunction with imagery from the visible wave bands, in order to give some measure of the vegetation cover (Moran et al., 1994; Gillies et al., 1997; Goward et al., 2002; Wan et al., 2004; Verstraeten et al., 2006).

Methods for deriving soil moisture from thermal infra-red measurements evolved essentially in two directions (i) use of Soil Vegetation Atmosphere Transfer models to define the relationship between radiant temperature of the vegetation-bare soil mix and soil moisture and (ii) use of time series of diurnal surface temperature cycles to determine the relationship between thermal inertia and soil moisture. These methods and their limitations are briefly described below.

The first approach consists of inverting a one-dimensional Soil-Vegetation-Atmosphere-Transfer (SVAT) model using thermal infra-red observations of surface temperature. This was attempted in several studies (Ottlé et al., 1989 and Demarty et al., 2005 to name a few), using SVAT models which calculated the surface fluxes, surface temperature and soil moisture content by solving simultaneously the energy budget equation at the soil surface and above the canopy. The thermal and hydraulic transfers were described by three important processes: thermal inertia, hydraulic diffusivity and evaporation. Atmospheric data necessary to run the model were daily variation in incoming radiation, air temperature, humidity and wind speed. The three key vegetation parameters of the SVAT model were the height of the vegetation, minimum leaf resistance to evaporation and the Leaf Area Index (LAI).

Alternative approaches which relax the need for avoiding complex modeling of the land soil-vegetation-atmosphere interaction were developed by Carlson et al., 1994) and extended by Gillies et al. (1997), who generated regression relations between Normalised Difference Vegetation Index (NDVI), soil moisture, and soil temperature by careful analyses of available data. Although a unique relationship between surface soil moisture availability and radiant temperature does not exist in the presence of vegetation cover, if the 0% and 100% vegetation cover limits can be evaluated for a particular study area and the fractional vegetation cover is defined amongst these two extremes through NDVI observations, then a fairly stable relationship between soil temperature and soil moisture availability can be established (Moran et al., 1994). This can be a simple linear relationship (Moran et al., 1994) or a non-linear relationship derived from simulations with a SVAT modeling (Carlson et al., 1994). In either case the NDVI extremes for the study area need to be deduced from analysing yearly variation of NDVI in order to capture the annual vegetative response to soil moisture changes. One major question arising from a global soil moisture monitoring perspective is whether this relationship between NDVI, soil temperature and soil moisture can be defined from coarse-resolution space observation (Gillies et al., 1997).

The second type of approach for deriving soil moisture from thermal infra-red measurements is based on the concept of thermal inertia. Thermal inertia is a property of a materials (in the context discussed here, the mix of soil and water), which describes their resistance to temperature variations. The method developed by Mitra and Majumdar (2004) and later applied by Verstraeten et al. (2006) to spaceborne data is based on estimation of an apparent thermal inertia (ATI) through the combination of measurements of spectral surface albedo and diurnal temperature range. The strategy to derive water content is then based on the rationale that high ATI values correspond to maximum soil moisture content (the diurnal temperature range is the denominator in the calculation of ATI). Therefore, if extreme ATI values can be derived from time series analysis over a specific area, a soil moisture saturation index can be defined and converted to a soil moisture estimate through knowledge of the soil type in the area and consequently the soil moisture at saturation and residual.

It must be noted that the use of thermal infra-red measurements is limited to cloud free areas and complicated by vegetation masking of the soil surface. Moreover, such methods require meteorological and atmospheric information such as daily variation in incoming radiation, air temperature, humidity and wind speed if SVAT based retrieval methods are used, or time series of daily temperature variations and/or NDVI values which are long enough to encompass the full range of values for both variables (i.e., from maximum to minimum) experienced by the area of interest. Although the studies discussed showed that combined visible/thermal infra-red approaches have the potential to sense soil moisture, implementation from space has not been accomplished so far, and a soil moisture product has not been envisioned for future optical/IR missions. To overcome the problems of thermal infra-red methods for satellite based soil moisture remote sensing, attempts have been made to couple these approaches with remote sensing methods which employ the microwave region of the spectrum (Chauhan et al., 2003).

Table 2.1. Microwave band designations (Lillesand and Kiefer, 1994).

Band Designation	*Wavelength (cm)*	*Frequency (GHz)*
K_a	0.75 – 1.10	40.0 – 26.5
K	1.10 – 1.67	26.5 – 18.0
K_u	1.67 – 2.40	18.0 – 12.5
X	2.40 – 3.75	12.5 – 8.0
C	3.75 – 7.50	8.0 – 4.0
S	7.50 – 15.0	4.0 – 2.0
L	15.0 – 30.0	2.0 – 1.0
P	30.0 – 100	1.0 – 0.3

2.2.3 Microwave Radiation

Microwave remote sensing measures the electromagnetic radiation in the microwave region of the electromagnetic spectrum, which has wavelengths between 0.75 and 100cm, corresponding to frequencies between 40GHz and 0.3GHz. This region is subdivided into bands, which are often referred to by a lettering system (see Table 2.1). The radiation in this region of the spectrum is highly correlated with the dielectric properties of the soil which are mainly determined by the amount of water volume present.

The fundamental basis of microwave remote sensing for soil moisture content is the contrast between the dielectric constant of water (about 80 at frequencies below 5GHz) and that of dry soil (about 3.5) (Ulaby et al., 1986). As the volume fraction of water in the soil increases, both the real and imaginary parts of the soil dielectric constant (respectively $\varepsilon_G^{'}$ and $\varepsilon_G^{''}$) increase, depending on the soil particle distribution (Ulaby et al., 1986). This is shown in Figure 2.1 for different soil textures.

If it is assumed that the target being observed by the microwave sensor is a plane surface with surface geometric variations and volume discontinuities much less than the wavelength, only refraction and absorption of the media need to be considered. Therefore the reflectivity to microwave radiation of the soil/air interface can be related to the ratio between the dielectric constant of air (known) and soil through the Fresnel reflection equations, the relationship being dependent on the viewing angle and the polarisation of the radiation (Njoku and Entekhabi, 1996a). The smooth surface reflectivity (Γ*) at vertical (V) and horizontal (H) polarisation can therefore be expressed as:

$$\Gamma_V^*(\vartheta) = 1 - \left| \frac{\varepsilon_G \cos\vartheta - \sqrt{\varepsilon_G - \sin^2\vartheta}}{\varepsilon_G \cos\vartheta + \sqrt{\varepsilon_G - \sin^2\vartheta}} \right|^2 \text{, and} \tag{2.1}$$

$$\Gamma_H^*(\vartheta) = 1 - \left| \frac{\cos\vartheta - \sqrt{\varepsilon_G - \sin^2\vartheta}}{\cos\vartheta + \sqrt{\varepsilon_G - \sin^2\vartheta}} \right|^2 , \tag{2.2}$$

where ε_G is the soil dielectric constant (relative to that of air) and ϑ is the viewing angle. Following Kirchoff's reciprocity theorem, the microwave emissivity (*e*) of the target can be related to its microwave reflectivity as $\Gamma=1-e$.

The two basic approaches used in microwave remote sensing are active and passive. Active systems, otherwise known as radars, send out a pulse of electromagnetic radiation and measure the amount that is scattered back in the direction of the sensor (reflectivity). That backscatter coefficient is then related to the characteristics of the target. In contrast, passive systems measure the natural emission (emissivity) of the land surface at microwave frequencies using detectors, referred to as radiometers. Given the low frequency, the spatial resolution that can be achieved from space with the current technology is low for passive sensors (~40km, Kerr et al., 2001). For active sensors, the spatial resolution can be as fine as 10m from space (Wagner et al., 2006). A description of the fundamental basis and main characteristics of the methods to obtain soil moisture information from active and passive microwave observations is presented in the following sections.

2.2.3.1 Active Microwave Remote Sensing

Active microwave remote sensing involves the use of a radar antenna, which transmits wave pulses and receives a return signal whose intensity

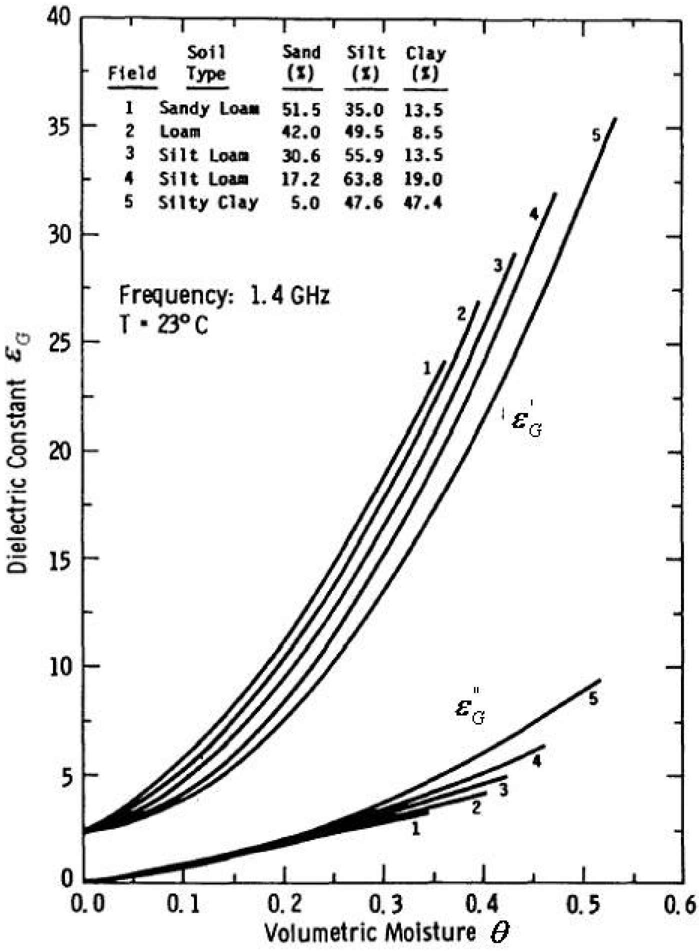

Figure 2.1. Real (ε_G') and imaginary(ε_G'') soil dielectric constant as a function of volumetric soil moisture content for five soils at 1.4GHz. Smooth curves were drawn through measured data points (from Ulaby et al., 1986).

varies with the target characteristics. The signals sent and received by aradar are usually polarised, either horizontally (H) or vertically (V). Possible combinations are HH, VV, HV and VH. The backscattering coefficients $\sigma^o_{PP,}$ where P is the polarisation, are used to describe the intensity of the reflected radiation from an object and are measured in decibel (dB) (Schmugge, 1985). The backscattering coefficients depend on wave polarisation, frequency and incidence angle (Schmugge, 1985) and are influenced by the dielectric constant of the soil (through surface reflectivity) and surface roughness for bare soils (Schmugge, 1985; Ulaby et al., 1986). For vegetation covered areas, the backscattering coefficients depend on the vegetation characteristics and on the soil's backscattering signal attenuated by the vegetation layer (Ulaby et al., 1982). Moreover, topographic relief has a significant effect on the backscattering signal (van Zyl et al., 1993).

The relationship between backscatter and dielectric constant is highly non-linear. The coefficients $\sigma^o{}_{vv}$ and $\sigma^o{}_{hh}$ increase with soil moisture at higher rates for lower dielectric constants, with $\sigma^o{}_{hh}$ shown to be less sensitive to variation in the dielectric constant than $\sigma^o{}_{vv}$. At approximately 35º-40º incidence angle, $\sigma^o{}_{hh}$ increases are typically about 5-6dB for a variation of dielectric constant between 3 and 30 (corresponding to a soil moisture range between 2% to 50%, depending on frequency and soil texture) as compared to an 8-10dB increase in $\sigma^o{}_{vv}$ (Hoeben et al., 1997; Shi et al., 1997). This range is fairly independent of the sensor frequency (Hoeben et al., 1997). The sensitivity of $\sigma^o{}_{vv}$ to changes in dielectric constant increases with incidence angles but becomes fairly stable in the 30º–50º range (Shi et al., 1997).

The effect of soil roughness on the backscattering signal is quantified through the surface height standard deviation (RMS). The effect of surface roughness may be synthesised by saying that, for a given frequency, the backscattering from soils with a higher RMS is less dependent on the value of the incidence angle (Ulaby et al., 1986). Therefore, the larger the incidence angle, the greater the sensitivity of the backscattering signal to RMS (Oh et al., 1992). In many cases the effects of roughness may be equal or greater than the effects of soil moisture on the backscattering (Engman et al., 1995). This might be more significant in ploughed fields, where the row structure generated by ploughing presents a regular pattern that can complicate data interpretation (Giacomelli et al., 1995). Furthermore, due to weathering, the surface roughness of agricultural fields is likely to change quickly in time between satellite overpasses, although for natural ecosystems it should not change significantly over relatively short time periods (Beaudoin et al., 1990; Sano et al., 1998). Roughness represents therefore a major issue in active microwave remote sensing. The soil moisture problem in active remote sensing becomes one of determining the roughness effect independently so that a model can be inverted to yield a measure of soil moisture (Oh et al., 1992; Engman et al., 1995; Jackson et al., 1996b).

The observations made with active microwave remote sensing are affected by vegetation cover that reduces the sensitivity of the return signal to the moisture content of the underlying soil (Wang et al., 1987; Engman et al., 1995). The return signal from the layer of vegetation is composed of four principal components: direct, reflected, direct-reflected and surface scattering (see Figure 2.2). All mechanisms include scattering and absorption of the signal by the vegetation components. The amount of absorption is primarily due to the water content of the vegetation (Schmugge, 1985), whilst the scattering is influenced by the vegetation shape and geometry (Engman et al., 1995; Giacomelli et al., 1995). The effect of vegetation is also greatly dependent upon the instrument's angle of incidence and on polarisation (Ulaby et al., 1986). Engman et al. (1995) showed that the attenuation of the backscattered signal for horizontal polarisation due to a corn canopy is relatively weak, but that the vertically polarised data are attenuated to a much greater degree because of their relationship to the canopy structure, which consists primarily of vertical stalks. Wang et al. (1987) have shown that the effect of vegetation cover does not play a significant role at low incidence angles. The influence of the vegetation on the radar signal can in general be diminished by decreasing the frequency. L-band (1-2GHz) measurements yield good results under various canopy types (Brown et al., 1992; Schmulluis and Furrer, 1992; van Zyl et al., 1993; Giacomelli et al., 1995), whereas for C-band (4-8GHz) even a thin vegetation cover may distort the measurement (Schmulluis et al., 1992).

Surface topography affects active microwave remote sensing observations mainly by changing the incidence angle due to the local slope (Hinse et al., 1988) and by changing the pixel size when, as is common, data are processed with a flat earth assumption (van Zyl et al., 1993). The

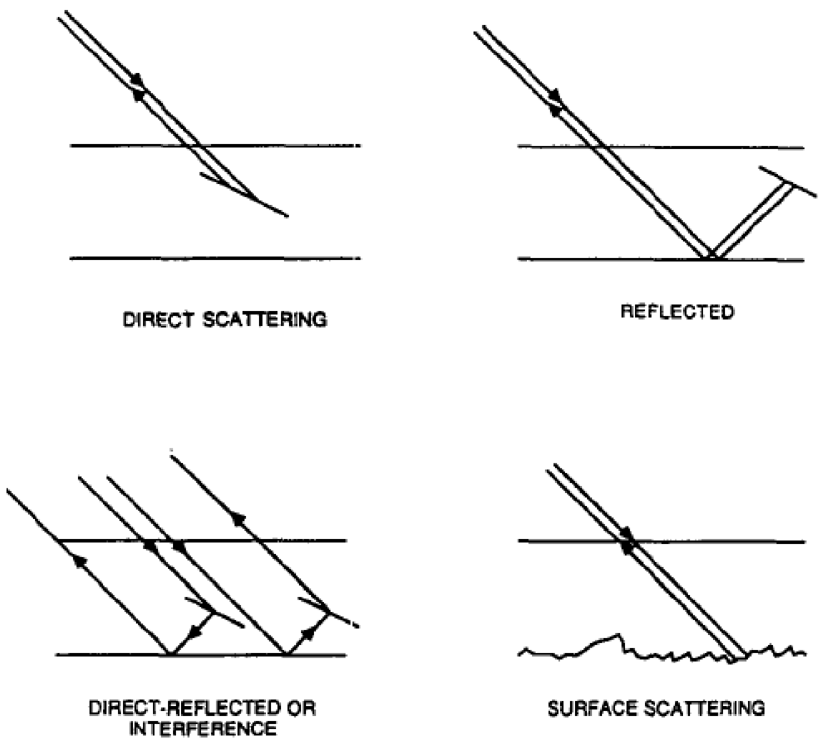

Figure 2.2. Dominant scattering mechanism from a vegetation layer Engman et al., 1995.

problem is more important for airborne systems than for spaceborne systems. However, it has been shown that these effects can be taken into account if a digital elevation model is available (Hinse et al., 1988; van Zyl et al., 1993).

Due to the sensitivity of the active microwave backscattering signal to surface roughness and vegetation cover, and the competing effect of frequency and incidence angle discussed in this section, there has been a great deal of discussion in the literature about an "optimum" configuration for active microwave remote sensing with satellites. In this section it has been discussed how the larger the incidence angle, the larger the sensitivity to soil moisture content, but also the higher the influence of both surface roughness and vegetation. Therefore there must be a compromise. Also, as frequency is increased the active microwave remote sensor becomes more sensitive to vegetation and the sensitivity to soil moisture content decreases. Moreover, the $\sigma^o_{vv.}$ Backscattering coefficient is generally more sensitive to soil moisture content than the $\sigma^o_{hh.}$ coefficient. Given that low incidence angles (i.e., reduced effect of vegetation and surface roughness) are very unlikely on a spacecraft system, as the resolution gets coarser with decreasing incidence angle according to $1/\sin\vartheta$ (Autret et al., 1989), it has been suggested that an active microwave remote sensing system characterised by an incidence angle of approximately 20°, *vv* polarisation and frequency of 5.3GHz (C-Band) would be the optimal configuration (Ulaby et al., 1978; Dobson and Ulaby, 1986; Dobson et al., 1992; Altese et al., 1996).

It should be noted that the radar configuration adopted by the upcoming NASA's Soil Moisture Active Passive (SMAP) mission will instead consist of an L-band radar at ~40° looking angle. This choice was driven by economical consideration (the need to utilise a shared antenna for the radar and the L-band radiometer) and scientific requirements dictating the need for a large incidence angle in order to ensure a three-day revisit time.

2.2.3.2 Passive Microwave Remote Sensing

Passive microwave remote sensors are radiometers that measure the thermal emission from the ground at microwave frequencies. As already discussed, the microwave emissivity (e) of a surface can be related to its microwave reflectivity Γ_P through Kirchoff's reciprocity theorem. The microwave reflectivity can in turn be related to the soil relative dielectric constant.

The dielectric constant can be computed as a function of soil moisture and other soil parameters such as soil moisture, soil salinity, bulk density and soil texture. Two main models have been developed to related the dielectric constant to soil moisture for the low frequency range (1–20GHz) by Wang and Schmugge (1980) and Dobson et al. (1985). These models have been found to be accurate except for the case of frozen soils, for which a specific model was developed by Hallikainen (1984), and for dry sandy soils, for which a simplified approach was proposed by Mätzler (1998).

Therefore the emissivity of a smooth bare soil surface at a given polarisation and angle can be defined once its volumetric soil moisture content and particle size distribution is known. The intensity of the radiation at microwave frequencies measured by a radiometer (usually called brightness temperature or radiobrightness, T_B, and measured in kelvin) viewing a smooth bare soil surface is given by:

$$T_{BP} = e_{GP} * T_S \,, \tag{2.3}$$

where P is the radiation polarisation, e_{GP} the polarised smooth surface emissivity and T_S is the soil temperature. (2.3) derives from Plank's blackbody radiation law through the Rayleigh-Jeans approximation for microwave frequencies (Schmugge, 1985; Njoku et al., 1996a).

The variation in soil emissivity exhibits a range from about 0.95 for dry soil (5%v/v) to 0.6 or less for wet soil (40%v/v) (Schmugge, 1985; Jackson and Le Vine, 1996a; Njoku et al., 1996a). For soil at a temperature of 300K, this variation in emissivity corresponds to a brightness temperature variation of 90K, which is much larger than the noise sensitivity threshold of a microwave radiometer, being typically less than 1K (Njoku et al., 1996a).

The simple expression in (2.3) between sensor measured radiation and soil moisture is complicated in an operational scenario by roughness of the soil surface, non-uniform soil moisture and temperature vertical profiles and presence of vegetation and/or litter layer above the soil (Choudhury et al., 1979; Jackson and Schmugge, 1991; Njoku et al., 1996a; Njoku et al., 1996b; Saleh et al., 2006a).

2.2.3.2.1 Impact of Surface Roughness

Field measurements made by Newton and Rouse (1980) and Wang et al. (1983) have indicated that rougher soil surface increases soil emissivity and decreases the sensitivity to soil moisture content (see Figure 2.3). This increase in emissivity can be attributed to the increase in soil surface area that interfaces with the air (Schmugge, 1985). Wang et al. (1983) noted that the effects of surface roughness decreases with the frequency.

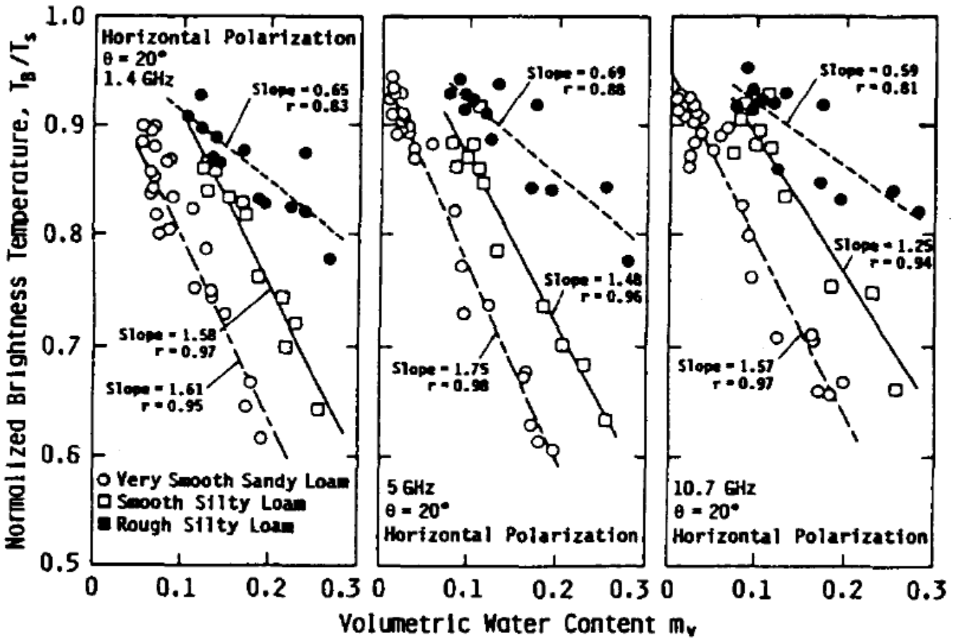

Figure 2.3. Variation in brightness temperature as a function of moisture content; for soils of different roughness at 1.4GHz, 5GHz, and 10.7GHz. (from Wang et al., 1983).

In order to account for this effect, (2.1) and (2.2) need to be modified to take into account the scattering of the radiation at the soil-air interface. Thereflectivity (Γ_P) of a rough surface is the sum of two components: (i) the non-coherent component, computed by integrating over the upper hemisphere the bistatic scattering coefficient which characterise the scattering of radiation from any direction to any other direction, and (ii) the coherent components, which depends on the smooth reflectivity (see (2.1) and (2.2)) and the standard deviation of the surface heights (Shi et al., 2002). Shi et al. (2002) showed that roughness effects differ strongly at different incidence angles and polarisations. At large incidence angles (ϑ~50°), the emission was found to increase at H polarisation as the geometric surface roughness increases. This confirmed earlier experimental observations (Choudhury et al., 1979; Wang, 1983; Wang et al., 1983). Conversely, at V polarisation, the emission was found to decrease. In the perspective of satellite application, it is difficult to compute the emissivity using this rigorous approach, as this requires complex theoretical approaches (such as the Advanced Integral Equation Model, AIEM) to derive expressions for the scattering coefficients over large and heterogeneous areas such are satellite pixel.

A simpler, semi-empirical expression for the rough surface reflectivity (Γ_P) was proposed by Wang and Choudhury (1981). This is based on two best fit parameters: a height parameter, H_R (which is related to the standard deviation of surface heights), and a polarisation mixing parameter, Q_R:

$$\Gamma_P(\vartheta) = \left[(1 - Q_R(\vartheta))\Gamma_P^*(\vartheta) + Q_R(\vartheta)\Gamma_Q^*(\vartheta)\right]\exp(-H_R(\vartheta)\cos^2\vartheta), \quad (2.4)$$

where the subscripts Q and P indicate V or H polarisations.

Wang et al. (1983) considered in a more detailed study that the $\cos^2\vartheta$ dependence was much too strong. Also, in the approach given by (2.4), considering that H_R increases with surface roughness effects leads to consider that emissivity increases with roughness at both H and V polarisations, which is in contradiction with theoretical analysis (Mo and Schmugge, 1987 ; Shi et al., 2002). The H_R parameter should be thus considered as dependent on angle and polarisation. Therefore a generalised semi-empirical formulation of roughness effects can be written as (Wigneron et al., 2007):

$$\Gamma_P(\vartheta) = \left[(1 - Q_R(\vartheta))\Gamma_P^*(\vartheta) + Q_R(\vartheta)\Gamma_Q^*(\vartheta)\right]\exp(-H_{RP}(\vartheta)\cos^{N_{RP}}\vartheta) \quad (2.5)$$

In this generalised formulation, the dependence of Q_R and H_R on ϑ and polarisation is accounted for and the N_{RP} exponent is inserted in the exponential term.

2.2.3.2.2 Impact of Vertical Soil Moisture and Temperature Profiles

The simple expression in (2.3) assumes constant soil moisture and temperature throughout the soil profile contributing to the microwave emission. At low frequencies, this profile may consist of a layer of several centimeters (Njoku et al., 1996a). The temperature and moisture contents of soils exhibit natural variability as a function of depth. Therefore it is not strictly correct to represent soil brightness temperature and emissivity by such approximations. To take this into account, the effective soil temperature (T_{EFF}) contributing to the soil microwave emission can be computed from the radiative transfer theory as (Choudhury et al., 1982):

$$T_{EFF} = \int_0^\infty T_S(z)\alpha(z)\exp\left[-\int_0^z \alpha(z')dz'\right]dz\,, \tag{2.6}$$

where $T_s(z)$ is the soil temperature at depth z, and the attenuation coefficient $\alpha(z)$ is related to the soil dielectric constant as:

$$\alpha(z) = (4\pi/\lambda)\varepsilon_G''(z)/2(\varepsilon_G'(z))^{1/2}\,, \tag{2.7}$$

where λ is the wavelength of observation.

Using this physical approach, T_{EFF} can be computed using measured profiles of both soil moisture (which is used to compute the soil dielectric constant in (2.7)) and soil temperature. Due to the difficulties in obtaining accurate soil moisture and temperature profiles over large areas, a simple linear parameterisation was been developed using controlled experiments at L-band (Choudhury et al., 1982). This parameterisation makes use of temperature measurements at two depths and an empirical attenuation coefficient which is a function of the surface soil moisture content:

$$T_{EFF} = T_{DEPTH} + C_t(T_{SURF} - T_{DEPTH})\,, \tag{2.8}$$

where T_{DEPTH} is the deep soil temperature (approximately at 50 or 100cm) and T_{SURF} is the surface temperature (approximately corresponding to a depth interval of 0–5cm). Choudhury et al. (1982) suggested that the surface temperature may be estimated from thermal infra-red observations, or meteorological data of near-surface air temperature, while the deep soil temperature can be modelled based on geographic location and season. Choudhury et al. (1982) calibrated constant values of the C_t parameter for several frequency bands, with C_t being equal to 0.246 at L-band.

2.2.3.2.3 Impact of Vegetation

Vegetation emits microwave radiation, whilst it also absorbs and scatters the radiation coming from the soil. It therefore reduces the sensitivity of the observed brightness temperatures to soil moisture changes (Van de Griend et al., 1985; Jackson et al., 1996a). This attenuation increases as frequency increases (Jackson et al., 1996b; Wigneron et al., 1998). For a sufficiently thick layer of vegetation, only the radiation from the vegetation itself is observed (Schmugge, 1985).

In early theoretical studies, Basharinov and Shutko (1975) and Kirdiashev et al. (1979) modeled the soil-canopy system as a two-layer incoherent non-scattering medium with a negligible albedo. In this model the vegetation is treated simply as an absorbing layer at a temperature T_V Overlaying a soil layer of temperature T_S. The brightness temperature above the canopy is given by:

$$T_B = T_V + (e-1)\exp(-2\tau) + e(\frac{T_S}{T_V} - 1)\exp(-\tau)\,, \tag{2.9}$$

where τ is a one-way canopy absorption factor or optical depth which is dependent on the vegetation dielectric properties, plant shape and structure, frequency, polarisation and look angle A more sophisticated approach was later developed by Mo et al. (1982), who proposed the usually so called 'τ-ω' model, which makes use of two parameters to characterise the absorption and scattering of the soil signal through the vegetation canopy, the optical depth τ and the single scattering albedo ω. In this model the polarised brightness temperature observed above the canopy is written as:

$$\begin{aligned} T_{BP}(\vartheta) = {} & (1-\omega_P(\vartheta))(1-\gamma_P(\vartheta))(1+\Gamma_P(\vartheta)\gamma_P(\vartheta))T_V + \\ & +(1-\Gamma_P(\vartheta))\gamma_P(\vartheta)T_S\,, \end{aligned} \tag{2.10}$$

where the vegetation attenuation factor γ_P is written as a function of the optical depth τ as:

$$\gamma_P(\vartheta) = \exp(-\tau_P(\vartheta)/\cos\vartheta)\,. \tag{2.11}$$

The second term on the right hand side of (2.10) computes the attenuation of the microwave signal radiating up from the soil through the vegetation layer, while the first term accounts for (i) the upward vegetation radiation and (ii) the downward vegetation radiation reflected by the soil and attenuated by the vegetation in this upward path. At microwave frequencies the single scattering albedo term is almost zero, varying between 0.05 and 0.10 (Jackson et al., 1991; Wigneron et al., 2004; Wigneron et al., 2007).

This model is a zero-order solution of the radiative transfer equations as it assumes that the vegetation scattering phase matrix term can be neglected (Ulaby et al., 1986; Mätzler et al., 2006). The τ–ω model has been found to be an accurate approach to model the L-band emission from a vegetation canopy in numerous studies (Mo et al., 1982; Jackson et al., 1991; Wigneron et al., 1995; Van de Griend and Wigneron, 2004; Wigneron et al., 2004) and it is also a tractable tool for the process of inversion (Wigneron et al., 1995; Wigneron et al., 2000; Wigneron et al., 2003).

Various theoretical and empirical relationships have been proposed for the optical depth required by the τ–ω model. Basharinov et al. (1975) proposed that $\tau = l\alpha \sec\vartheta$, where l is the thickness of the vegetation layer with an absorptivity α. However, this simple parameterisation does not explain the observed polarisation and angular dependence of the vegetation effect on the microwave signal (Van de Griend and Owe, 1994; Wigneron et al., 1995; Wigneron et al., 2004), which may be significant for crops with predominant vertical plant structure. Therefore, Kirdiashev et al. (1979) and similarly Njoku et al. (1996a) proposed that the optical depth be computed as:

$$\tau_P(\vartheta) = \frac{Af\theta_{veg}\varepsilon''_{veg}}{\cos\vartheta}, \tag{2.12}$$

where A is a structure parameter related to the geometry of the vegetation, f is the observation frequency (Hz), θ_{veg} is the VWC (kg/m^2) and ε''_{veg} is the imaginary part of the dielectric constant of the vegetation. The parameter A can be obtained by modeling the vegetation as cylinders or discs with different orientations, but it is more commonly estimated empirically for specific vegetation types (Njoku et al., 1996a).

An empirical relationship between optical depth and VWC has been given by (Jackson et al., 1982; Jackson et al., 1991), by lumping all parameters in (2.12) except θ_{veg} into a regression parameter b which is unique to the type of vegetation, the radiation frequency, polarisation and incidence angle:

$$\tau_P(\vartheta) = b\theta_{veg} . \tag{2.13}$$

Jackson (1993) presented a plot of b for different frequencies and vegetation types as presented in Figure 2.4. An interesting observation of Figure 2.4 is that at low frequencies, b is found to be only weakly dependent on vegetation type. Based on these results, it would appear that at L-band (wavelength 15 to 30cm) a single value of b equal to 0.15 is representative of most agricultural crops (Jackson, 1993). Several studies have concentrated on the determination of suitable values of parameter b for a variety of vegetation types. At L-band a value of b=0.12±0.03 was found to satisfactorily represent the dependence of vegetation opacity (referenced to nadir, i.e. $\vartheta = 0$) on its water content for a range of grass and agricultural crops with θ_{veg} from 0.5 to 6kg/m^2 (Mo et al., 1982; Jackson et al., 1991; Van de Griend et al., 2004). Values of b reported in these studies are generally average values based on brightness temperatures measurements made at various incidence angles.

As the SMOS L2 soil moisture retrieval algorithm is based on bi-polarised, multi-angular measurements, it is important to account for the dependence of the optical depth on incidence angle and polarisation. More recent studies have indicated that although the main determinant of the b values appears to be vegetation type, the dependence of b on polarisation may also be significant over several crops and that while the dependence of b on incidence angle was observed to be generally low at H polarisation, it may be significant at V polarisation (Wigneron et al., 1995; Van de Griend et al., 2004; Wigneron et al., 2004; Wigneron et al., 2007). This will be discussed in more detailed in Chapter 3.

Several studies have also shown that the effect of litter on the microwave signal is significant (Schmugge et al., 1988; Jackson et al., 1991; Wigneron et al., 2004; Saleh et al., 2006a). Litter can be present below most vegetation

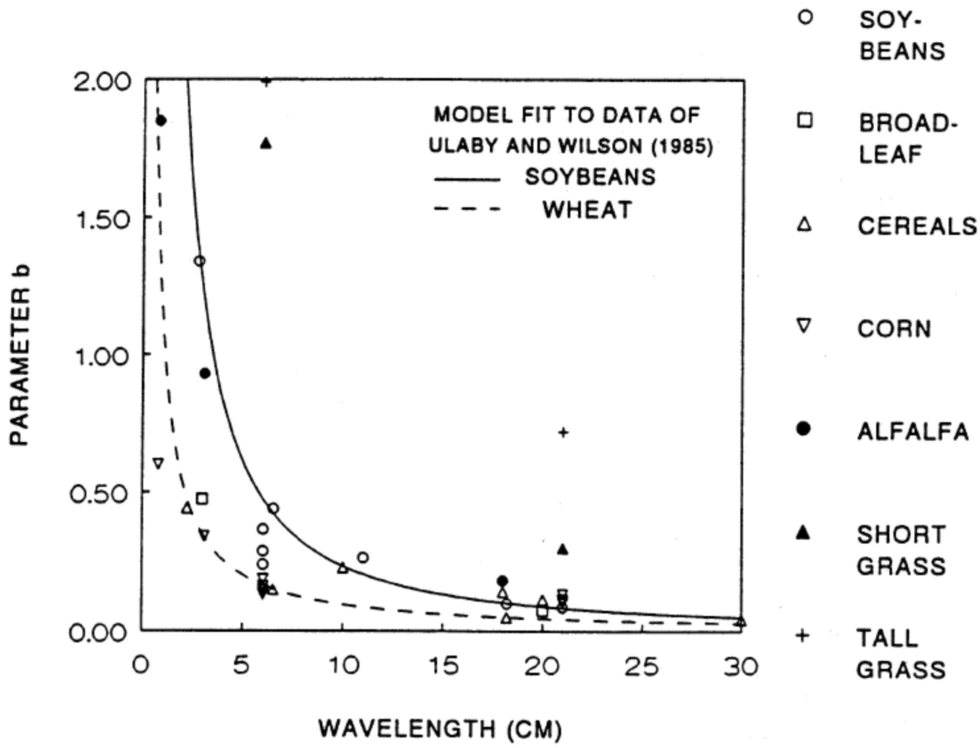

Figure 2.4. Observed values of the effects of vegetation on model parameter *b* as a function of wavelength (from Jackson, 1993).

canopies in fields which are not (or rarely) ploughed, like prairies or below non-agricultural canopies, natural covers and forests. Currently no method has been proposed to take into account the effect of litter, and this is generally considered implicitly by increasing the value of parameter *b* (Wigneron et al., 2007).

2.2.4 Applicability of Remote Sensing to Global Soil Moisture Monitoring

There is now a wide consensus in the scientific community that microwave remote sensing is the most promising technology for global soil moisture monitoring (Engman et al., 1995; Jackson et al., 1996b; Wigneron et al., 2003; Prigent et al., 2005; Wagner et al., 2006; Wagner et al., 2007). This is because this domain of the electromagnetic spectrum presents some major advantages over the infra-red and visible domains which make it appealing for global soil moisture monitoring purposes. The advantages of passive microwave remote sensing over the other methods are discussed hereby.

Microwave remote sensing offers a relatively direct means of assessing soil moisture since it exploits, like many *in situ* observation techniques (e.g., Time Domain Reflectometry probes or capacitance probes), the strong relationship between the moisture content and dielectric constant of the soil. This relationship is fairly well understood and depends only on soil texture at a given frequency (Wang et al., 1980; Wang et al., 1983; Ulaby et al., 1986). Conversely, infra-red and visible remote sensing technologies are based on a less direct relationship between the observed variable, soil surface temperature and albedo, respectively, and the retrieved variable, soil moisture. In the case of infra-red techniques, for example, the relationship between the diurnal cycle of surface temperature is not only associated with the thermal inertia determined by soil moisture but also strongly affected by micrometeorological conditions and to surface characteristics (vegetation, thermal conductivity K, and heat capacity C). For example, in areas where the surface temperature T_s is controlled by evaporation, not by thermal inertia, the T_s diurnal amplitude extracted from the infra-red observations is not well correlated with the soil moisture (Prigent et al., 2005).

Another important advantage of microwave techniques is that at lower frequencies the depth of soil layer which contributes to the emission, and therefore the depth of soil layer for which information can be retrieved by remote sensors, is greater. This is due to the fact that attenuation of an electromagnetic radiation through a medium is frequency dependent (Kong, 1990). For the microwave frequencies considered optimal for soil moisture retrieval (1-3GHz), the contributing depth is theoretically between 10cm and 1m, although field experiments suggested that the actual contributing depth is closer to about 1/4 the wavelength (based on a wavelength range of 2-21cm) (Jackson et al., 1996b). This is nevertheless a greater contributing depth than that of infra-red and visible radiation, which is of the order of 1mm (Idso et al., 1975). Several studies has shown that the soil moisture information provided by remote sensing technology for the near-surface layer can be used in combination with land surface modeling to retrieve the soil moisture content at much greater depth (e.g. Houser et al., 1998;

Walker et al., 2001), further extending the benefits of improvements in remote sensing technology

As discussed in previous sections, the effect of vegetation on electromagnetic radiation is amongst the most serious problem for all remote sensing techniques presented. Nevertheless, visible and infra-red measurements are hampered by perturbation of the signal by the vegetation in a more serious way than microwave measurements (Sadeghi et al., 1984). At microwave frequencies instead vegetation appears semi-transparent. Jackson et al. (1991) showed that theoretically the sensitivity of L-band (1.4GHz) microwave observations to soil moisture at a VWC of 3kg/m^2 (typical of a mature crop) is only halved with respect to that over a bare soil. It appears that 7kg/m^2 in plant water content is the limiting situation, reducing the sensitivity to about 25% of the bare soil case (Schmugge et al., 2002). However, as the frequency increases the sensitivity of microwave observations to soil moisture is more strongly affected the vegetation layer. For example, at C-band (4-8GHZ) passive microwave observations appear to be insensitive to changes in soil moisture for a canopy with a VWC of 1-2kg/m^2 (Guha and Lakshmi, 2002; Jackson et al., 2005).

Microwave measurements have the significant advantage of being independent of solar illumination, and therefore can be made at any time of the day or night (Jackson et al., 1996b; Schmugge et al., 2002). It has been shown that night time observations may prove more accurate for soil moisture retrieval from spaceborne platforms due to the more homogeneous vertical and horizontal temperature profiles (Owe et al., 2001; Draper et al., 2009). Moreover, air, vegetation and soil temperature are almost in equilibrium at sunrise (Kerr et al., 2001), minimising the perturbation of gradient between soil and vegetation canopy on the microwave signal.

The attenuation of the radiation by atmospheric gases and clouds in the atmosphere is negligible for microwave frequencies below 3GHz (Schmugge, 1985). In the case of visible and thermal radiation, clouds as well as atmospheric temperature and water vapour add serious perturbations to the signal, therefore requiring pre-processing of the observations to mask cloud and correct for atmospheric attenuation (Wan and Li, 1997; Wan and Dozier, 1996; Wan et al., 2004; Verstraeten et al., 2006).

Therefore, implementation of soil moisture retrieval from satellite using visible and infra-red measurements has been so far limited to determination of draught onset through monitoring of plant water stress, which is only indirectly related to soil moisture (Wan et al., 2004), or combination of visible/infra-red techniques with microwave observations (Chauhan et al., 2003; Verstraeten et al., 2006). A soil moisture product has not been slated for future optical/IR missions so far (Chauhan et al., 2003).

2.2.5 Past and Current Microwave Space-Sensor

The afore mentioned advantages of microwave remote sensing have boosted research into the use of low frequency passive and active microwave technology on spaceborne platforms. From an operational point of view, the current generation of spaceborne microwave radiometers is not optimal for soil moisture sensing in terms of their spatial resolution and frequency. Under low vegetation conditions (less than 1-2kg/m^2), however, the 6.6 and 10.7GHz channels of the Scanning Multichannel Microwave Radiometer (SMMR, 1978-1987) and the 6.9 and 10.7GHz channels of the Advanced Microwave Scanning Radiometer (AMSR-E, 2002) have adequate sensitivity to surface soil moisture and have proved to be useful for monitoring of trends in surface soil moisture conditions despite their non-optimal frequencies (Owe et al., 2001; Owe et al., 2007; Rudiger et al., 2007; Wagner et al., 2007; Draper et al., 2009). Amongst the active microwave systems with configurations suitable for soil moisture remote sensing, several satellites that have been launched in the 1990s carrying a Synthetic Aperture Radar (SAR). Most spaceborne SAR systems have operated at C-band, such as the European Remote Sensing Satellites ERS-1/2 (1991) and Environmental Satellite ENVISAT (2002), and the Canadian RAdar SATellite RADARSAT (1995), but also L-band SAR systems have also been used, e.g. on the Japanese satellite Japanese Earth Resources Satellite JERS-1 (1992-1998). Nevertheless, given the difficulty of modeling the effect of vegetation and surface roughness on active microwave observations, it has not yet been demonstrated that currently available single-frequency C- and L-band SAR systems can be used for operational soil moisture applications at the field scale. This is mainly due to the lack of retrieval algorithms, that are both sophisticated enough to capture the complex scattering mechanisms involved, and of tractable tools for global application (Wagner et al., 2006).

The most important difference between active and passive microwave remote sensing systems is the ground resolution that can be achieved. Active sensors have the capability to provide fine spatial resolution (on the order of tens of meters from space platforms (Wagner et al., 2006)). On the other hand, the passive systems require larger antennas to be able to detect the relatively weak natural microwave emission of the earth surface (Kerr et al., 2001). As large antennas in orbit are an engineering challenge, resolutions achieved from space so far with passive microwave radiometers have been not better than ~50km at 6.9GHz frequency for the most recent passive microwave system (AMSR-E)(Njoku et al., 2003). Current meteorological and climate models use computational cells on the order of 10-100km, which may be well within the capacity of passive systems. However, for more detailed hydrologic process studies and partial area hydrology modelling is required, the passive data would appear to be of little use (Engman et al., 1995). It is in this context that the active systems appear promising. On the other hand active microwave systems are affected more seriously by surface roughness, topography and vegetation than passive systems. For active microwave the soil moisture retrieval capability appears to be limited to vegetation cover with less than about 0.5–1kg/m^2 water content (Dobson et al., 1986; Dubois et al., 1995; Oh et al., 1992).

2.2.6 SMOS and SMAP

Within the microwave region of the electromagnetic spectrum, the low frequency microwave range of 1-3GHz (30-10cm wavelength) is considered most suitable for passive microwave soil moisture sensing, owing to the reduced atmospheric and vegetation attenuation, deeper penetration depth, and higher soil moisture sensitivity (Wang et al., 1981; Schmugge, 1985; Jackson et al., 1996b). Most studies to date have focused on observations at 1.4GHz (L-band), as this is in a protected radio astronomy band where there is little Radio Frequency Interference (RFI). Numerous field experiments using ground-based and airborne L-band observations indicated a soil moisture retrieval capability of approximately 4%v/v accuracy or better for vegetation cover with water content up to about 5kg/m^2 for passive microwave systems (Wang et al., 1990a; Schmugge et al., 1992; Jackson et al., 1995a; O'Neill et al., 1996; Jackson et al., 1999; Mohanty et al., 2000a; Mohanty et al., 2000b; Guha et al., 2003; Uitdewilligen et al., 2003; Panciera et al., 2008b).

There is currently no passive microwave sensor in space with this optimal frequency. Nevertheless, two soil moisture specific satellite missions are planned for the next decade, the SMOS mission and NASA's Soil Moisture Active Passive (SMAP) mission, due to be launched respectively in 2009 and 2013 respectively, which will enable evaluation of the current satellite technology for soil moisture sensing at L-band frequency. In the case of SMOS, an innovative passive interferometric measurement principle is used to create a large "virtual" antenna by using a Y-shaped structure, a technique widely used in radio astronomy (Kerr et al., 2000). SMOS is the first mission to carry such a sensor in space which will provide new and significant capabilities, especially in terms of multi-angular viewing configuration. SMOS will in fact provide bi-polarised observations at several incidence angles (from nadir to ~55°) over almost the same location and will achieve a spatial resolution of better than 50km (Kerr et al., 2001).

SMAP will instead combine an L-band radiometer and an L-band radar sharing the same 6m wide conically rotating antenna/feed, allowing simultaneous active and passive microwave observation of the same portion of the earth surface at respectively 3 and 40km resolution (NASA, 2007). The innovative component of SMAP is the potential to provide fine-resolution (10km) soil moisture observations through combination of radar and radiometer measurements (NASA, 2007). Other objective of the mission include providing global measurements of soil moisture at 40km resolution through the radiometer, and providing global freeze/thaw state observations at 3km resolution through the radar.

For both missions, the radiometer footprint will cover an area of approximately 40km. However, as discussed in section 2.1, land surface exhibits considerable spatial heterogeneity at this scale. Thus, the observed brightness temperatures provided by SMOS and SMAP will be spatial averages of the various radiation components of the heterogeneous scene in the Field Of View (FOV) of the radiometer. Any retrieval based solely on these observations will result in 'average' retrieved quantities. As the effects on emitted microwave radiation of moisture, vegetation, and temperature combine in a nonlinear manner (see section 2.2.3.2), the retrieved 'average' quantities, such as soil moisture, will not in most cases represent true spatial averages of the actual quantities (Njoku et al., 1996a). SMAP proposes to partially overcome this problem by using the radar observations to obtain downscaled soil moisture information at 10km resolution. However, this is a relatively large scale at which retrieved soil moisture might still be affected by the problem of horizontal heterogeneities. There is little published literature on this topic, particularly concerning the coarse scales typical of satellite footprints and using real passive microwave observations, and it remains a much needed area for further study. In particular, it is of interest to estimate the errors introduced by the non-linearity inherent in the spatially averaged soil moisture obtained by current state-of-the-art retrieval methods based on (2.10).

2.3 Effect of Land Surface Heterogeneity on Passive Microwave Remote Sensing

The effect of surface heterogeneity on soil moisture retrieval can be illustrated with a very simple synthetic example. Let us consider the relationship between soil moisture and brightness temperature as predicted by a state-of-the-art radiative transfer model as shown in Figure 2.5, for a field which is divided in two fractions, one at 0.1%v/v and the other at 0.5%v/v soil moisture content, with every other land surface parameter constant between the two fractions. Given that the relationship is clearly non-linear, if soil moisture is retrieved from the average brightness temperature resulting from the direct emission of the two different fractions of the pixel (dashed gray lines in Figure 2.5), the retrieved soil moisture of the pixel (solid black line) will (in theory) present an error as large as 4%v/v, the total error budget for a satellite soil moisture mission, resulting solely from sub-pixel heterogeneity of soil moisture. It is readily observable that the error between retrieved and field mean soil moisture will vary depending on vegetation conditions and soil texture affecting the relationship between soil moisture and brightness temperature.

From purely theoretical considerations it can be deducted that surface heterogeneity should produce an error in soil moisture retrieval of large scenes (like that of a satellite footprint) only when the heterogeneous factor is one of those that affect the microwave emission (as modeled in the emission model) in a non-linear way. Heterogeneity in soil temperature and single scattering albedo, for example, should produce no error (although uncertainty on their exact average value would still produce absolute errors in soil moisture retrieval), as brightness temperatures scale linearly with these parameters. Other parameters, such as VWC, soil texture and roughness, instead, affect the surface microwave emission in a non-linear way, and therefore the brightness temperature curve of a mixed pixel will differ from that of the same pixel with arithmetic averages for VWC and soil texture, producing the above discussed error. The synthetic example shown here is a simplification of what would happen in the real world in three ways: (i) It assumes that the model is perfect, meaning that it simulates the exact brightness temperature-soil moisture relationship for given surface conditions; (ii) it considers only the heterogeneity of soil moisture within the field, while other factors like VWC and soil texture are considered uniform; (iii) it assumes that brightness temperature fields scale linearly with resolution, so that a coarse-resolution brightness temperature

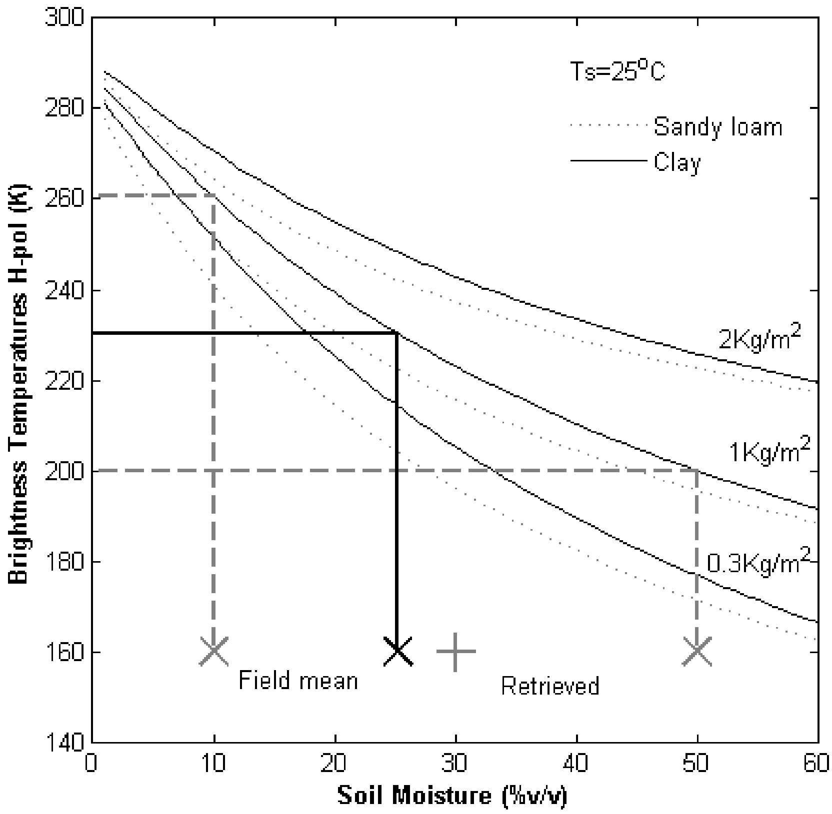

Figure 2.5. Illustrative example of the effect of radiative transfer non-linearities on soil moisture retrieval, for two different soil type, sandy loam and clay, both at 25ºCelsius and three different VWC (0.3,1 and 2kg/m^2). The model used to produce these curves is the L-band Microwave Emission of the Biosphere Model (SMOS mission).

observation can be derived from finer-resolution observations by simple linear averaging.

The error induced by land surface heterogeneity in a real application (like that of retrieval from a coarse satellite footprint) will also be affected by error in the radiative transfer model representation of the physics of microwave emission, and by the combined effect of heterogeneity in soil moisture and other land surface characteristics that contribute to the emission. Moreover, there will likely be a physical connection between the variability across the pixel of each land surface factor and that of soil moisture (e.g., sandy soils tend to exhibit drier conditions). This will result in an increase or decrease of the soil moisture retrieval error, depending on the relative effect of soil moisture and the land surface factor on the brightness temperature.

The studies which have dealt with the problem of land surface heterogeneity and its effect on soil moisture retrieval from coarse observations have approached the problem in three distinct ways: (i) analytical approaches which have used synthetic soil moisture and associated brightness temperature fields, (ii) simulation experiments which have coupled land surface models with more or less realistic land surface conditions to generate "real world" soil moisture distribution and microwave emission models to produce brightness temperature fields, and (iii) experimental studies which made use of real (airborne or spaceborne) brightness temperature data acquired over test sites. These three approaches and their main findings are discussed in the following sections.

2.3.1 Analytical studies

Initial studies addressed the effect of heterogeneity on soil moisture in a synthetic framework and analysed the effect of each land surface factor on the soil moisture retrieval separately. Njoku et al. (1996b) derived analytical expressions for the effects of the individual heterogeneity of soil moisture, soil temperature, and vegetation on the coarse-scale microwave sensor-averaged (or "effective") value of each individual parameter (i.e., the pixel average value that results in the same microwave radiation as that produced by the spatially heterogeneous field), which may be significantly different from the area-averaged (or "composite") parameters that are often assumed to be estimated by the remote sensors (like that obtained, for example, by simple averaging of the measured VWC over an area). This study showed that only in the case of emissivity and soil temperature are the coarse-scale effective values simple averages of the component parameters weighted by their fractional coverage areas as is often assumed (note that these two parameters affect brightness temperature in a linear way, as discussed in the previous section). In the case of vegetated surfaces, the retrieved effective optical depth was smaller than the composite one. This underestimation is greater for large VWC contrasts within the pixel. Soil moisture heterogeneity by itself had a negligible effect on the difference between field averaged and sensor-averaged soil moisture so long as the area was vegetation free (bare). The error was somewhat larger at higher frequencies (C-band) than at lower frequencies (L-band). This study concluded that in many situations, the differences between effective and composite surface parameters may be small and can be safely neglected. However, in some cases, particularly in semi-arid environments or agricultural areas where large parameter contrasts exist between bare and vegetated surfaces, unexpectedly large differences may occur that need to be addressed.

Through simulated spatially heterogeneous L-band radiometer footprints over a 15-day drydown, Galantowicz et al. (2000) addressed specifically the problem of soil type heterogeneity, previously ignored. The study concluded that the magnitude of the soil moisture retrieval error induced by soil type heterogeneity alone for bare soil regions was 0.7%v/v. This error is smaller than the error due to instrument noise for a typical radiometer (brightness temperature uncertainty 2K, soil moisture uncertainty of about 2%v/v) (Jackson et al., 1995a; Njoku and Li, 1999).

The first study to consider the combined effect of heterogeneity of different land surface factors was that of Bindlish et al. (2002), which synthetically analysed the effect of perturbations around the pixel mean value in soil moisture, soil temperature, NDVI (as a proxy for VWC) and soil texture on the coarse-scale soil moisture retrieval. In this study the mean VWC was made to vary from 0 to 4kg/m^2, with a fixed standard deviation of 0.5kg/m^2 for each level. Soil temperature varied between 5ºC and 35ºC, with a fixed standard variation of 5ºC. A variability of 15% in percent sand and clay was used for each of twelve different soil texture types. Beside confirming that with the set level of variance the individual effect of soil moisture, soil texture and soil temperature perturbations resulted in soil moisture errors that were within the instrument noise of the radiometer (approximately 2K for the ESTAR radiometer considered in this study), this study found that the effect of perturbations in VWC could induce errors in retrieved soil moisture as high as 15% around the mean value. Moreover, when considering the combined effect of the sub-pixel heterogeneity of the above factors, the absolute error between mean soil moisture and sensor retrieved soil moisture consistently exceeded the uncertainty in soil moisture estimates associated with the instrument error. Bindlish et al. (2002) also showed that the τ-ω based soil moisture retrieval algorithm used, (the common approach of Jackson et al., 1995a) scaled linearly with respect to the distribution of the vegetation biomass within the pixel, i.e., given a level of NDVI variance within the pixel, it was the average NDVI value and not its actual spatial distribution within the pixel that was important in determining microwave response of the footprint. This had been previously observed by Liou et al. (1998) who analysed 1.4GHz brightness temperatures simulated from a 50% mix of simulated bare and grassland (3.7kg/m^2), pixels with different distributions of the same mean vegetation amount throughout the pixel (tiled or randomly distributed). An important finding of Bindlish et al. (2002) was that surface heterogeneity produced the highest soil moisture retrieval error (12% around the mean soil moisture value of the synthetic footprint) when the VWC was high (~4kg/m^2) and/or when the land surface was cool and wet. As shown in Figure 2.5, under these circumstances the slope of the relationship between brightness temperature and soil moisture (and therefore the sensitivity of the brightness temperature to soil moisture) is reduced (see Figure 2.5), and so is the algorithm's ability to capture small changes in soil moisture.

The effect of land surface heterogeneity on soil moisture retrievals from multi-angle SMOS type observations has been explored with a synthetic scenario by only two studies so far (Van de Griend et al., 2003; Davenport et al., 2008). Davenport et al. (2008) approached this problem by generating single- and multi-angle synthetic scenes using the τ-ω modeling approach and analysed the effect of heterogeneity in three factors: soil surface roughness, soil moisture, and vegetation optical depth. Results indicated that heterogeneity in soil roughness had only a small effect on soil moisture retrieval from single-angle observations (0.5%v/v). It affected multi-angle data more seriously (2.1%v/v), but this error could be reduced by retrieving a representative value of soil roughness from the data (retrieved values are lower than the average of the real values). Reasonable spread in soil moisture (10%v/v) yielded small or negligible errors (0.5%v/v for single-angle observations, 1.7%v/v for multi-angle). The effect of vegetation optical depth heterogeneity (0-0.6) appeared to be significant (6.1%v/v error in retrieved soil moisture). It was observed that since the major effect of vegetation in the τ-ω model is to obstruct the target surface by exponential attenuation, a pixel containing areas with a range of vegetation optical depths will not have the same brightness temperature curve as a pixel with a single uniform optical depth with the same mean. Therefore a simplistic modification to the model was proposed, which represents vegetation as a weighted average of bare soil and vegetation, the relative fraction of which can be retrieved as an extra parameter by multi-angle data. This significantly reduced the error induced by vegetation heterogeneity (to 1%v/v), as not one uniform optical depth is used, but rather two, one set at zero (for the bare fraction) and one retrieved (for the vegetated fraction).

The key findings of Davenport et al. (2008) are that (i) single-angle retrievals are less affected by heterogeneity of all factors than multi-angle retrieval. This is because in multi-angle configuration, the composite brightness temperature curve does not correspond to a single τ-ω scenario, therefore the model distorts other variables (including soil moisture) to fit the curve; (ii) the highest errors are observed for scenarios with high soil moisture contents and high optical depth values (with the same spread of heterogeneity around the mean values); and (iii) the effect of heterogeneity can be taken into account when using multi-angle observations allowing for an “effective” optical depth to be retrieved (including the fractions of bare and vegetated areas). This will be smaller than the effective mean optical depth and compensate for heterogeneity. It should noted however Note that in this approach, the retrieved fraction and optical depths do not correspond to real physical quantities, but are rather fictional quantities used to compensate for the heterogeneity.

Similar results were obtained by Van de Griend et al. (2003). They showed that under wet soil conditions where the soil signal is weaker, the retrieval errors can be beyond the value of 4%v/v when assuming a single vegetation optical depth even for a 50% pixel fraction cover of a moderate vegetation density of $3kg/m^2$, typical of a mature crop

In all the above studies the land surface heterogeneity in the mixed pixel was simulated in a somewhat arbitrary manner which was not necessarily realistic (i.e., did not reflect physical links between land surface characteristics and soil moisture existing in the real world). In a real application, the amount of heterogeneity will vary from pixel to pixel, and there will be a physical link between soil moisture variability and, for example, heterogeneity in soil texture and vegetation density. The studies presented in the next sections analysed the effect of heterogeneity using more realistic land surface conditions, generally derived from land surface models.

2.3.2 Simulation Experiments

In the absence of real L-band satellite observations, the impact of complex land surface heterogeneity on soil moisture retrieval over large scales typical of satellite pixels has been mainly analysed using brightness temperatures simulated with microwave emission models given a more or less physically realistic soil moisture background derived from a land surface model. This was the approach used by Crow et al. (2001) and Lakshmi et al. (1997) in the case of C-band observations (like AMSR-E), and by Burke et al. (2004), Davenport et al. (2008), Loew (2008) and Van de Griend et al. (2003) for L-band, SMOS type observations.

Crow et al. (2001) performed a complete AMSR-E observation simulation experiment, including land surface heterogeneity over the entire $575,000km^2$ Red-Arkansas River basin in the south-central United States. Using a two-polarisation, single-channel retrieval (C-band) to retrieve coarse-scale soil moisture and comparing it with the average of fine-resolution soil moisture data produced by a land surface model, they found that errors due the spatial heterogeneity were positively correlated with the density of vegetation cover and that it was of the order of 3.1%v/v over areas where VWC was below 1.5kg/m^2 (at C-band, retrieval over denser canopy is highly affected by the reduced sensitivity of the microwave signal to soil moisture). These errors decreased at coarser spatial scales. Absolute error levels in soil moisture of 1.8%v/v and 1.1%v/v were found at 50 and 100km respectively, with a dry bias (retrieved soil moisture drier than the true one). At 50km scales, therefore, the error due to spatial heterogeneity was found to be smaller than other errors, such as that due to distributed point ground sampling used for validation (3%v/v) or that associated with obtaining gridded products from sampling heterogeneous fields with non-linear antenna gain functions. This is consistent with studies at L-band by Drusch et al. (1999b). Interestingly, Crow et al. (2001) observed that heterogeneity within large pixels results in the persistence of a relatively constant dry bias in simulated AMSR-E retrievals, suggesting that although spatial heterogeneity may produce inaccurate estimates of the field mean soil moisture at any given instant in time, it should not prevent validation and retrieval products from accurately representing temporal fluctuations in coarse-scale soil moisture

Burke et al. (2004) investigated the impact of the presence of different land covers (with prescribed, land cover specific VWC), on the accuracy of retrieved soil moisture, vegetation optical depth, and soil effective temperature. The study used multi-angle 50km brightness temperatures, simulated using soil moisture fields generated over North America by a land surface model at 12.5km resolution. Errors in retrieved soil moisture and optical depth were found to increase exponentially with increasing degree of heterogeneity (represented by the standard deviation of the optical depth within the pixel), with errors in retrieved soil moisture as high as 6%v/v for the maximum optical depth standard deviation of 0.25. In general, the retrieved parameters were smaller than the area-averaged parameters, confirming the theoretical predictions of Njoku et al. (1996b). Moreover, the study confirmed no apparent relationship between the error in retrieved effective temperature and degree of heterogeneity.

Loew (2008) used multi-angle bi-polarised L-band brightness temperature simulated with the MEM model (a precursor of the L-MEB model, based on the τ–ω approach (Wigneron et al., 1995)) and using soil moisture fields at 1km resolution generated by a land surface model in the Upper Danube catchment in Germany. The 1km brightness temperature data was aggregated at different spatial scales and additional simulated noise (2K for the radiometric uncertainy and up to 4K for uncertainty in soil temperature) was added to provide the most realistic simulations. These simulated L-band data were then used to retrieve surface soil moisture information at different scales and to quantify the soil moisture retrieval error. The analysis considered the combined effect of soil texture, land cover, VWC and soil moisture heterogeneity. However, no discussion on the individual effect of each factor was presented. Overall, the soil moisture retrieval error was below 4%v/v. Only high uncertainties in soil temperature values (4K noise) produced errors in excess of 4%v/v. Nevertheless, in this study the soil moisture variability generated by the land surface model within 1km pixels ranged between 2 and 12%v/v. The overall soil moisture variability was therefore generally low. The soil moisture retrieval error showed a strong dependency on the investigated scale. Below 10km, the errors showed a strong increase as the model spatial resolution got coarser. For coarser resolutions the errors remained almost stable.

The studies described thus far agree that errors due to land surface heterogeneity are expected to be generally less than 4%v/v, and smaller than other sources of error such as validation with in situ soil moisture data or nonlinear gridding of antenna gain. Nevertheless, they can be more serious in aggravating circumstances of wet and/or cold land surfaces with significant vegetation density, which increases the nonlinearity effect. A caveat in the type of analysis described so far is the implicit assumption that the retrieval algorithm used in forward mode to simulate the brightness temperature that will be produced by a mixed pixel is a reliable mathematical proxy of the radiometer. Some studies (e.g., Loew, 2008) partially alleviated this assumption by adding noise to the simulated T_B and ancillary data before performing coarse-scale retrieval from aggregated brightness temperatures. Nevertheless, the fact that the same model is used to simulate T_B and retrieve soil moisture estimates poses an implicit limitation to the investigation of errors due to model physics inaccuracy. Moreover, in the synthetic studies presented, the same parameters are generally used for generation of the brightness temperature and model inversion. In reality, ignoring the true radiative transfer parameterisation will constitute a major source of error in microwave soil moisture retrieval. This can be resolved using real brightness temperature data for diverse and heterogeneous landscapes.

2.3.3 Experimental Studies

Analysis of the effect of land surface heterogeneity using real brightness temperatures observation was initiated in the 1990's with the first large-scale airborne campaigns conducted in the US by the National Aeronautics and Space Administration (NASA) and United States Department of Agriculture (USDA). Beside preliminary, small scale campaigns such as HAPEX, FIFE, and MONSOON'90 campaigns (Wang et al., 1990b; Schmugge et al., 1992), of interest for coarse-scale soil moisture studies are the Washita'92 (Jackson and Schmugge, 1995b), Southern Great Plains'97 (Jackson et al., 1999) and Southern Great Plains'99 (Njoku et al., 2002) campaigns. These experiments provided L-band brightness temperature observations at resolutions ranging from 200m to 800m over areas as large as 10,000km^2, with the primary objective to evaluate the performance of L-band soil moisture retrieval algorithms at coarse spatial resolution (up to 30km) and provide the link in extrapolating previous results at finer resolution to the resolution of future satellite footprints, as well as test the results obtained from synthetic studies and simulation experiments.

The first step towards using airborne brightness temperature acquisitions to simulate satellite pixels was to verify that a simple linear aggregation is a realistic representation of the scaling of brightness temperature fields. This was verified with fairly consistent results (Jackson et al., 1995a; Drusch et al., 1999a; Jackson et al., 1999; Jackson, 2001; Guha et al., 2002). All these studies showed that (i) L-band and C-band brightness temperatures provide the same mean values for an area regardless of the spatial resolution of the original data, and (ii) the theory and soil moisture retrieval algorithms developed at fine resolution (tower radiometer) were also applicable at these coarse resolutions, although the radiative transfer parameters required adjustment for coarse pixels with mixed land surface conditions.

Uitdewilligen et al. (2003) used the SGP'97 fine-resolution brightness temperature observations (200m) to retrieve soil moisture estimates using the parameters of the soil moisture retrieval algorithm calibrated by Jackson et al. (1999) for the coarse-resolution (800m) observations. It was observed that using parameters estimated at 800m to estimate soil moisture at 200m would lead to underestimation of the ground-measured soil moisture. The parameters derived by Jackson et al. (1999) had to be redefined. In particular, the roughness parameter and vegetation parameter *b* had to be increased to compensate for this effect. As the vegetation optical depth is directly related to parameter *b* and VWC, this means the coarser the resolution (i.e., the higher the sub-pixel heterogeneity), the lower the effective optical depth or the effective roughness of a mixed pixel.

Burke and Simmonds (2003) performed a mixed analytical-experimental study by applying a simplified emissivity-soil moisture relationship derived from a coupled soil–vegetation–atmosphere–transfer scheme and microwave emission model to analyse the effect of soil texture and vegetation optical depth heterogeneity. The analytical results were then verified with three SGP'97 800m brightness temperatures observations. In the case of bare soil pixels, sub-pixel heterogeneity in soil moisture and soil particle size distribution had minimal impact on the retrieved soil moisture. However, in the case of a vegetated pixel, it was shown that variability in VWC could produce soil moisture errors as high as 8%v/v under extreme conditions (high variability in optical depth). Nevertheless, when analysing real data from SGP'97 it was found out that the soil moisture errors were of the order of 3%v/v.

A key point made by Burke and Simmonds (2003) is that under extreme conditions (high variability in optical depth) the physical connection between vegetation cover (and hence optical depth), soil texture and soil moisture (wetter soils under denser canopies) worked to reduce the magnitude of the errors by reducing the variability of emissivity. This had not been considered in previous studies, where each factor's variability was either treated individually, or the combined effect of the heterogeneity in land surface characteristics was considered at once, without attention to the physical connection between them. For example, soils with a greater percentage of sand usually have lower soil moisture and vice versa, but at the same water content a sandier soil will have a lower microwave brightness temperature than a more clayey soil (see Figure 2.5). Similarly for the optical depth, lower soil moisture (higher emissivity) is generally associated with lower vegetation density, which tends to decrease the emissivity, smoothing out the variability. Burke and Simmonds (2003) concluded that real world errors should be less than theoretical ones, where this physical connection is not accounted for. Moreover, they pointed out that even if non-linearity errors are theoretically high when the variability in optical depth is significant, the microwave brightness temperature is not very sensitive to changes in surface soil moisture under elevated optical depth, even for a uniform pixel. Therefore the inaccuracies in the retrieval algorithm may be higher than the error due to heterogeneity.

All studies presented thus far regarding the effect of land surface heterogeneity on L-band soil moisture retrieval were based on the SGP'97 or Washita'92 data sets, which were relatively benign with respect to vegetation effects (less than approximately 2.5kg/m^2 VWC (Njoku et al., 2002)). More recent field efforts by USDA included the SGP'99 experiment and the sequence of Soil Moisture Experiments (SMEX'02,'03'04 and '05), which were undertaken in regions with more severe land cover conditions (vegetation water contents ranging from 0 to 5kg/m^2). However, these experiments had the primary objective of validating the soil moisture product from the AMSR-E radiometer, and therefore focused mainly on C-band frequencies (Jackson and Cosh, 2003; Jackson et al., 2005; Bindlish et al., 2008; Jackson et al., 2008). Only a few studies have so far investigated soil moisture retrieval from L-band observations over dense canopies (i.e., forests with VWC >5kg/m2), Ryu et al. (2007) using the SMEX'03 data and Saleh et al. (2004) using data from the EuroSTARRS airborne campaign conducted at different sites in Spain and France. Both studies showed that the radiometric sensitivity at L-band is sufficient to monitor realistic changes in soil moisture under dense vegetation. Moreover, making use of the 62.5m L-band observations collected during the present study Grant (2009) showed that soil moisture could be retrieved with an accuracy of 6%v/v over an Eucalypt forest. However, the footprint resolution was in all cases not superior to approximately 1km, and therefore these studies did not address the problem of land surface heterogeneity within satellite scale footprint

The review of existing literature presented has shown that vegetation is the main land surface factor whose heterogeneity affects to coarse-scale soil moisture retrieval due to non-linearity in state-of-the-art radiative transfer models. Heterogeneity in soil moisture, soil texture, surface roughness and soil temperature should have a minor effect, generally within the instrument error of a typical radiometer. The effect of increasing vegetation heterogeneity is to non-linearly increase the coarse-scale soil moisture retrieval error. This can be significant and higher than the instrument error of a typical radiometer in the case of cold, wet land with substantial vegetation. Only two studies to date have addressed the problem of land surface heterogeneity and its effect on L-band coarse-scale soil moisture retrieval using real data (Burke et al., 2003; Uitdewilligen et al., 2003). Both studies were based on the SGP'97 data set, which was relatively benign with respect to vegetation effects (consisting primarily of grasslands, pastures and winter wheat with less than approximately 2.5kg/m^2 VWC). Moreover, only one study considered the combined effect of heterogeneity in land surface when physical links between different land surface factors and soil moisture variability is taken into account. This is mainly due to difficulties in monitoring soil moisture, vegetation characteristics, surface roughness, soil temperature and soil properties at scales typical of satellite footprints and resolution sufficient to capture the above physical links. There is therefore a pressing need for thorough investigation of the problem of land surface heterogeneity using real data on a wider range of surface conditions, including higher variability in vegetation cover than that observed so far, supported by detailed ground sampling. In particular, it is important to understand how the physical links between land surface factors and soil moisture variability work toward reducing or enhancing the coarse-scale soil moisture retrieval error through their combined effect on the non-linear response of large, mixed pixel.

2.3.4 Methods to Account for Heterogeneity

Amongst the studies discussed in the previous section, only one study proposed a technique to correct for the effect of land surface heterogeneity on soil moisture retrieval at coarse scale (Davenport et al., 2008). The technique was proposed for multi-angle SMOS type observations and consists of representing vegetation as a weighted average of bare soil and vegetation, the relative fraction of which can be retrieved as an extra parameter by multi-angle data. The technique was shown to significantly reduce the error induced by vegetation heterogeneity, as not one uniform optical depth was used, but rather two, one set at zero (for the bare fraction) and one equal to the vegetated fraction (retrieved). Nevertheless, as will be extensively discussed in Chapter 3, multi-parameter retrieval from SMOS might not be always feasible. This is because the number of incidence angles and their angular range available from SMOS, which depends on the position of the footprint in the swath, is very wide (0º and 50º) only near the centre of the swath, while it reduces significantly when the area of interest closer to the edges of the swath. Depending on the ancillary data available and the position of the area of interest within the swath therefore, only a one- or two-parameter retrieval might be feasible (soil moisture and another parameter), not allowing retrieval of the extra parameter for correction the effect of vegetation heterogeneity. Moreover, the extra parameter retrieved in the method of (Davenport et al., 2008) is not a usable quantity but rather a tuning parameter used to compensate for the heterogeneity.

A different approach was proposed by Zhan et al. (2008). Based on the recognition that simple averaging of fine-resolution ancillary parameters (e.g., VWC) can induce significant errors in footprint-scale soil moisture by Chehbouni et al. (1995) and Njoky et al. (1996b), Zhane et al. (2008) derived and tested an analytically-based alternative rule for aggregating VWC and optical depth from fine-resolution ancillary data to satellite-footprint resolution. Despite showing promising improvement in satellite-footprint soil moisture retrieval when tested with a single-angle simulation experiment, validation of these theoretical results using real satellite data and extension of the technique to multi-angle observations will be necessary before they can be applied in operational soil moisture retrieval algorithms.

The soil moisture retrieval approach proposed for the SMOS mission to account for land surface heterogeneity is based on the physically-based method proposed by Kerr and Njoku (1993) and Njoku (1996a). In this method the observed brightness temperature over a heterogeneous surface, $\overline{T}_{BP}$ can be expressed as:

$$\overline{T}_{BP} = \sum_{i=1}^{N} a_i T_{BP_i} , \tag{2.14}$$

where T_{BPi}, are the brightness temperatures of the different pixel fractions, a_i are the spatial weights of the fractions such that $\sum_{i=1}^{N} a_i = 1$, and N is the number of significantly distinct homogeneous radiative fractions within the pixel. The weights a_i correspond to the fractional spatial areas covered by each component within the footprint. In SMOS the fractions a_i will correspond to areas with uniform land cover and will be determined using land cover maps at 4km resolution. The SMOS L2 algorithm will be described in detail in the next Chapter. In this context it suffices to say that the method, as implemented in SMOS, relies on two main assumptions: These are that (i) land cover is the major source of land surface variability which can affect the coarse soil moisture retrieval, and that (ii) the retrieved parameters (i.e., soil moisture alone or soil moisture and optical depth) are uniform amongst different scene components.

Despite been adopted by the SMOS mission, the technique proposed by Njoku et al. (1996a) has thus far received little consideration in literature. Drusch et al. (1999a) tested the core concept of fractional coverage of Njoku et al. (1996a) with the SGP'97 airborne data set to analyse soil moisture retrieval scaling effects at L-band. However, the method as applied in this study only considered a limited number of cases, these being pixels with 100% vegetation cover and pixels with 80% vegetation cover (the rest bare soil), which do not represent the large variety of conditions that will characterise SMOS observations. Moreover, the vegetated fraction was composed of moderate vegetation conditions, i.e., mainly rangeland and pasture with some areas of crops, and the analysis was not supported by detailed information on land surface heterogeneity within each coarse pixel in order to understand the land surface factors which are critical for coarse-scale retrieval. Before application to SMOS data, it is imperative that the method, as currently implemented in the SMOS L2 soil moisture retrieval algorithm, and its fundamental assumptions are tested with real L-band observations at resolutions comparable to that of SMOS.

2.4 Proposed Approach

The review of existing literature presented in the previous sections has highlighted several shortcomings in the understanding of the impact of land surface heterogeneity on satellite-scale soil moisture retrieval. Specifically, in view of the upcoming availability of SMOS data there is a pressing need for:

- investigation of the impact of land surface heterogeneity on L-band satellite-scale soil moisture retrieval using real observations on a wide range of surface conditions, supported by adequate ground sampling of soil moisture and land surface conditions;

- understanding how the physical links between land surface characteristics and soil moisture distribution within satellite pixels affect the coarse-scale soil moisture retrieval; and
- testing the soil moisture retrieval approach proposed for SMOS to account for land surface heterogeneity and its fundamental assumptions with real L-band observations over highly heterogeneous landscape;

To address these shortcomings, in this study the soil moisture retrieval approach proposed for SMOS will be tested using simulated SMOS pixels based on airborne observations, and a technique will be proposed, applicable to SMOS, to reduce the soil moisture retrieval error due to land surface heterogeneity. The first part of this study included the collection of an extensive data set of airborne, L-band passive microwave observations and ground data to satisfy the scientific requirements outlined above. This was done during the NAFE'05 experiment (described in Chapter 4 and in Panciera et al., 2008a) conducted in the Goulburn catchment in Australia.

The NAFE'05 data set is unprecedented in its relevance to address the scientific questions of this study, and represents a substantial step forward with respect to the Washita'92 and SGP'97 and SGP'99 data sets in terms of the range of vegetation conditions mapped and the detail of the ground sampling: Airborne L-band observations were acquired over a large area, typical of a future L-band satellite pixel (40km) presenting highly heterogeneous vegetation conditions, ranging from nearly bare to forested areas. Airborne observations at multiple resolutions (62.5m to 1km) of focus areas provided data to analyse the scaling properties of the brightness temperatures over heterogeneous land surface to support aggregation of airborne data to simulate coarse L-bands pixels. All the airborne monitoring was supported by highly detailed ground soil moisture measurements ranging from the paddock scale (6.25m spacing) to the regional scale (2km spacing), as well as monitoring of all the land surface characteristics understood to affect the microwave emission. During the observation period, a full range of soil moisture conditions was experienced by the area.

The methodology followed in this study consists of three main phases: (i) processing of the NAFE'05 airborne and ground-based field data to create a SMOS scenario; (ii) testing of the soil moisture retrieval approach proposed for SMOS and its assumptions with real data, and (iii) development and testing of a new approach to better account for the sub-pixel heterogeneity of land surface conditions in the soil moisture retrieval from SMOS data. The three phases are individually described in the following sections and summarised schematically in Figure 2.6.

2.4.1 Creation of a SMOS Scenario

In the fist phase, aircraft and ground field data from the NAFE'05 field campaign will be composed to create coarse-resolution, SMOS-like passive microwave observations. This will be done by aggregation of airborne L-band data. Prior to the aggregation, the scaling properties of the L-band spatial fields will be analysed in order to assess the reliability of a simple linear aggregation of 1km airborne brightness temperatures for simulation of satellite footprints. Although a few studies indicated that multiple resolution observations should result in the same mean brightness temperature for a given area, these studies were limited to the SGP'97 or Washita'92 areas in the United States, which were relatively benign with respect to vegetation conditions (less than approximately 2.5kg/m^2 VWC). In the present study a large data set of brightness temperatures at 62.5m, 250m, 500m and 1km resolution acquired over portions of the study area will be analysed to properly address the scaling properties of the L-band spatial fields.

Coarse footprints will then be simulated by aggregation of 1km airborne brightness temperatures to resolutions ranging from 5km to 40km (SMOS resolution). These footprints cover the whole range of land surface conditions present in the NAFE'05 study area (agricultural, non-agricultural and forested areas) and the full range of soil moisture conditions (from

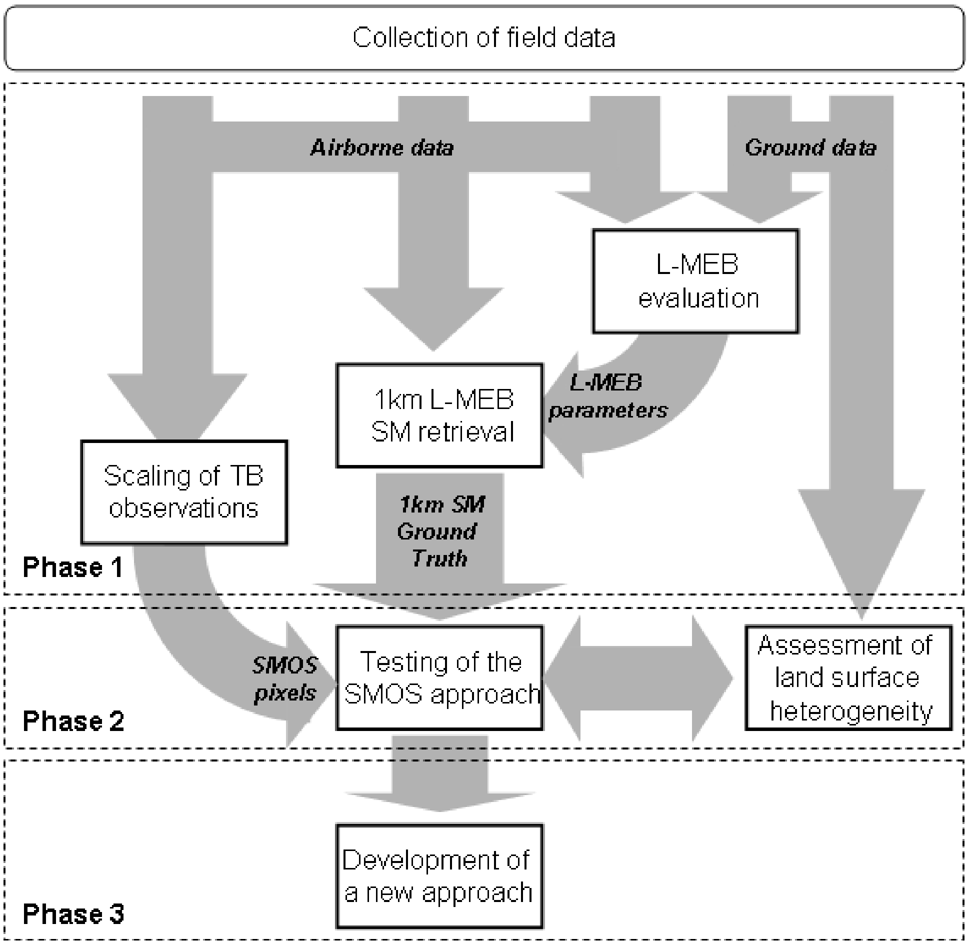

Figure 2.6. Schematic diagram of the methodology adopted in this thesis to test the soil moisture retrieval approach proposed for SMOS and develop a new approach to account for land surface heterogeneity.

saturated to residual soil moisture content) experienced during the November 2005 field campaign. They represent therefore an excellent data set for investigation of soil moisture retrieval in the presence of land surface heterogeneity.

The soil moisture retrieval from brightness temperature data in this study will be performed using a state-of-the-art microwave emission model, the L-band Microwave Emission of the Biosphere Model (L-MEB), which will be the core of the SMOS L2 soil moisture retrieval algorithm. Full details on the L-MEB model and the SMOS L2 algorithm are presented in the next Chapter. The model is based on the τ-ω parameterisation presented in section 2.2.3.2, and has been developed and tested nearly exclusively on

European, temperate conditions (Ferrazzoli et al., 2002; Saleh et al., 2006a; Saleh et al., 2006b; Escorihuela et al., 2007; Grant et al., 2007a; Grant et al., 2007b; Saleh et al., 2007; Wigneron et al., 2007; Grant et al., 2008). Before applying the model to the NAFE'05 airborne data, the model parameterisation will be therefore evaluated over the land surface conditions in the study area using 62.5m and 1km resolution brightness temperatures supported by very detailed ground sampling of soil moisture, VWC, soil temperature, soil texture and surface roughness monitored at eight supersites across the study area. After evaluation of its performance, the model will be applied to derive fine-resolution (1km) soil moisture maps of the entire simulated footprint to be used as "ground truth" soil moisture for verification of the methodology developed.

2.4.2 Testing of the SMOS soil moisture Retrieval Approach

In the second phase the error in the retrieval of soil moisture at coarse resolutions which is induced by the sub-pixel heterogeneity of land surface conditions will be assessed using the SMOS scenario created in the initial step. Initially, the land surface heterogeneity and its link to soil moisture variability in the study area will be assessed using ground soil moisture data and information on land cover, vegetation (NDVI), soil texture and topography. As discussed in section 2.3.3, it is important to understand these links as the combined effect of heterogeneity in soil moisture and other factors might decrease, or enhance, the impact on coarse-scale retrieval errors. Moreover, this analysis will provide an in-depth knowledge of the land surface heterogeneity in the study area, which will be in turn essential for interpretation of the outcomes of this study and definition of its applicability to other contexts.

A preliminary synthetic study will then be performed to analyse the impact of sub-pixel heterogeneity of different land surface factors on the soil moisture retrieval error performed with the L-MEB model. This is motivated by the fact that L-MEB presents some advances in terms of modeling of the microwave emission of soil and vegetation, the soil effective temperature and the surface roughness (see Chapter 3). Therefore, a proper investigation of the non-linearity of these advanced model physics is required prior to the assessment and interpretation of the non-linearity problem with real data. The error in the retrieval of soil moisture at coarse resolutions due to land surface heterogeneity will be finally analysed using the satellite footprint scenario derived from Phase 1 of this study. This will be done in two steps: first the classic method based on the assumption of pixel uniformity (i.e, no consideration is given to the land surface heterogeneity) will be tested, since this is the method adopted by the soil moisture products currently available. Then the soil moisture retrieval approach proposed for SMOS to account for the land surface heterogeneity will be tested. In both steps, soil moisture will be retrieved at coarse resolutions using a single-channel, two-polarisation retrieval of soil moisture and optical depth, and compared with the "ground truth" soil moisture, i.e., the 1km soil moisture maps created in Phase 1. This will be repeated at various resolutions for different portions of the study area. These land portions presents variable characteristics in term of soil moisture status and land surface heterogeneity. The aim of this analysis is three-fold:

1. Identify the land surface factor, or the combination of factors, which has the greater impact on the soil moisture retrieval error due to its heterogeneity within the footprint;
2. Test the effectiveness of the soil moisture retrieval approach proposed for SMOS to account for land surface heterogeneity and identify its weaknesses in relation with the assumptions of uniform soil moisture and optical depth within the pixel fractions;

2.4.3 Development of an Alternative Retrieval Approach

Based on the weaknesses of the SMOS approach identified in Phase 2, an approach will be developed to improve the soil moisture retrieval from SMOS data which is applicable to the SMOS L2 soil moisture retrieval algorithm. This will be done by testing different approaches, each relaxing one of the assumptions of the approach proposed for SMOS, these assumptions being of uniform soil moisture and uniform optical depth within the pixel fractions. It should be noted that, due to presence of relatively open Eucalypt forest in the NAFE'05 study area, this thesis specifically deals with the situation where the forested fraction of the SMOS pixel has a moderate density, in which case the assumptions of uniform soil moisture and uniform optical depth are made in the SMOS L2 algorithm. The improvement in soil moisture retrieval of each approach with respect to the SMOS approach in such case will be evaluated using the SMOS scenario created in Phase 1.

2.5 Chapter Summary

In this Chapter the potential of remote sensing for global soil moisture monitoring has been discussed. Different methods to obtain soil moisture from remote sensors were presented, including visible, thermal infra-red, active and passive microwave techniques, and their advantages and limitations discussed. It has been shown that low-frequency passive microwave remote sensing is the most promising method due to the direct link between microwave radiation and soil dielectric properties, its deeper penetration into vegetation, its all-weather capabilities and negligible atmospheric attenuation. However, the likely presence of land surface heterogeneity within the large passive microwave satellite footprints (40km) presents a challenge for the retrieval and validation of soil moisture over such large areas.

Recent work on the assessment and compensation of the effect of land surface heterogeneity on passive microwave soil moisture retrieval has been also discussed. This review showed that only a small number of studies has assessed the problem of land surface heterogeneity using real passive microwave data. Most studies have been undertaken at test sites with smooth topographic and vegetative conditions, and with limited ground sampling. Moreover, the review presented has shown that the soil moisture retrieval approach proposed for SMOS to account for land surface heterogeneity and the assumptions it relies on have not been extensively tested with real L-band observations over highly heterogeneous land surface conditions.

This study will address the shortcomings identified by the review presented in this Chapter using an unprecedented data set of airborne passive microwave observations and ground data, which was collected specifically during this study within the NAFE'05 field campaign. After detailed analysis of the land surface heterogeneity in the study area and identification of the weaknesses of the soil moisture retrieval approach proposed for SMOS approach and of its assumptions, this study will develop and test a new approach to account for land surface heterogeneity which is applicable to the SMOS L2 algorithm.

Chapter Three

3 The SMOS Mission

In this Chapter the Soil Moisture and Ocean Salinity (SMOS) mission and the algorithm adopted to retrieve soil moisture estimates operationally from SMOS data ("SMOS L2") are described. This provides the background to the soil moisture retrieval approaches which are tested in this thesis with airborne data. First, a general description of the mission science objectives is presented, followed by a description of the characteristics of the SMOS radiometer. The SMOS L2 soil moisture retrieval algorithm and the approach adopted by the algorithm to retrieve soil moisture estimates from SMOS observations are then reviewed in detail, together with their assumptions and limitations. The simplifications adopted in this thesis to test the SMOS L2 algorithm and its soil moisture retrieval approach to airborne data are also listed. Finally, the microwave emission model core to the SMOS L2 algorithm, the L-band Microwave Emission of the Biosphere model (L-MEB), is described in detail.

Using the data presented in Chapter 4, the L-MEB model will be evaluated with fine-resolution airborne data in Chapter 5 and used to produce "ground truth" fine-resolution soil moisture maps of the study area. After assessment of the land surface heterogeneity in the study area in Chapter 6, the fine-resolution soil moisture maps will be used in Chapter 7 to evaluate the error in soil moisture retrieval under the assumption of pixel uniformity and understand which land surface factors (or combination of factors) this error is mostly related to. The soil moisture maps will then be used in Chapter 8 to test the soil moisture retrieval approach proposed for the SMOS L2 algorithm and its weaknesses to account for the land surface heterogeneity will be identified. Based on those weaknesses, in Chapter 8 alternative retrieval approaches to improve the soil moisture retrieval accuracy from SMOS will then be proposed.

3.1 Mission Description

The SMOS mission was proposed to the European Space Agency (ESA) in the framework of the Earth Explorer Opportunity Missions (Kerr et al., 2001). The main objectives of SMOS are to deliver global and frequent coverage of key variables of the land surfaces (soil moisture, ice and snow), and of ocean surfaces (sea surface salinity). In this Chapter only the soil moisture component of the mission is described as that is the topic of this thesis. The SMOS mission is based on a dual polarised L-band radiometer using aperture synthesis (two-dimensional [2-D] interferometer**)**, so as to achieve a ground resolution of approximately 50km coupled with multi-angle acquisitions of the same land surface portion at V and H polarisations. This unprecedented multi-angle capability is expected to allow the retrieval of surface parameters with improved accuracy relatively to current, single-angle spaceborne sensors. SMOS is scheduled for launch in September 2009 and will be the first satellite mission with an optimal observing frequency (1.4GHz) for soil moisture estimation.

3.1.1 Science Objectives

SMOS aims at making measurements of soil moisture within the first few centimeters of the earth surface with sufficient accuracy, spatial and temporal coverage to serve hydrological, climatological, meteorological and agronomical sciences (Kerr et al., 2001). In summary SMOS requirements for soil moisture are (see also CESBIO, 2003):

- **accuracy of 4%v/v soil moisture or better**, for data outside mountainous, urban, and partially frozen or snow covered areas where the vegetation biomass is less than 5kg/m^2 (circa 65% of the Earth's continental areas). Simulation studies have demonstrated that such accuracy will be achievable in the central part of the SMOS Field of View (FOV) (Wigneron et al., 2000) where observations over a large range of incidence angles will be available (see next section). A soil moisture accuracy of 4%v/v has also been demonstrated by field observations at L-band (e.g., Jackson et al., 1995a; Njoku et al., 2002). Additionally, SMOS will aim at providing global maps of vegetation water content with an accuracy of 0.5kg/m^2 every six days;

- **spatial resolution better than 50km**. A 50km resolution is adequate for the purpose of providing soil moisture information to global atmospheric models and will allow hydrological modelling for the largest hydrological basins over the world. For most hydrological studies as well as mesoscale modelling, a finer spatial resolution is desired;
- **revisit time of 2.5-3 days**. This objective will satisfy temporal soil moisture sampling requirements for root zone soil moisture extrapolation and evapotranspiration estimation (Chanzy et al., 1995) and will allow tracking of the drying conditions after rainfalls most of the time (strictly a 1-2 days revisit time would be required for this application). Frequent coverage will be more important in dry tropical areas where water availability is much more important than at the equator, where the indicated revisit time is computed; and
- **overpass time at 6:00AM/PM local time**. This acquisition time has the advantage of presenting conditions as close as possible to thermal equilibrium in the soil-vegetation canopy layer, consequently making the retrieval more accurate. Moreover, the soil moisture gradient near the surface should be minimal at 6:00AM.

3.1.2 Instrument

The baseline SMOS payload is an L-band (1.4GHz) 2-D interferometric radiometer known as the Microwave Interferometric Radiometer with Aperture Synthesis (MIRAS). The interferometric design is inspired by the very large baseline antenna concept used in radio astronomy, and consists of deploying small receivers in a particular “Y-shaped” spatial arrangement, then reconstructing a brightness temperature (T_B) field with a resolution corresponding to the spacing between the outmost receivers. In MIRAS this is achieved through three deployable co-planar arms 120º apart. Each arm is 4.46m long (see Figure 3.1) and comprises three segments, each containing

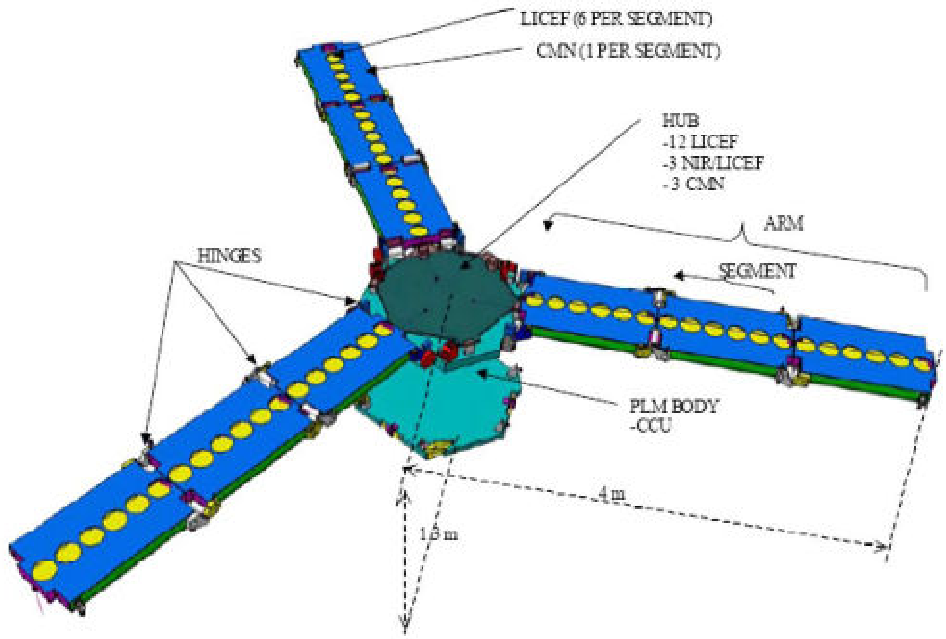

Figure 3.1. Deployed MIRAS configuration diagram (from McMullan et al., 2008).

six elementary L-band radiometers. The line of eighteen radiometers in each arm is complemented by a further four radiometers in the central hub, making a total of sixty-six radiometers, twelve in the hub and fifty-four in the arms (McMullan et al., 2008).

The instrument will be mounted on a PROTEUS platform and will be put in a sun-synchronous, 757km altitude orbit with a 6:00AM (±15 min) ascending equator crossing time, with a 25º tilt with respect to the orbital plane (i.e., a pitch rotation). This will allow the earth surface to be observed at larger incidence angles than a nadir-looking instrument. This configuration will generate records of T_B over incidence angles from 0º up to 55º across a 900km wide swath with a spatial resolution in the range of 30–50km. The SMOS radiometric sensitivity over land is currently estimated to be between 3.5 (at boresight, i.e. the physical axis of the directional synthetic antenna) and 5.8 K (within 32° from boresight) for a 1.2 s integration time (McMullan et al., 2008).

The instrument's instantaneous FOV will be 2-dimensional, extending

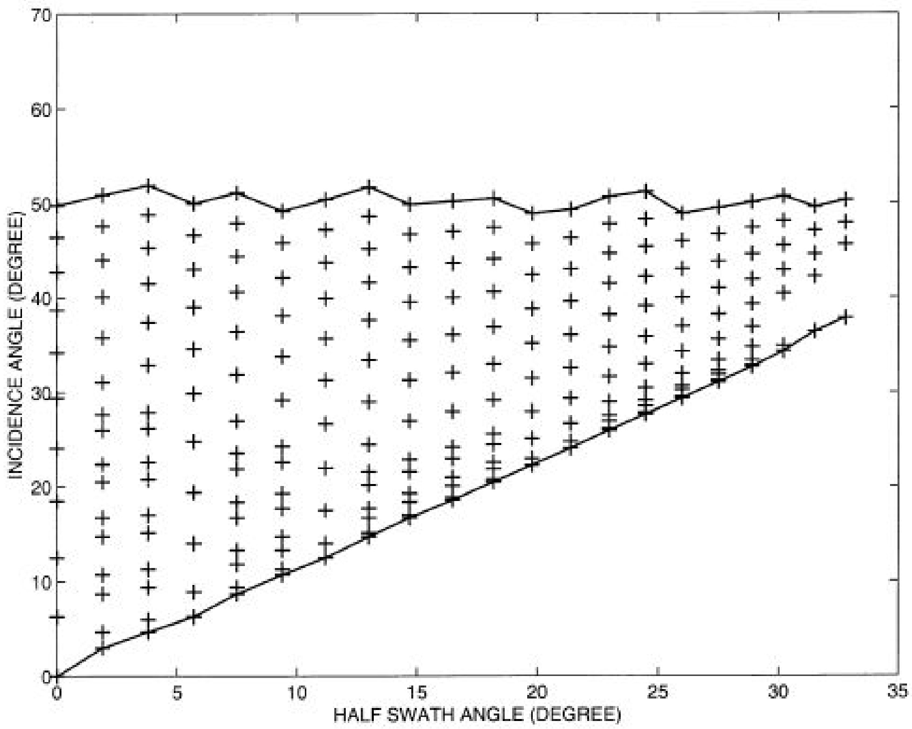

Figure 3.2. Simulated range of incidence angles of SMOS observations as a function of the equivalent half-swath angle η_m. Each cross corresponds to the incidence angle of independent SMOS observations acquired as the satellite moves along its track by 75km steps Angles are shown for successive half-swath angles η_m corresponding to increasing distances to the ground track by 25km steps (from Wigneron et al., 2000).

both along and across the satellite sub-track (i.e., the nadir projection of the satellite's trajectory on the earth). Such a FOV will be acquired every 3s. Consequently, as the satellite progresses along the orbit, any given location on the Earth's surface will be measured a number of times at different incidence angles and both V and H polarisations. The number of incidence angles and their angular range will depend on the distance of the footprint to the satellite sub-track. This position can be expressed in terms of the half-swath angle η_m. For locations on the satellite sub-track (η_m=0º), the full range of angles will be obtained, typically ten independent samples at angles between 0º and 55º from nadir (see Figure 3.2). The range of incidence angles will be reduced to approximately between 38º and 44º from nadir for a half-swath angle (η_m=33º) (Wigneron et al., 2000). Note that as the half-swath angle increases, the pixel resolution worsens. Resolution varies from

30km at satellite sub-track to over 60km at the edges of the swath (Wigneron et al., 2000).

3.1.3 Data Products

The tasks for transforming the actual raw interferometric measurements of the instrument into the final T_B images are summarised in the generic term “image reconstruction”. This includes converting the interferometric measurements (Level 1A product) to the T_B distribution across the FOV through a 2D inverse Fourier transform weighted by the antenna gain pattern. This is done in the SMOS antenna’s V and H polarisation reference frame and provides the Level 1B product. The T_B (V and H) in the antenna’s reference frame are then converted to the T_B (V and H) in the Earth’s reference frame, by taking into account the rotation of the electric fields, due to both geometrical considerations (orientation of the antenna’s V and H with respect to the earth surface’s V and H) and to the Faraday rotation induced by the ionosphere (Waldteufel et al., 2000). The final step consists of projecting the converted T_B onto a fixed grid on an Earth reference ellipsoid. This results in the Level 1C product (see Figure 3.3).

3.2 The SMOS L2 Algorithm

The principle of the approach used to retrieve land surface parameters from SMOS L1C T_B data is to use an iterative method to find the best suited set of soil moisture and vegetation characteristics that minimises the differences between the measured T_B and T_B simulated by a forward physical model of the surface microwave emission. The SMOS L2 is a complex algorithm which not only estimates soil moisture but also performs ancillary tasks such as data quality control and building of output data products. Moreover, given that it is built with a global perspective, it deals with the full range of land surface conditions that will be observed by SMOS and that are not of direct interest for soil moisture retrieval (including ocean, sea ice and snow covered areas). In this Chapter the discussion is limited to the component of SMOS L2 algorithm relevant for

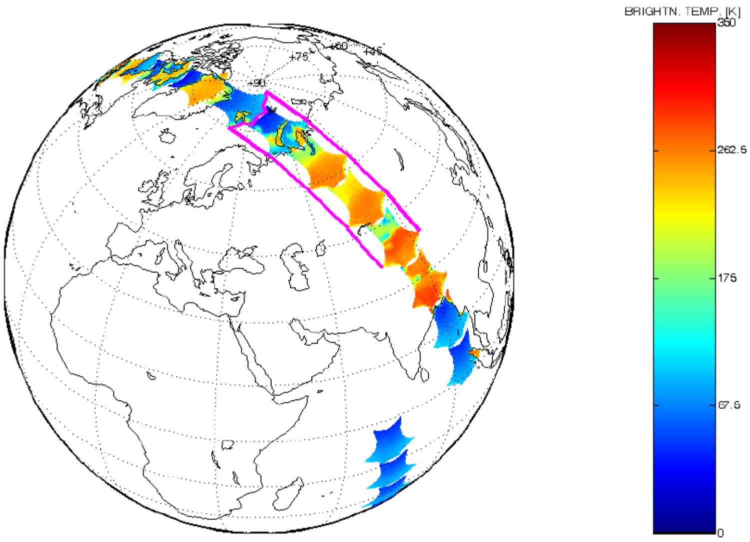

Figure 3.3. Illustration of SMOS L1C brightness temperature product (*courtesy of DEIMOS Engenharia, Lisbon, Portugal*).

understanding the results of this thesis: the retrieval of soil moisture from L1C T_B data over land areas which only include what is referred to as the "nominal case". The nominal case consists predominantly of low or moderately vegetated soil and forest and therefore do not include significant fractions of "non-nominal" surfaces like water bodies, mountainous, urban, and partially frozen or snow covered areas. Eventual "non-nominal" surfaces, if present, should cover areas small enough not to affect the retrievability of soil moisture over the nominal surface (this will be determined based on thresholds which are yet to be estimated). In the nominal case, the forward model used is the L-band Microwave Emission of the Biosphere Model (L-MEB). Although restricted with respect to the range of surface conditions which will be covered by SMOS observations, the nominal case is the most relevant case with respect to the SMOS science objectives as it is the one for which it is believed that soil moisture retrieval is feasible. Areas qualifying as "nominal" have been estimated to represent over 66% of the Earth's continental land mass (CESBIO, 2007). A complete description of the SMOS L2 algorithm can be found in the SMOS L2 Algorithm Theoretical Based Document (ATBD, http://www.cesbio.ups-tlse.fr/us/indexsmos.html). All the information contained in the following part of this Chapter has been derived from the ATBD, unless otherwise stated.

3.2.1 General Layout

In the iterative soil moisture retrieval approach, the objective is to minimise a cost function through minimising the sum of squared weighted differences between measured and modeled T_B observations at a range of incidence angles and at V and H polarisations of the same land portion. This is achieved by finding the set of parameters (e.g. soil moisture and vegetation characteristics) which yields the best match between T_B predicted by the model (L-MEB) and those observed. The retrieval is carried out at nodes of the fixed Earth surface grid onto which the L1C T_B have been projected.

It should be clarified here that each node represents purely the geographical location on the Earth's surface of the center of a cell of the global fixed grid. To each node corresponds what is referred to as a "SMOS pixel", which consists of the T_B observations at that node (i.e., that geographical location) and its spatial resolution on the Earth's surface, i.e., the 3dB surface characterised by the ellipse contour of the synthetic antenna footprint.

In a first step the input L1C data quality is assessed and all unwanted data are filtered out (e.g., data over ocean, L1C data quality flags etc.). Areas at the edge of the FOV which do not meet spatial resolution criteria (i.e., resolutions worse than 60km) are also filtered out at this stage. Next, auxiliary data is ingested, (e.g., meteorological data, vegetation optical depth and roughness maps from previous SMOS overpasses). Lastly, the soil moisture retrieval process is initiated. As different microwave emission forward models are used for different surface types (e.g., snow emission is simulated with a model different from that used for a vegetated soil for instance), the dominant land cover of a node must first be assessed. To this end a weighting function (which takes into account the incidence angle dependent ground area covered by each pixel) is used to determine the dominant cover type from a land use map with 4km resolution. This information initiates a decision tree which, step-by-step, selects the type of model to be used in accordance with surface conditions.

Each node is considered to be divided in two (sub) areas: one area where the soil moisture retrieval will take place (the nominal case) and one area where soil moisture cannot be retrieved from the microwave signal (e.g., water bodies or snow cover). In the case that soil moisture cannot be retrieved, the contributions to the overall node signal are estimated using external data, predetermined values of the surface characteristics or models other than L-MEB. Contributions from the second area are called the "default contributions" and the actual soil moisture retrieval is therefore made on the remaining area. Ideally three parameters are retrieved over this area: soil moisture, optical depth and surface roughness (the so-called "full retrieval"). If the algorithm does not converge satisfactorily, a new attempt is made with fewer parameters (i.e., soil moisture and optical depth or soil moisture alone by imposing the optical depth from ancillary data, "minimum retrieval") until either the results are satisfactory or the algorithm is considered to have failed. In some cases where retrieval of soil moisture is not possible due to the nature of the surface (e.g., iced surfaces) the so-called "cardioid" approach (Waldteufel et al., 2004) is used to attempt the retrieval of a proxy of the dielectric constant (the "dielectric constant index"). This can be a useful quantity as external information (from sources other than SMOS data) can then be used to retrieve the dielectric constant itself.

Depending on the data available (quality of ancillary data, range of incidence angles) and the nature of the SMOS pixel (surface conditions), the L2 processing will therefore result in the following basic categories: (i) no valid retrieval whatsoever can be attempted; (ii) soil moisture retrieval is attempted and succeeds, and values for soil moisture as well as for other parameters, typically vegetation optical depth, are obtained, (iii) retrieval is carried out for geophysical quantities which do not include soil moisture (e.g., dielectric constant) and succeeds, and (iv) retrieval is attempted and fails.

The components of the SMOS L2 algorithm which are relevant for understanding the findings of this thesis are the determination of the dominant land cover fraction within each SMOS pixel and the decision tree which determines (in the nominal case) which land surface parameters will be retrieved within this dominant fraction and which will be imposed *a priori* (e.g., full or minimum retrieval). These components are therefore described in detail in the following sections.

3.2.2 Land Surface Fractions

Land surface fractions (%) for each land cover are needed by the SMOS L2 algorithm for building the forward models to be used during retrieval. Land surface fractions within the SMOS instantaneous FOV are not straightforward (geometrical) surface ratios because the SMOS observed T_B is obtained from integrating radiances across the (directional) synthetic antenna pattern (see Figure 3.4). Therefore an antenna gain weighting function (WEF) has to be applied to every elementary land surface area (defined as the unitary 4km resolution land cover area) inside the SMOS pixel in order to give the proper weight to the contribution of each elementary area within the pixel to the overall observed up-welling radiation. This results in the calculation of incidence angle dependent fractions (“FV”).

However, prior to the retrieval, angle independent average fractions (“FM”) must be computed in order to allow running the decision tree and selecting the soil moisture retrieval approach options. This is done by applying a simplified WEF function, called “MEAN_WEF”, which represents the average SMOS pixel. In the case of MEAN_WEF, the weights will not vary within the SMOS swath, while in the case of WEF they will depend on the position in the swath (i.e., on the incidence angle of the antenna main lobe).

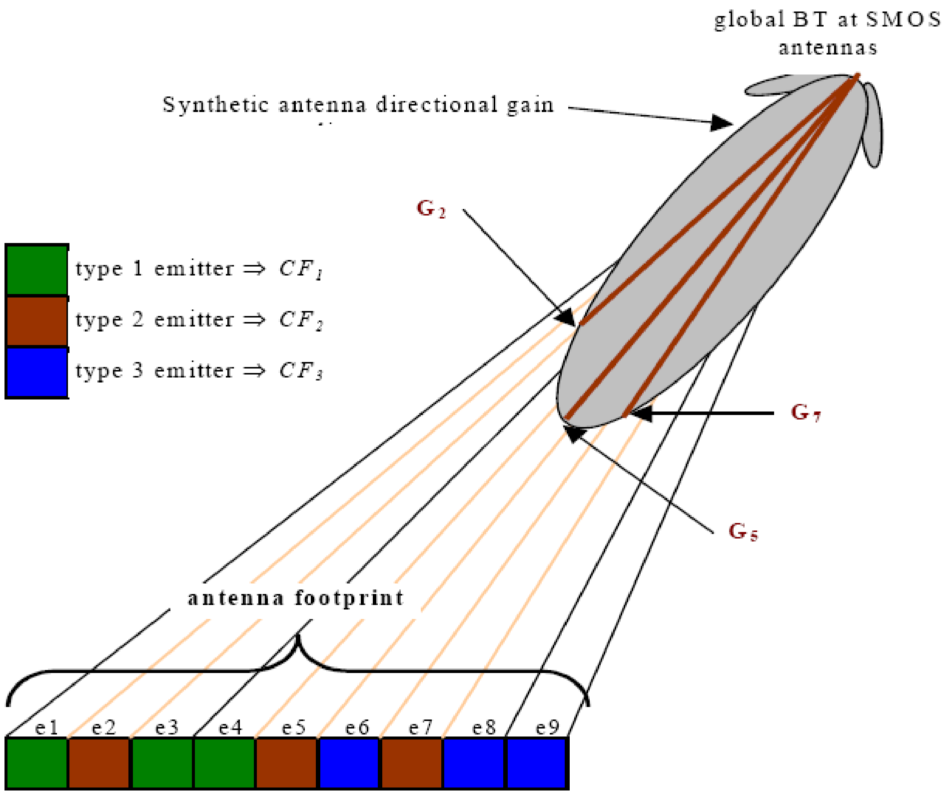

Figure 3.4. Schematic view of the determination of the weighted land surface fractions for each elementary 4km-resolution land cover area (emitter "e_i") within the pixel (i.e., footprint), depending on the SMOS synthetic antenna directional gain (WEF) (from CESBIO, 2007).

An illustrative example of this weighting procedure is shown in Figure 3.4. The surface fraction for the 4km-resolution land surface elementary areas "e1" and "e5" will be the same from a geometrical point of view (at the Earth's surface level). However, after weighting each elementary area with the WEF (or MEAN_WEF) function the FV5 (or FM5) fraction for the land surface elementary area "e1", will be greater than FV1 (or FM1), to account for the higher contribution of "e5" to the overall SMOS T_B given its position closer to the centre of the antenna main lobe. In the case of the FV fractions, the weights of e1 and e5 will change for different position across the swath, while in the case of the FM fractions, the weights will be the same across the swath.

3.2.3 Decision Tree

The decision tree of the SMOS L2 algorithm is applied to each node of the L1C grid after pre-processing of the data to select the type of retrieval to be performed. This is articulated in the following five main steps:

1. the decision tree procedure begins with determining the reference fractions (FM) for each land surface type within the SMOS pixel;
2. the dominant land surface fraction within the pixel is defined through a series of tests based on a series of thresholds concerning the magnitude of the various fractions;
3. the most appropriate microwave emission model is selected for the dominant fraction, which will be inverted to retrieve the free parameters. At the same time relevant models are selected for the remaining fractions, which will be run in forward mode with fixed parameters to provide the default contributions to the overall node signal;
4. from auxiliary data, reference values for spatially varying data input for all the relevant models selected for the pixel are obtained for every relevant fraction of the pixel; and
5. finally, a retrieval approach is finally selected, concerning the number of parameters to be retrieved (free parameters) and those to be imposed *a priori* (fixed parameters).

Each of the steps listed above is described in the following sections.

3.2.3.1 Computing Aggregated Fractions

First the average fractions (FM) within each SMOS pixel are determined by running the mean weighting function MEAN_WEF through a land cover map. The land cover map derives from an ECOCLIMAP land cover classification data set listing 218 land cover classes at 1km resolution (Masson et al., 2003). This has been aggregated into nine classes and the information stored in a 4km resolution grid for the entire globe together with each aggregated class's surface fraction within each 4km x 4km cell.

The aggregated ECOCLIMAP classes are summarised in Table 3.1. Therefore, in the SMOS L2 algorithm, surface areas are represented as aggregated (over the 4km grid) fractions for each of the nine land cover classes (aggregated from 218 ECOCLIMAP classes). The final fractions of each of the aggregated land cover classes within the entire SMOS pixel are simply computed as the mean of the 4km surface fractions over the pixel.

3.2.3.2 Surface Fraction Thresholds

Based on the incidence angle dependent fractions (FM), a series of tests is defined, based on a series of surface fraction thresholds concerning the magnitude of the various FM fractions. This results in one of several decision tree branches, depending on the predominance within the SMOS pixel of one of the land surface types. The selected branch establishes on which land cover fraction (the dominant) retrieval of land surface parameters (e.g., soil moisture, optical depth or dielectric constant) will be attempted and which other (minor) land cover fractions will be accounted for as default contributions.

Table 3.1. ECOCLIMAP fractions for continental areas over the entire globe (freezing conditions and ice are ignored in the calculation of the total fractions).

SMOS L2 Class Type	Main ECOCLIMAP classes	Fraction of Continental Area (%)
Low or moderately vegetated soil	Flat bare soil grassland tropical grassland C3 crops C4 crops irrigated crops	46.5
Snow	Permanent snow	31.1
Forest	Broadleaf tree coniferous tree tropical tree	20.0
Open Water	Water	8.7
Barren	Rocks	1.7
Wetlands	Park marshes	0.7
Urban	Urban	0.1
Frozen soil	Frozen soil	-
Sea ice	Sea ice	-

3.2.3.3 Selecting the Forward Microwave Emission Model

Based on the outcomes of the previous test, a retrieval approach is selected. In the selected approach, one model will be used to retrieve land surface parameters over the dominant land cover fraction in the pixel, while the emission from the remaining land cover fractions will be simulated using the relevant model but no retrieval will be attempted (default contributions). There are currently four models: Cardioid, L-MEB, a model for open water (with or without effect of salinity) and a model for snow. In the following we only describe the situation in which the L-MEB model is selected for retrieval (the nominal case). In practice this happens practically only when either the “low or moderately vegetated soil” fraction or the forest fraction are larger than 50% of the total pixel fraction. In both cases (“low or moderately vegetated soil” fraction dominant or forest fraction dominant) the retrieval is attempted on the dominant fraction, while the emission from the remaining fraction is estimated using *a priori* values. However, in the case when the density of canopy in the forest fraction is expected to be low, like is the case for the open Eucalypt forest present in the NAFE’05 study area, the free (i.e., retrieved) parameters are considered the same for both fractions, e.g., if soil moisture and optical depth are retrieved then soil moisture and optical depth are the same for both the vegetated soil and the forest fraction.

3.2.3.4 Computing Reference Values for Parameters

Reference values for all the spatially varying input data for the relevant forward model are obtained for every fraction of the pixel by aggregation of the ancillary data at their original resolution. In this phase the incidence angle dependent fractions (FV) are used to account for the antenna directional gain. In the nominal case, which is of interest of this thesis, these input data are soil moisture, soil texture, roughness parameters, vegetation parameters and soil physical temperature. Depending on the outcomes of the following steps of the decision tree, these values will be either passed to the forward model as *a priori* estimates (fixed parameters) or as initial guess values in the case they are retrieved (free parameters).

3.2.3.5 Determining Retrieval Conditions

The last step of the SMOS L2 decision tree is to determine the retrieval conditions for the pixel depending on the number of available T_B data (in terms of angles and polarisation), which determines how many parameters can be retrieved, and the range of initial/expected values of the vegetation optical depth. This step has four possible outcomes:

1. the L1C pixel is invalidated (no retrieval is attempted);
2. a "minimum" retrieval is attempted (only soil moisture or soil moisture and optical depth);
3. a "full" retrieval is attempted (soil moisture, optical depth and surface roughness); and
4. a "maximum" retrieval is attempted (soil moisture, optical depth and surface roughness plus other vegetation parameters).

In cases (2), (3) and (4), different retrieval options ("negligible", "moderate" and "forest") are selected depending on thresholds on the *a priori* value of the optical depth of the dominant fraction. The *a priori* value can be derived from previous retrievals over the same area or from ancillary data (e.g., LAI maps).

In the retrieval process, the retrieved parameters are constrained to initial guess values (also determined *a priori* from previous retrievals over the same area or from ancillary data). The constraint is applied through the cost function using uncertainties in the guess value for each parameter expressed in the form of *a priori* standard deviations (see section 3.2.4), so that large *a priori* values of standard deviation mean that the parameter is practically left free. Different *a priori* standard deviations are assigned to each retrieved parameter in cases (2), (3) and (4). These *a priori* standard deviations are summarised in Table 3.2 for all the retrieval options in those cases.

In the "minimum" retrieval case, only soil moisture is retrieved for surfaces with negligible optical depth. In moderate vegetation conditions,

Table 3.2. *A priori* standard deviations for all "retrievable" L-MEB parameter and for all SMOS L2 algorithm retrieval options: negligible vegetation cover, moderate vegetation cover and forest cover. Where not retrieved, parameters are indicated as "nil", while where retrieved parameters are indicated with their *a priori* standard deviation (in the parameter's measurement unit). The retrieval options are indicated for the nominal case of low or moderately vegetated soil or forest. The vegetation parameters in the 1st column are explained in section 3.4.5. The *a priori* optical depth thresholds TH_23 and TH_34 are defined in the text.

Parameter	**Units**	***A Priori* Optical Depth**	**Retrieval Options**		
			Min.	**Full**	**Max.**
Soil Moisture	%v/v	Negligible (<TH_23)	20	20	20
		Moderate (>TH_23 & <TH_34)	20	20	20
		Forest (>TH_34)	10	10	10
Soil Temperature	K	negligible	nil	nil	2.5
		moderate	nil	nil	2.5
		forest	nil	nil	2.5
Optical depth τ	-	negligible	nil	nil	nil
		moderate	0.1	0.5	0.5
		forest	0.5	0.5	0.5
Vegetation parameter tt_H	-	negligible	nil	nil	nil
		moderate	nil	nil	1
		forest	nil	nil	nil
Vegetation parameter $Rtt=tt_V/tt_H$	-	negligible	nil	nil	nil
		moderate	nil	nil	2
		forest	nil	nil	nil
Vegetation scattering ω_H	-	negligible	nil	nil	nil
		moderate	nil	nil	0.1
		forest	nil	nil	0.1
Vegetation scattering $\Delta\omega=\omega_V- \omega_H$	-	negligible	nil	nil	nil
		moderate	nil	nil	0.1
		forest	nil	nil	nil
Roughness H_R	-	negligible	nil	0.1	0.1
		moderate	nil	nil	nil
		forest	nil	nil	nil

retrieval is attempted of both soil moisture and optical depth but with a strong constraint on the optical depth (*a priori* standard deviation of 0.1). When the vegetation cover is significant (forest case), soil moisture is constrained (*a priori* standard deviation of 10%v/v) and only optical depth is left as a free parameter (*a priori* standard deviation of 0.5). In the "maximum" retrieval case due to the presence of good quality L1C T_B data for a variety of incidence angles the retrieval of several other parameters is attempted along with the retrieval of soil moisture and optical depth in the case of moderate vegetation conditions. The rationale behind this is that, for example, in the case in which forest is the dominant fraction and the expected optical depth is significant, soil moisture is not expected to vary significantly in time and can therefore be highly constrained to the value retrieved at a previous time-step in order to obtain a better retrieval of the optical depth of the forest.

The thresholds which are used to determine the retrieval options based on the *a priori* optical depth are TH_23, TH_34. (for easy reference, the nomenclature used in the ATBD (CESBIO, 2007) was adopted here). These are yet to be estimated at global scale. TH_23 should be fairly small, since if the expected optical depth is below this value, the pixel is considered bare. Values smaller than TH_23 should mainly correspond to ice or barren soil, i.e., surfaces where the optical thickness is known to be negligible. The TH_34 threshold corresponds to situations close to the limit of the validity domain (vegetation density too high to attempt any soil moisture retrieval). Hence it defines a trade-off between getting better estimates of soil moisture by constraining the optical depth and getting best estimates of the optical depth at the expense of undergoing some risk of bias on the retrieved soil moisture. To derive the retrieval conditions, the *a priori* optical depth of the dominant cover fraction of the pixel is compared with these thresholds (see Table 3.2).

3.2.4 Iterative Solution

Once the retrieval problem has been set by the decision tree, the retrieval itself is performed by minimising a quadratic cost function. This is more complex than a standard maximum likelihood estimation, because:

- constraints (*a priori* estimates and a priori standard deviations) are introduced for some of the retrieved parameters; and
- when several multi-angle T_B observations are available, a strong correlation between the T_B data must be accounted for, in such a way that the cost function becomes a quadratic form rather than a sum of weighted squared differences.

For each L1C pixel, the T_B are computed for each incidence angle (ϑ) and polarisation (*P*) by aggregating the T_B predicted for each surface cover fraction FV_i (which are incidence angle dependent) as a function of the surface physical parameters p_i of each fraction (including free and fixed parameters), such that:

$$\overline{T}_{BP}(\vartheta) = \sum_{i=1}^{N} FV_i * T_{BP}(\vartheta, p_i), \tag{3.1}$$

where N is the number of surface cover fractions FV_i present in the mixed L1C pixel. These aggregated T_B are as observed “above the canopy”. Atmospheric and sky contributions are then added to this aggregated signal to obtain the Brightness Temperature at the Top Of the Atmosphere ($T_{B\text{-}TOA}$) as described later in section 0. The retrieved parameters are those which minimise the cost function between simulated ($T_{BP\text{-}TOA}$) and measured brightness temperatures (T_{BPM}) at polarisation *P* expressed as:

$$CF = (T_{BPM\,n} - T_{BP-TOA}(\vartheta_n, p_i))^T * [COV_T]^{-1} * (T_{BPM\,n} - T_{BP-TOA}(\vartheta_n, p_i)) +$$
$$+ \frac{\sum_i (p_i - p_i^{ini})^2}{\sigma_P^2}, \tag{3.2}$$

where the $T_{BPM\,n}$ is an n x 1 vector including n T_B observations at n incidence angles, subscript “*T*” stands for matrix transposition, $[COV_T]$ is the n x n variance/covariance matrix for the T_{BPM} and p_i^{ini} are *a priori* estimates of the retrieval parameters, with *a priori* standard deviations σ_P set as in Table 3.2. The cost function *CF* is minimised using the Levenberg-Marquardt (L-M) algorithm.

After the parameter retrieval has been attempted, some post-processing analysis is undertaken which consists of computing the posterior error variance on the retrieved parameters, and checking consistency with other products and/or the expected range. If retrieval of geophysical parameters other than soil moisture has been successful (e.g., optical depth or roughness) these values are used to update the current maps for the specific parameters, so that the next retrieval over the same area will take advantage of these fine tuned reference values

3.2.5 Limitations of SMOS L2 algorithm

Even though the SMOS L2 algorithm is intended to be run in its operational version as described in this Chapter, it is also foreseen that after SMOS launch and the commissioning phase, a better knowledge of the whole system will result in changes in the approach outlined. Important limitations of the current set up which are relevant to this thesis are:

- direct models such as L-MEB, even when validated, are strictly valid only at local scale. However, due to the large size of the SMOS pixel average values have to be retrieved over heterogeneous targets and errors may be due to the non-linear behaviour of the model;
- the land cover type (forest, moderately vegetated soil etc...) is considered to be the only factor whose variability within the SMOS pixel can produce and error in the soil moisture retrieval due to non-linearity of the retrieval algorithm. The impact of the variability of other land surface factors, such as soil moisture itself or soil texture, is implicitly neglected by the approach; and
- for a mixed pixel composed of a fraction of moderately vegetated soil and a fraction of forest, and in the case when the density of canopy in

the forest fraction is expected to be low, the assumption is made that the retrieved parameters are the same for both fractions, while all other parameters (fixed parameters) are surface fraction specific. An illustrative example of this approach is shown in Figure 3.5, where the retrieval of soil moisture (θ) and optical depth (τ) is shown for a pixel with a mix of forest (fixed parameters p_1) and low vegetated soil (fixed parameters p_2) with other minor surface fractions. Both the assumptions of uniform optical depth and uniform soil moisture between the fractions are rather strong. Moderately vegetated surfaces like crops and grasses are known to have lower vegetation water content (which determines the optical depth) than the dense canopy of a forest (Njoku et al., 2002; Ryu et al., 2007). Moreover, the literature review presented in Chapter 2 gave strong evidence that differences in soil moisture are associated with different vegetation covers.

These limitations are addressed in this thesis through:

- a specific evaluation of the parameters of the L-MEB model for the surface conditions in the study area (Chapter 5);
- an evaluation of the model from local (62.5m) to satellite footprint scale (40km), accompanied by a detailed characterisation of the land surface heterogeneity within the footprints (Chapter 5, 6 and 7); and
- testing of the soil moisture retrieval approach proposed for SMOS at satellite footprint scale and investigation of alternative retrieval approaches for mixed pixels with areas of moderately vegetated soil and forest and in the case of low forest canopy density (Chapter 8).

The simplifications and assumptions made in applying the complex SMOS L2 algorithm to the airborne data are described in the next section.

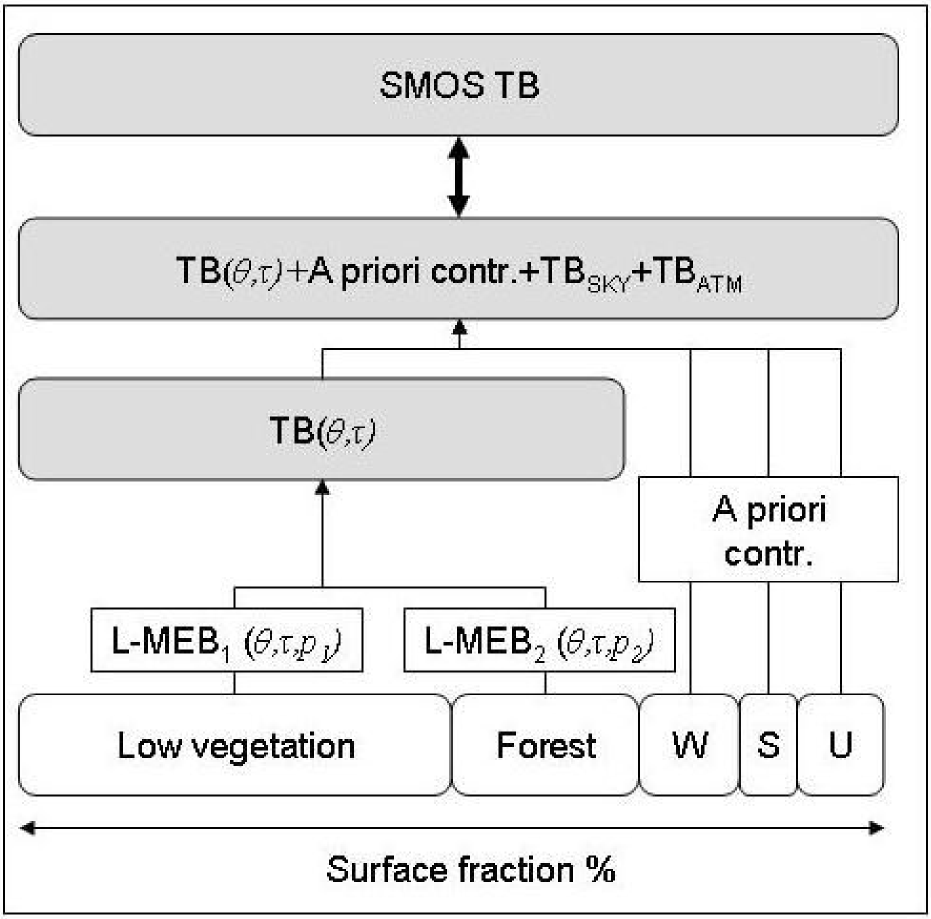

Figure 3.5. Schematic of SMOS L2 forward modelling approach for a nominal pixel and in the case of low forest density. θ=Soil Moisture, τ=Optical depth, p=fixed physical parameters, W=Water, S=Snow, U=Urban.

3.3 Application of the SMOS L2 Algorithm to Airborne Data

In order to apply the complex SMOS L2 algorithm to the airborne data collected across the NAFE'05 study area, several simplifications can be introduced to make the data processing easier without diminishing the significance of this thesis's findings for future real-world application of the algorithm. These simplifications are summarised in this section.

As already anticipated at the beginning of this Chapter, this thesis focuses on the so-called "nominal" case of land surface parameter retrieval from SMOS, i.e., the retrieval of soil moisture over mixed pixels which include predominantly low or moderately vegetated soil and forest, and therefore do not include a significant fraction of water bodies, mountainous, urban, and partially frozen or snow covered areas. Additionally, due to the nature of the NAFE'05 study area, this thesis is concerned with the case in which the sum of the vegetated soil and forest fractions is 100% and the density of the forest canopy is low.

In Chapter 7, SMOS pixels are simulated by aggregating 1km airborne T_B data. This approach has three main implications for the relevance of the results of this thesis to SMOS operational retrieval:

1. it by-passes the sequence of processing steps that leads from the raw interferometric measurements of the MIRAS instrument into the final SMOS L1C TB images (see section 3.1.3). Therefore, SMOS observations simulated in this thesis are considered free of the errors associated with image reconstruction, ionospheric (Faraday) rotation and sky and atmospheric contributions compensation, which are estimated to amount to a combined error of 0.5 K (CESBIO, 2007). Moreover, the radiometric uncertainty is that of the PLMR radiometer (2 K and 0.7 K respectively at V and H polarisation, see Appendix A3), which is lower than that of SMOS (estimated to be of 3.5 K at boresight and 5.8 K within 32° from boresight (McMullan et al., 2008). As the radiometric uncertainty is expected to be the main contribution to the error budget (CESBIO, 2007), the findings of this thesis should therefore be considered a best case scenario of SMOS operational retrieval;

2. given the fine spatial resolution of the airborne TB observations (1km), the SMOS pixels resulting from aggregation of such observations are equivalent to those that would be observed if the SMOS sensor had a uniform directional gain. Consequently no antenna gain weighting function (WEF, see section 3.2.2) is applied when aggregating ancillary data and the fraction-specific TB to SMOS pixel resolution. Any error which in SMOS will derive from the choice of the proper antenna gain weighting function WEF (which is an approximation of the synthetic antenna pattern) is

therefore ignored in this thesis. The results of a SMOS soil moisture retrieval study (Vergely, 2005) suggest however that the WEF function currently adopted for the SMOS L2 algorithm is a sufficiently accurate replicate of the antenna pattern and that therefore no significant error should result from this operation; and

3. the range of independent observations at multiple incidence angles that could be simulated was very narrow, and essentially consisted of bi-polarised observations at two different incidence angles. Therefore, only the "minimum" retrieval option described in section 3.2.3.5 can be analysed, in which the retrieval of only two parameters (soil moisture and optical depth) is attempted. This will be the most common retrieval scenario in SMOS, since to date the retrieval of more than three unconstrained parameters has proven to be difficult (Wigneron et al., 2000).

Finally, the land surface ancillary data used in this thesis differ from those which will be used operationally in the SMOS L2 algorithm. These data will be described in detail in Chapter 4 and in the relevant sections in Chapter 5 and Chapter 7. Here it is important to note that the best available ancillary data at the finest available resolution (finer than those used for the SMOS L2 algorithm) are used in this thesis (either collected during NAFE'05 or from other sources). This is motivated by the fact that the SMOS L2 algorithm has been designed to be flexible in accommodating any improvements, or changes, on the ancillary data currently adopted (i.e., finer resolution). Therefore, by adopting the best available ancillary data sets, this thesis will reduce uncertainties associated with the currently proposed data and at the same time the results will be relevant to SMOS operational conditions when better ancillary data sets will become available.

3.4 The L-MEB Model

The L-band Microwave Emission of the Biosphere model, L-MEB, is the core to the SMOS L2 algorithm described in the first part of this Chapter.

The L-MEB model was born from an extensive review of the current knowledge of the microwave emission of various land cover types (Wigneron et al., 2003) and is currently being developed and tested with tower based studies on mostly homogeneous land surface conditions of low to moderate vegetation density, such as crops and grass-type surfaces (Wigneron et al., 2007). Development is also ongoing for forested areas (Saleh et al., 2004; Grant et al., 2007b; Guglielmetti et al., 2007). In order to retrieve soil moisture estimates from SMOS data, the algorithm requires the input of ancillary information on soil temperature, soil texture, surface roughness and vegetation water content. Moreover a set of vegetation and surface type dependent parameters are needed which characterise the microwave properties of the top soil layer and the vegetation canopy. In the following section the L-MEB model structure is described, and the values of the model parameters used in this study and their derivation from the relevant literature are presented.

3.4.1 General

The L-MEB model is based on a widely recognised approach to simulating microwave emission from the land surface, based on a simplified (zero-order) solution of the radiative transfer equations (Ulaby et al., 1986). The model represents the soil as a rough surface in contact with the atmosphere and the vegetation as a homogeneous layer between the two, and models the complex interaction of the radiation emitted by the soil, the vegetation and the sky (see Figure 3.6).

The soil emission is controlled by the microwave reflectivity of soil, which depends on the dielectric properties of the soil-water mixture, while the vegetation layer scatters and absorbs part of this radiation, as well as emitting radiation itself. The radiation measured by the sensor in space (T_{B-TOA}) is the sum of (see Figure 3.6): (i) the upward atmospheric emission ($T_{B-ATM-UP}$), (ii) the surface level emission (T_B) attenuated by the atmosphere, (iii) the downward atmospheric emission ($T_{B-ATM-DOWN}$) reflected (scattered) at the surface and attenuated along the upward path by the atmosphere and finally (iv) the cosmic background emission (T_{B-SKY}) attenuated by the

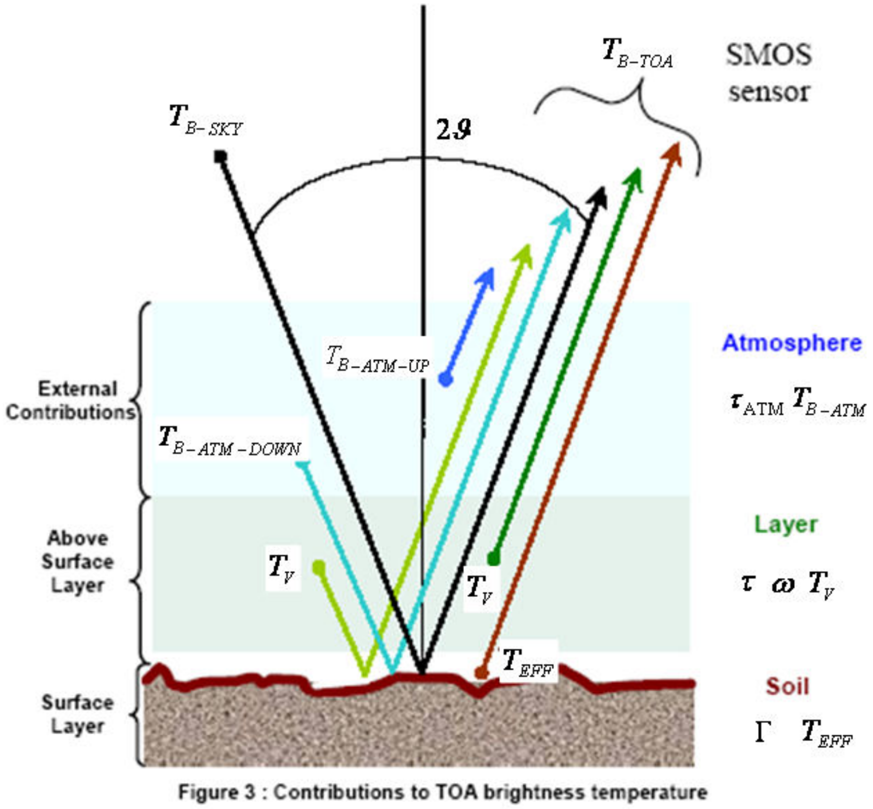

Figure 3.6. Schematic of the radiative transfer processes simulated by the L-MEB model (Adapted from CESBIO, 2006).

atmosphere, reflected/scattered at the surface and attenuated again along the upward path by the atmosphere according to:

$$T_{BP-TOA} = T_{BP}\exp(-\tau_{ATM}) + T_{BP-ATM-UP} +$$
$$+ (T_{BP-ATM-DOWN} + T_{BP-SKY}\exp(-\tau_{ATM}))\Gamma_P \exp(-\tau_{ATM})\,, \qquad (3.3)$$

where τ_{ATM} is the atmospheric optical thickness, and T_{BP} is the brightness temperature as observed "above the canopy" (the sum of the soil and vegetation contributions) and Γ is the surface reflectivity. All the terms of the above equation are functions of the frequency and the sensor observation angle ϑ (defined with respect to nadir and referred to earlier as the "incidence angle"). The subscript "P" indicates the polarisation (vertically, V, or horizontally, H). A simplified approach is used by L-MEB to compute the atmospheric and background contributions (Pellarin et al., 2003). Since the SMOS pixels that will be simulated in the present study derive from airborne data, the atmospheric component was not considered in this study.

Therefore, only the modeling of the above canopy T_B in L-MEB is discussed in detail here. This is done in the following sections by distinguishing between the cases of (i) bare soil, (ii) low or moderate vegetation cover and (iii) forest. The following sections rely on the description of the basic physics of microwave emission already presented in Chapter 2 and focus on the particular aspects of the L-MEB which distinguish it from other microwave emission models.

3.4.2 Soil Reflectivity

The polarised (subscript P) microwave emission of bare soil (T_{BP}) is written in L-MEB as a function of the soil microwave emissivity (e_{GP}) as (see also (2.3)):

$$T_{BP}(\vartheta) = e_{GP}(\vartheta, P)T_{EFF}\,. \tag{3.4}$$

where the soil temperature T_s in (2.3) in has been replaced with the effective soil temperature ($T_{EFF},$ see section 3.4.4). The soil microwave emissivity is computed as: e_G=1−Γ. For smooth soil surfaces and homogeneous soils, the soil microwave reflectivity can be approximated by using the soil reflectivity of a smooth surface (Γ*). This is related to the soil dielectric constant or permittivity (ε_G) and the incidence angle through the Fresnel equations (2.1) and (2.2) that define the behavior of electromagnetic waves at a smooth dielectric boundary.

The dependence of ε_G from the soil moisture content, soil density, and textural properties is accounted for in L-MEB using the Dobson dielectric mixing model (Dobson et al., 1985) which takes into account soil textural properties to simulate the dielectric behavior of the soil-water mixture. However, in particular conditions, such as dry sandy soils or frozen soils, this model is not sufficiently accurate and other models are used. For dry sandy soils the model proposed by Mätzler (1983) is used in L-MEB. The case of frozen soil is not treated here as such conditions were not encountered in the study area focus of this study.

3.4.3 Surface Roughness

The modeling of surface roughness in L-MEB is based on the semi-empirical approach developed by Wang and Choudhury (1983) and Wang et al. (1983) and has been presented in (2.5). More recent tower observations found that the polarisation mixing parameter Q_R in (2.5) can be safely neglected, having very small values at L-band (for three soil types the best fit values of Q_R were 0, 0.01 and 0.12) (Mo et al., 1987 ; Wigneron et al., 2001; Wigneron et al., 2007). The formulation used in L-MEB for rough reflectivity (Γ) is therefore a simplification of (2.5) expressed as:

$$\Gamma_P(\vartheta) = \Gamma_P^*(\vartheta)\exp(-H_R(\vartheta)\cos^{N_{RP}}\vartheta)\,. \tag{3.5}$$

where H_R is the surface height parameter and N_{RP} the roughness exponent.

The dependence of H_R on the surface roughness characteristics is not well understood. Wigneron et al. (2001) found that the best geophysical parameter to describe H_R over agricultural fields was the slope parameter (m= σ_S/L_C), dependent on the standard deviation of surface heights (σ_S) and the correlation length (L_C). Additionally, Wigneron et al. (2001) found that H_R exhibited soil moisture dependence. This was confirmed by detailed studies by Saleh et al. (2007) and Escorihuela et al. (2007). The dependence of H_R on soil moisture was explained by an effect of volume scattering: the spatial fluctuations of the dielectric constant within the soil volume are stronger during drying out, producing an important "dielectric" roughness effect. Therefore, it was proposed that H_R should be considered as an effective parameter that accounts for (i) "physical roughness" effects related to spatial variations in the soil surface height, and (ii) "dielectric roughness" effects related to variation of the dielectric constant in the near-surface soil layer.

3.4.4 Microwave Effective Soil Temperature

In L-MEB a soil profile temperature approximation is used to characterise the contribution of the whole soil layer contributing to the microwave emission. At L-band, this can in fact be much deeper than the actual observation wavelength, especially in dry conditions (Stiles et al., 2000; Mätzler et al., 2006). The formulation of the microwave effective soil temperature T_{EFF} contributing to the soil microwave emission is based on the parameterisation developed by Choudhury et al. (1982) and shown in (2.8). However, in L-MEB, the dependence of the empirical attenuation coefficient C_t in (2.8) on soil moisture (θ) is taken into account using a refinement of (2.8) proposed by Wigneron et al. 2001:

$$T_{EFF} = T_{DEPTH} + (T_{SURF} - T_{DEPTH}) * (\theta / w_0)^{b_0}, \tag{3.6}$$

where T_{DEPTH} is the deep soil temperature (approximately at 50 to 100cm) , T_{SURF} is the surface temperature (approximately corresponding to a depth interval of 0–5cm) and w_0 and b_0 are semi-empirical parameters depending on the specific soil characteristics (mainly soil texture). θ stands for the top 5cm soil moisture which corresponds well to the effective soil moisture value contributing to soil emission at L-band.

The formulation in (3.6) takes into account the variation in contributing depth depending on soil moisture conditions. If the soil is very dry, soil layers at depth (deeper than 1 meter for dry sand) contribute significantly to the soil emission, and $T_{EFF} \sim T_{DEPTH}$. Conversely, if the soil is very wet, the soil emission originates mainly from layers at the soil surface and $T_{EFF} \sim T_{SURF}$. Note that the formulation in (3.6) neglects multiple scattering effects within the soil layer. However, its effectiveness was tested over several L-band test sites at the seasonal to inter-annual temporal scales by De Rosnay et al. (2006b). Wigneron et al. (2001) showed that this approximation can result in error of the effective soil temperature estimate of approximately 1.3K.

3.4.5 Vegetation Modelling

When a vegetation layer is present over the soil surface, the vegetation layer scatters and absorbs part of the radiation emitted by the soil, as well as emitting radiation itself (see Figure 3.6). In L-MEB this is modeled using the 'τ-ω model', proposed by Mo et al. (1982) and already described in section 2.2.3.2.3. With the 'τ-ω' formulation, the above canopy brightness temperatures are written as (see also (2.10)):

$$T_{BP}(\vartheta) = (1-\omega_P(\vartheta))(1-\gamma_P(\vartheta))(1+\Gamma_P(\vartheta)\gamma_P(\vartheta))T_V +$$
$$+(1-\Gamma_P(\vartheta))\gamma_P(\vartheta)T_{EFF}\,, \tag{3.7}$$

where T_V is the effective vegetation temperature and ω the single scattering albedo which characterise the scattering of the soil microwave signal through the vegetation canopy.

The transmissivity of the vegetation layer γ_P is calculated from the vegetation optical depth τ_P as (see also (2.11)):

$$\gamma_P(\vartheta) = \exp(-\tau_P(\vartheta)/\cos\vartheta)\,. \tag{3.8}$$

In L-MEB a sophisticated modeling approach is used to account for the effect of vegetation structure on the dependence of the τ_P from polarisation and incidence angle, which was found to be significant in several studies (Wigneron et al., 1995; Van de Griend et al., 2004; Wigneron et al., 2004; Wigneron et al., 2007), particularly for stem-dominated crops like wheat and corn. Given that the most common crop types in the NAFE'05 study area are of this kind, it is important to consider this effect. Wigneron et al. (2001) proposed a simple formulation using a polarisation correction factor C_{pol} to parameterise the effect of a dominant vertical vegetation structure on the optical depth for cereal crops:

$$\tau_H(\vartheta) = \tau_{\mathrm{NAD}} \qquad\qquad ,\text{and} \tag{3.9}$$

$$\tau_V(\vartheta) = \tau_{\mathrm{NAD}}(\cos^2\vartheta + C_{pol}\sin^2\vartheta)\,, \tag{3.10}$$

where τ_{NAD} is the value of τ_P at nadir, independent of both incidence angle and polarisation. (3.9) and (3.10) were later refined by Escorihuela et al. (2007) and Saleh et al. (2007) by introducing the vegetation structure parameters tt_V and tt_H (or tt_H and the parameter $R_{tt}=tt_V/tt_H$) that correct the optical depth for non-nadir views at each polarisation by:

$$\tau_P(\vartheta) = \tau_{\mathrm{NAD}}(\cos^2\vartheta + tt_P * \sin^2\vartheta)\,. \tag{3.11}$$

A value of $tt_P>1$ or $tt_P<1$ will correspond, respectively, to an increasing or decreasing trend of τ as a function of the incidence angle ϑ. The particular case, $tt_H = tt_V = 1$, corresponds to the "isotropic" case where τ_P is assumed to be independent of both polarisations and incidence angle.

The nadir value of the vegetation optical depth τ_{NAD} is then related to the vegetation water content (VWC) using the empirical relationship between optical depth and VWC given by Jackson et al., 1991:

$$\tau_{NAD} = b * VWC \,. \tag{3.12}$$

using the parameter *b* which, given (3.11), can be considered unique to the type of vegetation and radiation frequency.

One caveat in using (3.12) for satellite applications is that it is difficult to provide estimates of VWC at global scale. An alternative approach proposed for the SMOS mission is to parameterise the optical depth through vegetation indices such as the Leaf Area index (LAI) or the Normalised Difference Water Index (NDWI). It is in fact much easier to construct global maps of LAI and NDWI from spaceborne remote sensing observations in the optical domain or from SVAT modeling (Wigneron et al., 2002) than construct maps of VWC directly. Moreover, recent studies have found good correlation between optical depth and LAI (Saleh et al., 2006a) and NDWI (Jackson et al., 2004).

3.4.6 Forest

In the case of dense vegetation cover like such as a forest canopy, the effects of attenuation and scatter of the vegetation layer become increasingly important and would require the consideration of more complex attenuation/scattering mechanisms than those simulated by the zero-order radiative transfer simplification used by L-MEB. However, in order to harmonise the methodology to be adopted for forests with the general SMOS L2 algorithm, a zero-order τ-ω approach has been adopted for forests by the SMOS L2 algorithm. Several L-band studies have analysed the radiative transfer properties of different types of forest (Ferrazzoli et al., 2002; Saleh et al., 2004; Della Vecchia et al., 2007; Grant et al., 2007b). The main findings of these studies are:

- the nadir equivalent optical depth for forest (τ_{FNAD}) can be considered as fairly constant with respect to polarisation and incidence angle (i.e., parameter $tt_V = tt_H \sim 1$). This is a result of the variability in orientation of branches and leaves in forest canopies;
- at L band, leaves are almost transparent, attenuation is mostly due to branches, and contributions from the soil may still be appreciable, unless the forest is very dense. Therefore, τ_{FNAD} can be considered as a "static" parameter which does not change in time. In the SMOS L2 algorithm, τ_{NAD} will be related to the annual maximum LAI through empirical parameters; and
- the scattering albedo ω can be considered as constant (i.e. independent of incidence angle, polarisation and time). However, it is not negligible, since its value is close to 0.1 (see next section).

In this study, values of the L-MEB parameters specifically calibrated for the Eucalypt forest in the NAFE'05 study area were used (Grant et al., 2008). This is addressed in the following section together with a description of the values of all the L-MEB parameters used in this study for the low and moderately vegetated soil case.

3.4.7 L-MEB Parameters

The review of the L-MEB model presented in the previous section identified several parameters that are needed to characterise the radiative transfer properties of low to moderately vegetated soil and forested surfaces. A summary of these parameters is presented in Table 3.3.

Specific values for each parameter need to be set *a priori,* or can be retrieved together with soil moisture if a sufficient number of concurrent multi-angular and/or bi-polarised observations are available. A considerable amount of research has been devoted in the past decade towards building a database of L-MEB parameter estimate for a variety of vegetation and surface types. Building upon these studies, J.P. Wigneron (pers. comm.) has completed a summary of 'best estimates' which will be the baseline for

Table 3.3. L-MEB input parameters to be set *a priori*. This table does not include ancillary data.

L-MEB component	Symbol	Description	units
Soil emission/ scattering	H_R	Roughness (section 3.4.3)	[-]
	N_{RP}	Roughness exponent at V/H polarisation (section 3.4.3)	[-]
Effective soil temperature	w_o	Texture parameters for effective soil temperature T_{EFF} computation (section 3.4.4)	[m^3/m^3]
	b_o		[-]
Vegetation emission/ scattering/ absorption	b	parameter of the relation τ_{NAD}/VWC (section 3.4.5)	[-]
	tt_P	Angular correction for τ at V/H polarisation (section 3.4.5)	[-]
	ω_P	Single scattering albedo at V/H polarisation (section 3.4.5)	[-]
	τ_{FNAD}	Nadir equivalent optical depth for forest (section 3.4.5)	[-]

SMOS operational soil moisture retrieval and which have been adopted in this study. This database is summarised in the following discussion and will be referred to in this thesis as the L-MEB ‘default’ parameter set:

Among the soil and vegetation parameters that appear in L-MEB, the roughness parameter H_R is amongst those which have the largest impact on the soil moisture retrieval accuracy. The dependence of this parameter on the surface roughness characteristics (standard deviation of heights σ_S, autocorrelation length L_C, etc.) is nevertheless not well known. Wigneron et al. (2001) proposed a simple incidence angle and polarisation independent parameterisation of H_R as a function of σ_S, L_C and soil moisture. Nevertheless, as estimates of two surface roughness parameters are required, the parameterisation cannot be applied directly for coarse-scale soil moisture retrievals due to the difficulty in determining the two surface roughness parameters over large areas. The dependence of H_R on soil moisture was confirmed by other studies (e.g., Saleh et al., 2007) which proposed an incidence angle and polarisation independent linear parameterisation $H_R=1.3-1.13*\theta$. This has been shown to be applicable to a variety of grass types with a litter layer. In the absence of litter, a constant value for H_R of 0.5 was found suitable for grass surfaces (Saleh et al., 2007). For crops, values of H_R have been shown to be in the range 0.1-0.2 for relatively smooth surfaces (wheat) and ~0.5 when rows at the surface are present (as for corn) (Van de Griend et al., 2004).

Estimates of the polarised (subscript P) roughness exponent N_{RP}, generally considered zero at L-band, have been recently updated through long time series observations over bare soils from the Surface Monitoring Of the Soil Reservoir Experiment (SMOSREX; De Rosnay et al., 2006a), with $N_{RV}=-1$ or 0 and $N_{RH}=0$ or 1 respectively (Escorihuela et al., 2007). These values were also found suitable for crops (Wigneron et al., 2004; Wigneron et al., 2007). For grasses $N_{RV}=0$ and $N_{RH}=1$ provided the best soil moisture retrievals (Saleh et al., 2006b; Saleh et al., 2007). However, the variability of these parameters across surface types and their impact on the soil moisture retrievals are relatively limited.

At L-band a value of $b=0.12\pm0.03$ was found to be representative of most agricultural crops for a variety of incidence angles (Jackson et al., 1991; Van de Griend et al., 2004). This estimate was later refined to 0.08 (Wigneron et al., 2007), after introduction of the incidence angle dependence of the vegetation optical depth (see (3.11)). Similar values (0.15) have been estimated over grasslands (Saleh et al., 2007). A few studies have reported that the effect of the litter layer common in grasslands might result in an increased value for b of up to 0.4, as a consequence of the attenuation effects of the water content in this layer (Jackson et al., 1991; Wigneron et al., 2004).

Values of ω have been found to be significantly larger than zero only for corn fields and grasslands at V-pol (ω_v =0.05), and negligible for all the other crop types and at H-pol (Ferrazzoli et al., 2002; Grant et al., 2007a). As the dependence of ω on the incidence angle has not been clearly demonstrated to date in the literature, the value of ω in L-MEB is tabulated only as a function of the vegetation type (i.e., any dependence on incidence angle is neglected).

The variation of the optical depth with incidence angle is modulated through two 'vegetation structure' parameters tt_V and tt_H which characterise the isotropy of the structure of the standing vegetation. These are generally set to '1' in the case of isotropic canopy like that of native grasses (Wigneron et al., 2007), while values as high as '8' for tt_V have been estimated for vertically dominated crops such as wheat and corns, with tt_H generally closer to 1 (Wigneron et al., 2007).

Parameters w_0 and b_0 were calibrated using data from two bare soil sites in southern France: a loam soil at the SMOSREX (De Rosnay et al., 2006a) and a silty clay loam at the site of the Institut National de Recherches Agronomiques near Avignon (INRA) (Wigneron et al., 2001). The value of w_0 was found to be close to 0.3m^3/m^3 at both sites. The value of b_0 was close to 0.3 over the INRA Avignon site and close to 0.65 over the SMOSREX site. It should be noted that recently the dependence of the parameters w_0 and b_0 as a function of soil texture was determined by analysis of a large number of soil types (Wigneron et al., 2008). However, in this thesis the values w_0=0.3m^3/m^3 and b_0 =0.3 were used as default values in L-MEB.

Values of parameters τ_{FNAD}, ω, tt, N_R, and H_R were specifically calibrated for the Eucalypt forest present in the NAFE'05 study area by J. Grant (pers. comm.). The optical depth of the Eucalypt canopy was calibrated to be 0.57, which is lower than that retrieved over coniferous and deciduous forests (Saleh et al., 2007), reflecting the lower density of the Eucalypt forest. Lower values were also calibrated for H_R (0.12), while tt_V and tt_H (0.46), ω (0.07) and N_R (1.5) were close to those retrieved for other types of forests.

3.5 Chapter Summary

This Chapter has presented a background description of the Soil Moisture and Ocean Salinity (SMOS) mission and the currently proposed SMOS L2 soil moisture retrieval algorithm. The approach used by the SMOS L2 algorithm to retrieve soil moisture (and potentially optical depth) estimates over heterogeneous areas has also been described, with focus at the vegetated surface types considered in this thesis. The assumptions that will be made in subsequent Chapters of this study to apply the SMOS L2 algorithm with airborne L-band data have been presented. Additionally, the L-MEB radiative transfer model, which is the core to the SMOS L2 algorithm, has been described in detail together with a review of its input parameters.

The approach adopted for the SMOS L2 algorithm to retrieve soil moisture estimates from SMOS data over heterogeneous pixels containing a mix of low or moderately vegetated soil and low density forest cover is based on some limiting assumptions which need to be verified and tested with realistic data sets. These assumptions are that (i) the land cover heterogeneity is the most important factor in terms of soil moisture retrieval at satellite scale, and (ii) soil moisture and optical depth are uniform between the moderately vegetated soil fraction and the forest fraction. Additionally, the L-MEB input parameters have been thus far calibrated using only tower radiometers and never verified at coarse resolutions typical of SMOS footprints.

The L-MEB model with the proposed parameters will therefore be evaluated with fine-resolution airborne data in Chapter 5, using the data to be described in Chapter 4. In Chapter 7 the model will be evaluated at the satellite scale and the error in soil moisture retrieval interpreted on the basis of the land surface heterogeneity which will be assessed in Chapter 6. In Chapter 8, the SMOS L2 algorithm approach will be tested at satellite scale in order to test the assumptions listed above and to develop an alternative soil moisture retrieval approach to better account for the land surface heterogeneity.

Chapter Four

4 The NAFE'05 Field Campaign

This Chapter describes the airborne and ground data collected during this study, which are used throughout this thesis to address the problem of soil moisture retrieval in the presence of land surface heterogeneity. This data was collected under the auspices of the National Airborne Field Experiment 2005 (NAFE'05), and consisted primarily of airborne L-band observations supported by ground sampling of the top 5cm soil moisture over an area as big as a future SMOS pixel. This Chapter only describes the data which are essential to interpret the analysis presented in the following Chapters are included. . Full details of the experimental design are included in the NAFE'05 Experiment Plan presented in Appendix A1. A summary description of this data set has also been published in Panciera et al.(2008a), and the data together with relevant documentation are available at the website www.nafe.unimelb.edu.au. While the NAFE'05 experiment was an international effort of several institutions with more than 40 participants, the author of this thesis played a central role in all aspects of the field campaign, including conceptualisation and planning of the airborne monitoring and ground sampling strategies, management of the ground sampling activities, and the post-processing, documentation and archiving of all collected data.

In parallel with NAFE'05, the European Space Agency (ESA) conducted the Campaign for validating the Operation of SMOS (CoSMOS) on the same study area, using a separate aircraft and L-band radiometer. Although the two airborne campaigns were operated in synergy, the CoSMOS data set is not described in this Chapter or used in this thesis. However, a summary of the CoSMOS data is provided in Panciera et al. (2008a).

4.1 Experiment Overview

The National Airborne Field Experiment 2005 (NAFE'05) was undertaken across a 4-week period, starting on October 31st and ending on

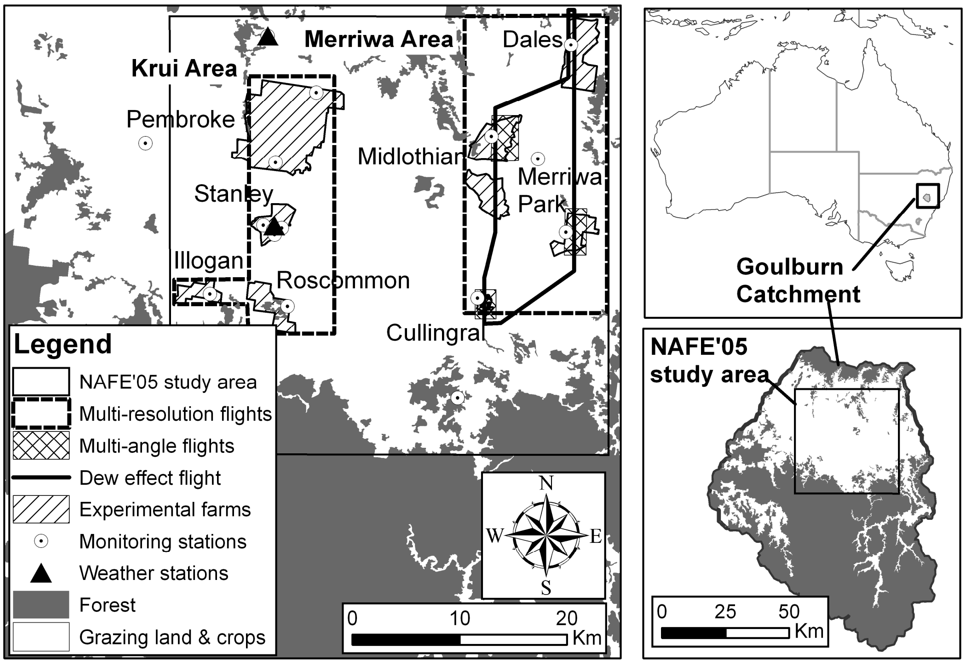

Figure 4.1. Location of the Goulburn catchment and study area (right panels) and overview of the NAFE'05 study area, permanent monitoring stations, experimental farms and flight coverages (left panel).

November 25th, in the Goulburn River catchment, located in south-eastern Australia (see Figure 4.1). The study area was a 40km x 40km area characterised by moderate to low vegetation cover (mainly grazing land and crops with a small fraction of forest) and gentle topography. The objective of the campaign was to provide simulated SMOS observations using an airborne radiometer, supported by soil moisture and other relevant ground data for i) development of the SMOS soil moisture retrieval algorithms, ii) developing approaches for downscaling the low-resolution data from SMOS, and iii) testing its assimilation into land surface models for root zone soil moisture retrieval. This thesis uses the data to address the first of these three objectives.

The airborne and ground data collected during the experiment used in this thesis consisted of:

- airborne data:
    - regional L-band airborne observations of the entire study area at 1km nominal resolution (section 4.3.3.1);

  - multi-resolution L-band airborne observations of focus areas at 62.5, 250, 500m and 1km nominal resolution (section 4.3.3.2);
  - multi-angle L-band airborne observations at 250m nominal resolution over three experimental farms (section 4.3.3.3); and
  - supporting thermal infrared and digital photography airborne observations;

- ground data:
  - spatial monitoring of near-surface soil moisture and temperature over the entire study area (2km spacing) concurrently with regional flights (section 4.4.1), flights over eight experimental farms (6.25m to 1km spacing) and with multi-resolution flights (4.4.1);
  - long-term observation of rainfall, soil moisture profiles (5cm-90cm) and near-surface temperature (2.5cm and 15cm) at seventeen permanent stations, together with associated meteorological data at two permanent stations (section 4.4.2);
  - continuous near-surface soil temperature at 1, 2.5 and 4cm together with leaf wetness at eight supplementary stations, with canopy thermal infrared temperature measurements also made at four of these stations (section 4.4.3); and
  - supporting data on vegetation biomass/water content, soil gravimetric water content, surface roughness, soil texture, vegetation type and land cover classification, surface rock cover and dew estimates (section4.4.4).

4.2 Description of the Study Area

The Goulburn catchment is a 6,540km^2 experimental area extending from 31°46'S to 32°51'S and 149°40'E to 150°36'E, with elevations ranging from 106m in the floodplains to 1,257m in the northern and southern mountain ranges. The terrain slope has a median of 8%, with a maximum of 71%. The Goulburn River runs generally from west to east with tributaries in a predominantly north-south orientation. Much of the original vegetation has been cleared to the north of the Goulburn River, where grazing and cropping are the dominant land uses (predominantly native grass, wheat and barley). In contrast, the southern portion of the catchment is largely un-cleared with extensive areas covered by open forest, consisting mainly of Eucalypt (see Figure 4.1). The soils in the area are primarily basalt derived clays in the north and sandstone derived sandy soils in the south. The general climate within the region can be described as sub-humid or temperate, with an average annual rainfall of approximately 650mm and temperatures varying from a monthly mean maximum of 30°C in summer to monthly mean minimum of 2°C in winter (see Appendix A1).

Aircraft and ground operations were concentrated on a 40km x 40km area in the northern part of the catchment (see Figure 4.1). This area was chosen to represent a single SMOS pixel, and was located in the mostly cleared northern part of the catchment, for its moderate to low vegetation cover and concentration of soil moisture monitoring stations, making it a candidate SMOS verification site. The area is characterised by a gently rolling landscape with mixed grazing and cropping land use.

The catchment has been the subject of hydrological monitoring for remote-sensing-related studies since 2001, and a complete description of the monitoring infrastructure can be found in Rüdiger et al. (2007). There are two weather stations and eighteen soil moisture profile stations within the area, with seven of the soil moisture stations concentrated in a 150ha study catchment at the Stanley experimental farm (see Figure 4.1), and the remainder uniformly distributed across the area.

For airborne and ground monitoring purposes the area was logistically divided into two sub-areas, the Krui and Merriwa study areas (see Figure 4.1), defined by the boundaries of two sub-catchments formed by the Krui and Merriwa Rivers. These areas were approximately 10km x 30km (Krui) and 20km x 30km (Merriwa) in size. Within these areas, eight of the farms hosting soil moisture monitoring stations were selected as experimental farms for intensive ground sampling and multi-resolution aircraft monitoring. These experimental farms were selected as being characteristic of the land cover and soil types present in the study area, and are also indicated in Figure 4.1. The farms ranged in size from 200ha to nearly 64km^2. The main characteristics of these farms are summarised in Table 4.1.

4.3 Airborne Data

The flights were carried out by a Diamond ECO-Dimona aircraft from the Airborne Research Australia (ARA) national facility, equipped with the Polarimetric L-Band Multi-beam Radiometer (PLMR) developed by ProSensing. All flights took off from the Scone Airport, situated approximately 50km east of the study area.

4.3.1 Instrument Characteristics

The PLMR is a dual polarised L-band radiometer. Due to the small instrument size and weight, a light aircraft can be used as the observing platform (see Figure 4.2), making it a suitable low-cost and flexible tool for environmental monitoring. The PLMR uses six pushbroom patch array receivers with incidence angles of +/-7°, +/-21.5° and +/-38.5, and measures both V and H polarised brightness temperatures (T_B) for each beam using a polarisation switch. The six beams can be oriented either across track (image) or along track (multi-angle). Apart from the multi-angle flights, the instrument was always flown in image (or "pushbroom") configuration. The change between these configurations was achieved in NAFE'05 by manually rotating the instrument through 90º prior to multi-angle flights, so that the beams pointed forward/backward with respect to the aircraft axis. The reduced antenna beamwidth coupled with an ability to fly low and slow allowed unprecedented ground spatial resolution, with a footprint size of approximately 62.5m (at 3db beamwidth) from a 625ft flying height, the lowest flying height during NAFE'05. On all flights, the payload also included a FLIR S60 thermal imager with 80° field of view lens. A Canon EOS 1Ds 11 Megapixel digital camera was installed specifically for a single aerial photography flight, conducted early in the campaign.

Table 4.1. Main characteristics of the eight experimental farms in the NAFE'05 study area.

Farm Name	Area (ha)	Topography	Land use (vegetation type)	Soil Type
Pembroke	6400	Hilly/Gently rolling	* Grazing * Crop *(wheat)*	Black basaltic clays
Stanley	720	Hilly	* Grazing	Black basalts and red basaltic clays
Roscommon	940	Flat/Gently rolling	* Grazing * Forest *(Eucalypt)*	Red basaltic clays and sandy soils
Ilogan	560	Flat/Gently rolling	* Crop *(barley, oats, wheat)*	Black basaltic clays w/ patches of red basaltic clays
Dales	1500	Flat/Hilly	* Grazing	Black basaltic clays
Midlothian	2000	Flat/Hilly	* Grazing * Crop *(sorghum, lucerne, wheat)*	Black basaltic clays
Merriwa Park	750	Hilly	* Grazing * Crop *(wheat)*	Black basaltic clays
Cullingral	220	Flat	* Crop *(wheat, lucerne)*	Black basaltic clays

Figure 4.2. the airborne facility: (a) View of the PLMR radiometer with the cover off; (b) the The Diamond ECO-Dimona aircraft with PLMR mounted under the fuselage and (c) view of the cockpit showing cockpit computer display.

4.3.2 Calibration of PLMR

Calibration of the radiometer was performed daily during the campaign against warm (ambient blackbody) and cold (sky) observations before and after every flight. At each calibration session, PLMR was left observing the target (sky or blackbody) for 15min. In warm calibration, PLMR beams were pointing downward to the blackbody box; in cold calibration, the PLMR beams were pointing at ~45º above the horizon looking at clear sky. Apart from the Sun, galactic background noise was not accounted for during the processing of the sky calibration data, as it is generally estimated to be less than 1K even when pointing exactly to the galactic plane. The effect of this assumption on calibration accuracy in the range considered is estimated to be less than one tenth of a kelvin, which is negligible in the context of soil moisture remote sensing. However, extreme care was taken to avoid sun or other terrestrial interferences in any of the six beams.

The accuracy of PLMR in the brightness temperature range observed over water and land during the NAFE'05 campaign (150–300K) was estimated to be better than 1K at H polarisation and 2.5K for V polarisation. Complete details about the calculation of the accuracy of PLMR, including plots and tables of accuracy for each individual beam are given in Appendix A3.

In-flight calibration checks were also performed by overpassing the nearby Lake Glenbawn immediately after take off in the morning and before landing in the evening (warm calibration), and sky-looks with the outermost beams through a series of steep turns (cold calibration). Lake Glenbawn is located 100km east of the Goulburn catchment, and was instrumented for monitoring of surface water temperature and salinity. Weekly water temperature and salinity transects over the lake were also undertaken to check for spatial gradients.

Beam-specific calibration coefficients were derived and applied for each day of the campaign by averaging the pre- and post-flight coefficients for each beam. The calibration drift during the flight (i.e., the difference between the coefficients calculated for pre- and post-flight calibration) was not found to be serious given the accuracy needed for soil moisture. The calibrated radiometer data have been geolocated taking into consideration the aircraft position, pitch, roll, and yaw information recorded for each measurement, with the beam centers projected onto a 250m Digital Elevation Model (DEM) of the study area. The effective footprint size and ground incidence angle has also been calculated, taking into consideration the aircraft attitude and terrain slope.

4.3.3 Airborne Monitoring

A total of approximately 100hrs of mission flights were conducted during the campaign. All flight lines were north-south oriented in order to be parallel to the geomorphology of the area and to avoid strong variation in terrain elevation, as well as direct sun glint in the outermost beams. Moreover, this orientation is similar to the planned SMOS flight path. Full coverage of the monitored area was guaranteed by allowing a full PLMR pixel overlap between adjacent flight lines, and by flying the nominal AGL altitude above the median elevation of the area. This was done to ensure that, even in areas of high elevation, the reduction of the pixel size due to terrain elevation did not jeopardise the overlap between adjacent flight lines. Five flight types were conducted: i) Regional, ii) Multi-resolution, iii) Multi-angle, iv) Dew effect and v) Aerial photography. Characteristics specific of each flight are summarised in Table 4.2.

4.3.3.1 Regional Flights

Regional flights were performed over the entire 40km x 40km study area. These flights were scheduled according to the local overpasses of the Aqua platform in order to provide supporting fine-scale passive microwave data for comparison with the C-band AMSR-E mission. The Flight altitude was 10,000ft Above Ground Level (AGL) with data generally acquired between 7:00AM and 9:30AM. These flights were undertaken every Monday and provided four maps of L-band microwave emissions at a nominal ground resolution of 1km. Due to the rough terrain, the effective pixel size varied between approximately 860m and 1070m, resulting from flying at constant altitude above the median elevation of the study area. The regional maps acquired are shown in Figure 4.3. For better display, the aircraft measurements shown were gridded to a reference 1km resolution grid and normalised for incidence angle to 38º (see Chapter 5 for details).

4.3.3.2 Multi-resolution Flights

The multi-resolution flight types were specifically designed to address L-band scaling issues by acquiring observations of the same area at various resolutions. This required mapping of the same area at different altitude flights on the same day. Due to the long flight time required, the entire study area could not be covered during these flights, therefore two focus areas of approximately 10km x 30km were selected for the alternate multi-resolution flights. These areas were the Merriwa and Krui study areas (see Figure 4.1).

Table 4.2. Characteristics of NAFE'05 flights. *The altitude and ground resolution indicated are the nominal ones (i.e., with respect to the median elevation of the monitored area).

Flight type	Area mapped	Altitude (ft AGL)*	Instrument (configuration)	Ground resolution (m)*	Monthly Schedule
Regional	Entire study area	10,000	PLMR (push-broom)	1000m	Once a week (Mon)
			Thermal Infrared	20m	
Multi-resolution	Krui or Merriwa areas (alter.)	10,000 5,000 2,500 625	PLMR (push-broom)	1000/500/250/62.5m	Krui area (Tue, & Thurs), Merriwa area (Wed & Fri)
			Thermal Infrared	20/10/5/1.25m	
Multi-angle	Merriwa Park farm	2,500	PLMR (multi-angle)	250m	Once a week (Wed)
			Thermal Infrared	5m	
Dew effect	Merriwa area (dew circuit)	5,000	PLMR (push-broom)	500m	Twice (4/11 and 25/11)
			Thermal Infrared	10m	
Aerial photography	Entire study area	2,500	Optical camera	0.5m	Once (2/11)

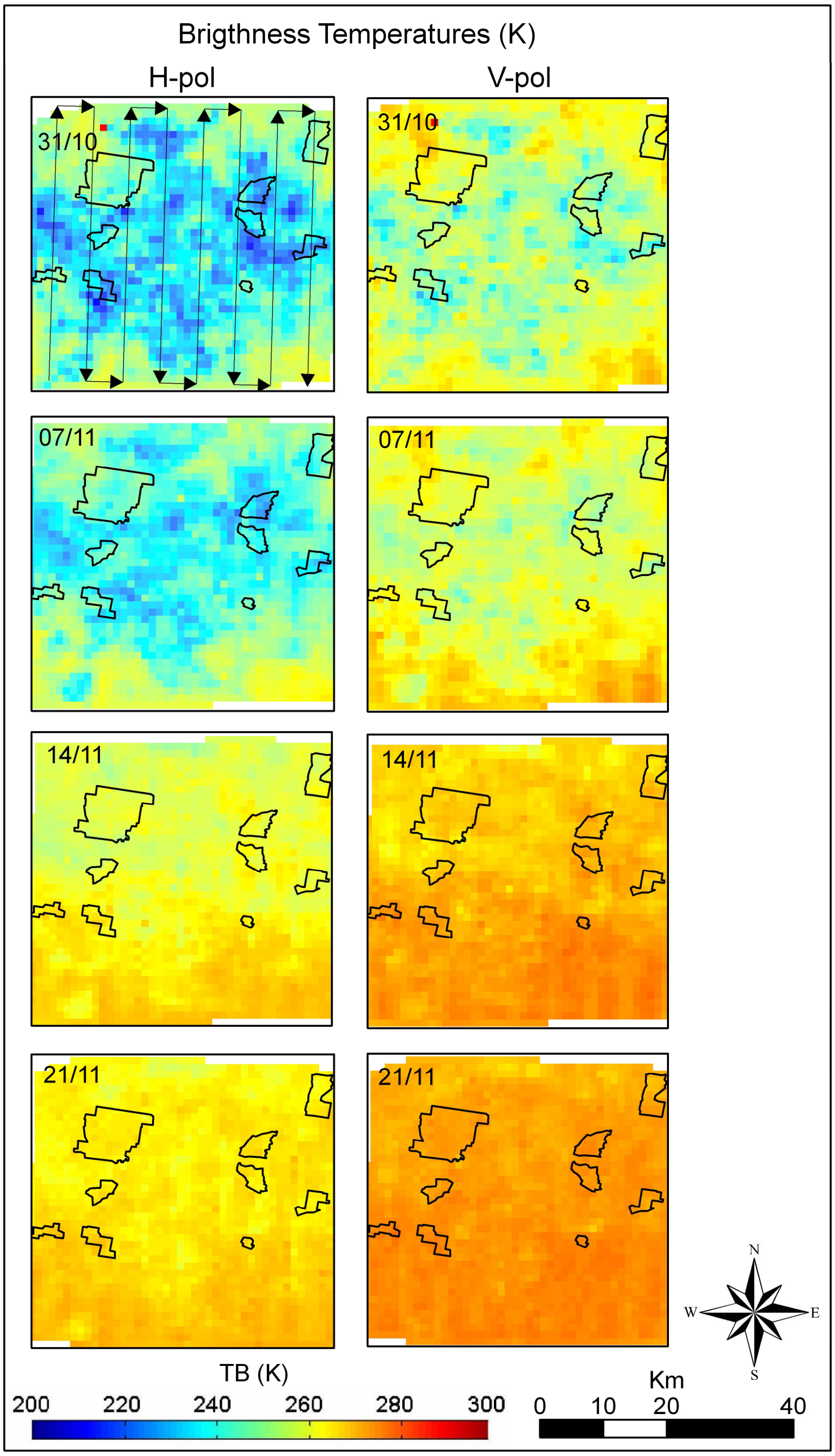

Figure 4.3. Regional brightness temperatures (kelvin) at Horizontal and Vertical polarisation (gridded at 1km resolution, normalised for incidence angle to 38° and for soil temperature changes to 8:00AM reference time). Flight lines are indicated in the top left panel. Boundaries of the experimental farms are also shown with solid lines.

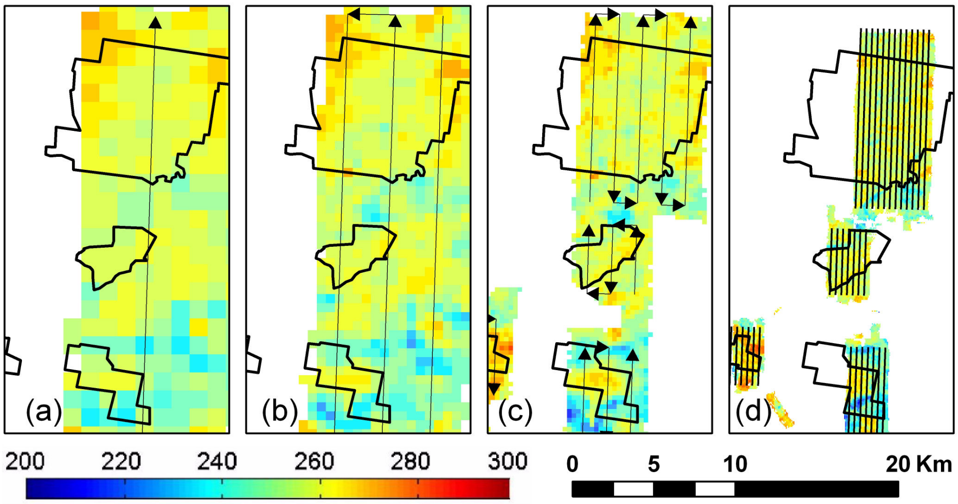

Figure 4.4. Multi-resolution flight lines and example of H-polarised brightness temperatures (kelvin) for the Krui area on November 1st. Maps are displayed by decreasing flight altitude from left to right: (a) 10,000ft/1km resolution; (b) 5,000ft/500m resolution; (c) and (c) 2,500ft/250m resolution, and (d) 625ft/62.5m resolution. Boundaries of the experimental farm are displayed in solid lines.

Multi-resolution flights were undertaken four times per week, alternating between the two focus areas. For each flight, the focus area was covered at four different altitudes in descending order (10,000ft, 5,000ft, 2,500ft and 625ft AGL), resulting in L-band maps at approximately 1km, 500m, 250m and 62.5m spatial resolutions and thermal infrared maps at approximately 20m, 10m, 5m and 1.25m resolution. In the Krui focus area, due to restriction in flight endurance the westernmost area (surrounding the Illogan farm, see Figure 4.1) could only be flown at the two lowest flight altitudes (2,500ft and 625ft).

Flights generally started at 6:00AM and finished at 11:00AM. To avoid gaps in the data due to the reduction in pixel size in the northern part of the study area (with higher terrain elevation), the flights were conducted with different flight altitude on each farm, this being obtained by flying the nominal altitude over the median elevation of each farm. An example of multi-resolution mapping over the Krui sub-area is shown in Figure 4.4 (the same data processing was applied here as in Figure 4.3)

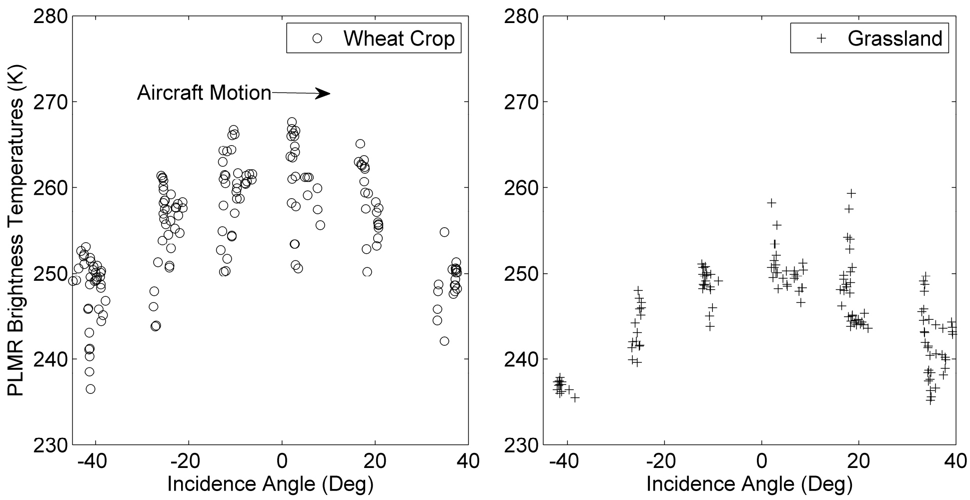

Figure 4.5. Example of multi-angle flight data (H-polarised brightness temperatures) over two uniform areas (250m x 250m) of the Merriwa Park experimental farm.

4.3.3.3 Multi-angle Flights

A total of six multi-angle flights were performed over three experimental farms in the Merriwa study area: Merriwa Park, Cullingral and Midlothian (see Figure 4.1). During these flights PLMR was mounted on the aircraft in the along-track configuration, yielding three forward and three backward looking beams (see Figure 4.5). These flights were flown at a nominal altitude of 2,500ft (AGL), resulting in a pixel size of approximately 250m, The farms were selected to have reasonably flat areas in order to avoid excessive topographic effect on the effective ground projected incidence angle. Moreover, uniform vegetation cover was sought in order to minimise the effect of land surface heterogeneity on the multi-parameter retrieval analysis. Multi-angle flights took place in the early afternoon immediately following the multi-resolution flights, between 12:00PM and 2:00PM approximately.

4.3.3.4 Dew effect Flights

Data from the dew effect flights were not used for the specific purpose of this study. Consequently, for more details about this type of data the interested reader can refer to Appendix A1.

4.4 Ground Data

The ground component of the NAFE '05 field campaign consisted of:

1. spatial soil moisture monitoring of near-surface soil moisture;
2. long-term observation of soil moisture profiles;
3. supplementary soil and canopy temperature monitoring stations; and
4. supporting data.

4.4.1 Spatial Monitoring of Near-Surface Soil Moisture

The soil moisture within the top 5cm of the soil profile was monitored coincident with each aircraft flight. Measurements were undertaken using a portable soil moisture spatial data acquisition system developed specifically for this research, named the Hydraprobe Data Acquisition System (HDAS, Figure 4.6). The system integrates (i) a Hydraprobe soil moisture device for measuring the top 5cm soil moisture, (ii) a GPS receiver for navigation to predefined sampling points, and (iii) a handheld system for storing the data in a GIS electronic format. Full details regarding this system have been included in Appendix A2. A site-independent calibration of the Stevens Water Hydraprobe sensor used by this system has been developed using gravimetric samples collected during the experiment and subsequent laboratory analysis, indicating that data is accurate to within ± 3.5%v/v Merlin et al., 2007.

Figure 4.6. The author taking measurements with the HDAS system.

On the four dates when regional flights were conducted (every Monday), the ground teams sampled soil moisture with the HDAS at approximately 2km spacing, covering a large portion of the NAFE'05 study area along the network of accessible roads in the area. Measurements were made at a

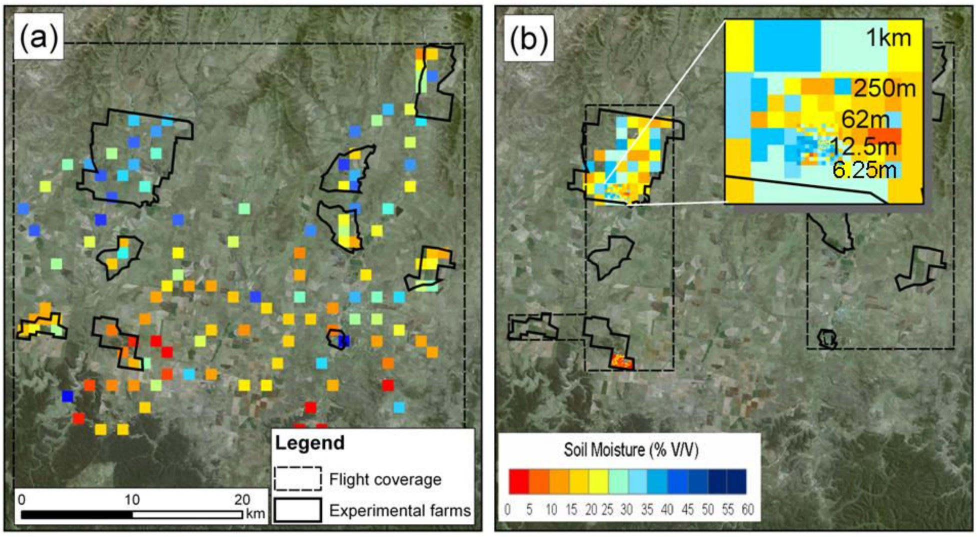

Figure 4.7. Example of spatial monitoring of soil moisture during (a) regional flights (Monday) and (b) Multi-resolution flights (only the Tuesday sampling strategy is shown). The inset magnifies the area surrounding the high-resolution area and indicates the increasing sampling spacing. HDAS Point measurements are displayed with grids of the size of the measurement spacing.

sufficient distance from the road in representative locations so as to avoid anomalous readings. An example of the data collected in November 14th is shown in Figure 4.7a.

On the other dates (concurrently with multi-resolution and multi-angle flights), the ground sampling was focused on two of the four experimental farms located in either the Krui or Merriwa focus area (depending on the schedule for multi-resolution flights shown in Table 4.2). Each farm was therefore mapped at least ones to two times every week. Very high resolution sampling was concentrated on a 150m x 150m area (called "High-resolution areas"), where soil moisture was measured at 12.5m (outer section) and 6.25m (75m inner square) spacing. The high-resolution areas on each farm were selected to capture local spatial variability of near-surface soil moisture associated with changes in vegetation cover, soil type or micro-topography. The area surrounding very high resolution sampling areas were sampled at intermediate resolutions (125m to 250m spacing). The remaining extent of the farm area was sampled at coarser resolution

(500m and/or 1km spacing). The relative extent of the areas sampled at each resolution was optimised by maximising the coverage at finer scale, while providing that the entire farm area was covered within a daily time window. An example of the soil moisture data collected on "multi-resolution" dates is shown in Figure 4.7b. To view the detailed sampling plans for each farm, please refer to Appendix A1.

4.4.2 Long-Term Soil Moisture Profile Stations

The pre-existing long-term soil moisture profile, rainfall and runoff monitoring infrastructure in the Goulburn Experimental catchment (Rüdiger et al., 2007) were upgraded for near-surface (top 5cm) soil moisture, temperature and more extensive rainfall monitoring, prior to the NAFE'05 experiment. A total of 26 monitoring sites were operating during the campaign. Of those, seventeen were distributed across the study area at locations chosen for typical vegetation, soil, and topographic aspect, so that they represented catchment average soil moisture locations (see Figure 4.1). Note that seven of these sites were concentrated in a 150ha study catchment at the Stanley farm, while the others were uniformly distributed across the area. Additionally, two automatic weather stations located in the area recorded meteorological data during the campaign (see Figure 4.1).

Each of the soil moisture sites had up to three vertically inserted Campbell Scientific CS616 water content reflectometers over depths of 0-30cm, 30-60cm and 60-90cm, respectively, together with a Stevens Water Hydraprobe, measuring the soil temperature at 2.5cm and soil moisture in the 0-5cm layer of soil. Additionally, a Campbell Scientific T107 temperature sensors measured soil temperature at 15cm depth. A typical installation for these sites is shown in Figure 4.8, whereas Figure 4.9 displays an example of soil moisture and rainfall time series collected at one of the sites during the campaign period. The CS616 reflectometers were calibrated against both laboratory and field measurements Rüdiger et al., 2009.

The automatic weather stations, located in the lower and upper reaches of

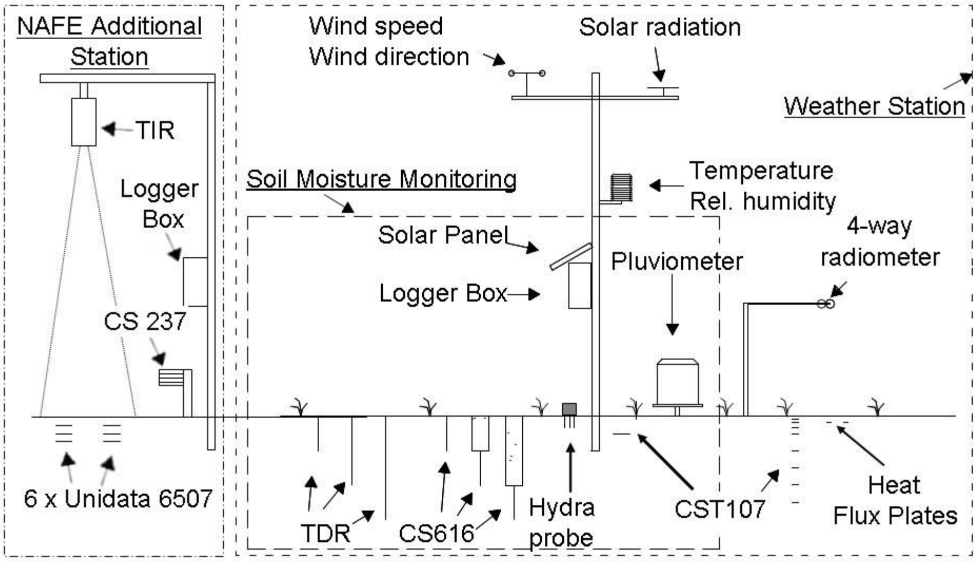

Figure 4.8. Schematic of the Goulburn River experimental catchment weather and soil moisture stations. The large box includes the instrumentation typically installed at weather stations while the smaller internal box shows the instruments typically installed at soil moisture monitoring sites. The supplementary NAFE instrumentation is shown in the left box

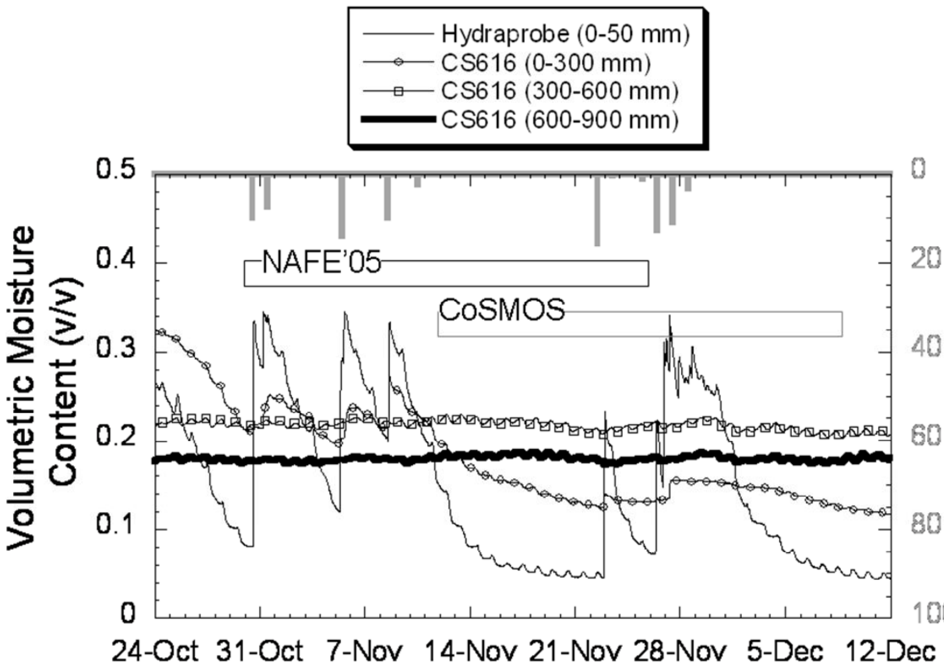

Figure 4.9. Example of soil moisture and rainfall time series data collected at the soil moisture monitoring sites during the campaign. The monitoring period of the ESA's CoSMOS campaign conducted in the study area is also indicated.

the Krui catchment respectively (see Figure 4.1) were operational during the experiment. Of interest to this study were only the three soil temperature sensors (15, 45 and 75cm). More details about the weather stations are given at www.nafe.unimelb.edu.au.

4.4.3 Supplementary Soil and Thermal Infrared Temperature Stations

Eight of the existing monitoring stations were supplemented with supplementary sensors for the duration of the experiment (see Figure 4.10). The primary purpose of this supplementary monitoring was to provide information on leaf wetness in response to dew and precipitation, and develop relationships between thermal infrared observations and near-surface soil temperature. Consequently, the eight stations were all supplemented with soil temperature profile measurements with sensors at 1cm, 2.5cm and 4cm (Unidata 6507A/10 sensors), duplicated in most cases. At four of these stations, thermal infrared radiometers (Ahlborn Thermalert TX or Everest Interscience Inc. Infrared Temp Transducers, Model 4000) were installed on 2m high towers (schematic of the setup is given in Figure 4.8). One of these was located at a bare soil site, while the other three were distributed amongst dominant vegetation types in the area (lucerne, wheat and native grass). Leaf wetness sensors (Measurement Engineering Australia 2040) were installed at the four monitoring stations located at experimental farms in the Merriwa area, where a dew effect flight was undertaken, and at two experimental farms in the Krui study area (Pembroke and Stanley) in order to check spatial variability of dew across the entire area.

A specific station was set up for rock temperature monitoring, to provide data for analysis of the effect of surface rock on L-band passive microwave emission. The station had four Unidata 6507A/10 thermocouples embedded in a surface layer of the rock at different locations and was installed at the Stanley experimental farm.

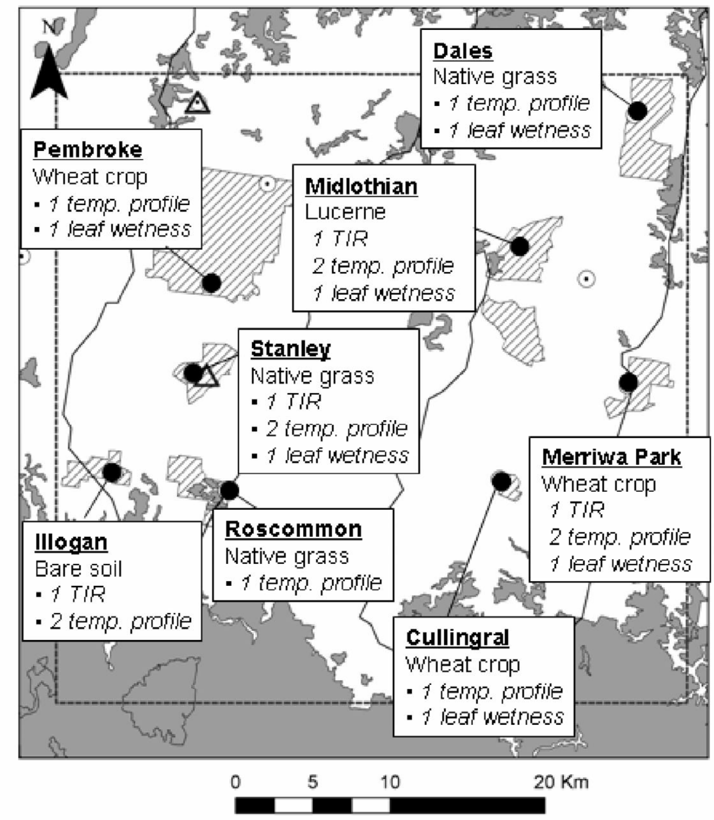

Figure 4.10. Supplementary instrumentation installed during NAFE'05. The map shows the Goulburn River Experimental catchment locations at which thermal infrared (TIR), soil temperature sensors at 1cm, 2.5cm and 4cm (temp. profile) and leaf wetness sensors were temporarily installed during November 2005.

4.4.4 Supporting Data

Supporting ground data collected during the campaign included vegetation biomass/water content, volumetric soil samples, surface roughness measurements, vegetation type and land use classification, surface rock cover and leaf wetness estimates.

4.4.4.1 Vegetation Data

On each experimental farm the spatial variability of vegetation biomass and water content was characterised by collecting between four and sixteen 0.5m x 0.5m quadrant samples across the high-resolution soil moisture sampling area, supported by a minimum of five quadrant samples of the dominant vegetation types across the farm. This was undertaken once a week at fixed locations in order to monitor temporal changes in vegetation

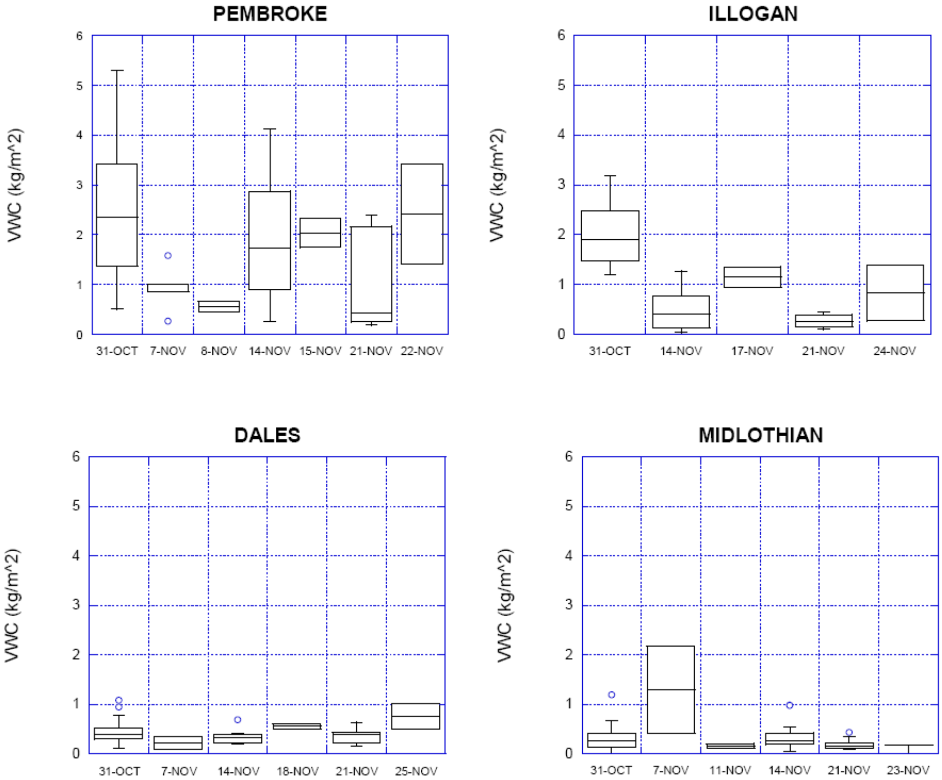

Figure 4.11. Example of Vegetation Water Content (VWC) data collected at the NAFE'0 5experimental farms. Data are shown for four farms: Pembroke (barley crop), Illogan (mix barley/oats), Dales (native grass) and Midlothian (mix lucerne/fallow).

biomass and water content. On all other days, vegetation water content samples were collected at two corners of the high-resolution areas, as a check on temporal changes of the farm vegetation water content. A detailed description of the vegetation sampling strategy is given in Appendix A1. An example of the vegetation water content (VWC) data collected is shown in Figure 4.11. The complete data can be viewed at www.nafe.unimelb.edu.au.

4.4.4.2 Surface Roughness

Surface roughness was estimated once during the campaign at a minimum of four locations on each experimental farm to capture the different roughness characteristics according to land cover type. Two 1m long roughness profiles were recorded for each measurement location, one north-south and one east-west oriented. The Root Mean Square of the pin profiler heights (average of the four locations) and the classical Choudhury

Table 4.3. Average RMS of pin profiler measurements and calculated Choudhury roughness parameter for all the experimental farms,

Farm	Average RMS	Choudhury parameter
Stanley	1.07	0.46
Pembroke	0.84	0.28
Roscommon	0.62	0.14
Illogan	0.97	0.39
Midlothian	0.82	0.29
Dales	0.89	0.31
Cullingral	0.65	0.18
Merriwa Park	0.63	0.15

roughness parameter (Choudhury et al., 1979) for all farms are indicated in Table 4.3.

4.4.4.3 Soil Gravimetric Samples and Soil Texture

Top 5cm volumetric samples of soil were collected across the study area for both soil textural analysis and calibration of the Stevens Water Hydraprobe. A total of 20 samples were collected at each experimental farm, aimed at characterising different soil types and wetness condition across the farm. On two dates, further soil samples were collected across the entire study area, for a total of 120 samples. Soils were oven-dried for 24hrs in order to calculate the thermogravimetric water content. Locations of the samples across the study area and complete data can be found at www.nafe.unimelb.edu.au

4.4.4.4 Vegetation Type, Land cover, Rock Cover and Dew

Dominant vegetation type, land cover and surface rock cover were recorded at each HDAS soil moisture sampling location. This was undertaken for both regional and farm sampling grids. Dew presence was estimated visually, and recorded daily as no dew, moderately wet, or very wet, in order to support the leaf wetness measurement made at the monitoring stations. Complete data can be found at www.nafe.unimelb.edu.au.

4.4.4.5 Vegetation LAI and NDVI

Vegetation reflectance and leaf area index were also measured for the high-resolution areas of each experimental farm, with the objective to develop relationships for vegetation water content and biomass estimation from satellite sensors. This was done at least once during the campaign at each farm. Locations of the measurements across the study area and complete data can be found at www.nafe.unimelb.edu.au

4.5 Other Data

Other data not specifically collected by the NAFE'05 experiment but used in this thesis are listed below: all these data can be found at www.nafe.unimelb.edu.au.

- Landsat-5 TM scene Acquired on October 21st, 2005;
- Digital Elevation model of the study area (Australian Surveying and Land Information Group, 2001, GEODATA 9 second DEM); and
- Daily Atmospherically corrected Surface Reflectance from the MODerate resolution Imaging Spectroradiometer (MODIS), 16-day composite product (November 1st to November 16th, and November 17th to December 2nd) at 250m resolution, kindly provided by Dr. Stefan W. Maier, Satellite Remote Sensing Services, Department of Land Information Western Australia.

4.6 Chapter Summary

This Chapter has presented the airborne and ground data collected during this study in the National Airborne Field Experiment 2005 (NAFE'05). The data described here will be used in the following Chapters to address the problem of soil moisture retrieval in the presence of land surface heterogeneity:

In Chapter 5, multi-resolution L-band airborne observations (62.5m and 1km) will be used to evaluate the L-MEB model. Supporting data on vegetation water content, near-surface soil temperature and surface roughness measurements will be used to characterise the soil-canopy microwave emission. HDAS spatial measurements of near-surface soil moisture will then be used for evaluation of the L-MEB retrieved soil moisture. Finally regional L-band airborne observations will also be used to derive soil moisture maps of the entire study area, together with supporting data on near-surface soil temperature, canopy land cover and soil texture.

In Chapter 6 the heterogeneity of the land surface conditions in the NAFE'05 study are will be investigated using continuous observation of top 5cm soil moisture, rainfall data, HDAS spatial measurements of near-surface soil moisture at the experimental farms and at regional scale, and soil texture data together with terrain elevation and Normalised Difference Vegetation index derived from MODIS.

In Chapter 7 multi-resolution observations will be used to investigate the scaling properties of brightness temperatures, Moreover regional L-band airborne observations will be aggregated to simulate SMOS pixels. The effect of land surface heterogeneity on the retrieval from simulated SMOS pixels will then be analysed in Chapter 7 and Chapter 8 using soil texture and land cover data.

Chapter Five

5 Evaluation of the L-MEB Model

In this Chapter the L-MEB radiative transfer model, being the core of the SMOS L2 algorithm described in Chapter 3, is evaluated using the L-band airborne brightness temperature (T_B) observations from the Polarimetric L-Band Microwave Radiometer (PLMR) and the ground data collected during the NAFE'05 field campaign presented in Chapter 4. The objective is to evaluate the accuracy of the L-MEB model for the land surface conditions encountered in the study area, before applying the model to produce soil moisture maps of the entire area from airborne data at 1km resolution. This 1km soil moisture product will serve as soil moisture ground truth in Chapters 7 and 8 in order to evaluate the error in coarse-scale soil moisture retrieval due to the presence of land surface heterogeneity across the study area.

For the evaluation of the model, this Chapter first focuses on the eight focus sites located at the NAFE'05 experimental farms where soil moisture and land surface conditions were monitored with exceptional detail. Here, the L-MEB model is first evaluated using high-resolution (62.5m) airborne T_B observations and the L-MEB 'default' values for the parameters. The parameters of the model that characterise the radiative transfer properties of different land surfaces are then tuned to the particular conditions of the NAFE'05 study area and the L-MEB model with calibrated parameters is evaluated using coarser-resolution (1km) airborne T_B observations over the same eight sites. The work specifically presented in the first section of this chapter has been published in Panciera et al. (2008b). Finally, 1km soil moisture maps of the entire NAFE'05 study area are produced by applying the L-MEB model to 1km airborne T_B observations. This is the first time the L-MEB model is applied to airborne data and evaluated for Australian conditions.

5.1 Evaluation of the L-MEB Model with High-Resolution Airborne Observations

The first evaluation of the L-MEB model was performed using the high-resolution airborne observations (62.5m footprint[1]) and ground soil moisture data acquired at the eight high-resolution soil moisture monitoring sites in the NAFE'05 experimental farms. At these sites all the factors known to affect the microwave emission were well monitored, and the spatial variability of soil moisture within the aircraft footprint was known in great detail (6.25m and 12.5m spacing). Direct comparison of the L-MEB model soil moisture retrieval with ground measured soil moisture therefore allowed detailed evaluation of the model physics and its parameterisation on a variety of typical land surface covers, with minimum uncertainty in the ancillary data used and in the soil moisture heterogeneity within the pixel. The location and characteristics of experimental farms, the ground sampling strategy, and the airborne observations have been thoroughly described in the relevant sections of Chapter 4. A brief review of the data used in this Chapter is presented here.

5.1.1 Airborne and Ground data

A total of four concurrent airborne and ground monitoring dates were available for each high-resolution site across the four week long campaign. The location and extent of these sites were carefully chosen with the objective of characterising the variety of land covers, soil type, and topography present in the study area. The characteristics of the high-resolution sites relevant to this section are summarised in Table 5.1, together with an overview of the vegetation, soil texture and surface roughness measured at each site. Roscommon was considered a 'control' site as it

[1] In this chapter, the term "observation" refers to the actual brightness temperature measurement, while the term "footprint" refers to the area on the ground which is within the radiometer field of view and contributes to the observed brightness temperature. The standard footprint size definition is that of the area on the ground from where 50% of the total power is received by the antenna.

Table 5.1. Characteristics of the high-resolution ground sampling sites and monitoring dates. Roughness parameters are indicated with the mean and standard deviation (in brackets) of eight measurements taken across the farm. (*) Soil textural data estimated from 5cm soil samples.

Site Name (Sampling Dates)	Land cover	Topo-graphy	VWC range (Kg/m^2)	% sand	% clay	Roughness heights (mm)	
						Stand. Dev.	Corr. length
Roscommon (1,8,15,22)	Grassland	Flat	1.1-0.4	67*	15*	6.3 (1.0)	64.7 (36.8)
Stanley (3,10,17,24)	Grassland	Sloping	0.4-0.1	6	54	10.8 (3.7)	93.9 (45.1)
Dales (4,11,18,25)	Grassland	Sloping	0.8-0.2	31	51	9.1 (2.3)	65.4 (37.6)
Midlothian (2,11,16,23)	Fallow /Lucerne	Flat	0.3-0.1	10	69	8.3 (3.6)	83.9 (38.1)
Merriwa Park (2,9,16,23)	Wheat	Gently sloping	2.0-1.2	21	36	7.5 (2.7)	93.4 (54.2)
Cullingral (4,9,18,25)	Wheat /Barley	Flat	0.9-0.4	30*	26*	6.6 (2.4)	104.8 (53.4)
Illogan (3,10,17,24)	Oats /Barley	Across Gully	1.1-0.3	26	23	9.8 (3.6)	61.7 (43.5)
Pembroke (1,8,15,22)	Wheat /Barley	Gently sloping	2.4-2.0	6	71	8.5 (2.8)	98.0 (53.6)

exhibited uniform, flat, short grass conditions. All other sites were characterised by either heterogeneous land cover (Midlothian, Cullingral, Illogan and Pembroke) or significant topography (Stanley, Dales and Merriwa Park). Spatial distribution of the top 5cm soil moisture was monitored at each site once a week concurrently with airborne T_B observations. A 150m x 150m core high-resolution area was sampled on a very fine regular grid (6.25m and 12.5m spacing) for evaluation of the soil moisture retrieval from the high-resolution airborne T_B observations (see Figure 5.1). Soil moisture ground sampling took approximately 6-8 hours daily (8:00AM-2:00PM), and flights over the sites were timed so that they always fell within this time window (9:00AM-11:00AM). Surface soil moisture can vary significantly on a diurnal basis, especially for short vegetation. Daily changes in soil moisture during the ground sampling time window were therefore monitored at the eleven monitoring stations across the study area (all on native grass). Soil moisture did not change significantly between 8:00AM and 2:00PM, with a mean soil moisture decrease across all stations and all sampling days of less than 1.1%v/v. Given that the airborne acquisitions were generally within the time window when this variation occurred, the differences between soil moisture at the time of aircraft overpass and that of the ground monitoring will be even smaller than that indicated above.

High-resolution airborne T_B observations at each site were collected at approximately the same time every day between 9:00AM and 11:00AM. The calibrated PLMR data were geolocated taking into consideration the aircraft position, pitch, roll, and yaw information recorded for each measurement, with the beam centers projected onto a 250m digital elevation model of the study area. The effective footprint size and ground incidence angle were also calculated taking into consideration the aircraft attitude, the terrain slope and the beam geometry. Final processing included filtering data with elevated aircraft roll angles (higher than 10° from horizontal) corresponding to steep turns of the aircraft. This also minimises sun glint effects in the external beams. High-resolution footprints covering each site were extracted using the geolocation information of each footprint, making sure that only the footprints entirely contained in the 150m x 150m high-resolution area were considered (see Figure 5.1). Approximately 5-8 daily independent, bi-polarised T_B observations of the high-resolution area were available for each site. These were at a variety of incidence angles, due to local topography and small variation in aircraft roll between parallel overpasses of the area.

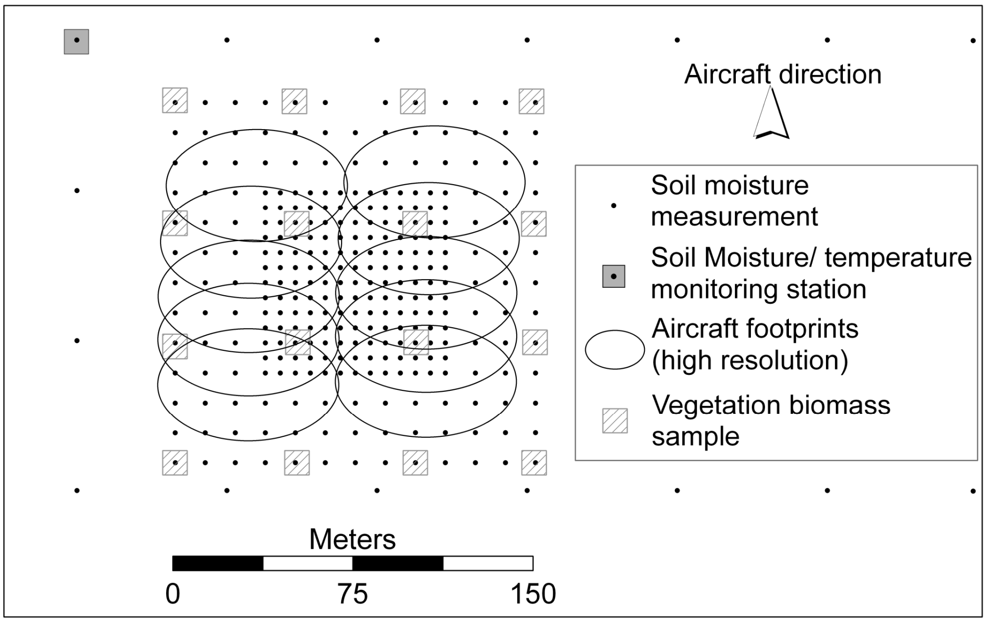

Figure 5.1. Schematic of airborne T_B observations and ground measurements at the high-resolution ground sampling sites for high-resolution evaluation of the L-MEB model.

As explained in Chapter 3, in order to retrieve soil moisture estimates from T_B, the L-MEB model requires information on vegetation water content (VWC), soil texture, soil temperature and surface roughness. All these factors affect the microwave emission of a given surface at particular soil moisture contents. Vegetation biomass and VWC were monitored throughout the campaign using 50cm x 50cm biomass samples collected at the end of each sampling day at two fixed locations chosen to be representative of the site vegetation conditions. On two occasions during the campaign, the first and the last weeks, the spatial variability of the VWC across all high-resolution sites was also characterised with sixteen biomass samples (see Figure 5.1).

Surface and deep soil temperature for each T_B observation was extracted from the continuous soil temperature records at 2.5cm and 15cm depth at the nearby monitoring stations, making use of the PLMR time reference. Due to the lack of soil temperature measurements deeper than 15cm at all the soil moisture monitoring stations, in the present study it had to be assumed that the value of soil temperature at 15cm depth is a good estimate of soil temperature at (50cm) for which the L-MEB parameters for the calculation of the soil effective temperature (w_0 and b_0, see section 3.4.7) have been calibrated. This assumption was verified with soil temperature data at 15cm and 60cm collected at a meteorological stations located at the Stanley farm. The 60cm temperature was found to have a positive bias of 0.9K with respect to that at 15cm, with an error standard deviation of 1.1K. This impacts the calculation of T_{EFF} only in very dry conditions (when the effect of T_{DEPTH} is important), yielding an error of less than 0.6K, which is not significant for soil moisture retrieval purposes.

Soil texture was determined by hydrometer analysis of 30cm deep soil samples collected at or near the high-resolution sites. Despite the availability of similar 5cm deep samples, the 30cm samples were preferred as the laser mastersizer particle size analysis performed on 5cm samples was found to consistently underestimate clay content. The 5cm sample was used in two cases only (Roscommon and Cullingral sites), as the 30cm samples were too far from the high-resolution sites to be representative. Finally, roughness parameters for each site were estimated from 1m-long transects of surface heights at various locations in close proximity to the high-resolution area. These were taken in two perpendicular directions at each location in order to account for anisotropy in surface roughness.

The VWC ranged from a minimum of 0.1kg/m^2 for the short lucerne at Midlothian to a maximum of 2.4kg/m^2 for the mature wheat crop at Pembroke, with an average of 0.4kg/m^2 for grassland sites and 2kg/m^2 for crop sites. The spatial variability was generally small for all the grassland sites (standard deviation of 0.15kg/m^2) and most crop sites (0.4kg/m^2), but was significant in the case of the Pembroke site (1kg/m^2). The VWC is also known to have diurnal variation, mainly associated with the presence of dew on the plants in the early hours of the morning. To ensure that this would not interfere with the aircraft microwave observations, leaf wetness sensors were installed at each high-resolution site to continuously record the presence of dew. These data (confirmed also by field observation) indicated that at all eight high-resolution sites dew had completely evaporated by 8:00AM throughout the campaign. Therefore the VWC samples taken at the end of each sampling day were considered representative of the conditions observed at the time of aircraft overpasses.

Soil types covered the whole range present in the study area, from the very sandy soil at Roscommon to the fine black clay at Pembroke. Surface roughness heights and correlation lengths were fairly uniform across the eight sites, with a standard deviation of surface roughness heights ranging from 6.3mm at the flat Roscommon site to 10.8mm at the Stanley site.

In order to verify the accuracy of the L-MEB soil moisture retrieval, a value of ground soil moisture was calculated for each T_B observation by averaging all the ground measurements falling within the footprint. The number of ground measurements per footprint varied due to local topographic conditions affecting the effective footprint size but was generally in the range of 50-100 points per footprint. This is an unprecedented ground sampling density for airborne evaluation studies.

Figure 5.2 shows the temporal change of the mean V-pol and H-pol T_B recorded by the PLMR radiometer at the eight high-resolution sites, together with the mean and standard deviation of the ground measured soil moisture. Figure 5.2 gives an overview of the range of soil moisture conditions encountered at the high-resolution sites and the sensitivity of the PLMR radiometer T_B to surface soil moisture condition, as well as the impact of vegetation density on the T_B dynamics. For better visualisation, the mean T_B shown in this plot have been calculated after compensating for the effect of the different incidence angle on the observed T_B, i.e. after normalising the observations as if they had been all observed at the same incidence angle (38º). This has been done using the procedure described in detail in section 5.3.2.1. Heavy rainfall delivered approximately 20mm of rain throughout the study area on October 30th and 31st (i.e. the beginning of the experiment). There was also a second event of approximately the same magnitude on November 5th and a few minor events (November 8th, 10th and 22nd). This is reflected in the very wet conditions observed at all sites on the

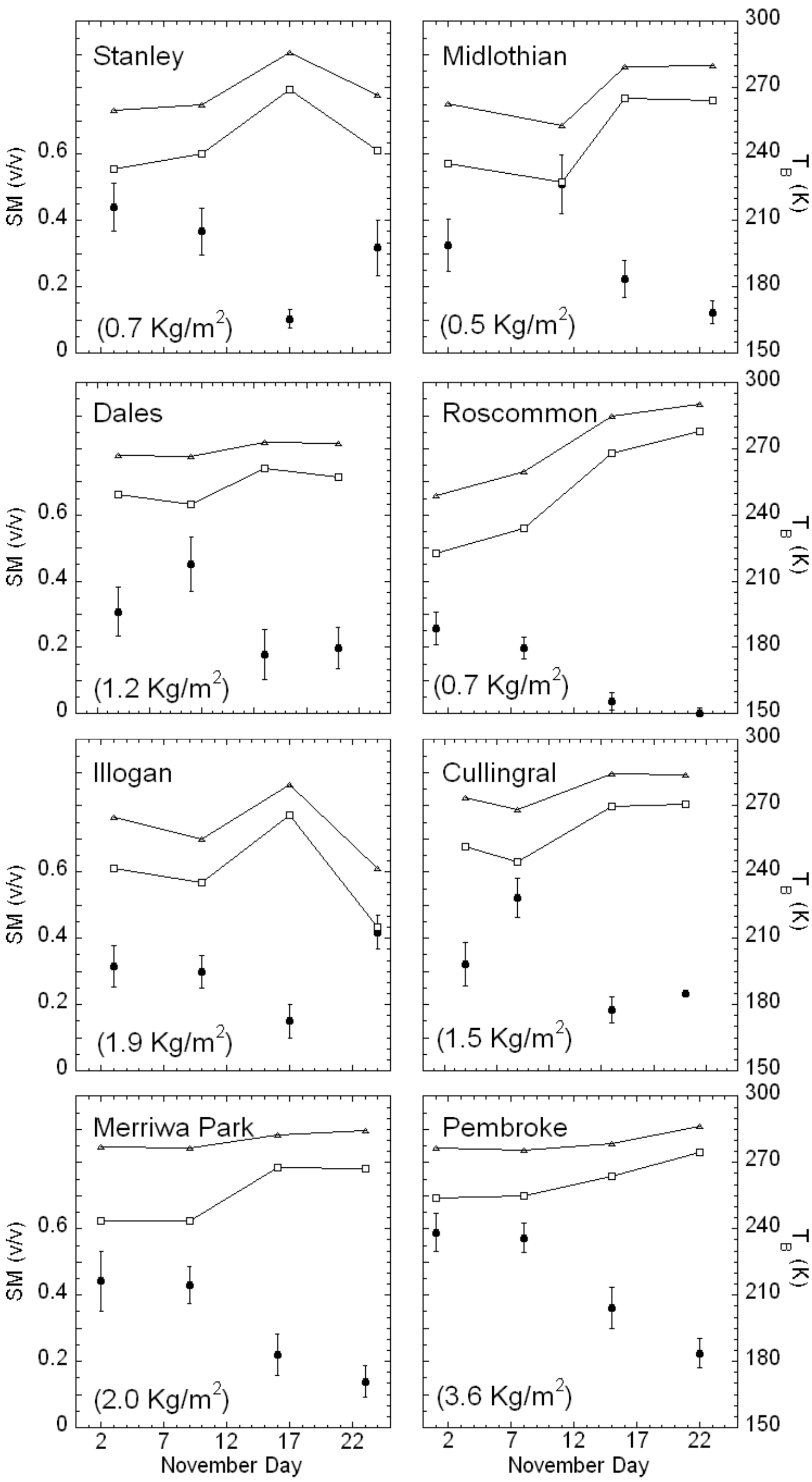

Figure 5.2. Mean of the high-resolution brightness temperatures (T_B, lines) and mean and standard deviation of ground measured soil moisture (SM, solid symbols) plotted daily at the eight high-resolution sites. Triangles are V-pol and squares are H-pol brightness temperatures. The temporal mean of the vegetation's undried biomass recorded throughout the campaign at each site is indicated in brackets as a reference of the canopy density.

first two sampling dates, prior to November 10th, particularly at the sites characterised by clay soils (Pembroke and Stanley). The November 5th event was more intense in the Merriwa area, determining wetter conditions at the eastern sites (i.e., Midlothian, Cullingral and Dales) on the second sampling day, while the western sites (Stanley, Roscommon, Illogan and Pembroke) experienced lighter rainfall on November 5th, maintaining nearly constant wetness conditions between the first and second sampling day. After November 10th and until the last recorded rainfall event, November 22nd, a gradual drydown was observed at all sites. On November 23rd another rainfall event produced moderately wet conditions which were recorded at the two sites monitored after that date (Stanley and Illogan).

The whiskers in Figure 5.2 indicate the standard deviation of the ground measured soil moisture within the high-resolution footprint (averaged over the 5-8 footprints falling within each high-resolution site and fully ground-monitored at high-resolution. The soil moisture standard deviation was on average 5.6%v/v. Maximum spatial variability was recorded at Midlothian (10.0%v/v) due to the strong contrast in soil moisture between the different land cover in the two halves of the high-resolution site (fallow field and a mature lucerne crop). High spatial variability was also recorded at Stanley (9.4%v/v) and Dales (8.8%v/v), which were on steep hillsides. Minimum soil moisture heterogeneity was recorded at the Roscommon 'control' site (3.1%v/v).

The PLMR radiometer data showed significant sensitivity to the top 5cm soil moisture, with higher values of T_B associated with dry soil conditions and lower values for wet conditions. The range of T_B was slightly higher at H-pol than at V-pol. This effect is partially smoothed here by the angle 'correction' applied to the T_B data. The H-pol T_B show a range of approximately 40K for a variation in soil moisture around 25%v/v over low-vegetated grasslands (e.g., Roscommon). This range was nearly halved to approximately 25K at sites with crops of higher vegetation biomass (Pembroke and Merriwa Park); as expected, the presence of a mature crop above the ground reduced the sensitivity of T_B to soil moisture.

Nevertheless, sensitivity to the soil wetness conditions was still exhibited and was used to retrieve soil moisture estimates under mature crops.

5.1.2 Optimisation Scheme

A detailed description of the L-MEB model has been presented in Chapter 3. In this Chapter L-MEB is applied by accounting only for the dominant vegetation type within each pixel, meaning that each pixel is considered uniformly covered by the vegetation type having the highest cover fraction, as calculated from high-resolution thematic maps of land use (from Landsat).

In the following sections the L-MEB model is used to solve two different problems: (i) the retrieval of soil moisture given *a priori* (prescribed or calibrated) values for the vegetation and soil surface dependant parameters given T_B; and (ii) the calibration of model vegetation and soil surface parameters given ground measured soil moisture and T_B. The number of parameters that can be retrieved simultaneously depends on the number of simultaneous and independent T_B observations available. Since the PLMR radiometer provides two T_B observations (V and H) per incidence angle, two parameters can potentially be retrieved at once (e.g. retrieval of soil moisture and vegetation optical depth if roughness is assigned *a priori*, or optical depth and roughness given the soil moisture). In this study both soil moisture retrieval and calibration problems were solved through iterative least squares minimisation of the cost function:

$$CF = \frac{\sum (T_{BP}^{o}(\vartheta) - T_B(\vartheta))^2}{\sigma_{T_{BP}}^2} + \frac{\sum_i (p_i - p_i^{ini})^2}{\sigma_P^2} \,. \tag{5.1}$$

This cost function includes the classical cumulative squared error between simulated and measured brightness temperatures (T_{BP} and $T_{BP}°$ respectively), and an additional term which accounts for the squared error between the current value (p_i) and the initial guess (p_i^{ini}) of each retrieved quantity (e.g. soil moisture in the soil moisture retrieval problem or parameters H_R, b, etc. in the calibration problem).

The second term in (3.2) allows the user to constrain the retrieved values about a physically plausible estimate for each parameter (p_i^{ini}) through the standard deviation associated with this estimate(σ_P). This optimisation method has been developed for the retrieval of surface parameters from SMOS data, where the possibility of constraining parameter values stems from the availability of the values retrieved on previous overpasses (Jackson et al., 1999; Wigneron et al., 2007). However, in this study, unless otherwise stated it was decided to work without constraints (i.e. no *a priori* knowledge was assumed), in order to find the 'real' optimum for each quantity. Therefore the value σ_P= 1 was used in most cases. Since all the quantities retrieved in this chapter (soil moisture and parameters H_R, b), have values generally much smaller than 1, a value σ_P= 1 represent a very mild constraint, effectively leaving the parameter free. Note that (5.1) is an adaptation of the SMOS L2 algorithm cost function (3.2) to airborne data, where the variance/covariance matrix COV_T of the observed T_B has diagonal elements all equal to $\sigma^2_{T_{BP}}$ (which is the square of the PLMR radiometer radiometric uncertainty) and zero off-diagonal elements (i.e., the airborne observations at different angles are independent, being taken at different instants and not in one single "shot" as in SMOS).

5.1.3 Evaluation of the L-MEB Model with Default Parameters

The L-MEB soil moisture retrieval was first evaluated using the L-MEB default values for the surface type dependent parameters, which were described in detail in Chapter 3. Based on the land cover information visually estimated for each of the NAFE'05 high-resolution sites (see Table 5.1), a set of radiative transfer parameters was extracted from the L-MEB default database. The resulting parameter sets are given in Table 5.2.

The eight sites fell into one of three tabulated surface types: crop (wheat type), grassland with litter and grassland without litter. For all the crop sites, the most suitable parameters were found to be those estimated over crops with mainly vertically oriented plant structure like wheat. In the NAFE'05

Table 5.2. L-MEB default parameters and high-resolution evaluation of the L-MEB soil moisture retrieval. Parameters (all dimensionless) are: roughness (H_R); polarisation mixing (Q_R); roughness exponent (N_R), vegetation structure (*tt*) and scattering albedo (ω), all at H and V pol), and vegetation parameter (*b*). Error statistics are calculated on all T_B observations across four dates; bias is calculated as the difference between the mean retrieved and the mean observed soil moisture (θ).

L-MEB surface type	High-resolution site	L-MEB Default parameters									Soil moisture retrieval (%v/v)		
		H_R	Q_R	N_{RH}	N_{RV}	tt_H	tt_V	ω_H	ω_V	b	RMSE	r^2	Bias
Grassland without litter *(Saleh et al., 2007)*	Roscommon	0.5	0	0	0	1	1	0	0.05	0.15	1.6	0.98	-1.3
Grassland with litter *(Saleh et al., 2007)*	Stanley	1.3-1.13*θ	0	1	0	1	1	0	0.05	0.12	1.3	0.99	0.6
	Dales										3.7	0.85	1.7
	Midlothian										7.4	0.68	2.8
Crop- wheat *(Wigneron et al., 2007)*	Merriwa P.	0.2	0	0	-1	1	8	0	0	0.08	21.4	0.94	-19.5
	Cullingral										19.4	0.87	-19.2
	Illogan										9.9	0.96	0.4
	Pembroke										32.5	0.95	-30.8

study area the predominant crop is wheat followed by barley which has a very similar plant structure (vertical stems). Given that no specific parameters are available in literature for oats, which covered approximately ½ of the Illogan site, together with barley, this site was assigned the same wheat-type crop parameters, as oats is also characterised by a predominantly vertical structure. Stanley and Dales were characterised by grazing lands covered by very tall grass, hence the presence of litter on the ground Roscommon was a very short grass site with exposed, un-littered bare soil between the grass clumps. Midlothian was split between a nearly bare fallow field (approximately 30% of the high-resolution ground sampling area) and a mature, short lucerne field (60% of the area). In the absence of specific literature parameters for the radiative transfer properties of lucerne, it was assumed that the anisotropic leaf structure of lucerne was similar to that of grass clumps. Therefore the site was treated as grassland. Note that the significant spatial heterogeneity of vegetation cover at this site could potentially affect the soil moisture retrieval, due to the non-linear response of the L-MEB model with respect to vegetation water content and soil moisture.

Soil moisture was retrieved at all high-resolution sites using a two-channel retrieval (H-pol and V-pol) applied individually to each of the 5-8 T_B observations available on every monitoring day. The soil moisture retrieved from each T_B observation was compared with the mean ground observed soil moisture within the T_B footprint. As different T_B footprints covered different portions of the high-resolution area (see Figure 5.1) which had been ground-sampled at fine spacing, this retrieval approach provided an extensive evaluation data set for each land cover type. All the ancillary input data were assumed to have uniform values across the 150m x 150m high-resolution area. The value of soil temperatures at 2.5cm and 15cm required by the model for the calculation of the soil effective temperature were obtained from the nearest permanent monitoring station using the time reference of the T_B acquisition. The value of the VWC estimated daily from the biomass samples collected at the high-resolution site was used to characterise the temporally varying contribution of the vegetation to the emission. Alternatively, a value for the high-resolution area was estimated using the two biomass samples consistently collected at two corners of the high-resolution area on each monitoring day (see section 4.4.4.1). The temperature of the vegetation canopy was assumed to be in equilibrium with the soil temperature at 2.5cm; this is a commonassumption in passive microwave soil moisture retrieval studies due to the lack of adequate canopy temperature measurements (e.g., Njoku et al., 1996a, Van de Griend et al., 2003). The consequences of this uncertainty in canopy temperature estimation for the soil moisture retrieval are discussed later in this section.

Figure 5.3a shows the scatter plot between L-MEB soil moisture retrieval using the default parameters and the ground measured soil moisture. At most of the grassland sites (Stanley, Dales and Roscommon) the L-MEB model achieved fairly accurate retrieval, with errors smaller than the standard deviation of ground measured soil moisture within the footprint (which was on average 5.6%v/v). This indicates a correct parameterisation of the model for grassland surfaces. Nevertheless at the crop sites (Merriwa Park, Cullingral, Illogan and Pembroke) the model underestimated soil moisture overall, particularly during wet conditions. The error is particularly high for Pembroke, Merriwa Park and Cullingral, being smaller at Illogan. These errors are quantified in Table 5.2. The Root Mean Square Error (RMSE), bias and correlation coefficient shown in the table were calculated considering all the retrieved-observed soil moisture pairs across the four mapping dates for each site (approximately 20-40 pairs per site in total). The RMSE between observed and estimated soil moisture was better than the proposed SMOS accuracy (4.0%v/v) for most grassland sites, with the exception of Midlothian. However, for crop sites errors between 10%v/v and 32.5%v/v were obtained. As shown in Table 5.1, the crops sites were characterised by significantly higher VWC than the grassland sites. This suggests that the cause of such large retrieval errors could reside in a wrong parameterisation of the relationship between vegetation characteristics and vegetation optical depth for crops.

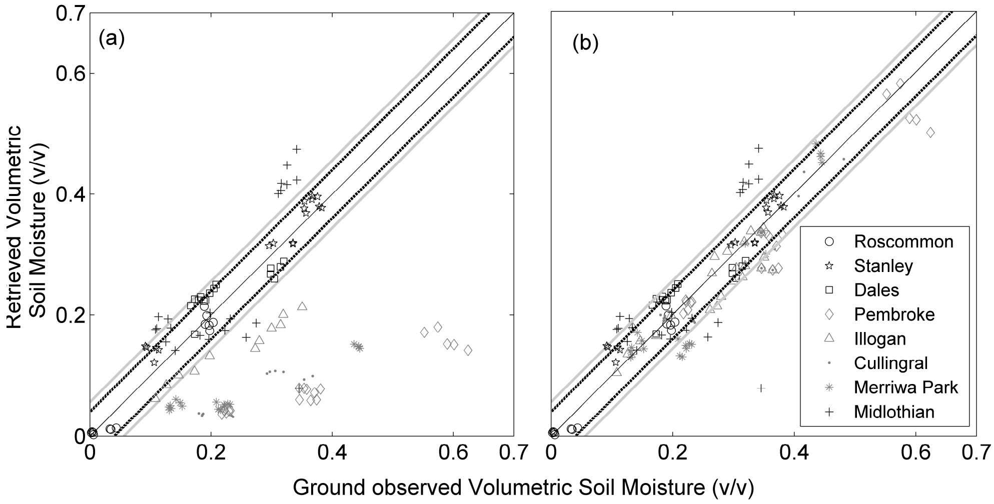

Figure 5.3. Evaluation of L-MEB soil moisture retrieval with high-resolution airborne T_B observations using (a) L-MEB default parameters and (*b*) calibrated roughness parameter H_R (see section 5.1.5.3). Grey symbols indicate sites classified as crops; black symbols sites are classified as grassland. Black dashed lines indicated the SMOS target accuracy (4%v/v). Grey lines indicate the typical standard deviation of the ground-monitored soil moisture within aircraft footprints (5.6%v/v)**.**

The parameterisation of the roughness parameter H_R as a function of soil moisture permitted an accurate soil moisture retrieval at the grassland sites, although in the case of Roscommon a successful retrieval was achieved using a constant H_R value (0.5). This might be due to the relatively limited soil moisture range exhibited at the site (below approximately 20%v/v) due to its sandy soil texture. A relatively high retrieval error was obtained for Midlothian. Midlothian was a site with unique land cover conditions in the study area, including a mix of lucerne (70% of the high-resolution area), for which no parameters were available in literature, and fallow (30%), characterised by significant dead biomass at the surface. This resulted in a strong discontinuity of soil moisture at the boundary (~20%v/v), and the highest variance of soil moisture observed amongst the eight sites (10%v/v standard deviation). It is likely that the combination of these three factors (incorrect parameterisation, the effect of the dead biomass layer and strong soil moisture gradient) cause the observed size of the error.

The results presented suggest that the set of L-MEB default surface parameters are directly applicable for uniform Australian native grasses. For the Australian wheat-type crops considered in this study, and particularly for Pembroke, Merriwa Park and Illogan, use of the default parameters led to large soil moisture retrieval errors. Crops cover a small, but significant portion of the study area, and are generally concentrated in large patches, more than a km across. These will likely occupy several of the 1km PLMR pixels which will be used in this and later Chapters to retrieve soil moisture estimates across the entire study area. Therefore, in order to obtain a reliable soil moisture retrieval across the study area, further investigation is required as discussed in the following sections.

5.1.4 Error Analysis

There are a number of factors that could be the cause of the large errors obtained over crops: (i) Error in the values of ancillary parameters input to the L-MEB model such as soil effective temperature, canopy temperature, soil texture and vegetation water content; (ii) Erroneous values of the L-MEB default parameters. Moreover, the effect of land surface heterogeneity within the PLMR pixel could have an impact, as shown in the case of Midlothian. In order to understand which of these factors could lead to the large errors observed over crops, the impact of each input (L-MEB parameters and ancillary data) on the soil moisture retrieval was assessed through sensitivity analysis. To this end, starting from a reference scenario with fixed values for all parameters, the values of the L-MEB parameters and ancillary data were changed individually within the expected range of values, while keeping all other values fixed at their reference values. At each step the retrieved soil moisture was then compared to that of the reference scenario to estimate the impact of each input parameter on the soil moisture retrieval. The process was repeated for four selected scenarios. These were the mature crop field at Pembroke and the short grassland site at Roscommon, which represent extreme conditions across the high-resolution sites in terms of above ground vegetation biomass and soil texture. Wet and dry conditions were considered for both sites. The results of the sensitivity analysis are shown in Figure 5.4 for each parameter individually and will be discussed below.

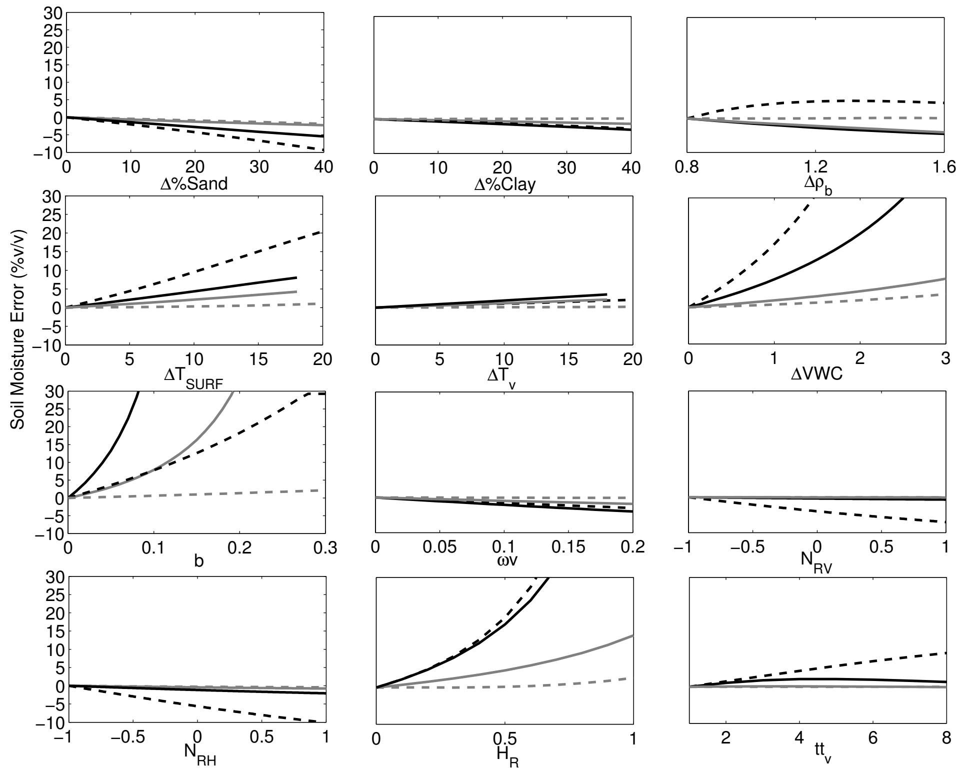

Figure 5.4. Analysis of the L-MEB microwave emission model sensitivity to errors in the ancillary data (top two rows) and changes in the L-MEB parameters (bottom two rows). Errors are indicated in %v/v from four reference scenarios: a crop site (VWC=3.6kg/m^2, solid lines) and a grassland site (VWC=0.7kg/m^2, dashed lines), both on wet (black line) and dry (grey line) conditions. ρ_b= soil bulk density (g/cm3); T_{SURF}= soil temperature at 2.5cm (K), T_v= vegetation canopy temperature (K), VWC=vegetation water content (kg/m^2).

As discussed earlier, the top 2.5cm and 15cm soil temperatures were estimated using data from monitoring stations which were not always immediately adjacent to the high-resolution sites, but could be as much as 1-km distant. This could lead to error in the estimation of the soil effective temperature in the direct emission model. The maximum spatial difference in soil temperature between monitoring stations recorded on sampling days was 6.5K. It can be reasonably assumed that this is the maximum error in soil temperature estimation due to the distance between the closest monitoring station and the high-resolution area. Sensitivity analysis showed that the associated soil moisture error should not be greater than approximately 5%v/v.

Analysis of the canopy infrared measurements recorded at some of the monitoring stations showed that at the time when the high-resolution acquisitions considered here were undertaken (9:00-11:00AM), the difference between the canopy and the top 2.5cm soil temperature was significant; more so in the case of crops (13K mean difference) than that of grasses (6K). Sensitivity analysis revealed that the soil moisture error associated with the assumption that the canopy temperature is in equilibrium with the top 2.5cm soil temperature should not be greater than approximately 3%v/v, as this is the maximum soil moisture error observed in Figure 5.4 for errors in canopy temperature up to 13K.

The soil textural properties which were derived from 30cm deep soil samples collected at or nearby the high-resolution sites might be different from those of the top 5-10cm layer which contributes to the soil microwave emission at L-band. A sensitivity study showed that large errors in soil textural properties estimation can lead to significant errors in retrieved soil moisture. In the case of crops, respectively 5%v/v and 3%v/v error for a 40% estimate error in sand and clay content. Although such a large variation in % sand and clay content is unlikely over such a shallow depth, in the absence of data for verification this error cannot be dismissed. Nevertheless, even in the case in which such a large error in soil properties estimation was committed, the associated soil moisture error (5%v/v) would only marginally explain the large soil moisture retrieval errors subject of this discussion.

The VWC sampling technique used (daily 50cm x 50cm biomass samples at two fixed locations in the high-resolution site, see section 5.1.1) could lead to an error in VWC estimation due to both the small sample size (bound to be heterogeneous in the case of crops, for example) and the spatial variation of the VWC across the area. Analysis of this error using the sixteen samples taken on several occasions at each site showed the daily value of the VWC used for crops could be underestimated by approximately 0.12kg/m^2 for most crops (Cullingral, Illogan and Merriwa Park) and as much as 1kg/m^2 for Pembroke. The impact of these biases on the soil moisture retrieval was investigated by adding them to the daily VWC recorded at each sites and repeating the retrieval. Results indicated that increasing the VWC reduced the RMSE of soil moisture retrieval at Pembroke by 4.1%v/v, while at the other crop sites the improvement was only 0.4%v/v. It is evident that the problem of VWC sampling only marginally accounts for the large errors at the crop sites, although the spatial variation of the VWC across the high-resolution sites might explain the scatter observed in daily errors at the same area (Figure 5.3).

Although the errors associated with ancillary data estimation discussed in the previous section were in some cases significant and certainly affected the overall accuracy of the soil moisture retrieval presented, it was evident that they could only partially explain the large errors observed at the crop site, which was of the order of 10-32.5%v/v. This suggests that the errors could be due to inadequacy of the default L-MEB parameters.

5.1.5 Calibration of the L-MEB Parameters

Amongst the L-MEB parameters, parameters b and H_R are those with the highest impact on the L-MEB soil moisture output (Figure 5.4). A site-specific calibration of the parameters b and H_R was therefore performed for the crop sites Pembroke, Merriwa Park, Illogan and Cullingral, using all the bi-polarised T_B observations of the high-resolution area available for each site, extracted from the airborne data set as described in section 5.1.1.

5.1.5.1 Calibration Option 1: b and H_R

Initially, both b and H_R parameters were calibrated at once. Given that H-pol T_B is known to be more sensitive to soil moisture while V-pol responds more to the canopy signal (this was also observed when commenting Figure 5.2), the simultaneous retrieval of b and H_R is expected to allow decoupling the soil surface (parameter H_R) from the vegetation (parameter b) component of the observed T_B. To this end, the multiple, bi-polarised high-resolution T_B observations were used to calibrate both parameters on each observation day, using the ground soil moisture and the ancillary data on VWC, soil texture, soil temperature and surface roughness described in the previous sections. As explained in detail in the description of the L-MEB model in Chapter 3, both *b* and Hr parameters can be considered incidence angle independent, as their angular dependence is treated in L-MEB through specific equations. This implies that one single value of each parameter can be retrieved by using the five to eight T_B observations available over each site on each day. A mean value for each parameter was then calculated by averaging the values obtained across different days. These average values were finally verified by running the L-MEB soil moisture retrieval for each sampling day.

The resulting calibrated values for each parameter and the respective soil moisture retrieval errors are shown in Table 5.3 ('Calibration 1') and compared with the retrieval using L-MEB default values for *b* and H_R. The calibration of *b* and H_R significantly improved the retrieval for most sites. For the site with the highest vegetation biomass (Pembroke) the retrieval accuracy was improved from 32.5%v/v to 8.9%v/v. The calibrated values of *b* and H_R were significantly higher than the default ones indicating that the proposed SMOS parameters (i) underestimate the effect of the vegetation in masking the soil signal and (ii) underestimate the scattering of the soil signal at the surface. At the Cullingral site very high values of *b* were obtained. It should be noted that the T_B observations available at this site were mostly within a narrow range of incidence angles close to nadir. At these angles the polarisation difference is reduced and consequently the algorithm is less able to decouple the vegetation and soil signal. For the remaining sites, the retrieved values for *b* were in the range 0.2-0.5 while H_R was in the range 0.2-0.6. These values allowed retrieval of soil moisture with accuracy better than 8.9%v/v.

5.1.5.2 Calibration Option 2: H_R

The coupled *b* and H_R calibration presented in the previous section determined a sensible improvement of the L-MEB soil moisture retrieval using default parameters over crops. Nevertheless, the accuracy achieved is still far from the 4.0%v/v target accuracy of SMOS. A second approach was

Table 5.3. Site-specific calibration of parameters *b* and H_R for the NAFE'05 crop sites. All calibrated values shown are the average of the values calibrated from four different dates. θ indicates soil moisture. 'Calibration 1'= Calibration of both *b* and H_R; 'Calibration 2'= Calibration of only H_R, *b* fixed to L-MEB default value; 'Calibration 3'; = Calibration of H_R as a linear function of soil moisture with *b* fixed to L-MEB default value.

High-Resolution Site	Range of Incidence Angles	Parameter Set	b	H_R	Soil Moisture RMSE (%v/v)
Merriwa P.	5°-42°	Default	0.08	0.2	21.4
		Calibration 1	0.26	0.46	6.4
		Calibration 2	0.08	1.03	5.1
		Calibration 3	0.08	H_R =1.5-1.6*θ	4.8
Cullingral	6°-23°	Default	0.08	0.2	19.4
		Calibration 1	1.15	0.46	18.2
		Calibration 2	0.08	1.29	14.5
		Calibration 3	0.08	H_R =1.6-1.0*θ	3.0
Illogan	3°-44°	Default	0.08	0.2	9.9
		Calibration 1	0.48	0.19	7.2
		Calibration 2	0.08	0.49	3.5
		Calibration 3	0.08	H_R =0.7-0.9*θ	2.9
Pembroke	16°-39°	Default	0.08	0.2	32.5
		Calibration 1	0.19	0.57	8.9
		Calibration 2	0.08	1.12	8.0
		Calibration 3	0.08	H_R =1.6-1.2*θ	4.0

to assume that the default value of parameter *b* proposed for crops (0.08) is correct and thus calibrate only H_R. This was justified by three reasons: (i) the value 0.08 for wheat-type crops resulted from an extensive review of estimates of *b* at L-band for various crop types, and therefore it is expected to be quite accurate; (ii) correct estimates of parameter H_R and their link to geophysical variables (soil type, surface roughness and soil moisture) are still the object of debate and have not yet been well understood; and (iii) parameter b, dependent on plant structure and independent on soil conditions, is expected to be less variable than parameter H_R across the similar wheat-type crops present in the study area.

The results of this second calibration approach (see Table 5.3, 'Calibration 2'), show a significant improvement in soil moisture accuracy at all sites when calibrating H_R alone, as compared to the calibration of both b and H_R. Soil moisture error decreased for all sites, with an improvement of at least 1.0%v/v and up to 3.7%v/v in some cases. Calibrated values of H_R were in the range 0.5 – 1.3, being much higher than both the L-MEB default values (0.1 – 0.2) and those obtained in 'Calibration 1' (0.2 – 0.5). These results suggest that the L-MEB default values of parameter H_R for crops, estimated by the SMOS team exclusively at European sites, represent conditions which are too smooth than those encountered in the NAFE'05 study area. Different ploughing and tilling practices in Australia could be the cause of rougher surfaces in the wheat crops reflected in the higher values calibrated for H_R.

5.1.5.3 Calibration Option 3: Soil Moisture Dependent H_R

In calibration 1 and 2 the parameters b and H_R were considered stable in time, i.e., one average value was calculated from the calibration on individual days to evaluate the soil moisture retrieval. An examination of the retrieved values of both parameters across the four sampling dates showed that while parameter b was fairly constant over time (as was expected given that it relates to the vegetation structure) the values of parameter H_R exhibited a notable variation in time, which was fairly well correlated with the soil moisture conditions, i.e., higher values of H_R were calibrated over dry conditions. As already discussed in Chapter 3 when describing the L-MEB default parameterisation for grasslands, this is consistent with several previous studies over crops and grasslands (Wigneron et al., 2001; Escorihuela et al., 2007; Saleh et al., 2007). The dependence of H_R on soil moisture is explained by an effect of volume scattering: the spatial fluctuations of the dielectric constant within the soil volume are stronger during drying out, producing an important "dielectric" roughness effect. Therefore, it has been proposed that H_R should be considered as an effective parameter that accounts for (i) "physical roughness" effects in relation with spatial variations in the soil surface height, and (ii) "dielectric roughness" effects in relation with the variation of the dielectric constant in the near-surface soil layer. In these studies it is also pointed out that this effect might be very "local", i.e., it should be smoothed out at larger resolution and is probably negligible at satellite scales.

Given that the evaluation of L-MEB presented in this Chapter had the objective to support the regional soil moisture retrieval presented in section 5.3 and the coarse-scale retrieval presented in Chapter 7 and 8, the problem of soil moisture dependence of H_R was not regarded as crucial, as long as a sufficiently accurate soil moisture prediction could be obtained over crops. Therefore, in line with previous studies, a simple linear regression was developed in this Chapter and used to model the relationship between H_R and soil moisture over crops in the study area. A detailed analysis of the relationship between parameter H_R was undertaken with the data presented here, and it has been included in Appendix A4.

The site-specific coefficients of the regression between H_R and soil moisture are shown in Table 5.3 ('Calibration 3'). Improvement in soil moisture retrieval accuracy was achieved at all sites after calibration of the soil moisture dependence of H_R. In particular, RMSE was reduced by 11.5%v/v at Cullingral and by 4.0%v/v at Pembroke, bringing the retrieval error at both sites below 4%v/v. For Merriwa Park and Illogan the improvement was not significant indicating that at these sites a fairly accurate soil moisture retrieval is achieved without the need for a soil moisture dependent parameterisation of H_R. Scatter plots of the retrieved versus ground measured soil moisture after calibration is shown in Figure 5.3b.

The coefficients of the regression of H_R as a function of soil moisture obtained were quite uniform across the four crop sites. In particular, the slope of the relationship for the different crops was in the range 0.9-1.6, which is close to the 1.3 already observed for grasslands by Saleh et al. (2007). The resulting value of H_R decreased on average from 1.3 on very dry soils (5.0%v/v) to 0.8 on very wet soils (50.0%v/v). At Illogan, low values of both the slope and intercept of the regression were retrieved, resulting in lower and more stable values of H_R with respect to soil moisture.

5.1.6 Soil Moisture Retrieval over Forest

The L-MEB model was thus far evaluated at grassland and crop sites. However, the NAFE'05 study area presented also a significant fraction of forest (24.3%, see section 5.3.1.1). Although ground sampling of soil moisture under forest canopy was not undertaken during the NAFE'05 field campaign at fine resolution, a small patch of forest, approximately 2km^2 in size, was sampled in the Roscommon experimental farm. The soil moisture ground sampling in the Roscommon forested area was more limited and at coarse spacing than that undertaken at the high-resolution sites and presented in earlier sections. Approximately 10-15 measurements were taken throughout the forest area per day, on an irregular grid with a variable spacing (on average 200m).

These data were used by Grant (2009) to perform a rigorous evaluation of the L-MEB model over the forested area at the Roscommn site, using the 62.5m T_B observations collected in the present study. Results indicated that soil moisture could be retrieved with an accuracy of 6%v/v for all soil moisture conditions, confirming earlier results by Ryu et al. (2007) and Saleh et al. (2004) at European and American sites which indicated good sensitivity of L-band observations to soil moisture changes under dense canopy forest.

In the following section, the L-MEB model with the parameters for grasslands and crops (including the soil moisture dependent linear regression for parameter H_R) calibrated with high-resolution airborne data are applied to low-resolution (1km) airborne data at the eight high-resolution sites. This is a crucial step for the application of L-MEB to regional soil moisture mapping which is performed in section 5.3.

5.2 *Evaluation of the L-MEB Model with Low-Resolution Airborne Observations*

Before applying the L-MEB model to retrieve soil moisture estimates over the entire study area, the model was evaluated using the 1km resolution T_B observations acquired by the PLMR radiometer over the high-resolution sites. This allowed evaluation of the L-MEB soil moisture retrieval at the same resolution which will be used for the regional soil moisture mapping in section 5.3, but with the support of detailed ground soil moisture data. Low-resolution T_B observations were acquired on the same days of high-resolution observations acquisition with a lag of 2-3 hours, 1km T_B being acquired earlier in the morning, at approximately 7:00-9:00AM. Flight lines were designed so that each of the eight 150m x 150m high-resolution sampling areas would fall within the field of view of the nadir beams of the radiometer (flown in push broom configuration). Given the low aircraft speed and the high rate at which the radiometer takes readings, the 1km footprints were highly oversampled, and therefore approximately 20-25 T_B observations covering each high-resolution site were available on each sampling day. Due to flying time restrictions, no low-resolution observations were acquired over Illogan.

Figure 5.5 gives an overview of the land surface conditions within the areas surrounding the high-resolution sites which fell within the 1km T_B footprints considered in this section. The 1km footprint centers are indicated, together with the locations at which ground soil moisture was measured for evaluation. The low-resolution T_B footprints covered a much larger portion of the land surface than the high-resolution ones (approximately the red squares in Figure 5.5), and were therefore characterised by a wider range of land covers, topography and soil type conditions.

Soil moisture was retrieved using the L-MEB model together with the site-specific surface and vegetation parameters calibrated in the previous section (‘Calibration 3’; *b* fixed to L-MEB default values and a site-specific

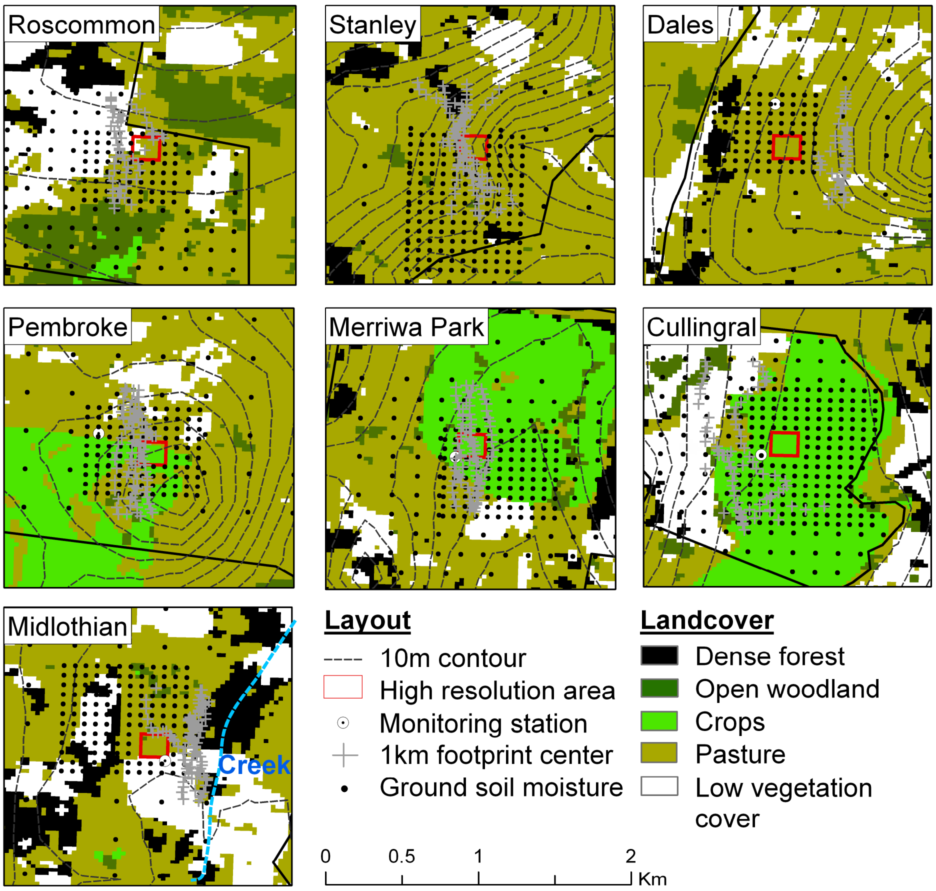

Figure 5.5. Land surface conditions and locations of airborne and ground sampling measurements in the areas surrounding the high-resolution sites. The centres of the 1km footprints are shown for all acquisition days and the locations at which soil moisture was monitored on the ground are displayed. High-resolution soil moisture measurements at 6.25m and 12.5m spacing covering the high-resolution areas (red rectangles) are not shown for clarity.

linear regression for H_R) and the same ancillary data used for the soil moisture retrieval with high-resolution T_B observations, except for the soil temperatures. These were extracted for the time of low-resolution acquisition from the local monitoring station time series, as described in the previous section. It should be noted that, since the 1km resolution T_B observations used in this section are completely independent from the 62.5m observations used in the previous section to calibrate the L-MEB parameters, this section represent an independent validation of the calibrated values of parameters b and H_R.

The retrieved soil moisture was compared with the average ground soil moisture measured at the 150m x 150m fields and surrounding areas. On average, 300-500 points at resolutions ranging from 6.25m to 250m fell within each 1km footprint. The standard deviation of the ground measured soil moisture within the low-resolution footprints was on average 7.2%v/v, as opposed to 5.6%v/v within the high-resolution footprints. Maximum soil moisture spatial variability was recorded at Cullingral (9.1%v/v) and Midlothian (9.2%v/v) while more uniform soil moisture conditions were recorded at Roscommon (3.1%v/v).

Figure 5.6 and Table 5.4 show respectively the scatter plot and error statistics of the comparison between L-MEB soil moisture retrieval and ground measured soil moisture. Very good agreement between retrieved and observed soil moisture was obtained at all the sites. At most sites the RMSE was better than 4.0%v/v, with a maximum error of 6.0%v/v at Stanley. The correlation coefficient exceeded 0.89 for most sites. This demonstrated excellent accuracy of the model despite the land surface heterogeneity observed at the scale of low-resolution footprints. Moreover, the soil moisture dependent parameterisation of parameter H_R calibrated with high-resolution T_B observations provided accurate soil moisture retrieval at all the crop sites.

It is interesting to note that negative biases (i.e. retrieved values less than observed values) were obtained at all the sites, indicating a tendency of the L-MEB model to underestimate soil moisture in the presence of land surface heterogeneity. This agrees with results by Van de Griend et al. (2003) over synthetically generated heterogenous pixels with a mix of vegetation densities. In the last column of Table 5.4 the difference between the RMSE obtained at low resolution and that obtained at high resolution is also shown, in order to highlight the change in accuracy with decreasing resolution. Overall the soil moisture accuracy was comparable with that obtained at the higher resolution. It is worth noting that in the case of Midlothian, the highly heterogeneous site for which the highest soil moisture retrieval error

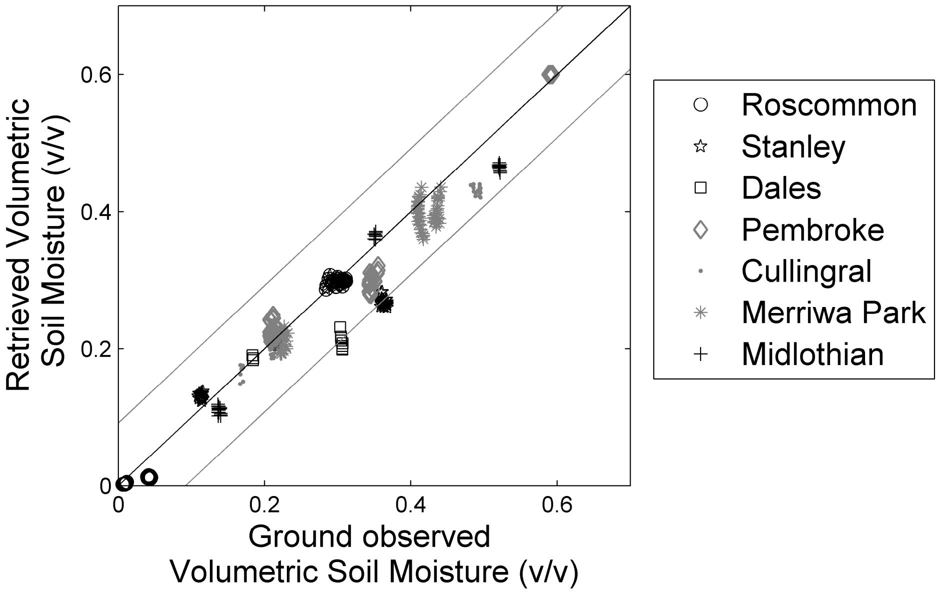

Figure 5.6. Evaluation of L-MEB soil moisture retrieval with low-resolution airborne T_B observation and L-MEB default parameters and calibrated roughness parameter H_R. Grey symbols indicate sites classified as crops, black symbols represent sites classified as grassland. Grey lines indicate the maximum standard deviation of the ground-monitored soil moisture within low-resolution footprints (recorded at the Midlothian site)**.**

Table 5.4. Low-resolution evaluation of the L-MEB soil moisture retrieval. 'Δ RMSE' is the difference between error at low and high resolution.

High-Resolution Site	**Soil Moisture Retrieval (%v/v)**			**ΔRMSE Low-High Resolution**
	RMSE	**r^2**	**bias**	
Roscommon	1.8	0.99	-1.2	+0.2
Stanley	6.0	0.89	-3.2	+4.6
Dales	5.3	0.45	-2.9	+1.6
Midlothian	3.7	0.99	-2.6	-3.7
Merriwa Park	3.0	0.98	-2.3	-1.8
Cullingral	3.8	0.99	-2.3	+0.8
Pembroke	3.1	0.98	-0.7	-0.9

had been obtained at high resolution (7.4%v/v) the retrieval accuracy improved significantly at low resolution (3.7%v/v improvement). This is likely due to the predominance within the 1km footprints field of view of large native grass areas surrounding the lucerne field, which was of limited extent (~500m).

As the site had been assigned the L-MEB parameter set relative to native grasses, due to the absence of existing estimates for lucerne type crops, this would have resulted in a better soil moisture retrieval at low resolution. It should be pointed out that in the context of the coarse-scale soil moisture retrieval which will be performed in the next Chapters, the poor parameterisation of the lucerne crop is a negligible problem. To the knowledge of the author the lucerne field at Midlothian was the only presence of lucerne in the entire study area, which was instead dominated by wheat, barley and oats crop for which accurate soil moisture retrieval was obtained in this Chapter.

5.3 Regional Soil Moisture Retrieval

In this section, the L-MEB model is applied to the airborne brightness temperatures (T_B) observations made with the PLMR radiometer across the NAFE'05 study area, being approximately a 40km by 40km area mapped at 1km nominal resolution. These observations will be hereby referred to as the 'Regional' airborne observations. The objective is to produce soil moisture maps of the entire study area at 1km resolution which will be used as soil moisture ground truth in Chapter 7 and Chapter 8 in order to assess the effect of land surface heterogeneity on the soil moisture retrieval from coarse-scale footprints. Soil moisture maps derived from 1km airborne data have two major advantages with respect to ground point measurements (monitoring stations or spatial monitoring): (i) they have large extent, covering the entire study area and therefore characterise the soil moisture variability within all the coarse-scale pixels to be analysed in Chapter 7 and Chapter 8 and (ii) each soil moisture observation represents an integrated value over a 1km land surface area, therefore overcoming the limitation of point data which only provide information on the horizontal domain immediately surrounding the ground probe (a few centimeters). These features make the airborne data highly desirable for ground truthing coarse-scale (40km) soil moisture retrieval. It should be noted that in both cases (airborne observations and ground probe) the vertical domain is the same (a few centimeters).

This section builds upon the evaluation of the L-MEB model with multi-resolution T_B observations performed in previous sections, since the L-MEB radiative transfer parameters used here are those evaluated at the high-resolution sites. In the following sections the ancillary data, the airborne observations and the retrieval approach adopted are described. Finally the soil moisture maps are presented.

5.3.1 Ancillary Data

In order to obtain soil moisture from T_B observations, the L-MEB model requires ancillary data on land cover, near-surface soil and canopy temperature, and soil textural properties. The ancillary data used in this thesis were (i) collected during the NAFE'05 field campaign, (ii) obtained from existing databases or (iii) derived from available satellite imagery available, and have been described in Chapter 4. Consequently, this section is limited to describing how those ancillary data were processed in order to make them suitable for soil moisture retrieval over the entire study area. As already noted in Chapter 3, the ancillary data used in this thesis differ from those which will be used by the SMOS mission; in principle, ground data were given priority where possible. In the case that satellite imaginary was the only source of information, the data sets with the finest available resolution (finer than those used by SMOS) were chosen. Consequently the results presented represent a best case scenario for SMOS retrieval.

5.3.1.1 Land Cover

A land cover map of the study area derived from the 30m resolution Landsat 5 Thematic Mapper scene acquired on October 21st, 10 days before the beginning of the airborne and ground monitoring operations, was used in this study. The land cover map, was produced by P. Maisongrande and G. Boulet at the Centre d'Etudes Spatiales de la BIOsphère (CESBIO), through

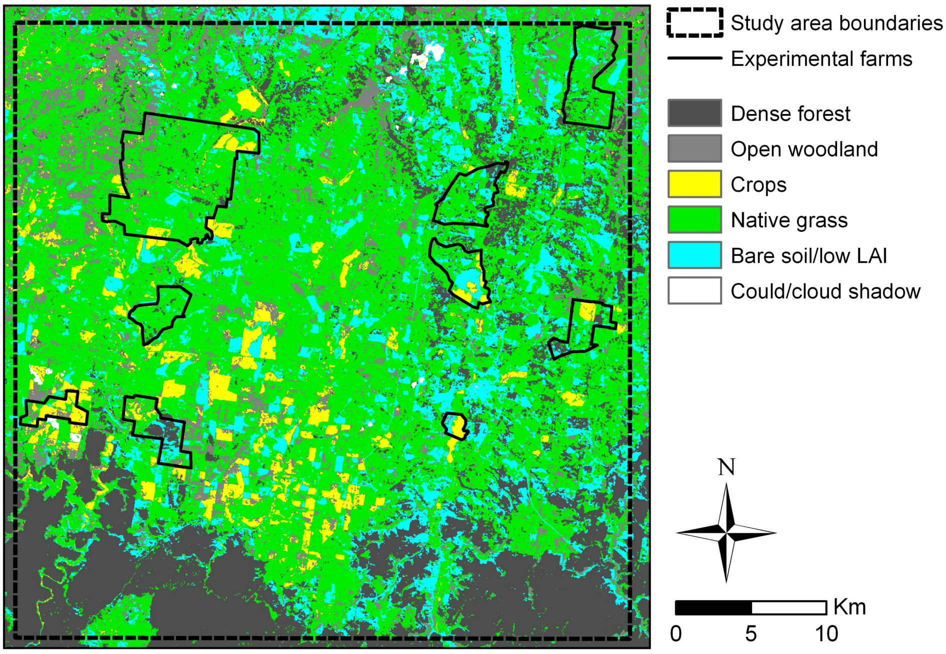

Figure 5.7. Land cover classification of the study area derived from Landsat 5 Thematic Mapper.

a supervised classification to define five land cover types (dense forest, open woodland, native grass, bare soil/very low LAI, crops), based on thirteen spectral classes derived from un-supervised spectral analysis of the six optical bands of Landsat.

The resulting Landsat thematic map is shown in Figure 5.7. The dominant land cover types in the study area are native grass (50.7%) and dense forest (24.3%), with the latter concentrated along the southern edges of the study area. The rest of the area is occupied by bare soil or vegetation with very low LAI (12%) and open woodland (8.5%). Cropped areas occupy only 4.5% of the area and are concentrated in the western part of the study area. The dense forest consisted mainly of Box (*Eucalyptus spp.*), Ironbark (*Eucalyptus spp.*) and some Black Cypress-pine (*Callitris endlicheri*). Fish-eye photographs were taken of the Eucalypt vegetation, from which the leaf area index (LAI) was estimated at LAI = 2.5). MODIS images showed that forest LAI did not noticeably change during the experiment (J. Grant, pers.

Table 5.5. Evaluation of the Landsat Thematic Mapper land cover with ground visual observations. The numbers in each cell indicate the count of the locations where a particular known land cover was assigned a particular Landsat land cover class.

		Land Cover Observed on the Ground				
		Bare	**Native grass**	**Crop**	**Forest**	**Open Woodland**
Landsat Thematic Map	**Bare**	0	27	3	0	2
	Native grass	2	75	7	0	4
	Crop	0	1	2	0	0
	Forest	0	4	0	0	2
	Open Woodland	0	6	2	0	1

comm.). The white areas in Figure 5.7 are areas classified as cloud (and associated cloud shadow); these areas could not be assigned a land cover type, and were therefore excluded from the analysis.

This thematic map was evaluated based on the ground visual observations of land cover performed by the ground team at 122 locations across the study area. Results of this comparison are shown in Table 5.5. The Landsat classification matched the ground visual observations in 64% of the 122 cases. Most errors were associated with locations classified as 'bare soil or very low LAI' and 'open woodland' in the Landsat thematic maps, being recorded as native grass by the ground team. Based on these results, it was decided in this thesis to combine 'bare soil or very low LAI' and 'open woodland' classes with 'native grass'. In this way the classification accuracy was increased to 80%.

5.3.1.2 Soil Texture

Detailed spatial characterisation of soil texture was possible through soil particle analysis with a Malvern Mastersizer 2000 performed on 88 soil samples (7cm in diameter, 5cm deep) collected across the study area. These were collected on two of the regional sampling days; November 14th and

November 21st, with each day being a subset of the soil moisture sampling locations. Soil texture in the study area is extremely variable, ranging from black basalt-derived cracking clays in the northern part to the sandstone derived soils in the southern part of the study area.

The Malvern Mastersizer 2000 has been reported to underestimate the fine (clay) fraction in inverse proportion to the amount of fine fraction present while accurately reporting the coarse fraction (Campbell, 2003). Therefore the reported clay fraction was adjusted using the quadratic fit expression reported by Campbell (2003), which is based on the only existing experimental data set of real clay fraction and Malvern Mastersizer 2000 data. Thus the clay fraction was corrected as:

$$C = -0.0116 \cdot C_{\mathrm{LM}}{}^{2} + 2.0071 \cdot C_{LM} + 6.0018\,, \tag{5.2}$$

where C is the corrected clay fraction (in % mass) and C_{LM} is the clay fraction reported by the Laser Mastersizer 2000. The RMSE of the fit in (5.2) was of 1.8% clay fraction.

In order to upscale the soil texture point data obtained from the gravimetric samples to the entire study area, the data were interpolated using the inverse distance with a 1km reference grid, to match the grid used for the airborne T_B data (see section 5.3.2). An estimate of the error involved in the interpolation and gridding process was obtained by comparing the final 1km soil texture grid with the original point data. The errors in clay fraction and sand fractions were 5.7% and 6.3% fraction respectively. The sensitivity analysis of the L-MEB model presented in section 5.1.4 indicates that such an error in soil texture has a negligible impact on the soil moisture retrieval accuracy, producing an error smaller than 1.5%v/v, which is smaller than that due to the PLMR radiometer noise (approximately 2K, see Appendix A3, resulting in approximately 2%v/v for a moderately vegetated soil). The resulting 1km soil texture grids are shown in Figure 5.8, together with the point gravimetric data.

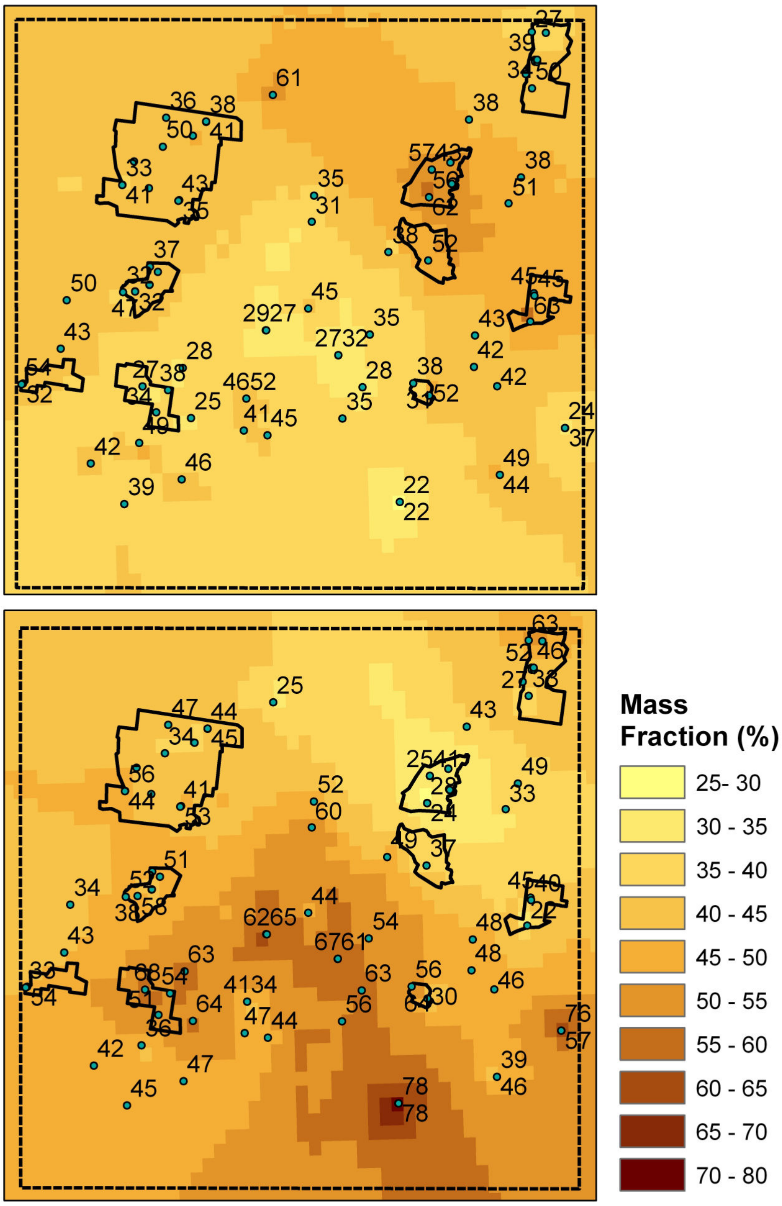

Figure 5.8. Soil texture data for the NAFE'05 study area; clay content (top panel) and sand content (bottom panel). The gravimetric samples point data are shown as well as the 1km soil texture grids derived by interpolation of the gravimetric samples. The thick dashed line delineates the study area boundaries while the solid lines indicate the experimental farms.

5.3.1.3 Soil Temperature

The L-MEB model requires input of soil temperatures at two depths, near-surface (at approximately 2.5cm) and deep (at approximately 50cm). However, as noted earlier, due to the lack of soil temperature measurements deeper than 15cm at all the soil moisture monitoring stations, in the present study it had to be assumed that the value of soil temperature at 15cm depth is a good estimate of soil temperature at (50cm). The spatio-temporal variability of the soil temperature at the available depths recorded at the eleven permanent monitoring stations during the time window of regional observations (7:00AM-9:30AM) is shown as an example in Figure 5.9 for November 14^{th}. The 2.5cm soil temperature had greater temporal and spatial variation than the soil temperature at 15cm, which was basically stable in the regional observation window. Moreover, during this time window the soil temperature spatial variability (indicated by the standard deviation of soil temperature amongst the stations in Figure 5.9) was smaller than the variation in time.

Spatial and temporal variability is summarised for all regional observation dates in Table 5.6, with the temporal variability quantified using the difference in average temperature between the stations at 9:30AM andthe average over the regional observation window. The spatial variability is quantified using the average of the standard deviations amongst the stations calculated for each temporal step (20min). The temporal variation of the surface temperature was greater than that spatial variation for all dates, and achieved a maximum (2.6K) for intermediate soil moisture conditions (November 14^{th}, 20.5%v/v), being minimum in very wet conditions (0.6K and 40.6%v/v). Spatial variability achieved a maximum on the same date as the temporal variability (November 14^{th}, 1.5K). The temporal variability of the deep soil temperature during the regional observation window was negligible (less 0.04K on all dates) as was the spatial variation (less than or equal to 1K in all cases).

Given this observed variability, three options were considered for estimating the surface temperature across the entire study area: (i) Use the MODIS land surface temperature product to estimate the surface temperature; (ii) Extrapolate the point measurements at the monitoring stations to the entire study area through correlation with geophysical quantities and (iii) Use daily averages of the soil temperatures at the monitoring stations recorded during the regional observation window.

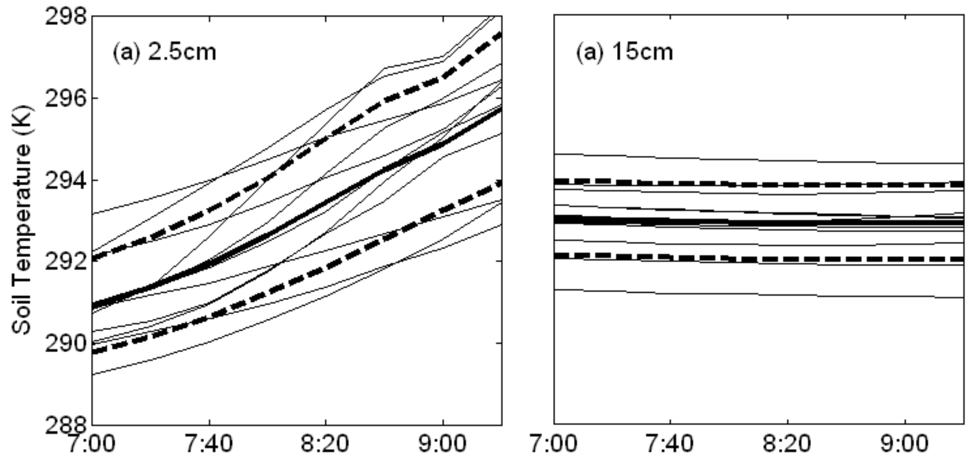

Figure 5.9. Soil temperature time series at the permanent monitoring stations on November 14th and during the regional airborne observations window. (a) Near-surface soil temperature (2.5cm); (b) Deep soil temperature (15cm) are shown. Thick lines indicate the average temperature (solid) and standard deviation (dashed) of the temperatures observed at the stations at each time step (20min).

Table 5.6. Summary of temporal and spatial variability of soil temperatures recorded at the permanent monitoring stations during regional airborne observations (7:00AM-9:30AM) at 2.5cm and 15cm depth. The quantification of temporal and spatial variability is is explained in the text.

Date	**Average Soil Moisture (%v/v)**	**Temporal Variability 2.5cm (K)**	**Spatial Variability 2.5cm (K)**	**Temporal Variability 15cm (K)**	**Spatial Variability 15cm(K)**
31/10	40.6	0.6	0.6	-0.04	0.7
7/11	35.1	1.9	0.7	-0.01	0.6
14/11	20.5	2.6	1.5	-0.03	0.9
21/11	10.8	1.9	1.3	-0.02	1.0

MODIS scenes of the NAFE'05 study area were available for only three of the four days of regional observations, and two of these scenes were affected by significant cloud cover, (only the MODIS November 21st scene was cloud free), making this data set unsuitable to estimate soil temperatures across the study area. Moreover MODIS observations only give a "leaf" temperature which would need to be correlated with the near-surface soil temperature.

The potential to extrapolate the point measurements of soil temperature to the entire study area was assessed by analysing correlation between the spatial distribution of the 2.5cm soil temperatures recorded at the monitoring stations and geophysical properties expected to affect the spatial distribution of soil temperature. However, the correlation coefficient was found to be very low for all the geophysical properties considered: elevation (r^2=0.01), aspect (r^2=0.04) and soil texture (through % clay content, r^2=0.006). Therefore the extrapolation was not considered a suitable method for estimating the surface temperature across the entire study area

Daily averages of monitoring station data was the approach finally adopted to estimate soil temperature across the study area, as the spatial variation was found to be only 1.5K. The impact of the observed spatio-temporal variability in soil temperature on the regional soil moisture retrieval was assessed by plotting the changes in retrieved soil moisture due to changing the input value of 2.5cm soil temperature of L-MEB for land surface conditions typical of the study area. Consequently, grassland and crop conditions were assessed with the Vegetation Water Content (VWC) equal to the average measured from biomass sampling (respectively 0.4 and 2kg/m^2). The results from this analysis are shown in Figure 5.10 (this plot is similar to the one presented in Figure 5.4, but is presented here in greater detail). Clearly the impact of errors in the 2.5cm soil temperature is greater in wet conditions, when the effect of soil temperature changes is enhanced by the lower soil emissivity. Moreover, this effect is stronger under a grassland canopy, due to the reduced contribution of the canopy to the overall signal and therefore the higher sensitivity to the soil signal.

Using Figure 5.10 together with Table 5.6, a first-order estimate of the impact of spatial and temporal variability of near-surface soil temperature on the regional soil moisture retrieval can be considered. Specifically, two alternate options can be assessed: (i) soil temperature uniform in space and time and (ii) soil temperature uniform in space but variable in time. Table 5.6 shows that, by using option (i), the maximum difference to be expected

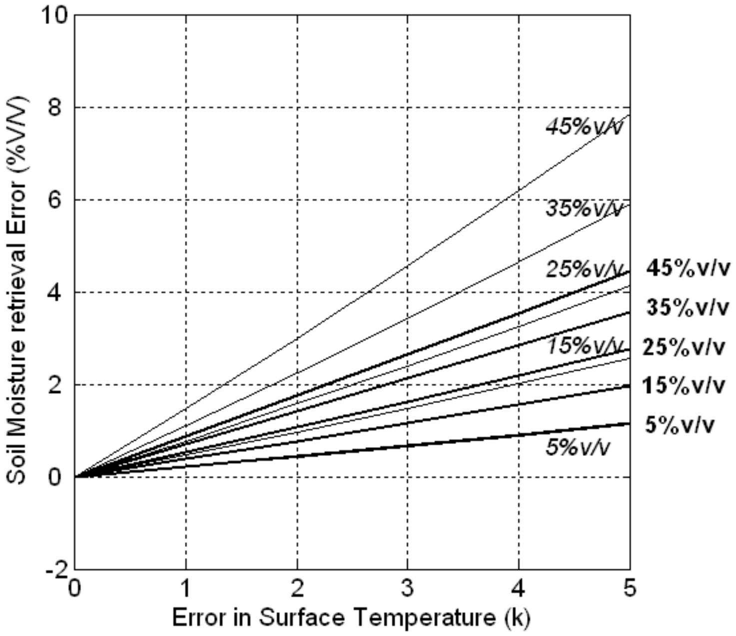

Figure 5.10. Sensitivity of the L-MEB soil moisture retrieval to changes in 2.5cm soil temperature input for different soil moisture conditions. Cases considered are grassland (thin lines, italic labels) and mature crop (thick lines, regular bold labels).

between the assumed soil temperature and the real soil temperature, based on monitoring stations measurements, would be of 4.1K (November 14th). This is estimated by adding the variation in time (3rd column) to the spatial standard deviation (4th column). By considering average soil temperatures at discrete points through time instead (i.e., option (ii)) the difference in soil temperature is reduced to the spatial standard deviation component only, i.e. 1.5K on November 14th. Figure 5.10 shows that the soil moisture retrieval error is reduced from 1%v/v to 6%v/v (depending on soil moisture conditions) for a 4.1K error in 2.5cm soil temperature, to a less than 2%v/v error in all cases for a 1.5K soil temperature error. Note however, that this analysis assumed, in the absence of additional data, that the standard deviation of soil temperatures recorded at the stations is representative of the spatial variability across the study area. This is believed to be a reasonable assumption since the stations were spread uniformly across the study area (see Figure 4.1).

This analysis has highlighted the importance of accurately accounting for temporal variation of soil temperature during the airborne acquisitions, while the spatial variation can safely be neglected (at least in the NAFE'05 area). In this Chapter, temporal variation of soil temperature was accounted for in the soil moisture retrieval as a two-step process:

1. the airborne T_B observations were normalised to an intermediate reference time (8:00AM) by means of the ground measured temporal variation in near-surface soil temperature presented here; and
2. the spatially uniform 2.5cm soil temperature calculated as the average temperature between the monitoring stations at the reference time (8:00AM) are used as input to L-MEB.

The normalisation produced T_B fields that were equivalent to those that would be observed at the reference time across the entire study area. Details about this pre-processing of the airborne data are given already in section 5.1.1. This two-step process has two advantages: (i) it accounts for the impact of soil temperature temporal variability during regional observations, shown earlier to have a significant impact on the soil moisture retrieval, and (ii) it prevents the presence of sub-pixel spatial heterogeneities in the coarse TB pixels (obtained in Chapter 7 from aggregated 1km TB data) induced by the temporal variability of soil temperature instead of by real spatial variability of TB.

The 8:00AM soil temperature recorded at 15cm depth at the permanent monitoring stations was used as the deep soil temperatures input of L-MEB. The implications of using the 15cm soil temperature as an approximation of the 50cm soil temperature have been already discussed in section 5.1.1. It suffices to say that the error in effective soil temperature estimation due to this assumption is less than 0.6K. Moreover, given the negligible small spatial variation of the 15cm temperature in the study area during the regional observation window (see Table 5.6) the 8:00AM average of the 15cm soil temperature between the monitoring stations was used in the regional soil moisture retrieval.

5.3.1.4 Canopy Temperature

Due to the difficulty of measuring the canopy temperature over large areas, it is common in passive microwave soil moisture retrieval studies to assume that this is equal to the air temperature and/or the soil surface temperature (Njoku et al., 1996a; Van de Griend et al., 2003). Since this is generally observed to be true at sunset and sunrise (Kerr et al., 2001). The NAFE'05 airborne observations were undertaken as early in the morning as possible possible while minimising the possible complications from dew, i.e., between 7:00A.M and 9:30AM. Consequently, canopy temperature was assumed to be the same as the 2.5cm soil moisture measurements.

The soil-canopy temperature differences were continuously monitored at various locations which represented the different vegetation types across the study area. This was undertaken using thermal infrared towers and near-surface soil temperature sensors installed at several depths. The sensor characteristics and locations of the towers have been described in detail in section 4.4.3. In summary, these stations included thermal infrared sensors mounted on 2m high towers pointing vertically down towards the vegetation canopy, with soil temperature sensors installed at three depths (1,2.5 and 4cm) within the infrared sensor's field of view. A total of four thermal infrared sensors were installed over different land covers: bare soil, lucerne crop, wheat crop and native grass. Figure 5.11 shows an example of the diurnal variation of soil and canopy temperature for the wheat field at the Merriwa Park experimental farm. As expected, the canopy temperature exhibited stronger daily variation than the near-surface soil temperature, being warmer during the day and colder at night. Thermal equilibrium between canopy and soil was reached at approximately 7:00A.M and 6:00P.M in the particular case of a wheat cover.

The differences between soil and canopy temperatures within the regional airborne observation window (7:00AM-9:30AM) are summarised for the four monitoring stations in Table 5.7. For the most common crop in the study area (wheat), differences were less than 3.2K, while for the native

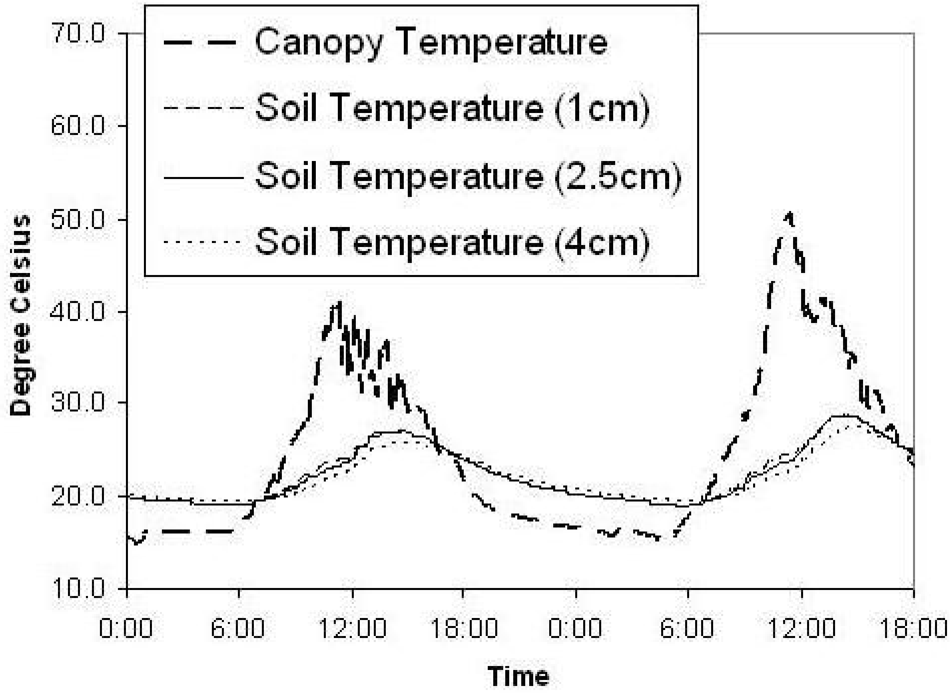

Figure 5.11. Example of diurnal cycles of thermal infrared canopy temperature and near-surface soil surface temperature at three depths. Data are from the thermal infrared station installed in the wheat field at Merriwa Park.

grass they could be up to 7.3K. It is notable how the differences changed appreciably going from wet (4K) to dry (11K) conditions (<20%v/v).

The sensitivity of the L-MEB soil moisture retrieval to differences between canopy and near-surface (2.5cm) soil temperature input was also tested, similarly to what was done for the 2.5cm soil temperature in the previous section, in order to estimate the impact of the assumption of soil-canopy thermal equilibrium. This was done by plotting the changes in L-MEB retrieved soil moisture due to changes in canopy temperature for land surface conditions typical of the study area: a grassland and a crop, with VWC equal to the average measured amount (respectively 0.4 and 2kg/m2). The results are shown in Figure 5.12. While a similar plot has been already presented in Figure 5.4, this plot shows the impact in greater detail. Here it can be clearly seen that despite differences between soil and canopy temperature of up to 11K in dry conditions, the impact on the soil moisture retrieval is small, yielding a soil moisture retrieval error less than 2%v/v. In

Table 5.7. Temperature difference (K) between the soil surface (average of the 0-5cm sensors) and the thermal infrared temperature on regional airborne observations dates for the four monitoring stations installed on. W=wheat, L=Lucerne, NG=Native Grass, and BS=Bare Soil. Empty cells are missing data due to instrument faults. The average of the soil moisture (SM, %v/v) recorded at the continuous monitoring stations is indicated for each day.

		Soil-Canopy Temperature Difference (K) at 7:00AM				**Soil-Canopy Temperature Difference (K) at 9:30AM**			
Date	**SM**	W	L	NG	BS	W	L	NG	BS
31/10	40.6	2.1	5.7	-	2.3	0.3	3.9	-	-0.7
7/11	35.1	2.5	3.7*	7.3**	1.8	-4.0	-3.3*	3.9**	-9.4
14/11	20.5	3.2*	6.3	-	0.2	-11.1*	-10.5	-	-14.3
21/11	10.8	2.3	-	6.2	3.8	-8.0	-	0.4	-4.1

**Data missing, value taken from ±1 day*

***Data missing, value taken from November 24th (mean SM=30%v/v)*

wet conditions, temperature differences of up to 3.2K for wheat crops and up to 7.3K for native grasses result in errors less than 1.2%v/v.

It has been shown therefore that the assumption of thermal equilibrium between soil and canopy, despite being not strictly correct, is not expected to produce errors in soil moisture retrieval higher than 2%v/v during the time window of regional airborne observations used here (7:00M.-9:30AM). The canopy temperature was therefore set as equal to the 2.5cm soil temperature when retrieving soil moisture estimates from regional airborne observation in the following sections.

In summary, the errors which will affect the regional soil moisture retrieval are: 1.5%v/v due to uncertainty in soil texture estimation, 2%v/v due to the assumption of uniform near-surface soil temperature and 1.2%v/v due to the assumption of thermal equilibrium between near-surface soil temperature and canopy temperature.

5.3.2 Airborne Data

Regional airborne observations were undertaken at 1km nominal resolution over the entire study area on October 31st, November 7th, 14th and

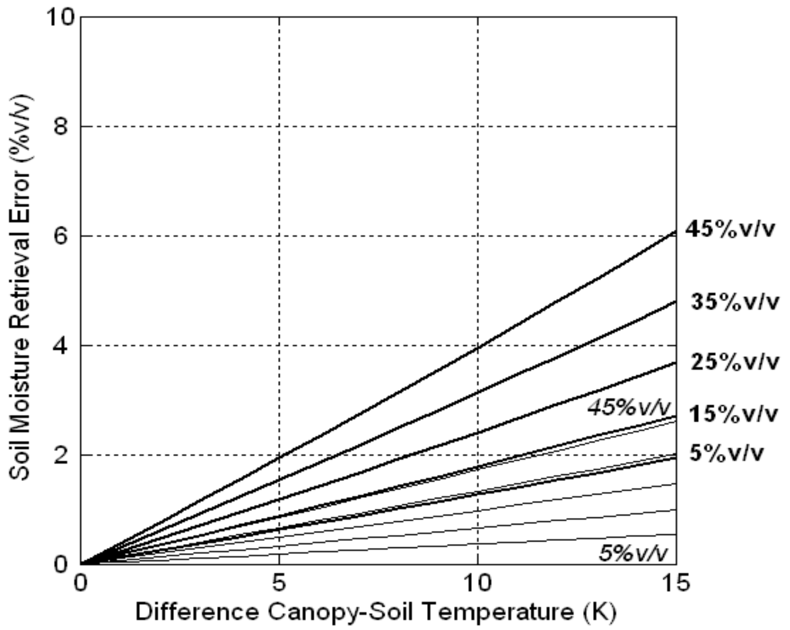

Figure 5.12. Sensitivity of the L-MEB soil moisture retrieval to absolute differences between canopy and near-surface (2.5cm) soil temperature for different soil moisture conditions. Cases considered are grassland (thin lines, italic labels) and mature crop (thick lines, regular bold labels).

21^{st}. The 40km-long, north-south oriented flight lines were flown at 10,000ft between approximately 7:00AM and 9:30AM. This time window was chosen as it is close to the SMOS overpass time (6.00AM), yet not expected to be complicated by dew, and therefore well replicates the mission soil moisture retrieval conditions. The radiometer was flown in 'pushbroom' configuration, yielding six across-track observations from each aircraft location. A full pixel overlap between adjacent flight lines was guaranteed in order to avoid data gaps and ensure full coverage of the entire area. The calibrated regional PLMR data were processed in the same way as the high-resolution data (see section 5.1.1), with a calibration error 1K at H polarisation and 2.5K for V polarisation (see Appendix A3).

In order to effectively use pushbroom radiometer data for soil moisture mapping, it is desirable to account for the effect of varying beam angles through a normalisation procedure and for the effects of varying soil temperature during the acquisition window which has been discussed in section 0. Once these two effects are taken into account, the T_B acquisitions can be gridded to a reference grid with uniform resolution. This is convenient since all the ancillary data to be used in the retrieval can be gridded to the same reference grid, and the soil moisture retrieval can then be performed for each cell of the grid. Moreover, by averaging several individual T_B acquisitions into one value of T_B for each cell, the signal noise is reduced. These pre-processing steps are described in the following sections before presenting the soil moisture retrieval.

5.3.2.1 Normalisation for Incidence Angle

It is well known that over a homogeneous bare soil target the measured T_B is affected by the viewing angle (Ulaby et al., 1986). This angular variation can be described by the Fresnel equations and differs depending on the land surface conditions. In previous studies using similar instrument designs (Jackson et al., 1999; Jackson, 2001), it has been shown that a normalisation procedures can be applied to mixed land covers. This procedure normalises the data to an equivalent angle of choice, by assuming that the deviation between beam positions is due to the Fresnel effect and calibration errors for individual beams, and that for a given day the Fresnel effect for a particular beam is approximately constant for the range of soil moisture and vegetation present. There are some circumstances when using a limited data set for this correction, say a single flight line, can lead to errors. This can occur when a land surface anomaly (such as a small water body in observed particular beam and not by the others. In the studies mentioned above it was assumed that by using a daily average for all data the area potential errors due to anomalies would be minimised. This assumption should be correct in the NAFE'05 study area, since there were no large water bodies or other features that exhibited significantly different microwave response.

With this assumption, a normalisation procedure was applied as follows:

- the daily average T_B was computed for all six beams;
- a reference beam was chosen to which all T_B observations will be normalised, representing a specific incidence angle; and

- a correction factor is computed for each beam by subtracting the reference average from each beam average. Since incidence angles of the six PLMR beams are symmetric with respect to nadir, the reference beam average is calculated as the average of all T_B observations taken by the two beams having the same incidence angle (e.g., ±38.5°).

All data from each beam on each day are then corrected using these correction factors as in:

$$T_{Bi}^{N} = T_{Bi} - (\overline{T_{Bi}} - \overline{T_{BREF}}), \tag{5.3}$$

where T_{Bi} is the individual T_B acquisition to be normalised, T_{Bi}^{N} is the normalised value, and $\overline{T_{Bi}}$ and $\overline{T_{BREF}}$ are the daily average T_B of respectively the beam to be normalised and the beam taken as reference.

Figure 5.13 shows the average T_B values for each of the six PLMR beams plotted for the study area on each date. The angular reflects the Fresnel effect. However, it can also be seen that the left beams (negative angles) recorded slightly lower T_B at H polarisation (about 3K). This is not visible at high T_B values (November 14th and 21st), and given that what is plotted in Figure 5.13 is the daily average of the T_B measured over the entire study area, it is unlikely that this was an effective difference in land surface emission observed by the different beams, pointing instead to a calibration problem. The anomaly in the 7° beam at V polarisation is related to a problem with loss of gain of the receiver after the factory calibration. This could not be fully corrected during daily calibration. However, an excellent symmetry about nadir was observed for all the other beams.

Before applying the normalisation procedures described above to the regional airborne observations, the procedure was tested using the multi-angle T_B observations made over the Merriwa Park farm at 250m nominal resolution on November 2nd, 9th, 16th and 23rd (see section 4.3.3.3). Since on

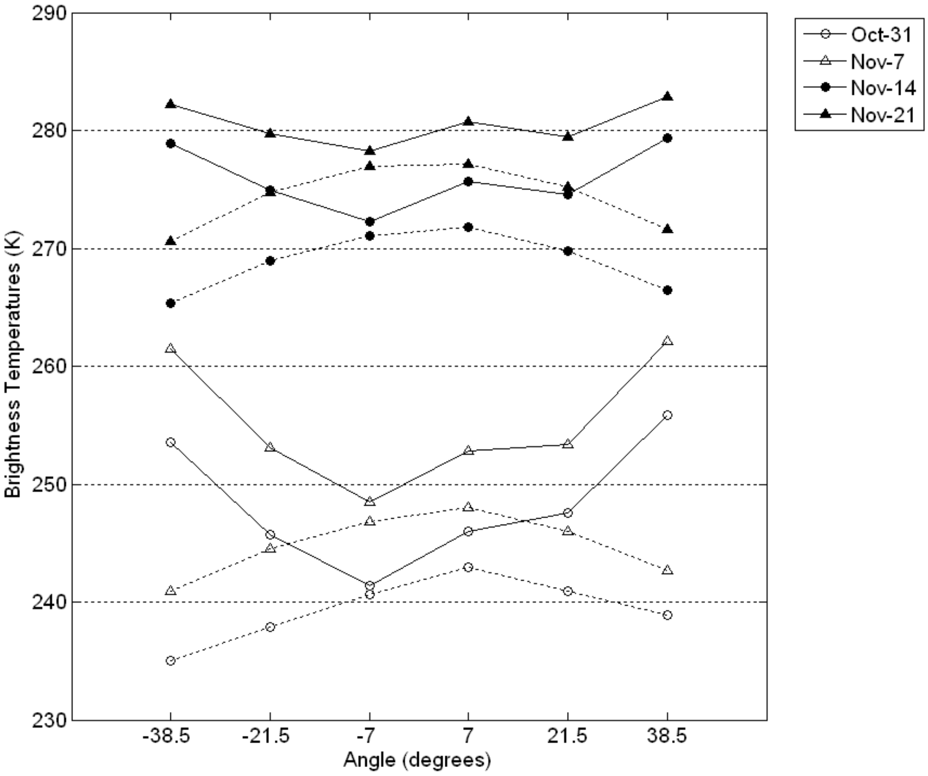

Figure 5.13. Daily average of PLMR 1km brightness temperature plotted versus angle at V (solid lines) and H (dashed line) polarisations (negative sign indicates left beams).

these flights PLMR was rotated by 90º with respect to pushbroom configuration, with the specific purpose to make multi-angular observations, every location on the farm was measured by all beams, therefore allowing a direct comparison between the T_B observations normalised to a particular angle using the procedure described above and the T_B observed at that angle. Two dates were selected for the analysis, a wet day (November 2nd, mean soil moisture 42%v/v) and a dry day (November 23rd, mean soil moisture 13%v/v). On each day three data sets were created by normalising the observations of each beam to the three reference angles of PLMR beams (±7º, ±21.5º and ±38.5º) using (5.3). Each normalised"data set was then compared with the direct T_B observations over the area from the reference beams. Results are shown in Figure 5.14, where the T_B normalised to each angle are compared with the T_B observed at that angle. Results indicate an

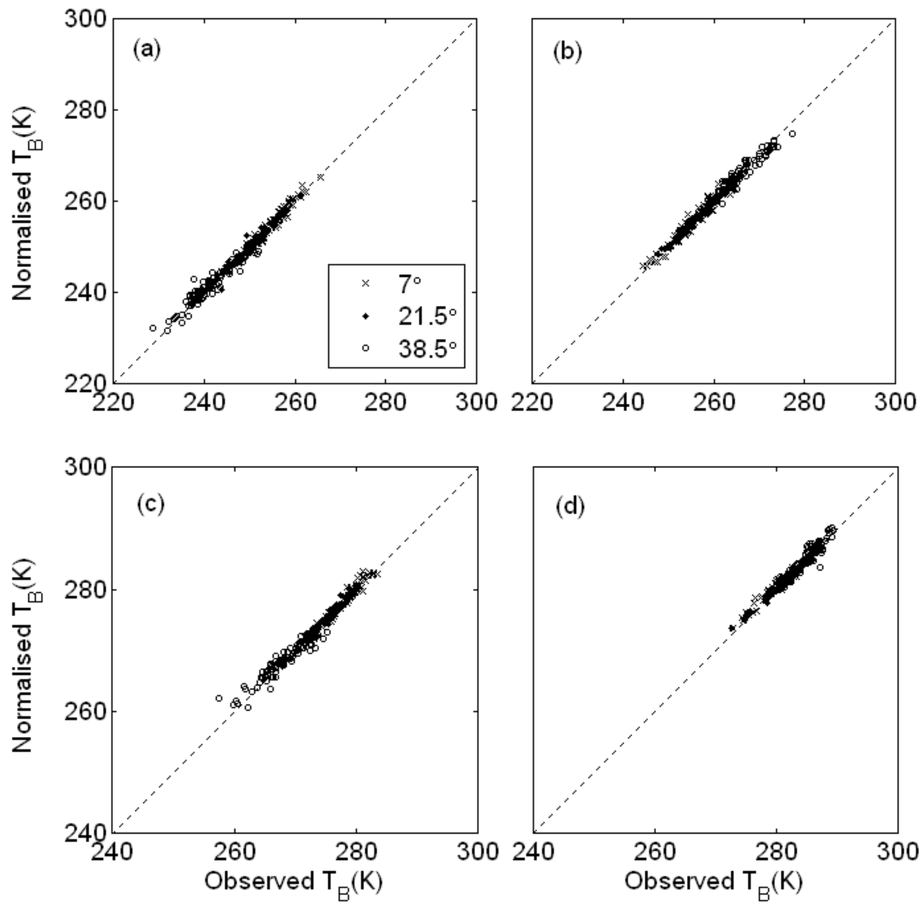

Figure 5.14. Comparison between normalised and observed brightness temperatures at Merriwa park on November 2nd at H (a) and V (b) polarisation and November 23rd at H (c) and V (d) polarisations.

excellent agreement between normalised and observed T_B, with a RMSE less than 1.5K in all cases. As a cross wind on the day forced the aircraft to fly with a small yaw angle with respect to the flight path, the areas covered by each individual beam did not exactly overlap in this comparison, potentially degrading the results.

This test showed that the normalisation procedures adopted can be used to produce T_B maps at a constant reference angle from pushbroom radiometer data using (5.3), under the assumption that for a given day the Fresnel effect for a particular beam is constant for the range of soil moisture and vegetation conditions present. The regional T_B observations were therefore normalised to the incidence angle of the radiometer outermost beams (±38.5°) using the procedure described above. This choice of angle was motivated by the fact that at close-to-nadir incidence angles the V and H-pol T_B values are very similar (see Figure 5.13), while at off nadir incidence angles V-pol T_B values are generally higher than H-pol values (this difference will vary depending on the land surface conditions). By using wider incidence angles, therefore, the retrieval accuracy of the L-MEB algorithm is improved since the polarisation difference yields information on the polarising effect of the vegetation canopy (Wigneron et al., 2000).

5.3.2.2 Normalisation for Soil Temperature

Airborne T_B observations were normalised to an intermediate reference time (8:00AM) using the temporal variation of the near-surface soil temperature recorded at the monitoring stations discussed in 0 and the radiometer time reference. Given that the effect of soil temperature on TB is linear (see radiative transfer equation (2.3) and Figure 5.10), the normalisation procedure was as follows:

- for each day, the average near-surface soil temperature between the stations was calculated for each logging time step (20min) between the start and end time of the regional airborne acquisition;
- a normalisation factor was then calculated for each time step as the ratio between the average soil temperature at 8:00AM and that at that time step, and
- each T_B acquisition was normalised to the reference time by multiplying the T_B value by the relevant normalisation factor, using the closest normalisation factor to the T_B acquisition time.

An example of the results of this procedure is shown in Figure 5.15 for November 14th. Despite the large variation of T_B due to spatial gradients, the original data show generally an increasing trend with time which is of the order of 5K, consistent with the observed average temporal increase of near-surface soil temperature for that day (see Figure 5.9). This trend is smoothed in the normalised data while the spatial gradients are maintained.

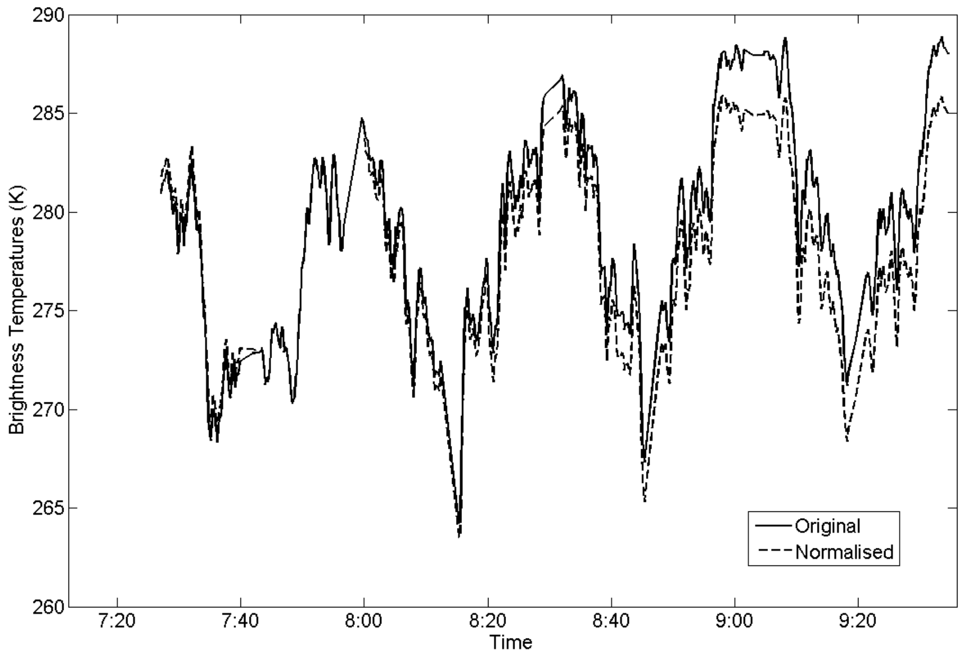

Figure 5.15. Example of normalisation of brightness temperatures for soil temperature temporal change. Shown are the original and normalised data for November 14th, V-pol (observations from all beams averaged every one minute for display).

This procedure produced T_B fields that were equivalent to those that would be observed at the reference time across the entire study area. The regional airborne observations normalised to the reference angle and reference time were then gridded to a regular 1km grid. Given the high rate at which individual TB acquisition were taken (0.6secs) by the instrument and the low aircraft speed (~50m/s, 180km/h), each 1km grid cell was greatly oversampled, with an average of 34±14 acquisitions falling in each 1km grid cell. Therefore a simple linear average was used to calculate a TB value for each grid cell. The TB maps of the study area have been already shown in Figure 4.3.

5.3.3 Soil Moisture Retrieval

Soil moisture was retrieved for each cell of the T_B grid using L-MEB together with the ancillary data described in section 5.3.1. Given the availability of two observations for each cell (V-pol and H-pol), a two parameter retrieval of soil moisture and vegetation optical depth was performed. The L-MEB vegetation-specific radiative transfer parameters for crop and native grass derived from the high-resolution sites (section 5.1 and 5.2) were adopted here, with the following considerations:

- all the crops in the study area were assigned the L-MEB default parameters for vertically dominated wheat-type crops. This was mainly motivated by the fact that a clear distinction between different crops could not be done based on the Landsat thematic map used to define land cover across the study area. Therefore, the parameters for the most common crop type in the area (wheat) were applied to all crops. In section 5.1.3 and 5.1.5 it was shown that the parameters for wheat apply well to other crops present in the study area, such as mixed wheat/barley and mixed oats/barley fields;
- all the native grass surfaces in the study area were assigned the L-MEB default parameters for surfaces with a litter layer (Saleh et al., 2007), as this parameterisation gave the most accurate soil moisture retrieval for most of the high-resolution native grass sites; and
- specific parameters for the Eucalypt forest present in the study area were those described in section 3.4.7, obtained by J. Grant (pers. comm.).

The L-MEB parameters used for each surface type are summarised in Table 5.8. Moreover, the following additional assumptions were made:

- the soil moisture output of the L-MEB algorithm was limited to a maximum soil moisture value of 58%v/v. This was derived from analysis of the maximum soil moisture achieved at the permanent monitoring stations (see Chapter 6), and matches well with the maximum porosity of the soils in the study area (determined by soil particle analysis), which was of 55% for the clay soils in the northern part of the study area. Conversely, no lower limit was imposed on the retrieved soil moisture;
- given the relatively small scale of the pixels (1km) each pixel was assumed to be uniform and covered by the land cover with the

Table 5.8. L-MEB surface type parameters for different vegetation covers. Native grass includes also 'bare soil' and 'woodland' classified pixels. θ is soil moisture. (*) the value of optical depth adopted is shown instead of that of parameter b.

Surface Type	H_R	Q_R	N_{RH}	N_{RV}	tt_H	tt_V	ω_H	ω_V	*b*
Crop	1.6-1.1*θ	0	0	-1	1	8	0	0	0.08
Native Grass	1.3-1.13* θ	0	1	0	1	1	0	0.05	0.12
Forest	0.12		0	0	0.46	0.46	0.07	0.07	0.57*

dominant fraction as calculated from the Landsat derived land cover map; and

- over forested pixels, retrieval of both soil moisture and the vegetation optical depth may be highly inaccurate, depending on the density of the canopy (i.e., the vegetation optical depth). It was therefore decided to constrain the retrieval by imposing the value of the vegetation optical depth calibrated with the detailed forest study by J. Grant (pers. comm.) (Table 5.8) and to retrieve only soil moisture. This is expected to yield a better soil moisture retrieval accuracy than the case in which retrieval of both soil moisture and vegetation optical depth was to be attempted over the forest.

The four maps of L-MEB retrieved soil moisture and vegetation optical depth for the NAFE'05 study area are shown in Figure 5.16. The spatial patterns can be interpreted using the spatial plots of ancillary data described earlier in this Chapter and summarised in Figure 5.17 for reference. The retrieved soil moisture shows interesting spatio-temporal dynamics. It reflects the temporal rainfall regime experienced by the area during the experiment, with wet conditions on October 31st and November 7th associated with the heavy rainstorms that crossed the study area at the beginning of the experiment (20mm over October 30th and 31st), followed by more intense rainfall on November 5th (21mm). The period between

November 5th and 23rd was characterised by little or no rainfall and accordingly drier soil moisture conditions were retrieved for November 14th and 21st.

The retrieved vegetation optical depth was more stable in time and less sensitive to the rainfall regime. This is expected as the optical depth is related to the water fraction of the plant biomass (or vegetation water content, VWC) and this should vary less in time (i.e. much slowly) than soil moisture, being biochemically linked to the plant matter. The daily average retrieved optical depth for crops and grasslands achieved a maximum of 0.19±0.05 on October 31st and a minimum of 0.15±0.05 on November 7th. This temporal variation is consistent with the variation of the ground measured VWC (to which optical depth is linearly correlated) at the high-resolution sites (see for example **Figure 4.11).**

The spatial distribution of the retrieved soil moisture across the study area shows a significant association with land cover and soil texture. In particular, the large forested area in the southern part of the study area exhibited drier conditions than the rest, while the cropped areas, more dense in the western part of the study area, maintained wet conditions throughout the month. This is consistent with the analysis of ground soil moisture data, which will be discussed in detail in Chapter 6.

The large native grass areas which cover the greatest fraction of the study area exhibited highly variable patterns where the influence of soil texture, and to a lesser extent topography can be identified; During the drydown period between November 14th and 21st, the southern part of the study area, which is characterised by a low flat plateau with sandstone derived soils, dried more quickly than the northern part, characterised by steeper hills and Black clay soils. This could be due to the higher water retention properties of the clay with respect to sandy soils, in addition to surface shading effects due to topographic aspect in the northern part, reducing evaporation.

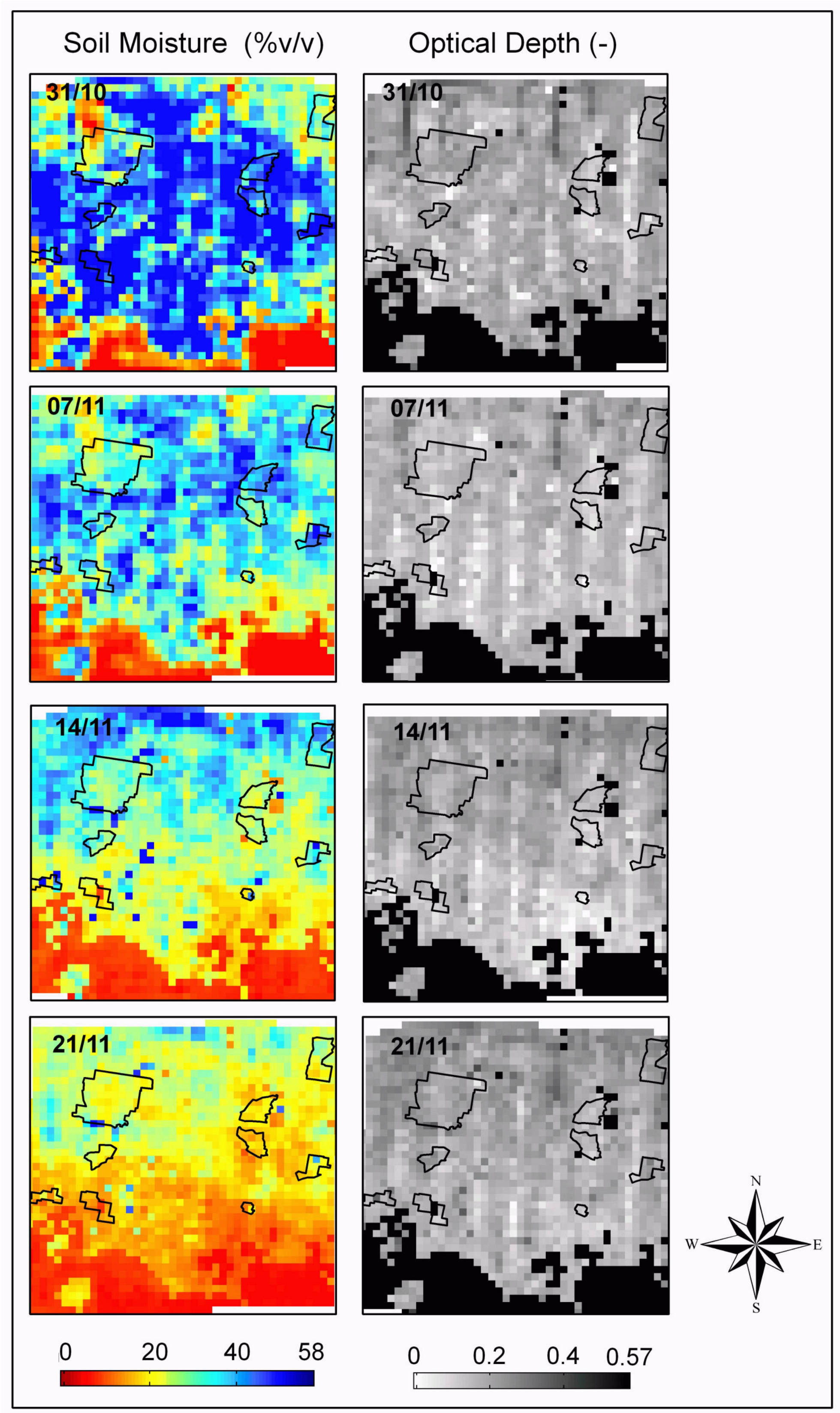

Figure 5.16. L-MEB retrieved soil moisture and optical depth from regional airborne observations (1km resolution). The boundaries of the experimental farms are shown with solid lines.

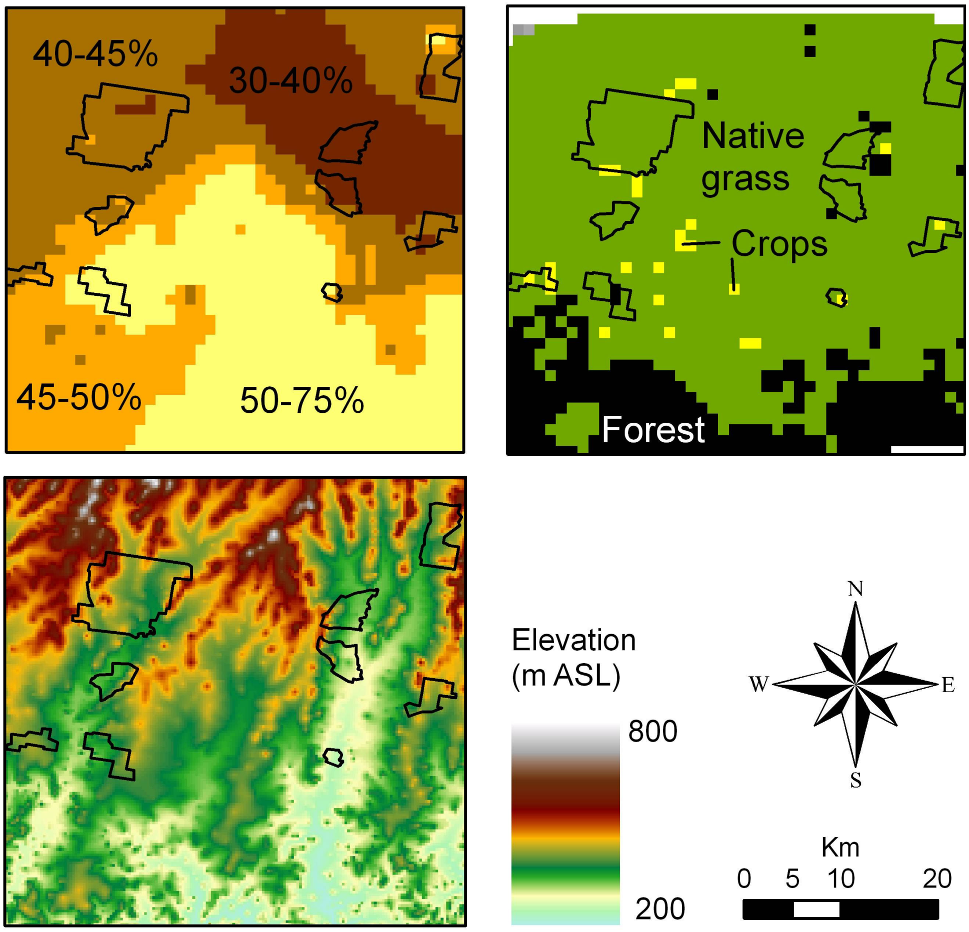

Figure 5.17. Spatial distribution across the study area of sand content (top left), Landsat land cover map (top right) and terrain elevation map (bottom right) of the NAFE'05 study area

The ability to observe these large-scale patterns in soil moisture demonstrates the utility of the regional soil moisture maps presented here, characterising the spatial distribution of soil moisture at a scale similar to that of typical satellite footprints. The daily statistics of the retrieved soil moisture are presented in **Table 5.9**, together with complementary statistics on the aircraft TB observations used for deriving this product. The average soil moisture conditions in the area decreased from 43.5%v/v (October 31st) to 14.0%v/v (November 21st), with the soil moisture standard deviation across the 40km x 40km study area decreasing from 14.1%v/v in wet

Table 5.9. Statistics of the regional L-MEB soil moisture product and ground soil moisture sampling. For each quantity on each date, average values are given as well as standard deviations across the study area.

Date	T_B (H)	T_B (V)	Retr. Soil Moist. (%v/v)	Retr. Opt. Depth (-)	Ground Soil Moist. (%v/v)	Rain (mm)
31/10	237.7 ±11.9	255.3 ±10.0	43.5 ±14.1	0.25 ±0.16	47.9 ±12.5	16.1 the day before
7/11	241.4 ±10.1	261.3 ±7.5	36.1 ±13.2	0.22 ±0.17	36.4 ±13.2	21.3 two days before
14/11	264.7 ±6.5	277.8 ±5.1	16.2 ±10.2	0.24 ±0.16	19.0 ±10.3	4.1 five days before
21/11	270.9 ±4.0	282.2 ±2.9	14.0 ±8.4	0.26 ±0.15	11.0 ±7.2	0 since the 14/11

conditions to 8.4%v/v in dry conditions. This data set is particularly interesting as it covers the full dynamic soil moisture range.

Table 5.9 presents equivalent statistics for the 2km-spaced ground soil moisture measurements collected on each regional observation day by the ground teams using the Hydraprobes. Given the point nature of the data and the distance between individual measurements, comparison with the L-MEB soil moisture product on a point-by-point basis is neither straightforward nor useful. The ground soil moisture data were mainly collected to analyse the large-scale soil moisture spatial variability as presented in Chapter 6.

The soil moisture variability within an area as big as an aircraft footprint (1km) can in fact be so high that the individual ground measurement are not typically representative at all of the surrounding areas, unless the sampling locations were carefully selected based on previous knowledge of the soil moisture variability within the area. Consequently a detailed analysis of the spatial variability of soil moisture within various 1km aircraft footprint was conducted using the high-resolution ground sampling data covering the experimental farms, collected concurrently with the multi-resolution flights during NAFE’05 (see Chapter 4). Although a detailed report on the results has been omitted here, it was found that that the soil moisture variance at 1km was typically of 13.4%v/v in wet conditions (November 8th) and 9.0%v/v in dry conditions (November 22nd). This is of the same order as the variability of soil moisture across the entire study area (Table 5.9), making it difficult to validate 1km retrieved soil moisture using one or two ground measurements falling within the footprint.

Nonetheless, the average of many such ground measurements across the entire area can be used as a rough check for the L-MEB soil moisture retrieval at 1km resolution which was properly evaluated at the high-resolution sites (see sections 5.1 and 5.2). The comparison of the L-MEB derived product and the ground measurements shows good agreement, both in terms of average soil moisture and standard deviation across the area. The overall difference between the two sources of soil moisture up exceeds 3.0%v/v only for the wettest day (4.4%v/v difference, October 31st).

5.4 Chapter Summary

This Chapter has presented an evaluation of the L-MEB radiative transfer model, core to the SMOS L2 soil moisture retrieval algorithm, for the specific land cover conditions in the NAFE'05 study area. The model has been evaluated using high (62.5m) and low (1km) resolution L-band observations at eight heavily monitored experimental farm in the study area. After evaluation of the model, high-resolution (1km) soil moisture maps of the entire study area have been produced.

Results have shown that the L-MEB model with its default values for the vegetation- and surface-specific parameters is suitable for soil moisture retrieval over the grass types in the NAFE'05 study area (maximum error 3.7%v/v). In the case of crops, the default parameters led to significant underestimation of soil moisture (between 10%v/v and 32.5%v/v). It was shown that the L-MEB default values of H_R are too low for the crops present in the study area (wheat, barley and oats). A linear soil moisture dependent parameterisation of H_R has been calibrated to achieve soil moisture accuracy better than 4.8%v/v for crop sites. This is consistent with previous results obtained using tower mounted radiometers both over grasslands and crops in Europe (Wigneron et al., 2001; Saleh et al., 2007) and is also in line with observations over the NAFE'05 study area by an independent study using the EMIRAD radiometer (Saleh et al., 2009). After site-specific calibration of the soil moisture dependent linear parameterisation of H_R, soil moisture has been retrieved with an accuracy better than 4.8%v/v at all the sites analysed except Midlothian (RMSE=7.4%v/v), which presented a unique type of crop, not present anywhere else in the study area.

This Chapter has also demonstrated the ability to retrieve soil moisture estimates at 1km resolution with an average soil moisture accuracy of 3.8%v/v and in all cases better than 6%v/v over a all the land surface conditions in the study area, including crop, grasslands and forest. The L-MEB model has therefore been used to produce soil moisture maps of the entire NAFE'05 study area from airborne data at 1km resolution. This soil moisture product has the advantage of overcoming the point nature and limited extent of traditional ground sampling techniques. Consequently, it will be used in Chapters 7 and 8 as soil moisture ground truth to address the problem of coarse-scale soil moisture retrieval from simulated satellite pixels in the presence of land surface heterogeneity.

Chapter Six

6 Land Surface Features Control on Soil Moisture Variability

This Chapter explores the spatio-temporal variability of near-surface soil moisture in the NAFE'05 study area using the ground-measured soil moisture data and information on land surface properties described in Chapter 4. The objective is to gain understanding of the land surface processes that dominate the control of soil moisture spatial variability in the study area at the scale of an L-band satellite footprint. This information will be crucial when analysing the error in soil moisture retrieval from simulated SMOS pixels induced by land surface heterogeneity discussed in Chapter 7. The results from this Chapter will also be used in conjunction with those from Chapter 7 to test alternative soil moisture retrieval approaches for SMOS in Chapter 8, which may reduce soil moisture retrieval by partially compensating for land surface heterogeneity.

In particular, this Chapter addresses the following questions:

- can spatial patterns of near-surface soil moisture be determined a-priori from spatial patterns of land surface features such as soil texture and/or land cover? And
- how does the role of these land surface features in determining near-surface soil moisture spatial distribution change in time and with spatial scales?

Initially, continuous point measurements undertaken at the monitoring stations throughout the NAFE'05 study area are analysed, providing insight to the temporal evolution of land surface control at discrete points. This is followed by an assessment of the spatial relationship between soil moisture and land surface factors using detailed soil moisture spatial monitoring data across the NAFE'05 experimental farms. Finally, the spatial relationship between soil moisture and land surface factors is analysed at the spatial extent of the typical satellite footprint, covering the wide range of land surface characteristics that characterise the NAFE'05 study area.

6.1 Data Overview

At a particular point in time soil moisture is influenced by: (i) the precipitation history, (ii) the texture of the soil, which determines its drainage rate and water holding capacity, (ii) the local topography, which affects runoff and infiltration, and (iv) the vegetation and the land cover type, which influence evapotranspiration and deep percolation. Moreover, rainfall spatial patterns and soil temperature differences due to local terrain aspects and its effect of the solar radiation at the surface are known to influence soil moisture.

The three ground data sets used in this Chapter to explore the spatio-temporal variability of soil moisture have been described in detail in Chapter 4 and consisted of (see also Figure 6.1):

1. a total of seventeen soil moisture monitoring stations operating during the NAFE'05 experiment, measuring soil moisture at 0-5cm depth through Stevens Hydraprobes (see section 4.4.2). Due to instrument faults, only eleven of those stations provided good quality and continuous data and are therefore used in this study;
2. spatially distributed soil moisture measurements at the eight experimental farms, undertaken on nested sampling grids with variable spacing, ranging from 6m in the center of the high-resolution area to 1km, over an area as big as 10km on each farm on sixteen dates; and
3. spatially distributed soil moisture measurements across the study area, undertaken at approximately 2km spacing on four dates.

6.2 Point-scale Variability

The available information on soil texture, topography, the land cover

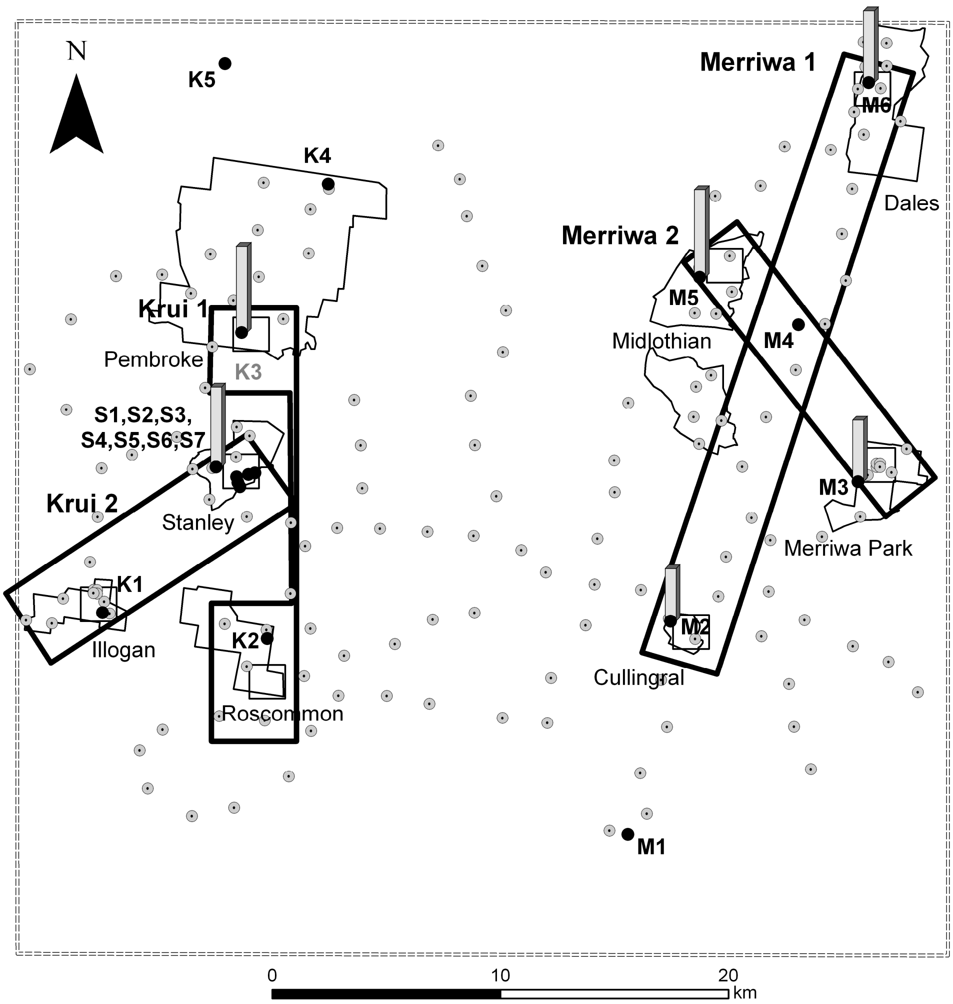

Figure 6.1. Layout of ground soil moisture measurements in the NAFE'05 study area. Permanent stations are indicated with gray circles and corresponding station ID. Farm boundaries and farm scale monitoring extent are shown in thin solid lines, while the grouping of the farms considered in the large satellite footprint scale analysis are indicated with thick solid lines. Gray points with black centre indicate the locations of the 2km-spaced sampling of the study area scale. Vertical bars indicate the relative amount of cumulative rainfall at each available rain gauge during the NAFE'05 period.

type and vegetation green biomass for each monitoring station is summarised in Table 6.1. Soil textural properties were derived from soil particle analysis of 30cm deep samples collected at each station. In this analysis the soil textural properties considered are the % sand and clay content. Topographic slope and elevation were calculated from a 250m DEM of the study area. As all stations for which continuous data are available were installed on grass fields, the effect of land cover type on the

Table 6.1. Land surface characteristics at the monitoring stations. *=data derived from a 250m resolution Digital Elevation model of the area.**=average of two MODIS 16-day reflectance at 250m resolution during November 2005."n/a" indicates rainfall data not available or incomplete due to instrument problems. The columns are ordered by ranking based on the value of mean relative difference described later in the section. The last column indicates the correlation coefficient between mean relative differences and each land surface property.

Station ID	**M2**	**S3**	**M3**	**S5**	**S4**	**S6**	**K3**	**S7**	**M6**	**M5**	**S1**	**r**
% Sand	94	31	21	12	32	31	6	32	31	10	6	-0.72
% Clay	0	41	36	46	16	41	71	16	51	69	54	+0.62
Elev. (m)*	261	412	423	378	454	405	419	432	394	365	329	+0.08
Slope (deg.)*	22	36	41	39	31	46	23	18	34	44	18	-0.08
NDVI**	0.60	0.56	0.60	0.52	0.58	0.52	0.74	0.53	0.62	0.57	0.56	-0.08
Cum. Rainfall (mm)	40	n/a	47	n/a	n/a	n/a	66	n/a	55	67	61.4	+0.76

soil moisture variability could not be analysed with this data set. It was investigated with the spatial soil moisture measurements later in this Chapter. In order to quantify the effect of vegetation on soil moisture variability the NDVI index was used. The NDVI index, proposed by Rouse et al. (1973), has been shown to be correlated with the "vigour" of the vegetation, in particular the live green vegetation (Ceccato et al., 2002; Jackson et al., 2004). NDVI values can range from 0 for bare soils to 1 to a very dense canopy. NDVI mapping of the study area was available from the MODIS sensor onboard the Terra and Aqua platforms as a 16-day composite product at 250m resolution. NDVI values were extracted for each station (see Table 6.1).

This data set encompassed a wide variety of conditions in terms of soil texture (from clay to sand), local terrain slope (from 20 to 46 degree slope) and topography (from relatively flat valley bottoms to ridge tops). The range of elevations (261m-454m) is relatively narrow compared to the overall range within the study area (180m-806m). Nevertheless, this data set is reasonably representative of the elevations observed in the study area as approximately 70% of the area falls within the range 297m-475m, with the exception of some mountain ridges in the northern part. NDVI values varied little across the sites and are overall in the 0.5-1 range, indicating fairly lush grasslands. Comparison of MODIS NDVI with the vegetation water content (VWC) samples taken throughout the study area indicated that these values of NDVI correspond to a VWC of approximately 0.5kg/m^2 for grasslands.

The time series of soil moisture recorded at the stations are plotted in Figure 6.2. Also plotted is the average cumulative precipitation recorded at rain gauges throughout the study area. Rainfall information has also been provided in Figure 6.1 to illustrate the spatial distribution of rainfall within the study area. A wide range of wetness conditions was encountered by all stations throughout the NAFE'05 period, since heavy rainfall delivered approximately 20mm of rain throughout the study area on October 30th and 31st, at the start of the experiment, followed by another rainfall event of approximately the same magnitude on November 5th and a few minor rainfall events (November 8th, 10th and 22nd). Significant increases in soil moisture were observed at all stations in response to these rainfall events, which maintained moderate to wet conditions throughout the study area during the first 10 days of November, followed by a gradual drying period from November 10th to November 22nd. While many of these stations were raised to about the same moisture content at the start of the experiment, the rate of decrease in soil moisture during the inter-storm periods was different between stations, reflecting different drainage and evaporative conditions associated with soil texture, topography and vegetation cover.

The variability of soil moisture observed across the stations at any instant in time was significant. This is shown in Figure 6.3 where the coefficient of

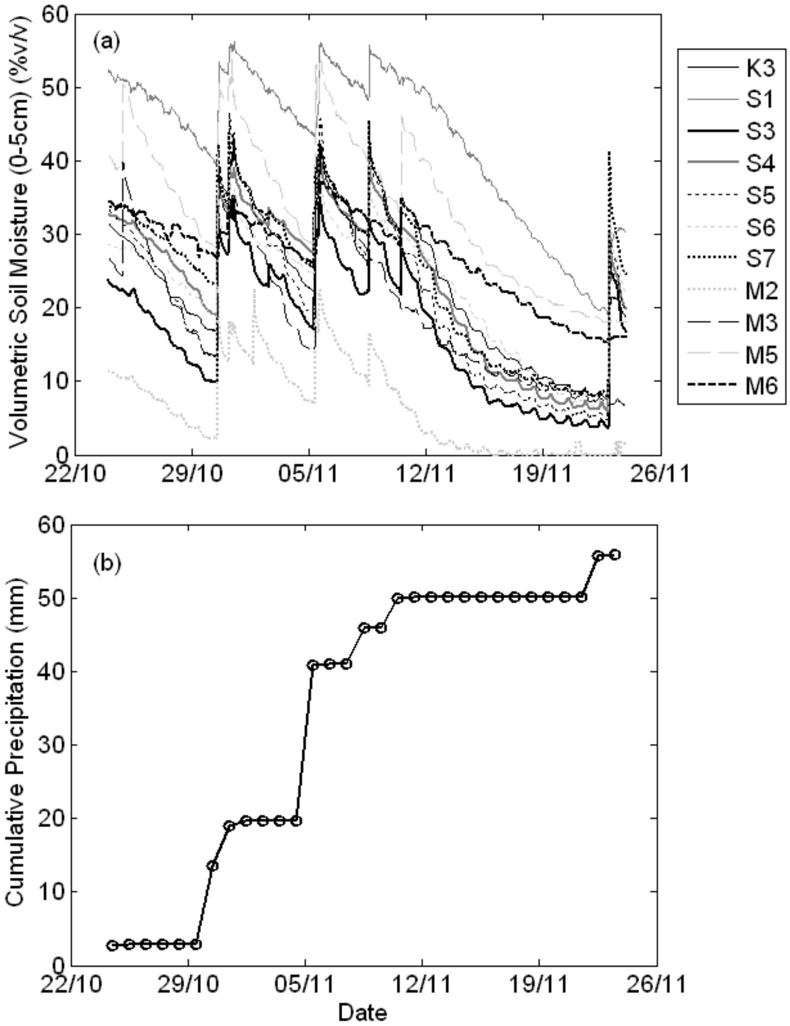

Figure 6.2. (a) Time series of 0-5cm soil moisture at the monitoring stations; (b) Cumulative precipitation (average of all rain gauges).

variation (CV) of soil moisture (defined as the standard deviation normalised by the mean across stations at any instant in time) is plotted against the mean soil moisture. In the figure a reference CV is also shown calculated using constant soil moisture standard deviations of 5, 10 and 15%v/v. The CV exponentially decreased as the mean soil moisture increased for intermediate to wet conditions, indicating that the scaled spatial variability was greater in dry conditions than in wet conditions. Note that different values of the CV are associated to the same mean soil moisture content due to different spatial distributions during wetting and drying phases, leading to different standard deviations. The CV reached a plateau in very dry conditions (less than 20%v/v), due to a decrease in absolute

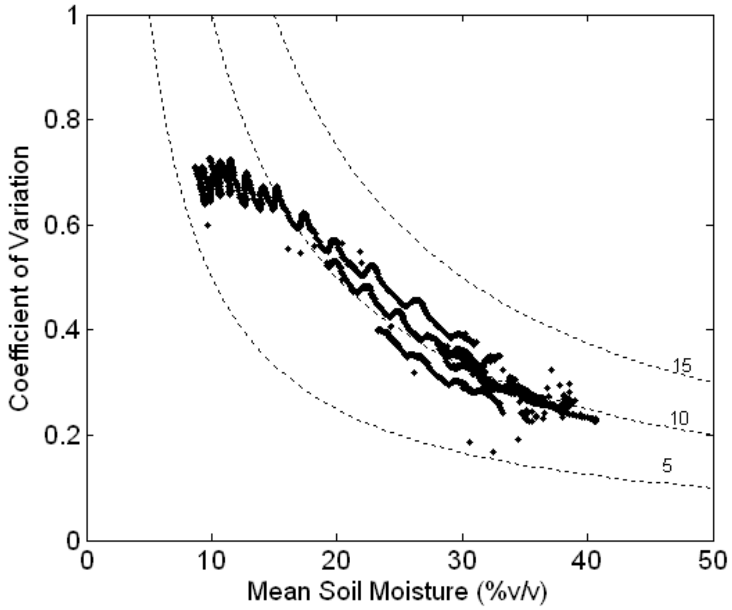

Figure 6.3. Relationship between mean 0-5cm soil moisture at the monitoring stations and coefficient of variation. The superimposed dotted lines show the theoretical relationship when using constant standard deviation values of 5, 10 and 15%v/v.

spatial variability. This result is consistent with previous studies at several US sites with similar soil moisture networks (Choi et al., 2007). However, the NAFE'05 soil moisture data encompass a wider range in soil moisture conditions and greater spatial variability (i.e., standard deviation) than in those watersheds, making this data set very suitable to analyse the relationship between the spatial distribution of soil moisture and associated land surface factors.

In order to gain insight into the sources of soil moisture spatial variability between the monitoring locations in the study area, temporal stability analysis was performed to determine which sites recorded consistently wetter or drier soil moisture conditions than the catchment average. These results were subsequently analysed in terms of the land surface characteristics observed at each site, in order to determine which factors were responsible for the observed deviation from the area-average conditions.

The term "temporal stability" was introduced by Vachaud et al. (1985) and has been further developed by Grayson and Western (1998). Temporal stability occurs if covariance exists between spatial pattern of soil moisture and a deterministic factor such as topography or soil texture. If this occurs, the soil moisture patterns are temporally stable (i.e., wetter locations are consistently wetter, drier locations are consistently drier). The mean relative difference is defined as:

$$\bar{\delta}_i = \frac{1}{t}\sum_{j=1}^{t}\frac{\theta_{i,j} - \hat{\theta}_j}{\hat{\theta}_j}, \qquad (6.1)$$

where $\theta_{i,j}$ is the jth soil moisture sample at the ith site of n sites within the study region and $\hat{\theta}_j$ is the computed soil moisture average among all n sites for a given date and time, j (j =1 to t):

$$\hat{\theta}_j = \frac{1}{n}\sum_{i=1}^{n}\theta_{i,j}\,. \qquad (6.2)$$

This variable directly measures how a particular site compares to the average of a larger region, whether it is consistently greater or less than the mean. Its standard deviation indicates how variable that relationship is. The mean relative differences of each station in the NAFE'05 study area are plotted in Figure 6.4 by rank (in order of mean soil moisture relative difference), with error bounds of one standard deviation of the relative differences. The data points of the plot can be interpreted in terms of the land surface characteristics of the stations shown earlier in Table 6.1, where the stations are listed in the same order as in Figure 6.4, based on the rank of mean relative difference (dry to wet).

Figure 6.4 shows that many sites were temporally stable in time (i.e., their relative difference has small standard deviation) and the watershed was highly temporally stable over this period. K3, a mid-slope location in the northwestern part of the study area with the highest % clay content recorded amongst the stations, had a mean relative difference close to zero and a small standard deviation, indicating a close correlation between K3 soil

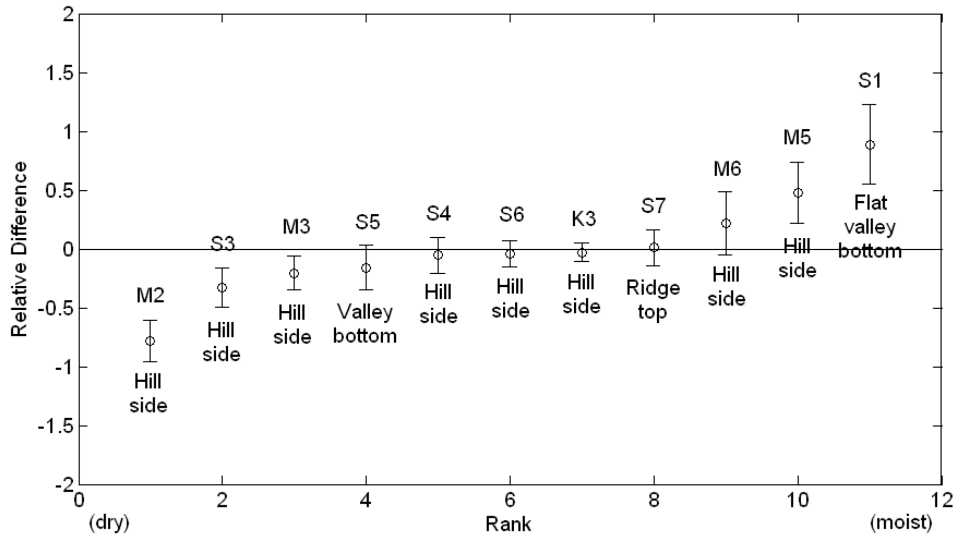

Figure 6.4. Mean and standard deviation of the relative difference of soil moisture recorded at each of the monitoring stations.

moisture conditions and the average of surface soil moisture across the entire study area. M5 and S1, clayey sites situated respectively on a hillside and at the flat outlet of a small watershed, both consistently overestimated the area-average conditions. On the contrary, M2, a mid-slope location in the southeastern part of the area with the highest sand content recorded amongst the stations, had mean relative difference that was lower than the area-average.

Weak or no relationship could be observed between mean relative difference in soil moisture and elevation or topography. This is indicated in the last column of Table 6.1 with the correlation coefficient between each land surface characteristic and the mean relative difference. A significant correlation was instead found between mean relative difference and soil textural properties (% sand and % clay content). Although these soil properties are somewhat correlated, they affect in a different way the hydrological properties of the soil: a high sand content determines high percolation rate and quick lateral and vertical drainage of the water through the profile, while higher % clay content means elevated water holding capacity of the soil during drying conditions.

This finding is significant in the context of this study, as it indicates that observed spatial patterns of soil moisture in the NAFE'05 study area can be connected to spatial patterns of soil textural properties. No correlation could be observed between mean relative difference and elevation, terrain slope, or NDVI. It has already been suggested that, while terrain attributes might play an important role when soil moisture variability is observed at the small scale (100m-1km) and during or immediately after storms, at larger scales (satellite footprint scale) they should be less important (Grayson et al., 1998; Kim et al., 2002b). Finally, the effect of vegetation cover, as quantified through the NDVI index, could not be explored very well in this case due to the small range in NDVI values across the stations and the fact that all stations had the same land cover type (native grass).

It is also evident in Table 6.1 that a strong correlation existed between the mean relative difference and the cumulative precipitation at the subset of stations where good quality and complete rainfall information was available (M2, M3, M5, M6, K3 and S1). Sites with higher cumulative precipitation tended to exhibit conditions wetter than the area-average. This is confounding as it partially explains the soil moisture difference observed between the sandiest site (M2) and the least sandy site (S1), which cannot therefore be solely attributed to soil texture differences. This will be further discussed later in this section. Moreover, given the high spatial and temporal variability in precipitation fields, rainfall is likely to introduce nearly random spatial variability in soil moisture conditions during and after rainfall events, limiting therefore the ability of this kind of analysis for determining land surface control on soil moisture variability.

In order to gain better understanding into the temporal variation of the correlation between soil moisture and land surface properties as well as into the relative importance of rainfall input and soil texture in determining soil moisture spatial distribution, the correlation between (i) the relative difference of soil moisture recorded at each station and the area-average, and (ii) the land surface properties was determined individually for each

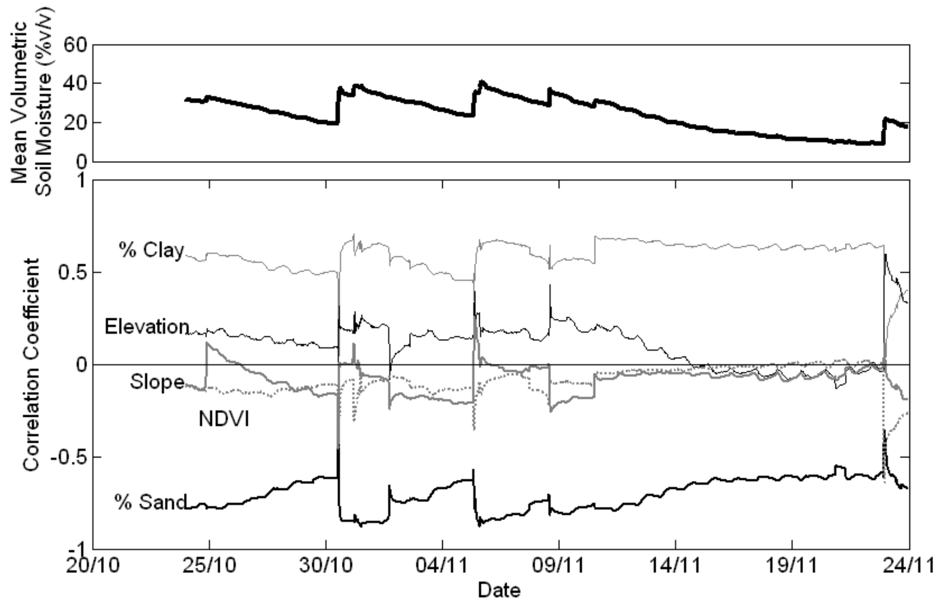

Figure 6.5. Temporal change of the correlation coefficients between soil moisture at the monitoring stations and relative difference for each date and time according to land surface features.

time step of soil moisture acquisition at the monitoring stations. The time series of the individual correlation coefficients with each land surface property are plotted in Figure 6.5. In this plot, a negative correlation coefficient means that an increase in that property is associated with soil moisture conditions drier than the area-average. A plot of the area-average soil moisture has been added at the top of Figure 6.5 to show the rainfall regime. Note that small-scale fluctuations in the values of the correlation coefficients are due to the small effect of daily soil temperature fluctuations on the soil moisture dielectric measurements. Several key observations could be drawn from this plot:

The observed correlation with sand content was dominant throughout the month, but more so in wet conditions. In dry conditions (after November 14th) this correlation decreased. The correlation with clay content, although slightly smaller than that with the sand content in wet conditions, was more persistent throughout the drying period and was the more important factor in dry conditions. This is likely to be associated with the greater water holding capacity of clay soils, which retain water for a longer period after rainfall.

As mentioned earlier in this section when discussing the mean relative difference analysis, the rainfall spatial distribution in the study area masked the effect of soil texture on the soil moisture distribution, as sites with higher sand content received overall a smaller amount of rainfall. In Figure 6.5 the persistence of the correlation between soil moisture and soil texture throughout the month, particularly after many days from the last rainfall event (e.g., after November 14^{th}) is notable. This supports the conclusions that soil texture is effectively the most important factor determining persistent spatial patterns of soil moisture in the study area, once the temporary effect of rainfall spatial distribution is exhausted. Even if during or immediately after storm soil moisture patterns are expected to be correlated with the spatial distribution of rainfall, in fact, during a long drydown period like that following November 14^{th}, the effect of the spatial distribution of the last rainfall event would get weaker until disappearing.

Little or no correlation was again observed with elevation, slope and NDVI, although some correlation with elevation was observed for the wet period in the first half of the month. This is likely to be due to the correlation between rainfall and elevation, which has been discussed earlier, as there is no other obvious reason why locations at higher elevation (and with generally smaller upslope drainage area) should be wetter than locations at lower elevation. Interestingly, in dry conditions the sign of the correlation with elevation inverted, indicating the tendency of higher elevations to produce drier areas (topographic effect).

The advantage of doing this type of analysis with continuously recording monitoring stations is that the effect of rainfall on temporal stability can easily be analysed. During, and immediately after storms, two important effects could be observed: (i) the correlations with sand/clay content decreased strongly, to be re-established within a time lag of 3-4hours and (ii) the correlation with elevation, slope and NDVI increased (correlation coefficients nearly doubles). This is die to several factors: (i) the soil texture is the main factor affecting drainage, but during rainfall events the hydrologic regime is dominated by the rate at which water is input at the soil surface, which is independent of soil texture, (ii) locations at higher elevations tend to receive more precipitation and therefore have wetter soils, (iii) steeper slopes determine quicker lateral flow which drains the surface layer at a higher rate, and (iv) denser vegetation cover intercepts more rainfall that will not reach the ground surface thus leaving the soil drier.

In summary this section identified sand content as the most important factor in determining spatial variability in soil moisture at spatial extents beyond 10km. Soils with higher sand content values tended to exhibit drier conditions than the area-average. Quantitatively, a difference of 88% sand content between two locations in the study area produced a soil moisture difference of 8.3%v/v on dry conditions of the area (5%v/v) and of 41.7%v/v on intermediate conditions (25%v/v). This finding is significant in the context of this study as it suggests that observed spatial patterns of soil moisture in the NAFE'05 study area can be connected to spatial patterns of soil textural properties. This correlation decreased strongly during and immediately after rainfall events (1-2days), when the influence of elevation, terrain slope and vegetation became sensible. After a long period of no rainfall, the clay content became the most important factor, determining wetter-than-average conditions.

The results discussed in this section have been limited by (i) the point nature and scarcity of the soil moisture measurements taken at the monitoring stations, which limited the ability of this kind of analysis to fully capture the large-scale variability in soil moisture within a typical L-band satellite footprint, and (ii) the fact that all the monitoring stations for which continuous data were available were installed at grass fields, limiting the possibility to investigate the effect of the land cover type on soil moisture variability. The spatially distributed soil moisture measurements collected during the NAFE'05 campaign are therefore used in the following sections to extend the results obtained thus far over the wide range of land surface conditions in the study area.

6.3 Farm-Scale Variability

6.3.1 High-Resolution Areas

Each of the eight, 150m x 150m high-resolution areas in the NAFE'05 experimental farms was specifically chosen to study the effect of a particular land surface property on soil moisture spatial distribution. However, the basis for area selection was limited to land cover type and topography, as only these properties could be readily assessed by visual inspection. The areas were chosen so that the other land surface properties could be considered uniform across the sampling area, and therefore soil moisture spatial variability could be directly associated to the variability of either the land cover type or topography. In the following discussion, the name of the experimental farm where the high-resolution area was located will be used to indicate the high-resolution area itself.

A detailed description of the high-resolution areas has been given in **Table 5.1**. Of the eight high-resolution areas, three cases were selected for analysis here:

- "Roscommon": A flat site characterised by uniform short grass and sandy soil, located in the south-western part of the study area in the Roscommon farm (see Figure 6.1);
- "Midlothian": A flat site characterised by a sharp contrast between a lucerne crop and a fallow field (respectively 70% and 30% of the high-resolution area), located in the north-eastern part of the study area in the Midlothian farm; and
- "Stanley": A hillslope site characterised by tall grass, located in the western part of the study area in the Stanley farm.

The Illogan and Pembroke high-resolution areas presented both mixed vegetation type conditions and micro-topographic conditions (e.g., a gully). Dales presented very similar conditions to Stanley, and therefore did not add extra information to this analysis. Merriwa Park presented uniform vegetation and a very gentle slope, making it unsuitable for analysis of the

Figure 6.6. Soil moisture patterns (% v/v) at the high-resolution areas during November 2005: Roscommon area (first row) Midlothian area (second row) and Stanley area (third row). The white cells in the bottom part of the Roscommon area on November 1st are missing data due to the suspension of the sampling during heavy rainfall. The double line in the middle row indicates the fence that separated the fallow from the lucerne field. The arrow in the bottom row indicates the maximum down slope direction.

topographic effect. Cullingral was a flat area with variable land cover type, but the two crops (wheat and barely) between which the high-resolution area was split comprised plants with very similar characteristics, which did not show in significant spatial variability. For the aboves reasons, although these areas were useful for the evaluation of the L-MEB presented in Chapter 5, they were not suitable for the current analysis of soil moisture spatio-temporal variability.

For all sites it was assumed that soil type is approximately uniform, i.e., soil type does not vary significantly over the 150m sampling distance. Moreover, the soil type for each site was determined from 30cm soil samples at the nearby monitoring station or, when the stations were too far from the high-resolution area, from 5cm soil samples taken at the closest sampling location of the 2-km spaced regional soil moisture data set (see section 4.4.1). There were not enough data to verify the assumption of uniform soil type within the 150m area.

An overview of the soil moisture spatial patterns collected weekly at the three sites during November 2005 is shown in Figure 6.6. Also indicated in the plots is the discontinuity in the land cover type for the Midlothian site and the direction of maximum slope for the Stanley area. Despite the large distance between the three sites (~10-20km), the three areas experienced similar soil moisture conditions, with wet conditions in the first two weeks followed by a drydown in the following two weeks. It should be noted that the patterns in Week 1, Week 2 and Week 3 were all between one and three days after rainfall events, while Week 4 sampling was at least five days after the last rainfall event.

The Roscommon control area exhibited very uniform soil moisture conditions, due to the absence of significant topographic relief and uniform land cover type. It should be noted that rainfall interrupted the sampling operations at Roscommon on November 1st, so only one-third of the high-resolution area could be sampled. Most notable is that the Midlothian area exhibited a significant soil moisture gradient at the boundary between the lucerne and fallow field, particularly in Weeks 2, 3 and 4, showing a vegetation control on soil moisture variability. This is further confirmed by the fact that the spatial variability within each field was smaller than the overall variability across the two fields. Moreover, the lucerne field, having denser vegetation than the fallow field, exhibited drier soil moisture conditions. In the case of the Stanley area, no soil moisture variability due to topographic relief was observed. The soil moisture distribution in the area was dominated by small-scale variability, not directly associated with the direction of maximum slope (i.e., lateral drainage), but most likely associated with very small-scale topographic relief (or surface roughness). This was confirmed by the standard deviation of surface heights measured with a pin profiler at the Stanley site, which was the highest recorded

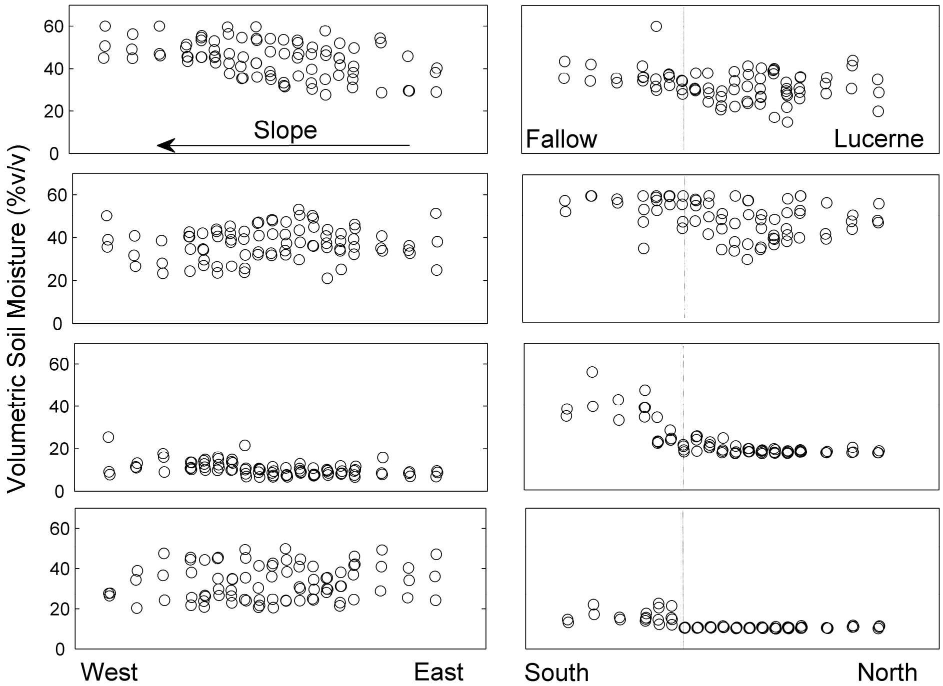

Figure 6.7. Soil moisture distribution along transects at Stanley (left panels, East-West transect) and Midlothian (right panels, North-South transect) for week 1-4 along rows. The arrow in the top left panel indicates the down slope direction

amongst the eight experimental farms (1.1cm as opposed to 0.8cm and 0.6cm at Midlothian and Roscommon respectively).

Volumetric soil moisture is plotted in Figure 6.7 along two transects (10m wide) oriented in the North-South direction at Midlothian (across the lucerne-fallow boundary) and in the East-West direction at Stanley (very close to the maximum slope direction). For Stanley the plot shows little correlation of soil moisture with the location along the hillslope, with slightly wetter conditions in the downward direction on week 1 and week 3. This was nevertheless masked by large variance of soil moisture at short distances. For Midlothian, a strong soil moisture gradient was associated with the boundary between the two fields. This became more evident in week 2 and 3 as the conditions became drier, and it was likely the result of the higher evapotranspiration from the lucerne field, accelerating the drying. Moreover, as already noted in Chapter 5, the fallow field had significant dead biomass at the surface. It has been already noted that this creates a

Table 6.2. Summary statistics of volumetric soil moisture at Roscommon (uniform), Midlothian (variable vegetation cover) and Stanley (micro-topography). Values of mean and standard deviation are in %v/v.

	Roscommon			
	01/11	**08/11**	**15/11**	**22/11**
Nr points	89	290	274	141
Mean	27.7	20.7	4.1	1.6
St. Dev.	5.7	3.0	2.4	1.4
Skewness	-0.032	-0.230	0.572	1.347

	Midlothian			
	02/11	**11/11**	**16/11**	**23/11**
Nr points	297	218	294	291
Mean	33.9	48.0	24.8	13.0
St. Dev	6.9	7.7	9.0	4.5
Skewness	-0.316	-0.346	1.227	2.705

	Stanley			
	03/11	**10/11**	**17/11**	**24/11**
Nr points	292	295	293	293
Mean	43.9	35.8	10.4	31.5
St. Dev	7.1	7.3	3.0	8.1
Skewness	-0.207	0.130	1.681	0.591

masking layer which can shade the soil surface and therefore keep it moist (Saleh et al., 2006a).

Statistical analysis of the four soil moisture maps for the three areas is summarised in Table 6.2. Overall, the Roscommon area showed very small variability (standard deviation in the table) and a relatively small skewness (asymmetry from normal distribution), as expected for a uniform soil moisture field. The standard deviation at Midlothian was significantly higher and increased in Weeks 1 and 2 to peak in Week 3 (November 16^{th}), when highest was the difference in soil moisture between the two fields (see

Table 6.3. Vegetation Water Content (VWC) measured from ground biomass samples collected at Midlothian (kg/m^2). Values indicated are the mean and standard deviation of eight samples or the mean of two samples when standard deviation is indicated as "N/A".

Date	Lucerne		Fallow	
	Mean	**Std. Dev.**	**Mean**	**Std. Dev.**
31/10	0.22	0.14	N/A	N/A
11/11	0.21	N/A	N/A	N/A
12/11	N/A	N/A	0.11	N/A
14/11	0.30	0.14	0.00	0.00
16/11	0.27	N/A	0.00	N/A
21/11	0.14	0.09	0.00	0.00
23/11	0.17	N/A	0.00	N/A

Figure 6.7). Stanley had also a significantly higher standard deviation than Roscommon, indicating strong spatial variability.

The impact of the vegetation cover on the soil moisture distribution at the Midlothian site was investigated through the VWC ground-sampled in both fields (Lucerne and fallow), taken as a proxy to the vegetation density and its impact on the soil moisture distribution. It should be noted that the fallow field had nearly always zero VWC, associated with the dead biomass at the surface. The results, shown in Table 6.3, highlights that the spatial variability of soil moisture was very well correlated with the VWC difference between the two fields, as this achieved a maximum on November 14th-16th, where the VWC of the Lucerne field was maximum. Although the connection between VWC and the physical interaction between the plant and the soil (water retention and extraction by the roots and shading of the soil surface by the foliage) are not entirely understood, in this analysis VWC seems to be a good indicator of the impact of the vegetation cover on soil moisture spatial distribution.

The soil moisture spatial distribution at Midlothian also showed the highest skewness amongst the areas, more so in intermediate and dry conditions (Weeks 2 and 3). To better understand the significance of this, histograms of soil moisture for all the areas were calculated (see Figure 6.8). The Midlothian area showed bimodality in Weeks 2 and 3, when the VWC

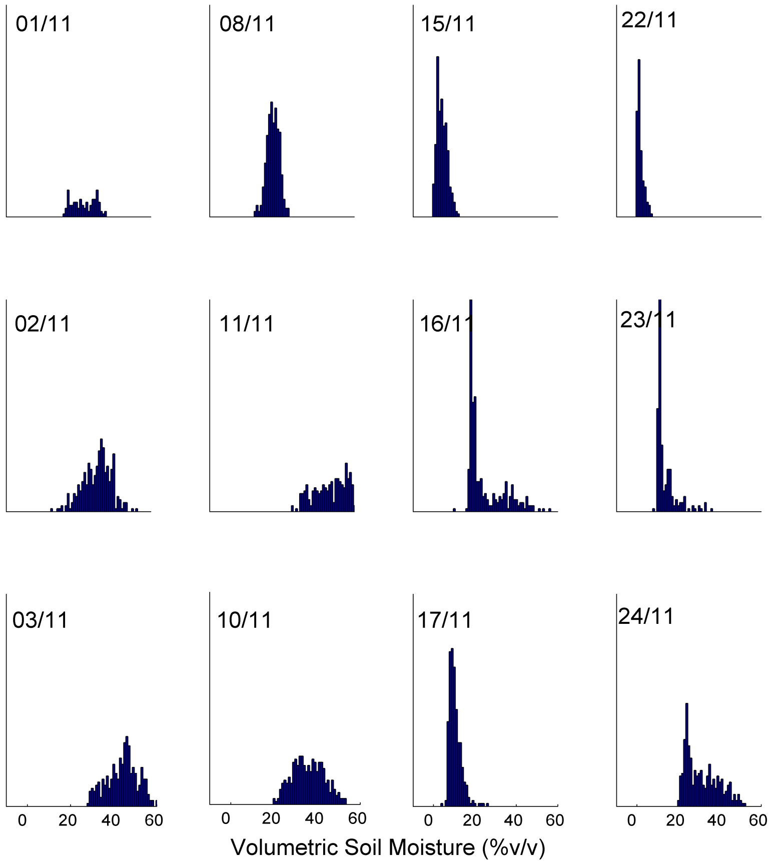

Figure 6.8. Histograms of soil moisture (% v/v) at the high-resolution areas: Roscommon area (first row) Midlothian area (second row) and Stanley area (third row).

of the lucerne field and the soil moisture spatial variability reached their highest values. In Weeks 1 and 2, with higher soil wetness and relatively small VWC values, the distribution was unimodal and the effect of vegetation variability on soil moisture distribution was not visible. Table 6.2 showed that Stanley had a significantly higher standard deviation than Roscommon. Nevertheless, analysis of the histograms revealed a unimodal distribution throughout most of the month. This confirms the absence of topographically driven spatial distribution, which would have resulted in at least two different modes (drier areas at higher elevation and wetter areas at lower elevation).

To further confirm these findings, semivariograms were calculated for each area and each day. The semivariogram is the expected value of the square of the differences of soil moisture between locations which are separated by a distance h. This is very effective tool for evaluating the two-dimensional spatial correlation structure of a soil moisture field. Following Matheron (1963), the semivariogram is calculated as:

$$\gamma(h) = \frac{1}{2N_P} \sum_{i}^{Np} \left[\theta(x_i) - \theta(x_{i+h}) \right]^2 , \tag{6.3}$$

where the γ values at distance h are known as semivariances. The volumetric soil moisture values, $\theta(x)$, are taken at pairs of sample points x_i and x_{i+h}, which are separated by a distance h for a total of N_p pairs of increments in two dimensions. For this application, the experimental semivariograms calculated with (6.3) were normalised by the total spatial variance of surface soil moisture for each day, in order to compare semivariograms for different days with different total field variances. The general shape of a semivariogram is an increase of the semivariance as the lag h increases, until a point beyond which this does not change anymore (the semivariance corresponding to this distance is called the “sill”). The distance h at which the semivariance becomes stable is called the “range”, and it is an approximation of the correlation length of the spatial field. Locations with distances higher than the range are considered uncorrelated, and if the semivariance sills to the total field variance, the field is defined as “spatially stationary” (it has a constant mean and variance for a certain distance h). The semivariance at short distances is called the “nugget”). The nugget is due to the variance of the measuring device as well as the variance of soil moisture at scales smaller than the minimum sampling space (6.25m here) which can not be resolved by the semivariogram.

The semivariograms for the three high-resolution areas are shown in Figure 6.9. One common restriction in semivariogram calculations is that the maximum separation distance should not exceed half the minimum dimension of the data field considered. Therefore the semivariograms shown in Figure 6.9 extend to 75m. Several key conclusions can be drawn from the plots. For Roscommon as well as for Stanley, the range was very small (of

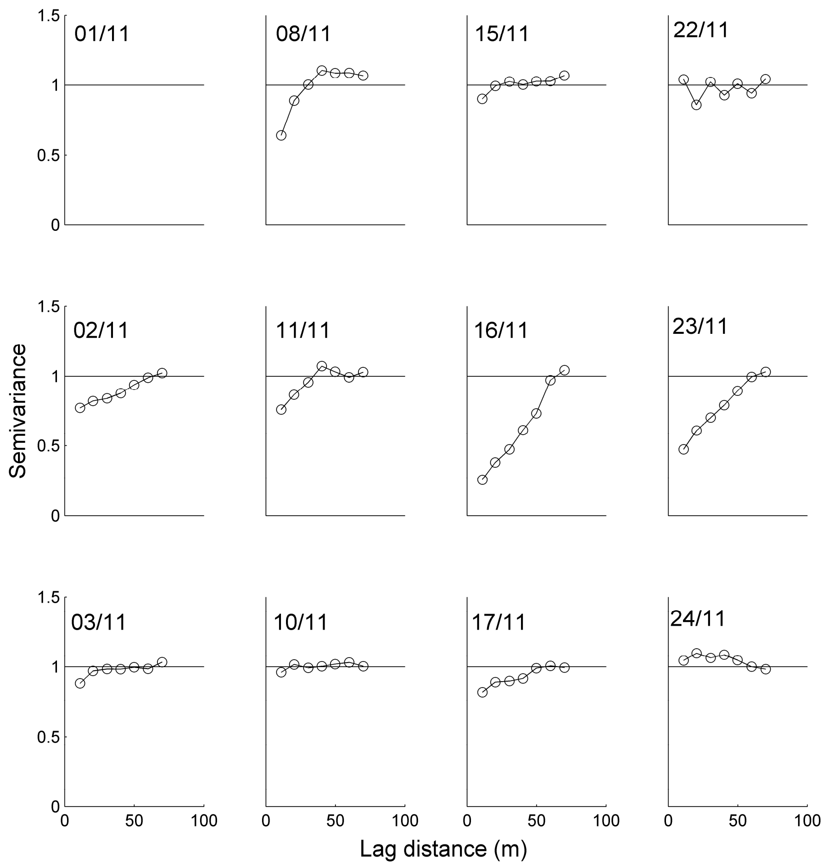

Figure 6.9. Semivariograms of the high-resolution areas by area and by day. Each semivariance value is normalised by the variance of the moisture field. Plots are for Roscommon area (first row) Midlothian area (second row) and Stanley area (third row). The semivariograms for Roscommon on November 1st is not shown due to the limited amount of data collected.

the order of 10m), and the field total variance was already achieved at distances smaller than 20m. Exceptions are Weeks 1 and 3 for Stanley, where the range slightly increased (up to 50m), probably due to the weak topographically driven soil moisture distribution already observed. Nevertheless, overall small-scale variability dominates the spatial distribution in both areas. In the case of Midlothian, the range was much greater than 10m, and more so in Weeks 2 and 3, in association with the higher soil moisture variability between the Lucerne and fallow fields observed earlier. This indicates that due to the discontinuity in the land cover type, the soil moisture field exhibited spatial correlation at larger scales than in the case of Roscommon and Stanley (>50m). In Weeks 3 and

4 at Midlothian, the nugget was also very small compared to the overall variance, indicating a relatively uniform spatial distribution within the lucerne and fallow fields at small scale.

In summary, this section has shown that strong soil moisture spatial variability can be associated with spatial variation in the land cover type. The case presented, of a lucerne field adjacent to a fallow field, showed that a difference in vegetation cover corresponding to a difference of approximately 0.3kg/m^2 in VWC could produce a soil moisture variability of up to 20%v/v, over an otherwise flat area with uniform soil type. This was particularly evident in drying conditions for soil moisture content below 30%v/v. However, the analysis of the soil moisture distribution along a 150m hill slope showed only a weak correlation between soil moisture and position along the slope. It was also noted that in the present case small-scale variability associated with surface roughness dominated the soil moisture distribution. Here the variability associated with topography was significantly less than the noise due to small-scale variability except in very dry conditions (10%v/v).

6.3.2 Experimental Farms

In this section the analysis of spatial variability in soil moisture is extended to the distributed soil moisture measurements undertaken across the broader area of the eight experimental farms. These measurements were undertaken on each farm on nested sampling grids with spacing ranging from approximately 6m in the center of the high-resolution area to 1km, over an area of at least 2km^2 (Cullingral farm) and up to 64km^2 (Pembroke farm) (see section 4.4.1). However, this analysis is limited to the areas covered by ground sampling with spacing smaller than 125m, which ranged between 0.5 and 3km^2 in size, depending on the farm. The reason for this choice is that the spatial resolution of the ancillary data used to characterise the impact of vegetation and topography on the soil moisture distribution was 250m for both MODIS NDVI and the DEM of the study area. Therefore, if ground soil moisture data with spacing larger than 125m had been included, the analysis would have been affected by the measurement uncertainty that occurs when only one ground point is used to characterise the wetness conditions of a 250m x 250m area. As shown in section 6.3.1, a strong variability of soil moisture can exist even over such a short distance. Limiting the analysis to 125m resolution ensured that every DEM and NDVI pixel was compared with at least four soil moisture measurements, hence reducing the uncertainty due to variability of soil moisture at scales smaller than 250m.

Since terrain elevation alone is not always suitable to characterise the impact of topography on soil moisture distribution, a Compound Topographic Index (CTI) was also calculated from the 250m DEM. The CTI is a steady state wetness index (also named Topographic Wetness Index) and it is a function, at any given location in the landscape, of both the slope and the upstream contributing area per unit width orthogonal to the flow direction as per (see also Koster et al., 2000):

$$CTI = \ln\left(\frac{\alpha}{\tan\beta}\right), \qquad (6.4)$$

Where the term α is the upstream area that contributes flow, and β is the local topographic slope. Locations higher values of CTI will have greater upslope area and smaller slope. This is in general associated with valley bottoms, where the convergence of subsurface flow is known to maintain moist conditions (Beven et al., 1979; Grayson et al., 2001

In order to investigate the relationship between soil moisture and land surface features, all data were interpolated to the 250m DEM grid, and the average of the ground soil moisture measurements within each grid cell calculated. The correlation coefficients between soil moisture and the land surface features (elevation, CTI, NDVI, and % sand and clay content) were then calculated individually for each farm and each monitoring day, and their variation in time analysed.

It should ne noted that, although the nominal maximum spacing of the ground soil moisture sampling was 125m, in reality this was variable and sometimes higher than that, due to problems with access to certain locations by the sampling teams. Consequently, only pixels which contained at least four ground points were considered in this farm-scale analysis, in order to guarantee accurate ground sampling of each pixel. It should also be noted that while NDVI and topographic attributes are available at a 250m resolution soil texture was only available the locations where gravimetric samples used for soil texture analysis were collected (over an irregular, 2km spaced grid, see **Figure 5.8).** Therefore, interpolation at 250m resolution of soil texture data may have introduced uncertainty in soil texture estimation. So rather than interpolate the soil texture data, it was decided to include in the correlation analysis only those 250m pixels for which a gravimetric soil texture sample had been obtained, assuming that the sample was representative of the 250m x 250m area. Consequently, the correlation between soil moisture and soil texture was determined with a significantly lower number of points than that with NDVI and topographic attributes. However, in order to keep a statistically significant number of data points, all pixels were considered in the case of soil texture (i.e., even those with only one ground soil moisture measurement).

An example of the correlation between soil moisture and elevation, CTI, NDVI, and % sand and clay content is shown in Figure 6.10 for the Dales farm. This was a 2km x 2km area situated on a steep hill slope culminating a ridge top, covered with uniform native grassland. Here soil moisture exhibited a significant correlation with elevation, with decreasing soil moisture values at increasing elevation. The correlation persisted to November 11th after a rainfall event on November 9th wetted the area (see Figure 6.10, panel a), and was mantained throughout the following drydown until November 18th. Soil moisture exhibited a significant correlation with the sand content on wet conditions (November 4th and 11th, panel d). However, differently than what observed when analysing the monitoring stations (see section 6.2), the correlation here was positive, indicating wetter conditions associated with higher sand content. Detailed analysis of the data points on November 4th and 11th revealed that these corresponded to four

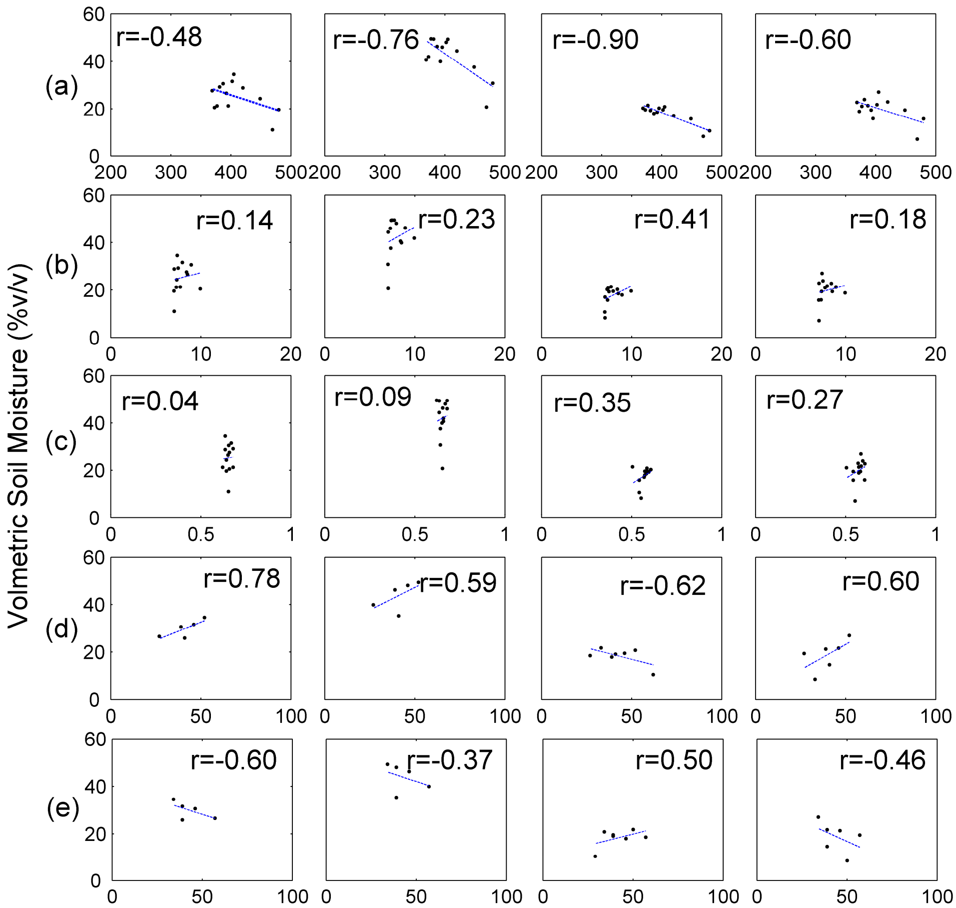

Figure 6.10. Scatter plots and correlation coefficients between ground measured soil moisture and (a) Elevation (m), (b) Compound Topographic Index, (c) NDVI, (d) % sand and (e) % clay content at the Dales farm on November 4th, 11th, 18th and 25th (left to right). The linear regression for each day and each data set is shown with a blue line, and the correlation coefficient for each regression is indicated in each box.

soil texture measurements very close to each other (~150m). It is possible that small-scale variability of soil moisture affected these results.

No significant correlation was observed between soil moisture and CTI (panel b), indicating that the CTI might not be an efficient wetness index when dealing with such a shallow soil layer (5cm) as that considered here. Moreover, the basic assumption of steady state on which is based might not apply to the NAFE'05 observation period, which was characterised by several rainfall events (see section 6.2). Consequently, the CTI index was not considered further in this analysis. No correlation was also observed between soil moisture and vegetation NDVI (panel c). It should be noted, however, that the range of NDVI values exhibited by the uniform grassland cover at this farm was very narrow (see Figure 6.10).

The correlation coefficients were calculated for all the four monitoring days on each farm. Temporal series of these coefficients are shown in Figure 6.11. Also plotted on this graph is the area mean soil moisture content to indicate the wetness regime. Overall, soil moisture exhibited a strong correlation with elevation. This was observed for the Cullingral, Merriwa Park, Dales and Stanley areas, which all have a significant relief (~100m). Of these, Dales and Stanley had very small variability in NDVI values, while Merriwa Park and Cullingral had a significant range in NDVI values (0.4-0.7), indicating significant variability in vegetation density across the farm. However, in both cases soil moisture was more strongly correlated with elevation than with NDVI, indicating a dominant role of topography in soil moisture distribution at this scale.

The correlation between soil moisture and elevation was observed to peak at intermediate wetness conditions (15-35%v/v from November 9th to 22nd). In these conditions, a relief of approximately 100m produced a difference in soil moisture of 15-20%v/v for Merriwa Park, Stanley and Dales, and a difference greater than 30%v/v between the hillside and valley bottom at Cullingral. It is to be noted that, in contrast to the results of the analysis of the monitoring stations, soil moisture was observed here to be inversely correlated with elevation (i.e. drier conditions at higher elevation, while at the large scale of the monitoring stations wetter conditions were associated with higher elevations). This is more in line with previous studies (Grayson et al., 1997b; Western et al., 2004), and indicates that while at the farm scale the effect of elevation on soil moisture is associated with drainage from upslope areas to downslope areas (which is more pronounced during inter-storm periods), at larger scales the effect of elevation is more associated with its impact on rainfall patterns, determining wetter conditions at higher elevation. This was confirmed by the rain gauge data, which showed higher cumulative precipitation at higher elevations.

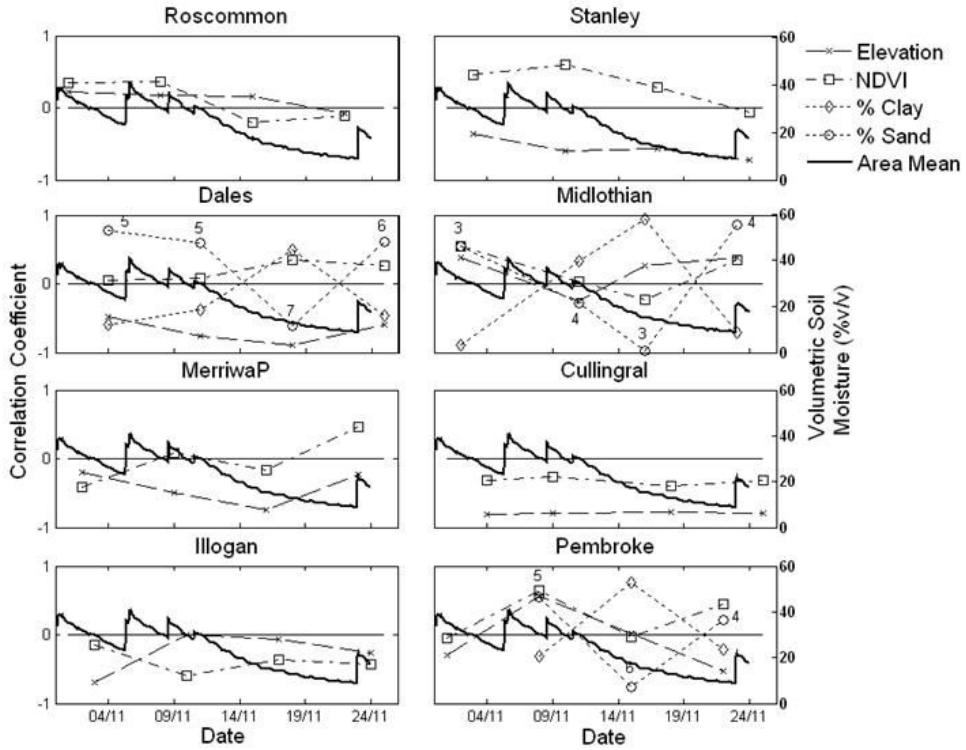

Figure 6.11. Time series of correlation coefficients between soil moisture and elevation, NDVI and soil texture (left axis) in the NAFE'05 experimental farms. On the right axis the temporal variation of mean soil moisture over the entire study area is plotted. Correlation with sand and clay content is shown only in the cases where a sufficient number of data points were available for calculation of the coefficient. The numbers on the sand content data points indicates the number of pixels available for calculation of the correlation coefficients.

The correlation of soil moisture with NDVI exhibited strong variability. It is worth here to limit the discussion to those farms with a significant range in NDVI values (i.e. Midlothian, Merriwa Park, Cullingral and Illogan), because in the other cases the narrow range of NDVI makes the calculation of the correlation coefficient less reliable. These farms all presented a mix of native grass and cropped areas. Moreover, Illogan was a highly cropped farm with strong variability in NDVI (0.5-0.8, corresponding to a range of vegetation water content of 0.5-3kg/m^2) and a very small relief (30m). This was in fact the only case in which soil moisture exhibited higher correlation with NDVI than with elevation, with drier soil associated with higher NDVI values (more "vigorous" vegetation). Despite the wide range of vegetation conditions, however, the resulting soil moisture variability appeared relatively small, with a 10%v/v soil moisture variation on November 10th, where the correlation with NDVI was highest. In all the other cases presented, the correlation with NDVI was found to be small and highly variable in sign. When compared to the soil moisture differences between the lucerne and fallow fields in section 6.3.1, these results suggest that the presence/absence of vegetation, i.e., the land use distribution, might be a more important control on soil moisture than the “vigor” of the vegetation growth (associated with NDVI).

Despite the small number of soil texture data points available, the correlation of soil moisture with soil texture showed consistent results. However, the only farms at which a sufficient number of data points were available were Midlothian, Dales and Pembroke. Of the other farms, Cullingral was the only farm with some soil texture data points, but too few to be used here for correlation analysis. They were nevertheless considered in the large-scale analysis presented in the next section. Of the three farms with usable data, Dales and Pembroke were characterised by significant variability in soil texture (30-50% sand content), while Midlothian had a narrow range (25-35% sand content) and a smaller number of soil texture data points available. However, for these three farms soil moisture exhibited a significant correlation with the sand content, which changed from positive during wet conditions (wetter soil associated with higher sand content) to negative during drying conditions (drier soil associated with higher sand content). A positive correlation was again observed after the rainfall on November 22nd. This is in contrast with what was observed at the large scale (monitoring stations), where drier soils were consistently associated with higher sand contents. However, the analysis of the monitoring stations also showed that the effect of sand content on soil moisture variability during the wet period until November 11th was confounded by other factors which had a non-negligible impact (NDVI and elevation, see Figure 6.5). The confounding effect of these other factors could therefore be the reason for the observed positive correlation between soil moisture and sand content during this period at the three farms. During the drying phase after

November 11th, instead, sand content became dominant in determining spatial distribution, hence the expected negative correlation. Although relatively narrow, the range of sand content at the Dales and Pembroke farms (30-50%) determined significant soil moisture variability (15-30%).

In summary this section identified elevation as the most important factor in determining spatial variability in soil moisture at spatial extents up to 3km^2. Soil moisture was observed to be inversely correlated with elevation, i.e. drier conditions at higher elevation, and to be a more dominant control than vegetation "vigorous" growth (i.e., NDVI). Morevoer, soil moisture exhibited a significant correlation with soil texture (% sand and clay content) which was predominant on the topographic effect during drying conditions.

6.4 Satellite Footprint Scale Variability

While the analysis conducted to this point has provided insight into the factors determining soil moisture spatial variability through time and over spatial extents smaller than 3km^2, the primary objective of this Chapter is to determine the controls on soil moisture spatial variability within a typical L-band satellite footprint, i.e. up to 40km. Therefore this section expands the analysis to an area of 40km x 40km by simultaneously using all the spatially distributed soil moisture measurements made from different farms on the same day. Moreover, the regional soil moisture sampling undertaken on four occasions across the entire study area are also analysed.

6.4.1 Direct Correlation Analysis

The eight experimental farms were grouped into four different ways (see Figure 6.1): two in the Krui subcatchment ("Krui 1" and "Krui 2") and two in the Merriwa subcatchment ("Merriwa 1" and "Merriwa 2"). The rationale behind this division is that each of these areas included two farms approximately 10-30km apart, simultaneously mapped on the same day by separate teams in a consistent manner. Consequently these areas represent landscape units with defined characteristics in term of topography, vegetation, soil texture and rainfall regime. Each area was originally to be ground-monitored on four occasions during the month. However, for logistical reason, in the case of Merriwa 1 and Merriwa 2 only three simultaneous mappings of soil moisture were obtained using the groupings identified for were sampled in their entirety only three times.

The land surface characteristics for each area are summarised in Table 6.4. Merriwa 1 is the area with the largest distance between the two farms (25km), and is also characterised by the largest range of elevations (214m) and soil texture (34% range in sand content). It is therefore most representative of the variability that is to be expected across the 40km x 40km study area. Note that this is also the only area where soil texture data points were available at both farms in sufficient number for correlation purposes. The other three areas present limited variability in land surface conditions, had a much smaller spatial extent and not enough soil texture data points to carry out a comprehensive comparison of the correlation between soil moisture and the land surface features considered here. With a procedure identical to that used for the farm-scale analysis, the temporal variation in correlation coefficients between soil moisture and the land surface features (all gridded to the 250m DEM reference grid) were calculated individually for each area (see Figure 6.12).

In the Merriwa 1 area soil moisture exhibited stronger correlation with soil texture than with elevation or NDVI. This was not true for the third day, November 25th, which was proceeded by a significant rainfall event. These results are consistent with the analysis of station data, where at large spatial extent (>10km) soil moisture variability was observed to be mostly correlated with the % sand and clay content, with this correlation decreasing significantly during and after rainfall events. A soil moisture variability of over 30%v/v was produced in the Merriwa 1 area by a range of sand content of 34%. This variability is higher than that observed at the farm scale (15-30% for a sand content range of 30-50%) but consistent with that observed at the monitoring stations (30.4% soil moisture difference induced by a difference in sand content of 25%).

Table 6.4. Land surface properties of the large scale areas.

Area	**Extent (km)**	**Elevation (m)**			**NDVI**			**% sand**		
		Mean	**St.Dev.**	**Range**	**Mean**	**St.Dev.**	**Range**	**Mean**	**St.Dev**	**Range**
Krui 1	15	400	22	83	0.6	0.1	0.3	33	7	17
Krui 2	8.5	391	24	91	0.6	0.1	0.4	29	5	14
Merriwa 1	25	316	68	214	0.6	0.1	0.4	41	11	34
Merriwa 2	11	386	43	120	0.6	0.1	0.4	34	8	20

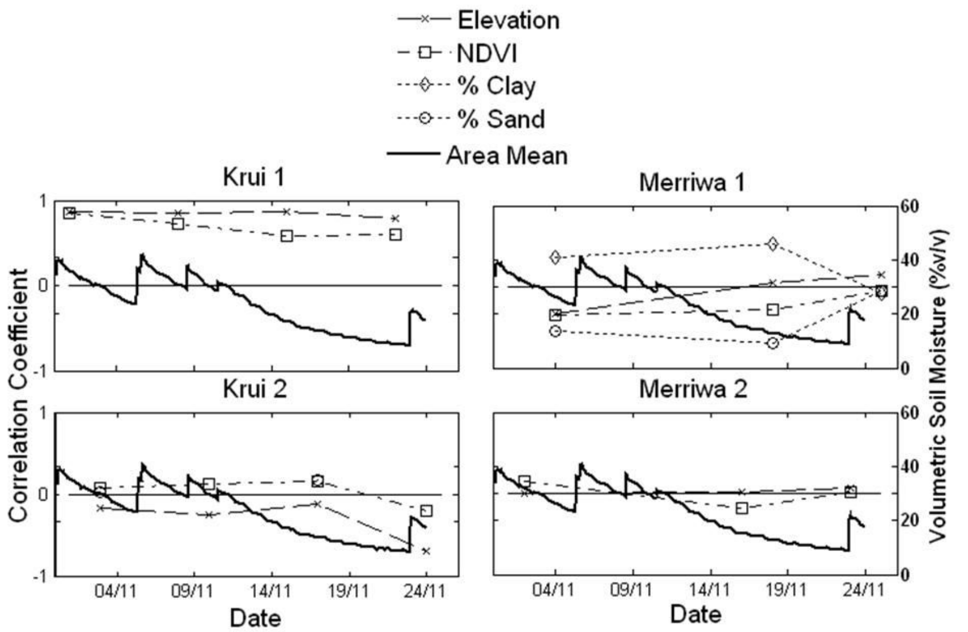

Figure 6.12. Time series of correlation coefficients between soil moisture and elevation, NDVI and soil texture (left axis) in the NAFE'05 large-scale areas. On the right axis the temporal variation of the mean soil moisture over the entire study area is plotted.

In the Krui 2 and Merriwa 2 areas, little or no correlation was observed with NDVI and elevation, while in the Krui 1 area soil moisture exhibited a significant correlation with elevation, and to a lesser extent with NDVI. The Krui 1 area presents a relative small range of elevations (83m, see Table 6.4). Nevertheless, it had a significant amount of cumulative rain in the northern, more elevated portion with respect to the other gauged stations (66mm at station K3, Table 6.1). Despite the lack of complete rainfall time series for the southern part of the area (stations K1 and K2 had several data gaps), it is expected that this is much smaller and comparable to site M2, which is situated on the same large flat plateau occupying the southern part of the study area. Therefore the high correlation of soil moisture with elevation is likely to be due to the correlation between rainfall and elevation at larger scales, as discussed in the analysis of the station data.

The analysis here has confirmed that soil texture was a dominant factor in determining soil moisture variability at the extent of interest of this study (>10km), while being still important but confounded by other factors such as elevation and vegetation distribution at smaller extents (<3km). The analysis has nevertheless been limited by the small number of soil texture points available in the near vicinity of soil moisture measurement locations and the relatively small extent of the spatially distributed soil moisture measurements (below 30km). In the next section the analysis is extended to a yet wider domain, that of the entire study area (approximately 40km extent), using the soil moisture measurements undertaken at approximately 2km spacing across the study area on October 31st, November 7th, 14th and 21st.

6.4.2 Semivariogram Analysis

The 2km-spaced soil moisture measurements had the advantage of covering the study area fairly extensively. Nevertheless, the single point nature of each measurement is a limitation when used to characterise the soil moisture condition of the surrounding 2km large area. Consequently, rather than trying a direct correlation analysis between soil moisture and land surface properties as performed in the previous section, it was decided to investigate the spatial structure of the soil moisture fields and their relationship with that of vegetation, topography and soil texture through a semivariogram analysis. This has the advantage of using information from several different combinations of data points to provide an estimate of the variability of soil moisture for a given lag distance, thereby reducing the uncertainty associated with the point-scale sampling of large areas. The rationale behind semivariogram calculation has already been already described in section 6.3.1.

Semivariograms were calculated for each of the ancillary data and compared with the empirical semivariograms of soil moisture. This is shown in Figure 6.13. For the gridded products (DEM and MODIS NDVI) semivariograms lags were determined using multiples of the grid resolution (250m). These semivariograms will evidently have a nugget corresponding to the variance of the values of adjacent cells. Due to the scarcity of the locations at which soil textural properties were measured, a semivariogram model had to be fitted to the empirical semivariogram by minimising the root mean square differences. The empirical semivariogram was calculated using the % sand content, which was chosen as representative of the spatial structure of soil textural properties. A common exponential type semivariogram model was found to fit well the empirical sand content semivariogram, with a RMSE of 4.6% sand content. The % sand content empirical semivariogram and exponential fit are shown in Figure 6.14. Due to the common restriction in semivariogram calculations that the maximum separation distance should not exceed half the minimum dimension of the data field considered (40km), the empirical semivariogram in the figure extends to approximately 20km, while the exponential one has been extended further to highlight the sill. The semivariogram has a nugget at approx 8.4% sand content (obtained as the square root of the variance at zero lag, i.e., the y axis intercept in Figure 6.14), and a sill of 14% sand content at approximately 20km.

Similarly, soil moisture semivariograms were calculated using the large-scale soil moisture measurements at 1-2km spacing for November 7th, 14th and 21st. Due to heavy rainfall conditions which strongly affected the sampling, data for October 31st were very limited in extent and were not used. Semivariograms were binned at a 1km lag (h) ensuring that a fairly constant number of data points would fall within each bin. Note that these semivariograms were not interpolated with a model in order to be able to resolve the variation of the variance with distance in a comprehensive way. Given that the minimum distance between large-scale soil moisture

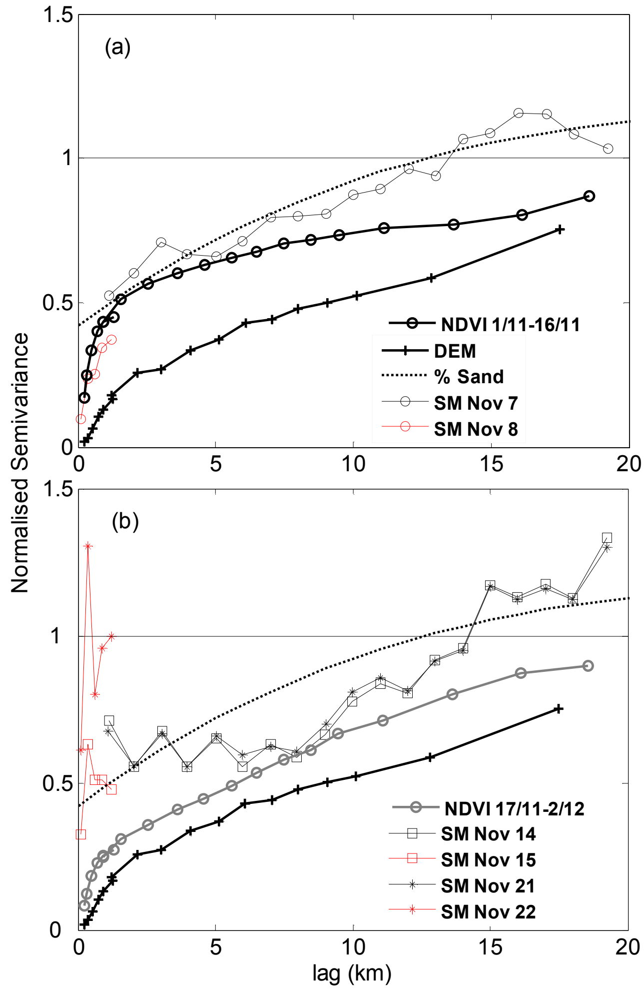

Figure 6.13. Comparison of soil moisture (SM) empirical normalised semivariograms and NDVI, soil texture and elevation normalised semivariograms. Panel (a) displays data for the November 1st to November 16th period, Panel (b) data for the November 17th to December 2nd period. DEM and % Sand semivariograms are invariant between the two panels and are labelled as indicated in panel a.

measurements was 1km, the semivariograms were extended to smaller lags by means of the farm-scale soil moisture measurements undertaken on each day following a large-scale mapping. Semivariograms extending to 1km were then calculated for November 8th, 15th and 22nd. In Figure 6.13 it can be seen that at the 1km lag these semivariograms match fairly well with the large-scale semivariograms of November 7th, 14th and 21st despite the lag of one day.

All semivariograms were then normalised to the total variance of the field to allow inter-comparison (i.e., in this kind of plot, the sill corresponds to value 1). The MODIS NDVI product was available in a 16-day composite product (November 1st to November 16th, and November 17th to December 2nd), therefore the comparison was performed separately for these two periods. The first period matched fairly well with the wet conditions of the area in the first half of the month, with the second period corresponding to the drydown to very dry conditions on November 21st. The spatial soil moisture monitoring on November 7th followed closely a significant rainfall event on November 5th, leading to fairly wet conditions (mean=36.4%v/v, standard deviation=13.1%v/v). November 14th and 21st were instead characterised by drier conditions (mean=10.9 and 11.1%v/v and standard deviation=7.3%v/v).

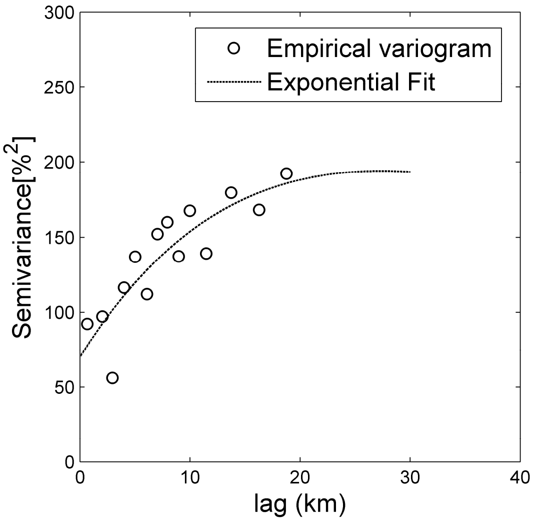

Figure 6.14. Exponential fit of the % sand content experimental semivariograms from the soil texture data across the NAFE'05 study area

The semivariograms are compared in Figure 6.13a for the November 1st to November 16th period, and in Figure 6.13b for the November 17th to December 2nd period. Note that the sand content semivariogram model and the DEM semivariogram are invariant between the two figures. The analysis was limited to 20km (½ of the study area dimension). NDVI appeared to be mostly stationary on wet conditions (panel a) with a range of approximately 1km. Sand content showed significant large small-scale variability (i.e. large nuggets) with a range of approximately 20km, while topography exhibited high spatial correlation until the 2-3km lag but was non-stationary at the 20km scale (i.e., the semivariance kept increasing).

In wet conditions, soil moisture exhibited a spatial structure similar to elevation and NDVI at the small scale, becoming mostly stationary at around 1-3km lags. Nevertheless, at scales larger than 1-3km variability increased steadily, reaching the sill at approximately 15-20km. Note how this matched fairly well the variance increments and lag at which the soil texture semivariogram sills. In dry conditions (panel b), the range of NDVI increased significantly, up to approximately 15km. This means that the variability of the NDVI field is mostly associated with large-scale variation in the value of NDVI. The spatial structure of soil moisture was very similar for November 14th and 21st, and had no definable range as in the case of wet conditions, but rather an elevated variance, quite stable from very small lags up to a lag of approximately 10km. At this scale the variance started increasing steadily and continued until approximately 15-20km, where the semivariogram seems to reach the sill. This matched fairly well the variance increments and the distance at which the soil texture semivariogram reaches the sill.

These results are in good agreement with the analysis performed in previous section and demonstrated that at the scales of interest of this study (~40km), the spatial structure of soil moisture fields resembled very closely that of soil texture, here investigated using the sand content. As observed during the analysis of the station data, this is consistently observed from wet to dry conditions.

6.4.3 Mean Relative Difference Analysis

In the analysis presented thus far on the role of land surface features in determining soil moisture patterns in the NAFE'05 study area, little consideration has been given to an important land surface property which is expected to play a significant role in this context, being the land cover type. The effect of land cover type was investigated only at the very small scale of the high-resolution areas (see section 6.3.1) and found to have a strong influence on soil moisture distribution. However, in the large-scale analysis presented in section 6.4, the effect of the land cover type could not be included because (i) all the monitoring stations for which continuous time series were available had been installed on native grass sites, allowing no comparison between the soil moisture dynamics produced by different land covers, (ii) land cover is not a monotonically varying physical quantity (like for example the sand content or the elevation) but rather a categorisation of the land surface into vegetation classes (grass, crop, forest, urban areas and so on). This makes it difficult to include in a direct correlation analysis such as that in the previous sections.

Here the impact of the land cover type on soil moisture variability is analysed to understand its role compared to soil texture. To this end, the spatial soil moisture ground measurements were grouped by land cover class, and the soil moisture distribution within each class was compared to the area average soil moisture. Each soil moisture point was classified as bare soil, grass, crop or forest using a 30m resolution Landsat five Thematic Mapper scene of the study area acquired on October 21st. To this end Landsat bands were converted into a land cover map by supervised classification using the ground visual estimation of land cover performed by the ground sampling team during the campaign (see section 5.3.1.1). Mean relative difference analysis was then performed on each class, by calculating the mean and standard deviation across the NAFE'05 period of the difference between mean soil moisture within each land cover class and mean soil moisture over the monitored area. This analysis is similar to that performed for the monitoring stations, but now covers a much wider range of land surface conditions and land covers.

For comparison, mean relative difference analysis was also performed with the other ancillary data considered in this Chapter, by grouping the ground measurements within ranges of elevation, NDVI and % sand and clay content, and considering the mean and standard deviation in time of the relative difference between soil moisture within each range and the daily average soil moisture. Results are shown in Figure 6.15. Mean relative difference analysis indicates which locations (or in this case, which classes or ranges of land surface properties) exhibit soil moisture conditions consistently higher or lower than the area mean, and and the variability of this relationship.

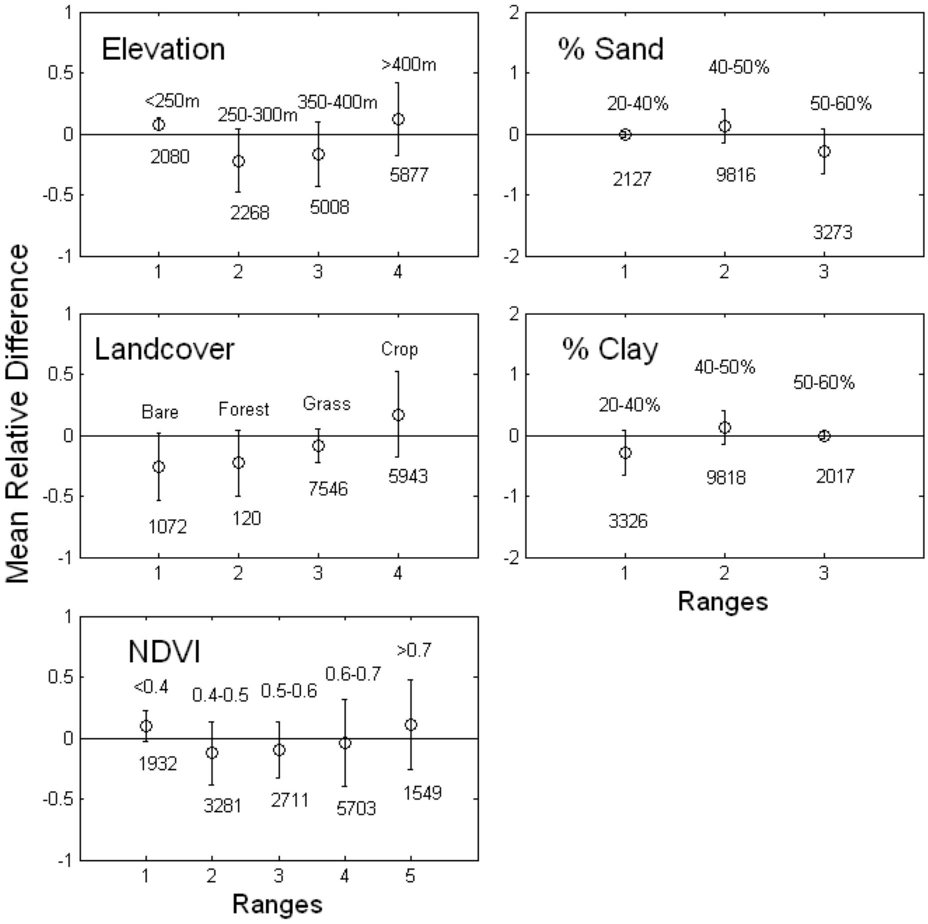

Figure 6.15. Mean and standard deviation of the relative difference between soil moisture within land cover classes, ranges of elevation, soil texture and NDVI and the daily mean soil moisture. The number under each bar indicates the number of points falling within each class.

Several key conclusions can be drawn from this plot. Ranges of elevation and NDVI showed very variable relationships with respect to the area mean. This means that even when considering a portion of the landscape with fairly uniform NDVI or elevation range, this will present a large range of soil moisture conditions, confirming that these are not the main factors determining spatial variability of soil moisture at large scale. When considering soil texture, it was observed that areas characterised by soils with sand content lower than 40% (and clay content higher than 50%) exhibited relatively higher temporal stability than soils with higher sand content, because the standard deviation of their relative difference in time is smaller. Moreover, the soil moisture relative difference of these areas was close to zero, indicating that these areas were consistently representative of the area average wetness conditions. Conversely, areas with high sand content (>50%), despite exhibiting a significant variation in relative difference, were characterised in general by drier conditions than the rest of the area. This confirms the strong correlation between soil moisture and soil texture over large areas previously observed at the various analysis extents in this Chapter, as well as the association soil moisture patterns with patterns of soil texture at the scale of a typical L-band footprint.

Another key result is related to the effect of land cover type on the soil moisture distribution. Areas of very low vegetation cover (classified as "bare") and forests were consistently characterised by conditions drier than average. It should be noted however that very few soil moisture measurements were undertaken under forest canopy (120). Therefore the results concerning the forested areas, although indicative of the behavior of these areas, should be taken with caution. Conversely, cropped areas were very densely monitored and exhibited clearly wetter-than-average conditions. This indicates that crops maintain moist soil conditions, most probably through decreased evaporation due to shading of the soil surface. The balance of these processes is expected to vary throughout the growing season, and therefore these conclusions are far from general. Nevertheless, in the period of the NAFE'05 campaign being considered by this thesis, cropped areas maintained overall wetter conditions than grasslands, forested areas and very low vegetated surfaces, although there was no significant soil moisture variability identified within a specific land cover class in response to variations in NDVI. Moreover, grassland areas exhibited the highest temporal stability across the land cover classes considered, having a small standard deviation and relative difference close to zero. This is most likely an effect of the vastly larger number of soil moisture measurements taken on grassland areas, which occupy the majority of the NAFE'05 study area (see data points tag in Figure 6.15). However this does not affect the relative difference in mean soil moisture conditions between grassland and the other land cove types.

Figure 6.16 focuses on the effect of land cover and soil texture distribution alone in determining soil moisture variability, and quantifies their relative importance their relative importance in terms of absolute soil moisture differences instead of mean relative difference. Here the difference between the average soil moisture within each of the land cover and soil type patches shown in Figure 6.15 and the area average soil moisture (i.e, the soil moisture anomalies) are plotted in time. The top panel of this plot shows how the presence of crops in the study area induced soil moisture conditions up to 20%v/v wetter than the average conditions in the study area, and up to 30-40%v/v wetter than the surrounding areas of very low vegetation ("bare soil"), grass and forest. Such anomalies were not stable in time and were correlated with the rainfall regime. Maximum soil moisture anomalies occurred in inter-storm periods (e.g., November 4^{th}-8^{th} after the big rainfall event, and November 11^{th}-22^{nd}) while rainfall events tended to decrease the soil moisture difference between land cover patches (e.g., November 8^{th}-11^{th}, November 23^{rd}). This is in agreement with the results obtained using the monitoring stations. Moreover, as the study areas dried down (November 11^{th} -22^{nd}) the soil moisture difference between land cover types decreased. As a result of this, the soil moisture difference between crops and the other land cover types was reduced to 20% on dry conditions (10%v/v)

The variability in soil moisture induced by soil texture distribution is shown in the middle panel of Figure 6.16. Soils with higher sand content (50-60%) exhibited drier-than-average conditions. Moreover, the maximum soil moisture difference with respect to soils with lower sand content (20-50%) was observed during inter-storm periods when the area is in wet conditions, amounting to approximately 35%v/v soil moisture difference. This differences decreased strongly during and after rainfall events (e.g., November 8^{th}-11^{th}, November 23^{rd}) and when approaching dry conditions

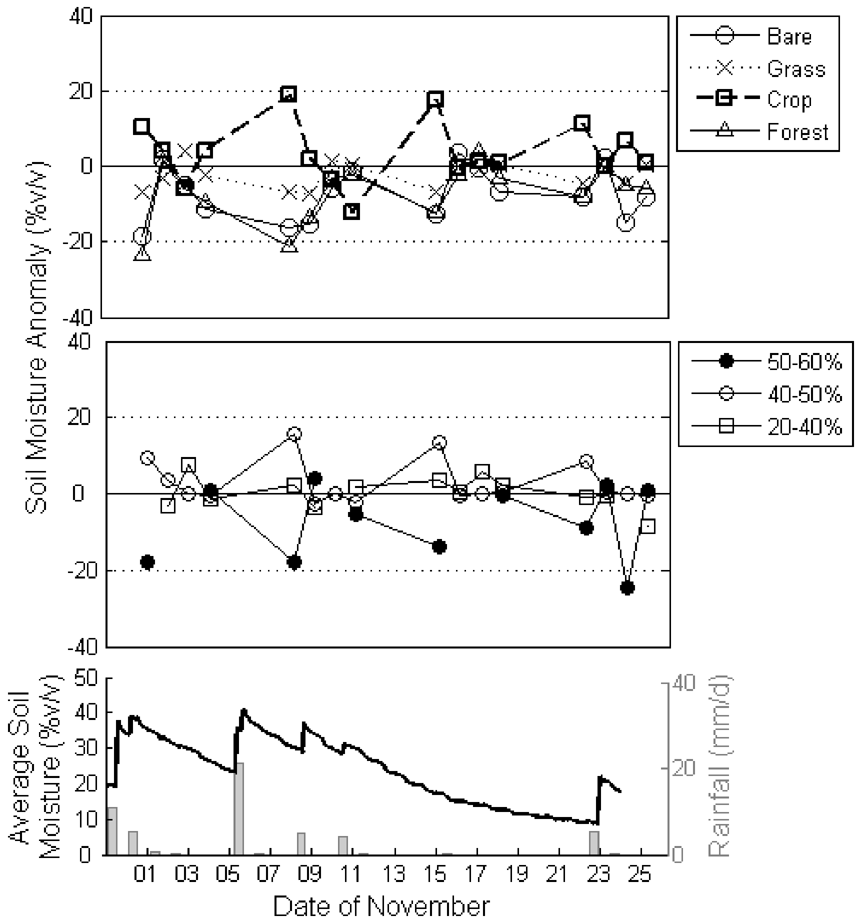

Figure 6.16. Time series of soil moisture anomalies (difference between average soil moisture within land surface patches and the average soil moisture in the study area). Land surface patches are determined by land cover type (top panel) and soil texture ranges (% sand content, middle panel). The area average soil moisture and daily rainfall is plotted the bottom panel. The time series in the middle panel have discontinuities due to the scarcity of the gravimetric samples used for soil textural analysis.

(November 11th -22nd). At the end of this drydown period (10%v/v area average soil moisture) the soil moisture difference between sandy and clay locations is reduced to 10-15%v/v. Note that these estimates are in very good agreement with those resulting from the analysis of the monitoring stations data, where it was estimated that a moderate difference in sand content, 25% between station S1 and S3 produced a difference in soil moisture between the two stations of 6.1%v/v and 30.4%v/v respectively on dry (5%v/v) and wet (25%v/v) average conditions of the study area.

6.5 Chapter Summary

This Chapter has analysed the spatio-temporal variability of near-surface soil moisture in the NAFE'05 study area at a range of scales, from the farm scale (<3km) to the satellite footprint scale (~40km), The purpose of this analysis was to understand the important factors determining the spatial variability of soil moisture and how the relative importance of these factors changes in time and with the spatial domain of observation.

It has been shown that soil texture (expressed in terms of % sand and clay content) and land cover type were the most important factors to determine soil moisture spatial distribution at the satellite footprint scale (40km). Soils with higher sand content exhibited drier soil moisture conditions than soils with lower sand content and higher clay content. Moreover, the range of soil texture in the area (variability in sand content of 35-40% variability in sand content), produced a soil moisture spatial variability ranging from 40%v/v soil moisture in wet conditions right after rainfall events throughout the study area to 10%v/v in dry conditions at the end of a 10 day drydown.

Land cover was also found to have a strong influence on soil moisture distribution at the local scale and the satellite footprint scales. Specifically, cropped areas exhibited consistently wetter-than-average conditions while bare ground and forested areas exhibited drier-than-average conditions. The difference in soil moisture conditions between crops and grasslands was as much as 30%v/v wet conditions while the difference between crops and bare soil or forested areas was up to 40%v/v. Both differences reduced to around 20%v/v in dry conditions.

The relationship between soil moisture variability and land cover and soil texture patterns varied significantly in time. Moreover, when decreasing the spatial domain of observation from the satellite footprint to individual farms, other factors came to play an important role in determining soil moisture distribution. The correlation between soil moisture variability and land cover or soil texture patterns was stronger during inter-storm periods, while it diminished during and immediately after rainfall events. At the farm extent (3km), the effect of soil texture and land cover on soil moisture variability was not always dominant. Rather, elevation had a significant impact on soil moisture distribution at the farm scale in the presence of significant relief (at least 100m over an area of 3km x 3km). Such features resulted in a difference of 15-20%v/v soil moisture, with drier conditions at higher elevation.

Consequently, this Chapter has demonstrated that soil moisture variability in the NAFE’05 study area at the scale of an L-band satellite footprint can be related to spatial patterns of land cover type and soil texture. Moreover, this Chapter has quantified the magnitude of soil moisture variability associated with those land surface factors and has shown that, contrary to the assumption made by the SMOS L2 algorithm, significant soil moisture heterogeneity occurs as a consequence of land cover variability. Consequently, Chapter 7 will investigate how the heterogeneity of land surface characteristics and the associated soil moisture heterogeneity affect the core model of the SMOS L2 algorithm (L-MEB) over large heterogeneous areas. Chapter 8 will then test the effectiveness of the SMOS L2 algorithm and its assumptions to account for the land surface heterogeneity. An alternative approach will then be developed in Chapter 8 to improve the accuracy of the algorithm by accounting for the land surface factors analysed in this Chapter.

Chapter Seven

7 Effect of Land Surface Heterogeneity on Soil Moisture Retrieval

This Chapter tests the L-MEB radiative transfer model, core to the SMOS L2 algorithm, at resolutions typical of a future SMOS footprint (40km), and assesses the error in the L-MEB soil moisture retrieval resulting from sub-pixel land surface heterogeneity under the assumption of pixel uniformity, which is typical of current soil moisture retrieval techniques. Moreover, the land surface factors most directly linked to this retrieval error in the NAFE'05 study area are identified. To this end, the NAFE'05 airborne data described in Chapter 4 are aggregated to produce Brightness Temperatures (T_B) observations at various pixel resolutions (5, 10, 20, 30, 40km) for a variety of land surface conditions, and the L-MEB model described in Chapter 3 is used to retrieve coarse-scale soil moisture from those observations. The error in soil moisture retrieval is estimated by comparison with the 1km soil moisture maps presented in Chapter 5, and then related to the land surface heterogeneity within each observation pixel through an analysis of multiple pixels with varying degrees of land surface heterogeneity.

This Chapter is organised as follows:

- a synthetic study is performed to understand how and to what extent the heterogeneity of each land surface factor affects the soil moisture output of the L-MEB model;
- coarse T_B observations are simulated by aggregation of 1km airborne data, after verifying the scaling of T_B fields using multi-resolution airborne observations; and
- soil moisture is retrieved from the coarse T_B observations, and the retrieval error analysed in terms of the sub-pixel heterogeneity of land surface conditions.

7.1 Synthetic Study

Before assessing the effect of the sub-pixel heterogeneity on the L-MEB soil moisture retrieval with real data, a simplified synthetic scenario was considered in which the effect of heterogeneity in each land surface factor on the L-MEB retrieval was assessed individually, separated from that of other confounding factors, such as uncertainties in model physics, model parameters and ancillary data.

Here, sub-pixel heterogeneity in soil moisture, vegetation cover, soil temperature, soil texture and surface roughness were considered separately. Moreover, the variability of vegetation cover was considered in two ways:

1. variability of vegetation water content (VWC) within individual land cover types (i.e., pixels with a single land cover type such as grassland, crop or forest), and
2. variability in land cover type (i.e., pixels with a mixture of cover types including crop, grassland and forest cover).

Case (2) is considered as two different land cover types having the same VWC and soil moisture would have different microwave emission due to different absorption/scattering characteristics which are highly dependent on the plant structure. The absorption/scattering mechanisms are defined in L-MEB through the parameters (see also section 3.4): b (VWC/optical depth ratio), tt_P (P polarised vegetation structure), and ω_P (single scattering albedo). Therefore, in case (1) these four parameters were held uniform across the pixel, whereas in case (2) they were land cover type specific, and the values used for the parameters were those evaluated each land cover types in the study area by evaluation of the L-MEB at fine resolution (see Table 5.2).

A schematic of the procedures adopted for this synthetic experiment is shown in Figure 7.1. A synthetic scenario was created using an arbitrary 10 cell x 10 cell grid which was assumed to constitute a single observation pixel. In order to analyse the effect of the heterogeneity of each individual

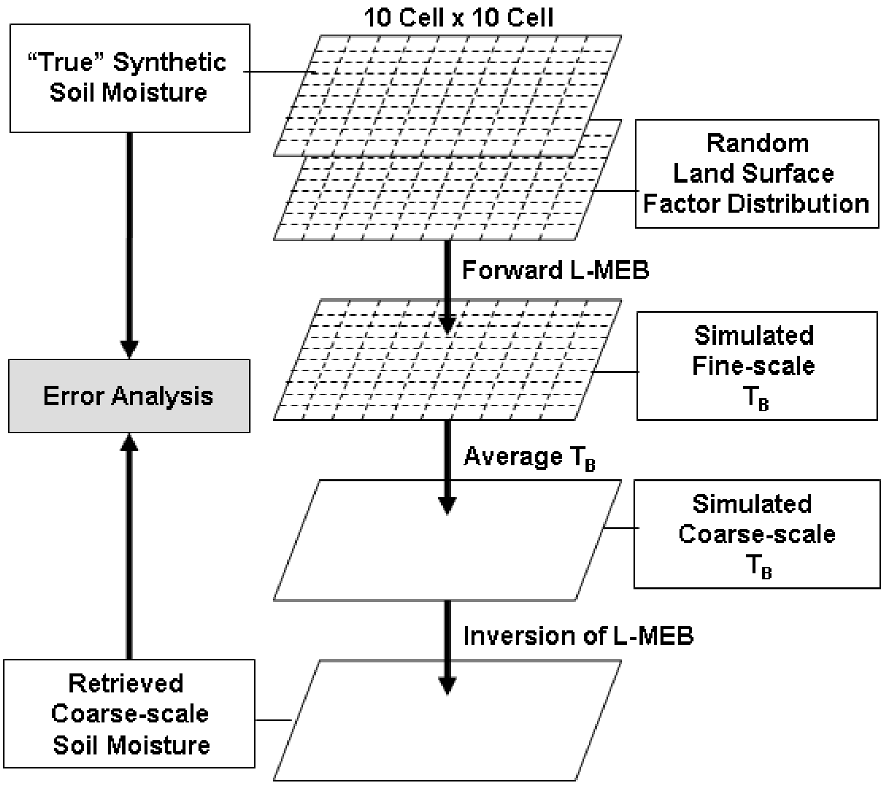

Figure 7.1. Schematic describing the strategy adopted to investigate the sensitivity of the L-MEB model to the sub-pixel heterogeneity of land surface factors.

land surface factor on the retrieval of the pixel average soil moisture, each factor (i.e., soil moisture, VWC, land cover, % sand and clay content, surface roughness and temperature) was perturbed randomly around a mean value and across the grid, with perturbations applied in such a way that the original pixel mean was conserved. Only one factor was perturbed at a given time, while all the other land surface factors were held at the reference values (uniform across the grid). Several pixel mean values and levels of perturbation were analysed for each factor in order to cover as many realistic degrees of heterogeneity encountered in a typical study area as possible. A summary of all the synthetic cases considered, including input values for each land surface factor and levels of perturbation is presented in Table 7.1.

Table 7.1. Summary of heterogeneous synthetic scenarios tested. The perturbation was applied to each mean values listed. The error indicated is the maximum expectable for the magnitude of heterogeneity expected in the study area and in the worst of the three soil moisture scenarios. Symbols are: T_{S1}=Surface soil temperature, F=Forest, C=Crop, G=Grassland, Cl=Clay, Sa=Sand.

Factor	**Mean values**	**Perturbation**	**Soil Moisture Conditions (%v/v)**	**Mean Error ±St.Dev. (%v/v)**
Soil Moisture (%v/v)	10,20,30,40	0, 5,10,15,20	10,20,30,40	-2.1±0.2
Vegetation Water Content (kg/m^2) and optical depth (τ)	0.4(G)	0,0.5,1(G)	5,20,40	1.4±0.2(G)
	2I	0,0.5,1,1.5,2 I		1.5±0.2I
	τ=0.57(F)	0,0.1,0.2,0.3,0.4,0.5, 0.6 (F)		4.8±0.5(F)
Land cover fraction (%)	5-100	Grass Crop Forest	5,20,40	19.8±2.1 -10.9±2.0
Soil Texture Sa(%), Cl(%)	(10 60) (35 35) (60 10)	0,5,10,15,20,25,30	5,20,40	2.0±0.2
Surface Roughness (-)	0.1,0.3,0.5	0,0.05,0.1,0.15,0.2	5,20,40	2.8±0.35
Soil Temperature T_{SURF}(°C)	10,25,40	0,5,10,15,20	5,20,40	-1.6±0.8

For each case (i.e., a determined mean value of the perturbed factor and a level of perturbation) L-MEB was applied to the synthetic fields in forward mode to generate the corresponding brightness temperature fields, which were in turn averaged to obtain a single value of brightness temperature for the pixel. An incidence angle of 38º (from nadir) was considered in all cases.

Using the simulated coarse-scale pixel average T_B, a pixel average soil moisture value was estimated by inversion of the L-MEB model and using the pixel average values for all the factors as input to the model (both the perturbed factors and the uniform ones). The retrieved pixel average soil moisture was then compared with the "true" pixel average soil moisture and the error related to the level of perturbation applied. The "true" synthetic soil moisture was in all cases a background soil moisture value uniform across the grid, unless when the heterogeneity of soil moisture itself was analysed.

For each case (i.e., mean value of the land surface factor and level of perturbation), 100 Monte-Carlo simulations were performed by creating 100 different random grids. This was done in order to obtain a statistically significant number of data points and also to check whether the retrieval algorithm converges to a stable solution. The mean error for each case was then calculated as the mean of the 100 errors between the output of the L-MEB inversion for all the Monte-Carlo simulations and the "true" synthetic soil moisture. For all the cases analysed, the results are given in terms of mean error ± the standard deviation of the errors of the 100 Monte-Carlo simulations.

The results of the analysis of heterogeneity of each individual land surface factor are discussed in the following sections. A summary of the maximum error observed for each synthetic cases considered is presented in Table 7.1 together with the input values for each land surface factor and levels of perturbation. In the following sections, the values of the L-MEB inputs which were not perturbed were taken as those of a reference case, unless otherwise stated; this consisted of a soil texture of 20% and 35% for sand and clay content respectively, VWC of 0.4kg/m^2 and 2kg/m^2 for grassland and crop land cover types respectively, and a value of 27ºC of soil and canopy temperature. These values of mean VWC for each land cover types were derived from the ground sampling of VWC at the high-resolution sites (see Chapter 5).

7.1.1 Soil Moisture Heterogeneity

The effect of sub-pixel heterogeneity in soil moisture was investigated by simulating heterogeneous soil moisture fields of bare soil having average soil moisture conditions of 10, 20, 30 and 40%v/v. Each case was randomly perturbed with four levels of perturbation, corresponding to a soil moisture standard deviation of 5, 10, 15 and 20%v/v about the mean value, together with a reference case where the mean soil moisture was uniformly distributed across the pixel. The maximum value of standard deviation of 20%v/v was a conservative choice since the maximum standard deviation observed in the study area was 13.2%v/v (see Table 5.9). The larger value was chosen as the actual standard deviation might in fact be higher than that observed value, given the large spacing of those samples.

All soil moisture cases were simulated with two different values of VWC (held uniform across the pixel). The value of VWC considered for the grassland was VWC =0.4kg/m^2 (optical depth ~0.06). As ground measurements of VWC were not available for the forest in the NAFE'05 study area, the effect of the canopy cover was simulated imposing directly the value of the optical depth (τ) 0.57, estimated for the Eucalypt forest in the NAFE'05 study area by J. Grant (pers. comm.). It should be noticed that τ is linearly related to VWC in L-MEB.

Figure 7.2 shows the mean error of soil moisture retrieval as a function of the perturbation level for the different average soil moisture conditions. Results show that the heterogeneity of soil moisture results in underestimation of the pixel average soil moisture, with the effect being greatest during wet conditions (30-40%v/v). The maximum error is 2.9±0.3%v/v when soil moisture has a standard deviation of 20% within the pixel. At a standard deviation of 15%v/v, which matches approximately that recorded across the NAFE'05 study area (see Chapters 4 and 6), the mean error is 2.1±0.2%v/v. The results for forest (see Figure 7.2b) are very similar to those for grassland. This indicates that, although high values of VWC (or τ) reduce the sensitivity of T_B to soil moisture changes (see Figure 2.5) they

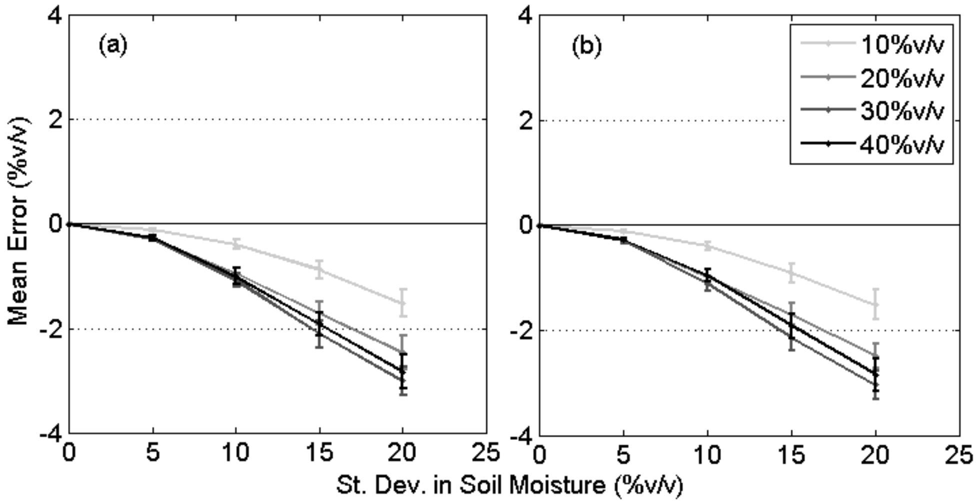

Figure 7.2. Mean error of L-MEB soil moisture retrieval due to the sub-pixel heterogeneity of soil moisture in four different average soil moisture conditions for (a) a grassland with VWC=0.4kg/m^2 and (b) a forest with τ=0.57. Vertical error bars indicate the standard deviation of the error of 100 Monte-Carlo simulations for each case.

have limited impact on the L-MEB soil moisture error due to soil moisture heterogeneity underneath the canopy.

The lack of impact of VWC (or τ) values on the error due to soil moisture heterogeneity could be due to the fact that in this synthetic scenario exact knowledge of the VWC was assumed during the retrieval process, eliminating the error due to the uncertainty in the knowledge of the VWC. Moreover, when only soil moisture is heterogeneous and all other parameters are uniform within the pixel, all the soil moisture-emission curves (see Figure 2.5) of the individual cells used for the simulation of the fine-scale T_B will be the same, and the single emission curve of the mixed pixel (i.e., the 10 cell x 10 cell grid), which is used for the retrieval, will be equal to those curve. Therefore, the error due to soil moisture heterogeneity is only dependent on the curvature of the soil moisture-emission curve, which does not change significantly with different VWC values imposed for the grid. Conversely, in the case when a land surface factor other than soil moisture is heterogeneous across the grid (like in the following sections), the soil moisture-emission curves of the individual cells will be all different, and the single emission curve of the mixed pixel used for the retrieval will not correspond to any of the individual cell curves.

7.1.2 Vegetation Water Content Heterogeneity

Pixels with heterogeneous VWC were simulated for the case of uniform grassland cover (mean VWC=0.4kg/m^2), a uniform crop cover (mean VWC=2kg/m^2) and a uniform forest cover (τ=0.57). The maximum level of perturbation around the mean value was different for each land cover type. In the case of grassland and crop the maximum level of perturbation (1kg/m^2 and 2kg/m^2 respectively) was chosen as two times the maximum VWC standard deviation from ground samples at the high-resolution sites (0.5kg/m^2 and 1kg/m^2 respectively). Perturbation scenarios from 0kg/m^2 to the maximum perturbation level were simulated for both land cover types with 0.5kg/m^2 increment. The maximum perturbation level for the forest optical depth (0.6) was set as two times the optical depth standard deviation (0.3) estimated in the NAFE'05 study area by J. Grant (pers. comm.), and perturbation scenarios from 0 to the 0.6 were simulated with 0.05 increment.

Figure 7.3 shows the mean error of soil moisture retrieval as a function of the VWC perturbation level for three different average soil moisture conditions (5%v/v, 20%v/v and 40%v/v). Results show that the heterogeneity of VWC results in an overestimation of the pixel average soil moisture, this being greatest in wet conditions (30-40%v/v). In the case of moderate vegetation cover (grass and crop) the maximum error is 1.4±0.2%v/v. However, when considering the VWC standard deviation observed during the NAFE'05 experiment (<1kg/m^2), the mean error is smaller than 1%v/v. For the forest cover, the mean error is generally higher than for the moderate vegetation cover, and increases considerably in wet conditions. At the magnitude of spatial variability observed in the Roscommon area (standard deviation in optical depth equals 0.3) the mean error achieves a maximum of 4.8±0.5%v/v in wet conditions (40%v/v).

As discussed earlier, the large errors for forest are due to the fact that the soil moisture-emission curves of the individual cells are very different due

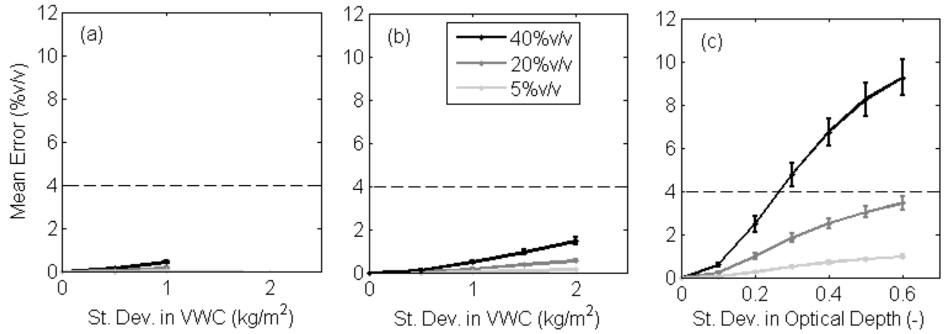

Figure 7.3. Mean error of L-MEB soil moisture retrieval due to the heterogeneity of the vegetation water content (VWC) in different soil moisture conditions for (a) grassland (VWC=0.4kg/m^2), (b) crop (VWC=2kg/m^2) and (c) forest (τ=0.57). Dashed horizontal lines indicated SMOS target accuracy. Vertical error bars indicate the standard deviation of the absolute error for the 100 Monte-Carlo simulations of each case.

to the differences in optical depth. Therefore, the single emission curve of the mixed pixel used for the retrieval of a pixel average soil moisture will not correspond to any of the curves of the individual cells, determining the retrieval error. It should be stressed that, since this a synthetic analysis, this error is strictly due to the heterogeneity of the optical depth within the pixel, and does not account for retrieval errors due to, for example, poor sensitivity of the microwave signal to soil moisture under dense canopy which would affect the retrieval of soil moisture under the forest canopy.

7.1.3 Land Cover Type Heterogeneity

Pixels with heterogeneous land cover type were simulated by mixing three land cover types with pixel fractions between 0 and 100%, with a 5% step. The three land cover types were grassland, crop and forest. To keep the simulation simple, each land cover type was assigned a fixed value of optical depth. For crop and grassland, these were calculated by multiplying the default L-MEB parameter "*b*" (ratio between the optical depth and VWC) for each vegetation type by the average VWC ground-sampled in the study area (respectively 0.4kg/m^2 and 2kg/m^2 for grassland and crop). The forest was instead assigned the fixed value of optical depth of 0.57 estimated by J. Grant (pers. comm.). For each combination of the three land cover types, the resulting pixel brightness temperature was simulated by aggregating of the brightness temperatures simulated for each land cover type weighted by the respective pixel fraction. The soil moisture retrieval was performed under the L-MEB default assumption of a uniform pixel, therefore assuming that the pixel was uniformly covered by the land cover type with the highest fraction.

Note that in the forward L-MEB modeling, the land cover specific L-MEB parameters used were those evaluated for the NAFE'05 study area in Chapter 5. Therefore the effect of land cover heterogeneity discussed here implicitly includes the cumulative effect of the sub-pixel heterogeneity of vegetation optical depth, vegetation scattering albedo (L-MEB parameter ω_P) and vegetation structure (L-MEB parameter tt_P).

Results are shown in Figure 7.4, where the mean error of soil moisture retrieval is shown for all combinations of grassland, crop and forest pixel fractions and for three soil moisture conditions (5%v/v, 20%v/v and 40%v/v, uniform across the pixel). The soil moisture retrieval error is as much as 4.3%v/v in dry conditions (panel a), increases to 10%v/v in intermediate conditions (panel b) and achieves a maximum of 19.8%v/v in wet conditions (panel c). The error is smaller in the case of mostly uniform land cover and is maximum in the case of the pixel split approximately in half between a forest cover and a land cover type with moderate canopy density (crop or grassland).

The cases where the error is at a maximum can be identified in Figure 7.4 as the boundaries between three regions: Each region includes the cases where each land cover type, having the highest pixel fractions is assumed uniform within the pixel by the retrieval algorithm (areas marked with letters "G", "C" and "F"), and along the boundaries of these regions are the cases where the fractions of two or more land cover types are very similar. When "moving" across these boundaries (i.e., varying the pixel fractions) the retrieval algorithm switches between one land cover type and the other. As a result of this a strong discontinuity in the error is observed at the

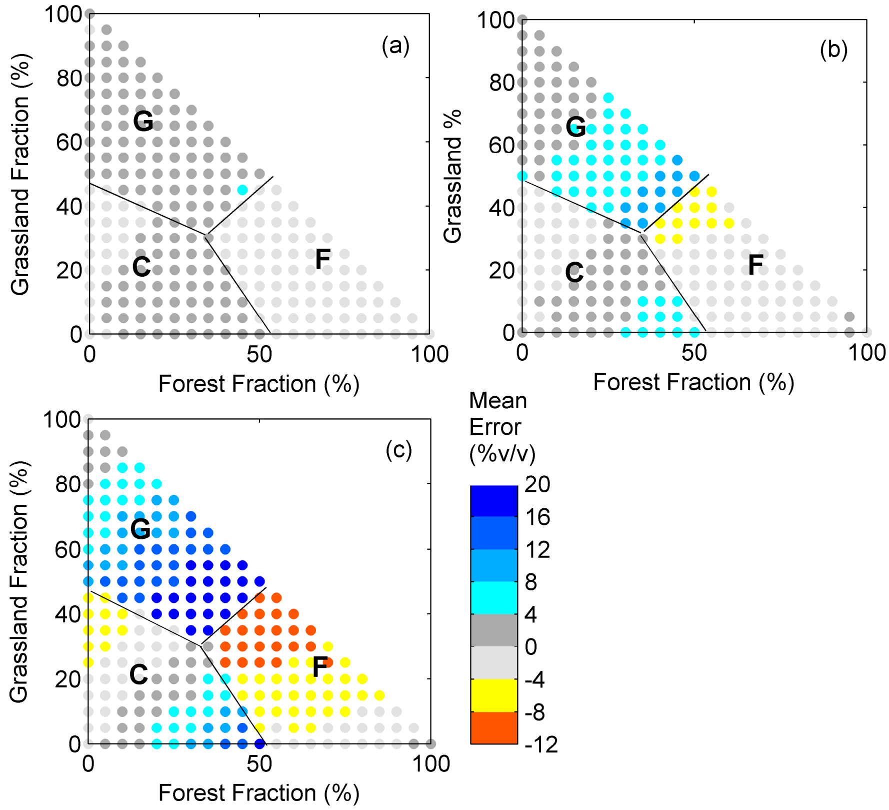

Figure 7.4. Mean error of L-MEB soil moisture retrieval due to heterogeneity of land cover type for all combinations of grassland, crop and forest pixel fractions and for various soil moisture conditions: (a) 5%v/v, (b) 20%v/v and (c) 40%v/v. The three regions delineated by solid lines and marked with letters identify the cases where the dominant land cover type in the pixel is G=grassland, C=crop or F=forest.

boundaries of these regions. In particular, the soil moisture retrieval algorithm is found to overestimate the pixel average soil moisture when the land cover type with the lower VWC is considered for the retrieval (e.g., pixel split in half between grassland and forest or in between crop and grassland and grassland assumed in the retrieval). Conversely, the pixel average soil moisture is underestimated by the retrieval algorithm when the land cover type with the higher VWC is considered for the retrieval (e.g., pixel split in half between grassland and forest and forest assumed in the retrieval or pixel split in half between crop and grassland and crop assumed in the retrieval). The underestimation is higher (-10.9±2.0%v/v error) when the difference between the mean VWC between the two land covers is higher (e.g., forest and grassland mixed pixels have higher error than forest/crop and crop/grassland mixed pixels).

7.1.4 Soil Texture Heterogeneity

Pixels with heterogeneous soil texture were simulated for a uniform grassland pixel (VWC=0.4kg/m^2) starting from three reference soil types, a clay (10%/50% sand/clay content), a clay loam (35%/35%) and a sandy loam (60%/10%). For each case the percentages of sand and clay content across the pixel were perturbed randomly around their mean values with increasing standard deviation from 0% up to 30% with steps of 5%. This was repeated for dry, intermediate and wet soil moisture conditions (5%v/v, 20%v/v and 40%v/v). The perturbations were applied to the sand content and the clay content was perturbed accordingly by imposing constant silt content (30%).

Results are shown in Figure 7.5. The error induced by the heterogeneity of soil texture is smaller than 2.0±0.2%v/v even for the worst case of a sandy loam soil in dry conditions (5%v/v). The error is clearly associated with the increased sand content, since the clay soil type in the same soil moisture conditions presents negligible error. It should be noted that, although the errors increase non-linearly with increasing soil texture heterogeneity, the mean error is always smaller than 1%v/v at the standard deviation of 11% sand content observed in the NAFE'05 study area from gravimetric soil samples (see Table 6.4).

7.1.5 Surface Roughness Heterogeneity

Heterogeneity in surface roughness was simulated by varying the L-MEB surface roughness parameter H_R. As discussed in Chapter 5 when calibrating the L-MEB model, the link between parameter H_R and surface geophysical quantities is not well understood. Moreover, it was demonstrated in Chapter 5 that the parameter has a strong dependence on soil moisture conditions (see section 5.1.5.3).

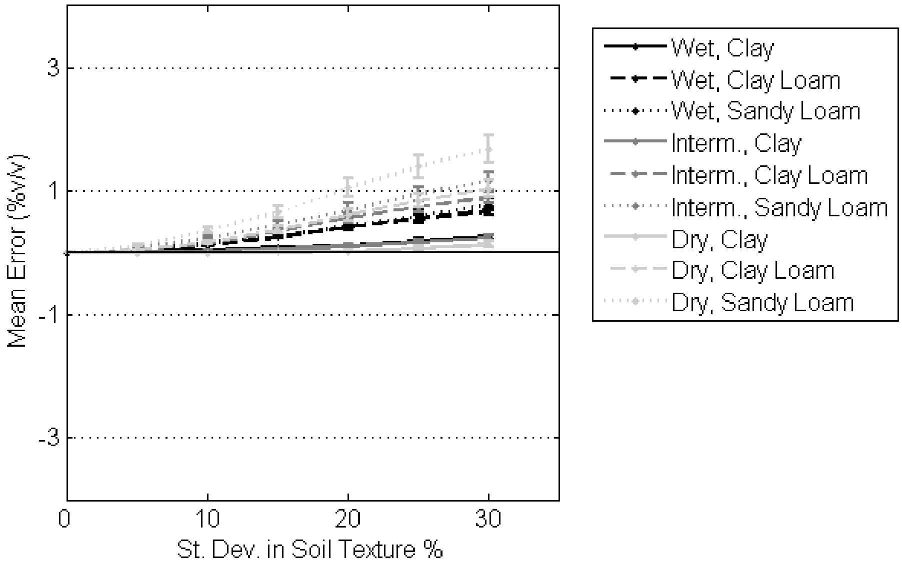

Figure 7.5. Mean error of L-MEB soil moisture retrieval due to heterogeneity of soil texture for three soil types in wet (40%v/v), intermediate (20%v/v) and dry (5%v/v) soil moisture conditions. Vertical error bars indicate the standard deviation of the error for the 100 Monte-Carlo simulations of each case.

In order to establish physically realistic values of spatial heterogeneity of H_R for this synthetic analysis, the spatial variation of the classical Choudhury roughness parameter (Choudhury et al., 1979) was calculated from the pin profiler measurements taken at several locations on the experimental farms (see section 4.4.4.2). This was found to range between 0.14 and 0.46 across the experimental farms, with a standard deviation of 0.11. Therefore, heterogeneous pixels of surface roughness were generated considering three pixel average values of parameter H_R (0.1, 0.3 and 0.5) each one perturbed about the mean value with standard deviation between 0 and 0.3. This perturbation, considerably higher than that measured with the pin profiler, was conservatively set in order to account for the heterogeneity unresolved by the scarcity of the pin profiler sampling locations. Each case was considered for dry, intermediate and wet conditions (5%v/v, 20%v/v and 40%v/v).

Results are shown in Figure 7.6. The error induced by the heterogeneity of parameter H_R increases non-linearly with the degree of heterogeneity and

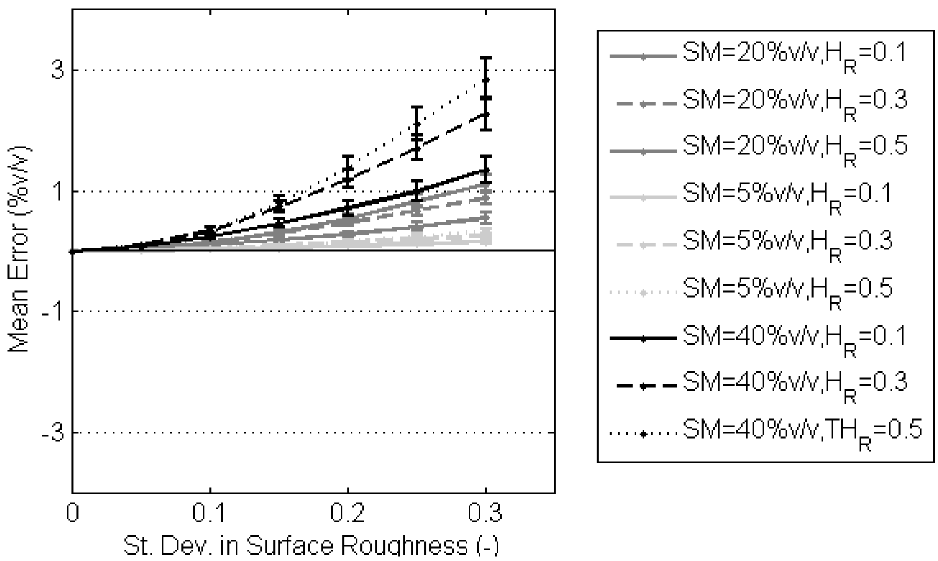

Figure 7.6. Mean error in L-MEB soil moisture retrieval due to heterogeneity of surface roughness for three pixel average surface roughness conditions (0.1, 0,3 and 0.5) in wet (40%v/v), intermediate (20%v/v) and dry (5%v/v) soil moisture conditions. Vertical error bars indicate the standard deviation of the error for the 100 Monte-Carlo simulations of each case.

is at a maximum in wet conditions (2.8±0.35%v/v). It is also notable that the mean error increases significantly going from smooth (H_R=0.1) to intermediate roughness conditions (H_R=0.3) but the increase is relatively small from intermediate to rougher conditions (H_R=0.5). This indicates that even in conditions rougher than those considered here, the error will not increase significantly. It must also be noted that in dry conditions, where the impact of surface roughness on the microwave emission was found to be higher (see Chapter 5), the error induced by the heterogeneity of the parameter H_R is found to be negligible for all the cases considered here. This indicates that when considering a decay of H_R with increasing soil moisture conditions, the error due to the heterogeneity of surface roughness will be even smaller than 2.8±0.35%v/v.

7.1.6 Soil Temperature Heterogeneity

The L-MEB model uses temperature at two depths, 2.5cm and 50cm, in order to calculate an effective soil temperature, depending on soil moisture conditions. However, it is reasonable to assume that the spatial heterogeneity of the soil temperature at 50cm is much smaller than that at 2.5cm. This is supported by the analysis of the spatial variation of soil temperature recorded at the NAFE'05 monitoring stations (see section 0), which showed a decay of soil temperature standard deviation with depth across the study area, from 2.6K (at 2.5cm depth) to 1K (at 15cm depth) in the 7:00-9:00AM time period. Pixels with heterogeneous soil temperature were therefore simulated by considering uniform deep soil temperature (at 50cm) and by perturbing only the near-surface temperature (at 2.5cm).

Three mean pixel temperatures were considered, 10ºC, 25ºC and 40 ºC, corresponding to respectively the monthly minimum, average, and maximum soil temperature recorded at 2.5cm depth at monitoring stations in the study area during November 2005, and three soil moisture conditions, 5%v/v, 20%v/v and 40%v/v. In each case soil temperature across the pixel was perturbed about the mean values with a standard deviation of up to 20ºC.

Results are shown in Figure 7.7. In the presence of strong heterogeneity in soil temperature, the L-MEB algorithm tends to underestimate the pixel average soil moisture conditions. This effect is stronger when the soil is cold and wet, producing an error of -11.8±1.4%v/v in conditions of strong heterogeneity (standard deviation of 20ºC). This is because in wet conditions the L-MEB soil moisture retrieval is more sensitive to changes in soil temperature (see section 0).

However, such extreme conditions were not encountered during the NAFE'05 experiment. The airborne data used in the analysis later in this Chapter were collected in the early hours of the morning, approximately between 7:00AM and 9:30AM. The lowest 2.5cm soil temperature recorded during November 2005 within this time window was 14ºC and 17ºC at 7:00AM and 9:30AM respectively. However, soil temperature heterogeneity was generally very small at that time, with a maximum standard deviation during the month of 1.3ºC and 2.8ºC respectively. Under such conditions the spatial heterogeneity of soil temperature would therefore not produce an

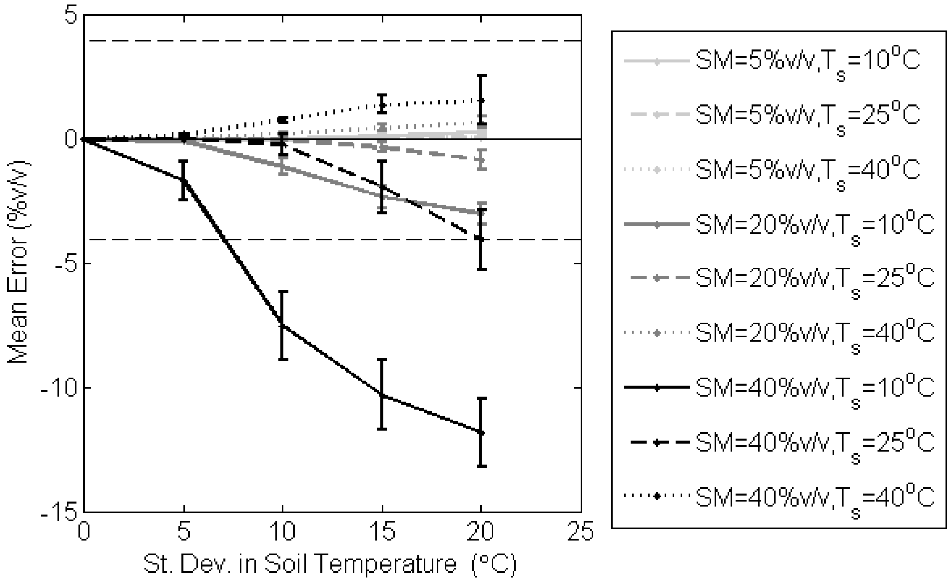

Figure 7.7. Mean error of L-MEB soil moisture retrieval due to heterogeneity of soil temperature for three pixel average surface roughness conditions (0.1, 0,3 and 0.5) in wet (40%v/v), intermediate (20%v/v) and dry (5%v/v) soil moisture conditions. Dashed horizontal lines indicated SMOS target accuracy. Vertical error bars indicate the standard deviation of the error for the 100 Monte-Carlo simulations of each case.

error of soil moisture higher than 1.6±0.8%v/v (underestimation), this being the mean error observed in Figure 7.7 for the case of cold soil (10ºC) and for soil temperature standard deviation of 5ºC.

7.1.7 Summary of Synthetic Analysis

The results for all the land surface heterogeneity scenarios discussed in this synthetic analysis are summarised in Table 7.1. In line with previous synthetic studies (Njoku et al., 1996b; Bindlish et al., 2002; Van de Griend et al., 2003; Davenport et al., 2008), it was observed that the sub-pixel heterogeneity of soil moisture, soil, texture, surface roughness and soil temperature has a minor impact on the retrieval of a pixel average soil moisture, with individual retrieval errors less than 2.8%v/v. In real world applications such errors would be comparable to the radiometer noise, which was of approximately 2K for the PLMR radiometer (see Appendix A3), resulting in approximately 2%v/v for moderately vegetated soil. The effect of the sub-pixel heterogeneity of VWC within land cover types was observed to be significant, but only in the case of heterogeneous forest canopy (mean error of 4.8%v/v), while the heterogeneity of VWC within a grassland or crop covered pixel had a minor impact (mean error smaller than 1.5%v/v). The effect of the heterogeneity of VWC was that of causing an overestimation of the pixel average soil moisture in all cases.

However, the sub-pixel heterogeneity of land cover type was observed to have the highest impact on the L-MEB soil moisture retrieval amongst the land surface factors analysed, with errors well beyond the SMOS target accuracy of 4%v/v and up to 19.8%v/v. The conditions producing the highest errors were wet soil (40%v/v) with the pixel divided in half between grassland and forest. The sub-pixel heterogeneity of land cover generally resulted in overestimation of the pixel average soil moisture for most combinations of grassland, crop and forest pixel fractions. However, when a crop or forest dominant cover type was assumed by the model to be uniform across the pixel in the presence of a significant fraction of grassland, the model underestimated the pixel average soil moisture.

The strong effect of the sub-pixel heterogeneity of land cover type observed in this section has not been reported in previous synthetic studies (Njoku et al., 1996b; Bindlish et al., 2002; Van de Griend et al., 2003; Davenport et al., 2008). This is because those studies simulated variable land cover only through the variability of VWC. In this section instead the effect of the presence within the pixel of different land covers with different VWC but also different radiative transfer properties (i.e., land cover specific parameters in L-MEB) was considered, and therefore included the cumulative effect of the sub-pixel heterogeneity of vegetation optical depth, vegetation scattering albedo (L-MEB parameter ω_P) and vegetation structure (L-MEB parameter tt_P), which are characteristics specific to each land cover types.

It should be noted that, although the impact of individual heterogeneity in soil moisture, soil, texture, surface roughness, soil temperature and VWC (in grasslands and crop) was found to be overall of the order of magnitude of the measurement error due to the radiometer noise, the combined heterogeneity of several of these factors could result in significant errors. A complete analysis of the impact of heterogeneity in land surface factors is a complicated problem, not only because it would be difficult to include all the possible combinations of six variables, but also because there are not enough data to define which of these combinations are physically realistic and actually occur in the study area.

However, the analysis of the effect of land surface heterogeneity with real T_B data performed later in section 7.3 will allow observing the combined effect of the land surface factors here analysed individually. The comparison with the simplified scenarios presented in this section will then be crucial to distinguish the land surface factors having a predominant effect and selecting an approach to account for those land surface factors.

7.2 Aggregation of Airborne Data to Coarse-Scale Pixels

In order to analyse the effect of the sub-pixel heterogeneity of land surface conditions on the soil moisture retrieval at coarse resolutions, coarse pixels were derived from aggregation of 1km resolution airborne observations. These were the 'regional' airborne brightness temperature (T_B) observations, collected across the entire NAFE'05 study area at 1km resolution on four dates.

The aggregation of T_B observations to coarser resolutions is an approach which has been used extensively for passive microwave scaling studies to compensate for the lack of L-band satellite data (Drusch et al., 1999a; Guha et al., 2002; Loew, 2008). However, very few studies verified the scaling properties of T_B observations collected concurrently over the same area at different resolution, and only one study used L-band data (Jackson, 2001). Consequently, the scaling properties of the T_B observations across the NAFE'05 study area are here assessed before aggregating the regional airborne observations of NAFE'05 to coarse pixels (section 7.2.2).

All the airborne data analysed hereby were collected, calibrated and processed as detailed in section 4.3. Therefore, only the more pertinent details are recalled in the following sections.

7.2.1 Scaling of Brightness Temperature Fields

During the NAFE'05 field campaign, a total of sixteen multi-resolution flights were conducted between October 31st and November 25th for use in investigating the scaling properties of T_B fields. On each date one of two focus areas of the NAFE'05 study area, either the "Krui" or the "Merriwa" area, were covered alternatively. Each of these areas was approximately 10km wide and 30km long in the south-north direction (for the location and extent of these areas, see Figure 4.1). On each date, airborne T_B observations were collected at four different altitudes in descending order (10,000ft, 5,000ft, 2,500ft and 625ftm AGL); this resulted in T_B maps at nominal resolution of 1km, 500m, 250m, and 62.5m of the same area and on the same day. Actual resolutions varied slightly depending on terrain elevation and are indicated in Table 7.2.

Ideally, observations of the same area at the same time of the day and with the same instrument configuration should be compared in order to analyse the scaling of the T_B fields. In reality, these were taken at a range of view angles, as the instrument was flown in "pushbroom" configuration, acquiring six concurrent observations at the PLMR beam angles (±7º, ±21.5º, and ±38.5º). Before comparing the T_B maps collected at different resolutions, the effect of varying beam angles was therefore accounted for with the normalisation procedure proposed by Jackson et al. (1999). This procedure assumes that the deviation between beam positions is due to the Fresnel effect and calibration errors for individual beam positions, and that for a given day the Fresnel effect for a particular beam is constant for the range of soil moisture and vegetation present. Using this procedure, T_B observations were normalised to the incidence angle of the radiometer outermost beams (±38.5º) in order to produce maps of T_B with uniform angle. The method was tested with multi-angular data in section 5.3.2.1 and found to be accurate to within 1.5K.

Table 7.2. Characteristics of the Multi-resolution flights. ($^+$) Average of all sixteen dates.

Flight Altitude (ft AGL)	Start Time$^+$ (AM)	End Time$^+$ (AM)	Pixel Dimension at 3dB (m)		
			Nomin.	**Mean$^+$**	**St.Dev.$^+$**
10,000	7:21	7:40	1000	992	105
5,000	7:44	8:30	500	560	68
2,500	8:34	8:53	250	303	37
625	9:17	11:13	62.5	90	14

The T_B observations at the different resolutions were also undertaken at different times (see Table 7.2). This means that soil temperature changes might be significant during these periods, producing differences in the T_B which are not due to scaling. In order to account for changes of soil temperature, the observations were normalised to an intermediate reference time (9:00AM) using the temporal variation of surface soil temperature recorded at the monitoring stations and the procedure described in detail in Chapter 5; the method consists of calculating correction coefficients for each T_B acquisition time as the ratio between the average surface temperature over the study area at the reference time and that at the time of acquisition.

The resulting data set consists of sixteen multi-resolution T_B maps, eight for each of the Merriwa and Krui focus areas. An extract of this multi-resolution data set is shown in Figure 7.8 for the Krui focus area taken on a wet and a dry day (respectively November 1st and 22nd). The rainfall regime experienced by the NAFE’05 study area during the monitoring period allowed observation of a full drydown period, which is reflected in the highest T_B on November 22nd. It should be noted that the areas could not be entirely mapped at the finest resolutions (250m and 62,5m) due to flight time limitation. These flights therefore targeted the NAFE’05 experimental farms, and the analysis presented here was limited to these areas (i.e., areas covered by mapping at all resolutions). These areas are indicated in Figure

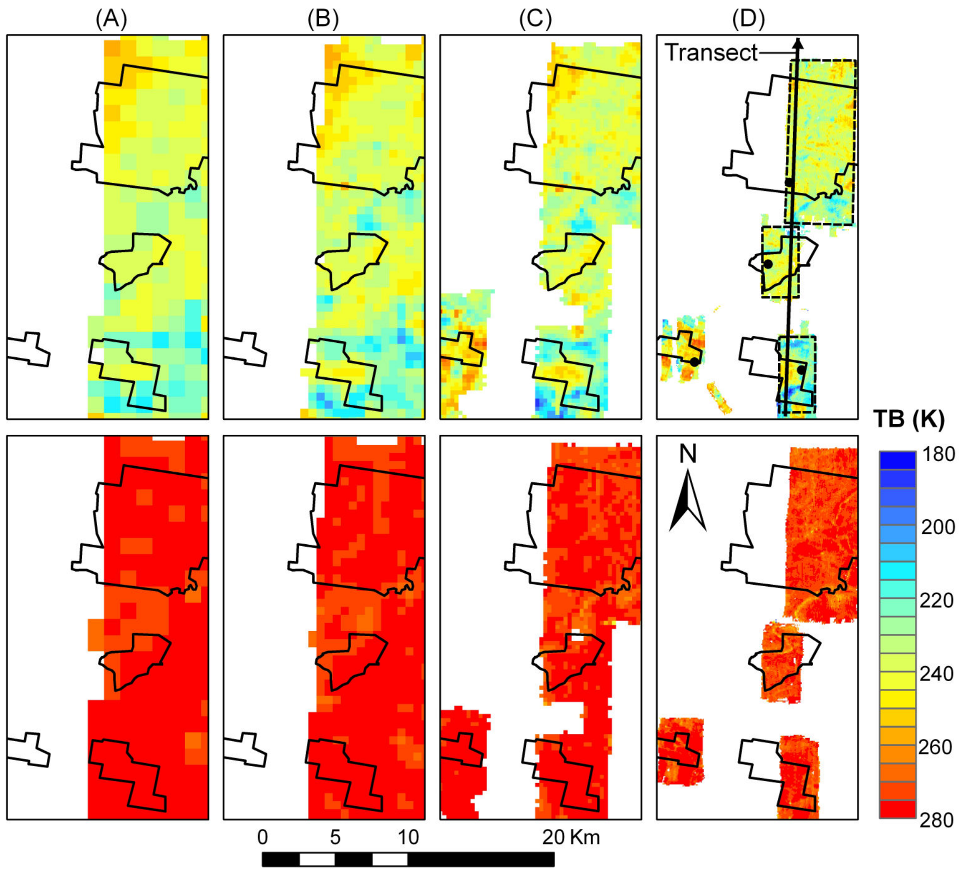

Figure 7.8. Example of multi-resolution T_B data set for the Krui area on November 1st (top row) and November 22nd (bottom row). Maps are displayed by decreasing flight altitude from left to right: 10,000ft and 1km resolution (column A); 5,000ft and 500m resolution (B); 2,500ft and 250m resolution (C) and 625ft and 62.5m resolution (D). Boundaries of the experimental farms are displayed in solid lines. In the top right panel; the black dots indicated the locations of the soil temperature monitoring stations, polygons with dashed lines show the areas covered by mapping at all altitudes and the black arrow indicates the flight line analysed in Figure 7.9.

7.8 (top right panel), and had a total surface area of 70km^2 in the Krui and 60km^2 in the Merriwa area. The consistency between patterns of T_B at different resolutions is notable, although many fine-resolution features are lost in the high-altitude observations due to the coarser resolution. However, the main spatial features of the T_B fields are retained as the resolution becomes coarser.

Figure 7.9 gives an indication of the changes that might be expected as the resolution gets coarser. Here the T_B collected along an high-altitude

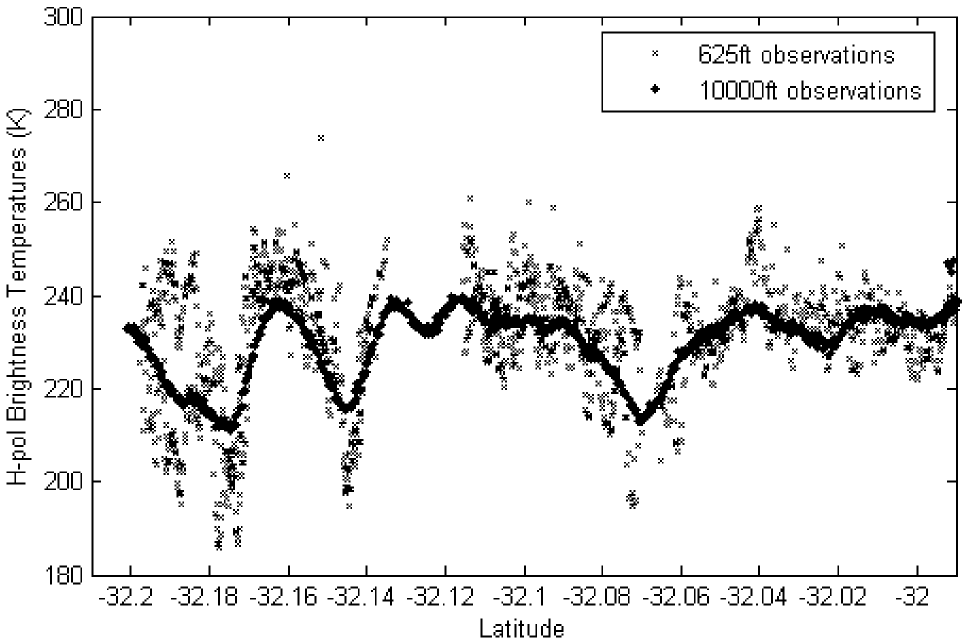

Figure 7.9. Comparison of H-pol brightness temperature observations at two different flight altitudes along the transect shown in Figure 7.8 for November 1st.

(10,000ft) transect (see top right panel in Figure 7.8) are compared with those collected at low-altitude (625ft); to this end, the fine-resolution pixels (from 625ft) falling within each coarse-resolution pixels (from 10,000ft) along the transects were extracted. The figure shows the consistency between T_B spatial variation as measured at different altitudes. An important feature in these plots is that the range of observed T_B decreased as the altitude increased. This is the result of surface features with extreme values of T_B (e.g., areas with localised soil saturation, treed area) filling the radiometer field of view at lower altitudes but not at higher altitudes.

The average and standard deviation of the T_B fields at both polarisation and for each resolution and date are listed in Table 7.3 and Table 7.4 for the Krui focus area. Analysis of the Merriwa data is omitted for reasons of simplicity but the results are analogous. The statistics were calculated considering only the common areas covered by observations at all resolutions. Note that for this analysis the geolocated but un-gridded data were used. Given the large areas analysed and the high density of individual T_B acquisition (approximately 30-40 acquisitions for an area corresponding

Table 7.3. Mean and standard deviation of brightness temperatures at H polarisation over the Krui area for each flight altitude.

Date	10,000ft Alt. 1000m Res.		5,000ft Alt. 500m Res.		2,500ft Alt. 250m Res.		625ft Alt. 62.5m Res.	
	Mean	**St.Dev.**	**Mean**	**St.Dev.**	**Mean**	**St.Dev.**	**Mean**	**St.Dev.**
1/11	232.3	7.4	230.6	8.8	230.7	8.0	229.8	10.5
3/11	246.4	5.2	245.7	6.8	243.6	7.2	240.3	9.4
8/11	247.5	5.0	246.9	6.7	246.2	7.0	243.9	9.2
10/11	248.7	6.9	248.1	7.7	247.4	8.5	244.2	10.2
15/11	265.0	4.1	265.3	5.0	263.1	6.0	260.8	6.8
17/11	266.7	3.5	266.3	4.3	265.3	5.6	263.6	5.9
22/11	271.8	2.9	271.9	3.6	270.7	4.6	267.9	5.1
24/11	252.8	6.7	253.4	7.8	254.6	7.4	252.0	10.9

Table 7.4. Mean and standard deviation of brightness temperatures at V polarisation over the Krui area for each flight altitude.

Date	10,000ft Alt. 1000m Res.		5,000ft Alt. 500m Res.		2,500ft Alt. 250m Res.		625ft Alt. 62.5m Res.	
	Mean	**St.Dev.**	**Mean**	**St.Dev.**	**Mean**	**St.Dev.**	**Mean**	**St.Dev.**
1/11	256.9	6.3	255.9	6.7	255.8	6.8	254.3	8.9
3/11	268.7	4.5	267.7	5.1	266.1	5.5	263.3	7.7
8/11	266.6	4.1	266.2	4.9	265.7	5.4	264.3	7.4
10/11	269.9	6.2	269.0	6.0	268.9	6.4	266.0	8.3
15/11	280.4	3.9	280.5	3.9	278.6	4.6	276.3	5.5
17/11	280.5	3.3	279.8	3.5	279.4	4.1	277.7	4.7
22/11	285.1	2.7	285.1	2.9	284.0	3.4	281.5	3.9
24/11	272.2	5.1	272.2	5.5	273.1	5.2	271.2	8.4

to the nominal pixel size), the gridding process would not have affected the results presented.

Table 7.3 and Table 7.4 shows how the T_B detected over a large area varies with the sensor altitude (i.e., ground resolution). It is shown that the average emission was fairly constant with resolution on all the monitoring dates, corresponding to wetness conditions going from near saturation (November 1st) to near residual soil moisture content (November 22nd). Due to the local differences between the signal detected at different altitudes already discussed above for a single flight line, the standard deviation of T_B consistently decreased going towards coarser resolution. The change between the average T_B measured at the coarser and finer resolution (respectively 1km and 62.5m) was on average 3.6K (H-pol) and 3.2K (V-pol), with a maximum change of respectively 6.1K and 5.4K. This significant change occurred on only one day (November 3rd). On all the remaining days the difference was below 4.5K for both polarisations.

It is important to note in Table 7.3 and Table 7.4 that the largest difference in T_B occurred between the 62.5m observations and the 250m observations. This was 2.4K on average at H-pol compared with 3.6K as the total difference between the 62.5m and 1km resolutions. The difference in average T_B between the 250m resolution observations and the 1km observations was on average only 1.2K (H-pol) and 1.1K (V-pol). This difference is below the PLMR radiometer noise (approximately 2K, see Appendix A3), therefore suggesting that the average T_B mapped at resolutions between 250m and 1km is essentially constant over areas of the order of 70km^2.

The difference observed between the average T_B at 62.5m and 250m is attributed to the normalisation for soil temperature changes applied to the data. This was done for each T_B acquisition by calculating the ratio between the average soil temperature at the reference time (9:00AM) and that at the time of the acquisition, with the soil temperatures taken from four monitoring stations across the focus areas (these are indicated in Figure 7.8). Since these monitoring stations certainly did not characterise the spatial variation of the soil temperature across an area as large as 70km^2, the normalisation procedure may have introduced errors due to a mismatch between average and local soil temperature changes. This would strongly affect the high-resolution observation, since these were undertaken later in the morning (see Table 7.2) when spatial gradients in soil temperature are more significant. The normalisation procedure would instead be more accurate for the 1km, 500m and 250m observations, since these were collected earlier in the morning with more uniform soil temperatures.

The objective of the present analysis was to support the aggregation of 1km airborne observation to resolutions of a typical SMOS pixel. Although the results presented are limited to resolutions from 62.5m to 1km, and therefore cannot be directly extrapolated to 30-50km resolutions, it can be noted that the difference in average T_B between the four resolutions analysed here strongly decreased going toward coarser resolutions. In particular, the average difference in measured H-pol T_B was 2.4K between 62.5m and 250m resolution observations, 0.8K (250m-500m observations) and 0.4K (500m-1km observations). Results for V-pol were analogous. These results, obtained on areas some 20km x 30km in size encompassing the range of land surface conditions observed across the entire study area, support the conclusion that the aggregation of 1km airborne observation to resolution typical of a future SMOS footprint (40km x 40km) will produce realistic coarse-scale T_B observations. These results are consistent with those of Jackson (2001), who observed that the area-averaged V-pol T_B values over test sites of a few km^2 consisting of pasture and wheat stubble were the same regardless of the spatial resolution (200m-1km). The results presented here extend that analysis to areas which are an order of magnitude larger, covering a variety of crops of land surface conditions and include H polarisation, which is more sensitive to soil moisture changes than V polarisation.

7.2.2 Aggregation of Brightness Temperatures

Building upon the verification, in the previous section, that the same average T_B values are observed over the same area at different resolutions, in this section coarse-resolution (5, 10, 20, 30, 40km) T_B observations were produced by aggregating of the 1km regional T_B airborne observations. Regional T_B observations were described in Chapter 4 and Chapter 5 where they were used to retrieve soil moisture maps of the study area at 1km resolution. The relevant information is briefly recalled here.

Regional observations were collected on October 31st, November 7th, 14th and 21st, with 40km-long north-south oriented flight lines flown at 10,000ft between approximately 7:00AM and 9:30AM. This time window was chosen to be close to SMOS overpass time (6.00AM) and therefore replicate the observation conditions, yet not affected by vegetation dew. Before aggregating the T_B observations to coarser resolutions, the effect of varying beam angles was accounted for through the normalisation procedure proposed by Jackson et al. (1999) and tested on the NAFE'05 study area in Chapter 5.

Using this procedure, the T_B observations were normalised to the incidence angle of the radiometer outermost beams (±38.5º). This choice was motivated by two reasons:

- at close-to-nadir incidence angles the V and H-pol T_B are very similar (see Figure 5.13), while at off-nadir incidence angle V-pol T_B are generally higher than H-pol (this variation depends on the land surface conditions). By using larger incidence angles, therefore, the retrieval accuracy of the L-MEB algorithm is improved since the polarisation difference yields information on the polarising effect of the vegetation canopy (Wigneron et al., 2000); and
- the number of incidence-angles and their angular range at which SMOS observations will be available will depend on the distance of the pixel to the sub-satellite track. This position can be expressed in terms of the half-swath angle, and the range varies approximately between 0º and 50º for a sub-satellite track and approximately between 38º and 44º for a half-swath angle of 33º. Therefore, the 38.5º reference angle chosen is representative of the SMOS observations that will be available for a large fraction of the earth surface.

Prior to aggregation, the 1km T_B observations were also normalised for soil temperature changes to a reference time (8:00AM), using the temporal variation of surface soil temperature recorded at the monitoring stations as described in detail in Chapter 5. This is desirable since when aggregating 1km T_B observations to coarse resolution these will include observations taken at different times, which when considering very coarse pixels (30km and up) could be as far apart as 2.5 hours. Omitting this normalisation would introduce soil temperature differences across the aggregated pixels which do not correspond to actual soil temperature variability that would exist in SMOS pixels. Note that in Chapter 5 the 1km T_B observations were also normalised for soil temperature changes to the same reference time before retrieving the soil moisture maps used in this Chapter as ground truth.

The 1km T_B observations were aggregated using a “moving window” approach. The aggregation consisted of an arithmetic average of the 1km T_B observations falling within windows at various resolutions, namely 5, 10, 20 30km, which were “moved” across the study area with spatial steps of 5km. Moreover, the T_B observations were also aggregated within a single, 40km x 40km window covering the entire area mapped during each of the regional flights. This was repeated for each of the four regional flight days, obtaining coarse pixels at five resolutions for four different dates. The total number of pixels available (over four dates) was 256, 196, 100, 36 and 4 at respectively 5, 10, 20, 30 and 40km resolution. T_B observations were aggregated at both V and H polarisation to produce bi-polarised coarse T_B observations.

While the 5, 10 and 20km resolutions are finer than that of a future SMOS pixel (30-50km), they were chosen to allow the analysis of a much wider variety of conditions of land surface heterogeneity than possible with pixels at 40km resolution (i.e., uniform pixels as well as heterogeneous pixels, and heterogeneity of different land surface factors). Moreover, this choice resulted in a considerable increase in the number of pixels available for analysis. The approach adopted in the following sections therefore consisted of (i) focusing the analysis on the finer-resolution pixels (5km); (ii) extrapolating the conclusions drawn at fine resolution to SMOS resolution using subsequently coarser pixels (10, 20, 30km), and finally (iii) verifying those conclusions using the 40km sized pixels.

7.2.3 Retrieval Scheme

The soil moisture retrieval approach used here is the same as that used in Chapter 5 to retrieve soil moisture estimates at 1km resolution. The L-MEB model was applied to the coarse (5-40km), bi-polarised T_B observations described in the previous section to retrieve soil moisture and vegetation optical depth estimates assuming that the pixel was uniform in terms of land cover, soil texture, soil temperature, canopy temperature and surface roughness. Then aim was to understand the effect of the sub-pixel heterogeneity of land surface conditions on the soil moisture retrieval at coarse resolutions when no consideration is given to this heterogeneity in the retrieval approach.

The ancillary data and radiative transfer parameters input of the L-MEB model were the same as those adopted for the regional 1km soil moisture retrieval described in section 0. These are listed hereafter.

- Land cover: Landsat derived land cover map at 30m resolution**.** Each coarse pixel was assigned the land cover type (native grass, crop or forest) which occupied the highest fraction of the pixel area.
- Soil texture: 1km resolution maps of percentage of sand and clay content derived from soil particle analysis of 88 5cm deep soil samples.
- Soil temperatures (2.5cm and 15cm): Spatial average of the soil temperature recorded at the eleven permanent monitoring stations across the study area at 8:00AM This was the reference time to which all T_B observations were normalised as described in section 7.2.2.
- Canopy temperature: Set equal to the 2.5cm soil temperature, assuming thermal equilibrium between soil and canopy.

The sensitivity analysis of the L-MEB soil moisture retrieval to soil temperature and canopy temperature errors presented in Chapter 5 showed that the errors in soil moisture associated with the assumption of spatial uniformity of surface soil temperature and of thermal equilibrium between soil and canopy were both smaller than 2%v/v.

Values of the L-MEB ancillary data for each coarse-resolution pixel were calculated with by averaging the spatially distributed values of each quantity within the pixel. Moreover, the standard deviation of the quantity was used to quantify the sub-pixel heterogeneity of each land surface factor.

On the basis of the land cover classification, a set of L-MEB radiative transfer parameters were selected from the values derived for specific land cover conditions in the NAFE'05 study area in Chapter 5. The explicit assumption made here was that the parameters are uniform within each land cover type. Implicitly, the assumption was also made that the parameters are scale invariant, i.e., the impact they have on the model output does not change with the resolution of observation over a uniform surface, and therefore they can be applied to coarser resolutions up to the satellite pixel scale (40km). This assumption was supported by the evaluation of the L-MEB model and its parameterisation at 60m and 1km resolution performed in Chapter 5. Although those results do not directly imply that the scale invariance can be extrapolated to resolutions coarser than 1km, this assumption is necessary as the scale invariance of the L-MEB parameters cannot be verified unless actual coarse-resolution observations are available over fairly uniform land surface conditions.

7.3 Effect of Heterogeneity on Coarse-Scale Soil Moisture Retrieval

In Figure 7.10 the soil moisture retrieved from the coarse T_B observations at 5, 10, 20 and 30km is compared with the soil moisture ground truth, i.e., the 1km L-MEB soil moisture product covering the whole study area obtained from 1km airborne data (Chapter 5), averaged to the respective spatial resolution. While there is a reasonable agreement between retrieved soil moisture at all resolutions and soil moisture conditions, there are many examples of pixels having errors higher than the SMOS target accuracy (4%v/v).

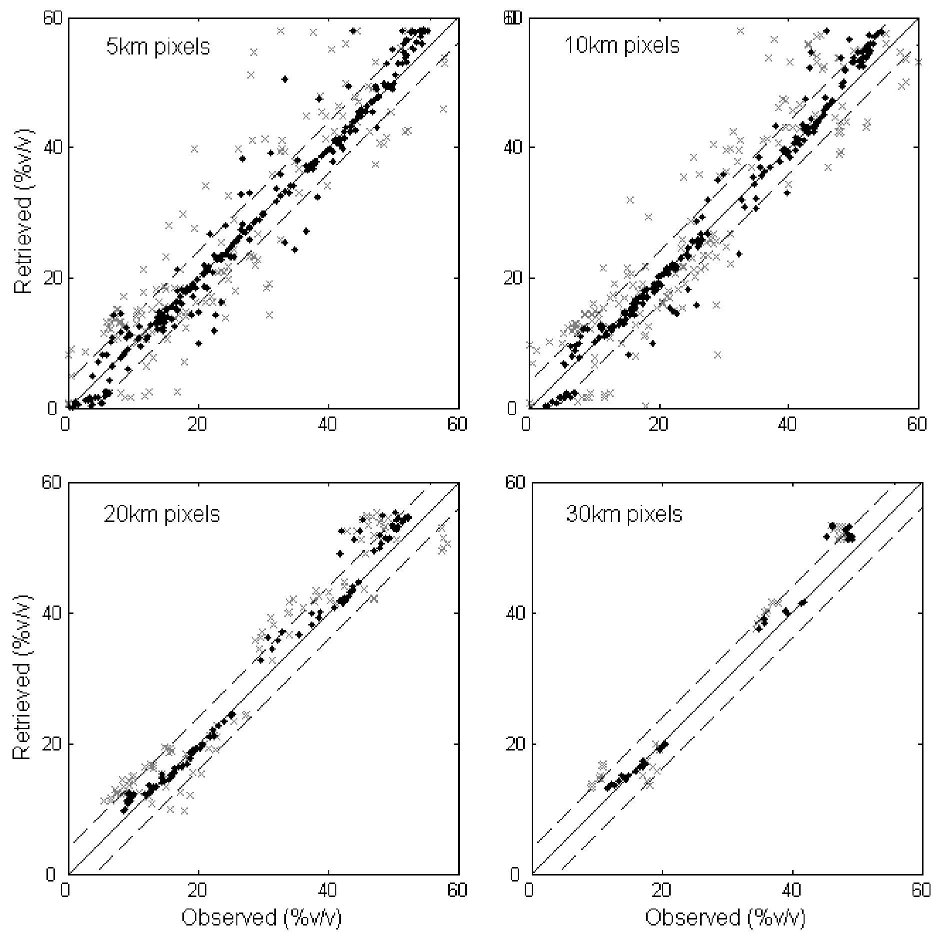

Figure 7.10. Comparison of the soil moisture retrieved for each 5, 10, 20 and 30km resolution pixel against the average within each coarse pixel of the 1km L-MEB product (black dots) and the regional ground sampling (gray crosses) are shown as ground truth. Dashed line indicate the SMOS target accuracy (4%v/v)

In Figure 7.10 the retrieved soil moisture for each coarse pixel is also compared with the average of the regional soil moisture measurements (at 2km spacing) falling within the pixel. It is notable that, when using the averaged ground measurements, the error appeared substantially higher and

the scatter was significant. This increased noise is due to the fact that when using the ground measurements only a few sampling points are compared with the soil moisture retrieved at coarse resolution, therefore demonstrating the advantage of using the 1km L-MEB soil moisture product as ground truth. However some characteristics of the coarse-scale retrieval error can be identified regardless of the ground truth data set used. The error tended to be

Table 7.5. Error statistics of the comparison between soil moisture retrieved at various resolutions and the 1km L-MEB soil moisture ground truth. All soil moisture values are in %v/v. Error sign "+" indicates overestimation of the soil moisture ground truth

Pixel size (km)	Nr. Of Pixels (*4 Dates)	RMSE	Mean Error	Median Error	Max Error (Abs.)	r^2
5	256	3.1	0.1	-0.12	+17.2	0.97
10	196	3.0	0.1	-0.10	+12.2	0.97
20	100	2.7	1.3	0.26	+10.6	0.98
30	36	2.6	1.5	0.97	+7.2	0.99

greater in wet conditions and was characterised by overestimation of the pixel average soil moisture. In dry conditions the error was smaller and was generally associated with an underestimation of the pixel average soil moisture.

The error statistics of Figure 7.10 are shown in **Table 7.5**. At the finest resolution (5km), the RMSE was below the SMOS target accuracy and the error distribution had no significant bias (0.1%v/v). As the resolution got coarser, the retrieval was more accurate (RMSE decreased to 2.6%v/v at 30km resolution) but the distribution of the error tended to be positively biased. The maximum retrieval error was 17.2%v/v at the finest resolution and decreased rapidly as the resolution got coarser, being of 7.2%v/v at 30km resolution. However, it should be noted that this decrease in error might be a result of the NAFE'05 study area being largely occupied by native grass (73%) with only a small fraction of forest (22.1%) and crops (4.6%), therefore presenting rather uniform land cover conditions as opposed to several of the finer-resolution pixels. For this reason, in the following section the analysis focuses on the 5km resolution pixel, while the extrapolation to coarser pixels will be discussed in more detail in section 7.3.2).

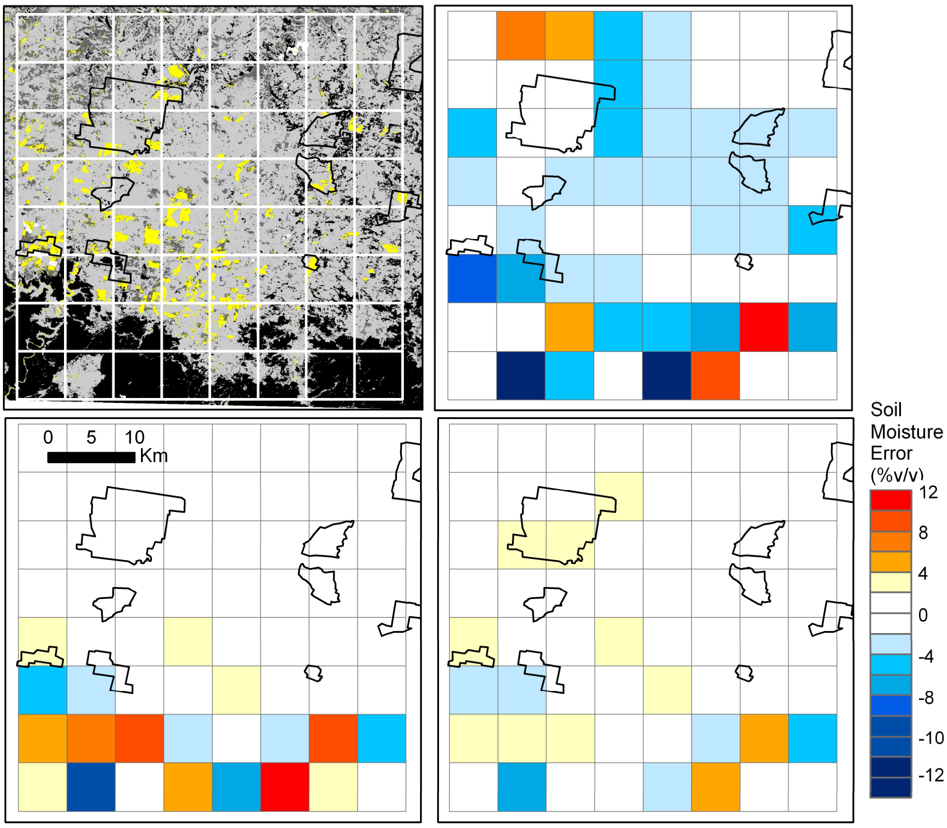

Figure 7.11. Spatial distribution of the coarse-scale (5km) soil moisture retrieval error across the study area on October 31st (top right), November 7th (bottom left) and November 14th (bottom right). Red colours indicated underestimation of the pixel average soil moisture, blue colours indicated overestimation. The top left panel shows the Landsat land cover map (black=forest, grey=native grass, yellow=crops). Boundaries of the experimental farms are indicated in solid black lines.

7.3.1 Retrieval at 5km Resolution

Figure 7.11 shows the spatial distribution of soil moisture retrieval error at 5km resolution for three of the four dates (November 21st is omitted as it is very similar to November 14th) together with the Landsat derived land cover map of the study area. As observed in Figure 7.10, the error was generally higher in wet conditions (October 31st) than dry conditions (November 14th). Moreover, there was persistence in the spatial patterns of the error. In particular, the error was typically higher in the southern part of the study area, especially at the edge of the forested area. The pixels with more homogeneous land cover (mostly covered by forest or moderate vegetation cover, i.e., crop and/or native grass) had a smaller error. This is particularly evident in intermediate and dry conditions (bottom row of Figure 7.11). It is notable how the error at the boundary between forest and moderate vegetation covers was variable in sign but within each pixel the sign of the error was persistent through time. These observations indicate persistency of soil moisture retrieval error in pixels which are across the boundaries between forest and moderate vegetation covers and stronger on wet conditions. These findings are consistent with the synthetic study performed in section 7.1, which indicated that the sub-pixel heterogeneity of land cover type had the highest impact on the L-MEB retrieval amongst the land surface factors analysed, producing a strong error (up to 19.8%v/v) on a pixel with wet soil (40%v/v) when the pixel land cover was approximately half native grass and half forest.

In order to further investigate the association between land cover type heterogeneity and soil moisture retrieval error, the retrieval error at 5km resolution was analysed in terms of fractions of each land cover type within the pixel (to characterise land cover heterogeneity as done in the synthetic analysis) as well as standard deviation of soil moisture, vegetation optical depth and soil texture within the pixel. This is shown in Figure 7.12. In this plot, the effect of heterogeneity of soil temperature and surface roughness was omitted. The reasons behind this were that: (i) throughout this study soil temperature was considered spatially uniform across the entire study area due to the small spatial variability observed between the data recorded at the continuous monitoring stations (see section 0), and (ii) the surface roughness parameter in L-MEB does not strictly represent a "physical roughness", but rather includes a dielectric component which cannot be easily mapped in space in order to characterise its sub-pixel heterogeneity (this is extensively discussed in section 5.1.5.3 and Appendix A4). However, the synthetic analysis showed that the sub-pixel heterogeneity in both these factors had a negligible impact on the soil moisture retrieval error.

Figure 7.12 indicates that, as suggested by the synthetic analysis, there is

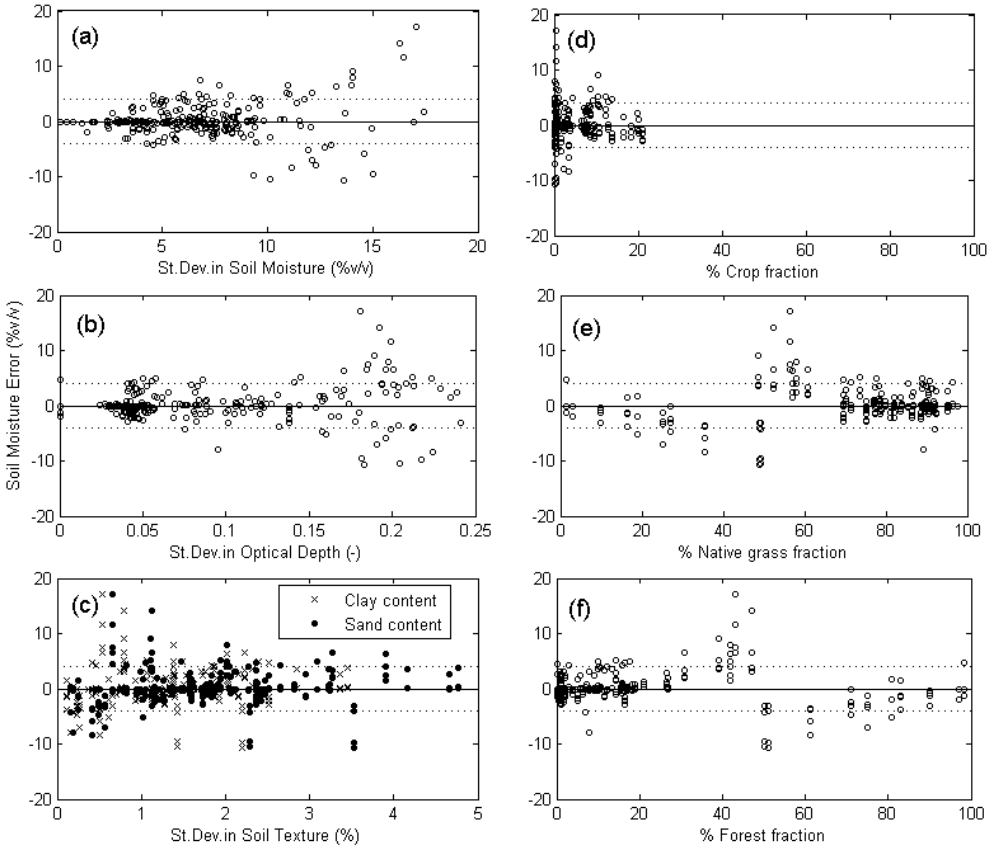

Figure 7.12. Relationship between coarse-scale (5km) soil moisture retrieval error for each 5km pixel and the sub-pixel heterogeneity (standard deviation) of (a) soil moisture at 1km resolution (b) vegetation optical depth at 1km resolution, (c) clay and sand content at 1km resolution and percentage of pixel fraction of land cover type crop (d), native grass (e) and forest (f). Dashed horizontal lines indicate the soil moisture target accuracy (±4%v/v).

a significant correlation between the soil moisture retrieval error and the variability of land cover type within the pixel. In particular a strong correlation was observed with the fraction of the pixel occupied by native grass and forest (panel e and f), while no correlation was observed with the fraction of crops. However, it should be noted that at this resolution the maximum percentage of crop fraction was quite small (20%). Therefore, the effect of the presence of a large fraction of cropped area could not be assessed, although it can be inferred from the lack of correlation of the error with the crop fraction up to 20%. Consequently, the errors are not expected to increase at higher crop fractions. Note that panels "e" and "f" in Figure 7.12 yield very similar information; in the presence of a small crop fraction and since no other land cover types were present in the study area the native grass and forest fraction are nearly complementary. In panel "f", for very low forest fraction (i.e., more uniform pixels mostly occupied by native grass and eventually small amount of crops) the retrieval errors were below SMOS target accuracy. However, as the forest fraction increases (i.e., pixel split between native grass and forest and eventually a small amount of crops) the mean retrieval error increased linearly (in absolute terms) and exceeded SMOS target accuracy when the forest fraction was above approximately 30% and achieved a maximum (overestimation) of +17.2%v/v at approximately 50% native grass fraction. A further increase in forest fraction produced a strong discontinuity in the error, which became an underestimation (-10%v/v) and decreased quickly until going below the SMOS target accuracy when the pixel is mostly occupied by forest.

This error pattern, and in particular the strong correlation of the retrieval error with the sub-pixel heterogeneity of the land cover and the discontinuity of the error sign for highly heterogeneous pixel (approximately 50% grass and 50% forest) has been observed in the synthetic study (section 7.1.3 and Figure 7.4). It was explained there that the discontinuity occurs in the case of pixels with equivalent sub-pixel fractions of native grass and forest (~50%); in this case the retrieval algorithm switches between the two land cover types as the one used in the forward modeling (and thus considered uniform across the pixel) depending on the predominance of either sub-pixel fraction. As a result of this, the pixel average soil moisture is overestimated when a pixel containing a significant amount of forest is modeled as having a uniform native grass cover and underestimated when the pixel is modeled as having a uniform forest cover.

It should be noted that there was good agreement between the values of the maximum errors observed (+17.2%v/v and -10.0%v/v) and those determined through synthetic analysis (+19.8%v/v -10.9%v/v, see Table 7.1). This is because the synthetic analysis was done using "realistic" values for the ancillary data derived from analysis of the ground conditions in the study area. These results therefore confirmed with actual T_B observations the significant effect of the sub-pixel heterogeneity of land cover type on the coarse-scale soil moisture retrieval which was suggested by the synthetic analysis.

In Figure 7.12 no correlation was observed with the sub-pixel heterogeneity of vegetation optical depth (panel b) and percentage of clay and sand content (panel c). The synthetic analysis had already indicated that the sub-pixel heterogeneity of VWC (to which optical depth is linearly related through vegetation parameter "*b*") and percentage of sand and clay content should have a minor effect on the retrieval (less than 2%v/v, see Table 7.1). Note that the synthetic study indicated that a significant error (4.8%v/v) could derive from the heterogeneity of optical depth within a forested area. However, this could not be verified here with real data, as the optical depth used in Figure 7.12 was that retrieved together with soil moisture at 1km resolution in Chapter 5; in the case of forested pixels, the optical depth had been imposed *a priori* in order to ensure better soil moisture retrieval over dense canopy.

In Figure 7.12 the error in retrieval increased with increasing sub-pixel heterogeneity of soil moisture (panel "a"). However, this was more noisy than that with the land cover type fraction and evident only for elevated soil moisture heterogeneity (standard deviation above 10%v/v). Moreover, the synthetic study indicated that the direct effect of the sub-pixel heterogeneity of soil moisture is that of producing negative errors (underestimation), while in panel "a" of Figure 7.12 the errors are both negative and positive. It seems therefore likely that the relationship of the error with the soil moisture heterogeneity could be an indirect effect of the correlation between soil moisture spatial distribution and the land cover, which has been observed in the study area and discussed in detail in Chapter 6. There it was shown that the spatial distribution of land cover type, together with that of sand and clay content, is the main factor determining the spatial distribution of soil moisture.

In order to understand the relative importance of the sub-pixel heterogeneity of land cover and soil moisture in determining the error, Figure 7.13 reproduces panel “a” of Figure 7.12 with the data points colour-coded using the value in the x-axis of panel ”e” and vice versa. This helps to visualise the relationship between the retrieval error and each factor when the other factor is kept constant. It can be seen from this plot that the error in coarse-scale soil moisture cannot be simply attributed to heterogeneity in land cover or soil moisture, but rather to a combination of the two factors.

In the top panel of Figure 7.13, the retrieval error exhibits correlation with the soil moisture standard deviation for pixels having a very similar fraction of native grass. However, this relationship is very variable; depending on the amount of native grass fraction (i.e., degree of land cover heterogeneity), the relationship can be a non-linear increase in error due to increase in soil moisture standard deviation (e.g., top panel of Figure 7.13, data points with native grass between approximately 60-70%) or a linear decrease (data points with native grass between approximately 40-50%). Moreover, when the land cover is fairly uniform (e.g., data points with native grass below 25% or above 75%) a weak or zero correlation between the error and the soil moisture heterogeneity is observed.

The comparison between the panels of Figure 7.13 also indicates that, despite the confounding effect between the two land surface factors, the sub-pixel heterogeneity of land cover had a predominant effect. The heterogeneity of soil moisture in fact caused a significant soil moisture retrieval error, but only in conjunction with a strong heterogeneity of land cover. In the top panel of Figure 7.13, it was the heterogeneity of land cover which determined the sign of the error, since the points with native grass fraction higher than approximately 50% (i.e., pixels where native grass is the dominant land cover type within the pixel) are mostly above the x-axis (overestimation error), and vice versa. Moreover, small soil moisture retrieval errors occurred in pixel with even strong soil moisture

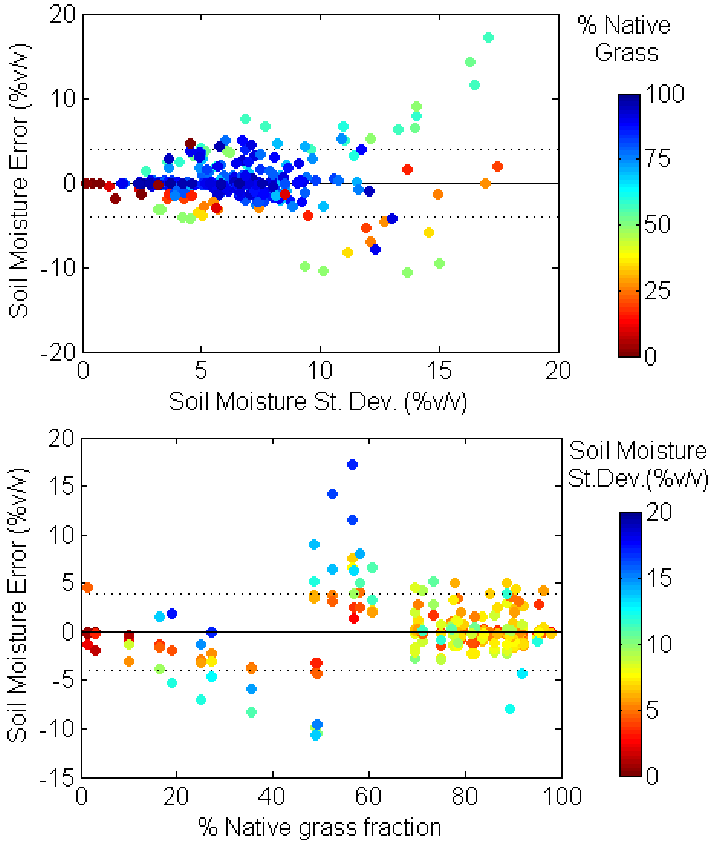

Figure 7.13. Relationship between the soil moisture retrieval error for each 5km pixel and the sub-pixel heterogeneity (standard deviation) of soil moisture (top panel) and percentage of native grass (bottom panel). In each plot, data points are colour coded using the x-axis of the other plot.

heterogeneity but fairly uniform land cover (e.g., top panel, data points with native grass below 25% or above 75%). This is the case, for example, of soil moisture heterogeneity induced by land surface factors other than land cover type (e.g., soil texture or topography as seen in Chapter 6). Conversely, in the bottom panel of Figure 7.13, an increase in land cover heterogeneity (i.e., in this case increase of native grass fraction up to 50%) caused an increase of the retrieval error regardless of the soil moisture standard deviation within the. The observation that the heterogeneity of soil moisture caused a significant soil moisture retrieval error only in conjunction with a strong heterogeneity of land cover can be interpreted in light of the results of Chapter 6, where it was shown, through analysis of ground soil moisture data, that the forested area tended to exhibit consistently drier soil moisture conditions than the native grass areas. Since drier soil moisture conditions cause higher microwave emission, and areas with dense canopy such as forest have generally higher emission, the combination of the two factors further increases the difference in emission between the forest and the native grass areas, causing the increase in error observed in Figure 7.13. These results are in contrast with those of Burke and Simmonds (2003), one of the few studies to link the effect of heterogeneity on coarse-scale passive microwave retrieval to the spatial distribution of soil moisture induced by vegetation type. They observed that the physical connection between vegetation cover and soil moisture worked to reduce the effect of heterogeneity estimated analytically by reducing the variability of emissivity. However, they only analysed one study site of mixed bare and moderate vegetation cover (crop), with a much weaker contrast of optical depth than that analysed here over large areas.

The synthetic analysis presented earlier in this Chapter also highlighted that retrieval errors induced by the sub-pixel heterogeneity of land cover (as well as heterogeneity in all other factors) significantly depends on the pixel-average soil moisture conditions, with higher retrieval errors associated with wetter pixel conditions. However, what is investigated here is a different effect, where the heterogeneity of soil moisture acts in synergy with that of land cover type to increase the error, since soil moisture was kept uniform between the land cover types in the synthetic analysis. The dependence of the retrieval error on the pixel-average soil moisture conditions is analysed in Figure 7.14. The plot shows that a direct dependence of the error on soil moisture conditions as observed with synthetic analysis is not visible when using real data. The highest errors are, however, mostly associated with intermediate and wet soil moisture conditions, where there is the greatest sub-pixel soil moisture variability.

The analysis of the effect of the land surface heterogeneity at 5km resolution soil moisture retrieval has thus far led to five important observations:

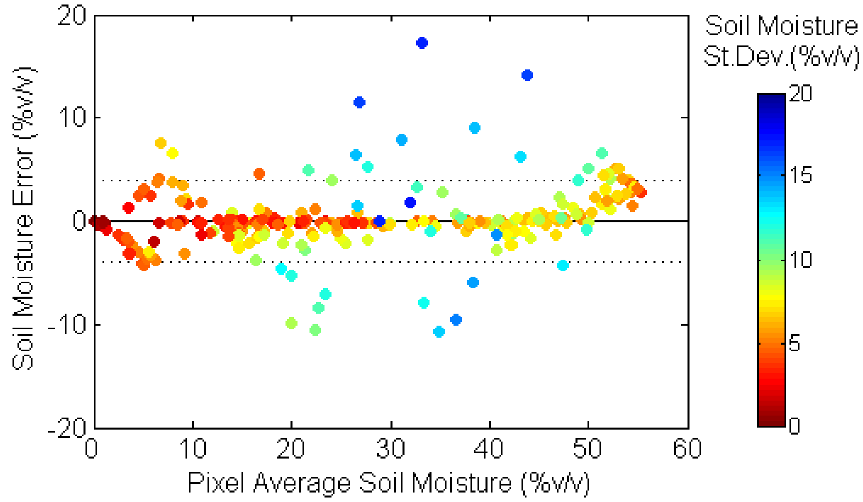

Figure 7.14. Relationship between the soil moisture retrieval error for each 5km pixel and the average pixel soil moisture conditions. The data points are colour coded by the soil moisture standard deviation within the pixel.

1. there was significant correlation between the soil moisture retrieval error and the heterogeneity of land cover type within the pixel; since in the study area the only land cover types were native grass, crop and forest, and that the crop fraction was generally small, this meant that a strong correlation could be established between the retrieval error and the percentage of pixel area occupied by forest (and the nearly complementary percentage of pixel area occupied by native grass);
2. the sign of the retrieval error due to land cover heterogeneity depended on the predominance of forest or native grass within the pixel, i.e., the pixel average soil moisture was overestimated when a pixel containing a significant amount of forest was modelled as having a uniform native grass cover and underestimated when the pixel is modelled as having a uniform forest cover;
3. the retrieval error was above SMOS target accuracy for a forest fraction exceeding 30%v/v in a pixel otherwise occupied by native grass (and eventually a relatively small fraction of crop), and achieved a maximum (+17.2%v/v and -10.0%v/v) when the fractions of native grass and forest were close to 50%;

4. in the presence of critical land cover conditions (fractions of native grass and forest close to 50%) the error was highly sensitive to the heterogeneity of soil moisture within the pixel, with higher error associated with higher sub-pixel heterogeneity of soil moisture; and
5. the L-MEB soil moisture retrieval was not significantly affected by the sub-pixel heterogeneity of soil texture or by the sub-pixel heterogeneity of soil moisture related to soil texture variability (shown in Chapter 6**).**

7.3.2 Extrapolation to 40km Resolution

The analysis was conducted thus far by considering only pixels with relative fine resolution (5km), so as to analyse the largest possible variety of land cover conditions. The next step is to establish how these findings can be extrapolated to pixel resolutions more similar to that of a SMOS pixel (40km). Since at 5km resolution the error was found to be mainly determined by the relative sub-pixel fractions occupied by forest and native grass, it is expected that errors of the same magnitude will be observed at coarser resolutions, provided that the conditions producing the higher errors (~50% native grass and ~50 forest fraction) were also present at the coarser resolution. This is of course subjected to the presence of patches of forest and native grass large enough to occupy at least 50% of the pixels at each resolution. However, given that only a small fraction of the NAFE'05 study was occupied by forest, the critical conditions might not occur when considering the 40km simulated pixel over the area.

To verify this, the maximum sub-pixel fraction for each land cover type was calculated amongst all the pixels analysed at each resolution. Table 7.6 shows these maximum sub-pixel fractions together with the maximum soil moisture retrieval error observed at each resolution. The fraction showed here for each land cover type is the maximum fraction amongst all the pixels analysed at each resolution, therefore the three fractions (crop, native grass and forest) do not necessarily amount to 100% at each resolution, since they correspond to different pixels. However, the table indicates how as the

Table 7.6. Variation with the pixel resolution of the maximum sub-pixel fractions of each land cover type (columns 1-3), the maximum soil moisture retrieval error (column 4) and the soil moisture error for pixels with sub-pixel fractions equal to the 40km pixel (column 5).

Pixel Res.	(1) Native Grass %	(2) Forest %	(3) Crop %	(4) Maximum Retrieval Error (%v/v)	(5) Retrieval Error for conditions* (%v/v)
5km	97.8	98.2	20.9	+17.2	+6.6
10km	94.4	70.0	17.3	+12.2	+7.3
20km	90.2	38.5	11.0	+10.6	+6.7
30km	85.8	25.1	7.4	+7.2	+7.2
40km	73.0*	22.1*	4.6*	+5.5	+5.5

resolution gets coarser the maximum fraction of every land cover type decreases. This is because when observing the landscape at coarser resolutions, less pixels have uniform conditions (i.e., with fraction of one particular land cover type close to 100%) and more pixels present a mix of land cover types (i.e., fractions smaller than 100%).

While at 40km the maximum fraction of native grass is reduced to approximately 25% of the maximum native grass fraction observed at 5km, in the case of forest and crops the decrease is more substantial, respectively 77% and 78% of their value at 5km resolution. This is due to the NAFE’05 study area being largely occupied by native grass. Consequently, in the NAFE’05 study area the chance of having pixels with the critical conditions of land cover heterogeneity (~50% native grass and ~50 forest fraction) is decreased as the resolution gets coarser.

The critical conditions of land cover heterogeneity could therefore not be directly observed at the coarser resolution, due to the limited amount of forest present in the NAFE’05 study area. This explains why the maximum retrieval error in Table 7.6 decreases as the resolution gets coarser. In order to understand whether the maximum retrieval error that can be produced by the heterogeneity of land cover at the resolution of a typical SMOS pixel is equal to that observed at 5km, the error for pixels with land cover fractions similar to those of the 40km pixel simulated across the entire study area (73.0% native grass, 22.1% forest and 4.6% crop) were extracted at each resolution and compared.

This is shown in the last column of Table 7.6. The error produced by the same conditions of land cover heterogeneity (~73% native grass, ~22.1% forest and ~4.6%crop) was very similar at all the resolutions, varying by less than 1.1%v/v from 5km to 40km sized pixels. This indicates that the effect of the heterogeneity of land cover is invariant with resolution, demonstrating at the scale of a typical SMOS pixel land surface heterogeneity would produce a soil moisture retrieval error greater than that actually observed in the study area (5.5%v/v), and most likely as high as that observed at 5km resolution for critical conditions (~50% native grass and ~50 forest fraction), had these conditions been observed at 40km resolution within the NAFE'05 study area.

7.4 Chapter Summary

This Chapter has assessed the magnitude of the L-MEB soil moisture retrieval error that is likely to exist at the resolution of a SMOS pixel as a consequence of unaccounted sub-pixel heterogeneity in land surface conditions, i.e., when the pixel is assumed to be uniform. Moreover, the land surface factors which are mostly responsible for this error have been identified. This assessment was made in two ways: (i) using synthetic data to analyse the effect of sub-pixel heterogeneity of each land surface factor in turn, and (ii) using real airborne data and ground ancillary data collected during the NAFE'05 field campaign to confirm the synthetic results and assess the interplay between different land surface factors.

It has been shown for the conditions encountered during the NAFE'05 field campaign there was a significant correlation between the soil moisture retrieval error and the sub-pixel heterogeneity of land cover type; retrieval errors exceeded the SMOS target accuracy for a fraction of forest larger than

30% of the pixel area, in a pixel otherwise occupied by native grass and crops. Moreover, retrieval errors achieved a maximum of +17.2%v/v and -10.0%v/v for pixels with highly heterogeneous land cover type (approximately 50% native grass and forest fraction). The sign of this error depended on whether forest or native grass was the dominant land cover within the pixel, i.e., the pixel average soil moisture was overestimated when a pixel containing a significant amount of forest was modeled as having a uniform native grass cover and underestimated when the pixel was modeled as having a uniform forest cover. The errors observed in this Chapter are higher than those reported by the few previous studies that analysed the effect of heterogeneity in passive microwave soil moisture retrieval using real T_B data (Drusch et al., 1999a; Burke et al., 2003; Uitdewilligen et al., 2003). However, it must be noted that the present analysis was undertaken on a wider variety of land surface conditions with a stronger variability of canopy density.

An important finding of this Chapter has been to show that one of the assumptions made by the SMOS L2 algorithm, that land cover is the only sources of error due to its sub-pixel heterogeneity, is not verified. It was in fact shown that the sub-pixel heterogeneity of soil moisture also affects the retrieval, although only when in conjunction with critical land cover heterogeneity conditions (approximately 50% native grass and forest fraction). Under those conditions the physical link between land cover and soil moisture spatial distribution (see Chapter 6) worked toward further increasing the retrieval error. This had not been observed before because: (i) synthetic studies had either considered soil moisture constant across the mixed pixel (Bindlish et al., 2002; Van de Griend et al., 2003) or the effect of soil moisture heterogeneity was considered individually (Njoku et al., 1996b; Davenport et al., 2008), or (iii) studies using actual T_B data had been performend at sites with relatively benign vegetation conditions (Drusch et al., 1999a; Burke et al., 2003; Uitdewilligen et al., 2003).

This Chapter has also shown that the impact of the heterogeneity of land cover type on the soil moisture retrieval is invariant with resolution. This demonstrated that the assumption of pixel uniformity can lead to significant soil moisture retrieval errors at the scale of SMOS pixels (up to 17%v/v). In Chapter 8, the ability of the SMOS L2 retrieval approach to compensate for these errors will be assessed and a new approach will be developed to reduce the error in SMOS soil moisture retrieval due to land cover heterogeneity.

Chapter Eight

8 A Proposed Extension to the SMOS L2 algorithm

This Chapter tests the SMOS L2 soil moisture retrieval algorithm presented in Chapter 3 using the SMOS observations simulated on regional monitoring days from PLMR data. The SMOS L2 algorithm seeks to account for the sub-pixel heterogeneity of land surface conditions by dividing the pixel in fractions of uniform land cover, for which the microwave emission is simulated individually. The method is based on the assumption that: (i) Land cover is the only land surface factor whose sub-pixel heterogeneity affects the coarse-scale soil moisture retrieval in a significant way, and (ii) in the case where the canopy density of the forest fraction of the pixel is low, the retrieved parameters (soil moisture and optical depth) are uniform amongst different land cover types. In Chapter 7 it was demonstrated that a significant error in soil moisture retrieval can result from the heterogeneity of the land cover within a SMOS footprint when the pixel is considered uniform by the retrieval algorithm. However, it was shown that land cover type is not the only factor affecting the retrieval. The heterogeneity of soil moisture contributes to the retrieval error when associated with critical land cover heterogeneity conditions (more than approximately 30% forest fraction).

Consequently, in this Chapter the ability of the SMOS L2 algorithm and its main assumptions to reduce the error resulting from the land surface heterogeneity is tested. Two novel retrieval approaches which relax those assumptions are then proposed and tested in order to overcome the limitations identified in the retrieval approach proposed for the SMOS L2 algorithm in the case of pixels composed of a mix of moderately vegetated soil (crops and grasslands) and moderately dense Eucalypt forest, typical of the Australian environment.

8.1 Description of the Retrieval Approaches

The baseline technique adopted in the SMOS L2 soil moisture retrieval algorithm to reduce the error due to land surface heterogeneity has been described in detail in Chapter 3. All the retrieval approaches tested in this Chapter are based on this baseline technique, and differ only in regards to the parameters which are retrieved. The main characteristics and assumptions of the SMOS baseline technique are briefly reviewed in this section, while the soil moisture retrieval approach proposed for the SMOS L2 algorithm (hereafter referred to as the "SMOS approach") and the two proposed alternative approaches are described in the following three sections (see also the summary in Table 8.1). It should be noted that the nomenclature used in Table 8.1 and throughout the present Chapter to indicate the different approaches is particular to this thesis and therefore does not correspond to that found in any SMOS technical document. While the retrieval approaches tested in this Chapter have been given a short name code (such as "2P-U", see relevant section for each approach), the uniform pixel approach was indicated simply as "uniform pixel", for consistency with the way it is indicated in Chapter 7.

The SMOS baseline technique consists of applying the L-MEB microwave emission model separately for each land cover type present in the pixel using land cover specific parameters to simulate fraction-specific T_B's, which are then linearly aggregated to give a weighted-average pixel T_B. These land cover fractions are determined using high-resolution thematic maps of land use (at 4km resolution). Given the availability of multiple observations of the same SMOS footprint (multi-angle and bi-polarisation), parameters other than soil moisture itself can be theoretically retrieved. In the "minimum" and "full" retrieval options (see Table 3.2), these parameters will be soil moisture, optical depth and eventually surface roughness (highly constrained and only in the "full" retrieval).

In testing of the SMOS L2 algorithm, the following simplifications are made:

Table 8.1. Summary of the retrieval approaches tested in this Chapter with simulated SMOS data; θ=soil moisture, τ=optical depth. Subscripts indicate that the parameter is retrieved for the entire pixel (*pixel*), for the moderate vegetation fraction (*mod*) or for the forest fraction (*for*). All the parameters not indicated are set *a priori*. Note that the nomenclature utilised does not correspond to that of any SMOS technical document.

Retrieval Approach	Retrieved Parameters	*A priori* Parameters	Main Assumptions
Uniform pixel	θ_{pixel}, τ_{pixel}	-	• Only dominant land cover type modeled
2P-U	θ_{pixel}, τ_{pixel}	-	• θ uniform in pixel • τ uniform in pixel
2P-S	θ_{pixel}, τ_{mod}	τ_{for}	• θ uniform in pixel
3P-S	θ_{mod}, θ_{for}, τ_{mod}	τ_{for}	

1. only the “nominal” case of the SMOS L2 algorithm is considered, i.e., when either the “low to moderately vegetated soil” or the “forest” land cover classes are dominant within the SMOS FOV (see Chapter 3). This means that the case when land surface conditions that are not of direct interest for soil moisture retrieval (e.g., ocean, sea ice, snow-covered or urban areas) are dominant within the SMOS FOV is not considered. The “low to moderately vegetated soil” (hereby referred to as “moderately vegetated surface”) included both the crops and grassland land surface types on which the L-MEB model was evaluated in Chapter 5. Due to the nature of the NAFE’05 study area, this analysis is concerned with the case in which the forest, grassland and crop fraction sum up to 100%. Therefore, when running the L-MEB model in forward mode to optimise the retrieved parameters, the model is applied separately for the grassland, forest and crop fraction of the footprint;
2. due to the limited number of independent observations at different incidence angles that could be obtained from the NAFE’05 airborne data (in terms of incidence angle), in this study only a limited amount of parameters could be retrieved at once, namely soil moisture and

vegetation optical depth. Therefore only the "minimum" retrieval case of the SMOS L2 algorithm is considered (see Table 3.2); and

3. several assumption are made in terms of the synthetic SMOS data used as discussed in detail in Chapter 3: (i) Observations are considered free of the errors associated with image reconstruction, ionospheric (Faraday) rotation and sky and atmospheric contributions compensation; (ii) the radiometric uncertainty considered is that of the PLMR radiometer (2 K and 0.7 K respectively at V and H polarisation); and (iii) no antenna gain weighting function (WEF, see section 3.2.2) is applied when aggregating the fraction-specific modelled T_B to SMOS pixel resolution. The fractions used for the aggregation are geometrical surface fractions estimated from the 30m resolution Landsat-derived land cover map described in detail in Chapter 5.

The criteria used to assess the SMOS L2 algorithm at coarse resolution and to compare it with alternative approaches are those suggested in the SMOS L2 algorithm validation plan (CESBIO, 2006): that is, the Root Mean Square Error (RMSE) and bias between retrieved soil moisture and optical depth at coarse resolution and the average of the soil moisture and optical depth "ground truth". The "ground truth" soil moisture and optical depth are taken as the 1km L-MEB product evaluated in Chapter 5; unless otherwise stated, for each coarse pixel the arithmetic average of the 1km soil moisture and optical depths across the coarse pixel are used as "ground truth".

Finally, it should be anticipated that, due to the relatively limited extent of the crop fields in the study area and the coarse resolution of the analysis (5km-40km), crops never constituted the dominant fraction of the pixel, with the maximum pixel fraction occupied by crops being 20% of the pixel area (at 5km). This poses certain limitations to the applicability of the results of this thesis. However, the crop fraction is considered in the forward modeling weighted by its pixel fraction.

8.1.1 The SMOS Approach (2P-U)

The retrieval approach proposed for the SMOS L2 algorithm in the "nominal" case scenario is that of retrieving one or two parameters (soil moisture alone or soil moisture and optical depth, depending on the quality and quantity of available concurrent observations) which, when the density of the forest fraction eventually present in the pixel is expected to be low, as is the case for the open Eucalypt forest in the NAFE'05 study area, are considered to be uniform amongst the sub-pixel land cover fractions, which are modeled individually. This means for example that if soil moisture and optical depth are retrieved they are considered to have the same value in both the moderately vegetated (including grassland and crops) and the forest fraction. This approach will be hereby referred to as the 2P-U approach (2-Parameters Uniform). All other physical parameters (fixed parameters of the forward L-MEB model, see Table 5.8) are fraction-specific. In some cases, when the number and quality of multi-angle observations are high, the retrieval of up to eight parameters might be attempted by SMOS. However, that will happen on a limited number of locations, mainly on the satellite sub-track (i.e., at the centre of the swath). Therefore, in this thesis only the more common one-parameter and two-parameter retrieval scenarios are considered, which are relevant for most of the swath.

During the retrieval from SMOS data, the values of soil moisture and optical depth are not left free, but rather they are constrained to a variable extent. The two parameters are constrained to the values derived from previous retrievals over the same area, with user-defined standard deviations to specify the uncertainty in that value (through the objective function described in Chapter 3). The standard deviations are determined through some user-defined threshold against which the expected optical depth of the pixel is compared prior to the retrieval. The retrieval options and the thresholds have been described in detail in Table 3.2 and section 3.2.3.5. The thresholds on the expected optical depth are TH_23, TH_34 (the nomenclature is that of the SMOS L2 algorithm description document (CESBIO, 2007)). The retrieval conditions are determined by comparing the pixel optical depth from previous retrievals over the same with those thresholds.

Values of optical depth smaller than TH_23 should mainly correspond to ice or bare soil, i.e., cases where the optical thickness is known to be negligible and the pixel treated as bare soil. Since that type of surface was not present in the NAFE'05 study area, TH_23 was here set to zero. The TH_34 threshold corresponds instead to situations close to the limit of the validity domain (vegetation density too high to attempt any soil moisture retrieval). Since most of the NAFE'05 study area is occupied by "nice" areas where the retrieval of soil moisture is considered feasible (grassland and crops), the value of TH_34 was set to 0.8, higher than that of the forest (0.57, J. Grant, pers. comm.), so that all the pixels corresponded to the "moderate" retrieval case (see Table 3.2). In this case the retrieval of soil moisture is attempted (with a constraint of 20%v/v, which is a very mild constraint for a 2-3 days nominal overpass, effectively leaving the parameter free) whereas the optical depth is constrained to that retrieved on previous days with a standard deviation of 0.1. It should be noted that on the first day, October 31st, given the absence of previous observations of the area a free retrieval was performed (i.e., no constraints on either soil moisture or optical depth). On the subsequent three days the approach was applied as described above. October 31st therefore represents a "spin up" day.

The 2P-U approach is based on two main assumptions: (i) Land cover is the only land surface factor causing an error in the soil moisture retrieval due to its heterogeneity within the footprint and (ii) the two retrieved parameters (in the case simulated here, soil moisture and optical depth) are considered uniform amongst the modeled pixel fractions, i.e., optical depth is the same in the moderately vegetated and the forest fraction and so is soil moisture. These assumptions have been shown to be not realistic in Chapter 6 and 7, where it was shown that the physical link between land cover and soil moisture results in a higher soil moisture retrieval error than that from the land cover heterogeneity alone. Additionally, the assumption of soil moisture and optical depth uniformity is restrictive, as demonstrated in

Chapter 6 using the NAFE'05 ground data. There it was shown that moderately vegetated surfaces, like grassland and crops, generally exhibit wetter conditions than the soil under the forest canopy. In this thesis two alternative approaches are therefore proposed to relax those assumptions. These are described in the following two sections.

8.1.2 Two-Parameter, Split Optical Depth Approach (2P-S)

The first alternative approach proposed and tested in this thesis consists of a two-parameter retrieval of soil moisture (considered uniform amongst the sub-pixel fractions) and optical depth of only the moderately vegetated fraction (grass or crop). The optical depth of the forest fraction is assumed to be known, e.g., retrieved on previous overpasses of the area or derived from Leaf Area Index (LAI) maps, and is imposed *a priori* in the forward modeling of the forest fraction.

The rationale for this 2P-S approach derives from the temporal stability of the optical depth of forest as observed in recent forest studies, which was attributed to the dominance of the branch system over the leafy part of the plant in absorbing/emitting radiation at L-band (Ferrazzoli et al., 2002; Della Vecchia et al., 2006). In this approach it is therefore hypothesised that the soil moisture retrieval error resulting from assuming an *a priori* value of the forest optical depth, which may have some small error in it, should be much smaller than that resulting from assuming a single value of optical depth, this being the same for the forest and the moderately vegetated fraction of the pixel.

It should be stressed upfront that this new approach does not involve an improvement of the modeling of the physics behind the radiative transfer properties of heterogeneous pixels. Rather, it is based on the hypothesis that the non-linear effect of land surface heterogeneity on the L-MEB radiative transfer model can be moderated by fixing certain variables of the system to plausible values (i.e., the optical depth of forest). This retrieval approach is expected to improve the soil moisture retrieval accuracy over the mixed pixel depending on the quality of the *a priori* information on the forest optical depth. If this information is rather accurate, it is expected to lead to improved soil moisture retrieval accuracy when compared with the 2P-U approach described in Section 8.1.1.

8.1.3 Three-Parameters, Split Optical Depth and Soil Moisture Approach (3P-S)

This second alternative approach consists of a three-parameters retrieval of (1) soil moisture of the moderate vegetation fraction (including crop and grassland), (2) soil moisture of the forest fraction, and (3) optical depth of the moderate vegetation fraction. As for the 2P-S approach, the optical depth of the forest fraction is imposed *a priori*. This approach relaxes the assumption of uniform soil moisture between the two fractions on which the previous approaches are based by considering separate soil moisture values for the moderate vegetation fraction and the forest fraction.

The rationale for this approach derives from the observations presented in Chapter 6 and Chapter 7, where it was demonstrated that:

- land cover type had a strong influence on soil moisture distribution at the scale of a typical SMOS footprint, with forested areas exhibiting consistently drier conditions than areas with moderate vegetation, this difference being between 20 and 40% in the case of crops and 5 to 15% in the case of grasslands; and
- the soil moisture spatial variability within the footprint produced by the land cover distribution increases the error in soil moisture retrieval produced by land cover heterogeneity.

However, this approach introduces the burden of an extra retrieval parameter (the additional soil moisture), and that is the reason why the intermediate 2P-S approach was tested along with the 3P-S approach. Since the retrieval of three parameters is attempted in 3P-S, it is necessary to have a minimum of three concurrent observations. These can be obtained, for example, using bi-polarised observations at two different incidence angles. However, the regional airborne data were collected with the radiometer in "pushbroom" configuration in order to allow monitoring of a large area within one day, implying that only two observations for every ground location were available (single-angle, V and H-pol). Therefore, in order to apply the 3P-S approach, SMOS observations were simulated at 7º incidence angle in addition to the 38.5º observations used for the 2P-U and 2P-S approaches, using the incidence angle normalisation procedures described in section 5.3.2.1. From a SMOS operational point of view, the approach should be feasible at least on satellite sub-track locations where a wealth of observations at multiple angles will be available.

8.2 Testing of the SMOS Approach (2P-U)

This section tests the ability of the SMOS approach (2P-U) to reduce the error due to land surface and soil moisture heterogeneity, as compared with the uniform pixel approach tested in Chapter 7. Initially only 5km resolution observations are considered. The analysis is then expanded to coarser resolutions.

The soil moisture values retrieved using the uniform pixel approach and the 2P-U approach are plotted in Figure 8.1 against the soil moisture "ground truth" for three example resolutions (5, 20 and 40km). Figure 8.1 shows that the 2P-U approach was able to significantly reduce the large errors obtained with the uniform pixel approach at the finer resolutions (5km), which in Chapter 7 were shown to be due to the combined effect of heterogeneous land cover within the pixel (~50% forested area and 50% moderate vegetated areas) and soil moisture variability associated with that heterogeneity. However, the 2P-U approach both significantly increased the scatter of the points about the 1:1 line and resulted in a bias in the retrieved soil moisture which was not present in the uniform pixel approach.

At coarser resolution (~40km) the errors were fairly small using the uniform pixel approach. As already commented in Chapter 7, this was because the crucial conditions of land cover heterogeneity were not met at this resolution, since only a small fraction of the pixel was occupied by

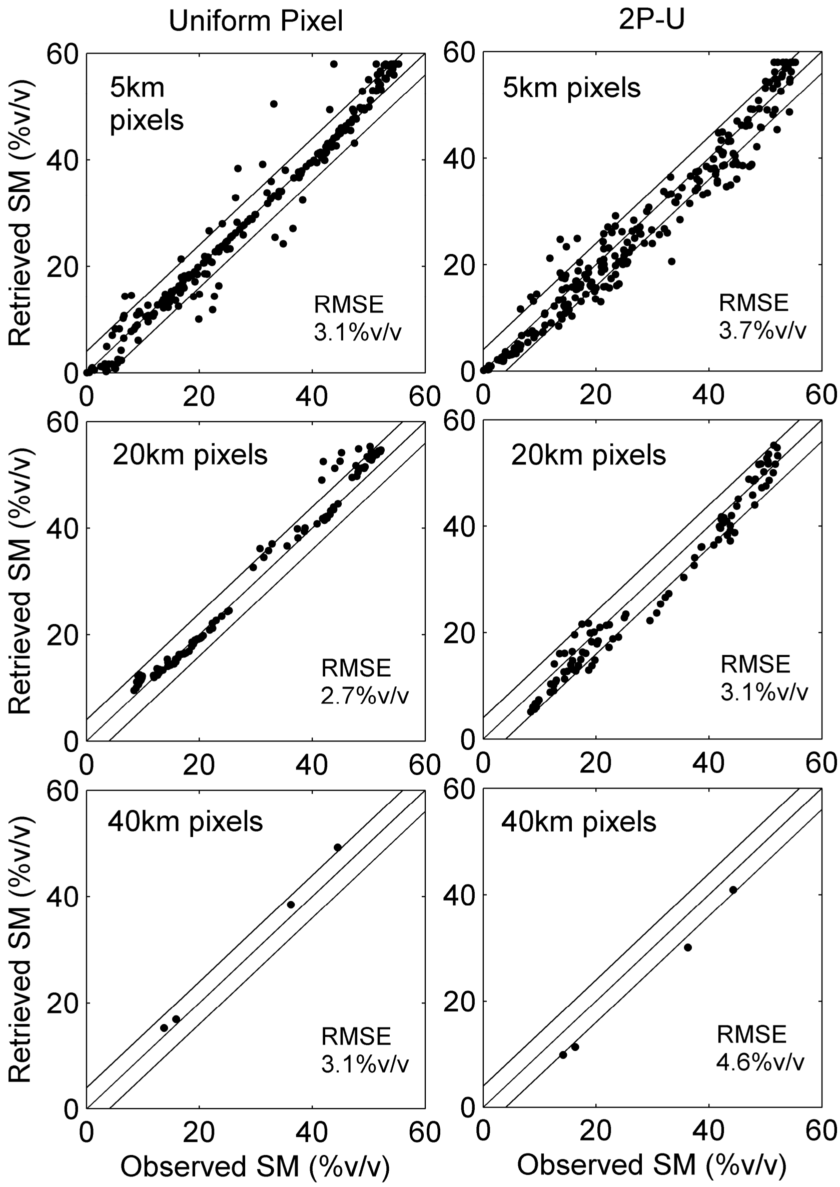

Figure 8.1. Observed vs. retrieved soil moisture (SM) at different resolutions using a uniform pixel approach (left column) and the SMOS approach (2P-U).

forest. In these conditions the 2P-U approach introduced a significant bias (underestimation).

The error statistics of the soil moisture retrieval at 5km resolution for the uniform pixel and the 2P-U approach are compared in Table 8.2, together with the error in retrieved optical depth. Note that the "observed" optical depth here is the arithmetic average of the optical depths of the different components of the pixel. In this table the 5km pixels are grouped according

Table 8.2. Errors in retrieved soil moisture (SM) and optical depth (TAU) at 5km resolution for different land cover categories when using the uniform pixel and 2P-U approaches.

		Uniform Pixel Approach			2P-U		
Group	**Date**	**SM RMSE (%v/v)**	**SM Bias (%v/v)**	**TAU RMSE**	**SM RMSE (%v/v)**	**SM Bias (%v/v)**	**TAU RMSE**
A. Forest <40%	31/10	2.9	2.2	0.02	3.8	0.2	0.02
	7/11	1.0	-0.2	0.02	4.0	-2.6	0.01
	14/11	0.9	-0.3	0.03	4.4	1.0	0.06
	21/11	1.0	-0.4	0.02	3.1	-2.2	0.01
B. Forest >40% <60%	31/10	11.6	4.3	0.14	5.5	-3.8	0.06
	7/11	8.4	1.1	0.15	5.7	-5.3	0.09
	14/11	3.7	1.2	0.16	1.6	-1.5	0.13
	21/11	4.6	1.6	0.12	2.0	-1.8	0.09
C. Forest >60%	31/10	2.8	-0.1	0.10	1.6	0.2	0.04
	7/11	5.0	-4.4	0.08	3.2	-2.9	0.09
	14/11	2.3	-1.8	0.16	1.1	-0.9	0.14
	21/11	2.0	-1.6	0.07	0.8	-0.7	0.11
Total		3.1	0.2	0.06	3.7	-1.2	0.06

to the percentage of pixel fraction occupied by the forested area (the remaining part of the pixel being occupied by grassland and crop in some cases): group A, pixels occupied predominantly by moderate vegetation (forest fraction<40%); group B, heterogeneous pixels with land cover conditions shown in Chapter 7 to be critical for the retrieval (forest fraction between 40-60%) and group C, pixels occupied predominantly by forest (forest fraction>60%). In the following sections, the results for the "critical" group B (heterogeneous) pixels are discussed first, followed by group A and C (homogeneous) pixels.

8.2.1 Heterogeneous Pixels (Group B)

Table 8.2 shows that the 2P-U approach significantly reduced the RMSE of both soil moisture and optical depth in the case of highly heterogeneous pixels (group B). The RMSE of soil moisture was reduced from a maximum of 11.6%v/v using a uniform pixel approach to 5.7%v/v using the 2P-U approach. This was a result of the more accurate retrieval of the mixed pixel optical depth due to the fractional forward modeling in the 2P-U approach. The RMSE of the retrieved optical depth was in fact reduced significantly, by as much as 0.08 (as a reference, the optical depth of a typical grassland with 1kg/m^2 is 0.15 and that of a forest is ~0.5). However, the error using the 2P-U approach was greater than 4%v/v on October 31st and November 7th, when the study area was characterised by wet conditions. As also shown in Figure 8.1, the reduction in soil moisture error came at the expense of a negative bias (underestimation), which was between -1.8%v/v in dry conditions (November 21st) and -5.3%v/v in wet conditions (November 7th).

8.2.2 Homogenous Pixels (Group A and C)

Compared to the uniform pixel approach, a slightly degraded retrieval was obtained with the 2P-U approach over moderately vegetated pixels having a small fraction of forest (group A). In these cases the RMSE increased from 0.9-2.9%v/v for the uniform pixel approach to 3.1-4.4%v/v for the 2P-U approach, depending on the day. Again, the 2P-U approach introduced a negative bias for most days, as seen by the increased scatter about the 1:1 line and negative bias in Figure 8.1.

Conversely, the 2P-U approach showed an improvement with respect to the uniform pixel approach in the case of pixels with a predominant forest fraction (group C), since in these cases the error obtained using the uniform approach was greater than in the case of moderately vegetated pixels group A. However, the 2P-U approach was able to improve the accuracy over such pixels, with the RMSE and bias decreasing from 3%v/v to 1.4%v/v and from -2%v/v to -1.1%v/v on average respectively. These results suggest that the fractional forward modeling, which is the innovative aspect of the 2P-U approach, improves the retrieval over forest-dominated pixels by accounting for the contribution of the moderately vegetated fraction but decreases the accuracy over moderate vegetation-dominated pixels when accounting for the contribution of the small forest fraction.

8.2.3 Limitations of the SMOS Approach

Since the moderate vegetated fraction of group A pixels consisted of a

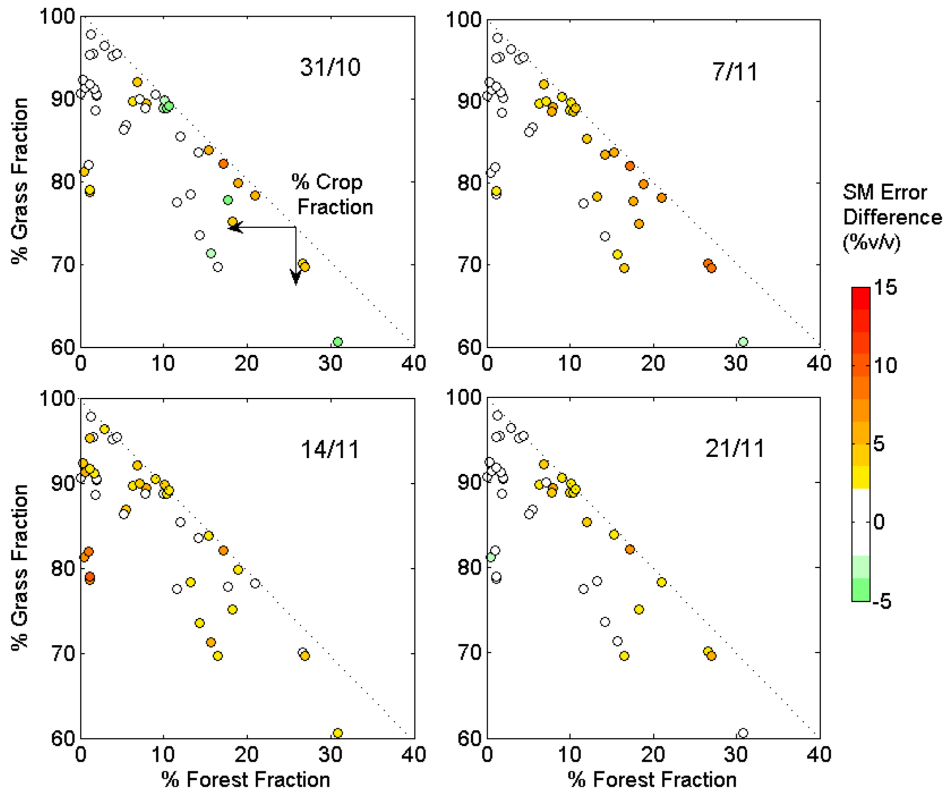

Figure 8.2. Difference in absolute soil moisture error between the 2P-U and the uniform pixel approach for "group A" pixels (5km resolution) plotted as a function of the sub-pixel land cover fractions on each date. Green coloured dots (negative differences) indicate cases where the 2P-U approach improved the retrieval, white coloured dots are cases where the two approaches give similar results (±2%v/v), and yellow-red coloured dots (positive differences) are cases where the 2P-U approach has a higher error than the uniform pixel approach. The number of the colour legend results from subtracting the error using the 2P-U approach to the error using the uniform pixel approach.

mix of crop and grassland surfaces, the error induced by the 2P-U approach in this group was analysed in detail in terms of the sub-pixel land cover fractions of grassland, crop and forest. This is shown in Figure 8.2, where the difference between the errors obtained with the 2P-U and the uniform pixel approach is shown as a function of the sub-pixel fractions of forest (x-axis) and grassland (y-axis). Each point in the plot represents a pixel, and the error between the two approaches in that pixel is quantified by subtracting the retrieval error of the uniform approach to that of the 2P-U approach, both taken in absolute value. Therefore a positive value of this difference indicates that in that pixel the 2P-U approach had a retrieval error higher than the uniform pixel approach. In the space of Figure 8.2, the crop fraction corresponds to the vertical distance of each dot from the diagonal line (i.e., the dots falling on the diagonal line have zero crop fraction).

The plots confirm the overall lower accuracy of the 2P-U approach with respect to the uniform pixel approach in group A pixels, already observed in Table 8.2. However, the plot shows that this general trend varies depending on the relative mix of forest, crop and grassland fractions. The 2P-U approach tended to have a soil moisture accuracy comparable to the uniform pixel approach when either grassland was dominant (>90%, top left corner in each plot), or when the pixel was a mix of grassland and crop, provided the forest fraction was close to zero (dots along the y axis). Moreover, the increased RMSE values in Table 8.2 (group A) were due to the points lying along the diagonal line, being pixels with crop fraction close to zero and a mix of grassland and forest.

An exception to these observations was November 14th, where the accuracy of the 2P-U approach was poor for a larger number of cases than on the other days. It can be seen in Table 8.2 that on November 14th a higher error in retrieved optical depth (0.06 compared to 0.01-0.02 for the other days) was also obtained. Analysis of the residuals between the observed and simulated T_B at 5km resolution on November 14th revealed a poor performance of the optimisation routine, with residuals of 1.4±1.7K (average for all pixels) and maximum of 6.1K, as compared to the 0.05±0.2K average residuals for the other three days. This suggests that the change in land surface `conditions between November 7th and 14th might have been too strong, so that the algorithm could not match well the simulated with the observed T_B due to the constraint imposed on the optical depth or the soil moisture by the 2P-U approach (see Table 3.2). This was confirmed by the strong change of average soil moisture conditions recorded by the ground monitoring stations between November 7th and 14th, which was the highest amongst the four dates, being approximately 20%v/v as compared to less than 10%v/v between all other dates (see Table 5.9). Since the focus of this analysis is on the ability of the 2P-U approach to deal with varying degree of land surface heterogeneity, the retrieval for November 14th was repeated without constraining soil moisture. As expected, this led to an improvement, with a RMSE of 3.1%v/v for soil moisture and 0.02 for optical depth.

It should be stressed that in all the cases displayed in Figure 8.2 (group A; forest fraction <40% and grassland+crop fraction>60%), the uniform pixel approach treated the 5km pixels as uniform grassland surfaces, since crops never constituted the dominant fraction. Therefore, the results presented indicate that on pixels with a large fraction of grassland, the fractional forward modeling of the 2P-U approach did not result in a significant improvement to the retrieval of the pixel averaged soil moisture as compared to using the uniform pixel approach. This was true even when a relatively small fraction of the pixel was occupied by another moderate vegetation land surface type (crop in this case). However, in the presence of even a small fraction of forest in a pixel that is largely occupied by grassland, the 2P-U approach led to higher retrieval errors than the uniform pixel approach.

These observations are quantified in Table 8.3, where the soil moisture RMSE for the two approaches is shown for group A pixels as a function of the pixel forest fraction (for pixels with very small crop fraction) and as a function of the crop fraction (for pixels with very small forest fraction). The two approaches performed similarly for very homogenous conditions (crop and forest fraction<5%). However, the presence of a 5-10% fraction of forest was sufficient to increase the error beyond the SMOS target accuracy (4%v/v) when using the 2P-U approach, with the negative bias increasing with increasing forest fraction. As the forest fraction increased beyond 40% (group B pixels in right-most column), the error using the uniform pixel approach increased significantly, while the 2P-U approach effectively compensated for the strong land cover heterogeneity (as observed for group B pixels in Table 8.2). Table 8.3 also indicates that the increasing fraction of crops in pixel otherwise occupied by grassland (forest fraction<5%) had the

Table 8.3. Soil moisture retrieval RMSE for group A pixel (5km resolution) as a function of (1) forest fraction for pixel with crop fraction<5% and (2) crop fraction for pixel with forest fraction<5%. The soil moisture bias is also indicated for each case in smaller italics font. ($^+$) Heterogeneous group B pixels are shown as reference.

(1)		Crop Fraction<5%					
	Forest fraction (%)	0-5	5-10	10-20	20-30	30-40	40-50$^+$
	Uniform approach	1.1	2.0	1.7	1.2	-	7.8
		0.2	*-0.4*	*0.6*	*0.9*	*-*	*6.5*
	2P-U	1.7	4.9	4.4	6.0	-	3.9
		-0.2	*-3.8*	*-3.0*	*-5.2*	*-*	*-2.7*

(2)		Forest Fraction <5%		
	Crop fraction (%)	0-5	5-10	10-20
	Uniform approach	1.2	1.7	1.7
		0.3	*0.3*	*-0.8*
	2P-U	2.0	2.4	2.9
		0.6	*1.4*	*1.7*

effect of introducing a wet bias. This a similar effect to that observed in the case of increasing forest fraction in pixels otherwise occupied by grassland (crop fraction>5%), but of inverted sign. The dry bias due to the increasing crop fraction was much smaller than that due to the increasing of the forest fraction, being of 1.7%v/v for a 20% crop fraction in contrast with a -3%v/v for a 20% forest fraction. Since the largest crop fraction observed in the NAFE’05 area at 5km resolution was of 20%, the contribution of crops to the error of the 2P-U approach in group A pixels could not be investigated further. However, it indicates that the 2P-U approach and its assumptions might result in significant retrieval errors also in pixels occupied by a mixed crop and grassland with small amount of forest.

A simple schematic example can help explain the reason for these biases in the case of a mix of forest and grassland. Figure 8.3 shows the simple retrieval case of a pixel with uniform soil moisture and land surface parameters (i.e., 45%v/v soil moisture, 25ºC soil temperature, 21% sand content and 36% clay content) but split in two fractions, (50% forest and 50% grassland), with different optical depths (0.57 and 0.05 respectively).

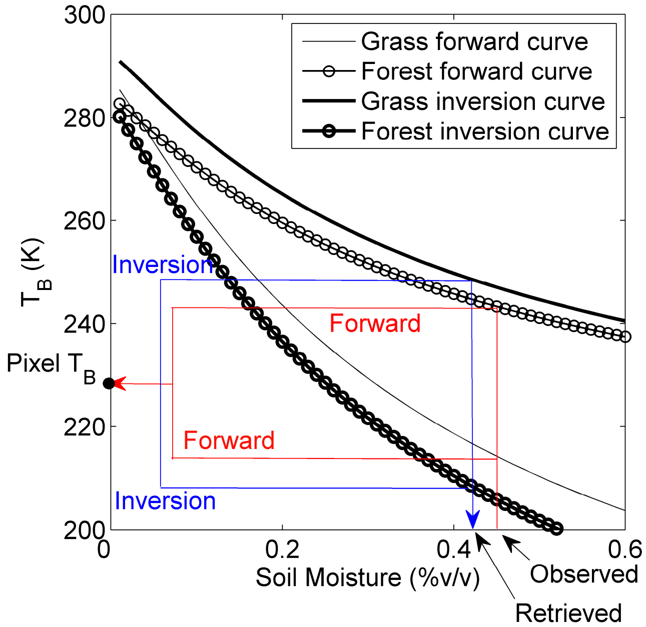

Figure 8.3. Schematic example that illustrates the effect of retrieving one single optical depth value for a mixed pixel using the 2P-U approach.

In the plot the soil-moisture-emission curves are shown for the grass and forest fraction. The forward curves are those calculated using the original optical depth, while the inversion curves are calculated using the single (hence same for grass and forest) value of retrieved pixel optical depth using the 2P-U approach. The forward curves have the characteristic that, given the different optical depth of the two fraction, each soil moisture content results in a much higher T_B for the forest fraction than the grassland fraction (due to higher vegetation emission).

The red lines show the forward simulation of T_B for each fraction at 45%v/v soil moisture (value that we want to eventually retrieve using the 2P-U approach), given the input land surface conditions and the original optical depths. The forward simulated T_B's were then aggregated linearly to produce a "pixel T_B", which is exactly the average of the forward T_B's, since the pixel fractions are the same for grass and forest. The 2P-U approach is then used to retrieve a uniform soil moisture and optical depth value for the pixel (blue lines). It can be seen that as a result of retrieving a single pixel optical depth, the soil moisture is underestimated because the soil-moisture-emission curve of the forest (thick line with circles) has been distorted by the algorithm much more than that of the grass (thick line) from the respective original curve (thin lines, which in this scenario corresponds to the "true" emission curve) in order to accommodate a single optical depth. Therefore, the retrieved soil moisture is distorted as well and this results in a bias.

It was also shown in this section that the bias observed for the 2P-U approach in heterogeneous group B pixels appeared to be greater in wet conditions. Note that, in homogeneous group A pixels, the bias did not change with wetness conditions. The link between pixel wetness conditions and the bias was thus far postulated only in terms of the entire study area, using the daily average soil moisture retrieved over the entire study area (see Table 8.2). Given the large variability of soil moisture within the study area, the correlation between retrieval error and wetness conditions is analysed in Figure 8.4 for individual pixels. Here the retrieval error is also plotted as a function of the sub-pixel standard deviation of soil moisture. This is because in Chapter 7 it was shown that the sub-pixel standard deviation of soil moisture contributed to the retrieval error when associated with the critical land cover conditions (group B pixels). Therefore the effect of the sub-pixel heterogeneity of soil moisture is a possible explanation for the residual error in the 2P-U approach on October 31st and November 7th.

It can be seen in Figure 8.4 that for homogenous group A pixels the retrieval error was weakly correlated with pixel average soil moisture conditions, with underestimation in most conditions, and overestimation only occurring for very dry and very wet conditions, approximately below 10 and above 50%v/v soil moisture content. In these cases no correlation between the retrieval error and the sub-pixel heterogeneity of soil moisture was observed (bottom row, left panel). However, this could be because group A pixels were characterised by generally small sub-pixel heterogeneity (<10%v/v). Conversely, the maximum retrieval error in heterogeneous, group B pixels occurred in wet and heterogeneous conditions (compare top and bottom panel of the middle column of Figure 8.4).

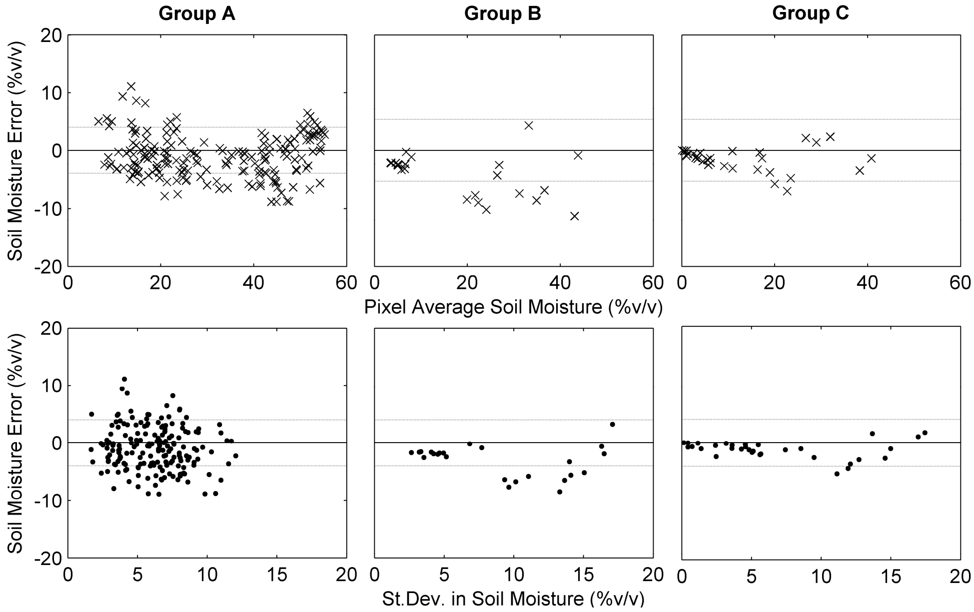

Figure 8.4. Error of soil moisture retrieval at 5km resolution obtained with the 2P-U approach, plotted as a function of the pixel average soil moisture (top panel) and the sub-pixel standard deviation of soil moisture (bottom panel). The three pixel groups are shown by column. Dashed lines represent SMOS target accuracy.

8.2.4 Conclusions on the Applicability of the SMOS Approach

In summary, the comparison of the SMOS approach (2P-U) and the uniform pixel approach showed that the 2P-U approach significantly reduced the error in retrieved soil moisture with respect to a uniform pixel approach on pixels with highly heterogeneous land cover (group B, 40-60% Forest) and when the forest fraction was predominant (group C, forest>60%). For example, the RMSE for group B was reduced to 5.7%v/v, as much as 6.1%v/v less than that obtained with the uniform pixel approach in the same land surface conditions; the RMSE for group C was reduced to 3.2%v/v, as much as 1.8%v/v less than that obtained with the uniform pixel approach. However, three major limitations were identified in the approach:

- on highly heterogeneous pixels (group B, 40-60% forest), the 2P-U approach showed a dry bias. This bias was greater on days when the study area was characterised by wet conditions, i.e., October 31st and November 7th. On these days the RMSE of the 2P-U retrieved soil moisture was 5.7%v/v and 5.5%v/v respectively, and the bias was -3.8%v/v and -5.3%v/v respectively;

- the 2P-U approach was found to be less accurate than the uniform pixel approach in the case of more uniform, moderately vegetated pixels (group A, forest<40%). In such cases the 2P-U approach resulted in a RMSE between 3.1-4.4%v/v as compared to a RMSE of 1.0-2.9%v/v when using the uniform pixel approach. This RMSE was also accompanied by a dry bias (underestimation), which increased according to forest fraction; and
- the constraint of 20%v/v imposed on the retrieved soil moisture in the "moderate" retrieval case appeared too restrictive. In particular, it resulted in significant errors in both the soil moisture and optical depth retrieval on November 14^{th}, as a consequence of a strong change in soil moisture conditions between November 14^{th} and the previous retrieval on November 7^{th} (area-average soil moisture approximately 20%v/v drier). In a SMOS operational context, such a long revisit time (7 days), and hence such significant difference in soil moisture conditions due to drydown is less likely occur. However, a rainfall event might easily produce an increase in soil moisture conditions of similar magnitude, even within a nominal SMOS revisit time of 2-5 days.

These results indicate that the presence of a significant forest fraction in a pixel otherwise occupied by moderate vegetation (grass or crop), the 2P-U approach results in an underestimation of the pixel average soil moisture conditions. In contrast, when the pixel is split between land cover types of moderate vegetation (crop and grass), the 2P-U approach achieves a similar accuracy to the uniform pixel approach. Moreover, a dry bias is introduced by the 2P-U approach that increases according to forest fraction in the pixel. Due to the limited extent of cropped areas in the study area, the influence of the presence of large fraction of crops in the pixel could be only partially addressed. Nevertheless the results presented suggested that the 2P-U approach results in a wet bias when significant fraction of crop is present in the pixel.

8.3 Improvements to the SMOS Approach

In order to overcome the problems of the 2P-U approach highlighted in the previous section, and with the objective of reducing the errors in heterogeneous group B pixels and in homogenous, moderately vegetated group A pixels, in the following sections two new approaches are proposed and tested with the NAFE'05 experimental data. These two approaches relax one-by-one the two assumptions on which the 2P-U approach is based. The assumptions made by the 2P-U approach are that (i) the retrieved optical depth is the same in both the modeled pixel fractions, and (ii) soil moisture is the same in both the modeled pixel fractions.

8.3.1 The 2P-S Approach

In this alternative approach, one value of soil moisture and optical depth are retrieved for the mixed pixel, with soil moisture considered uniform across the pixel as in the 2P-U approach. However, the optical depth of the forest fraction is assumed *a priori* in the forward modeling. Consequently, the retrieved optical depth corresponds only to that of the moderate vegetation fraction (grass or crop). This approach is expected to improve the soil moisture retrieval accuracy over the mixed pixel depending on the quality of the *a priori* information on the optical depth of forest. From an operational point of view, this information will derive from ancillary maps of LAI. If this information is sufficiently accurate, it might lead to improved soil moisture retrieval accuracy when compared with the 2P-U approach. If this information is not so accurate, a lower accuracy might be obtained.

The performance of the 2P-S approach is compared to that of the 2P-U approach in Table 8.4. As a first attempt, it was assumed that the optical depth of the forest fraction is known with great accuracy, and was consequently set to the value specifically obtained over the NAFE'05 Eucalypt forest by J. Grant (pers. comm.), being 0.57. Later (section 8.3.2) the impact of uncertainties in this *a priori* information are analysed. It should be noted that here the 2P-S approach is applied using values of the optical depth thresholds such that all pixels fall in the "moderate" retrieval case of Table 3.2 However, on October 31st, a free retrieval is performed,

Table 8.4. Errors in retrieved soil moisture (SM) and optical depth (TAU) at 5km resolution and for different land cover categories obtained with the 2P-U and 2P-S approaches.

		2P-U			2P-S		
Group	**Date**	**SM RMSE (%v/v)**	**SM Bias (%v/v)**	**TAU RMSE**	**SM RMSE (%v/v)**	**SM Bias (%v/v)**	**TAU RMSE**
A. Forest <40%	31/10	3.8	0.2	0.02	3.6	2.1	0.03
	7/11	4.0	-2.6	0.01	2.1	-0.6	0.01
	14/11	4.4	1.0	0.06	5.0	2.8	0.06
	21/11	3.1	-2.2	0.01	2.2	-1.5	0.02
B. Forest >40% <60%	31/10	5.5	-3.8	0.06	4.6	2.6	0.04
	7/11	5.7	-5.3	0.09	2.8	-0.2	0.05
	14/11	1.6	-1.5	0.13	2.6	0.5	0.12
	21/11	2.0	-1.8	0.09	1.3	-1.0	0.07
C. Forest >60%	31/10	1.6	0.2	0.04	3.3	2.4	0.09
	7/11	3.2	-2.9	0.09	1.1	0.5	0.06
	14/11	1.1	-0.9	0.14	0.6	-0.4	0.06
	21/11	0.8	-0.7	0.11	0.6	-0.5	0.12
Total		3.7	-1.2	0.06	3.3	0.7	0.05

given the absence of "previous" retrievals. This is identical to that of the 2P-U approach.

Table 8.4 shows that the use of correct *a priori* information on the optical depth for the forest fraction led on average to an improvement of the soil moisture retrieval accuracy with respect to the 2P-U approach. The overall RMSE across all days and land surface conditions decreased by 0.4%v/v. More importantly, the strong dry bias which affected the 2P-U approach was corrected, going from -1.2%v/v to 0.7%v/v (average across all dates and groups). Moreover, on uniform moderately vegetated group A pixels, the reduction was from 4.0%v.v to 3.4%v/v for the RMSE and from -1.0%v/v to 0.6%v/v for the bias. On heterogeneous group B pixels, the RSME went from 3.7%v/v to 2.8%v/v and the bias was significantly reduced from -3.1%v/v to 0.5%v/v. On forested group C pixels the improvement was smaller, with the RMSE going from 1.7%v/v to 1.4%v/v and the bias from -1.1%v/v to 0.4%v/v. The largest errors of the 2P-S approach were obtained on the wettest day, October 31st (for all groups of pixels) and on November 14th for group A pixels. November 14th was also the only day in which the 2P-S approach was less accurate than the 2P-U approach (for group A and B pixels).

It is expected that the retrieval errors of the 2P-S approach on November 14th and October 31st are due to different effects. Specifically (see also section 8.2.2), the error obtained on November 14th could be linked to the constraint on soil moisture (20%v/v) imposed by the "moderate" retrieval case in the SMOS L2 algorithm, which might be too restrictive since a significant change in soil moisture was observed with ground data between November 7th and 14th (approximately 20%v/v decrease in the area-average soil moisture). This cannot be the case for the error on October 31st, since on that day soil moisture and optical depth were retrieved as free parameters, given the lack of previous retrieval dates. In this case, the error is expected to be associated with the algorithm not being able to retrieve both parameters without any constraints together with residual effects of land surface heterogeneity not being fully accounted for by the 2P-S approach.

In order to check whether the constraints imposed on the retrieved parameters are the cause of the observed error on November 14th, the retrieval was repeated with different constraints imposed by the SMOS L2 algorithm. Soil moisture and optical depth were alternatively left free (without any constraint) and the retrieval repeated for all dates. The resulting RMSE of soil moisture and optical depth are compared in Table 8.5 for the different options. As expected, relaxing the constraint on the retrieved parameters resulted in a better accuracy for November 14th, while the results on all other dates were unchanged. The best option was that of relaxing the constraint on soil moisture, with a decrease in RMSE of 2.9%v/v and 1.5%v/v respectively for group A and B pixels on November 14th.

Relaxing only the constraint on the retrieved optical depth did not make a substantial difference when compared with using a 0.1 constraint, although

Table 8.5. RMSE in retrieved soil moisture (SM) and optical depth (TAU) at 5km resolution using the 2P-S approach with different constraints on the retrieved parameters. "Constr." Means a standard deviation of 20%v/v for soil moisture and of 0.1 for optical depth.

		SM constr. TAU constr.		**SM free TAU constr.**		**SM constr. TAU free**	
Group	**Date**	**SM RMSE (%v/v)**	**TAU RMSE (-)**	**SM RMSE (%v/v)**	**TAU RMSE (-)**	**SM RMSE (%v/v)**	**TAU RMSE (-)**
A. Forest <40%	31/10	3.6	0.03	3.6	0.03	3.6	0.03
	7/11	2.1	0.01	2.0	0.02	2.1	0.01
	14/11	5.0	0.06	2.1	0.02	5.0	0.11
	21/11	2.2	0.02	2.2	0.02	2.2	0.02
B. Forest >40% <60%	31/10	4.6	0.04	4.6	0.04	4.6	0.04
	7/11	2.8	0.05	2.6	0.05	2.9	0.06
	14/11	2.6	0.12	1.1	0.08	2.6	0.21
	21/11	1.3	0.07	1.5	0.07	1.4	0.07
C. Forest >60%	31/10	3.3	0.09	3.3	0.09	3.3	0.09
	7/11	1.1	0.06	0.9	0.05	1.2	0.11
	14/11	0.6	0.06	0.8	0.08	0.6	0.12
	21/11	0.6	0.12	0.6	0.12	0.6	0.13
Total		3.3	0.05	2.5	0.04	3.4	0.07

the accuracy was slightly degraded (0.1%v/v) in some cases (i.e., group A, November 7th and 21st). The results obtained when relaxing the constraint on both parameters (not shown in Table 8.5) were equivalent to those of relaxing only the constraint on soil moisture. One caveat in this analysis is that the four regional data sets used represent a gradual drydown from very wet to very dry conditions, not do not include a situation in which a fairly dry area is brought to intermediate or wet conditions by a rainfall event in between subsequent observation dates. It is likely that in that situation, the 2P-S approach will present similar limitations to that observed for November 14th where there was a significant decrease in soil moisture.

Apart from November 21st, the 2P-S approach was able to reduce the soil moisture retrieval error below the SMOS target accuracy for most cases and land surface conditions analysed (see Table 8.4). The only exception was

October 31st, the earliest monitoring day of the NAFE'05 data set, which was also the wettest of all dates, having average soil moisture conditions measured on the ground of 43.5±14.1%v/v (the second wettest day, November 7th, recorded 36.1±13.2%v/v). The soil moisture retrieval error on October 31st could stem from two causes: (i) Poor sensitivity of the L-MEB radiative transfer algorithm to changes in soil moisture in wet conditions due to the lower soil emissivity, resulting in poor convergence of the optimisation algorithm to a solution, or (ii) residual effect of land surface heterogeneity not fully accounted for by the 2P-S approach. The poor model sensitivity in wet conditions could also be aggravated by the lack of initial input values for October 31st, when a free retrieval (i.e., without constraints on soil moisture and optical depth) was performed

In order to verify whether the model sensitivity is the cause of the error on October 31st, the retrieval was repeated with the 2P-S approach after adding a Gaussian noise to the input coarse-resolution T_B values, which were perturbed around their observed values with a standard deviation of 2K, equal to the PLMR radiometric uncertainty (V and H polarisation were considered fully correlated when adding the noise). The model sensitivity was then assessed by calculating the variance of the soil moisture error for each pixel around its average value when the T_B is perturbed with the 2K noise. It is expected that if the greater error on October 31st was due to model sensitivity, the error variance would be greater in wet rather than in dry conditions.

In Table 8.6 the error variance (expressed in square root to match dimensionality with the soil moisture value) is presented for each group of pixels and date. Note that the RMSE and the variance in Table 8.6 are not correlated quantities. The value of error variance shown is the average of the individual error variances obtained for each pixel. The soil moisture RMSE is instead is calculated using the error in soil moisture retrieval of all the pixels in each group of pixels and date. The error variance was higher in wet conditions (October 31st and November 7th) indicating poorer model sensitivity. This was stronger in the presence of a significant forest fraction

Table 8.6. Square root of the average error variance (σ) of soil moisture (SM) retrieved with the 2P-S approach, after introduction of a 2K Gaussian noise to the 5km T_B observations. The average soil moisture in the study area and the RMSE of soil moisture retrieval for each land cover class and date is also shown.

Group	Date	Average Ground SM (%v/v)	SM RMSE (%v/v)	σ of the error with 2K noise (%v/v)
A. Forest <40%	31/10	49.0	3.6	2.4
	7/11	41.5	2.0	2.9
	14/11	19.7	2.1	3.2
	21/11	17.0	2.2	3.3
B. Forest >40% <60%	31/10	37.1	4.6	3.4
	7/11	23.5	2.6	2.6
	14/11	4.7	1.1	1.5
	21/11	6.0	1.5	1.7
C. Forest >60%	31/10	26.4	3.3	3.2
	7/11	15.9	0.9	2.2
	14/11	3.2	0.8	1.2
	21/11	2.9	0.6	1.3

(group B and C), while on moderately vegetated pixels the error variance was fairly stable with respect to the soil moisture conditions. In dry conditions (November 14th and 21st) the soil moisture RMSE obtained with the 2P-S approach was smaller or equivalent to the error variance resulting from the radiometric uncertainty. In wet conditions instead, the error variance explained only approximately 60-85% of the RMSE. This indicates that the error on October 31st might not be explained only by poor convergence of the retrieval algorithm.

Based on the findings of Chapter 7, it is hypothesised that this residual error is due to the heterogeneity of soil moisture within the pixel, which the 2P-S approach is unable to account for as a consequence of the assumption that soil moisture is uniform within the pixel (and hence between the different land cover fractions). This hypothesis is supported by the fact that it was demonstrated, both in Chapter 7 and in section 8.2.3, that the sub-pixel heterogeneity of soil moisture increased the soil moisture retrieval error, when associated with strong variability in land cover (group B pixels), for both the uniform pixel approach and the 2P-U approach. Moreover, in Chapter 7 it was also shown that the heterogeneity in other surface factors which contribute to the microwave emission of the surface had a negligible or minor impact on the retrieval of soil moisture from coarse resolution.

In order to verify this hypothesis, Figure 8.5 plots the error in soil moisture retrieval using the 2P-S approach against the sub-pixel standard deviation of soil moisture for each group of pixels. A strong correlation of the error with the sub-pixel standard deviation of soil moisture can be seen for pixels with a significant forest fraction (group B and C). In such cases, the increasing soil moisture standard deviation resulted in greater errors. As expected from the observations in section 6.3.3, these pixels were characterised by higher values of soil moisture standard deviation since the presence of forested areas, which generally exhibits conditions drier than crop and grasslands, resulted in more heterogeneous soil moisture distribution within the pixel. Moderately vegetated group A pixels were characterised by more uniform soil moisture conditions (standard deviation less than 10%v/v) and showed no correlation of the error with the sub-pixel standard deviation of soil moisture.

8.3.2 Sensitivity of the 2P-S Approach to the *a Priori* Optical Depth

The 2P-S approach was applied thus far under the assumption that the optical depth of the forest fraction of the pixel, which is imposed *a priori,* was known with good accuracy. This *a priori* value (0.57) was set to that calibrated specifically for the forest type of the study area (J. Grant., pers. comm.).

In an operational context, the optical depth of forest might be derived, for example, from maps of LAI using auxiliary sensors such as MODIS. Since the effect of a dense forest canopy on the microwave signal is expected to be more stable in time than that of crops and grasslands (Ferrazzoli et al., 2002; Della Vecchia et al., 2006), it has been proposed (CESBIO, 2007; Wigneron et al., 2007) to relate the forest optical depth to the maximum LAI observed

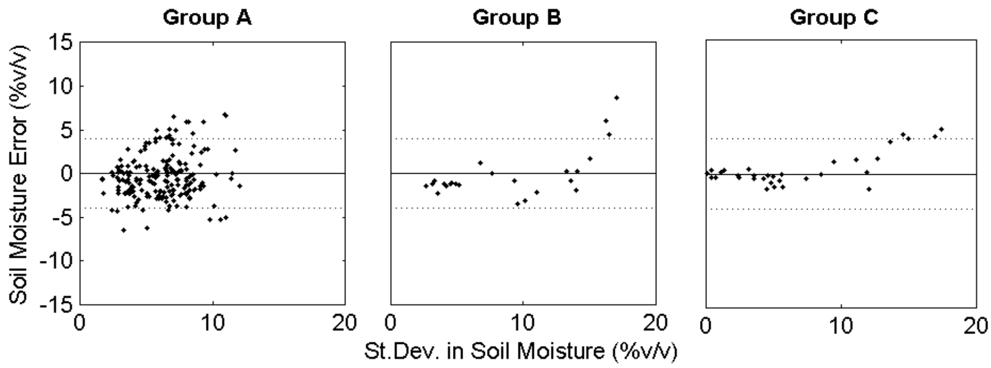

Figure 8.5. Error of soil moisture retrieval at 5km resolution using the 2P-S approach, plotted as a function of the sub-pixel standard deviation of soil moisture. The three pixel groups are shown by column. Dashed lines represent SMOS target accuracy (4%v/v).

during the year. It is therefore of interest to understand how the accuracy of the 2P-S approach would degrade with increasing uncertainty of the forest optical depth estimate.

The sensitivity of the soil moisture retrieval using the 2P-S approach to error in the *a priori* information on the optical depth of the forest was analysed by simulating increasing level of uncertainty on the optical depth of the forest. This was simulated by creating random distribution of optical depth of the forest, normally distributed around the correct value (0.57) and with increasing standard deviation (0.1, 0.2, 0.3 and 0.4). A set of 100 random *a priori* values of forest optical depth were created for each standard deviation. Using these input values soil moisture was estimated for each 5km NAFE'05 observations using the 2P-S approach.

The soil moisture RMSE and bias of the 2P-S approach with increasing level of uncertainty in the optical depth of the forest fraction are shown in Figure 8.6 and compared with those of the two other approaches tested in this Chapter (2P-U and the uniform pixel approach; the 3P-S approach was excluded from the analysis since it was shown to be less accurate). Results indicated that the accuracy of the *a priori* information on the optical depth of forest has little impact on the soil moisture retrieval for pixels mainly occupied by moderately vegetated surface types and with a forest fraction less than 40% (group A). In these cases, the soil moisture RMSE using the

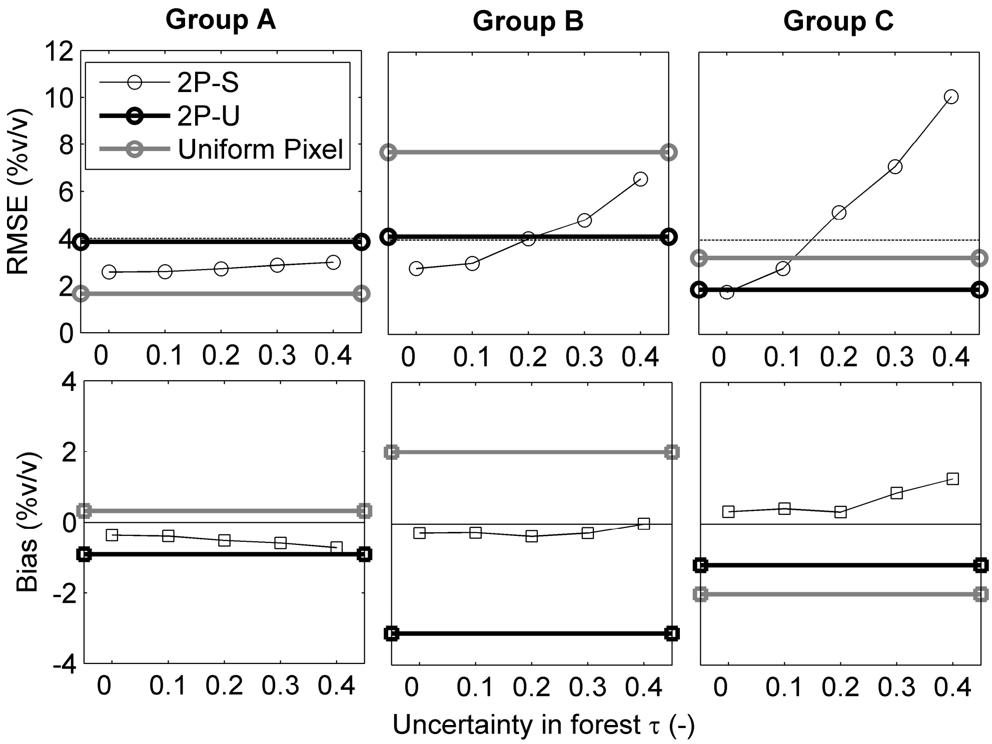

Figure 8.6. Impact of uncertainty in the *a priori* information on the optical depth of forest (expressed as standard deviation of the Gaussian distribution around the correct value) on the soil moisture retrieval error obtained with the 2P-S approach. The soil moisture Root Mean Square Error (RMSE, top row) and bias (bottom row) are shown for all pixels of group A (forest fraction<40%, left column), group B (forest fraction=40-60%, middle column) and group C (forest fraction>60%, right column). The RMSE and bias using the other methods tested in the Chapter are also shown for comparison and the SMOS target accuracy (4%v/v) is shown in the top row with a thin solid line.

2P-S approach was only slightly degraded (by 0.4%v/v) from the case where the optical depth of forest is known with high accuracy. As commented earlier, in these pixels the uniform pixel approach performed better than all the other approaches considered.

In pixels with land cover split in equivalent fractions of both moderately vegetated and forested surfaces (group B) the accuracy of the 2P-S approach decreased significantly as the uncertainty about the optical depth of forest increased. Moreover, the soil moisture RMSE increased exponentially with increasing uncertainty, although this did not result in an increased bias. The 2P-S approach was however more accurate than the 2P-U approach while the optical depth of forest was known with an accuracy better than 0.2, which corresponds to an error of 35%. For higher uncertainties the 2P-S approached the RMSE of the uniform pixel approach.

In pixels mostly covered by forest (Group C), the accuracy of the 2P-S approach degraded quickly with increasing uncertainty about the value of the optical depth of forest. The 2P-S approach was only slightly more accurate than the 2P-U approach when the optical depth of forest is known with high accuracy and became less accurate than the uniform pixel approach when the uncertainty was greater than 0.1 (relative error of 17.5%).

It is important to notice that while the 2P-U and uniform pixel approaches led to significant soil moisture biases in group B and C pixels, the 2P-S approach was able to correct for these biases. Even with the highest uncertainty (70%) on the estimate of the forest optical depth analysed, the soil moisture bias using the 2P-S approach was in no case higher than 1%v/v.

8.3.3 Conclusions on the Applicability of the 2P-S Approach

In summary, this section has shown that the proposed 2P-S approach was effective in reducing the error in soil moisture retrieval produced by the sub-pixel heterogeneity of land cover, which was previously shown to significantly affect the SMOS approach (2P-U). In particular, the 2P-S approach reduced the RMSE on uniform from 4.0%v/v to 2.6%v/v and the bias from -1.0%v/v to -0.3%v/v for moderately vegetated group A pixels. On heterogeneous group B pixels, the RSME was reduced from 4.1%v/v to 2.8%v/v and the bias significantly reduced from -3.1%v/v to -0.3%v/v. On forested group C pixels the improvement was smaller, with the RMSE going from 1.9%v/v to 1.8%v/v and the bias from -1.2%v/v to 0.4%v/v. In order to achieve this accuracy it was necessary to relax the constraint imposed on the retrieved soil moisture by the SMOS L2 algorithm (i.e., retrieve soil moisture as a free parameter). Despite the fact that the constraint imposed by SMOS L2 algorithm in the “moderate” retrieval case is a rather mild constraint, it nonetheless resulted in an error higher than that obtained with the 2P-U approach on November 14th, a day characterised by a change in soil moisture conditions of approximately 20%v/v on average across the study area from the previous date November 7th.

It was also shown that the 2P-S approach was affected by residual errors beyond the SMOS target accuracy of 4%v/v. This occurred within the group A and B pixels. For group A pixels, of all the approaches analysed in this Chapter thus far the uniform pixel approach led to the highest accuracy (RMSE=1.8%v/v, bias=0.3%v/v). A clear explanation for the error obtained with the 2P-S (as well as the 2P-U) approach in group A pixels was not found. It must evidently be associated with the forest component in the forward modeling of the 2P-S and 2P-U approaches, although small, which distorts the retrieved soil moisture and introduces an error not observed when the pixel is simply treated as uniform moderate vegetation cover.

The residual errors of the 2P-S approach in the case of heterogeneous group B pixels were observed to be correlated with the sub-pixel heterogeneity of soil moisture between the different land cover types. Therefore an alternative approach to 2P-S was proposed and tested, that aimed at reducing the soil moisture retrieval error by relaxing the second assumption of the 2P-U approach, being that of uniform soil moisture within the land cover fractions of the pixel.

8.3.4 The 3P-S Approach

The second alternative approach tested in this thesis consists of performing a three-parameters retrieval: the retrieved parameters are (i) the soil moisture of the moderate vegetation fraction, (ii) the optical depth of the moderate vegetation fraction and (iii) the soil moisture of the forest fraction. The optical depth of the forest fraction is imposed *a priori* as in the 2P-S approach.

It was found that there was no case where the 3P-S approach yielded more accurate results than the 2P-S approach. Therefore, a detailed report of the application of the approach to the NAFE'05 data is here omitted. However, the interested reader can find a detailed description of the findings summarised hereby in the Appendix A5. Additionally, the RMSE and bias of soil moisture retrieval using the 3P-S approach are included in the summary Table 8.7.

The poor accuracy of the 3P-S approach was associated with the difficult convergence of the retrieval algorithm when concurrently retrieving separate soil moisture values for the moderately vegetated and the forest fraction of the pixel. This was particularly marked in dry conditions, and for the land cover type having the smallest fraction in the pixel. As a result of this, the 3P-S approach resulted in larger errors than the 2P-S approach. Although the approach was tested with a small number of observations available for each simulated SMOS pixel (4 observations, being bi-polarised observations at 7º and 38.5º incidence angle), the results of a synthetic test indicated that the use of multiple observations (bi-polarised observations and up to 10 different incidence angles) did not improve the algorithm convergence and soil moisture accuracy.

8.4 Evaluation of the Approaches at Different Resolutions

All the analysis conducted thus far focused on the T_B observations at 5km resolution, since these provided a large number of study cases, in a variety of land surface conditions. In this final section, the conclusions drawn in previous sections are extended to the coarser observations at 10, 20, 30 and 40km over the study area.

In Table 8.7 the uniform pixel approach tested in Chapter 7 and the three approaches tested in this Chapter are compared in terms of soil moisture RMSE and bias over the entire observation period. The results are shown for different land cover conditions making use of the classification based on the forest fraction within the pixel adopted in this Chapter (i.e., pixel of group A with forest fraction smaller than 40%, group B with forest fraction between 40 -60%, and group C with forest fraction larger than 60%). It is shown that

Table 8.7. Overall soil moisture Root Mean Square Error (RMSE) and bias obtained for the study period with all the approaches tested in this Chapter and at each resolution of observation. For each resolution and each group a value of RMSE and bias is given considering the entire observation period. For each resolution and each group of pixels, the best results are indicated in bold. All values are in %v/v soil moisture content. Grey shaded cells indicate that no pixels of that group exist at that resolution. *= no constraint on the retrieved soil moisture and no uncertainty on the *a priori* optical depth of forest; **=without *a priori* information on the forest soil moisture.

Pixel Resolution ***(Nr. of pixels)***	**Approach**	**Group A Forest<40%**		**Group B Forest-40-60%**		**Group C Forest>60%**	
		SM RMSE	**SM Bias**	**SM RMSE**	**SM Bias**	**SM RMSE**	**SM bias**
5km *(254)*	Unif.	**1.8**	**0.3**	7.7	2.0	3.2	-2.0
	2P-U	4.0	-1.0	4.1	-3.1	1.9	-1.2
	2P-S*	2.6	-0.3	**2.8**	**-0.3**	**1.8**	**0.4**
	3P-S**	2.8	1.3	4.2	2.2	4.2	2.4
10km *(196)*	Unif.	**2.2**	**0.7**	7.0	-2.1	4.7	-4.2
	2P-U	3.5	-1.2	4.2	-3.7	3.2	-2.6
	2P-S*	2.4	-0.3	**2.8**	**-0.5**	**2.0**	**0.0**
	3P-S**	3.2	1.1	3.8	1.5	4.1	2.3
20km *(100)*	Unif.	2.7	1.3				
	2P-U	3.1	-1.8				
	2P-S*	**2.5**	**0.3**				
	3P-S**	3.1	1.1				
30km *(36)*	Unif.	2.6	1.5				
	2P-U	3.1	-2.7				
	2P-S*	**2.4**	**-0.6**				
	3P-S**	2.8	1.1				
40km *(4)*	Unif.	3.1	2.5				
	2P-U	4.6	-4.5				
	2P-S*	**2.5**	**-1.4**				
	3P-S**	3.1	2.0				

the main observations drawn from the analysis at 5km resolution hold well at coarser resolutions. In particular:

- the 2P-U approach partially reduced the error due to the heterogeneity of land cover in heterogeneous group B and forested group C pixels. However, it introduced a dry soil moisture bias;
- of the four approaches proposed in this thesis, the 2P-S approach (retrieval of a single soil moisture value uniform across the pixel and the optical depth of the moderately vegetated fraction, with the optical depth of the forest fraction imposed *a priori*) provided the most accurate soil moisture retrieval in heterogeneous group B and forested group C pixels. The improvement with respect to the 2P-U approach was stronger on group B pixels, while on group C pixels, it was only marginal, since the 2P-U approach was fairly accurate in those conditions. In these conditions the 2P-S approach was able to significantly reduce the error due to the heterogeneity of land cover within the pixel which affected the uniform pixel approach and the 2P-U approach; and
- the second approach proposed in this thesis, the 3P-S approach (retrieval of two different soil moisture values for the moderately vegetated and the forest pixel fractions and the optical depth of the moderately vegetated fraction, with the optical depth of the forest fraction imposed *a priori*), did not improve the soil moisture retrieval accuracy of the 2P-S approach;

An important outcome of this multi-resolution comparison is that the accuracy of 2P-S approach was substantially constant across resolutions (with only an increase in dry bias, not superior to -1.4%v/v), whereas that of the uniform pixel approach degraded significantly as the resolution gets coarser (overall RMSE for the study period increasing from 1.8%v/v to 3.1%v/v). As a result of this, the 2P-S approach proposed in this thesis was more accurate than the uniform pixel approach in pixels at resolutions coarser than 10km, in contrast with what was observed at resolutions finer than 10km. These results also strongly suggest that, although the analysis in the case of group B and C land cover conditions was here limited to resolutions finer than 10km resolutions (Table 8.7), the 2P-S approach should be more accurate were such land surface conditions be observed at resolutions more typical of SMOS.

However, it should also be considered that as the resolution gets coarser the coarse pixels become particular cases (in terms of land cover type fractions) of the group A land cover conditions observed at 5km resolution. For example, the 40km resolution, single pixel covering the NAFE'05 study area (sampled on four occasions) is one particular case within group A, having 22% forest fraction, 4.6% crops and 73% grassland. It is therefore difficult with this data set to understand whether the improved accuracy of the 2P-S approach at coarse resolutions is due to a change in the impact of land surface heterogeneity on the soil moisture retrieval at such resolution or simply due to the fact that the coarse pixels are a particular case of the variety of cases analysed at 5km resolution.

8.5 Chapter Summary

This Chapter has tested the SMOS L2 soil moisture retrieval algorithm using simulated SMOS pixels from 1km resolution airborne L-band observations, aggregated to spatial resolutions from 5km to 40km. While it was demonstrated that the retrieval approach proposed for the SMOS mission (2P-U) was able to reduce the soil moisture retrieval errors of a uniform pixel approach (Chapter 7) under the case of 40-60% forest (overall RMSE of soil moisture retrieval for the study period was reduced from 7.7%v/v to 4.1%v/v), the results were still larger than the SMOS target accuracy and displayed a significant dry bias.

Two major shortcomings were identified in the 2P-U approach, and subsequently addressed by a practical alternative approach. First, the assumption that a single value of optical depth can be retrieved for all the land cover fractions within the pixel when the expected optical depth of the forest fraction is low led to an underestimation of the pixel average soil moisture, resulting in a dry soil moisture bias for the study period of up to -3.1%v/v, depending on the fraction of forest. This resulted in the 2P-U approach being less accurate than a uniform pixel approach in pixels mainly covered by moderate (grassland and crop) vegetation, but having a small fraction of low density forest. Second, the 2P-U approach presented errors greater than the SMOS target accuracy of 4%v/v in the case of pixels characterised by mixed land cover (forest fraction between 40% and 60%) and strong sub-pixel heterogeneity of soil moisture (above 10%v/v). This condition led to a RMSE of respectively 5.7%v/v and 5.5%v/v on the 5km retrievals performed on the two wettest days, and an overall error for the study period of 4.1%v/v.

Two alternative retrieval approaches were proposed to reduce the soil moisture errors obtained with 2P-U approach in the case of low density forest fraction within the pixel; the 2P-S approach which imposed the optical depth of forest *a priori* and retrieved only the pixel average soil moisture and the optical depth of the moderately vegetated fraction, and the 3P-S approach which relaxed the assumption of uniform soil moisture retrieved between the different land cover types within the pixel. However, the 3P-S approach did not lead to further improvement with respect to the 2P-S approach, due to the poor sensitivity of forest emissivity to soil moisture. Conversely, the 2P-S approach led to highly improved soil moisture retrieval with respect to the 2P-U approach with an overall RMSE and bias for the study period of 2.8%v/v and -0.3%v/v (for less than 40% forest fraction), 2.6%v/v and -0.3%v/v (for 40-60% forest fraction) and 1.8%v/v and 0.4%v/v (for more than 60% forest fraction). The strength of the 2P-S approach was that it strongly reduced the error due to land cover heterogeneity in pixels with a forest fraction between 40% and 60% which affected the uniform pixel approach as well as eliminating the negative bias in soil moisture retrieval which affected the 2P-U approach. The downside of the 2P-S approach was that an estimation of the optical depth of forest is required. However, it was demonstrated that with even a crude estimate of the optical depth of forest the SMOS target accuracy could be met and the retrieval accuracy significantly improved from that of the 2P-U approach.

This Chapter therefore concludes that the best approach to reduce the error of soil moisture retrieval in areas characterised by strong variability in land cover type (i.e., equivalent fractions of forest and a moderately vegetated surface), is to retrieve a uniform soil moisture for the entire pixel together with the optical depth of the moderately vegetated surface, using *a priori* information on the optical depth of the forest fraction (2P-S approach). However, in the case of pixels mostly covered by a moderately vegetated surface, assuming a uniform surface generally leads to more accurate soil moisture retrieval. Finally, for pixels mostly covered by forest, using *a priori* information on the optical depth of the forest fraction (2P-S approach) leads only to a slight improvement with respect to the 2P-U approach.

Chapter Nine

9 Conclusions and Future Directions

This thesis has developed a soil moisture retrieval approach to reduce the error in near-surface soil moisture estimates from the future Soil Moisture and Ocean Salinity (SMOS) mission, by accounting for the heterogeneity of land surface conditions within the sensor field of view. After evaluating the core soil moisture retrieval model and main assumptions of the soil moisture retrieval approach proposed for SMOS, this thesis has found that the assumption of a uniform vegetation optical depth within the SMOS pixel resulted in a soil moisture retrieval error beyond the SMOS target accuracy (4%v/v) in the case considered of pixels occupied by a mix of moderately vegetated soil (crops and grasslands) and moderately dense Eucalypt forest, typical of the Australian environment. Therefore an approach was developed that relaxes this assumption using *a priori* information on the optical depth of the forest fraction of the pixel. Using SMOS pixels simulated from airborne data, this study has demonstrated that even with a crude estimate of the optical depth of forest, the proposed technique was able to significantly reduce the error in soil moisture retrieval due to land surface heterogeneity. In pixels presenting a 40-60% forest fraction, the approach reduced the overall RMSE of soil moisture retrieval for the study period from 4.1%v/v to 2.8%v/v, and the bias was reduced from -3.1%v/v to -0.3%v/v.

9.1 Conclusions

The conclusions of this thesis are presented hereafter in six categories: (i) Evaluation of the L-MEB radiative transfer model which is the core of the SMOS L2 soil moisture retrieval algorithm; (ii) Assessment of the scaling properties of the land surface brightness temperatures; (iii) Analysis of the link between the land surface and soil moisture heterogeneity in the study area; (iv) Assessment of the soil moisture error due to land surface and soil moisture heterogeneity under the assumption of pixel uniformity; (v)

Testing of the soil moisture retrieval approach proposed for SMOS; and (vi) Development of an alternative retrieval approach to account for the land surface heterogeneity. The limitations of the results of this thesis and their impact on further studies are also discussed.

9.1.1 Evaluation of the L-MEB Radiative Transfer Model

The L-MEB model, which is the core of the SMOS L2 soil moisture algorithm, was developed over the last 10 years from tower-based studies located mostly in European environments. Before applying the model to simulated SMOS pixels, it was therefore important in this thesis to undertake an evaluation at airborne resolutions (60m to 1km) for the land surface conditions of the study area. This was the first study to evaluate the model and its parameters at airborne resolutions and in Australian land surface conditions.

This study has demonstrated that the soil moisture accuracy of the L-MEB model, when applied to airborne data at high resolution (60m) and with the vegetation specific model parameters calibrated for European conditions, was better than 3.7%v/v over native grass sites. However, the accuracy over crop sites (largely wheat and barley) was between 10%v/v and 32.5%v/v. Moreover, there was one site (Midlothian) where the retrieval presented high errors (7.4%v/v), due to the particular vegetation type (lucerne) for which no parameters were available in the L-MEB parameter and therefore the parameters for native grass were used.

Through a sensitivity analysis of the L-MEB model it was found that the cause of the error for crops (wheat, barley and oats) resided in the very low values of the parameter characterising the soil surface roughness (parameter H_R). Following site-specific calibration of parameter H_R, it was found that this had to be increased from the value of 0.2 proposed for SMOS to a value of 1.6 for wheat and barley and 0.7 for oats. Moreover, the calibrated value of H_R was found to change with soil moisture conditions, being higher in dry conditions and decreasing in wet conditions, and therefore had to be modeled with a soil moisture dependent linear function. This function was similar to that already proposed for grassy surfaces (Wigneron et al., 2001; Escorihuela et al., 2007; Saleh et al., 2007) which was part of the L-MEB parameter set for native grasses tested in this study. Following site-specific calibration of parameter $H_{R,}$ the error over the crop sites was reduced to 4.8%v/v.

The L-MEB model was then applied to airborne observations at 1km resolution, using the soil moisture dependent parameterisation for H_R calibrated with 60m observations, yielding an average soil moisture accuracy of 3.8%v/v, and in all cases better than 6%v/v. This study has therefore demonstrated that the soil moisture dependent parameterisation of the L-MEB surface roughness parameters H_R reflects not only a "local" roughness effect (i.e., observable only at the resolution typical of tower radiometers), but needs to be accounted for at coarser resolutions. Additionally, this study has shown the soil moisture dependence of the L-MEB surface roughness parameters H_R was as important for cropped surfaces as it was for grassy surfaces.

The results of this study have important consequences for the parameterisation of H_R currently proposed for SMOS. This includes a soil moisture contribution in the form of a linear function, with the upper value of H_R (the dry end) to be defined as a function of the land cover type. However, this parameterisation is yet to be fully validated since it was verified so far only with tower-based radiometer (i.e., resolutions of 10's m) and on grassy surfaces. This study has not only provided the first experimental evidence at L-band that the change of H_R with soil moisture will be observed at SMOS resolutions, but it has also indicated that this will have to be considered for both cropped and grassy surfaces. Additionally, this study has provided strong evidence that the upper H_R value for cropped surfaces (at least in Australian conditions) will need to be set at a higher value (in the range 0.7-1.6) than that currently proposed for SMOS (0.2).

9.1.2 Scaling Properties of the Brightness Temperatures

The availability of concurrent L-band observations for large portions of the study area and at different resolutions was a novel component of the airborne data set acquired during this study. Such observations have allowed a demonstration that linear aggregation of airborne L-band data produces reliable simulation of SMOS observations at both vertical and horizontal polarisations. While a difference comparable to the radiometer noise was observed between the signal detected over common areas at 60m and 250m resolutions (2.4K), the difference was only 1.2K when the area-averaged observation over the same areas was compared between 250m and 1km resolution. This difference is well within the radiometric uncertainty of the instrument used.

9.1.3 Land Surface and Soil Moisture Heterogeneity

In order to interpret the error in soil moisture retrieval at SMOS resolution and to compare the different approaches tested in this study, it was crucial to understand how the land surface characteristics drive the near-surface soil moisture patterns in the study area. This study has found that there were different controls on the soil moisture variability depending on the scale considered. While topographically-driven soil moisture distribution was very important at small scales (~3km and below), at the scale of interest of SMOS the spatial patterns of near-surface soil moisture in the study area could be mostly linked to the spatial patterns of two land surface factors: land cover type and soil texture. Soils with higher sand content exhibited consistently drier soil moisture conditions than soils with higher clay content throughout the study period. Cropped areas exhibited overall wetter conditions with respect to areas with more moderate vegetation cover (such as grasslands), whilst forested areas were the driest across the study area. The link between near-surface soil moisture distribution, land cover and soil texture was weakened during and after rainfall events, but only for a short period of time (1-2 days). Here the spatial distribution of near-surface soil moisture was dominated by that of the rainfall fields.

This analysis has demonstrated that significant differences in soil moisture content were associated with different land cover types. Since the current satellite soil moisture products, as well as the soil moisture retrieval approach proposed for SMOS, are based on the assumption of uniform soil moisture and uniform optical depth amongst such areas, the error in soil moisture retrieval resulting from those assumptions was subsequently assessed.

9.1.4 Testing of the Uniform Pixel Assumption

Prior to evaluation of the soil moisture retrieval approach proposed for the SMOS mission, the error in soil moisture retrieval induced by land surface heterogeneity was assessed under the assumption of uniform pixel, as made by current soil moisture retrieval methods. A preliminary synthetic analysis was performed in order to analyse how the sub-pixel heterogeneity of each land surface factor affects the soil moisture retrieval as a result of the non-linearity of the L-MEB model. The analysis indicated that in a synthetic environment, and therefore with an otherwise "perfect" retrieval (i.e., exact model physics and no uncertainty in ancillary data), the heterogeneity of land cover type was the strongest source of difference between the pixel-average retrieved and observed soil moisture. Conversely the heterogeneity of soil moisture, soil texture, surface roughness, and soil temperature taken alone had a smaller impact on the retrieval, generally within the error resulting from the radiometric uncertainty of a typical radiometer (approximately 2K for the PLMR radiometer (see Appendix A3), resulting in approximately 2%v/v for moderately vegetated soil). The only exception was the error resulting from sub-pixel heterogeneity of vegetation optical depth, which was found to be significant within dense canopies. However, the heterogeneity of land cover type was simulated in this study in a physically plausible manner (i.e., using land cover specific parameters and typical vegetation water content values for each land cover type). Therefore, the observed retrieval error implicitly included the combined effect of the sub-pixel heterogeneity of vegetation optical depth, vegetation scattering albedo and vegetation structure, which are characteristics specific to each land cover type.

The conclusions drawn from the synthetic analysis were confirmed by the analysis of the error in soil moisture retrieval from simulated SMOS pixels. Significant correlation was observed between the soil moisture retrieval error and the sub-pixel heterogeneity of land cover type. Given the nature of the NAFE'05 study area, which was occupied by more than 73% native grasses, just over 4% crops, and 22% forest, the results of this study have been limited to pixels presenting mainly a mix of forest and grassland. However, this study has demonstrated that the error was strongly associated with the percentage of forest/grassland fraction within the pixel. The error raised beyond the SMOS target accuracy (4%v/v) for more than approximately 30% forest fraction, achieving a maximum of 17%v/v absolute error when the pixel was composed by 50% grassland and 50% forest fraction. The overall RMSE in soil moisture retrieval for the study period was of 7.7%v/v (with 2%v/v bias) for pixels with 40-60% forest fraction.

Additionally, the present analysis has demonstrated that the sub-pixel heterogeneity of soil moisture also affected the soil moisture retrieval from simulated SMOS pixels, but only when it occurred in conjunction with land cover heterogeneity. This can be explained by the link between land cover type and soil moisture spatial distribution observed in the study area. Drier soil moisture conditions consistently observed in forested areas interacted to determine a strong surface emission (dry soil and dense canopy), as opposed to the weak emission from the moderately vegetated fraction of the pixel which was generally wetter (low canopy density and wet soil). The soil moisture heterogeneity therefore affected the retrieval when in conjunction with the land cover type heterogeneity, since it enhanced the difference between the emissions from the forest and the moderately vegetated fraction already determined by the difference in vegetation density.

Another important conclusion of this analysis was that soil texture heterogeneity, which was shown in this study to be a major factor in driving the soil moisture variability through physical processes of water distribution, did not on the other hand have an impact on the soil moisture retrieval error comparable to that of land cover heterogeneity, nor did the heterogeneity of soil moisture caused by soil texture. Even strong soil moisture heterogeneity when occurring within pixels of homogeneous land cover did not result in a detectable soil moisture retrieval error.

These findings have important consequences for both the current soil moisture products based on the uniform pixel assumption and for the soil moisture retrieval approach proposed for SMOS. This study has demonstrated that the soil moisture retrieval under the assumption of uniform pixel will meet the SMOS target accuracy only for pixels with less than 30% forest with the remainder occupied by a mix of crops and grassland. In the presence of more than 30% forest, current soil moisture products are likely to be affected by soil moisture errors of up to 20%v/v.

While the soil moisture retrieval approach proposed for SMOS accounts for land surface type variability within the pixel, it does not account for the important contribution of variability in soil moisture and optical depth amongst land cover types, since these are assumed to be uniform amongst the pixel fractions.

9.1.5 Testing of the SMOS Soil Moisture Retrieval Approach

This study has tested the retrieval approach proposed for SMOS (approach “2P-U”) for the first time using simulated SMOS pixels based on airborne observations, with focus on the particular case of pixels composed of a mix of moderately vegetated soil (crops and grasslands) and moderately dense Eucalypt forest, typical of the Australian environment. It was found that the approach, which uses an inversion technique based on separate forward modeling for sub-pixel fractions of uniform land use, with the assumption of uniform optical depth and soil moisture between the fractions, was able to reduce the high soil moisture retrieval errors affecting the uniform pixel approach in the case of 40-60% forest, although only partially. The overall RMSE of soil moisture retrieval for the study period was in this case reduced from 7.7%v/v for the uniform pixel approach to 4.1%v/v. The approach also improved the retrieval in pixels where the forest fraction was predominant, i.e., higher than 60%, reducing the overall RMSE for the study period from 3.2%v/v to 1.9%v/v. However, the SMOS approach has been shown to have errors higher than a uniform pixel approach when the pixel was mainly occupied by a mix of moderately vegetated surfaces (crop and grassland) and the forest fraction was small (less than 40%). In these cases the overall RMSE was increased from 1.8%v/v to 4.0%v/v.

Two major shortcomings have been identified in the SMOS approach which have led to the improved approach developed in this study and discussed in the next section. The first shortcoming resided in the assumption that all land cover types in the pixel have the same optical depth. This has been shown to lead to a dry soil moisture bias in all pixels with a fraction of forest smaller than 60%, the bias increasing with increasing forest fraction and being as much as -3.1%v/v for the case 40-60% forest fraction. The reason for the bias was that the retrieved soil moisture was distorted by the algorithm in order to match the composite soil moisture-emission curve of the mixed pixel using one common optical depth. The second shortcoming was that for the case of 40-60% forest, despite the strong reduction in RMSE with respect to the uniform pixel approach, the SMOS approach was still affected by errors beyond the SMOS target accuracy in pixels characterised by strong soil moisture heterogeneity (standard deviation higher than 10%v/v). This was due to the interaction between canopy density and soil moisture discussed in the previous section, in pixels characterised by dry soil under forest canopy and wet soil in moderately vegetated areas.

This study has therefore demonstrated that the SMOS approach partially reduced the error of a uniform pixel approach due to land surface heterogeneity. However it resulted in underestimation of the pixel average soil moisture due to the contrast between the emission from forested and moderately vegetated areas (grassland or crop). This was mainly due to the difference in vegetation density and was enhanced by the generally drier soil moisture conditions under the forest canopy. Due to the erroneous assumptions of uniform soil moisture and optical depth between the two land cover fractions, the SMOS approach resulted in errors beyond the SMOS target accuracy in highly mixed pixels (40-60% forest), with an overall RMSE of 4.1%v/v (-3.1%v/v bias) and was less accurate than a uniform pixel approach in moderately vegetated pixels with 0-40% forest fraction, having an overall RMSE of 4.0%v/v (-1.0%v/v bias).

9.1.6 Development of an Alternative Retrieval Approach

This thesis has proposed an alternative approach ("2P-S") for soil moisture retrieval from SMOS and has tested its ability to reduce the soil moisture errors obtained with the approach proposed for SMOS. The approach consists of relaxing the assumption of uniform optical depth between the pixel modeled fractions, by imposing the optical depth of forest *a priori* and retrieving only the optical depth of the moderately vegetated fraction and a uniform soil moisture value for the pixel. This approach led to highly improved soil moisture retrieval with respect to SMOS approach. A second alternative approach ("3P-S") attempted, that of relaxing the assumption of uniform soil moisture by retrieving different soil moisture values for the forest and moderate vegetation fractions did not lead to better results.

The proposed approach allowed retrieval of soil moisture from simulated SMOS pixels with an overall RMSE for the study period much smaller than the SMOS target accuracy and with negligible bias, being respectively of 2.6%v/v and -0.3%v/v (for less than 40% forest fraction), 2.8%v/v and -0.3%v/v (for 40-60% forest fraction) and 1.8%v/v and 0.4%v/v (for more than 60% forest fraction). The advantages of this approach are that (i) it strongly reduces the error due to land cover heterogeneity which affects the uniform pixel approach for the case of 40-60% forest, (ii) it eliminates the dry soil moisture bias which affect the SMOS approach in pixels with forest fraction smaller than 60%.

Such dry bias using the SMOS approach was shown to affect pixels with even small amount of forest cover, as little as 5% in an otherwise moderately vegetated pixel. In the perspective of 'global' soil moisture monitoring, this means that the approach proposed would improve the accuracy of SMOS soil moisture retrieval not only on areas with significant amount of forest (40-60%), but also on areas with a small amount of forest, as little as 5%. Given the spatial resolution of SMOS (40km), the advantages of the approach proposed would therefore extend to most pixels of temperate or semi-arid continental areas.

The downside of the proposed approach is that an estimation of the optical depth of forest is required. However, this study has demonstrated that with even a crude estimate of the optical depth of forest the 2P-S approach could meet the SMOS target accuracy of 4%v/v and correct the dry bias typical of the SMOS approach. From an operational point of view, a sufficiently accurate estimate of the optical depth of forest at L-band could be derived from routinely available maps of LAI, since forest-specific studies have observed that the main contribution to microwave emission and attenuation is due to tree branches at L-band (Ferrazzoli et al., 2002).

This thesis has therefore concluded that the best retrieval approach to reduce the error in SMOS soil moisture retrieval due to the sub-pixel heterogeneity of land surface is to retrieve a single soil moisture value for the pixel and the optical depth of only the moderately vegetated fraction of the pixel, whereas the optical depth of the forest fraction should be imposed using *a priori* information. In the case of pixels mostly covered by a moderately vegetated surface and with forest fraction smaller than 40%, a simple approach which treats the pixel as a uniform, moderately vegetated surface leads to the most accurate soil moisture retrieval. However, in such cases the application of the proposed approach will only slightly degrade the retrieval, while still amply meeting the SMOS target accuracy.

It should be highlighted that the improvement in SMOS soil moisture retrieval demonstrated in this thesis was not obtained through an improved modeling of the physics of radiative transfer of heterogeneous pixels, beside the extension of the soil moisture dependence of the L-MEB surface roughness parameter to crops as discussed earlier. Rather, the improvement derived from reducing the non-linear effect of land surface heterogeneity on the L-MEB radiative transfer model used by the SMOS L2 algorithm by fixing one of the variables of the retrieval (i.e., the optical depth of forest) to a plausible value. This was shown to improve the soil moisture retrieval by reducing the distortion of the variable of interest (soil moisture) during the optimization process, without changes in the representation of the physics of radiative transfer.

As a final comment, it must be acknowledged that the results presented and conclusions drawn are for the land surface conditions of a semi-arid catchment during a one-month observation period. Morevoer, it should be remembered that this study focused on the particular case where the density of the forest canopy is low, like is the case for the Eucalypt forest in the study area considered. Consequently, it is important that such analysis be conducted for different sites, in particular in temperate areas presenting forest canopy of higher density, and over longer time frames. However, the study area is representative of a large portion of the Australian continent and the complete range of soil wetness conditions was encountered. Additionally, the proposed approach has corrected the problem of a dry soil moisture bias in the presence of large microwave emission contrasts between forested areas and areas of moderate vegetation, which are characteristic of several climatic regions of the world.

9.2 Recommendations for Future Work

9.2.1 Surface Roughness Parameterisation in L-MEB

This study has shown that a soil moisture dependent parameterisation of the L-MEB surface roughness parameter H_R is needed to accurately estimate soil moisture from airborne data. These results extended previous results obtained with tower-based radiometers and suggested that such parameterisation will be necessary when using SMOS data. Further investigation in this sense is needed to confirm whether this corresponds to a physical effect, or rather is due to some deficiency of the L-MEB model. Shortcomings in the modeling of the vegetation optical depth in L-MEB, or poor skills of the dielectric model used to account for small-scale soil moisture heterogeneity might have resulted in a deficit in the emission budget, attributed during the calibration process to the surface roughness parameter. This could be done for example by analysis of the data presented using a different emission model or using L-MEB with more advanced dielectric models.

Once the nature of this effect is confirmed, investigation is needed in order to understand whether a linear decay (like that calibrated in this study and proposed for SMOS) is the best function to model the variation of the roughness parameter with increasing soil moisture. Additionally, a link should be established between the parameters of such a curve and soil texture or land cover ancillary information, in order to ensure the applicability of the function to global retrieval without the need for calibration of the roughness parameter prior to soil moisture retrieval. For SMOS it is currently envisioned to define the slope of the linear function based on some soil-texture-dependent thresholds, but these are still to be fully explored and validated. This was partially attempted during this study (see Appendix A4). Although a complete soil moisture dependent model for H_R could not be developed in this study, results suggest that the function that better describes the change of H_R with soil moisture can be parameterised depending on soil texture information. However, this appears to be a more complex function than that proposed for SMOS. While a simple linear monotonic relationship between H_R and soil moisture applied well to sandy soils, for clay soils a piecewise function appears more appropriate, with an increase of H_R going from very dry to intermediate conditions (<25%v/v) and a linear decrease for wetter conditions.

9.2.2 SMOS Soil Moisture Retrieval Approach

This study has indicated some deficiencies in the retrieval approach proposed for SMOS. The results presented are subjected to certain limitations stemming from (i) the use of airborne data to simulate SMOS pixels, and (ii) the particular land surface conditions in the study area. These are separately explained below.

Only SMOS pixels at one fixed incidence angle (38.5º) could be used in this analysis to test the retrieval approach proposed for SMOS, because the airborne data used to simulated SMOS pixels were taken with the instrument in "pushbroom" configuration Although multi-angle observations were part of the NAFE'05 experiment data set, these were undertaken only over a few small areas (three of the experimental farms) and at 250m resolution and therefore could not be used to simulate SMOS pixels. The relative importance of the heterogeneity of different land surface factors within the pixel might change with the incidence angle. If that change was significant, the use of several observations at different angles might complicate the correction for sub-pixel heterogeneity. For example, the impact of the sub-pixel heterogeneity of land cover, which was observed to be significant at 38.5º, might be less important close-to-nadir due to the different angular variation of the vegetation optical depth of different land cover types. In this study this could not be investigated in depth at SMOS resolution for the reason outlined above. However, it was demonstrated through a synthetic experiment that in the presence of sub-pixel heterogeneity, use of multiple observations at multiple incidence angles did not necessarily represent an advantage with respect to the use of few incidence angles. This warrants further investigation with both synthetic analysis and real data (the 250m multi-angle observations collected during NAFE'05 or actual SMOS data). Such analysis should assess the impact of the same heterogeneity conditions on the retrieval at different incidence angles, and eventually identify the range of incidence angles where the impact of land surface heterogeneity on the retrieval is smaller.

The study area comprised 73% grassland, 22% forest and 5% crops. Therefore only land surface conditions considered “nominal” for SMOS retrieval were investigated, i.e., surfaces with “normal soil with low vegetation, eventually a manageable amount of free water […] and therefore do not include water bodies, mountainous, urban, and partially frozen or snow covered areas” (CESBIO, 2007). The impact of non-nominal surfaces fractions within SMOS pixels might be significant and will need to be addressed. In particular, since no soil moisture retrieval will be attempted on non-nominal surfaces, further analysis is needed to understand how the presence of non-nominal surfaces will affect the retrieval of soil moisture over nominal surfaces also present in the pixel. Beside the possible use of real SMOS data to address these issues, the data collected during the NAFE’06 experiment in the Murrumbidgee catchment in Australia would be useful to this end, since the region monitored comprised some urban areas and an extensive irrigation area with flooded crops.

Another limitation related to the particular land surface conditions in the study area is the limited pixel fraction of cropped areas in the simulated SMOS pixels (less than 5%). This was partially compensated by analysing simulated pixels at 5km resolution. However, even at that resolution the fraction of crop examined never exceeded 20%. Moreover, the results suggest that the contrast between grassland and cropped areas will result in a wet bias under the assumption of uniform optical depth of the SMOS approach. Although the bias was only half that caused by the contrast between forested areas and moderately vegetated areas (including grassland and crop), in the presence of a fraction of crops higher than 20% of the pixel area the SMOS approach might result in errors beyond the SMOS target accuracy. A possible solution to be explored could be to apply the approach proposed in this study for forests, by using *a priori* information on the forest optical depth, but retrieve separate values of the optical depth for the crop and the grassland fraction. This is expected to improve the soil moisture retrieval since the same technique, when applied to retrieve different optical depth values for the forest and moderate vegetation, improved the retrieval of a uniform-optical-depth approach. Another option could be that of retrieving three different optical depth values (forest, grassland and crop), but this will require a wealth of observations, and might present problems of algorithm convergence.

9.2.3 Alternative Retrieval Approaches

The major limitation faced by this study was the lack of multi-angular observations at the SMOS resolution. This has limited the analysis to reproduce SMOS retrieval scenarios where observations with only two incidence angles and polarisations are available. Therefore, very little "extra" observations are left to allow the retrieval of extra parameters accounting for the effect of heterogeneity (other than a uniform soil moisture and a uniform optical depth). However, the current SMOS approach is that of devoting the extra observations to retrieval of other important radiative transfer parameters (e.g., surface roughness, scattering albedo). The analysis of SMOS data over well-monitored areas should investigate whether it is more efficient to use the extra observations to retrieve many parameters uniform amongst the pixel fractions, or retrieve fewer parameters, but consider them fraction-specific. This comes down to a trade-off between the impact of the sub-pixel heterogeneity of each parameter versus the importance of the estimation of the pixel average value of the parameter for the soil moisture retrieval. Moreover, the choice of the approach will also be subjected to consideration of the algorithm convergence.

The approach proposed in this study was shown to improve the soil moisture retrieval accuracy over that of the SMOS approach for all combinations of grassland and forest fractions within the pixel (although always less than 20% crop). However, strictly speaking this was demonstrated only with pixels at 5km resolutions. At the SMOS resolution, the only combination that could be analysed was the particular mix of land cover types present in the study area (73% grassland, 22% forest and 5% crops). Since the accuracy of the proposed method was found to be stable across resolutions, with the accuracy of SMOS algorithm retrieval degraded when going towards coarser resolution, it is likely that the results of this thesis will be valid for SMOS pixels with a larger fraction of forest. However, the results should be confirmed by applying the method proposed to areas of such nature.

References

Altese, E., Bolognani, O., Mancini, M. and Troch, P. A., 1996. Retrieving soil moisture over b33are soil from ERS-1 synthetic aperture radar data: Sensitivity analysis based on a theoretical surface scattering model and field data. *Water Resour. Res.*, **32**(3): 653-661.

Ambroise, B., Beven, K. J. and Freer, J., 1996. Toward a generalization of the TOPMODEL concepts: Topographic indices of hydrological similarity. *Water Resour. Res.*, **32**(7): 2135-2145.

Ångström, A., 1925 The albedo of various surfaces of ground. *Geograf. Ann.*, **7**: 323-342.

Autret, M., Bernard, R. and Vidal-Madjar, D., 1989. Theoretical study of the sensitivity of the microwave backscattering coefficient to the soil surface parameters. *Int. J. Rem. Sens.*, **10**(1): 171-179.

Barling, R. D., Moore, I. D. and Grayson, R. B., 1994. A quasi-dynamic wetness index for characterizing the spatial distribution of zones of surface saturation and soil-water content. *Water Resour. Res.*, **30**(4): 1029-1044.

Basharinov, A. Y. and Shutko, A. M., 1975. Simulation studies of the SHF radiation characteristics of soils under moist conditions. *NASA Tech. Transl.*, **TT F-16**.

Beaudoin, A., Le Toan, T. and Gwyn, Q. H. J., 1990. SAR observations and modeling of the C-band backscatter variability due to multiscale geometry and soil moisture. *IEEE. Trans. Geosci. Rem. Sens.*, **28**(5): 886-895.

Beljaars, A. C. M., Viterbo, P., Betts, A. K. and Miller, M. J., 1996. Anomalous rainfall over the United States during July 1993: Sensitivity to land surface parameterization and soil moisture anomalies *Mon. Wea. Rev.*, **124** 362-383.

Betts, A., Ball, J., Beljaars, A., Miller, M. and Viterbo, P., 1996. The land surface-atmosphere interaction: A review based on observational and global modeling perspectives *J. Geophys. Res.-Atmospheres*, **101** (D3:): 7209-7225

Betts, A. K., Ball, J. H., Baljaars, A. C. M., Miller, M. J. and Viterbo, P., 1994. Coupling between land-surface, boundary-layer parameterizations and rainfall on local and regional scales: lessons from the wet summer of 1993. *In: Proc. of Fifth Conf. on Global Change Studies*, Nashville, 174 -181

Beven, K. J. and Kirkby, M. J., 1979. A physically based, variable contributing area model of basin hydrology. *Hydrol. Sci. Bull.*, **24**(43-69).

Bindlish, R. and Barros, A. P., 2002. Subpixel variability of remotely sensed soil moisture: An inter-comparison study of SAR and ESTAR. *IEEE Trans. Geosci. Remote Sens.*, **40**(2): 326-337.

Bindlish, R., Jackson, T. J., Gasiewski, A., Stankov, B., Klein, M., Cosh, M. H., Mladenova, I., Watts, C., Vivoni, E., Lakshmi, V., Bolten, J. and Keefer, T., 2008. Aircraft based soil moisture retrievals under mixed vegetation and topographic conditions. *Remote Sens. Environ.*, **112**(2): 375-390.

Blazkova, S., Beven, K. J., Tacheci, P. and Kulasova, K., 2002. Testing the distributed water table predictions of TOPMODEL (allowing for uncertainty in model calibration): The death of TOPMODEL? *Water Resour. Res.*, **38**(11): 1257.

Brown, R. J., Manore, M. J. and Poirer, S., 1992. Correlations between X-, C- and L-band imagery within an agricultural environment. *Int. J. Rem. Sens.*, **13**(9): 1645-1661.

Burke, E. J. and Simmonds, L. P., 2003. Effects of sub-pixel heterogeneity on the retrieval of soil moisture from passive microwave radiometry. *Int. J. Rem. Sens.*, **24**(10): 2085-2104.

Burke, E. J., Shuttleworth, W. J. and Houser, P. R., 2004. Impact of horizontal and vertical heterogeneities on retrievals using multiangle microwave brightness temperature data. *IEEE Trans. Geosci. Remote Sens.*, **42**(7): 1495.

Campbell, J. R., 2003. Limitations in the laser particle sizing the soils. In: R. I.C (Eds), *Advances In Regolith*, CRC LEME, 38-42.

Carlson, T., Gillies, R. and Perry, E., 1994. A method to make use of thermal infrared temperature and NDVI measurements to infer surface soil water content and fractional vegetation cover. *Remote Sens. Rev.*, **9**: 161-173.

Castillo, V. M., Gómez-Plaza, A. and Martínez-Mena, M., 2003. The role of antecedent soil water content in the runoff response of semiarid catchments: a simulation approach. *J. Hydrol.*, **284**(1-4): 114-130.

Ceccato, P., Flasse, S. and Gregoire, J.-M., 2002. Designing a spectral index to estimate vegetation water content from remote sensing data Part 2. Validation and applications. *Remote Sens. Environ.*, **82**: 198–207.

CESBIO (2003). Mission objectives ans scientific requirements of the Soil Moisture and Ocean Salinity (SMOS) Mission. Technical Report. [Available online at http://www.cesbio.ups-tlse.fr/pdf/SMOS_MRD_V5.pdf], Centre d'Etudes Spatiales de la BIOsphère.

CESBIO (2006). Algorithm validation plan for SMOS L2 SMPPD. Technical Report. [Available online at www.cesbio.ups-tlse.fr/data_all/SMOS-doc/CBSA/L2-SM_algovalP_V015_1g.pdf], Centre d'Etudes Spatiales de la BIOsphère.

CESBIO (2007). SMOS level 2 processor for soil moisture Algorithm Theoretical Based Document (ATBD), version 3.a. Technical Report. [Available Online at http://www.cesbio.ups-tlse.fr/data_all/SMOS-doc/SM_ATBD_3-a.pdf], Centre d'Etudes Spatiales de la BIOsphère.

Chand, T. R. K. and Badarinath, K. V. S., 2007. Analysis of ENVISAT ASAR data for forest parameter retrieval and forest type classification: a case study over deciduous forests of central India. *Int. J. Rem. Sens.*, **28**(22): 4985-4999.

Chanzy, A., Bruckler, L. and Perrier, A., 1995. Soil Evaporation Monitoring: a possible synergism of microwave and infrared remote sensing. *J. Hydrol.*, **165**: 235-259.

Chauhan, N. S., Miller, S. and Ardanuy, P., 2003. Spaceborne soil moisture estimation at high resolution: a microwave/optical/IR synergistic approach. *Int. J. Rem. Sens.*, **24**(22): 4599-4622.

Chehbouni, A., Njoku, E. G., Lhomme, J.-P. and Kerr, a. Y. H., 1995. Approaches for averaging surface parameters and fluxes over heterogeneous terrain. *J. Climatol.*, **8**(5): 1386–1393.

Choi, M., Jacobs, J. M. and M.H., C., 2007. Scaled spatial variability of soil moisture fields. *Geophys. Res. Letters*, **34**(L01401).

Choudhury, B. J., Schmugge, T. J., Chang, A. and Newton, R. W., 1979. Effect of surface-roughness on the microwave emission from soils. *J. Geophys. Res.-Oceans and Atmosphere*, **84**(Nc9): 5699-5706.

Choudhury, B. J., Schmugge, T. J. and Mo, T., 1982. A parameterization of effective soil temperature for microwave emission. *J. Geophys. Res.*, **87**(C2): 1301-1304.

Conil, S., Douville, H. and Tyteca, S., 2007. The relative influence of soil moisture and SST in climate predictability explored within ensembles of AMIP type experiments. *Climate Dynamics*, **28**: 125-145.

Cosh, M. H. and Brutsaert, W., 1999. Aspects of soil moisture variability in the Washita '92 study region. *J. Geophys. Res.*, **104**(D16): 19751-19757.

Crow, W. T., Drusch, M. and Wood, E. F., 2001. An observation system simulation experiment for the impact of land surface heterogeneity on AMSR-E soil moisture retrieval. *IEEE Trans. Geosci. Remote Sens.*, **39**(8): 1622-1631.

D'Odorico, P., Laio, F., Porporato, A. and Rodriguez-Iturbe, I., 2003. Hydrologic controls on soil carbon and nitrogen cycles. II. A case study. *Adv. Water. Resour.*, **26**(1): 59-70.

Davenport, I. J., Sandells, M. J. and Gurney, R. J., 2008. The effects of scene heterogeneity on soil moisture retrieval from passive microwave data. *Adv. Water Resour.*, **31**(11): 1494-1502

De Rosnay, P., Calvet, J.-C., Kerr, Y., Wigneron, J.-P., Lemaitre, F., Escorihuela, M. J., Sabater, J. M., Saleh, K., Barrie, J., Bouhours, G., Coret, L., Cherel, G., Dedieu, G., Durbe, R., Fritz, N. E. D., Froissard, F., Hoedjes, J., Kruszewski, A., Lavenu, F., Suquia, D. and Waldteufel, P., 2006a. SMOSREX: A long term field campaign experiment for soil moisture and land surface processes remote sensing. *Remote Sens. Environ.*, **102**(3-4): 377-389.

De Rosnay, P., Wigneron, J.-P., Holmes, T. and Calvet, J.-C., 2006b. Parameterizations of the effective temperature for L-band radiometry. Intercomparison and long term validation with SMOSREX field experiment. . In: P. W. R. C. Mätzler, A. Battaglia, & J. P. Wigneron (Eds), *Thermal Microwave Radiation-Applications for Remote Sensing*, London, UK, 312−324.

de Troch, F. P., Troch, P. A., Su, Z. and Lin, D. S., 1996. Chapter 9: Application of remote sensing for hydrological modelling. In: M. B. Abbott, and Refsgaard, J. C. (Eds), *Distributed Hydrological Modelling*, Kluwer Academic Publishers, Dordrecht.

Della Vecchia, A., Ferrazzoli, P., Giorgio, F. and Guerriero, L., 2006. A large scale approach to estimate L band emission from forest covered surfaces. *In: Proc. of 2nd International Symposium on Recent Advances in Quantitative Remote Sensing*, Torrent (Valencia, Spain).

Della Vecchia, A., Ferrazzoli, P., Wigneron, J. P. and Grant, J. P. A. G. J. P., 2007. Modeling forest emissivity at L-band and a comparison with multitemporal measurements. *IEEE Geoscience and Remote Sensing Letters*, **4**(4): 508-512.

Demarty, J., Ottle, C., Braud, I., Olioso, A., Frangi, J. P., Gupta, H. V. and al., e., 2005. Constraining a physically based soil–vegetation–atmosphere transfer model with surface water content and thermal infrared brightness temperature measurements using a multiobjective approach. *Water Resour. Res.*, **41**(1).

Dobson, M. C., Ulaby, F. T., Hallikainen, M. T. and El-Rayes, M. A., 1985. Microwave dielectric behavior of wet soil-part II: Dielectric mixing models. *IEEE Trans. Geosci. Remote Sens.*, **GE-23**(1): 35-46.

Dobson, M. C. and Ulaby, F. T., 1986. Active microwave soil moisture research. *IEEE. Trans. Geosci. Rem. Sens.*, **GE-24**(1): 23-36.

Dobson, M. C., Pierce, L., Sarabandi, K., Ulaby, F. T. and Sharik, T., 1992. Preliminary analysis of ERS-1 SAR for forest ecosystem studies. *IEEE. Trans. Geosci. Rem. Sens.*, **30**(2): 203-211.

Draper, C. S., Walker, J. P., Steinle, J., de Jeu, R. A. M. and T.R.H., H., 2009. An evaluation of AMSR–E derived soil moisture over Australia. *Remote Sens. Environ.*, **113** (4): 703–710.

Drusch, D., Wood, E. F. and Simmer, S., 1999a. Up-scaling effects in passive microwave remote sensing: ESTAR 1.4 GHz measurements during SGP '97. *Geophys. Res. Letters*, **26**(7): 879-882.

Drusch, M., Wood, E. F. and Lindau, R., 1999b. The impact of the SSM/I antenna gain function on land surface parameter retrieval *Geophysical Research Letters* **26** (23): 3481-3484

Dubois, P. C., van Zyl, J. and Engman, T., 1995. Measuring soil moisture with imaging radars. *IEEE. Trans. Geosci. Rem. Sens.*, **33**(4): 915-926.

Dunne, T. and Black, R. D., 1970a. An experimental investigation of runoff production in permeable soil. *Water Resour. Res.*, **6**(2): 478-490.

Dunne, T. and Black, R. D., 1970b. Partial area contributions to storm runoff in a small New England watershed. *Water Resour. Res.*, **6**(5): 1296-1311.

Ellyett, C. D. and Pratt, D. A., 1975. *A review of the potential application of remote sensing techniques to hydrogeological studies in australia. Australian Water Resources Council Technical Paper No. 13*. Australian Gov. Publishing Service, Canberra, 147pp.

Engman, E. T., 1990. Progress in microwave remote sensing of soil moisture. *Canadian J. Rem. Sens.*, **16**(3): 6-14.

Engman, E. T., 1991. Application of microwave remote sensing of soil moisture for water resources and agriculture. *Remote Sens. Environ.*, **35**: 213-226.

Engman, E. T., 1992. Soil moisture needs in Earth sciences. *In: Proc. of International Geoscience and Remote Sensing Symposium (IGARSS)*, 477-479.

Engman, E. T. and Chauhan, N., 1995. Status of microwave soil moisture measurements with remote sensing. *Remote Sens. Environ.*, **51**(1): 189-198.

Entekhabi, D., Nakamura, H. and Njoku, E. G., 1993. Retrieval of soil moisture by combined remote sensing and modeling. *In: Proc. of ESA/NASA International Workshop on Passive Microwave Remote Sensing Research Related to Land-Atmosphere Interactions*, St. Lary, France, 485-498.

Entekhabi, D. and Rodrigueziturbe, I., 1994. Analytical framework for the characterization of the space-time variability of soil-moisture. *Adv. Water Resour.*, **17**(1-2): 35-45.

Entekhabi, D., RodriguezIturbe, I. and Castelli, F., 1996. Mutual interaction of soil moisture state and atmospheric processes. *J. Hydrol.*, **184**(1-2): 3-17.

Entin, J., Robock, A., Vinnikov, K., Hollinger, S., Liu, S. and Namkhai, A., 2000. Temporal and spatial scales of observed soil moisture variations in the extratropics *J. Geophys. Res.-Atmosphere*, **105**(D9): 11865-11877.

Escorihuela, M. J., Kerr, Y. H., de Rosnay, P., Wigneron, J. P., Calvet, J. C. and Lemaitre, F., 2007. A Simple model of the bare soil microwave emission at L-band. *IEEE Trans. Geosci. Remote Sens.*, **45**(7): 1978-1987.

Famiglietti, J. S., Devereaux, J. A. and Laymon, C. A., 1999. Ground-based investigation of soil moisture variability within remote sensing footprints during the Southern Great Plains 1997 (SGP97) hydrology experiment *Water Resour. Res.*, **35**(6): 1839-1851.

Ferrazzoli, P., Guerriero, L. and Wigneron, J. P., 2002. Simulating L-band emission of forests in view of future satellite applications. *IEEE Trans. Geosci. Remote Sens.*, **40**(12): 2700-2708.

Fitzjohn, C., Ternan, J. L. and Williams, A. G., 1998. Soil moisture variability in a semi-arid gully catchment: Implications for runoff and erosion control. *Catena*, **32**: 55-70.

Galantowicz, J. F., Entekhabi, D. and Njoku, E. G., 2000. Estimation of soil-type heterogeneity effects in the retrieval of soil moisture from radiobrightness. *IEEE Trans. Geosci. Remote Sens.*, **38**(1): 312-316.

Giacomelli, A., Bacchiega, U., Troch, P. A. and Mancini, M., 1995. Evaluation of surface soil moisture distribution by means of SAR remote sensing techniques and conceptual hydrological modelling. *J. Hydrol.*, **166**(3-4): 445-459.

Gillies, R. P., Kustas, W. P. and Humes, K. S., 1997. A verification of the 'triangle' method for obtaining surface soil water content and energy fluxes from remote measurements of the Normalized Difference Vegetation Index (NDVI) and surface e *Int. J. Rem. Sens.*, **18**(15): 3145 - 3166.

Goward, S. N., Xue, Y. K. and Czajkowski, K. P., 2002. Evaluating land surface moisture conditions from the remotely sensed temperature/vegetation index measurements - An exploration with the simplified simple biosphere model. *Remote Sens. Environ.*, **79**(2-3): 225-242.

Grant, J. P., Wigneron, J.-P., Van de Griend, A. A., Schmidl Søbjærg, S., Skou, N. and Balling, J., 2007a. Bray-2004 L-band radiometric field experiment in the Les Landes forest: microwave signal behaviour for varying conditions of ground moisture. *Remote Sens. Environ.*, **107**: 639−655.

Grant, J. P., Wigneron, J. P., Van de Griend, A. A., Kruszewski, A., Sobjaerg, S. S. and Skou, N., 2007b. A field experiment on microwave forest radiometry: L-band signal behaviour for varying conditions of surface wetness. *Remote Sens. Environ.*, **109**(1): 10-19.

Grant, J. P., Wigneron, J.-P., Panciera, R., Walker, J. P. and Van de Griend, A. A., 2008. L-band microwave emission model parameters for a Eucalypt forest. *In: Proc. of IEEE International Geoscience and Remote Sensing Symposium 2008 (IGARSS'08)*, Boston, Massachusetts, U.S.A.

Grant, J. P. (2009). Measurement and modelling of L-band forest emission for future soil moisture retrieval from SMOS signatures, PhD Thesis, Vrije Universiteit Amsterdam.

Grayson, R., Western, A., Chiew, F. and Bloeschl, G., 1997a. Preferred states in spatial soil moisture patterns: Local and nonlocal controls. *Water Resour. Res.*, **33**(12): 2897-2908.

Grayson, R., Bloschl, G., Willgoose, G. and McMahon, T., 1999. Observed spatial organization of soil moisture and its relation to terrain indices. *Water Resour. Res.*, **35**(3): 797-810.

Grayson, R. and Western, A., 2001. Terrain and the distribution of soil moisture. *Hydrol. Processes*, **15**(13): 2689-2690.

Grayson, R. B., Western, A. W., Chiew, F. H. S. and Bloschl, G., 1997b. Preferred states in spatial soil moisture patterns: Local and nonlocal controls. *Water Resour. Res.*, **33**(12): 2897-2908.

Grayson, R. B. and Western, A. W., 1998. Towards areal estimation of soil water content from point measurements: time and space stability of mean response. *J. Hydrol.*, **207**(1-2): 68-82.

Guglielmetti, M., Schwank, M., Mätzler, C., Oberdörster, C., Vanderborght, J. and Flühler, H., 2007. Measured microwave radiative transfer properties of a deciduous forest canopy. *Remote Sens. Environ.*, **109**(4): 523-532.

Guha, A. and Lakshmi, V., 2002. Sensitivity, spatial heterogeneity, and scaling of C-band microwave brightness temperatures for land hydrology studies. *IEEE Trans. Geosci. Remote Sens.*, **40**(12): 2626-2635.

Guha, A., Jacobs, J. M., Jackson, T. J., Cosh, M. H., En-Ching, H. and Judge, J., 2003. Soil moisture mapping using ESTAR under dry conditions from the Southern Great Plains Experiment (SGP99). *IEEE Trans. Geosci. Remote Sens.*, **41**(10): 2392–2397.

Hallikainen, M., Ulaby, F., Dobson, M. and El-Rayes, M., 1984. Dielectric measurements of soils in the 3- to 37- GHz band between −50 °C and 23 °C. *In: Proc. of International Geoscience and Remote Sensing Symposium, IGARSS'84*, Strasbourg, France, 163−168.

Hinse, M., Gwyn, Q. H. J. and Bonn, F., 1988. Radiometric correction of C-band imagery for topographic effects in regions of moderate relief. *IEEE. Trans. Geosci. Rem. Sens.*, **26**(122-132): 1988.

Hoeben, R., Troch, P. A., Su, Z., Mancini, M. and Chen, K., 1997. Sensitivity of radar backscattering to soil surface parameters: A comparison between theoretical analysis and experimental evidence. *In: Proc. of International Geoscience and Remote Sensing Symposium (IGARSS)*, Singapore, 1368-1370.

Houser , P. R., Shuttleworth , W. J., Famiglietti, J. S., H.V., G., Syed, K. H. and Goodrich, D. C., 1998. Integration of soil moisture remote sensing and hydrologic modeling using data assimilation. *Water Resour. Res.*, **34**(12): 3405–20.

Huszár, T., Mika, J., Lóczy, D., Molnár, K. and Kertész, Á., 1999. Climate change and soil moisture: A case study. *Physics and Chemistry of the Earth, Part A: Solid Earth and Geodesy*, **24**(10): 905-912.

Idso, S. B., Jackson, R. D., Reginato, R., J., Kimball, B. A. and Nakayama, F. S., 1975. The dependence of bare soil albedo on soil water content. *J. Appl. Met.*, **14**: 109-113.

Jackson, R. D., Idso, S. B. and Reginato, R. J., 1976. Calculation of evaporation ratesduring the transition from energy-limiting to soil-limiting phases using albedo data. *Water Resour. Res.*, **12**(1): 23-26.

Jackson, T. J., Schmugge, T. J. and Wang, J. R., 1982. Passive microwave sensing of soil-moisture under vegetation canopies. *Water. Resour. Res.*, **18**(4): 1137-1142.

Jackson, T. J., Schmugge, T. J. and O'Neill, P., 1984. Passive microwave remote sensing of soil moisture from an aircraft platform. *Remote Sens. Environ.*, **14**(1-3): 135-151.

Jackson, T. J., Hawley, M. E. and O’Neill, P. E., 1987. Preplanting soil moisture using passive microwave sensors. *Water Resour. Bull.*, **23**(1): 11-19.

Jackson, T. J. and Schmugge, T. J., 1991. Vegetation effects on the microwave emission of soils. *Remote Sens. Environ.*, **36**(3): 203-212.

Jackson, T. J., 1993. III Measuring surface soil moisture using passive microwave remote sensing. *Hydrol. Processes*, **7**: 139-152.

Jackson, T. J., Levine, D. M., Swift, C. T., Schmugge, T. J. and Schiebe, F. R., 1995a. Large-area mapping of soil-Moisture using the ESTAR passive microwave radiometer in Washita92. *Remote Sens. Environ.*, **54**(1): 27-37.

Jackson, T. J. and Schmugge, T. J., 1995b. Surface soil moisture measurement with microwave radiometry. *Acta Astronautica*, **35**(7): 477-482.

Jackson, T. J. and Le Vine, D. E., 1996a. Mapping surface soil moisture using an aircraft-based passive microwave instrument: algorithm and example. *J. Hydrol.*, **184**(1-2): 85-99.

Jackson, T. J., Schmugge, T. J. and Engman, E. T., 1996b. Remote sensing applications to hydrology: soil moisture. *Hydrol. Sci. J.*, **41**(4): 517-530.

Jackson, T. J., Le Vine, D. M., Hsu, A. Y., Oldak, A., Starks, P. J., Swift, C. T., Isham, J. D. and Haken, M., 1999. Soil moisture mapping at regional scales using microwave radiometry: The Southern Great Plains Hydrology Experiment. *IEEE Trans. Geosci. Remote Sens.*, **37**(5): 2136-2151.

Jackson, T. J., 2001. Multiple resolution analysis of L-band brightness temperature for soil moisture. *IEEE Trans. Geosci. Remote Sens.*, **39**(1): 151-164.

Jackson, T. J. and Cosh, M. H. (2003). SMEX02 watershed soil moisture data, Walnut Creek, Iowa. Digital Media. [Available online at http://nsidc.org/data/nsidc-0143.html.], National Snow and Ice Data Center, Boulder, Colorado.

Jackson, T. J., Chen, D., Cosh, M., Li, F., Anderson, M., Walthall, C., Doriaswamy, P. and Hunt, E. R., 2004. Vegetation water content mapping using Landsat data derived normalized difference water index for corn and soybeans. *Remote Sens. Environ.*, **92**(4): 475-482.

Jackson, T. J., Bindlish, R., Gasiewski, A. J., Stankov, B., Klein, M. A., Njoku, E. G., Bosch, D. A., Coleman, T. L., Laymon, C. A. and Starks, P. A., 2005. Polarimetric scanning radiometer C- and X-band microwave observations during SMEX03. *IEEE Trans. Geosci. Remote Sens.*, **43**(11): 2418-2430.

Jackson, T. J., Moran, M. S. and O'Neill, P. E., 2008. Introduction to Soil Moisture Experiments 2004 (SMEX04) special issue. *Remote Sens. Environ.*, **112**(2): 301-303.

Jacobs, J. M., Mohanty, B. P., Hsu, E.-C. and Miller, D., 2004. SMEX02: Field scale variability, time stability and similarity of soil moisture. *Remote Sens. Environ.*, **92**(4): 436-446.

Jawson, S. D. and Niemann, J. D., 2007. Spatial patterns from EOF analysis of soil moisture at a large scale and their dependence on soil, land-use, and topographic properties. *Adv. Water. Resour.*, **30**(3): 366-381.

Jin, X., Wang, S. and Zhou, Y., 2008. Microbial CO2 production from surface and subsurface soil as affected by temperature, moisture, and nitrogen fertilisation. *Australian Journal of Soil Research*, **46**(3): 273-280.

Kachanoski, R. G. and de Jong, E., 1988. Scale dependence and the temporal persistence of spatial patterns of soil water storage. *Water Resour. Res.*, **24**: 85-91.

Kerr, Y. and Njoku, E. G., 1993. On the use of passive microwaves at 37 GHz in remote sensing of vegetation. *Int. J. Rem. Sens.*, **14**: 1931-1943.

Kerr, Y., Font, J., Waldteufel, P., Camps, A., Bará, J., Corbella, I., Torres, F., Duffo, N., Vallossera, M. and Caudal, G., 2000. Next generation radiometers: SMOS a dual pol L-band 2D aperture synthesis radiometer. *In: Proc. of 2000 IEEE Aerospace Conference*, Big Sky, MT.

Kerr, Y. H., Waldteufel, P., Wigneron, J. P., Martinuzzi, J. M., Font, J. and Berger, M., 2001. Soil moisture retrieval from space: The Soil Moisture and Ocean Salinity (SMOS) mission. *IEEE Trans. Geosci. Remote Sens.*, **39**(8): 1729-1735.

Kim, G. and Barros, A. P., 2002a. Space-time characterization of soil moisture from passive microwave remotely sensed imagery and ancillary data. *Remote Sens. Environ.*, **81**(2-3): 393-403.

Kim, G. and Barros, A. P., 2002b. Downscaling of remotely sensed soil moisture with a modified fractal interpolation method using contraction mapping and ancillary data. *Remote Sens. Environ.*, **83**(3): 400-413.

Kirdiashev, K. P., Chukhlantsev, A. A. and Shutko, A. M., 1979. Microwave radiation of the earth's surface in the presence of vegetation cover. *Radio Eng. Electron. Engl. Transl.*, **24**: 256-264.

Kong, J. A., 1990. *Electromagnetic Wave Theory, 2nd*. Wiley-Interscience, New York.

Koster, R. D., Suarez, M. J., Ducharne, A., Stieglitz, M. and Jumar, P., 2000. A catchment-based approach to modeling land surface processes in a general circulation model 1. Model structure. *J. Geophys. Res.*, **105**(D20): 24,809-24,822.

Koster, R. D. and Suarez, M. J., 2003a. Impact of land surface initialization on seasonal precipitation and temperature prediction. *J. Hydromet.*, **4**(408-423).

Koster, R. D., Suarez, M. J., Higgins, R. W. and Van den Dool, H. M., 2003b. Observational evidence that soil moisture variations affect precipitation *Geophys. Res. letters*, **30**(5).

Lakshmi, V., Wood, E. F. and Choudhury, B. J., 1997. Investigation of effect of heterogeneities in vegetation and rainfall on simulated SSM/I brightness temperatures. *Int. J. Rem. Sens.*, **18**(13): 2763 - 2784.

Lakshmi, V., Bolten, J. and Narayan, U., 2004. Microwave remote sensing: a perspective from the last few field experiments. *In: Proc. of IEEE International Geoscience and Remote Sensing Symposium 2004 (IGARSS'04)*, 332-335.

Lanza, L. G., Schultz, G. A. and Barrett, E. C., 1997. Remote sensing in hydrology: Some downscaling and uncertainty issues. *Phys. Chem. Earth*, **22**(3-4): 215-219.

Le Vine, D. M., 1999. Synthetic aperture radiometer systems. *IEEE Transactions on Microwave Theory and Techniques*, **47**(12): 2228-2236.

Li, H., Robock, A. and Wild, M., 2007. Evaluation of Intergovernmental Panel on Climate Change Fourth Assessment soil moisture simulations for the second half of the twentieth century *J. Geophys. Res.-Atmospheres*, **112**(D6): 15.

Lillesand, T. M. and Kiefer, R. W., 1994. *Remote sensing and image interpretation 3rd ed.* John Wiley and Sons, New York, 750pp.

Liou, Y. A., Kim, E. J. and England, A. W., 1998. Radiobrightness of prairie soil and grassland during dry-down simulations. *Radio Science*, **33**(2): 259-265.

Loew, A., 2008. Impact of surface heterogeneity on surface soil moisture retrievals from passive microwave data at the regional scale: The Upper Danube case. *Remote Sens. Environ.*, **112**(1): 231-248.

Masson, V., Champeau, J.-L., Chauvin, F., Meriguet, C. and Lacaze, R., 2003. A global data base of land surface parameters at 1 km resolution in meteorological and climate models. *J. Climate*, **16**: 1261-1282.

Matheron, G., 1963. Principles of Geostatistics. *Econ. Geol.*, **58**: 1246-1266.

Matzler, C., 1998. Microwave permittivity of dry sand. *IEEE Trans. Geosci. Remote Sens.*, **36**(1): 317-319.

Mätzler, C., Rosenkranz, P. W., Battaglia, A. and Wigneron, J.-P., 2006. *Thermal Microwave Radiation — Applications for Remote Sensing*. IET Electromagnetic Waves Series 52, London, UK, 555pp.

McCabe, M. F., Wood, E. F. and Gao, H., 2004. Evaluation of AMSR-E-derived soil moisture retrievals using ground-based and PSR airborne data during SMEX02. *J. Hydromet.*, **6**(6): 864-877.

McCabe, M. F., Wood, E. F. and Gao, H., 2005. Initial soil moisture retrievals from AMSR-E: Multiscale comparison using in situ data and rainfall patterns over Iowa. *Geophys. Res. Letters*, **32** (L06403).

McMullan, K. D., Brown, M. A., Martin-Neira, M., Rits, W., Ekholm, S., Marti, J. and Lemanczyk, J., 2008. SMOS: The payload. *IEEE Trans. Geosci. Rem. Sens.*, **46**(3): 594-605.

McVicar, T. R. and Jupp, D. L. B., 1998. The current and potential operational uses of remote sensing to aid decisions on drought exceptional circumstances in australia: A review. *Agricultural Systems*, **57**(3): 399-468.

Merlin, O., Walker, J., Panciera, R., Young, R., Kalma, J. and Kim, E., 2007. Soil moisture measurement in heterogeneous terrain. *In: Proc. of International Congress on Modelling and Simulation (MODSIM)*, Christchurch, New Zealand.

Merlin, O., Walker, J. P., Kalma, J. D., Kim, E. J., Hacker, J., Panciera, R., Young, R., Summerell, G., Hornbuckle, J., Hafeez, M. and Jackson, T., 2008. The NAFE'06 data set: towards soil moisture retrieval at intermediate resolution. *Adv. Water. Resour.*, **31**(11): 1444-1455.

Mitra, D. S. and Majumdar, T. J., 2004. Thermal inertia mapping over the Brahmaputra basin, India using NOAA-AVHRR data and its possible geological applications. *Int. J. Rem. Sens.*, **25**(16): 3245-3260.

Mo, T., Choudhury, B. J., Schmugge, T. J., Wang, J. R. and Jacskon, T. J., 1982. A model for the microwave emission of vegetation-covered fields. *J. Geophys. Res.*, **87**(11): 229-237.

Mo, T. and Schmugge, T. J., 1987 A parameterization of the effect of surface roughness on microwave emission. *IEEE Trans. Geosci. Remote Sens.*, **25**(47−54).

Mohanty, B. P., Famiglietti, J. S. and Skaggs, T. H., 2000a. Evolution of soil moisture spatial structure in a mixed vegetation pixel during the Southern Great Plains 1997 (SGP97) Hydrology Experiment. *Water. Resour. Res.*, **36**(12): 3675-3686.

Mohanty, B. P., Skaggs, T. H. and Famiglietti, J. S., 2000b. Analysis and mapping of field-scale soil moisture variability using high-resolution, ground-based data during the Southern Great Plains 1997 (SGP97) Hydrology Experiment. *Water. Resour. Res.*, **36**(4): 1023-1031.

Mohanty, B. P. and Skaggs, T. H., 2001. Spatio-temporal evolution and time-stable characteristics of soil moisture within remote sensing footprints with varying soil, slope, and vegetation. *Adv. Water Resour.*, **24**(9-10): 1051-1067.

Moran, M. S., Clarke, T. R., Inoue, Y. and Vidal, A., 1994. Estimating crop water-deficit using the relation between surface-air temperature and spectral vegetation index. *Remote Sens. Environ.*, **49**(3): 246-263.

Narayan, U. and Lakshmi, V., 2008. Characterizing subpixel variability of low resolution radiometer derived soil moisture using high resolution radar data. *Water Resour. Res.*, **44**(6).

NASA (2007). Soil Moisture Active/Passive (SMAP) mission. Workshop Report. Arlington, Virginia., National Areonautic and Space Administration.

Newton, R. W. and Rouse, J. W., 1980. Microwave radiometer measurements of soil moisture content. *IEEE Transactions on Antennas Propogation*, **AP-28**(5): 680-686.

Njoku, E. G. and Entekhabi, D., 1996a. Passive microwave remote sensing of soil moisture. *J. Hydrol.*, **184**(1-2): 101-129.

Njoku, E. G., Hook, S. J. and Chehbouni, A., 1996b. Effects of surface heterogeneity on thermal remote sensing of land parameters. In: E. T. E. J. B. Stewart, R. A. Feddes, and Y. Kerr (Eds), *Scaling Up in Hydrology Using Remote Sensing*, Wiley, New York, 19-39.

Njoku, E. G. and Li, L., 1999. Retrieval of land surface parameters using passive microwave measurements at 6–18 GHz *IEEE Trans. Geosci. Remote Sens.*, **37**: 79–93.

Njoku, E. G., Wilson, W. J., Yueh, S. H., Dinardo, S. J., Li, F. K., Jackson, T. J., Lakshmi, V. and Bolten, J., 2002. Observations of soil moisture using a passive and active low-frequency microwave airborne sensor during SGP99. *IEEE Trans. Geosci. Remote Sens.*, **40**(12): 2659-2673.

Njoku, E. G., Jackson, T. J., Lakshmi, V., Chan, T. K. and Nghiem, S. V., 2003. Soil moisture retrieval from AMSR-E. *IEEE Trans. Geosci. Remote Sens.*, **41**(2): 215-229.

O'Loughlin, E. M., 1981. Saturation regions in catchment and their relations to soil and topographic properties. *J. Hydrol.*, **53**: 229-246.

O'Neill, P. E., Chauhan, N. and Jackson, T. J., 1996. Use of active and passive microwave remote sensing for soil moisture estimation through corn. *Int. J. Rem. Sens.*, **17**: 1851-1865.

Oh, Y., Sarabandi, K. and Ulaby, F. T., 1992. An empirical model and an inversion technique for radar scattering from bare soil surfaces. *IEEE. Trans. Geosci. Rem. Sens.*, **30**(2): 370-381.

Ottlé, C., Vidal-Madjar, D. and Girard, G., 1989. Remote sensing applications to hydrological modeling. *J. Hydrol.*, **105**: 369-384.

Owe, M., De Jeu, R. and Walker, J., 2001. A methodology for surface soil moisture and vegetation optical depth retrieval using the microwave polarization difference index. *IEEE Trans. Geosci. Remote Sens.*, **39**(8): 1643-1654.

Owe, M., De Jeu, R. and Holmes, T., 2007. Multi-sensor historical climatology of satellite-derived global land surface moisture. *J. Geophys. Res.*, **113**(F01002).

Panciera, R., Walker, J. P., Kalma, J. D., Kim, E. J., Hacker, J., Merlin, O., Berger, M. and Skou, N., 2008a. The NAFE'05/CoSMOS data set: Towards SMOS soil moisture retrieval, downscaling and assimilation. *IEEE Trans. Geosci. Rem. Sens.*, **46**(3): 736-745.

Panciera, R., Walker, J. P., Kalma, J. D., Kim, E. J., Saleh, K. and Wigneron, J. P., 2008b. Evaluation of the SMOS L-MEB passive microwave soil moisture retrieval algorithm. *Remote Sens. Environ.*, **113**(2): 435-444.

Pellarin, T., Wigneron, J.-P., Calvet, J.-C., Ferrazzoli, P., Douville, H., Lopez-Baeza, E. and al., e., 2003. Two-year global simulation of L-band brightness temperatures over land. *IEEE Trans. Geosci. Rem. Sens.*, **41**(9): 2135−2139.

Porporato, A., D'Odorico, P., Laio, F. and Rodriguez-Iturbe, I., 2003. Hydrologic controls on soil carbon and nitrogen cycles. I. Modeling scheme. *Adv. Water. Resour.*, **26**(1): 45-58.

Prigent, C., Aires, F., Rossow, W. B. and Robock, A., 2005. Sensitivity of satellite microwave and infrared observations to soil moisture at a global scale: Relationship of satellite observations to in situ soil moisture measurements *J. Geophys. Res.*, **110**(D07110).

Rahman, M. M., Moran, M. S., Thoma, D. P., Bryant, R., Holifield, C. C., Jackson, T. J., Orr, B. J. and Tischler, M., 2008. Mapping surface roughness and soil moisture using multi-angle radar imagery without ancillary data. *Remote Sens. Environ.*, **112**: 391-402.

Rodriguez-Iturbe, I., Vogel, G. K., Rigon, R., Entekhabi, D., CAstelli, F. and Rinaldo, A., 1995. On the spatial organization of soil moisture fields. *Geophys. Res. Letters*, **22**(20): 2757-2760.

Rouse, J. W., Haas, R. H., Schell, J. A. and Deering, D. W., 1973. Monitoring vegetation systems in the Great Plains with ERTS. In: E. P. M. S. C. Freden, & M. Becker (Eds.) (Eds), *Third Earth Resources Technology Satellite-1 Symposium. Technical presentations, section A.*, National Aeronautics and Space Administration (NASA SP-351). Washington, DC, 309–317.

Rudiger, C., Calvet, J.-C., Gruhier, C., Holmes, T., De Jeu, R. and Wagner, W., 2007. An intercomparison of ERS-Scat and AMSR-E soil moisture observations with model simulations over France. *J. Hydromet.*, **10**(2).

Rüdiger, C., Hancock, G., Hemakumara, H. M., Jacobs, B., Kalma, J. D., Martinez, C., Thyer, M., Walker, J. P., Wells, T. and Willgoose, G. R., 2007. Goulburn river experimental catchment data set. *Water Resour. Res.*, **43**(W10403).

Rüdiger, C., Western, A. W., Walker, J. P., Smith, A. B., Kalma, J. D. and Willgoose, G. R., 2009. Towards a general equation for frequency domain reflectometers. *J. Hydrol.*: Submitted.

Ryu, D., Jackson, T. J., Bindlish, R. and Le Vine, D. M., 2007. L-band microwave observations over land surface using a two-dimensional synthetic aperture radiometer. *Geophys. Res. Letters*, **34**(L14401).

Sadeghi, A. M., Hancock, G. D., Waite, W. P., Scott, H. D. and Rand, J. A., 1984. Microwave measurements of moisture distributions in the upper soil profile. *Water Resour. Res.*, **20**(7): 927-934.

Saha, S. K., 1995. Assesment of regional soil moisture conditions by coupling satellite sensor data with a soil-plant system heat and moisture balance model. *Int. J. Rem. Sens.*, **16**(5): 973-980.

Saleh, K., Wigneron, J. P., Calvet, J. C., Lopez-Baeza, E., Ferrazzoli, P., Berger, M., Wursteisen, P., Simmonds, L. and Miller, J., 2004. The EuroSTARRS airborne campaign in support of the SMOS mission: first results over land surfaces. *Int. J. Rem. Sens.*, **25**(1): 177-194.

Saleh, K., Wigneron, J.-P., de Rosnay, P., Calvet, J.-C., Escorihuela, M. J., Kerr, Y. and Waldteufel, P., 2006a. Impact of rain interception by vegetation and mulch on the L-band emission of natural grass. *Remote Sens. Environ.*, **101**(1): 127-139.

Saleh, K., Wigneron, J.-P., de Rosnay, P., Calvet, J.-C. and Kerr, Y., 2006b. Semi-empirical regressions at L-band applied to surface soil moisture retrievals over grass. *Remote Sens. Environ.*, **101**(3): 415-426.

Saleh, K., Wigneron, J. P., Waldteufel, P., de Rosnay, P., Schwank, M., Calvet, J. C. and Kerr, Y. H., 2007. Estimates of surface soil moisture under grass covers using L-band radiometry. *Remote Sens. Environ.*, **109**(1): 42-53.

Saleh, K., Kerr, Y. H., Richaume, P., Escorihuela, M. J., Panciera, R., Delwart, S., Boulet, G., Maisongrande, P., Walker, J. P., Wursteisen, P. and Wigneron, J. P., 2009. Soil moisture retrievals at L-band using a two-step inversion approach (COSMOS/NAFE'05 Experiment). *Remote Sens. Environ.*, **113**(6): 1304-1312.

Sano, E. E., Huete, A. R., Troufleau, D., Moran, M. S. and Vidal, A., 1998. Relation between ERS-1 synthetic aperture radar data and measurements of surface roughness and moisture content of rocky soils in a semiarid rangeland. *Water Resour. Res.*, **34**(6): 1491-1498.

Schmugge, T., 1985. Chapter 5: Remote Sensing of Soil Moisture. In: M. G. Anderson and T. P. Burt (Eds), *Hydrological Forecasting*, John Wiley and Sons, New York, 101-124.

Schmugge, T. J., Jackson, T. J. and McKim, H. L., 1980. Survey of methods for soil moisture determination. *Water Resour. Res.*, **16**(6): 961-979.

Schmugge, T. J., Wang, J. R. and Asrar, G., 1988. Results from the push broom microwave radiometer flights over the Konza Prairie in 1985. *IEEE Trans. Geosci. Remote Sens.*, **26**: 590−597.

Schmugge, T. J., Jackson, T. J., Kustas, W. P. and Wang, J. R., 1992. Passive microwave remote sensing of soil moisture: results from HAPEX, FIFE, and MONSOON'90. *ISPRS J. Photogramm. Remote Sens*, **47**: 127–143.

Schmugge, T. J., Kustas, W. P., Ritchie, J. C., Jackson, T. J. and Rango, A., 2002. Remote sensing in hydrology. *Adv. Water. Resour.*, **25**(8-12): 1367-1385.

Schmulluis, C. and Furrer, R., 1992. Frequency dependence of radar backscattering under different moisture conditions of vegetation-covered soils. *Int. J. Rem. Sens.*, **13**(12): 2233-2245.

Shi, J., Wang, J., Hsu, A. Y., O'Neill, P. E. and Engman, E. T., 1997. Estimation of bare surface soil moisture and surface roughness parameter using L-band SAR image data. *IEEE. Trans. Geosci. Rem. Sens.*, **35**(5): 1254-1266.

Shi, J., Chen, K. S., Qin, L., Jackson, T. J., O'Neill, P. E. and Leung, T., 2002. A parameterized surface reflectivity model and estimation of bare-surface soil moisture with L-band radiometer. *IEEE Trans. Geosci. Remote Sens.*, **40**(12): 2674-2686.

Shinoda, M. and Yamaguchi, Y., 2003. Influence of soil moisture anomaly on temperature in the Sahel: A comparison between wet and dry decades. *J. Hydromet.*, **4**: 437-447.

Sridhar, V., Hubbard, K. G., You, J. and Hunt, E. D., 2008. Development of the soil moisture index to quantify agricultural drought in Severity-area-duration assessment. *J. Hydromet.*, **9**(4): 660-676.

Stiles, J. M., Sarabandi, K. and Ulaby, F. T., 2000. Electromagnetic scattering from grassland—Part II: Measurement and modeling results. *IEEE Trans. Geosci. Remote Sens.*, **38**(1): 349-356.

Su, Z., Troch, P. A., de Troch, F. P., Nochtergale, L. and Cosyn, B., 1995. Preliminary results of soil moisture retrieval from ESAR (EMAC 94) and ERS-1/SAR, Part II: Soil moisture retrieval. *In: Proc. of Second workshop on hydrological and microwave scattering modelling for spatial and temporal soil moisture mapping from ERS-1 and JERS-1 SAR data and macroscale hydrologic modeling (EV5V-CT94-0446)*, Institute National de la Recherche Agronomique, Unité de Science du Sol et de Bioclimatologie, France.

Teuling, A. J. and Troch, P. A., 2004. Improved understanding of soil moisture variability dynamics. *Geophys. Res. Letters*, **32**(5): .

Troch, P. A., Vandersteene, F., Su, Z., Hoeben, R. and Wuethrich, M., 1996. Estimating microwave observation depth in bare soil through multi-frequency scatterometry. *In: Proc. of First EMSL User Workshop, SAI, JRC*, Ispra, Italy.

Turcu, V. E., Jones, S. B. and Or, D., 2005. Continuous soil carbon dioxide and oxygen measurements and estimation of gradient-based gaseous flux. *Vadose Zone J.*, **4**(4): 1161-1169.

Uitdewilligen, D. C. A., Kustas, W. P. and van Oevelen, P. J., 2003. Estimating surface soil moisture with the scanning low frequency microwave radiometer (SLFMR) during the Southern Great Plains 1997 (SGP97) hydrology experiment. *Physics and Chemistry of the Earth, Parts A/B/C*, **28**(1-3): 41-51.

Ulaby, F. T., Batliva, P. P. and Dobson, M. C., 1978. Microwave backscatter dependence on surface roughness soil moisture and soil texture; Part 1 - bare soil. *IEEE. Trans. Geosci. Elec.*, **GE-16**(4): 286-295.

Ulaby, F. T., Aslam, A. and Dobson, M. C., 1982. Effects of vegetation cover on the radar sensitivity to soil moisture. *IEEE. Trans. Geosci. Rem. Sens.*, **20**(4): 476– 481.

Ulaby, F. T., Moore, R. K. and Fung, A. K., 1986. *Microwave remote sensing: Active and passive. From theory to application, vol III*. Artech House, Dedham, MA.

Vachaud, G., Passerat De Silans, A., Balabanis, P. and Vauclin, M., 1985. Temporal stability of spatially measured soil water probability density function. *Soil Sci. Soc. Am. J.*, **49**: 822–828.

Van de Griend, A. A. and Engman, E. T., 1985. Partial Area Hydrology and Remote Sensing. *J. Hydrol.*, **81**: 211-251.

Van de Griend, A. A. and Owe, M., 1994. The influence of polarization on canopy transmission properties at 6.6 GHz and implications for large scale soil moisture monitoring in semi-arid environments. *IEEE Trans. Geosci. Remote Sens.*, **32**: 409–415

Van de Griend, A. A., Wigneron, J. P. and Waldteufel, P., 2003. Consequences of surface heterogeneity for parameter retrieval from 1.4-GHz multiangle SMOS observations. *IEEE Trans. Geosci. Remote Sens.*, **41**(4): 803.

Van de Griend, A. A. and Wigneron, J. P., 2004. The b-factor as a function of frequency and canopy type at H-polarization. *IEEE Trans. Geosci. Remote Sens.*, **42**(4): 786-794.

van Zyl, J. J., Chapman, B. D., Dubois, P. and Shi, J., 1993. The effect of topography on SAR calibration. *IEEE. Trans. Geosci. Rem. Sens.*, **31**(5): 1036-1043.

Vergely, J.-L. (2005). Soil moisture Retrieval Study,ACRI-ST, Sophia Antipolis, Final Report SMOS-FR-ACR-SA-007.

Verstraeten, W. W., Veroustraete, F., van der Sande, C. J., Grootaers, I. and Feyen, J., 2006. Soil moisture retrieval using thermal inertia, determined with visible and thermal spaceborne data, validated for European forests. *Remote Sens. Environ.*, **101**(3): 299.

Vijaya Kumar, P., Ramakrishna, Y. S., Bhaskara Rao, D. V., Sridhar, G., Srinivasa Rao, G. and Rao, G. N., 2005. Use of remote sensing for drought stress monitoring, yield prediction and varietal evaluation in castor beans (Ricinus communis L.). *Int. J. Rem. Sens.*, **26**(24): 5525-5534.

Vinnikov, K., Robock, A., Speranskaya, N. and Schlosser, A., 1996. Scales of temporal and spatial variability of midlatitude soil moisture *J. Geophys. Res.-Atmosphere*, **101**(D3): 7163-7174.

Wagner, W., Scipal K, Pathe C, Gerten D, Lucht W and B, R., 2003. Evaluation of the agreement between the first global remotely sensed soil moisture data with model and precipitation data. *JGR Atmos*, **108**(D19:4611).

Wagner, W., Bloschl, G., P., P., Calvet, J. C., Bizzarri, B., Wigneron, J. P. and Kerr, Y., 2006. Operational readiness of microwave remote sensing of soil moisture for hydrologic applications. *Nordic Hydrology*, **38**(1): 1-20.

Wagner, W., Naeimi, V., Scipal, K., de Jeu, R. and Martínez-Fernández, J., 2007. Soil moisture from operational meteorological satellites. *Hydrogeol. J.*, **15**(1): 121-131.

Waldteufel, P., Anterrieu, E., Goutoule, J. M. and Kerr, Y., 2000. Field of view characteristics of a microwave 2-D interferometric antenna, as illustrated by the MIRAS concept. In: P. P. a. S. Paloscia (Eds), *Microwave Radiometry and Remote Sensing of the Earth's Surface and Atmosphere*, Utrecht, The Netherlands, 477–483.

Waldteufel, P., Vergely, J.-L. and Cot, C., 2004. A cardioid model for multi-angular radiometric observations. *IEEE Trans. Geosci. Remote Sens.*, **42**: 1059-1063.

Walker, J. P., Willgoose, G. R. and Kalma, J. D., 2001. One-dimensional soil moisture profile retrieval by assimilation of near-surface measurements: A simplified soil moisture model and field application. *J. Hydromet.*, **2**(4): 356-373.

Wan, Z.-M. and Dozier, J., 1996. A generalized split-windows algorithm for retrieving land surface temperature from space. *IEEE Trans. Geosci. Rem. Sens.*, **34**: 892-905.

Wan, Z.-M. and Li, Z.-L., 1997. A physics-based algorithm for retrieving land surface emissivity and temperature from EOS/MODIS data. *IEEE Trans. Geosci. Rem. Sens.*, **35**: 980-996.

Wan, Z., Wang, P. and Li, X., 2004. Using MODIS land surface temperature and normalized difference vegetation index products for monitoring drought in the southern great plains, USA. *Int. J. Rem. Sens.*, **25**(1): 61-72.

Wang, J. R. and Schmugge, T. J., 1980. An empirical model for the complex dielectric permittivity of soils as a function of water content. *IEEE Trans. Geosci. Remote Sens.*, **GE-18**(4): 288-295.

Wang, J. R. and Choudhury, B. J., 1981. Remote sensing of soil moisture content over bare field at 1.4GHz frequency. *J. Geophys. Res.*, **86**: 5277-5282.

Wang, J. R., 1983. Passive microwave sensing of soil moisture content: The effects of soil bulk density and surface roughness. *Remote Sens. Environ.*, **13**(4): 329-344.

Wang, J. R., O'Neill, P. E., Jackson, T. J. and Engman, E. T., 1983. Multifrequency measurements of the effects of soil moisture, soil texture, and surface roughness. *IEEE Trans. Geosci. Remote Sens.*, **21**: 44-51.

Wang, J. R., Engman, E. T., Mo, T., Schmugge, T. J. and Shiue, J. C., 1987. The effects of soil moisture, surface roughness, and vegetation on L-band emissions and backscatter. *IEEE. Trans. Geosci. Rem. Sens.*, **GE-25**(6): 825-833.

Wang, J. R., Shiue, J. C., Schmugge, T. J. and Engman, E. T., 1990a. The L-band PBMR measurements of soil moisture in FIFE. *IEEE Trans. Geosci. Remote Sens.*, **28**: 906-914.

Wang, J. R., Shiue, J. C., Schmugge, T. J. and Engman, E. T., 1990b. The L-band PBMR measurements of surface soil moisture in FIFE. *IEEE Trans. Geosci. Rem. Sens.*, **28**(5): 906-914.

Western, A. W., Bloschl, G. and Grayson, R. B., 1998. Geostatistical characterisation of soil moisture patterns in the Tarrawarra a catchment. *J. Hydrol.*, **205**(1-2): 20-37.

Western, A. W., Zhou, S. L., Grayson, R. B., McMahon, T. A., Bloschl, G. and Wilson, D. J., 2004. Spatial correlation of soil moisture in small catchments and its relationship to dominant spatial hydrological processes. *J. Hydrol.*, **286**(1-4): 113-134.

Wigneron, J. P., Chanzy, A., Calvet, J. C. and Bruguier, N., 1995. A simple algorithm to retrieve soil moisture and vegetation biomass using passive microwave measurements over crop fields. *Remote Sens. Environ.*, **51**(3): 331.

Wigneron, J. P., Schmugge, T., Chanzy, A., Calvet, J. C. and and Kerr, Y., 1998. Use of passive microwave remote sensing to monitor soil moisture. *Agronomie*, **18**(1): 27-43.

Wigneron, J. P., Waldteufel, P., Chanzy, A., Calvet, J. C. and Kerr, Y., 2000. Two-dimensional microwave interferometer retrieval capabilities over land surfaces (SMOS mission). *Remote Sens. Environ.*, **73**(3): 270-282.

Wigneron, J. P., Laguerre, L. and Kerr, Y. H., 2001. A simple parameterization of the L-band microwave emission from rough agricultural soils. *IEEE Trans. Geosci. Remote Sens.*, **39**(8): 1697-1707.

Wigneron, J. P., Chanzy, A., Calvet, J.-C., Olioso, A. and Kerr, Y., 2002. Modeling approaches to assimilating L-band passive microwave observations over land surfaces. *J. Geophys. Res.*, **107**(D14).

Wigneron, J. P., Calvet, J. C., Pellarin, T., Van de Griend, A. A., Berger, M. and Ferrazzoli, P., 2003. Retrieving near-surface soil moisture from microwave radiometric observations: current status and future plans. *Remote Sens. Environ.*, **85**(4): 489-506.

Wigneron, J. P., Parde, M., Waldteufel, P., Chanzy, A., Kerr, Y., Schmidl, S. and Skou, N., 2004. Characterizing the dependence of vegetation model parameters on crop structure, incidence angle, and polarization at L-band. *IEEE Trans. Geosci. Remote Sens.*, **42**(2): 416-425.

Wigneron, J. P., Kerr, Y., Waldteufel, P., Saleh, K., Escorihuela, M. J., Richaume, P., Ferrazzoli, P., de Rosnay, P., Gurney, R., Calvet, J. C., Grant, J. P., Guglielmetti, M., Hornbuckle, B., Matzler, C., Pellarin, T. and Schwank, M., 2007. L-band Microwave Emission of the Biosphere (L-MEB) model: Description and calibration against experimental data sets over crop fields. *Remote Sens. Environ.*, **107**(4): 639-655.

Wigneron, J. P., Chanzy, A., de Rosnay, P., Rudiger, C. and Calvet, J. C., 2008. Estimating the effective soil temperature at L-band as a function of soil properties. *IEEE Trans. Geosci. Rem. Sens.*, **46**(3): 797-807.

Wood, E. F., Lin, D. S., Mancini, M., Thongs, D., Troch, P. A., Jackson, T. J., Famiglietti, J. S. and Engman, E. T., 1993. Intercomparisons between passive and active microwave remote-sensing, and hydrological modeling for soil-moisture. *Adv. Space Res.*, **13**(5): 167-176.

Yang, H., Shi, J., Li, Z. and Guo, H., 2006. Temporal and spatial soil moisture change pattern detection in an agricultural area using multi-temporal Radarsat ScanSAR data. *Int. J. Rem. Sens.*, **27**(19): 4199-4212.

Yoo, C., Valdes, J. B. and North, G. R., 1998. Evaluation of the impact of rainfall on soil moisture variability. *Adv. Water Resour.*, **21**(375–84).

Yoo, C. and Kim, S., 2004. EOF analysis of surface soil moisture field variability. *Adv. Water Resour.*, **27**(831–42).

Zhan, X., Crow, W. T., Jackson, T. J. and O'Neill, P. E., 2008. Improving spaceborne radiometer soil moisture retrievals with alternative aggregation rules for ancillary parameters in highly heterogeneous vegetated areas. *IEEE Trans. Geosci. Remote Sens.*, **5**(2): 261-265.

Zribi, M., Le Hetarat-Mascle, S., Ottle, C., Kammoun, B. and Guerin, C., 2003. Surface soil moisture estimation from the synergistic use of the (multi-incidence and multi-resolution) active microwave ERS Wind Scatterometer and SAR data. *Remote Sens. Environ.*, **86**(1): 30-41.

Zribi, M., Baghdadi, N., Holah, N. and Fafin, O., 2005. New methodology for soil surface moisture estimation and its application to ENVISAT-ASAR multi-incidence data inversion. *Remote Sens. Environ.*, **96**(3-4): 485-496

Appendix A1:
The NAFE’05 Workplan

empty page

National Airborne Field Experiment 2005

31 Oct – 25 Nov 2005

Jeffrey Walker and Rocco Panciera
University of Melbourne, Australia

Experiment Plan

October 2005

Contents

1 Overview and Objectives

The purpose of this project is to map near-surface soil moisture at a range of resolutions making use of passive microwave airborne and spaceborne remote sensors. The ultimate goal is to be able to provide reliable near-surface soil moisture observations at the paddock scale globally. Specifically, this involves positioning ourselves to capitalise on future remote sensing missions such as ESA's Soil Moisture and Ocean Salinity (SMOS) satellite scheduled for launch in 2007 and NASA's Hydrospheric States (Hydros) scheduled for launch in 2010.

This project is complementary with others around the world, including the series of SGP (Southern Great Plains) and SMEX (Soil Moisture Experiment) campaigns in the United States (http://hydrolab.arsusda.gov) and coSMOS (Campaign for validating the Operation of SMOS) activities in Europe (http://www.esa.int/esaLP/LPsmos.html). Specifically, the coSMOS activities planned for Europe in summer of 2005 have been moved to Australia in cooperation with the NAFE (National Airborne Field Experiment) activities planned for November 2005, as described in this document. NAFE '05 has been made possible through recent infrastructure (LE0453434 and LE0560930) and research (DP0557543) funding from the Australian Research Council. Initial setup and ongoing maintenance of the study catchment was funded by research grants (DP0209724 and DP0556941) from the Australian Research Council and NASA.

1.1 Overview

Internationally there has been a significant decline in the number of gauged basins over recent years, yet the demand for hydrologic prediction is greater than ever, particularly as we enter an era of uncertainty due to global climate change. The potential for reliable hydrologic prediction in ungauged basins exists only through an increasing ability to remotely sense land surface states, fluxes, and parameters that impact on basin prediction. For instance, it is now possible to measure evapotranspiration rates that determine soil moisture and baseflow, near-surface soil moisture content that controls rainfall partitioning into infiltration and runoff, snow water equivalent of the snow pack that determines spring-time runoff, vegetation parameters such as leaf area index and greenness that control evapotranspiration, land surface elevation and canopy height that impact on runoff routing and evapotranspiration, and so on. However, there are still many unanswered questions that need to be addressed, including validation of data products from new sensors, maturing of retrieval algorithms, developing techniques for downscaling, and merging remote sensing data with model predictions through the process of data assimilation.

To answer these important questions it is essential that field campaigns with coordinated satellite, airborne and ground-based data collection be undertaken, giving careful consideration to the diverse data requirements for the range of questions to be addressed. Moreover, it must be recognized that such invaluable data sets do not come without considerable effort and cost. Thus it is increasingly important that scientists collaborate nationally and internationally on the collection and subsequent analysis of such data to share in the burden and reap the benefits of more extensive data sets than are possible on an individual basis. To this end two month-long National Airborne Field Experiments (NAFE; see http://www.nafe.unimelb.edu.au) have been planned in consultation with scientists from diverse backgrounds (soil moisture, runoff, evapotranspiration, carbon, forestry, bushfires, water quality, irrigation and salinity) and organizations (several divisions of CSIRO, State Agencies, CRC's, national and international universities, NASA and ESA).

While there is a clear emphasis on soil moisture remote sensing in the two planned NAFE experiments (a primary objective of the research project which provides core funding), the nature of the airborne and supporting data to be collected makes these campaigns applicable to a wide range of environmental remote sensing disciplines and applications.

These coordinated field experiments are open to collaboration from all interested parties. In November 2005 (NAFE ’05) there will be participants from the University of Melbourne, University of Newcastle, Airborne Research Australia, and several European universities and organizations including the European Space Agency (ESA), undertaking research on soil moisture, flood forecasting, carbon budgets and ecohydrology. In November 2006 (NAFE ’06) it is anticipated that participants will undertake research on soil moisture, evapotranspiration, bushfire prediction and precipitation measurement. This document describes in detail the core soil moisture component to the NAFE ‘05 field campaign.

1.2 Objectives

Information on soil moisture may be obtained from three sources. First, ground-based soil moisture profile measurements may be made continuously at individual points. Unfortunately, these are rarely representative of the spatial distribution, and so are unsuitable for mapping of large areas. Second, remote sensing may be used to give measurements of soil moisture in the top few centimetres for areas with low to moderate vegetation cover but do not provide any direct information on root zone soil moisture. Third, land surface models may be used to predict the spatial and temporal variation of soil moisture (near-surface and root zone) but those estimates suffer from inadequate model physics, parameter estimates, and atmospheric forcing data. Clearly these different approaches are complementary, and so one approach has been to utilise all three sources of data, by assimilation of the remotely sensed near-surface soil moisture measurements into a land surface model, and relying on the point measurements for verification. While current progress on this approach has been good, application has been confined to large scale estimates with little appropriate data available for assimilation and/or field verification. **Therefore appropriate observation and verification data needs to be collected to mature this technology.**

Over the past two decades there have been numerous near-surface soil moisture remote sensing studies, using visible, thermal infrared (surface temperature) and microwave (passive and active) electromagnetic radiation. Of these, passive microwave soil moisture measurement has been the most promising technique, due to its all-weather capability, its direct relationship with soil moisture through the soil’s dielectric constant, and a reduced sensitivity to land surface roughness and vegetation cover. Due to the long wavelengths required for soil moisture remote sensing, space-borne passive microwave radiometers (both current and planned) have a coarse spatial resolution, being on the order of 25 to 50km, but have a frequent temporal resolution of 1 to 2 days. While this spatial resolution is appropriate for some broad scale applications, it is not useful for small scale applications such as on-farm water management, flood prediction or meso-scale climate and weather prediction. Thus methods need to be developed for reducing these large scale measurements to a smaller scale. This may ultimately be possible using information from other types of higher resolution sensors (eg. thermal and visible imagery from the MODerate resolution Imaging Spectrometer (MODIS) or LANDSAT Thematic Mapper), but any **downscaling approaches must first be developed and validated with direct high resolution passive microwave measurements and such data must be collected**.

May 2002 saw the launch of NASA’s Advanced Microwave Scanning Radiometer for the Earth observing system (AMSR-E) on the Aqua satellite. This is the first passive microwave sensor in space with appropriate frequencies for measuring near-surface soil moisture content since the Scanning Multi-channel Microwave Radiometer (SMMR) ceased operations in 1987. During the SMMR mission, soil moisture remote sensing was in its infancy, and so there were no dedicated field campaigns for verification of remotely sensed and derived root zone soil moisture. This lack of concurrent data has made evaluation of SMMR-based studies effectively impossible. It is therefore imperative that research programs are designed and undertaken now, in order to fully exploit the potential for retrieving important information on the spatial and temporal variation of soil moisture content from AMSR-E data. The Aqua satellite has an operational design life of 6 years, so there is only a narrow window of opportunity to undertake ground-based research. **Verification of space-borne observations at these coarse resolutions** can only be undertaken using airborne data with a ground resolution fine enough to allow its own accurate verification from ground-based measurements. All airborne soil moisture remote sensing campaigns to date have had spatial resolutions on the order of 1km – an order of magnitude greater than what will be achieved in the NAFE campaigns. Moreover, surface rock covers a large proportion of the Earth's surface and this is not currently considered in retrieval algorithms, leading to a potential underestimation in soil moisture.

In addition there are two dedicated soil moisture missions planned with optimal frequencies for soil moisture measurement. These are the ESA Soil Moisture and Ocean Salinity (SMOS) and NASA Hydrospheric States (HYDROS) sensors to be launched in 2007 and 2010 respectively. These new sensors each will have their own novel approach to soil moisture measurement, requiring algorithms to be developed and results verified using field data. The SMOS sensor will collect data at a range of incidence angles potentially alleviating some of the current assumptions and ancillary data requirements for soil moisture retrieval. Hydros will collect both accurate low resolution passive microwave data together with noisy high resolution active microwave data to produce a 10km soil moisture product. However, both of these missions are planned for 6am/pm overpass times and it is likely that dew will impact on the 6am soil moisture retrievals, but this process is not well understood. Thus it is **important that we prepare now so as to obtain maximum benefit from these dedicated soil moisture sensors when they come online.**

1.3 Ground Requirements

To answer the science questions outlined there are a number of ground data requirements to be considered (Fig. 1):

- long-term observation of soil moisture profiles and associated meteorological data for evaluation of derived root zone soil moisture
- extensive ground-based near-surface soil moisture and temperature data at a range of spatial scales during airborne campaigns for scaling studies, aircraft and satellite verification and algorithm development
- continuous near-surface soil moisture, soil temperature, and thermal infrared point observation for relating air-to-ground measurements throughout the day
- vegetation biomass/water content and dew observation for determining vegetation and dew effects

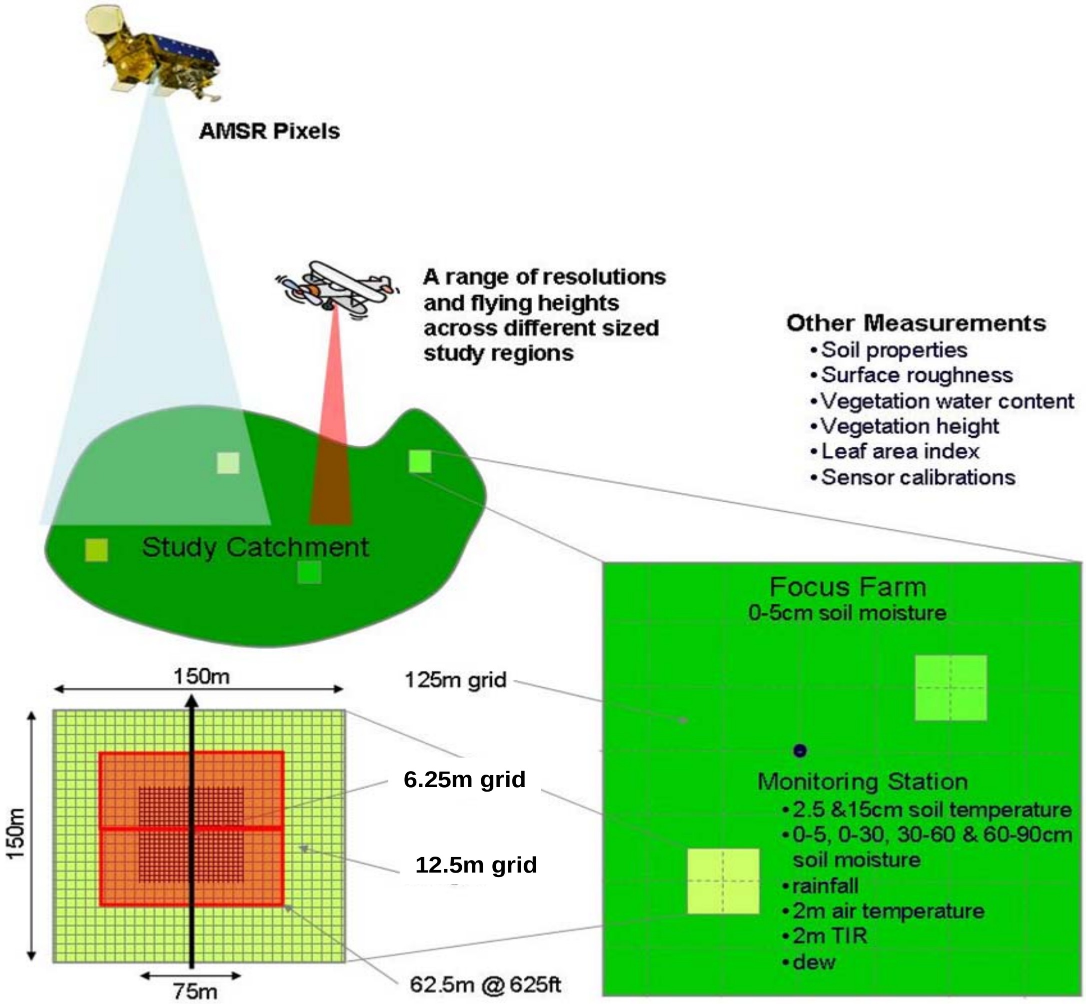

Figure 1. Schematic of the experimental design.

1.4 Air Requirements

To answer the science questions outlined there are also a number of airborne data requirements to be considered (Fig. 1):

- airborne passive microwave, thermal and NDVI data at a range of scales for algorithm development and satellite verification
- airborne lidar data for accurate topography and incidence angle information and vegetation height determination
- digital photography for land use and land cover information
- airborne observations coincident with ground observations and made as early in the morning as possible to ensure that soil and vegetation temperatures are more closely aligned, have a more uniform soil temperature profile, and to coincide more closely with AMSR-E (1:30am/pm) and SMOS/Hydros (6:00am/pm) overpass times
- airborne observations at a range of altitudes (625ft to 10,000ft) to achieve a range of ground resolutions (62.5m to 1,000m for passive microwave and 1m to 20m for thermal and NDVI) for scaling, algorithm development and satellite verification

- airborne observations with passive microwave radiometer in mapping and multi-incidence angle configurations for SMOS and HYDROS algorithm development

1.5 General Approach

The scientific objectives and data requirements of NAFE ’05 as addressed in the previous sections will be met by coordinating an aircraft remote sensing campaign with a ground data collection campaign. Furthermore, all collected data will support measurements taken from various spaceborne remote sensing platforms overpassing the study area. This is expected to provide appropriate and extensive datasets to address the scientific objectives of the project.

The aircraft remote sensing campaign will make use of a small environmental aircraft (see section 3) equipped with passive microwave, infrared and visible sensors to map the whole study area. The characteristics of such sensors in terms of spectral range, incidence angle and field of view are comparable with those onboard various existing and future satellite remote sensing missions. This will allow comparability between spaceborne and airborne measurements and therefore will ensure applicability of the outcomes of NAFE ’05 to future spaceborne missions. In order to address the scaling issues which are crucial to NAFE ’05, it is imperative to collect data at various resolutions and instrument configurations (in terms of incidence angle). This will be made possible by flying the aircraft at different altitudes, resulting in a variety of ground spatial resolutions ranging from satellite-footprint scale down to farm and paddock scale.

Airborne and spaceborne observations will be supported by ground data collected during the one-month long campaign. Ground measurements will include near-surface soil moisture for direct validation of the passive microwave remote sensors observations, as well as ancillary data such as vegetation biomass, land cover information, soil temperature and surface roughness. Ground sampling will be coordinated with aircraft and satellite overpasses times to minimise temporal lag between observations.

The study area of NAFE ’05 is the Goulburn River catchment, a subhumid to temperate area located in south-eastern Australian, approximately 300km north-west of the city of Sydney. A detailed description of the area is given in section 4. The area has been long monitored for hydrological and remote sensing purposes and thus constitutes a very suitable study site, in terms of both scientific requirements and logistical issues. An overview of the NAFE ’05 field campaign area is given in Fig. 2. The main study area includes a large portion of the northern part of the Goulburn Basin, approximately the size of a AMSR-E pixel. (these area will be hereby referred to as “AMSR sampling area” or alternatively “Regional sampling area”). Two focus areas delimited by the Merriwa River and Krui River catchment boundaries have been selected for more detailed analysis.. Within these areas eight farms have been chosen as the object of intensive farm-scale ground and aircraft monitoring (these areas will be hereby referred to as “Farm scale sampling areas”). The extent of mapping achieved by each flight altitude is also shown in the plot. The ground crew will be based in the township of Merriwa, located in the heart of the study area, and will set off from there for the daily sampling. The air crew will be based in Scone, near the airport used for the aircraft operations, approximately 1hour drive from Merriwa.

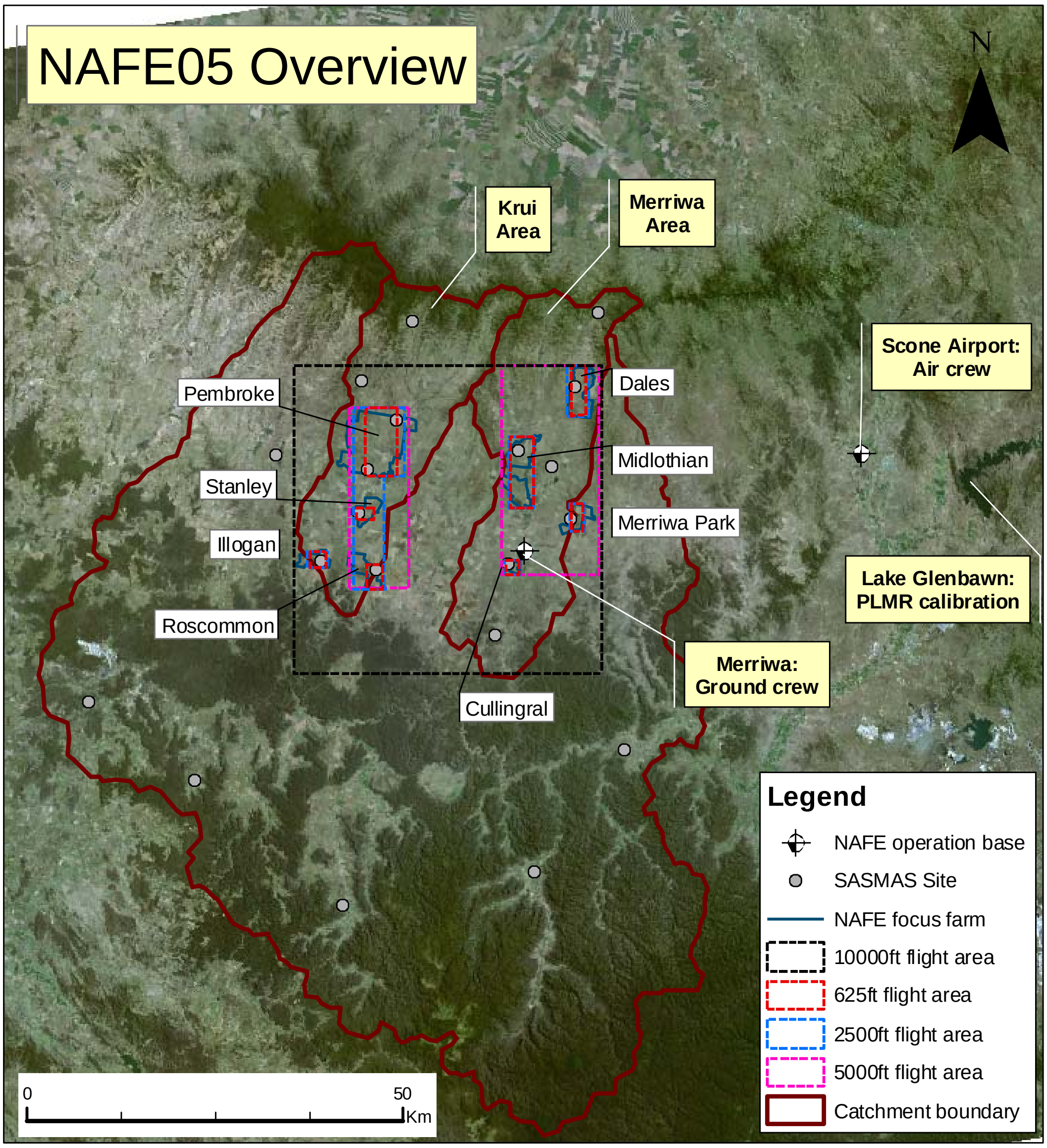

Figure 2. NAFE '05 overview. The map shows the location of the operation bases for the air and ground crews, the main study areas and the extents covered by the mapping from different altitudes. Permanent monitoring stations are also shown. The figure doesn't specifically show the coverage at 10,000ft of the two sub-study area of Krui and Merriwa catchment, being these basically the same as the 5,000ft coverage's for the two areas.

2 Satellite Observing Systems

The following summary of satellite observing systems is limited to those observing systems that provide data of potential relevance to soil moisture remote sensing and scaling. It covers not only a description of the observing systems but also the data collection and availability characteristics.

2.1 Advanced Microwave Scanning Radiometer for EOS (AMSR-E)

AMSR-E on Aqua (http://wwwghcc.msfc.nasa.gov/AMSR) is a multi-frequency dual polarisation microwave radiometer launched in May 2002, with frequencies of 6.925, 10.65, 18.7, 23.8, 36.5 and 89.0 GHz and spatial resolutions of 75, 48, 27, 31, 14 and 6km respectively. The most appropriate frequency for soil moisture measurement is the 6.925GHz or C-band channel, which does not show evidence of radio frequency interference in Australia as it does in the United States. The viewing angle of AMSR is a constant 55°. Aqua is in a 1:30am/pm equator crossing orbit with 1-2 day repeat coverage. Overpasses for the NAFE '05 region are summarized in Table 1. Fig 3. shows an example of global brigthness temperature data provided by AMSR-E

2.2 WindSat

WindSat (http://www.ipo.noaa.gov/Projects/windsat.html) is a multi-frequency polarimetric microwave radiometer with similar frequencies to the AMSR-E, with the addition of full polarisation for 10.7, 18.7 and 37.0 GHz channels and the lack of an 89.0 GHz channel. Developed by the Naval Research Laboratory, it is one of the two primary instruments on the Coriolis satellite launched on 6 January 2003 with an expected life cycle of three years. However, WindSat stopped responding earlier this year and is therefore not considered further in this experimental plan.

2.3 MODerate resolution Imaging Spectroradiometer (MODIS)

Another important instrument carried onboard Aqua is MODIS (http://modis.gsfc.nasa.gov), a passive imaging spectroradiometer with 36 discrete spectral bands between 0.41 (visible) and 14.2 micrometers (thermal infrared). These bands range in resolution from 250m to 1km, and are most useful for land cover and vegetation mapping. Details about MODIS bands are shown in Table 2. This instrument is also carried on the Terra (http://terra.nasa.gov) spacecraft. Aqua has a 1:30am/pm equator crossing time while Terra has a 10:30am/pm equator crossing time, meaning that MODIS data is typically available on a daily basis.

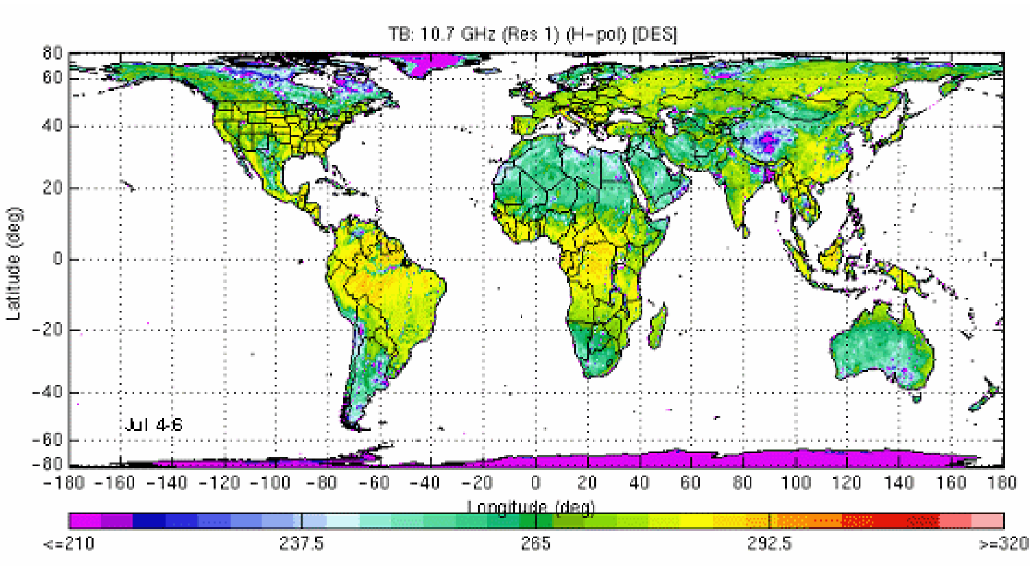

Figure 3. Example of AMSR-E brightness temperature image.at 10.7 GHz frequency, Horizontal polarization.

Table 1. Summary of Aqua overpasses for the Goulburn study area. Highlighted are the dates selected for regional sampling.

AQUA Overpasses			
Day of week	Date	Time of peak elevation (GMT + 10:00)	Peak spacecraft elevation above horizon
Sun	30-Oct-05	14:20:31	41.6
Mon	31-Oct-05	1:21:13	67.1
		13:25:40	46
Tue	1-Nov-05	14:08:20	57.4
Thu	3-Nov-05	13:56:08	79.4
Fri	4-Nov-05	0:56:49	64.7
Sat	5-Nov-05	1:39:36	40.9
		13:43:56	75.6
Sun	6-Nov-05	0:44:37	46.7
		13:31:44	54.3
Tue	8-Nov-05	14:14:23	48.8
Wed	9-Nov-05	1:15:04	79
Thu	10-Nov-05	14:02:11	67.7
Fri	11-Nov-05	1:02:52	76
Sun	13-Nov-05	0:50:41	54.9
Mon	14-Nov-05	1:33:20	48.2
		13:37:48	64.1
Tue	15-Nov-05	14:20:27	41.7
Wed	16-Nov-05	1:21:08	67.2
		13:25:28	46
Thu	17-Nov-05	14:08:15	57.5
Fri	18-Nov-05	1:08:56	87.7
Sat	19-Nov-05	13:56:03	79.4
Sun	20-Nov-05	0:56:44	64.5
Mon	21-Nov-05	1:39:24	41
		13:43:51	75.3
Tue	22-Nov-05	0:44:32	46.6
Wed	23-Nov-05	1:27:12	57
		13:31:31	54.2
Thu	24-Nov-05	14:14:11	48.9
Fri	25-Nov-05	1:14:52	78.9
Sat	26-Nov-05	14:01:59	67.8
Sun	27-Nov-05	1:02:40	75.8
Mon	28-Nov-05	13:49:47	87.4
Tue	29-Nov-05	0:50:28	54.7
Wed	30-Nov-05	1:33:15	48.3
		13:37:35	64

2.4 Advanced Spaceborne Thermal Emission and Reflection Radiometer (ASTER)

ASTER, carried onboard Terra, provides high resolution visible (15m), near infrared (30m) and thermal infrared (90m) data on request, prioritized by project. In general the data coverage occurs on the same day as Landsat 7 for a 60 km swath, but trailing by approximately half an hour. Data for this sensor have bee requested and are awaiting approval.

Table 2. Modis Bands

Primary Use	Band(s)	Wavelength	Pixel Size
Vegetation Index	1	620-670 nm	250 m
Vegetation Index	2	841-876 nm	250 m
	3	459-479 nm	500 m
	4	545-565 nm	500 m
Vegetation H_2O	5	1230-1250 nm	500 m
Vegetation H_2O	6	1628-1652 nm	500 m
	7	2105-2155 nm	500 m
Ocean Color	8 - 16	405-877 nm	1000 m
Atmospheric H_2O	17 -19	890-965 nm	1000 m
Thermal	20 -36	3.660-14.385 :m	1000 m

2.5 Landsat

The Landsat (http://landsat7.usgs.gov/programdesc.html) satellites collect data in the visible (30m), panchromatic (15m), mid infrared (30m) and thermal infrared (60 to 120m) regions of the electromagnetic spectrum. These data have an approximately 15day repeat cycle with a 10:00am equator crossing time. This data is particularly valuable in land cover and vegetation parameter mapping. However, due to an instrument malfunction onboard Landsat 7 in May 2003, it is now only able to provide useful image data within the central ~20km of the swath. As Landsat 5 is still in operation it is being increasingly relied upon. The significance of this is a decrease in spatial resolution of thermal infrared data. The Goulburn River Catchment is located on path 90, row 82 of the descending node of both Landsat 5 and 7. Overpass details for Landat 5 and Landsat 7 are given in Table 3. This data needs to be purchased and is not currently included as part of the budget allocation.

2.6 Soil Moisture and Ocean Salinity (SMOS)

The SMOS (http://www.esa.int/esaLP/ESAMBA2VMOC_LPsmos_0.html) satellite is scheduled for launch in 2007 and seeks to provide 3-day repeat soil moisture at 50km. SMOS is a synthetically generated L-band microwave radiometer instrument yielding a range of incidence angles from 0° to 55° at both V and H polarisations, and a 1000km swath width. This satellite will have a 6:00am/pm equator overpass time. A novel feature of this system is its multi-incidence angle capability, expected to assist in determining ancillary data requirements, including vegetation attenuation, surface roughness, soil texture, surface temperature etc.

2.7 Hydrospheric States (Hydros)

The Hydros (http://hydros.gsfc.nasa.gov/mission) satellite is scheduled for launch in 2010 and seeks to provide 3-day repeat soil moisture at 10km. Hydros has a 40km rotating L-band radiometer with a constant 40° incidence angle at both V and H polarisations, and a 3km L-band radar at VV, VH, HV, and HH polarisations. This satellite will also have a 6:30am/pm equator overpass time. The novel features of this system is i) the combination of active and passive observations to alleviate the ancillary data requirements and ii) the combination of high resolution noisy data with low resolution accurate data to yield a high resolution reliable product.

2.8 Advanced Synthetic Aperture Radar (ASAR)

ASAR provides both continuity to the ERS-1 and ERS-2 mission SARs and next generation capabilities. This C-band SAR is carried on board the Envisat (http://envisat.esa.int) satellite, launched into a sun synchronous orbit in March 2002, also carrying a visible and near infrared imaging system called MERIS. The exact repeat cycle for a specific scene and sensor configuration is 35 days. ASAR can provide a range of incidence angles ranging from 15° to 45° and can operate in alternating polarisation mode, providing two polarisation combinations (VV and HH, HH and HV, or VV and VH). Swath width is nominally 100 km and the product pixel size is 30m. ASAR data for NAFE ’05 have been requested and approved from ESA.

2.9 Advanced Along Track Scanning Radiometer (AATSR)

Also carried onboard Envisat, AATSR main objective is to establish continuity of the ATSR-1 and ATSR-2 data sets of precise sea surface temperature (SST). It makes use of four thermal infrared channels (centred on 1.6 microns, 3.7 microns, 10.7 microns, and 12 microns) for the SST. Additionally, with two visible channels (0.87 microns and 0.67 microns respectively) provides measurements of vegetation at 1 × 1km resolution at nadir. An additional visible channel at 0.55 microns indicates, from chlorophyll content, the growth stage and health of vegetation. AATSR data for NAFE ’05 have been requested and approved from ESA.

2.10 Compact High Resolution Imaging Spectrometer (CHRIS)

CHRIS provides, for the first time, remotely-sensed Multi-View-Angle data at high spatial resolution, and in superspectral/hyperspectral wavelength resolutions. The sensor is onboard ESA’s Project for On-Board Autonomy (Proba) launched on 22 October, 2001. CHRIS has a spectral range of 415-1050 nm, and provides observations at 19 spectral bands simultaneously, with a spatial resolution of 20m at nadir and a swath width of 14km. CHRIS data for NAFE’05 have been requested and proved from ESA.

3 Aircraft Observing System

Airborne measurements will be made using the small, low-cost, two-seater motor glider from

Table 3. Summary of Landsat 5 and Landsat 7 overpasses for the Goulburn study area.

Landsat 5

Day of week	Date	Time (GMT+10:00)
Fri	21-Oct-05	9:30:39
Sun	06-Nov-05	9:36:35
Tue	22-Nov-05	9:36:08
Thu	08-Dec-05	9:36:08

Landsat 7

Day of week	Date	Time (GMT+10:00)
Sut	29-Oct-05	9:25:33
Mon	14-Nov-05	9:37:27
Wed	30-Nov-05	9:30:39
Fri	16-Dec-05	9:36:35

Figure 4. The Diamond ECO-Dimona aircraft with PLMR mounted under the fuselage, and thermal imager, digital camera and NDVI scanner in an underwing pod.

the Airborne Research Australia national facility called Small Environmental Research Aircraft (SERA), shown in Fig. 4, together with the recently acquired Polarimetric L-band Multibeam Radiometer (PLMR; http://www.plmr.unimelb.edu.au) and thermal imager. This new infrastructure will allow for the first time, very high resolution passive microwave (~50m) and land surface skin temperature (~1m) observations to be made across large areas. There is no other capacity world-wide to make such high resolution measurements together with a range of other supporting data including a first-last return lidar, NDVI scanner and 11MegaPixel digital camera. An example of the data to be collected is given in Fig. 5..

The aircraft can carry a typical science payload of up to 120kg with cruising speed of 92-203km/h and range of 4-8hrs or 800-1500km. The aircraft ceiling is 3km or up to 7km with oxygen, under day or night VFR conditions. While the aircraft can take up to 2 crew (pilot/scientist + scientist), for maximum range and/or payload it is only possible to operate with 1 crew.

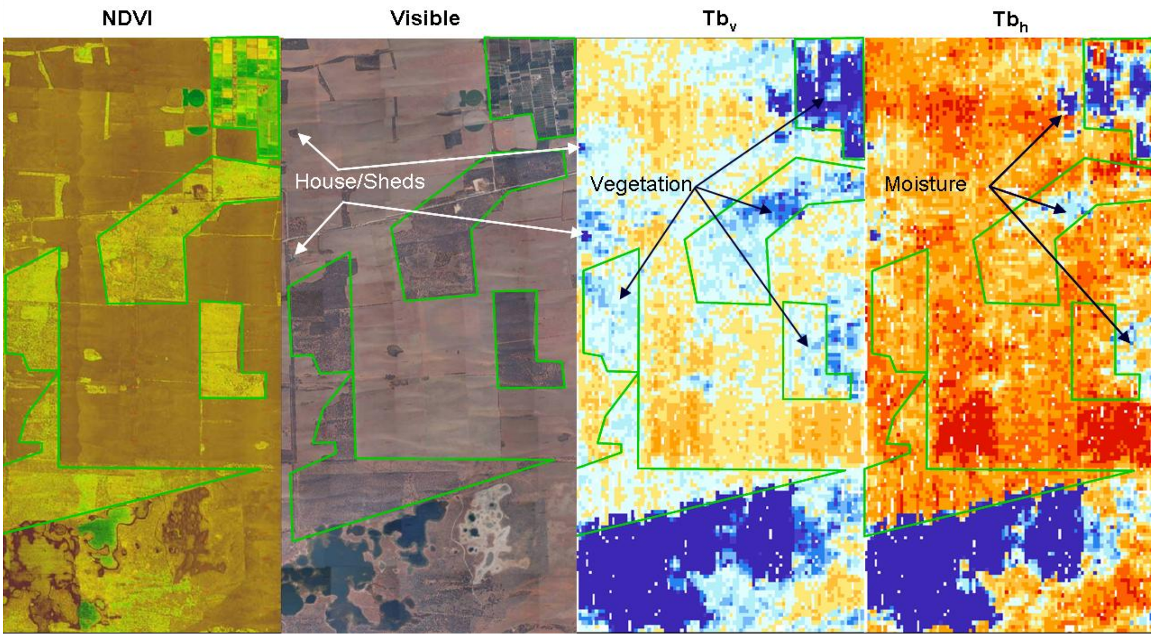

Figure 5. Example of airborne data collected from a trial campaign near Waikerie in South Australia. Note that the vertically (Tb_v) and horizontally (Tb_h) polarized passive microwave data are shown with a different colour scale.

Aircraft instruments are typically installed in one of the certified underwing pods (see Fig. 6) or the underbelly pod. Aircraft navigation for science is undertaken using a cockpit computer display that shows aircraft position relative to planned flight lines using the OziExplorer software. The aircraft has a Trimble TANS 4-way differential GPS system (antennae on each wing and both fore and aft on the fuselage) for position (georeferencing) and attitude (pitch, roll and heading at 0.1° resolution) interpretation. Additionally there is a Rockwell-Collins AHS-85 inertial navigation system yielding the more accurate attitude information required for interpretation of high resolution scanning instruments.

Figure 6. View of one of the underwing pod with the cover off, and view of the cockpit showing cockpit computer display.

Figure 7. View of PLMR with the cover off.

3.1 Polarimetric L-band Multibeam Radiometer

The PLMR (Fig. 7) measures both V and H polarisations using a single receiver with polarisation switch at incidence angles +/–7°, +/–21.5° and +/–38.5° in either across track (pushbroom) or along track configurations. The beamwidth is 17° resulting in an overall 90° field of view. The instrument has a frequency of 1.413GHz and bandwidth of 24MHz, with NEDT and accuracy better than 1K for an integration time of 0.5s and 1K repeatability over 4 hours. It weighs 46kg and has a size of 91.5cm × 91.5cm × 17.25cm.

3.2 Thermal Imager

The thermal imager is a FLIRTS ThermaCam S60 with spectral range 7.5 to 13μm, accuracy +/–2°C or +/–2% of reading and thermal sensitivity of 0.08°C. It has an 80° × 60° FOV lens with 1.3mrad IFOV, resulting in approximately 1m data from a 150m flying height. The thermal imager looks very similar to a digital video camera (Fig. 8), with a weight of 2kg and size of 10cm × 12cm × 22cm.

Figure 8. View of the S60 Thermal Imager.

3.3 Tri-spectral NDVI Scanner

The TSLS AWI/ARA Trispectral line scanner can operate in either of two modes - Visible (Red, Green and Blue) or Vegetation (Green, Red and Near-IR).The sensor offers a resolution of better than 0.5m. This is achieved using high pixel resolution of 2048 pixels per line, and an acquisition frequency of 50 lines per second (stored directly onto a hard disk). The scanner is a compact unit, measuring just 110mm x 110mm x 300mm. It has two lens option; a 28mm lens (45°) and a 50mm lens (24°). The 28mm lens will be used in this experiment to ensure maximum coverage, and flight lines will be planned to have a nominal 1/6th of a swath width overlap.

3.4 Digital Photography

The camera is a Canon EOS-1DS 11MegaPixel digital camera with two lens options; a 24mm lens (74° × 53°) and 50mm lens (40° × 27°). The 24mm lens will be used in this experiment to ensure maximum coverage.

3.5 Airborne Laser Scanner

The airborne laser (near infrared) scanner is a first pulse (vegetation) last pulse (ground) Riegl LMS-Q280i with range of 30m to 1500m, vertical accuracy of 30mm and resolution of 5mm. It has a maximum 60° FOV with 0.02° step width, yielding approximately 1m horizontal resolution when flown from a 150m flying height. The instrument is approximately 56cm × 20cm × 21cm and weighs approximately 20kg (Fig. 9).

Figure 9. View of the Riegl LMS-Q280i airborne laser scanner

4 Catchments

The 6,540km^2 Goulburn River experimental catchment (http://www.sasmas.unimelb.edu.au) is a tributary to the Hunter River in New South Wales, Australia (Fig. 10). This subhumid to temperate catchment extends from 31°46'S to 32°51'S and 149°40'E to 150°36'E, with elevations ranging from 106m in the floodplains to 1257m in the northern and southern mountain ranges. The catchment was chosen for i) its relative large area of predominantly low to moderate vegetation cover in the north of the catchment for satellite soil moisture remote sensing studies; ii) the lack of maritime effects in order to avoid mixed pixel responses from ocean and land data within satellite measurements; and iii) its relative proximity to the University of Newcastle.

Figure 10. Location of Goulburn River catchment.

The Goulburn River runs generally from west to east, with tributaries from the north and south, meaning the catchment is dominated by easterly and westerly aspects. The catchment has two more intensively monitored subcatchments, the Krui River ($562km^2$) and Merriwa River ($651km^2$) in the northern half of the catchment (Fig. 2). Additionally, a densely monitored 175ha micro-catchment is located on a property called "Stanley", located in the lower reach of the Krui River catchment.

4.1 Climate

The general climate within the region can be described as subhumid or temperate, with significant variation in the annual rainfall throughout the catchment. While the average annual rainfall in most of the catchments is approximately 700mm, it varies from 500mm to 1100mm depending on altitude (Fig. 11). Major rainfall events generally occur in October and November with an average precipitation of 50mm, while the monthly average precipitation in July is 40mm. The average annual Class A pan evaporation for the study region is about 1800mm. The minimum monthly pan evaporation is reached in July with an average of 75mm and the maximum can be observed in January reaching 250mm. Monthly mean maximum temperatures reach approximately 30°C in summer and 14°C in winter, with minimum values of 16°C and 2°C, respectively. Except for elevated areas, frost is unlikely to occur during daytime in winter, but night time minimum temperatures in winter are frequently less than 0°C.

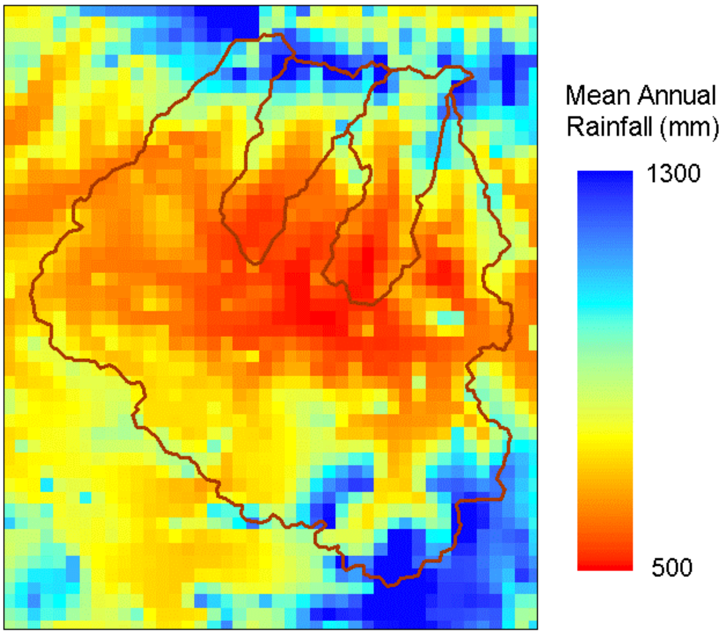

Figure 11 Map of mean annual rainfall for the Goulburn catchment.

4.2 Geology and Soils

The geology of the Goulburn River catchment can be distinguished into two types: the northern which is predominantly Tertiary basalt, a product of Cainozoic volcanism which took place throughout much of eastern Australia, and the southern which is dominated by rocks of the Triassic age laid down as sediments in lagoons and consisting of sandstone, conglomerate and shale. The regions geomorphology is largely dependent on its geological and climatic history with four main types of country identified; the Liverpool Range and Merriwa Plateau in the north and the Central Goulburn Valley and Southern Mountains in the south. The actual study area falls in the northern part of the Goulburn catchment, across the Liverpool Range and Merriwa Plateau. Situated at the northern extent, the Liverpool ranges are characterized by a rugged and basaltic landscape. The area rises over 1200m above sea-level, and localized plateaus exist despite the characteristic rugged topography. The Merriwa Plateau is located south of the Liverpool Range, presenting a rolling and hilly basaltic topography. Its elevation ranges between 450m to the north and 300m to the south.

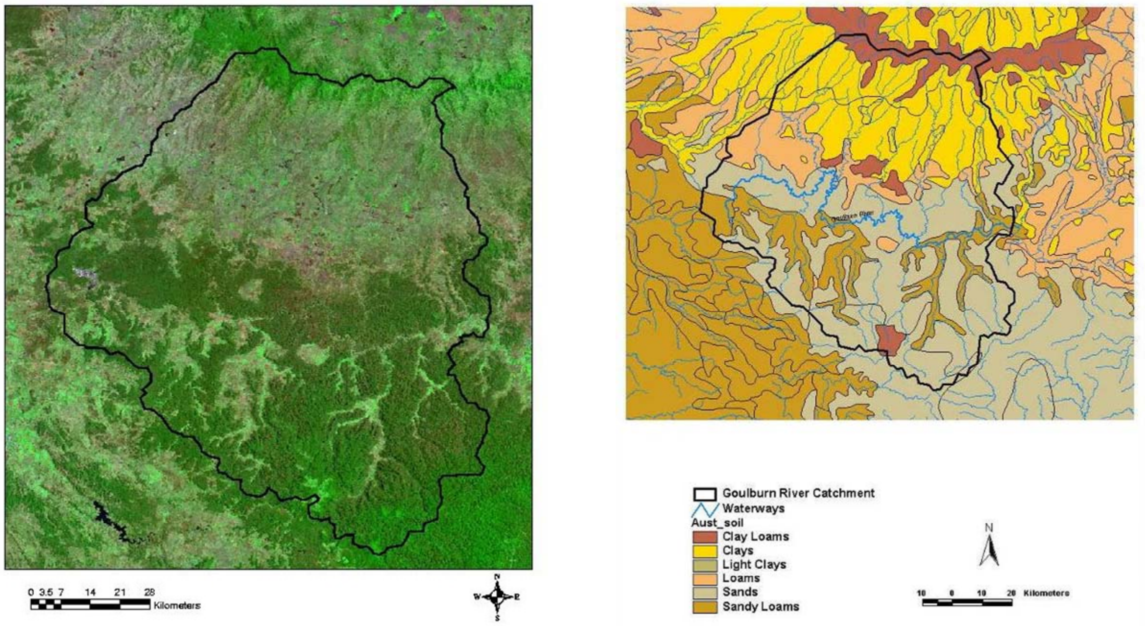

Figure 12. Vegetation (Landsat 5 false colour image) and soil characteristics of the Goulburn study area from the Atlas of Australian Soils.

The NAFE ’05 study area covers mainly the Merriwa Plateau and the southern fringes of the Liverpool Ranges. The northern part of the NAFE ’05 study area is therefore characterized by black basalt derived cracking clays, while the very southern part of the study area is characterized by sandstone derived soils (Fig. 12). Red basalt derived clays are also existent in southern regions of the study area.

4.3 Vegetation

Much of the original vegetation in the northern part of the Goulburn catchment has been cleared, the extent of which has largely been influenced by topography and soil type (Fig. 12). In the north where the terrain is rugged (the Liverpool Range), accessibility is restricted and the area has thus remained highly vegetated. To the south, clearing has been more extensive due to the rolling to hilly terrain ensuring greater accessibility (the Merriwa Plateau). Grazing and cropping activities dominate cleared areas, due to the high fertility of basaltic soils. The sandstone derived soils to the far south are largely uncleared as they are less fertile and productive.

4.4 Monitoring Infrastructure

The Goulburn River experimental catchment has been instrumented since September 2001 and will continue until at least January 2008. There have been several enhancements to the catchment instrumentation since its original installation and several more are planned and/or underway. The catchment monitoring includes surface and root zone soil moisture, soil temperature, meteorological and streamflow measurements.

A total of 26 soil moisture and temperature monitoring sites (Fig. 13) were chosen on the basis of being i) a representative monitoring site, ii) spatial distribution across the experimental catchment, and iii) accessibility. The representative monitoring site objective was addressed by choosing midslope locations with typical vegetation, soil, and aspect, so that they represented catchment average soil moisture locations. The spatial distribution was chosen to give a concentration of measurements in the open cropping and grazing land to the north for application to remote sensing measurements, while achieving a good distribution for model verification within the chosen focus catchments and the broader Goulburn catchment. The automatic weather stations were sited with regard to existing infrastructure and expected spatial variability, resulting in one at the centre of the Goulburn experimental catchment and a second in high terrain to the north of the catchment, supplementing sites to the south, east (Bureau of Meteorology) and west (Ulan Coal Mine). At the same time this resulted in having automatic weather stations located in both the upper and lower reaches of the Krui focus catchment and in the centre of the Stanley microcatchment. Five streamgauges were installed in the two focus catchments, adding to the 4 existing streamgauges operated by the New South Wales Department of Infrastructure, Planning and Natural Resources (DIPNR) allowing the main catchment to be subdivided into smaller modelling units. This included 3 subcatchments in the Krui, 3 subcatchments in the Merriwa, and a further 3 divisions in the Goulburn. Catchment runoff observations are also made at the Stanley microcatchment using a Parshall flume.

Each of the soil moisture sites have up to three vertically inserted Campbell Scientific CS616 water content reflectometers (http://www.campbellsci.com/cs616-l) over depths of 0-300mm, 300-600mm and 600-900mm, respectively (Fig. 14). The number of soil moisture sensors installed was determined by the depth to the bedrock, being less than 900mm in some cases. Sensors were installed by excavation and backfilling. These sensors ensured a continuous observation of the soil moisture profile, with sensors read and the values logged once every 20 minutes.

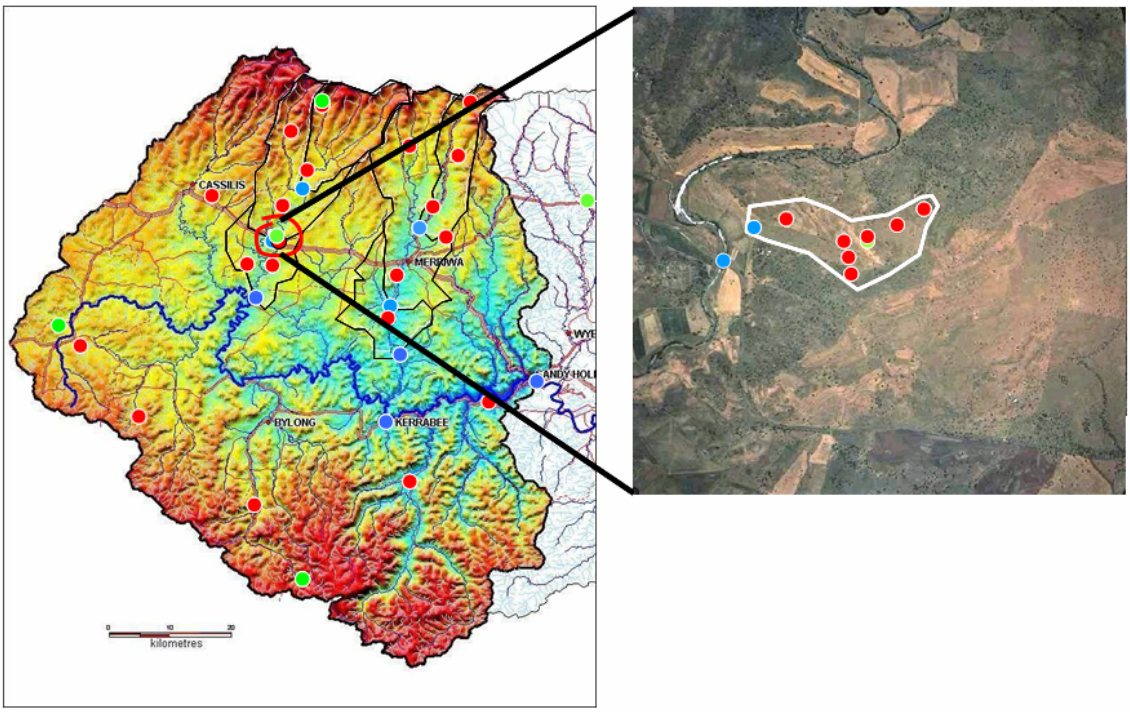

Figure 13. Soil moisture, climate and streamflow monitoring network in the Goulburn iver catchment, overlaying the elevation data. Inset shows the Stanley microcatchment.

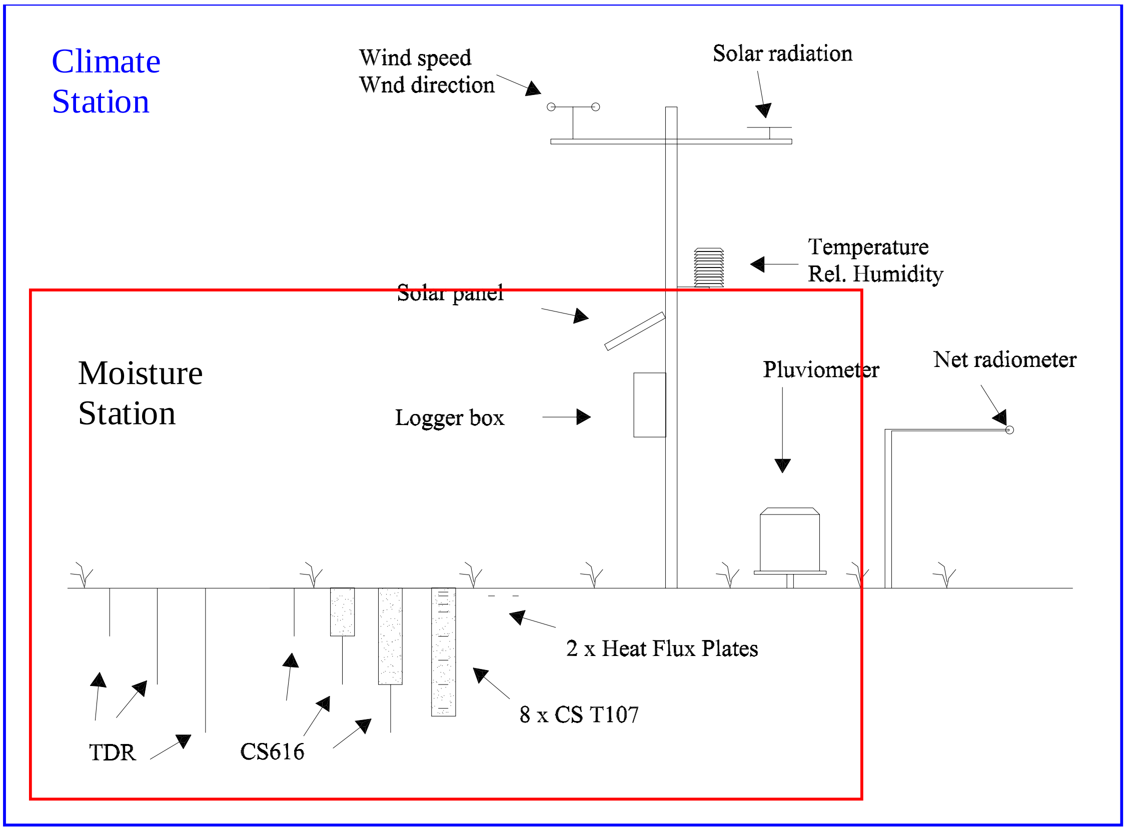

Figure 14. Schematic of monitoring stations.

Sensor response to soil moisture varies with salinity, density, soil type and temperature, so a detailed sensor calibration is being undertaken for each site using both laboratory and field measurements. As the CS616 sensors are particularly sensitive to soil temperature fluctuations Campbell Scientific T107 temperature sensors (http://www.campbellsci.com/107-l) were installed vertically with their midpoint at 15cm below the soil surface, providing a continuous record of soil temperature at a midpoint of the 0-30cm CS616 for each monitoring site. Deeper temperatures were assumed to have the same characteristics throughout the catchment and are therefore estimated from detailed soil temperature profile measurements made at the automatic weather station in the Stanley microcatchment, with a linear offset applied based on comparison of the two 15cm measurements. Fig. 15 displays an example of the collected datasets for years 2003 and 2004 at Spring Hill station, in the northern par of the study area.

Two focus catchments were created by establishing 7 soil moisture monitoring sites in each of the major subcatchments (6 individual sites in the Krui River catchment in addition to the Stanley microcatchment (with 7 sites) and 7 individual sites in the Merriwa Creek catchment), with a further 6 sites installed in the remaining Goulburn River catchment (Fig. 13). The intensively monitored Stanley microcatchment was designed to estimate the location of catchment average soil moisture sites within a catchment, as two groups of sites were located along lines at lower, mid and upper slope locations. Moreover, the higher density of soil moisture monitoring sites in the Krui and Merriwa catchments allows for work on the spatial organisation of soil moisture throughout the northern part of the catchment and supports work undertaken in the validation and scaling of satellite measurements and model simulation.

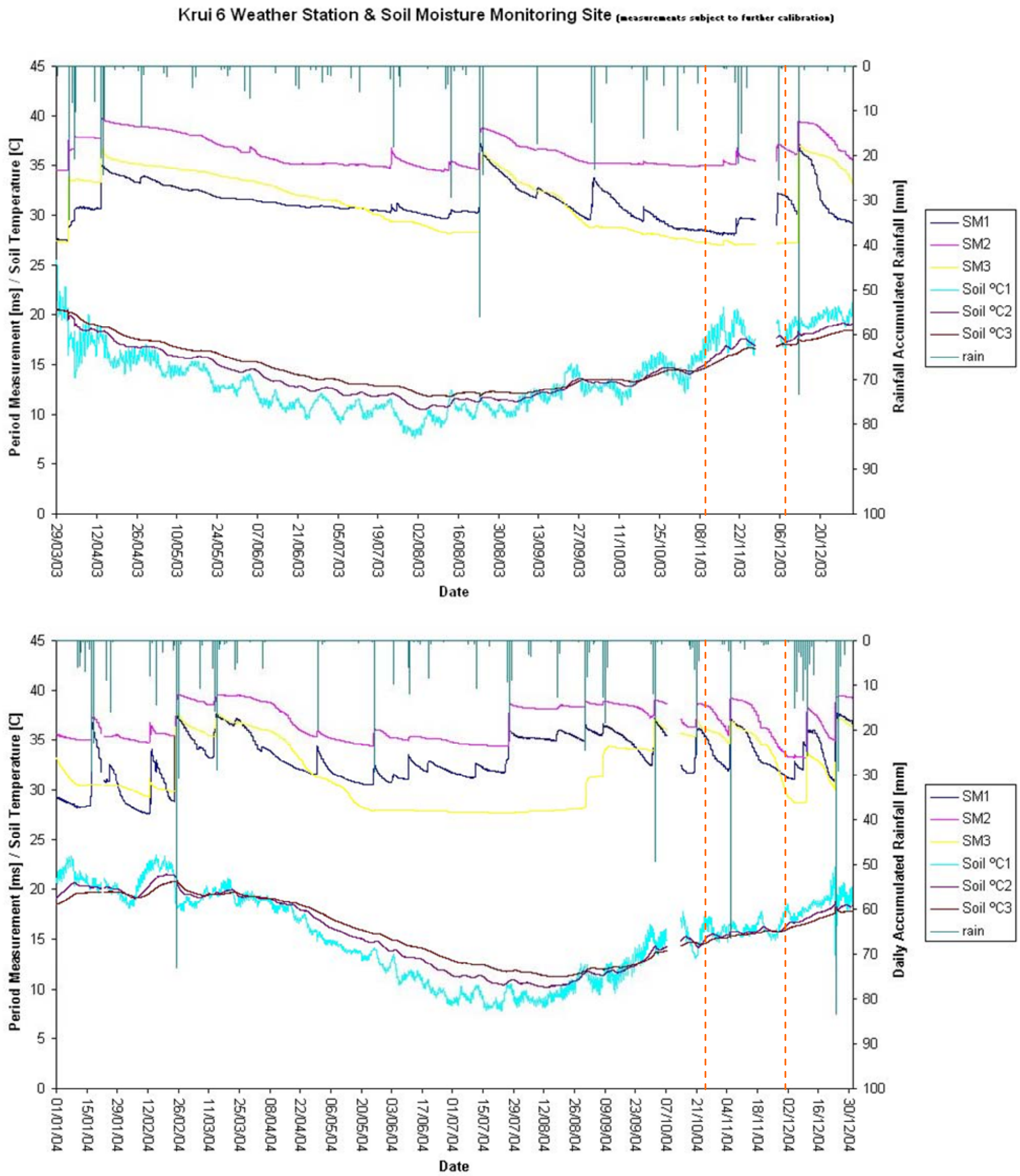

Figure 15. Example of data collected at SAMSAS sites. Plots show temporal variation of soil moisture and soil temperature at (1) 0-30cm (2) 30-60cm and (3) 60-90cm during 2003 (top panel) and 2004 (bottom panel). Daily rainfall is also indicated. Dashed red lines highlight the period in which NAFE'05 will take place.

NAFE'05 will take place in the period between October 31st and November 26th. The time frame was chosen in order to capture highly dynamic soil moisture stats. As evident in the panels of Fig. 15, storms are frequent in this period, at least in the upper part of the study area, resulting in a root-zone soil moisture content (0-30cm) variation within the month of about 7% (V/V). Given the buffer imposed by infiltration of water from the soil surface to these depths, the dynamics in the layer which affects remote sensing measurements (approximately 0-5cm), are expected to be even stronger.

5 Ground Monitoring

The ground component of the NAFE '05 field campaign consists of four aspects:

1. Network of continuous soil moisture profile monitoring stations;
2. Supplementary monitoring stations;
3. Spatial soil moisture mapping; and
4. Supporting data.

5.1 Soil moisture profile stations

The soil moisture and climate monitoring sites existing within the Goulburn River experimental catchment form the basis of all ground based monitoring activities. These monitoring sites have recently been upgraded with telemetry systems, Stevens Water

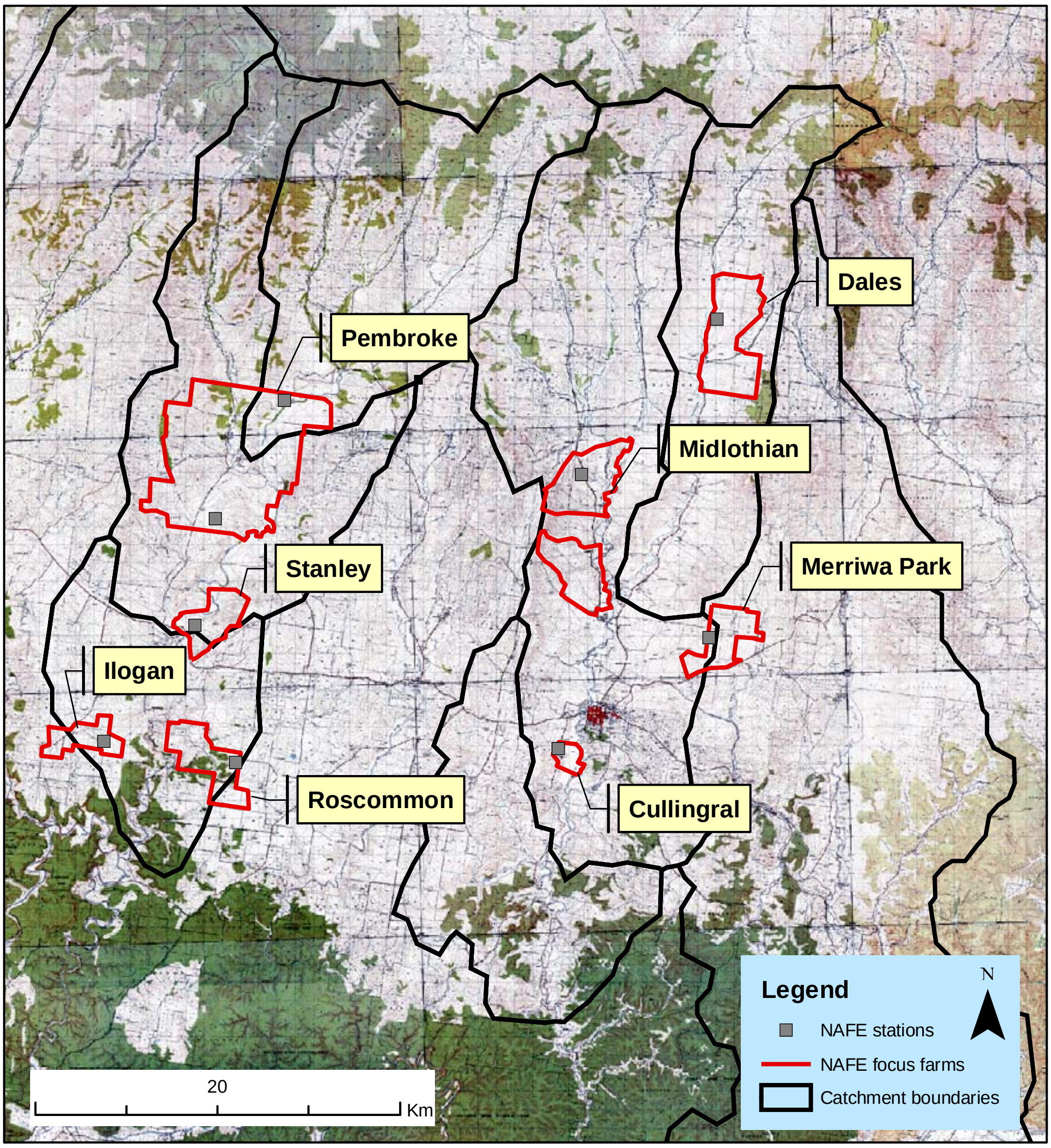

Figure 16. NAFE focus farms in the Northern Goulburn catchment area. NAFE mmonitoring stations are also indicated with squares.

Table 4. Main characteristics of target farms of the NAFE '05 campaign.

FARM NAME	AREA(ha)	TOPOGRAPHY	LANDUSES	SOILS
Pembroke	6400	Hilly/Gently rolling	• Grazing • Crop (wheat)	• Black basaltic clays
Stanley	720	Hilly	• Grazing	• Black basalts on flat; red basaltic clays on crests
Roscommon	940	Flat/Gently rolling	• Grazing	• Red basaltic clays and sandy soils
Ilogan	560	Flat/Gently rolling	• Crop (Barley, Oats, Wheat)	• Black basaltic clays with patches of red basaltc clays
Dales	1500	Flat/Hilly	• Grazing	• Black basaltic clays
Midlothian	2000	Flat/Hilly	• Grazing • Crop(Sorghum, Lucerne,Wheat)	• Black basaltic clays
Merriwa Park	750	Hilly	• Grazing • Crop (Wheat)	• Black basaltic clays
Cullingral	220	Flat	• Crop (Wheat, Lucerne)	• Black basaltic clays

HydraProbe® sensors (Stevens Water; http://www.stevenswater.com/catalog/stevensProduct.aspx?SKU='70030') for top 5cm soil moisture (inserted vertically from the soil surface) and tipping bucket raingauges. Because the HydraProbe temperature sensor is located in the exposed head of the probe, a supplementary temperature sensor has been installed at 2.5cm depth and temperature output from the HydraProbe discarded. Location of the NAFE '05 study area within the Goulburn River experimental catchment was chosen to encapsulate the majority of these stations, and eight focus farms for detailed measurements were chosen within the Krui and Merriwa sub-catchments according to spatial distribution and characteristics of farms hosting these stations (Fig. 16). As the dominant landuses are grazing and cropping, this region is very suitable for soil moisture remote sensing studies due to the moderate vegetation cover. Table 4 summarises the characteristics of each farm.

5.2 Supplementary monitoring stations

A total of eight of the existing monitoring stations (one at each of the eight focus farms) will be supplemented with additional sensors for the duration of NAFE '05 (hereafter referred to as NAFE stations). The primary purpose of this supplementary monitoring is to:

1. provide information on near-surface soil temperature profiles;
2. provide information on leaf wetness in response to dew and precipitation; and
3. develop relationships between thermal infrared observations and near-surface soil temperature

To capture the relevant information, there will be nominally:

- four stations that have thermal infrared radiometers (Two Ahlborn Thermalert TX® and two Everest Interscience Inc.® Infrared Temp Transducers, Model 4000), duplicate soil temperature sensors at 1cm, 2.5cm and 4cm (Unidata® 6507A/10 sensors), and leaf wetness sensors (Measurement Engineering Australia 2040®);

- two stations that have single soil temperature sensors at 1cm, 2.5cm and 4cm, and leaf wetness sensors;
- two stations that have single soil temperature sensors at 1cm, 2.5cm and 4cm; and
- one station that has 4 Unidata® 6507A/10 thermocouples attached to a rock (at Stanley farm)

This supplementary monitoring will in most cases be installed "within" the enclosure at existing monitoring station sites. In particular cases, they will be installed at nearby locations to capture land cover requirements not met at the existing sites; specifically for bare soil and at some crop sites. Fig. 17 shows the location of NAFE stations and the supplementary instrumentation to be installed at each. Fig. 18 shows a schematic of the instrumentation setup.

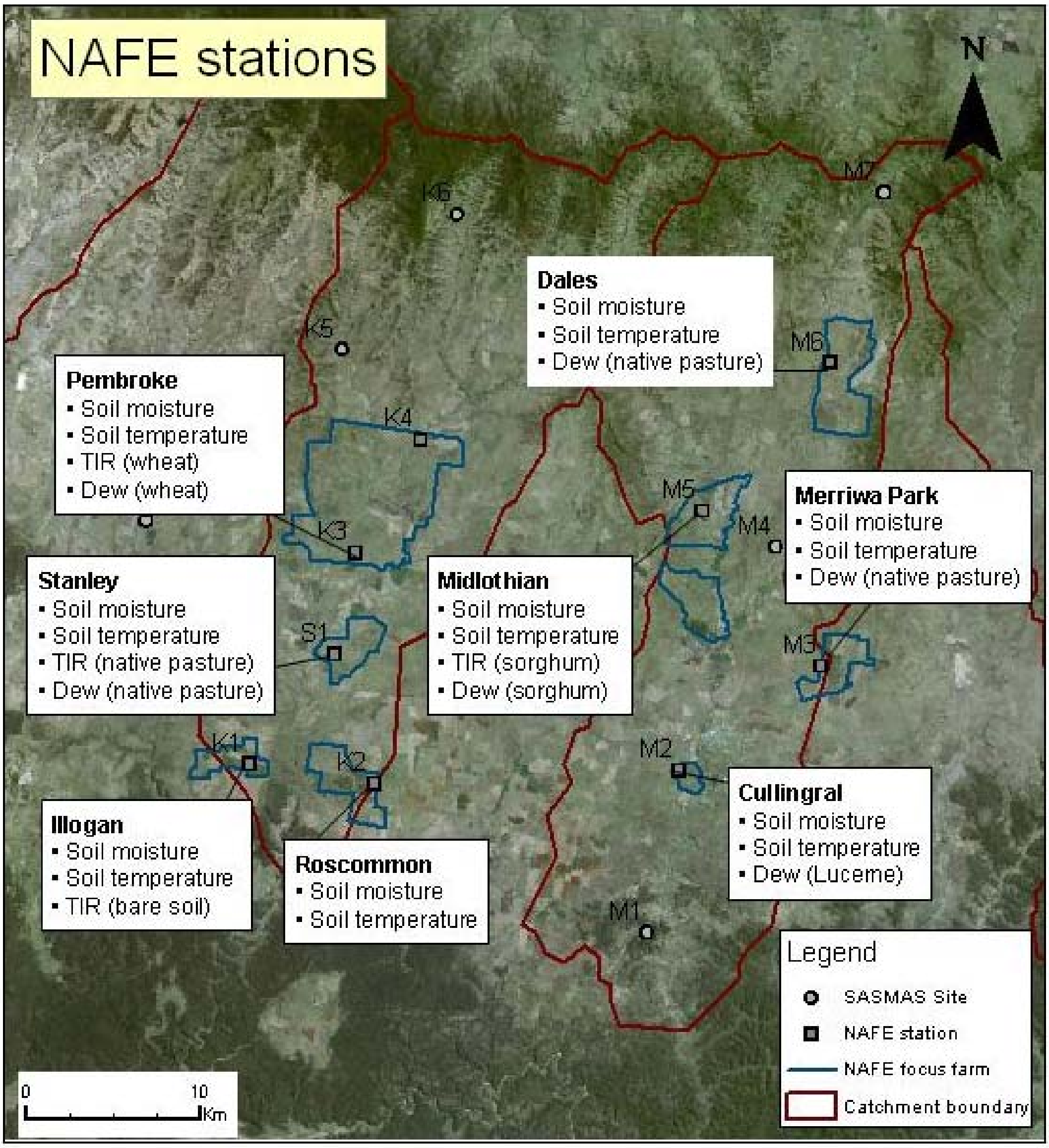

Figure 17. Location of additional ground instrumentations installed for the NAFE campaign. "TIR" stands for Thermal Infrared towers and "Dew" for Leaf wetness sensors.This figure doesn't display the rock surface temperature site at Stanley farm.

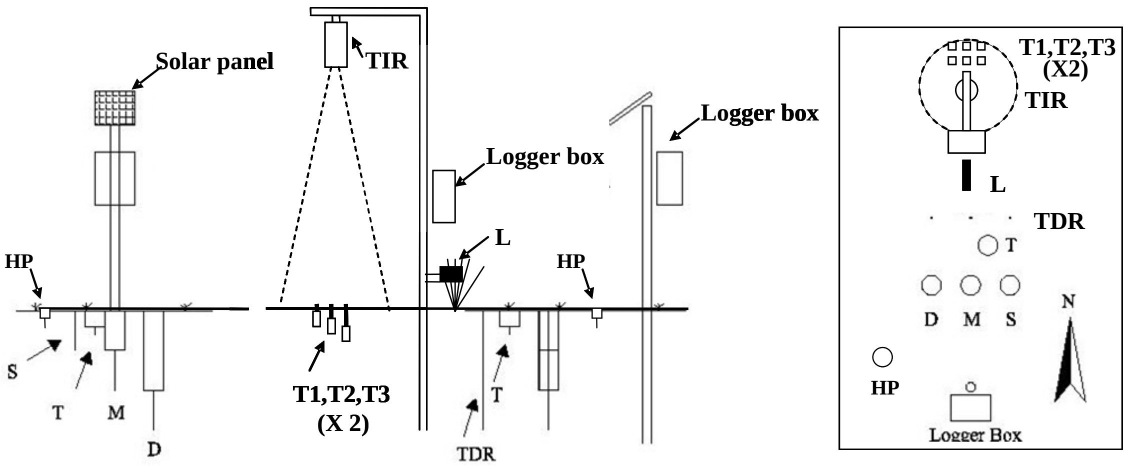

Figure 18. Typical set up of the supplementary monitoring site. (front view, side view and top view); showing shallow (S), medium (M), and deep (D) CS616 soil moisture sensors; 0-5cm Stevens HydraProbe (HP); CS T107 (T), 1 cm (T1), 2.5 cm (T2) and 4cm (T3) soil temperatures; Thermal infrared (TIR) and leaf wetness (L) sensors.

5.3 Spatial soil moisture mapping

Near-surface soil moisture will be measured across the NAFE study area at a range of spatial scales. This will provide an extensive multi-scale near-surface soil moisture dataset useful for addressing the objectives of the study as outlined in section 1.2. Specifically, there will be:

1. regional measurements for verification of airborne and satellite soil moisture retrieval;
2. farm wide measurements for:
    a. verification of scaling assumptions of radiobrightness equations;
    b. assessment of land cover impacts;
    c. development of multi-incidence angle algorithms;
    d. assessment of leaf water impact for 6:00am overpass times;
3. high resolution measurements across these farms for:
    a. understanding spatial variability and representativeness in individual ground measurements;
    b. developing downscaling techniques;
    c. understanding the impact of topography;
    d. understanding the importance of surface roughness;
    e. developing methods for vegetation water content assessment; and
    f. including the impact of surface rock.

Regional scale sampling will occupy an entire day once per week, while farm scale and high resolution area sampling will parallel in the same day on the same farm, four times a week, alternating between Krui and Merriwa area farms, as per the schedule in Table 5

During the 4 week experiment, ground crew will be organised into 4 teams of 3 people (with exception of the Pembroke farm which will have 4 people), each team acting independently within the daily schedule (apart from daily morning and evening briefings). Each team will be assigned 2 focus farms, one within the Krui and one within the Merriwa sub-catchments, and will be responsible for all sampling operations within the assigned areas, as well as general monitoring and reporting to the ground crew leader. Exact location of soil moisture sampling points will be provided – see section 7.

5.3.1 Regional scale sampling

One of the objectives of the NAFE '05 campaign is to provide ground verification data for the AMSR-E soil moisture retrieval algorithms. For this purpose, soil moisture measurements will be made at many locations within the focus farms and along the roadsides in the surrounding areas on days when there are both am and pm overpasses of AMSR-E for the study area. The main objectives are to:

1. Provide an estimate of the areal average and spatial variation of near-surface soil moisture content within an AMSR-E footprint (~50km) at the nominal time of satellite overpass.
2. Develop and verify approaches to downscaling low resolution near-surface soil moisture estimates such as those from AMSR-E to 1km or better resolution using higher resolution remotely sensed thermal and visible data.

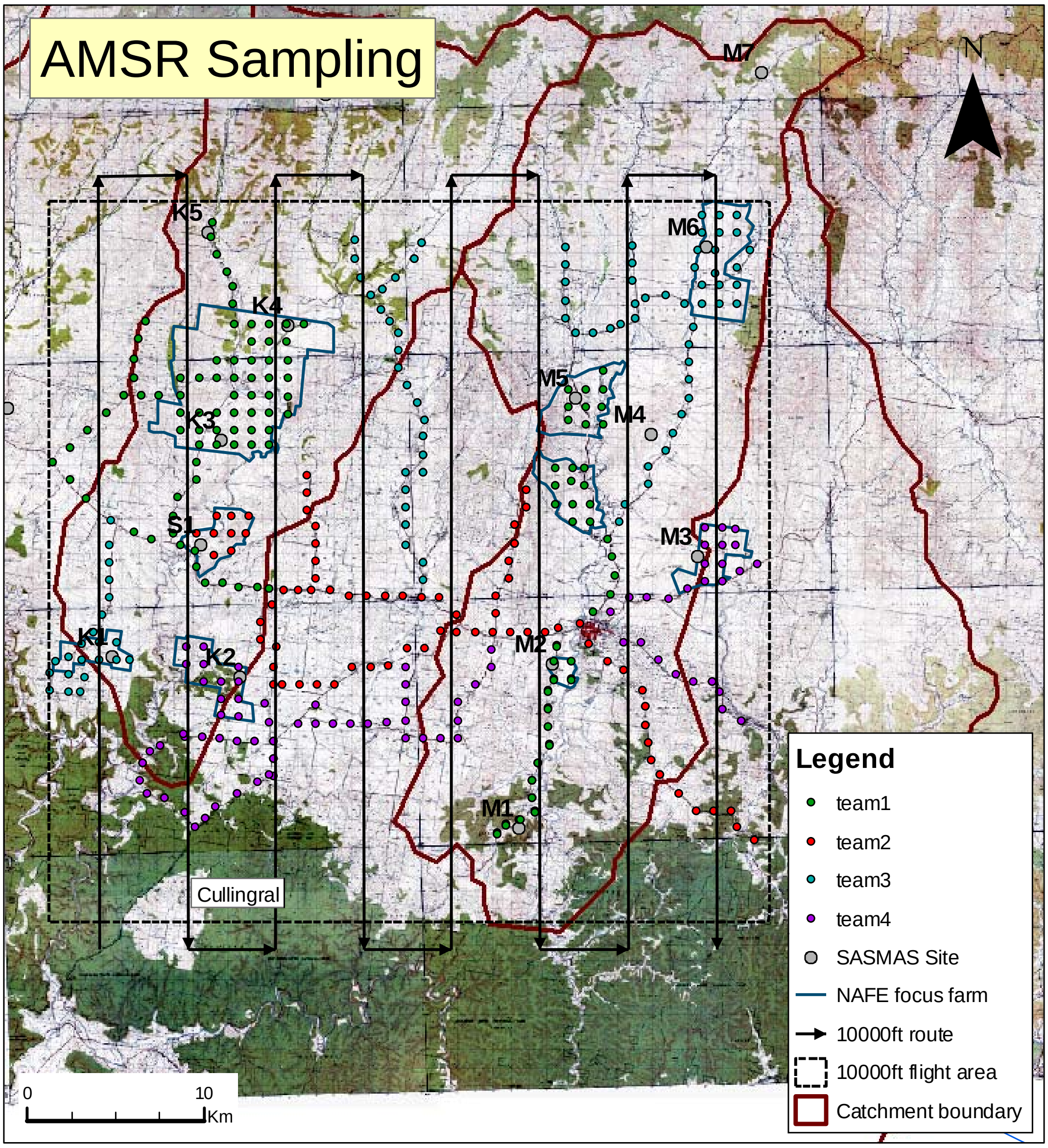

Figure 19. Planned sampling locations for regional scale soil moisture monitoring.

Table 6. Estimated regional sampling times. An average driving speed of 20 Km/h is assumed.

	Point N.	Distance (km)	Speed (Km/h)	Time (hrs)
team 1	122	121	20	6.1
team 2	116	115	20	5.8
team 3	130	129	20	6.5
team 4	99	98	20	4.9

Overpass dates and time are shown in Table 1. On these dates, PLMR flights with nominal 1km ground resolution will be undertaken concurrent with the regional ground sampling. Regional ground sampling of near-surface soil moisture will be undertaken by team leaders using iPAQ based HydraProbe systems (see section 7) at predefined GPS-located points approximately 1km apart. These points will be located in the respective two farms (one in each of the Krui and Merriwa sub-catchments) teams are responsible for and along the sides of main roads crossing the study area. The ground sampling grid according to team is shown in Fig. 19. Sampling will follow as closely as possible a regular 1km grid within the farm boundaries; sampling will occur mostly on the existent farm tracks in order to decrease the total sampling time. Outside the farm boundaries, sampling will be undertaken in the areas adjacent the road, at a distance from it sufficient to avoid localized moisture anomalies due to artefacts of the road. These sites would preferably be made “over the fence” to more closely represent the surrounding land use conditions, but without actually entering onto private land. The sampling illustrated in Fig. 19 is expected to take approximately 6 hours. See table 6 for detailed sampling times per each team.

Concurrently with soil moisture measurements, teams will collect the following supporting data across both focus farms in their responsibility during regional sampling days:

- Gravimetric soil moisture samples (also used for soil texture);
- Vegetation biomass samples;
- Vegetation type characterisation;
- Land use classification;
- Crop height measurements;
- Leaf wetness observations.

Table 5. Ground sampling calendar for NAFE.

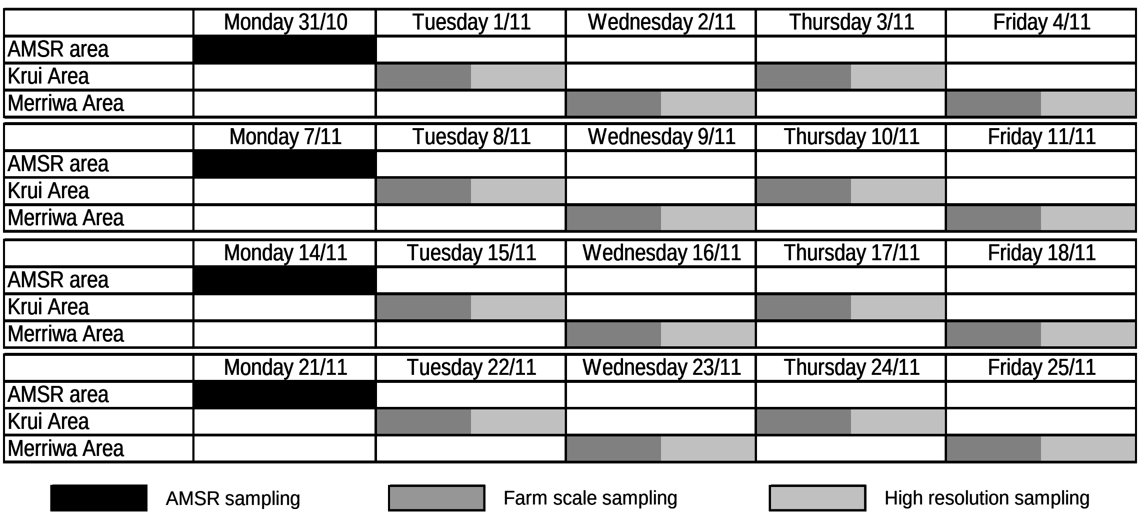

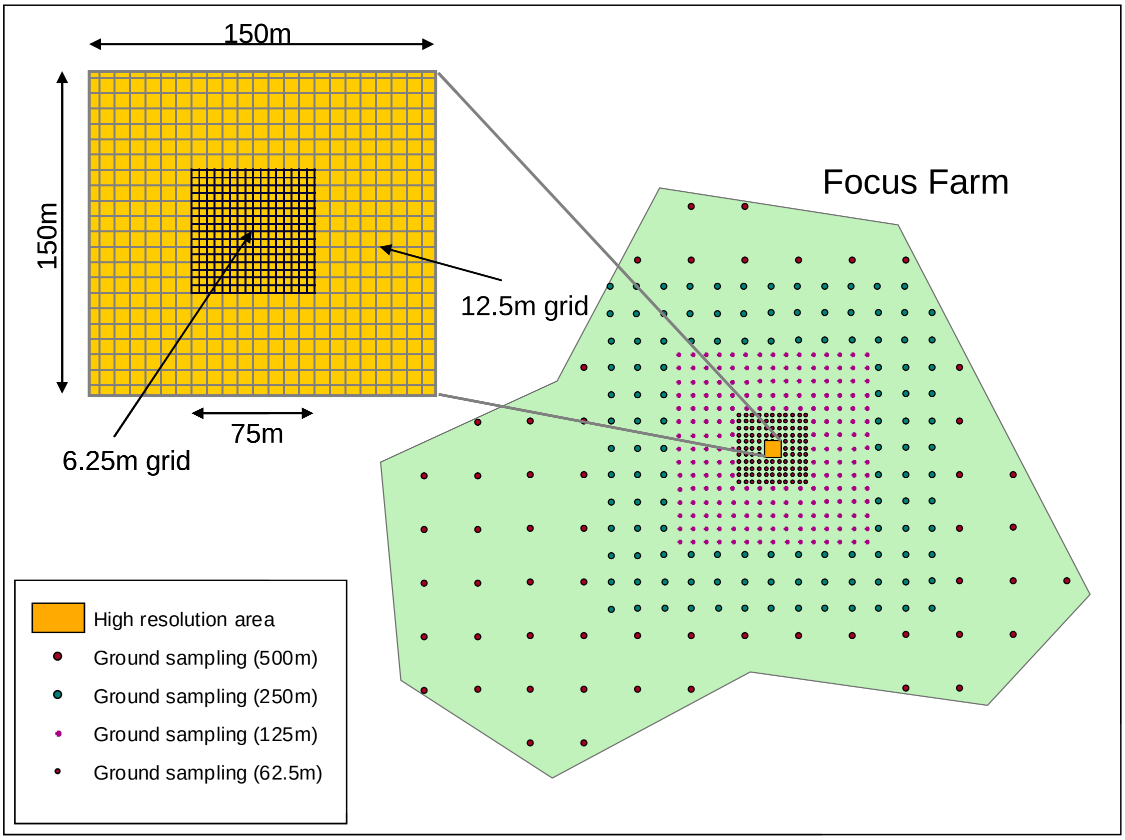

Figure 20. Schematic of farm scale soil moisture sampling strategy.

The following variables will be measured once only by each team for both farms, with instrumentation and/or personnel rotated between farms as necessary:

- Surface roughness measurements;
- LAI measurements;
- NDVI measurements;
- Surface rock cover estimation.

Detailed description of data sampling procedures can be found in sections 5.4 and 7. **For a summary of the daily measurements of each group refer to Tables B1 and B2 in Appendix B.**

5.3.2 Focus farms measurements

The purpose of farm scale sampling is to provide ground soil moisture and supporting data for verification of the aircraft soil moisture, soil temperature and vegetation mapping at different ground pixel resolutions. Near-surface soil moisture will therefore be measured across the focus farms concurrently with aircraft overpasses at a range of spatial scales. The objective is to cover as much of the farm extent and surface conditions present in the area as possible in a single day, with a combination of spatial resolutions. This will provide both direct ground and downscaling verification of the aircraft measurements with sufficient spatial detail to capture sub-pixel variability. The adopted sampling strategy (Fig. 20) is therefore a compromise between these objectives and logistic constraints such as number of ground personnel and time available.

Soil moisture measurements will be taken at many locations within the farm at various resolutions (500m, 250m, 125m and 62.5m), covering as much as possible of the range of land use, topographic, soil type and soil wetness conditions present across the farm. Furthermore, at each farm a small area of 150m by 150m size will be the focus of very intensive soil moisture sampling (12.5m and 6.25m). Each farm will be sampled in one day by one team, which will be divided into 2 groups:

- Group A (1 person) dedicated to the 500m, 250m and 125m sampling
- Group B (2 people) dedicated to the high resolution area sampling, in the morning, and the 62.5m sampling in the afternoon.

Exact sampling locations will be provided on the individual iPAQs. Group A will make use of the team vehicle to move across the farm, or walk to the sampling points in areas where driving is not feasible. Sampling points will be located by use of a GPS receiver link to the iPAQ. Similarly, Group B will identify the 62.5m sampling locations with the GPS and iPAQ system. As individual GPS receiver position accuracy is insufficient for the high resolution area, sampling locations will be clearly marked and labelled on the ground (see section 6.2). The farm scale sampling grid for all the focus farms are shown in Fig. 21 and 22.

The 150m x 150m areas herein referred to as “high resolution” areas will be sampled at very high resolution, down to 6.25m. This sampling approach has been chosen in order to (a) provide highly detailed ground information on the representativeness and variability expected from point soil moisture and vegetation biomass measurements used for accurate validation of the PLMR mapping and (b) validate the downscaling techniques with high

Table 7. Characteristics of the high resolution sampling areas

Farm	topography	vegetation cover	purpose	Soil type	Reference Lat(Deg)	Reference Long(Deg)
Pembroke	gently sloping/ contour bank	Native grass/ Wheat	vegetation cover variability	Black Basalt	150.1377	-32.0405
Stanley	slope	Native	topography	Red Basalt	150.1387	-32.0940
Roscommon	flat	Native	PLMR validation on native grass	Red Basalt	150.1460	-32.1754
Illogan	flat	Native grass/ Wheat	vegetation cover variability	Red Basalt	150.0572	-32.1454
Dales	sloping/creek	Native	topography	Black Basalt	150.4324	-31.9496
Midlothian	flat	Sorghum / Lucerne	vegetation cover variability	Black Basalt	150.3634	-32.0137
Merriwa Park	gently sloping	Wheat	PLMR validation on crop	Black Basalt	150.4335	-32.0979
Cullingral	flat	Lucerne	PLMR validation on crop	Black Basalt	150.3413	-32.1621

resolution ground data. For these reasons, the areas were selected in order to cover as many land cover conditions in the area as possible, while capturing detectable near surface

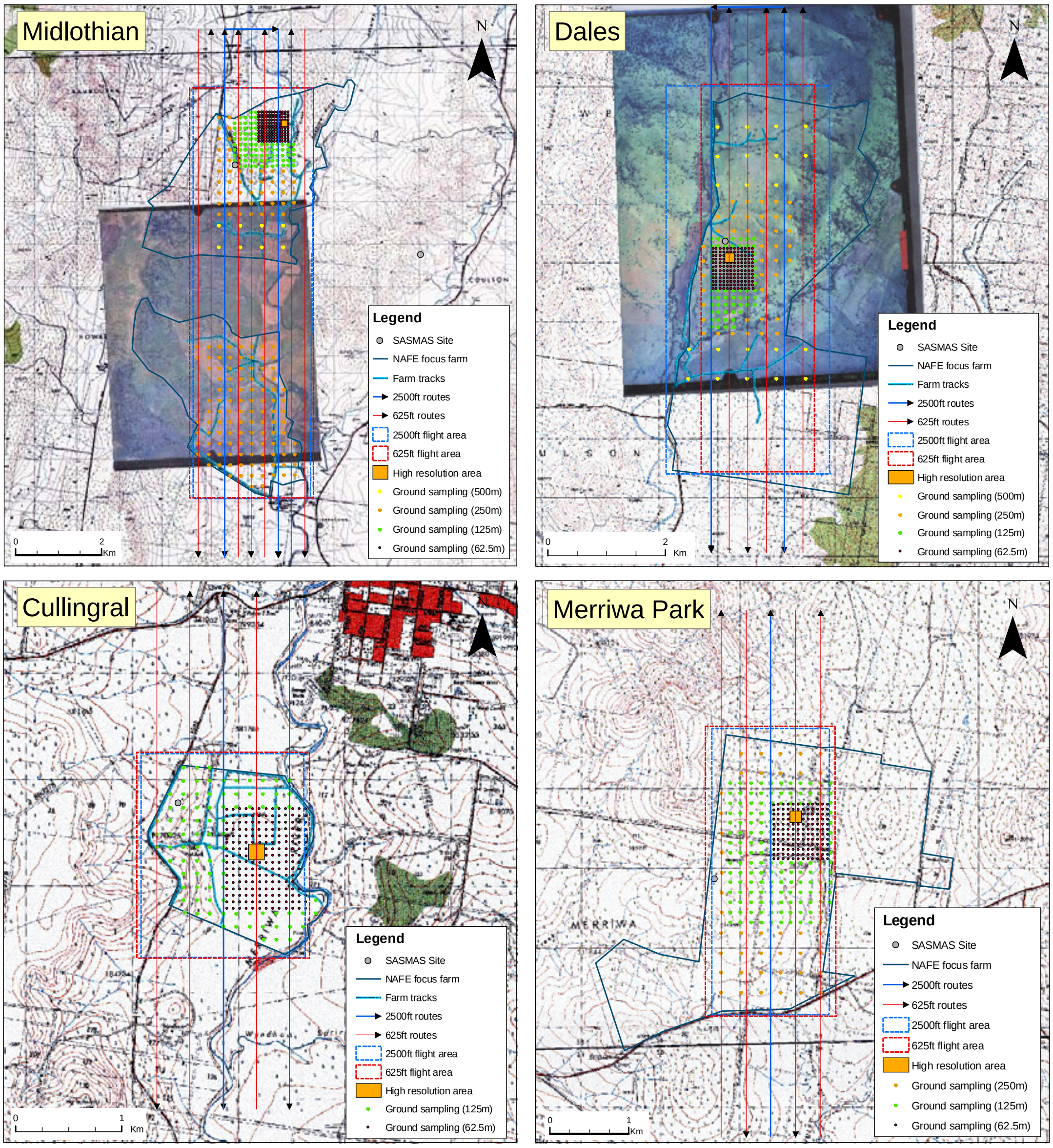

	Nr. Of Sampling points						Estimated sampling times (hrs)			
Farm	Hi-res area	62.5m	125m	250m	500m	1000m	person 1	person 2	person 3	person 4
Dales	289	140	58	41	21		6.5	6.5	6.8	none
Midlothian	289	140	86	157	8		6.5	6.5	6.5	6.7
Merriwa Park	289	140	138	41			6.5	6.5	6.8	none
Cullingral	289	197	89				7.1	7.1	5.5	none

Figure 21. Soil moisture sampling grids and estimated sampling times for all the four Merriwa area focus farms. High resolution PLMR flight lines are also indicated with the mapping coverage.

moisture patterns within the 150m x 150m area. The areas chosen represent microtopographic conditions and non-homogeneous vegetation covers and soil type which are expected to produce the desired soil moisture variability. Table 7 describes the characteristics of each high resolution area with the reference coordinate for their centre point. As shown, all predominant land cover types are included (with the exception of Barley and Oats crops, which will be generally very short or dead at this time of year and can therefore be considered as short native grasses), and various combinations of microtopography and non-uniform land cover are captured.

Teams will also collect the following supporting data at the focus farm on each farm sampling day:

- Gravimetric soil moisture samples;
- Vegetation water content samples;
- Leaf wetness observations and dew amount.

For a summary of the daily measurements of each group refer to Tables B1 and B2 in Appendix B.

The following section describes the methods use to sample these auxiliary data and their significance.

5.4 Supporting data

A number of auxiliary data sets are needed together with soil moisture in order to characterise the surface conditions within the study area. This information is necessary for various purposes:

- to provide auxiliary data required to model the soil microwave emission;
- to validate the observations from different remote sensors operating at different spectral bands which will be flown over the area;
- to calibrate the ground sensors that will be used during the campaign.

Supporting data that will be collected during the campaign include:

- Gravimetric soil moisture samples;
- Vegetation biomass and water content;
- Vegetation type;
- Landuse classification;
- Vegetation Leaf Area Index (LAI)
- Vegetation Normalized Difference Vegetation Index (NDVI)
- Surface roughness
- Soil textural properties
- Surface rock cover
- Leaf wetness

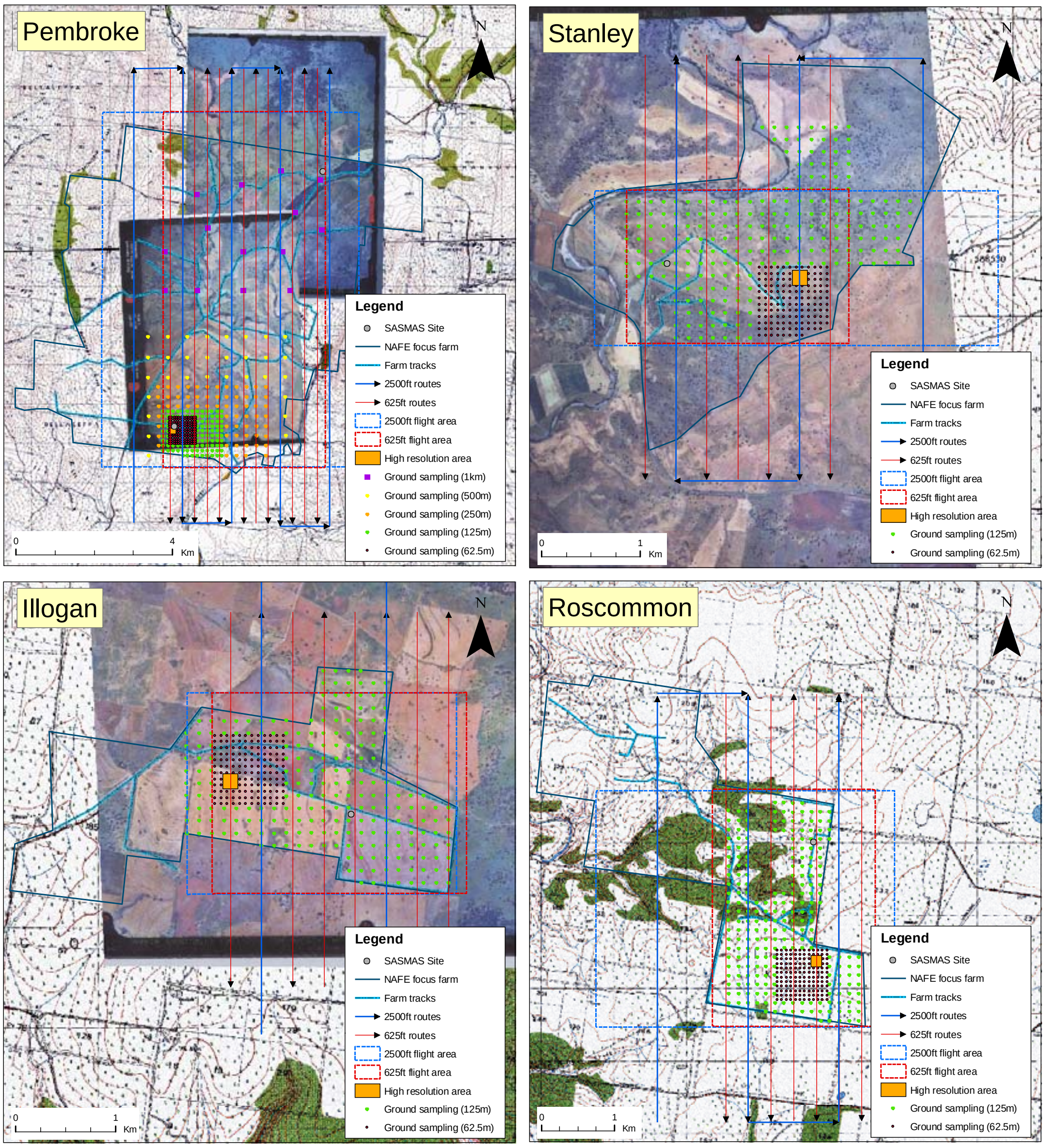

	Nr. Of Sampling points						Estimated sampling time (hrs)			
Farm	Hi-res area	62.5m	125m	250m	500m	1000m	person 1	person 2	person 3	person 4
Pembroke	289	140	101	64	31	14	6.5	6.5	7.1	7
Stanley	289	135	227				6.3	6.3	7.1	none
Roscommon	289	140	223				6.5	6.5	6.9	none
Illogan	289	140	228				6.5	6.5	7.1	none

Figure 22. Soil moisture sampling grids and estimated sampling times for the four Krui area focus farms. High resolution PLMR flight lines are also indicated with the mapping coverage.

The following sections discuss the significance of the above information and individual sampling strategies are described. **Details on how the measurement will be taken can be found in section 7.**

5.4.1 Thermogravimetric soil moisture samples

Volumetric samples of soil will be collected across the study area for both soil textural analysis and calibration of the Stevens Water HydraProbes®. Teams will collect soil samples both during both:

1. regional sampling days, requiring a minimum of 6 samples of different soil types and wetness condition combinations to be collected across each focus farm.
2. farm scale sampling, requiring a minimum of 2 samples of different soil types and wetness condition (1 dryish and 1 wetish) combinations to be collected across each focus farm.

In total, a minimum of 56 soil samples will be collected along the entire campaign. These volumetric samples (collected with a sampling ring for the same soil measured with the HydraProbe) will be dried in ovens at the end of each day to calculate the gravimetric water content and the bulk density. From there the volumetric water content will be compared with HydraProbe measurements taken at the same locations. These samples will cover a wide range of soil types and wetness conditions, providing a calibration equation for each farm if not the entire region.

5.4.2 Vegetation biomass and water content

The amount of vegetation biomass (Kg/m^2) and vegetation water content (g of water/g of biomass) present above the soil surface strongly affects the microwave emission observed. Information on the spatial and temporal variation of these two quantities is needed for microwave emission modelling and so that relationships with infrared and visible remote sensing observations can be established. An overview of the sampling approach is as follows, with detailed sampling procedures given in section 7:

1. During regional sampling days:
    - A total of 16 vegetation biomass "quadrant" samples will be collected on a grid across the high resolution area on both farms in weeks 1 and 4. These samples are intended to give an estimate of spatial variability in vegetation biomass and water content for a specific vegetation type.
    - A minimum of 6 vegetation biomass "quadrant" samples will be collected across each farm, with the aim of collecting at least one sample for every land cover class. Sampling locations should be the same for all four regional sampling days so they can be used to assess temporal variation in vegetation biomass and water content.
2. During farm scale sampling days:
    - A minimum of 2 vegetation water content "grab" samples will be collected for the farm reference vegetation at the end of the day. Sampling location and vegetation type will remain the same for all the sampling days. These samples are intended to give an estimate of temporal variability in vegetation water content for specific vegetation types.
    - Information about the plant height, using scale on HydraProbe pole.
    - Absence/presence of leaf wetness at start of day and time of burn off noted.

- During two of the Merriwa catchment sampling days there will also be an early morning "dew effect" flight (see Table 8). On these days 2 further vegetation water content "grab" samples will be collected for the farm reference vegetation at the beginning of the day. The purpose of these samples is to determine the amount of leaf water, so care must be taken not to shake the vegetation and loose this water.

5.4.3 Vegetation type

This information is important for the analysis of visual and infrared remote sensing observations, as well as general site characterisation. Dominant vegetation type will be recorded at each sampling site at least <u>once during regional and/or farm scale sampling</u> using the predefined list of vegetation types.

5.4.4 Land use classification

Land use is useful information that supports the interpretation of remotely sensed data of various nature. It is therefore important to characterize the main land uses in the study area, to complement land use mapping obtained from satellites like Landsat. Land uses will be characterized by visual observation during ragional sampling days, assigning every area sampled to one of the following subclasses (selected as the predominant land use classes in the region)

1. Native pasture
2. Improved pasture
3. Range land
4. Agricultural land: Fallow
5. Agricultural land: Wheat
6. Agricultural land: Sorghum
7. Agricultural land: Lucerne
8. Agricultural land: Canola
9. Agricultural land: Oats
10. Agricultural land: Barley
11. Forest land
12. Urban
13. Water body

5.4.5 Vegetation Leaf Area Index (LAI)

LAI assigns a quantifiable value to the amount of vegetation on the ground. Simply put, LAI is the leaf area per unit ground area as seen when looking down on vegetation. This parameter can be related to satellite and aircraft observations at infrared and visible wavelength to provide mapping of vegetation biomass over large areas. Given that the temporal variability of this parameter is expected to be moderate during the campaign, measurements of LAI will be undertaken across farms on only one occasion each, rotated between teams during <u>regional sampling</u> days (team 1 in week 1 through team 4 in week 4). Measurements will be made at 50m spacing at particular location in each farm, selected for high resolution LAI sampling. More extensive measurements will be made across the Stanley focus farm.

5.4.6 Vegetation Normalised Difference Vegetation Index (NDVI)

NDVI is a measure of the green, leafy vegetation density or the lushness of vegetation, and is a function of the difference between the visible and near-infrared sunlight that reflects off the vegetation. Ground measurements of this parameter can be used to verify satellite and aircraft observations, expected to provide vegetation biomass and downscaling information over large areas. Given that the temporal variability of this parameter is expected to be moderate during the campaign, measurements of NDVI will be taken together with the LAI measurements.

5.4.7 Surface roughness

Surface roughness affects the microwave emission from the soil by effectively increasing the surface area of electromagnetic wave emission. Although its effect on observations at L-band frequency has been shown to be very poor, it is important to characterise the spatial variation of this parameter across the different land cover types. As temporal variation in surface roughness is expected to be secondary to spatial variation, it will be estimated once only during the campaign at a minimum of 4 locations on each farm to capture the different roughness characteristics according to land cover type. Measurements will be made using a pin profiler which will be rotated between teams on regional sampling days (team 1 in week 1 through team 4 in week 4).

5.4.8 Soil textural properties

Information on soil textural properties is very important for modelling the microwave emission from the soil as it strongly affects the dielectric behaviour of the soil, a main factor in determining the microwave emission. Laboratory soil textural analysis will be performed on a subset of the soil samples for fraction of sand, clay and silt.

5.4.9 Surface rock cover

The effect of surface rock cover on microwave emission of the soil is still unclear and has not received special attention, despite the fact that large parts of the earth's surface has significant fractional surface rock coverage. One of the objectives of NAFE is to provide preliminary insight into this effect. This will be achieved by visually estimating the percentage of surface rock covered at all sampled sites on at least one occasion. Furthermore, rock temperature will be monitored by installing a set of sensors on a rock in the Stanley focus farm.

5.4.10 Leaf wetness

Passive microwave soil moisture retrieval algorithms generally rely on one fundamental assumption: that the temperature of the soil and the vegetation canopy are the same. This condition is more likely to be met early in the morning, when the effect of solar radiation is still minimal. For this reason, satellites missions are generally planned with local overpass times early in the morning and late in the evening (eg, 6:00am/pm for SMOS and Hydros). However, the presence of dew on vegetation at that time of day is likely to affect the accuracy of the passive microwave observation. One of the objectives of NAFE is to analyse the effect of dew on the microwave signal. This will be accomplished with two targeted "dew effect" aircraft flights during the campaign (see Table 8). On these days ground crew will additionally collect two vegetation samples at the start of the day when dew is still present (see section 7 for details). In order to support the leaf wetness measurement made by the permanent stations, ground crew will be required to provide a visual estimate of the leaf wetness conditions during the early hours of the day. This will be accomplished by assigning a value to the wetness state of the plants, ranging from 0= no dew, 1 = moderately wet, 3 = very wet.this values will be promted in the individual iPAQs

6 Airborne Monitoring

One of the major scientific components of the NAFE '05 field campaign is soil moisture mapping with the Polarimetric L-Band Multibeam Radiometer (PLMR) onboard the Small Environmental Research Aircraft (SERA). Technical details about the platform and scientific payload are presented in section 3.

PLMR will be flown together with the thermal imager on all flights. Additionally, for the Krui and Merriwa regions there will be NDVI scanner flights at the start, middle and end of the campaign, there will be digital photography at the start of the campaign only, and there will be lidar coverage undertaken most likely in February. The PLMR flights will be made at a range of flying heights/resolutions across areas of different size throughout the northern half of the Goulburn River experimental catchment (see Figs. 23 and 24, and Table 6).

In parallel with the flights of SERA, the area will be the object of a study conducted by a team from the ESA's SMOS project. This group will be flying an aircraft carrying the EMIRAD system, The airborne, imaging, polarimetric EMIRAD system employs Ku (16 GHz) and Ka (34 GHz) band polarimetric radiometers at 2 different incidence angle (0° and 40°) to measure microwave britghtness temperatures.

The aircraft will be based at Scone airport (Fig. 2) and will operate daily from there. The air crew will be based in Scone and will be responsible for all pre-flight and post-flight activities.

The most important component of the campaign is the high resolution soil moisture mapping

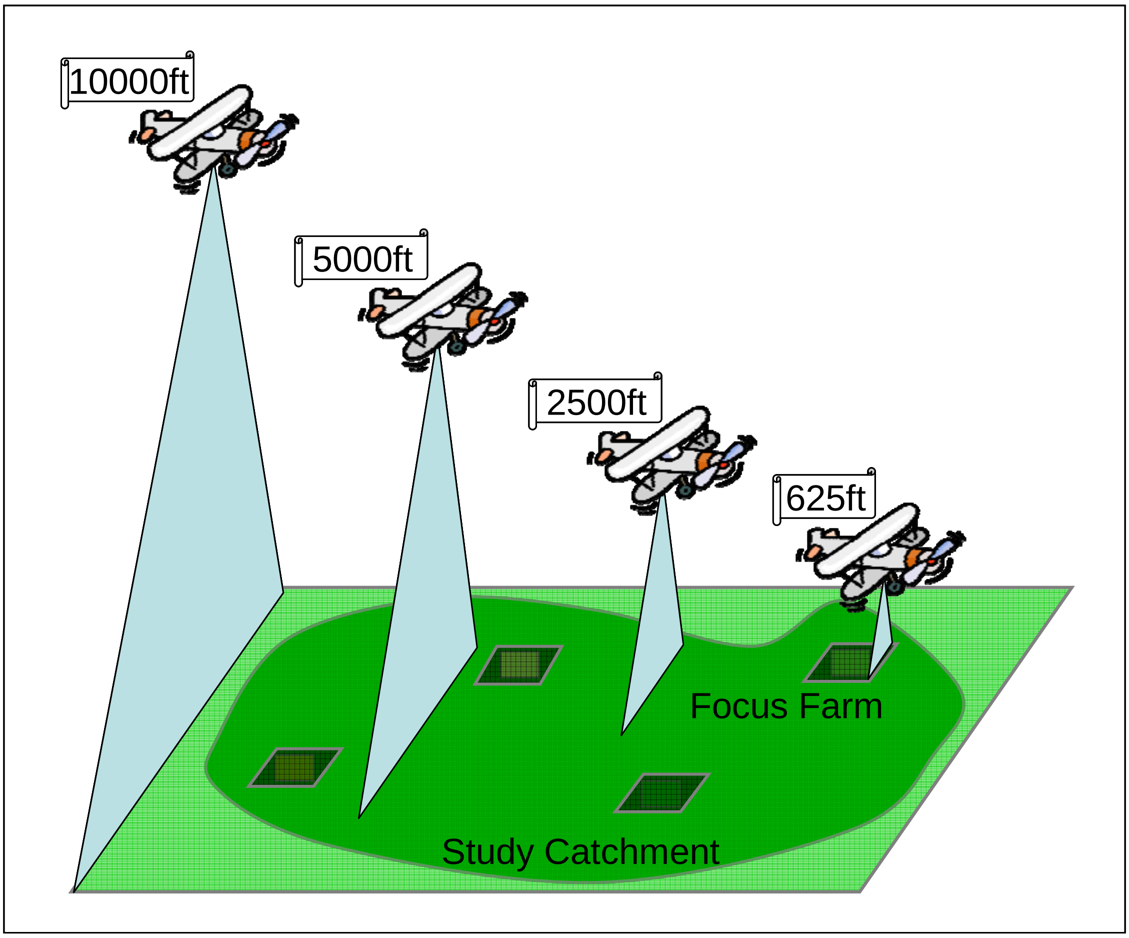

Figure 23. Schematic view of PLMR flights. Indicated flight heights are nominal mean altitudes above ground level.

Table 6. PLMR flight description. Labels for the flight lines naming convention are also indicated. See table C2 in Appendix C for details about Medium and high resolution actual flight altitudes ASL

FLIGHT NAME	FLIGHT ALTITUDE (AGL)	FLIGHT ALTITUDE (ASL)	NOMINAL GROUND RESOLUTION	SWATH	COVERAGE	LABEL
Low Resolution	10000ft	3430m	1000m	6000m	Regional plus Krui and Merriwa sub-areas	A
Intermediate Resolution	5000ft	1910m	500m	3000m	Krui and Merriwa sub-areas	B
Medium Resolution	2500ft	1050 - 1270m	250m	1500m	Farms	C
High resolution	625ft	480 -700m	62.5m	375m	Farms	D
Multi angle	2500ft	1210m	250m	1500m	Merriwa Park focus farm	E
Dew effect	5000ft	1910m	250m	1500m	Merriwa sub-area	F
NDVI	5000ft	1910m	2m	3000m	Krui and Merriwa sub-areas	G
Aerial photography	5000ft	1910m	0.5m	3000m	Krui and Merriwa sub-areas	G

over the focus farms. Such high ground resolution (62.5m) with an airborne passive microwave sensor is unprecedented (apart from a brief field trial). Therefore the scientific significance of this campaign will be outstanding. Intermediate, medium and low resolution flights will provide mapping of soil moisture at coarser scales but for larger areas, providing the linkage with satellite footprints, allowing the multiple scientific objectives of the NAFE '05 campaign to be addressed.

Before illustrating in detail the flight plans and schedules for NAFE '05, it is helpful to explain briefly the rationale behind the flight line planning.

6.1 Flight plans

Flight routes and coverage's at different altitudes have been carefully optimised in order to meet a number of objectives and logistic constraints. These objectives include:

- to cover as much of the study area at multiple ground resolutions during the campaign so as to obtain spatial soil moisture patterns at different scales for an extensive area;
- to map the same area at multiple ground resolutions within the same day to avoid so much as possible temporal differences between maps at different resolutions;

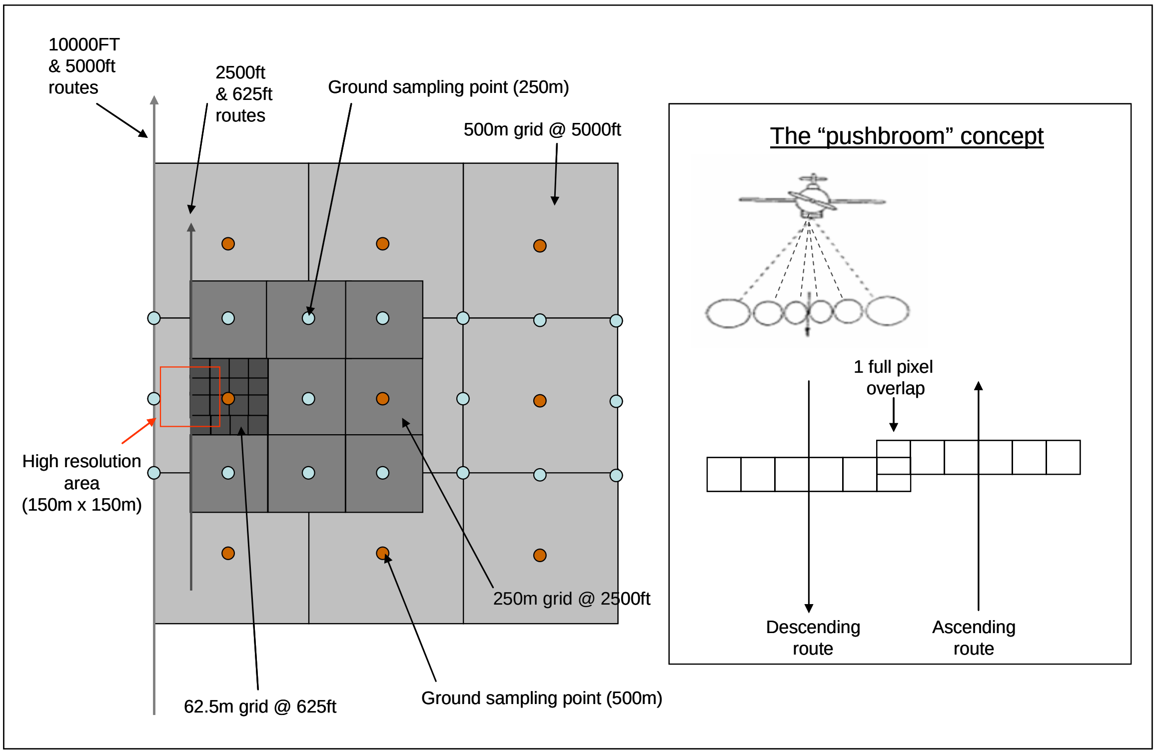

Figure 24. Schematic view of flight plan rationale.

- to obtain patterns of brightness temperature nested between different resolution for scaling purposes; and
- to have high resolution areas falling within the central pixels of the swath at each altitude (beam 1 or 2) to ensure they are not inadvertently missed due to diversions from planned flight paths and wing level attitude, or variations in ground elevation.

The main constraints include:

- to have sufficient overlap between adjacent flight lines in order to avoid areas of no data due to aircraft roll or variations in ground elevation;
- to have sufficient overlap to allow temporal correction of data back to a reference time;
- to have ground sampling points at the centre of aircraft pixels;
- to have a nested network of ground sampling grids linked between different ground sampling resolution (e.g. every second sampling point at 250m spacing is also a sampling point for 500m spacing);
- to keep the total number of mission flight hours for NAFE '05 below 92 hrs, due to legislative regulations; and
- to keep individual flights to not more than 4-5 hours and daily total flight hours below 6, to allow time for pre-flight and post-flight activities, avoid need for refuelling, and to allow the pilot to have a toilet break!!

Fig. 24 illustrates schematically the way flight lines at different altitudes and ground sampling points at different resolution are linked in order to meet the above criteria.

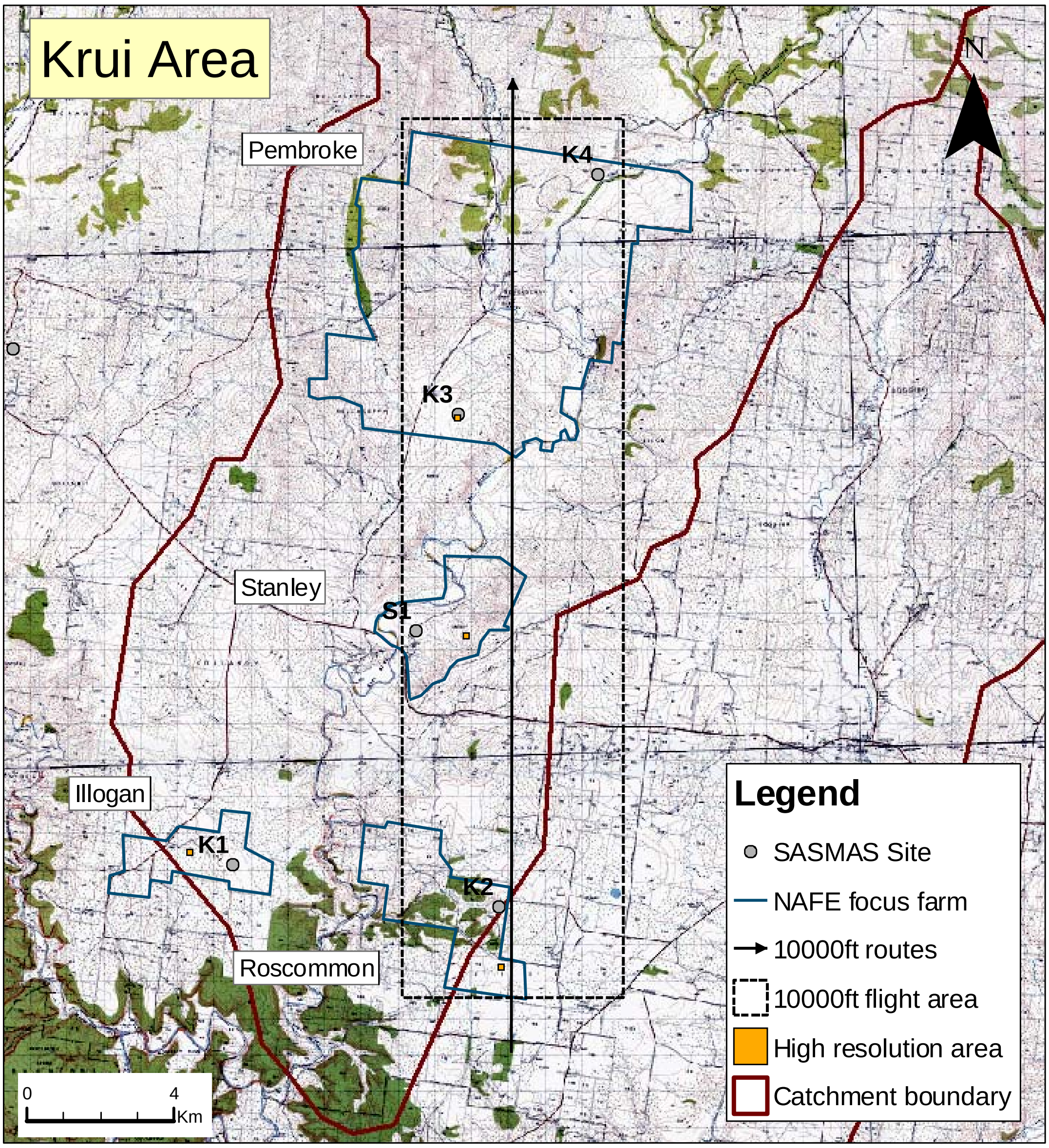

Figure 25. PLMR low resolution flightlines for farm scale days on Krui area. Black solid lines are the flight lines at 10,000ft altitude (AGL), dashed black lines are the areas covered by the mapping.

6.2 Low resolution mapping

One of the objectives of NAFE '05 is the mapping of soil moisture at satellite footprint scale from an airborne platform. This component of the airborne campaign will provide the necessary link between the passive microwave observations at high resolution and the equivalent spaceborne observation over large areas for scaling purposes. Furthermore, low resolution observations from the aircraft are easier to accurately validate than the satellite observations, due to the smaller ground pixel size achievable (1km against 50km). This will allow more accurate verification of the satellite-retrieved soil moisture over large areas by making use of the validated 1km product obtained with the aircraft. This will also provide invaluable data for verification of AMSR-E downscaling algorithms and exploring the scaleability of radiobrightness equations from tower to AMSR-E scales.

Low resolution mapping flights will be flown at a nominal altitude of 10,000ft AGL. Actual altitude above sea level will be of 3430m, which results from flying above the median

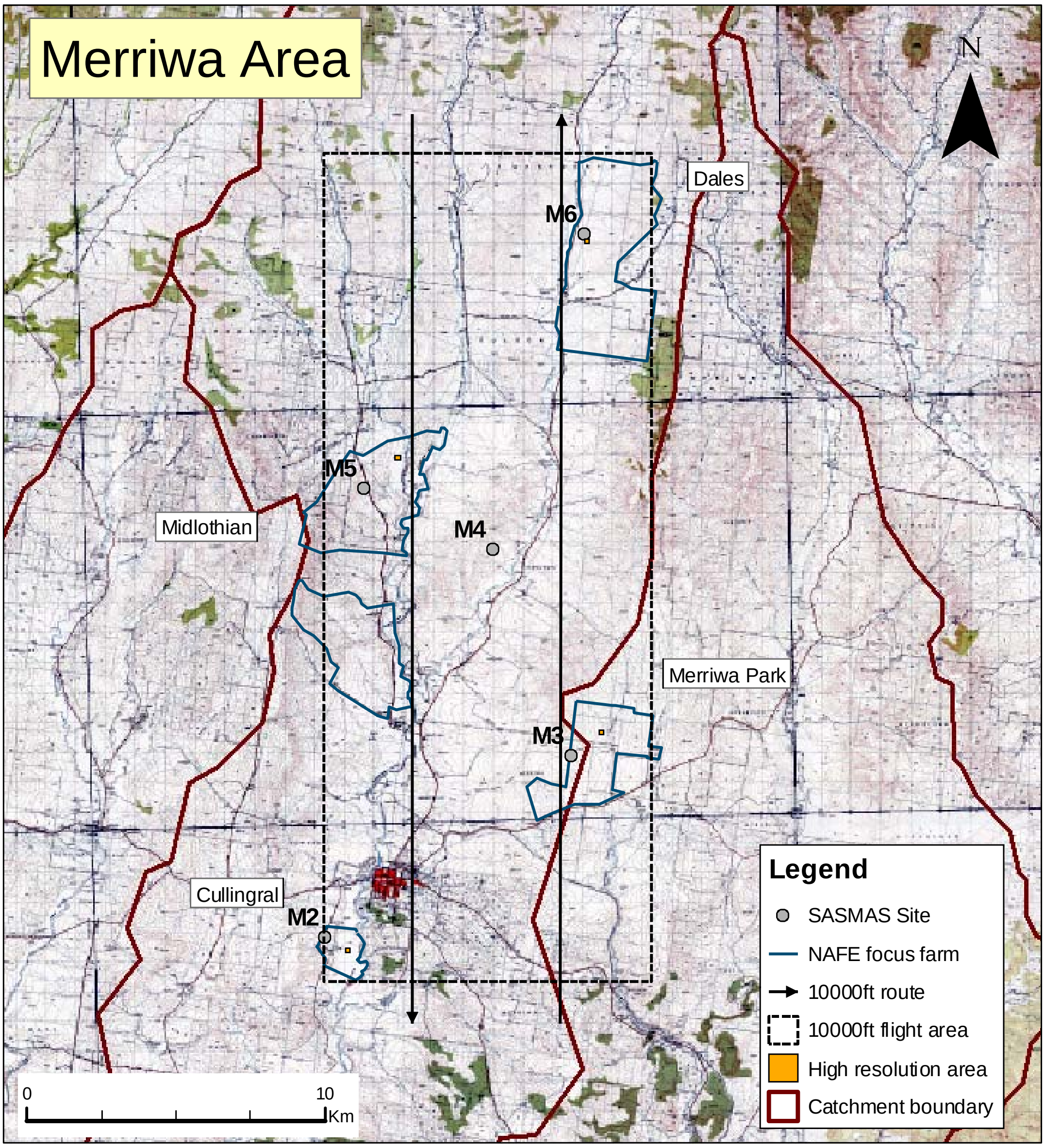

Figure 26. PLMR low resolution flight lines for farm scale days on Merriwa area. Black solid lines are the flight lines at 10,000ft altitude (AGL), dashed black lines are the areas covered by the mapping.

elevation of the terrain in the Northern Goulburn study area (see table C1 in Appendix C for details about terrain elevation and flight altitude). Ground pixel resolution will vary from approximately 861m to 1066m due to variable terrain elevation, with a mean resolution of 1km. Low resolution flights will be undertaken on various dates with different coverage's during the campaign:

- During regional days, low resolution flights will occupy the entire daily flying time and the coverage will be the area approximately covered by a satellite footprint (see Fig. 19 in section 5.3.1);
- During farm scale days, low resolution flight will be undertaken together with intermediate, medium and high resolution flights, with coverage being one of the two sub-catchment study areas, either Krui or Merriwa (see Figs. 25 and 26).

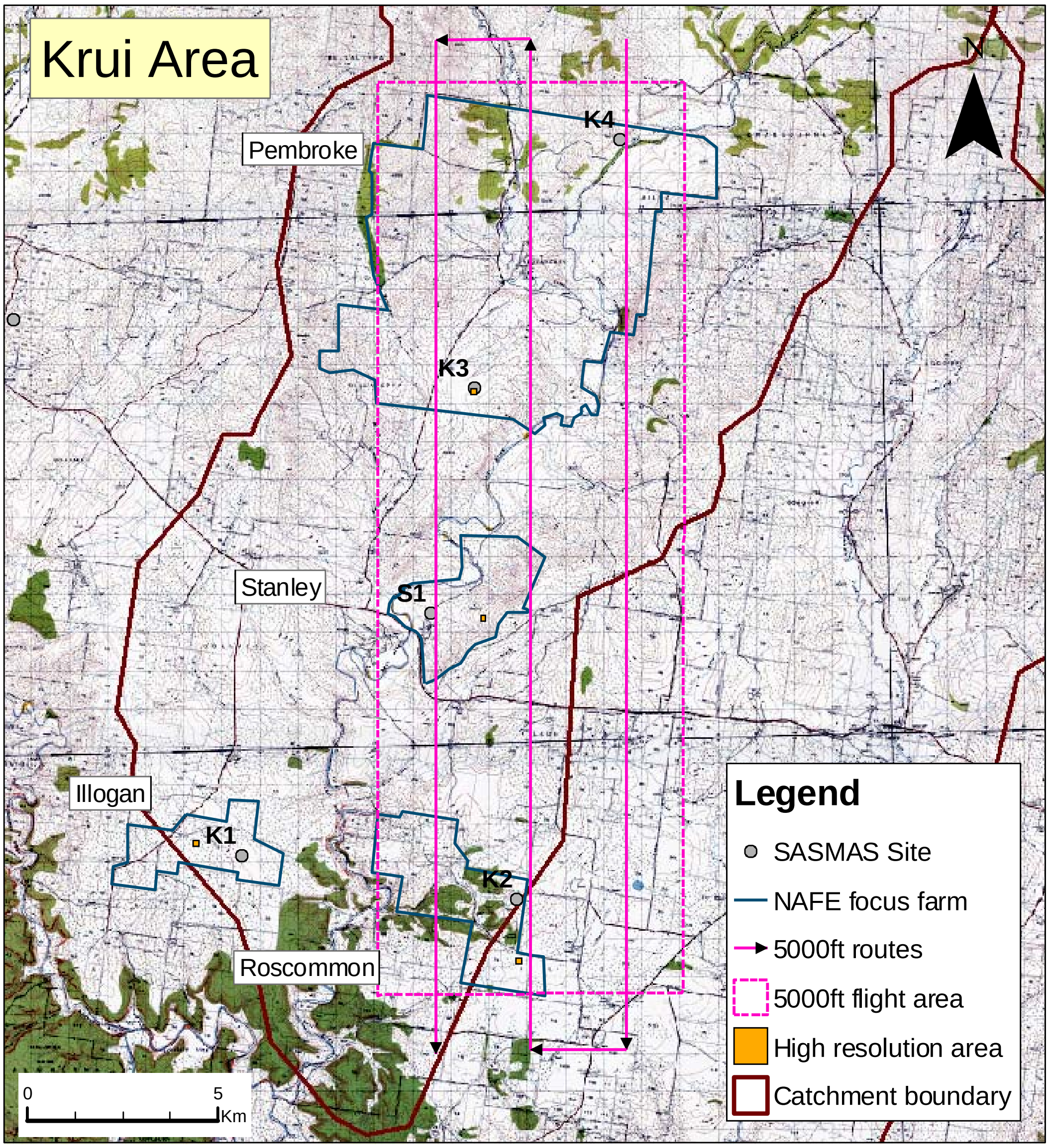

Figure 27. PLMR intermediate resolution flight lines over the Krui study area. Purple solid lines are the flight lines at 5,000ft altitude, dashed purple lines are the areas covered by the mapping.

A detailed flight schedule for NAFE05 is shown in Table 8. Coordinates for starting and ending points of all the sets of flight lines, together with reference coordinates for the mapping extents, are given in Appendix A. For low resolution flight lines refer to Table A1 (for regional days) and A2 (for farm scale days).

6.3 Intermediate resolution mapping

Flights at intermediate altitudes will allow investigation of the scaling nature of the microwave signature of soil moisture and will provide the link between regional scale microwave observations and the high resolution mapping, which is one main scientific objective of this campaign. The acquisition of microwave brightness temperatures at so many different resolutions is unprecedented. Investigation will focus on the relationship between brightness temperatures measured at different spatial resolution, down- and up-scaling issues.

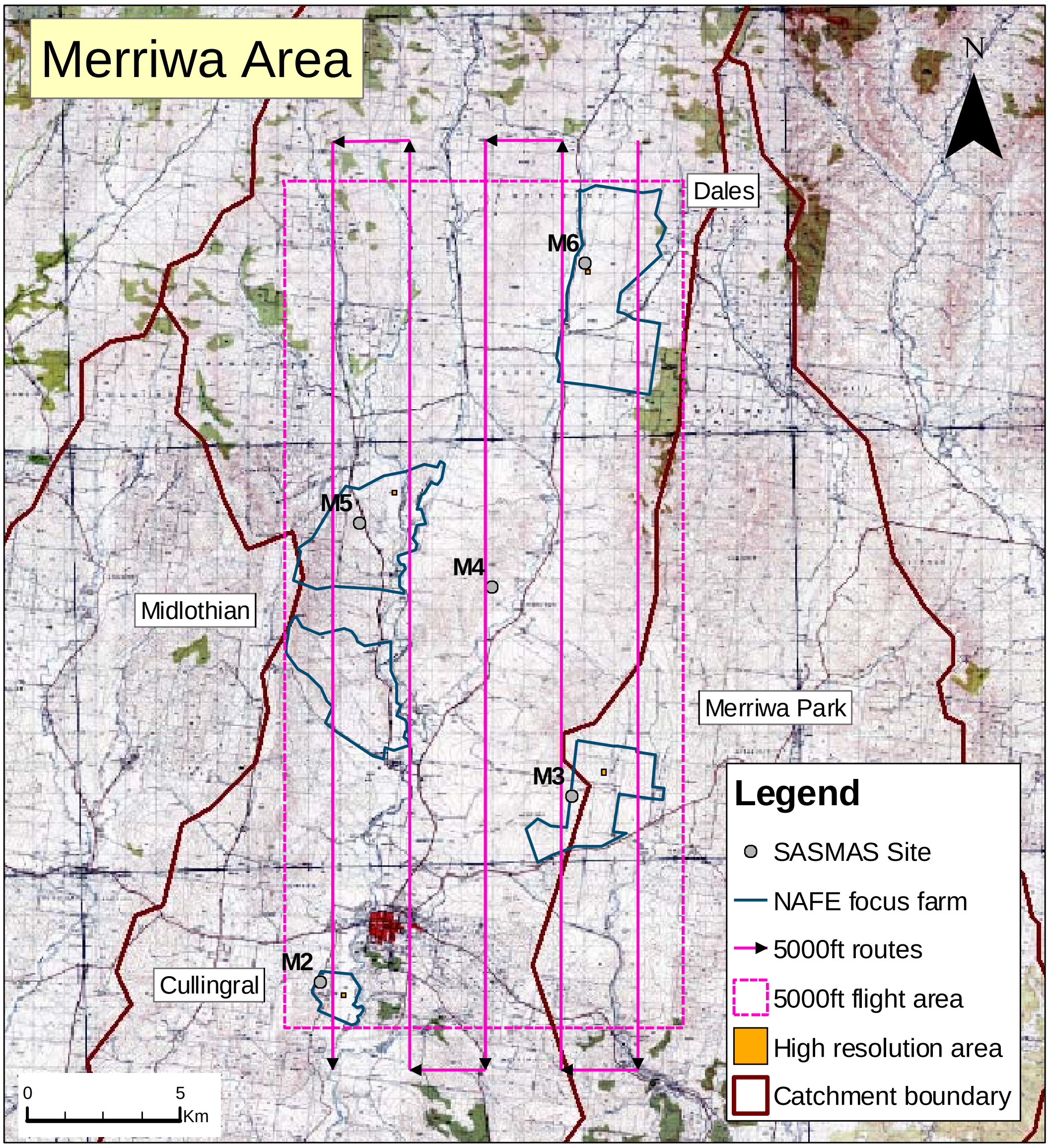

Figure 28. PLMR intermediate resolution flight lines over the Merriwa study area. Purple solid lines are the flight lines at 5,000ft altitude, dashed purple lines are the areas covered by the mapping.

Intermediate resolution mapping will include flights at a nominal 5,000ft AGL over 2 sub-areas in the northern half of the Goulburn River experimental study area, the Krui catchment and the Merriwa catchment. The actual planned flight altitude due to terrain elevation is 1910 ASL. This results from flying over the median terrain elevation of the Northern Goulburn study area. This reference elevation is the same for the low resolution and the intermediate resolution flights, and was chosen in order to maintain consistency between observations at different altitudes (i.e. linear scaling between ground pixels at different resolutions). These flights will entirely cover the NAFE focus farms and surrounding areas, and will therefore constitute an adequate medium resolution "frame" to the high resolution mapping of the individual farms. The only exception to this is the Illogan focus farm in the Krui study area. This farm is somewhat dislocated with respect to the other 4 farms in the area, being slightly isolated to the west. Given the restriction on the flight times, and the fact that the other 3 farms are aligned on a North-South corridor, a decision was made to exclude this farm from the 5,000ft and 10,000ft altitude flights. The farm is covered by the 2,500ft and 625ft flights.

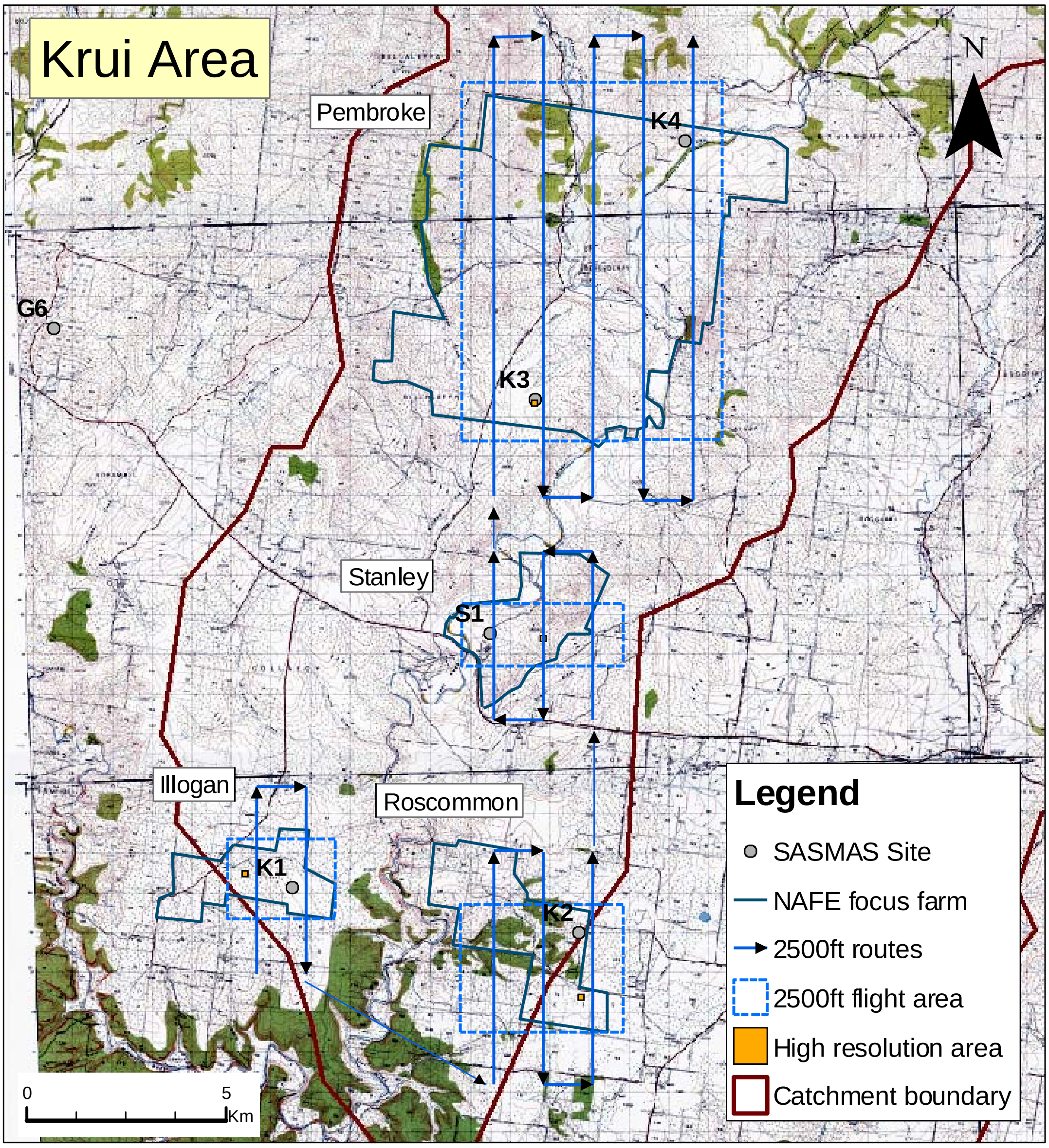

Figure 29. PLMR medium resolution flight lines over the Krui study area. Blue solid lines are the flight lines at 2,500ft altitude, dashed blue lines are the areas covered by the mapping**.**

Intermediate resolution flightlines will generally have different coordinates then those for low resolution flights. The lower altitude creates problems of a different nature which require dislocation of the flight paths (e.g, terrain elevation, matching with ground monitoring network and spatial sampling etc…). Tables A3 and A4 in Appendix A and Figs. 27 and 28

6.4 Medium resolution mapping

Flights at medium altitudes will allow investigation of the scaling nature of the microwave signature of soil moisture and will provide the link of the regional scale microwave observations with the high resolution mapping which is a main scientific objective of this campaign.

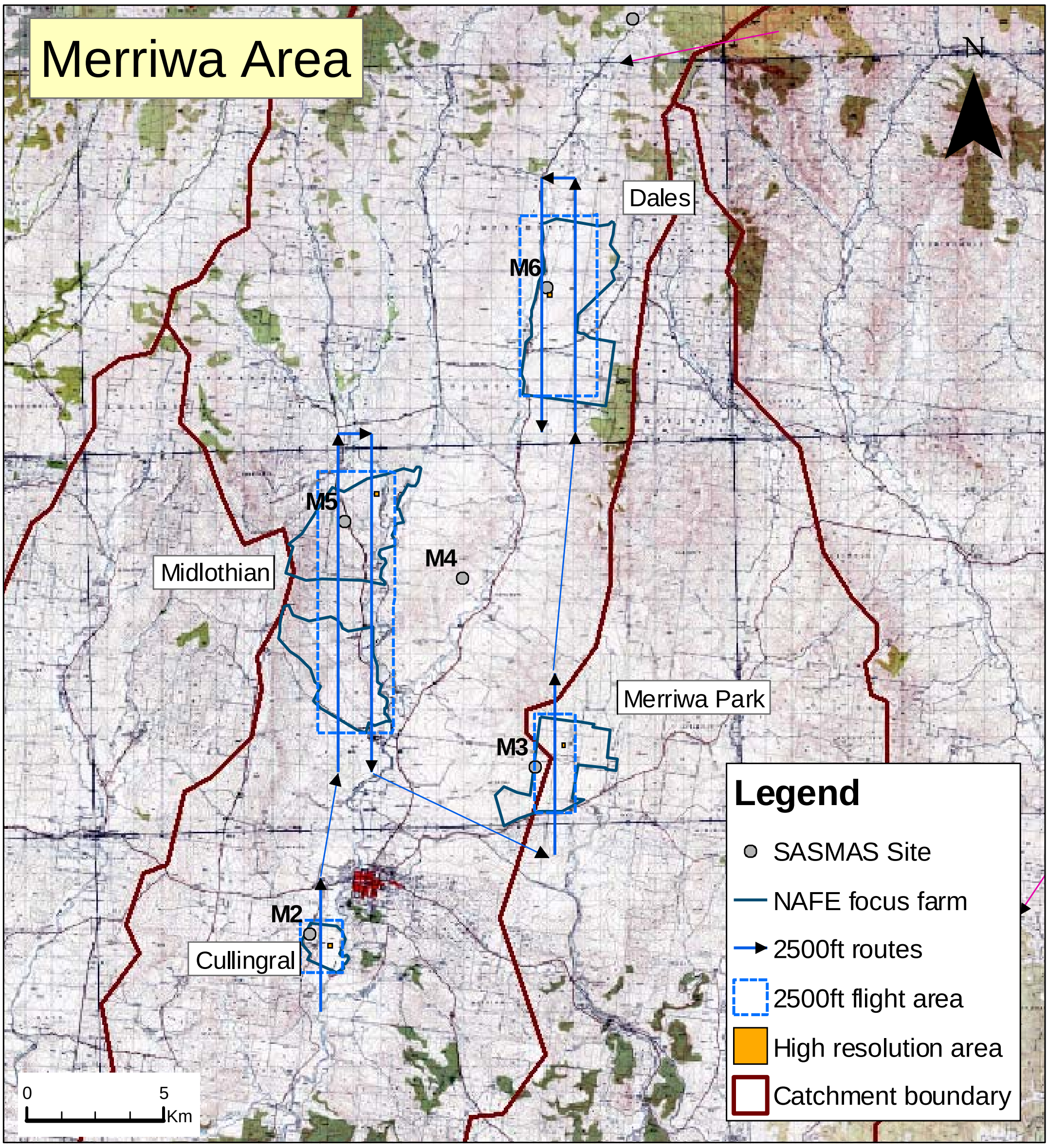

Figure 30. PLMR intermediate resolution flight lines over the Merriwa study area. Blue solid lines are the flight lines at 2,500ft altitude, dashed blue lines are the areas covered by the mapping.

Mapping at medium resolution will be undertaken at farm scale, at a nominal altitude of 2,500ft AGL, providing full coverage of all the NAFE focus farms at a ground resolution of approximately 250m. Actual flight altitude for these flights will be variable between farms, due to terrain elevation. Unlike for the low and intermediate flights, terrain elevation has a major impact on the ground resolution obtainable from these altitudes. In particular, due to the different mean elevations of the focus farms, it is not feasible to fly the whole medium resolution flight line set with constant altitude above sea level. This would in fact result in highly variable ground resolution. With the aim to maintain the highest possible consistency between the soil moisture maps, a decision was made to fly at 2,500ft (and 625ft for the high resolution flights) above the maximum elevation within each farm. This will guarantee greater uniformity in ground resolution as well as respect of the minimum flight altitude allowed without a low-level clearance, being 500ft. As for the medium resolution flight lines, flight altitude will vary between 1050m and 1270m ASL for the respective farms (see Appendix C),

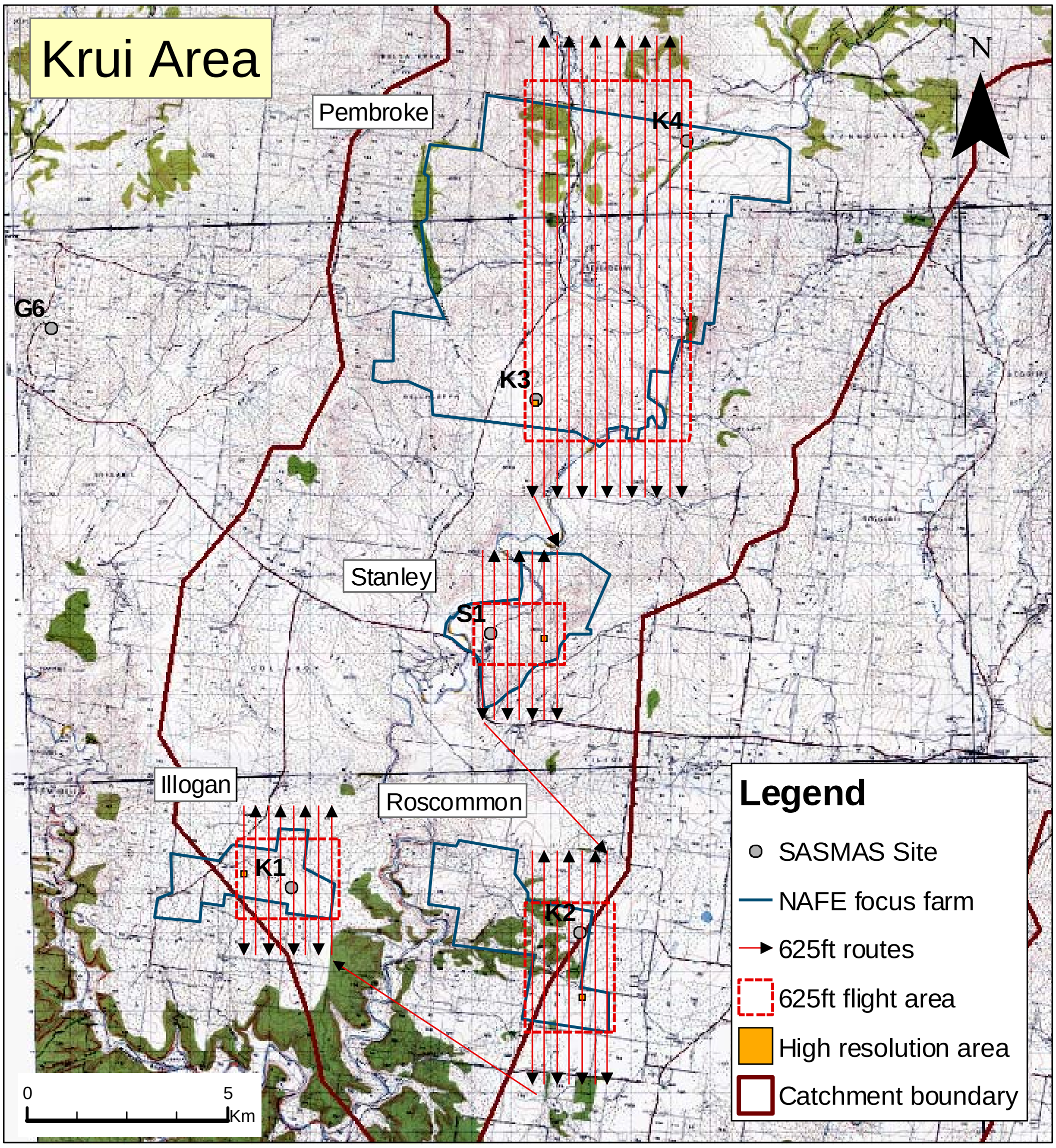

Figure 31. PLMR high resolution flight lines over the Krui study area. Red solid lines are the flight lines at 625ft altitude, dashed red lines are the areas covered by the mapping

resulting in a ground resolution between 240m and 308m.(see table C2 Appendix C for details) Medium resolution flight lines are described in Figs. 29 and 30 and Tables A5 and A6 in Appendix A.

6.5 High resolution mapping

The most important phase of the NAFE '05 campaign will be the monitoring of soil moisture at high resolution. PLMR will be flown at a nominal altitude of 625ft AGL to provide a nominal grid of 62.5m average near-surface soil moisture. Such a high resolution in passive microwave remote sensing is unprecedented, and will give the opportunity to study the microwave emission from the soil surface at very high detail. Together with the thermal-infrared, near-infrared and visible sensors onboard the SERA, the data provided by PLMR will allow development of downscaling techniques from coarser resolution measurement. The relatively small size of the ground pixels will also overcome one of the biggest problems faced by remote sensing validation campaigns in the past; relating ground point measurements

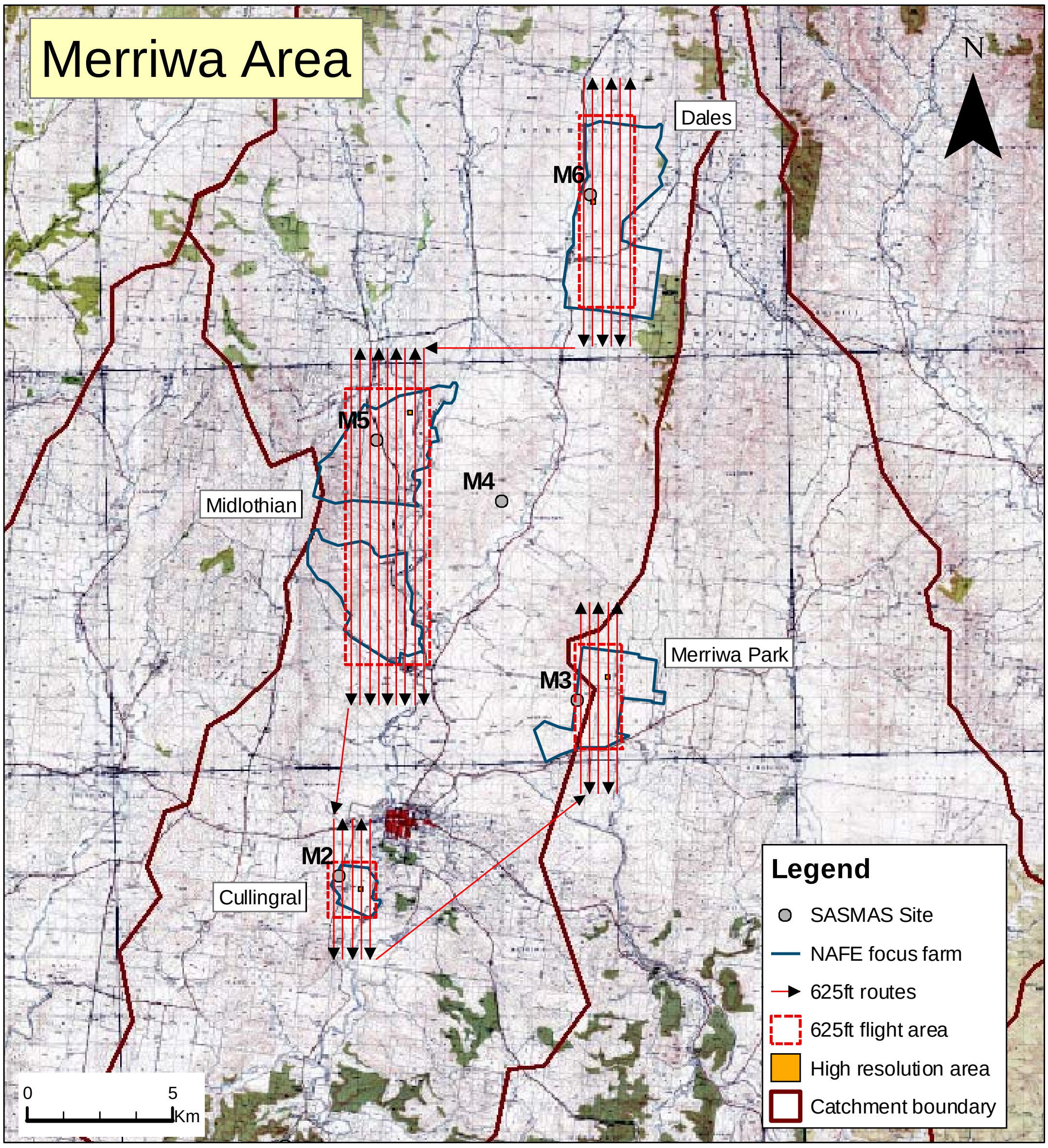

Figure 32. PLMR high resolution flight lines over the Merriwa study area. Red solid lines are the flight lines at 625ft altitude, dashed red lines are the areas covered by the mapping

as being representative of the soil moisture content for a much larger and non-uniform area for remote sensing validation. The validity of such an assumption is obviously weak and has been a constraint for accurate validation of satellite soil moisture products to date. During NAFE '05, intense ground sampling of soil moisture on the areas covered by high resolution aircraft mapping will provide highly detailed evaluation of the PLMR soil moisture product over a range of topographic and land cover conditions.

High resolution mapping flights will therefore be the core of the NAFE '05 aircraft campaign. Each farm will be mapped at 62.5m resolution twice a week (see Table 8) concurrently with intense ground monitoring of soil moisture as described in previous sections. The time to cover the single farm will be small (approximately 20 minutes) therefore there shouldn't be any appreciable time variation in soil moisture or temperature affecting the patterns. High resolution flight lines are described in tables A7 and A8 in Appendix A and illustrated in Figs. 31 and 32 for the Krui and Merriwa area focus farms. The actual flight altitude for this set of flights will vary between 480m and 700m ASL for the respective farms, resulting in a ground resolution between 51m and 121m (see table C3 Appendix C for details).

6.6 Multi-incidence mapping

A number of high resolution flights have been scheduled for the specific purpose of answering the important science question of multi-incidence angle retrieval of soil moisture. During these flights PLMR will be mounted on the SERA so as to have the 6 beams looking along the flight direction, 3 forward and 3 backward. In contrast to the "pushbroom" configuration, this set up will allow the same location on the ground to be remotely observed at three or more different incident angles. Given that every observation at a particular angle is bi-polarised, this will provide a set of six or more independent brightness temperature observations. The combination of these measurements potentially allows retrieval of auxiliary data in addition to soil moisture. Together with intensive ground sampling, these observations will provide a useful dataset to investigate multi-angle retrieval techniques.

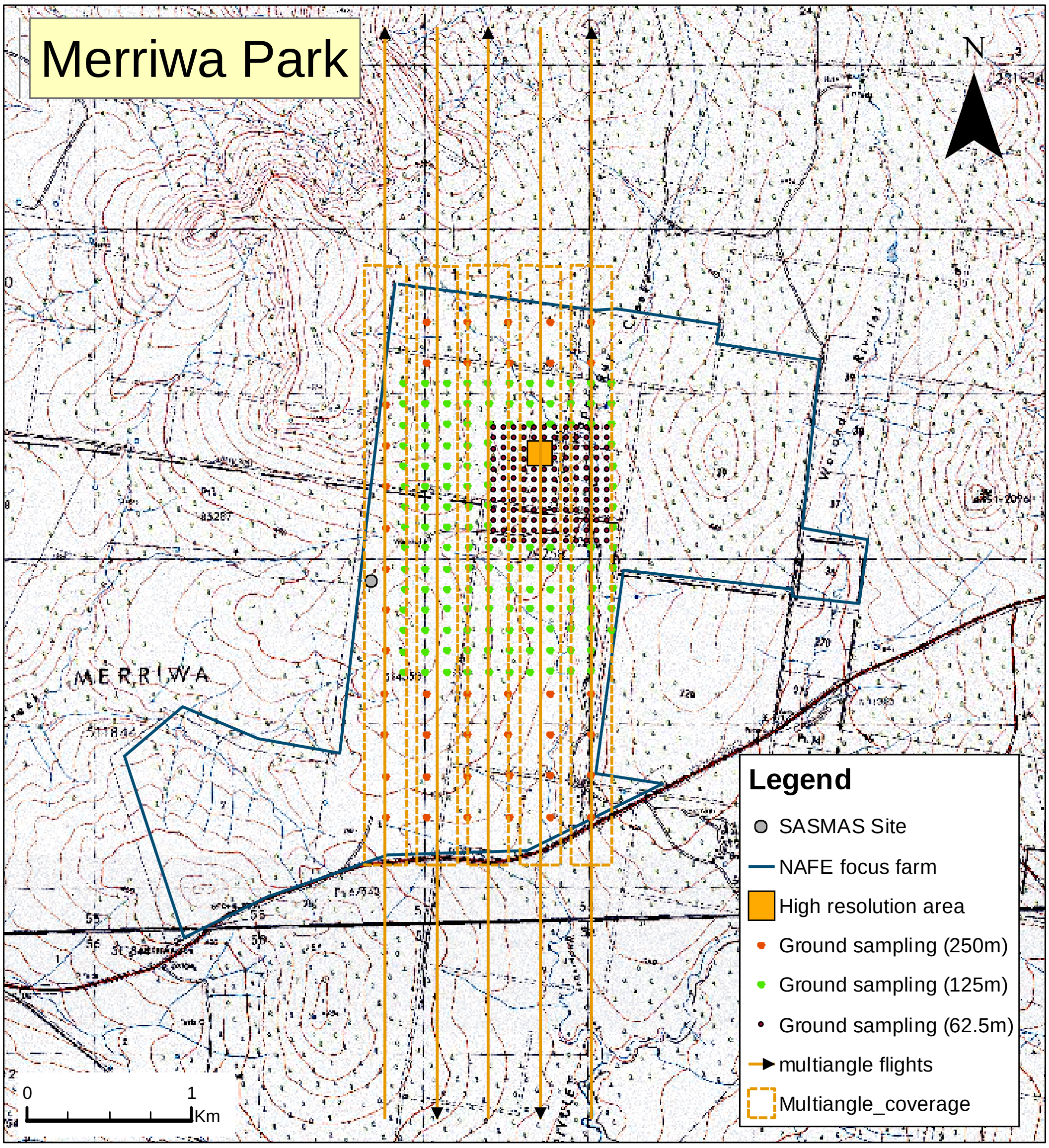

Figure 33. PLMR multi incidence angle flight lines over the Merriwa study area. Orange solid lines are the flight lines at 2,500ft altitude, dashed orange lines are the areas covered by the mapping in multi-angle configuration.

Multi-incidence observations will be undertaken at one particular farm, Merriwa Park in the Merriwa study area, on the same days when the area will be covered by multi-scale flights (see flight schedule in Table 8). Therefore, this experiment won't require extra ground sampling apart from the regular one. The Merriwa Park farm has been chosen for this experiment due to his smooth topography and easy accessibility, which makes it very suitable for the intensive farm scale ground sampling required for this experiment. Furthermore, due to is proximity to Scone Airport, this will make sure that multi-incidence angle flights won't interfere too much with the regular multi-scale flights held on the same day. For this experiment, PLMR will be flown following the high resolution routes over the farm, as described in previous sections, but at a nominal altitude of 2,500ft AGL.(1210m ASL) This will provide multi-angle coverage of the farm at a nominal resolution of 250m., with a range between 239m and 272m Fig. 33 illustrates this set of flight lines. As seen in the plot these flights are not expected to provide full coverage of the farm area, due to the distance between the flight lines being larger then the swath from that altitude. The start and end point coordinates are given in table A9 in Appendix A.

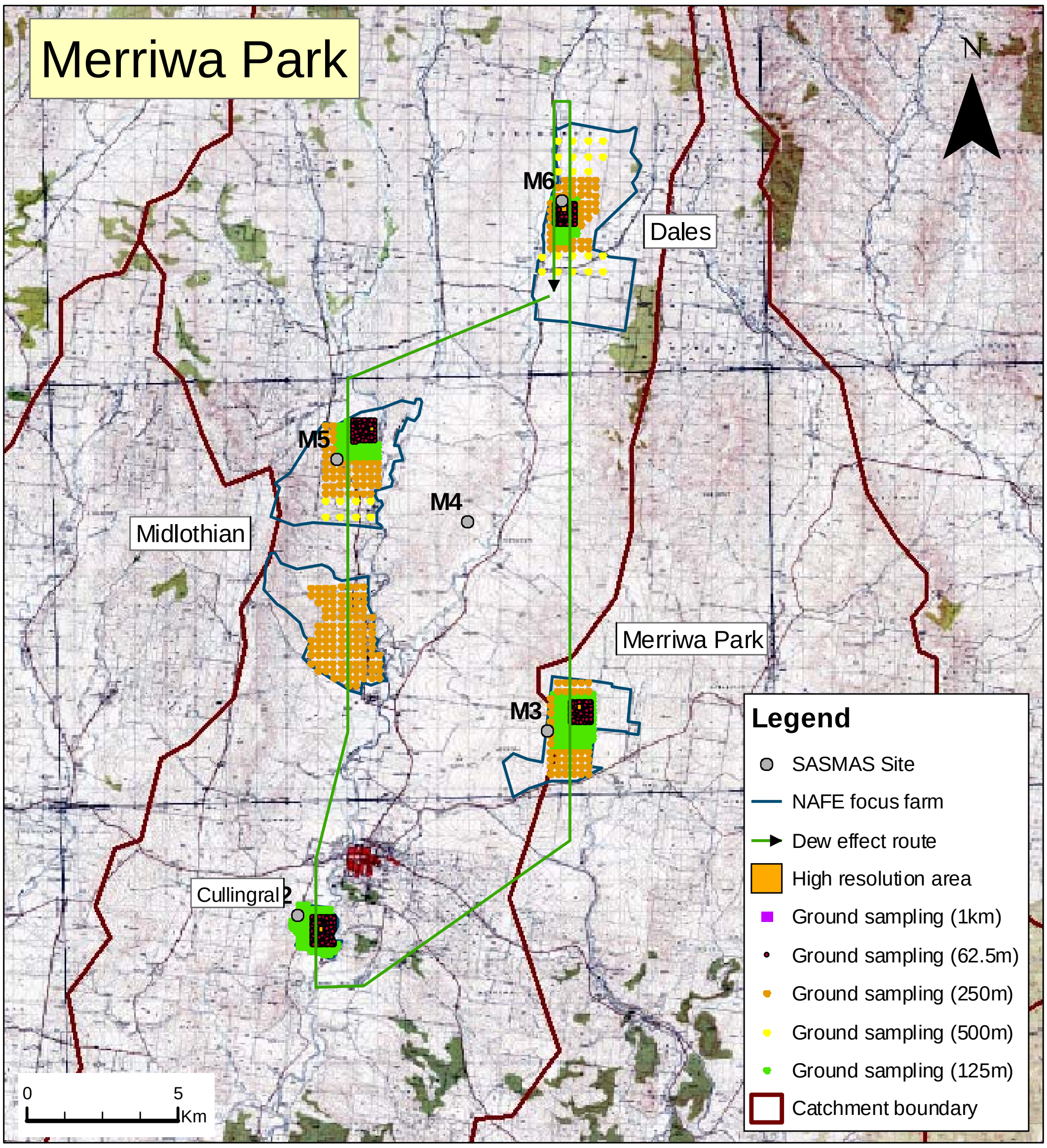

Figure 34. PLMR dew effect flight lines at 5,000ft over the Merriwa study area.

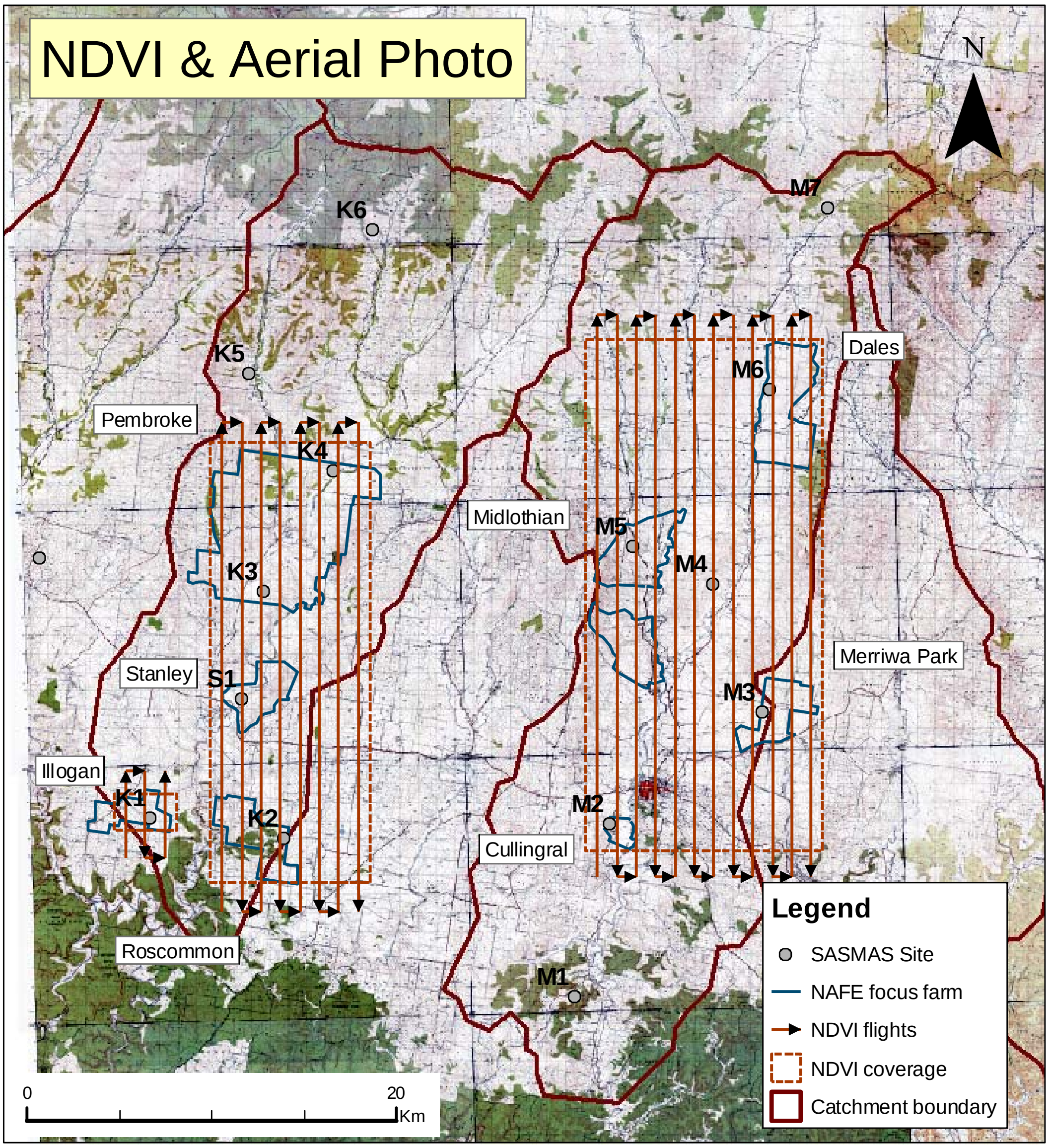

Figure 35. Flight lines for NDVI observations and aerial photography at 5,000ft over the Goulburn study area.

6.7 Dew effect

In order to analyse the effect of vegetation dew on the soil microwave signal, an early morning flight will be undertaken in the Merriwa area during some of Merriwa area sampling days. It is hypothesised that by comparison with the regular flights later in the day, this data will allow quantification of the role of vegetation dew on the microwave emission from the soil surface. Dew effect flights will include a loop covering the 4 focus farms in the Merrriwa area, as shown in Fig. 34. One single loop will be flown as early in the morning as possible. The nominal altitude for this flight will be 5,000ft AGL. This will allow direct comparison with the multi-scale 5,000ft flights over the area later on during the day. The actual flight altitude will be 1910m ASL, resulting from flying over the mean elevation of the Merriwa study area. This will result in a ground resolution between 405m and 554m. Subsequent to this loop the aircraft will return to Scone airport and take off for the regular multi-scale flights later in the day, when the dew has dried off. The coordinates of the main waypoints in the dew effect flight loop are listed in Table A10 of Appendix A.

6.8 NDVI

The Normalized Difference Vegetation Index, calculated from the visible and near-infrared radiation reflected by the vegetation, is a very useful parameter to characterise biomass density over large areas. For radiative transfer microwave modelling purposes, it is very important to collect information about the spatial and temporal variability of this quantity in order to properly quantify the masking of the microwave signal emitted from the soil by the vegetation canopy. For this purpose, the Tri-Spectral NDVI scanner onboard the SERA will be used to obtain high-resolution NDVI measurement for the study area. Given that NDVI is not expected to vary significantly over a 1 month time period, NDVI flights will be limited. On a date prior to commencement of the field campaign (~October 28th), a dedicated NDVI flight will be undertaken to cover the Krui and Merriwa sub-areas (see Fig. 35). This flight will have a nominal altitude of 5,000ft AGL, actual flight altitude 1910m ASL, resulting in a ground resolution of approximately 2m. Subsequently and depending upon instrument availability, two other full coverage flights are planned on two dates during and at the end of the campaign, to ensure temporal variation is captured. NDVI flight lines are described in Table A11 of Appendix A.

6.9 Aerial photography

High resolution aerial photo coverage of the Northern Goulburn study area will be undertaken concurrently with NDVI observations on the flight prior to the field campaign start only. Refer to section 6.8 for flight line details.

6.10 Calibration

The polarimetric L-band multibeam radiometer needs “warm” and “cold” calibration before, during and after each flight. The before and after flight calibrations are achieved by removing PLMR from the aircraft and making brightness temperature measurements of a calibration target and the sky (Fig. 36). The during flight calibration is accomplished by measuring the brightness temperature of the sky during a series of steep turns and of a water body. The water body is Lake Glenbawn, located approximately 100km east of the study area (Fig. 37). Ground requirement are the monitoring of the water temperature and salinity within the top 1cm layer of water. Both quantities will be monitored continuously during the campaign using a UNIDATA 6536B® temperature and salinity sensor connected to a logger, located at LAT & LONG to be defined. Furthermore, transects of water temperature and salinity in the top 1cm layer will be undertaken with a handheld temperature and salinity meter (Hydralab Quanta®) on four occasions. This will involve making 2km long north-south and east-west transects at 100m spacing once per week, centred on the monitoring station. The purpose of these measurements is to check for spatial variability. The air crew located at Scone airport will be responsible for these measurements.

Figure 36. Undertaking a sky cold point calibration with PLMR and the calibration box used for warm point calibration.

6.11 Flight schedule

All the flights described in the previous sections will be coordinated as per the calendar shown in Table 8. On regional days only low resolution flights will be undertaken covering the whole Northern Goulburn study area, concurrently with AMSR overpasses as described in section 2.1. The other days of the week will be occupied alternatively by multi-scale coverage of the two sub-areas, the Krui catchment and the Merriwa catchment. On these dates, flights will be undertaken at low, intermediate, medium and high resolution in this order. All the sub-area will be entirely covered at each altitude, before descending to the following altitude. In Table 8 tentative NDVI flights are also indicated.

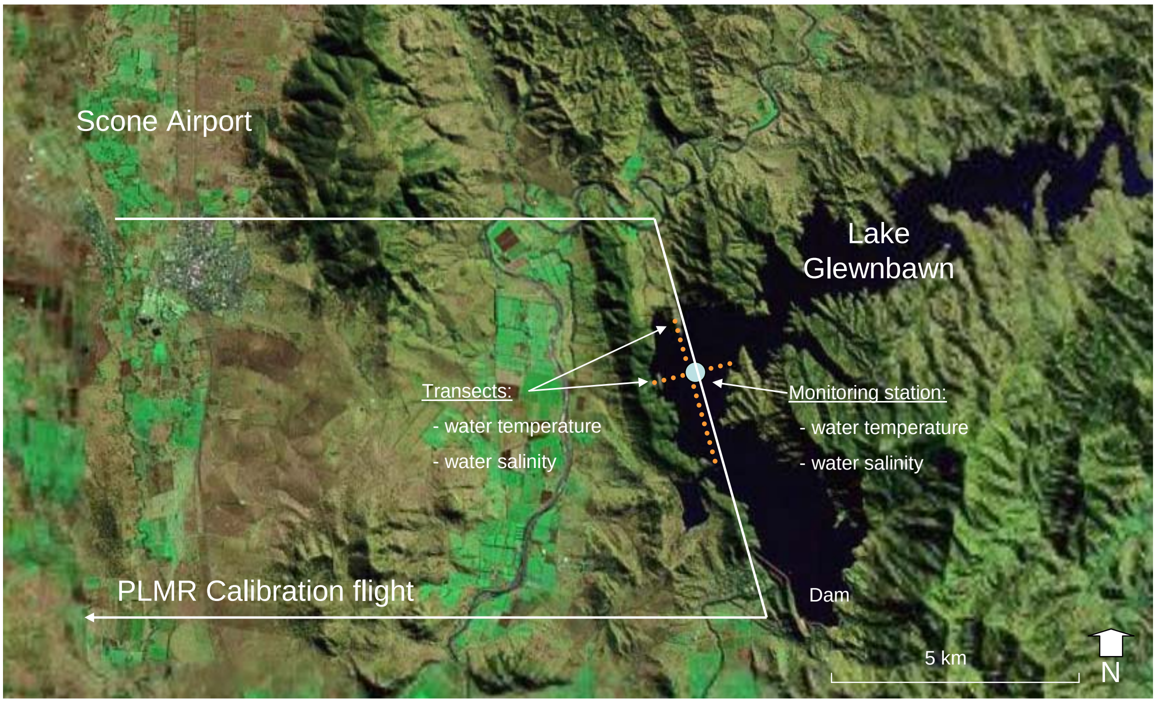

Figure 37. The location of Lake Glenbawn and Scone airport. The calibration flight line is schematically shown in solid white line. Dotted orange lines schematically indicate the planned water temperature and salinity transects. The approximate location of the permanent monitoring station is shown in blue.

Table 8. Schedule of flights during NAFE’05

	Mon 24/10	Tuey 25/10	Wed 26/10	Thur 27/10	Fri 28/10	Sat 29/10
Norhern Goulburn						
	Mon 31/10	Tue 1/11	Wed 2/11	Thur 3/11	Fri 4/11	Sat 5/11
Norhern Goulburn						
Krui Area						
Merriwa Area						
	Mon 7/11	Tue 8/11	Wed 9/11	Thur 10/11	Fri 11/11	Sat 12/11
Norhern Goulburn						
Krui Area						
Merriwa Area						
	Mon 14/11	Tue 15/11	Wed 16/11	Thur 17/11	Fri 18/11	Sat 19/11
Norhern Goulburn						
Krui Area						
Merriwa Area						
	Mon 21/11	Tue 22/11	Wed 23/11	Thur 24/11	Fri 25/11	Sat 26/11
Norhern Goulburn						
Krui Area						
Merriwa Area						

Low resolution Intermediate res. Medium res. High resolution

Multi-angle Dew effect NDVI & Photo NDVI (tentative)

This general schedule is likely to be affected by the weather conditions. In case of clouds, flights might be only partially completed, as per the following criteria

- On regional sampling days, flight altitude will be moved below the clouds. If clouds are lower than 5000ft no flights will be undertaken;
- On farm sampling days, only the flights with altitude lower then the clouds will be undertaken. If clouds are lower then the 2500ft no flights will be undertaken.

The flying time saved during these dates is expected to be used for extra NDVI mapping flights.

For logistic purposes, it is important to maintain the total number of hours flown in any single flight to around 4-5 hours and a daily total of not more than 6 hours, to allow time for pre-flight and post-flight activities on the PLMR and on the aircraft. This represented a major constraint in the planning of flight lines. Table 9 reports the estimated flight hours, including individual estimates for each set of flight lines and a summary of the daily total. As shown, the total number of hours is slightly higher then allowed (92 hours) for the whole field campaign. Nonetheless, the effective total is likely to be smaller due to possible adverse weather conditions resulting in cancelled flights and conservative flight time estimates. The estimates for NDVI/photography flights is not included in this total as the initial flight will be done on a separate aircraft, meaning that these hours do not count towards the aircraft maintenance requirement. While the second and third NDVI flights are planned for the same aircraft, it is expected that hours for this will become available due to cancellation of two or more days of flying as a result of poor weather conditions. The NDVI flights have been estimated at 4.4 hours.

Table 9. NAFE'05 flight times. Times have been calculated assuming the indicated aircraft speed.

Flight	Distance (Km)	Aircraft Speed (Km/h)	Flight Time (hrs)
Calibration	25.0	144	0.2
Ferry Scone airport-Krui area	143.1	180	0.8
Ferry Scone airport-Merriwa area	82.7	180	0.5
Ferry Scone airport-AMSR area	129.3	180	0.9
Low resolution regional area	385.4	144	2.7
Krui area			
Low resolution	26.5	144	0.2
Intermediate resolution	84.5	144	0.6
Medium resolution	129.8	144	0.9
High resolution	262.3	144	1.8
Merriwa area			
Low resolution	61.0	144	0.4
Intermediate resolution	162.5	144	1.1
Medium resolution	77.7	144	0.5
High resolution	250.0	144	1.7
Multiangle flights	35.0	144	0.9
Dew effect flights	64.4	144	1.1
Summary			
Regional days (Cal + Ferry + Low resolution)			**3.7**
Krui days (Cal+Ferry+Low+intermediate+medium+high)			**4.5**
Merriwa days (Cal+Ferry+Low+intermediate+medium+high)			**4.5**
Merriwa days + multiangle flights			**5.3**
Merriwa days + dew effect flights			**5.5**
TOTAL CAMPAIGN (4 weeks)			**93.8**

7 Field Work

7.1 General guidance

Sampling is conducted **every day**. It is canceled by the group leader if it is raining, there are severe weather warnings or a logistic issue arises.

- **Know your pace**. This helps greatly in locating sample points and gives you something to do while walking.
- All farmers in the area are aware of our presence on their property during the 4 weeks field campaign. However, if anyone questions your presence, politely answer identifying yourself as a scientist working on a University Of Melbourne soil moisture study with satellites. If you encounter any difficulties **just leave** and report the problem to the group leader.
- Although gravimetric and vegetation sampling are destructive, try to **minimise your impact** by filling holes. Leave nothing behind.
- When sampling on cropped areas, always sample or move through a field along the **row direction** to minimise impact on the canopy.
- Please be considerate of the landowners and our hosts. **Don't** block roads, gates, and driveways. Keep sites, labs and work areas clean of trash and dirt.

- Avoid driving through cropped areas.
- Beware of the possible presence of stocks in the sampling areas.
- Watch your **driving speed**, especially when entering towns. Be courteous on dirt and gravel roads, lower speed=less dust.
- Drive carefully and maintain a low speed (~4 km/h) when going through tall grass fields. Hidden boulders, trunks or holes are always a danger.
- When parking in tall grass for prolongated periods of time, turn off the engine. The catalytic converters can be a **fire hazard**.
- **Close any gate** you open as soon as you pass.
- **For your own security, carry a cell phone or UHF transmitter. Check the mobile phonecoverage over your sampling area** and be aware of the local UHF securityfrequencies.
- In case of breakdown of any part of the sampling equipment, **report immediately** to the group leader.

7.2 Focus farms

Sampling of the farm area is intended to provide near-surface (0-5cm) hydra probe soil moisture measurement across the farm at the highest possible resolution, provided all the accessible areas on the property are covered by sampling. Together with soil moisture, supporting information are needed, for purposes of microwave emission modelling and the characterization of the land cover distribution in the area.

The person responsible for farm scale sampling (generally this will be each team's leader, see Table 12) will be required to measure or characterise the following quantities (**for detailed description on the sampling procedures, please refer to section 7.5**):

- 0-5cm soil moisture using the Stevens water Hydra Probe® instrument at each sampling location;
- 0-5 cm gravimetric soil moisture (also used for soil texture and soil bulk density): a minimum of two samples are required, 1 dry and 1 wet. Location of these samples should vary from day to day in order to cover different soil types;
- Dew present at the location. A numeric code will be used to represent the amount: 0 = no dew; 1=some dew; 2=a lot of dew. This is a purely qualitative measure. (this is only required until dew dries off completely);
- Vegetation type at each location
- GPS locations of all sample point locations

The soil moisture measurements will be taken on grids that will generally vary between farms (see section 4.7.2). The planned sampling locations for each farm will be loaded onto the iPAQ, and visible with the GIS software ArcPad. Sampling will involve navigating to the sampling location through the use of the GPS receiver, which displays the real-time position on the same ArcPAd screen where the sampling grid is visible, and then once located the point takes all the required measurements. All the measurements will be electronically stored in the iPAQ, by prompting the values into forms. For details see section 7.5.1.

Each person responsible for the farm scale sampling will be equipped with the items listed below. The person will be individually responsible for the use and care of the equipment throughout the campaign, and must report any damage to the group leader immediately so that actions can be taken to repair or substitute the damaged item.

- 1 4WD vehicle or quad bike
- 1 iPAQ pocket PC
- 1 wireless GPS receiver
- 1 Stevens Water Hydra Probe Stevens water Hydra Probe®
- 1 Bumpack
- 1 Gel cell battery
- 1 Gel cell battery connector
- 1 spare gel cell battery
- 1 soil sampling kit including: sampling ring (approximately 7.5cm diameter and 5cm depth), hammer, garden trowel, blade, gloves, plastic bags, rubber bands, permanent markers;
- 1 hardcopy of the farm sampling plan
- 1 fieldbook
- 1 UHF receiver.
- Pen

7.3 High resolution focus areas

High resolution areas are 150m x 150m in size and are intended to provide high resolution near-surface soil moisture measurements for the validation of the PLMR high resolution passive microwave observations. Within each farm, 1 such area has been selected as explained in section 4.7.2. In every team there will be 2 people specifically dedicated to the sampling of these areas (in the morning) and the surrounding 62.5m grid (in the afternoon).

The personnel responsible for the focus areas will be required to measure or characterise the following quantities (**For detailed description on the sampling procedures, please refer to section 7.5**):

- 0-5cm soil moisture using the Stevens water Hydra Probe® instrument at each sampling location;
- GPS locations of all sample point locations (only in the afternoon for 62.5m sampling , NOT for high resolution areas)
- Vegetation water content: 2 samples ("grab" type, see section 7.6.4) at the end of the day at two corners of the high resolution areas (farm reference vegetation). The location of these samples will remain the same throughout the campaign.
- Vegetation dew: 2 samples ("grab" type) at the beginning of the day at two corners of the high resolution areas (farm reference vegetation). The location of these samples will remain the same throughout the campaign. These samples will be required only when dew effect flights are scheduled for the day (see Table 8).

Each person responsible for the farm scale sampling will be equipped with the items listed below. The person will be individually responsible for the use and the care of the equipment throughout the day, and must report any damage to the group leader immediately so that actions can be taken to repair or substitute the damaged item.

- 1 iPAQ pocket PC
- 1 wireless GPS receiver
- 1 Stevens Water Hydra Probe Stevens water Hydra Probe®
- 1 Bumpack
- 1 Gel cell battery
- 1 Gel cell battery connector

- 1 spare gel cell battery
- 1 vegetation sampling kit including: quadrant (50cm x 50cm), vegetation clipper, scissor, gloves, plastic bags, rubber bands, permanent markers
- 1 hardcopy of the farm sampling plan
- 1 fieldbook
- Pen

Morning

The high resolution areas will be clearly marked prior to the field campaign with 4 pegs (1.5m high) in the 4 corners of the 150m x 150m grid. Given that some of these areas will be in paddocks with crops up to 1m high, the top of the pegs will be coloured white, ensuring that they will are clearly visible. Pegs will remain in place during the entire campaign and are not to be removed. The area within the grid is to be sampled at two different resolutions: the whole grid (150m x 150m) will be sampled on a 12.5m grid, while an inner sub-grid (75m x 75m) will be the object of a 6.25m intensive sampling. The sampling resolution chosen is intended to maintain consistency between the PLMR observations (aboard the aircraft) and the ground sampling for data upscaling and downscaling purposes. The sampling will be undertaken using Stevens water Hydra Probe® to take one 0-5cm soil moisture reading at each point of the 12.5m and 6.25m grids. The probe readings will be stored electronically in the

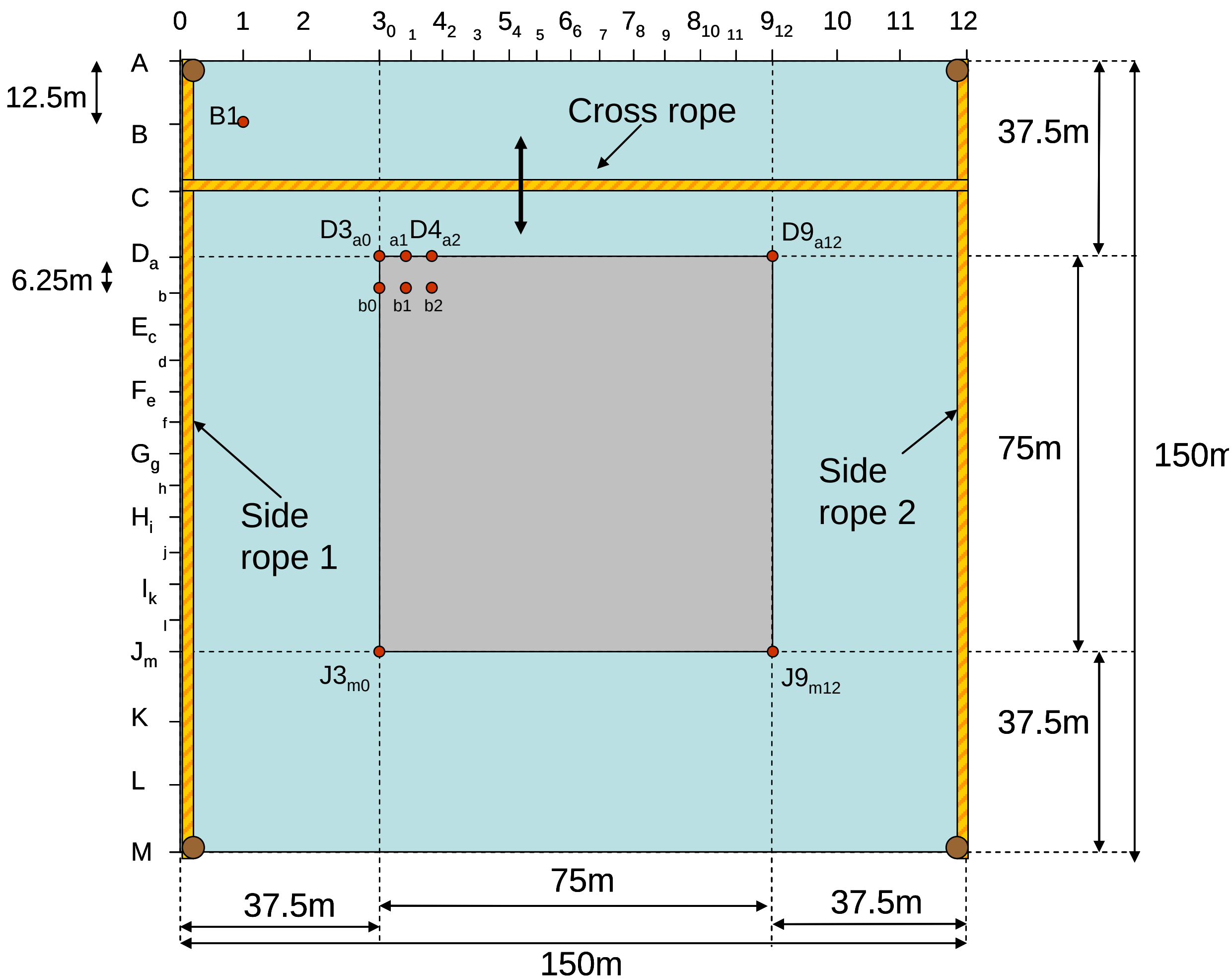

Figure 38. High resolution sampling scheme. In striped orange are indicated the ropes on the ground

iPAQ (see section 7.5.1).

The 12.5m and 6.25m sampling points will be marked by use of ropes labelled at 12.5m and 6.25m spacings. The system is explained hereby and illustrated schematically in Fig. 39. Two of the ropes (side rope 1 and side rope 2) will be laid prior to the field campaign and will remain in place for the entire four weeks. These ropes will be labelled with alphabetic characters; 12.5m points will be labelled with upper case, from “A” to “M”, 6.25m points will be marked with lower case letters, from “a” to “m”, starting at 37.5m from the edge of the high resolution area and forming an inner grid of 75m x 75m. The cross rope, will be removable, and will be laid at the beginning of each sampling day and collected at the end of the day, to be used on the other farm the next day. On this rope 12.5m points will be marked with large numbers from 0 to 12, while 6.25 m will be marked with small numbers from 0 to 12. Each point will therefore be uniquely identified by a letter/number combination (eg, B14). As shown in Fig.38, where a point belonging to the 12.5m grid will overlap a point belonging to the 6.25m grid, the point will be identified with both labels.

The sampling strategy for the two people dedicated to the high resolution areas will be the following:

- Upon arrival at the high resolution area in the morning, lay down the cross rope on row “A” between points A0 and A12.
- Sample row “A” converging to the middle from the side ropes (i.e. 1 person starts at A0, the other at A12, and meet in the middle)
- When finished the row, move the cross rope to next row “B” and repeat the sampling.
- When at row Da (beginning of 6.25m inner grid), sample all the points on the row in sequence
- When finished all the grid, remove the cross rope.

Some useful items on this sampling strategy are:

- Due to the length of the cross rope (150m) and the presence of vegetation (up to 1m high in places), the process of moving the rope sideways and tending it between the two side ropes can be difficult. It is suggested that the rope be moved in the following manner:
    1. When the two people sampling the hi-resolution grid meet in the middle of the rope, together, they should pick up the rope and walk approximately 12.5m (or 6.25m) in the direction the rope is to be moved
    2. Still holding the rope securely, each individual should walk back towards their respective side ropes
    3. Upon reaching the side rope untie the cross rope and move to the next sampling point along the side rope
    4. Pull the cross rope tight from each end so it clears the ground and then lay it down.
    5. Tie the cross rope to the side rope and begin sampling.
- In the inner 75m x 75m square, where the 12.5m grid is overlapped with the 6.25m grid, it is recommended to sample all the points in sequence as they appear on the rope, NOT the 12.5m before and the 6.25m after.

The planned sampling grids for each high resolution area will be loaded onto the iPAQ, and visible with the GIS software ArcPad. Sampling will involve navigating to the sampling location using the ropes and taking the measurements which will be electronically stored in the iPAQ, by prompting the values into forms. For details see section 7.5.1.

Afternoon

In the afternoon the people responsible for high resolution areas will be required to sample the 62.5m planned sampling grid, taking 0-5cm soil moisture sampling with Stevens water Hydra Probe® at each point. The 62.5m sampling grid will have to be divided between the two personnel by mutual agreement in order to optimise the sampling time.

The planned sampling locations for each farm will be loaded onto the iPAQ, and visible with the GIS software ArcPad. Sampling will involve navigating to the sampling location through the use of the GPS receiver, which displays the real-time position on the same ArcPAd screen where the sampling grid is visible, and then once located the point take all the required measurements. All the measurements will be electronically stored in the iPAQ, by prompting the values into forms. For details see section 7.5.1.

7.4 Regional sampling

Regional sampling will take place every monday and is intended to provide large scale (1km) near surface soil moisture measurements for validation of the PLMR and AMSR-E soil moisture product, as well as for scaling purposes as outlined in the objectives section of this work plan. On these dates, the sampling operations will be divided into 2 main phases:

- Soil moisture sampling across the region (including farms) at 1km resolution
- Vegetation sampling at the high resolution and surrounding areas

7.4.1 Soil moisture sampling at regional scale

Teams will sample at 1km spacing the two respective farms, one in the Merriwa and one in the Krui area (see Table 12), as well as the areas immediately adjacent to the main roads connecting the two farms. At each sampling location, teams will be required to measure or characterise the following quantities (**for detailed description on the sampling procedures, please refer to the section 7.6**):

- 0-5cm soil moisture using the Stevens water Hydra Probe® instrument at each sampling location;
- Landuse (on week 2 only);
- Vegetation type (on week 2 only);
- Dew present at the location. A numeric code will be used to represent the amount: 0 = no dew; 1=some dew; 2=a lot of dew. This is a purely qualitative measure. (this is only required until dew dries off completely);
- Percentage of surface rock cover: visual estimation and digital photography. This is to be done only on one occasion;
- GPS locations of all sample point locations

Furthermore, the following quantities will need to be measured throughout the day, following the indicated criteria.

- Vegetation Biomass: a minimum of 6 samples **per farm**, aiming at the dominant vegetation cover type in each farm;

- 0-5 cm gravimetric soil moisture (also used for soil texture and soil bulk density): a minimum of 6 samples **per farm** are required, aiming at different soil types and wetness conditions;
- Surface roughness using pin profiler: a minimum of 4 measurements per farm are required. This is to be done only on one occasion due to instrument availability

The soil moisture measurements will be taken on grids that will generally vary between farms (see section 4.7.2). The planned sampling locations for each farm will be loaded onto the iPAQ, and visible with the GIS software ArcPad. Sampling will involve navigating to the sampling location through the use of the GPS receiver, which displays the real-time position on the same ArcPAd screen where the sampling grid is visible, and then once located the point take all the required measurements. All the measurements, apart from the surface roughness, will be electronically stored in the iPAQ, by prompting the values into forms. For details see section 7.5.1.

Each person responsible for the soil moisture sampling during regional days will be equipped with the items listed below.

- 1 iPAQ pocket PC
- 1 wireless GPS receiver
- 1 Stevens water Hydra Probe®
- 1 Bumpack
- 1 Gel cell battery
- 1 Gel cell battery connector
- 1 spare gel cell battery
- 1 vegetation sampling kit including: quadrant (50cm x 50cm), vegetation clipper, scissor, gloves, plastic bags, rubber bands, permanent markers
- 1 soil sampling kit including: sampling ring (approximately 7.5cm diameter and 5cm depth), hammer, garden trowel, blade, gloves, plastic bags, rubber bands, permanent markers;
- 1 hardcopy of the farm sampling plan
- 1 fieldbook
- Pen

7.4.2 Vegetation sampling at the high resolution areas and surroundings

Intensive vegetation sampling will be undertaken at each farm's soil moisture high resolution area by at least 2 team members not involved in the soil moisture sampling. Every high resolution area will have to be sampled in half a day, one in the morning and one in the afternoon, accordingly with the farm visited by the team. Sampling will involve measurements of the following quantities: (**for detailed description on the sampling procedures, please refer to the section 7.6**):

- Vegetation biomass: a minimum of 16 samples ("quadrant" type, see section 6.6.4)
- Vegetation height at each vegetation sampling site. This will be done only on week1 and week 4
- Vegetation Leaf area index (LAI): at each vegetation sampling site. This will be done on one week only during the campaign due to instrument availability.

- Vegetation Normalised Difference Vegetation Index (NDVI) at each vegetation sampling site. This will be done on one week only during the campaign due to instrument availability.

There will be a specific ground crew member dedicated to the LAI and NDVI measurement, which will rotate through the teams on regional days (i.e. will make measurement of LAI and NDVI on each week on different farms).

All the above quantities will be initially measured on a 50m grid in the high resolution area, subsequently on two transects at 62.5m spacing (centred on the high resolution area) in the surrounding areas. These additional measurements will be depending on time availability. This sampling scheme is illustrated in Fig. 40. At each sampling location all the above quantities will be measured, with some repeats for the LAI and NDVI measurement as indicated in section 7.4.2.1 and 7.4.2.2 below. It is suggested to first sample the high resolution area, then transect 1 from west to east, followed by transect 2 from south to north.

The group responsible for vegetation sampling during regional days will be equipped with the items listed below (collectively):

- 1 iPAQ pocket PC
- 1 wireless GPS receiver
- 1 Bumpack
- 1 Gel cell battery
- 1 Gel cell battery connector
- 1 spare gel cell battery
- 1 vegetation sampling kit including: quadrant (50cm x 50cm), vegetation clipper, scissor, gloves, plastic bags, rubber bands, permanent markers
- 1 hardcopy of the farm sampling plan
- 1 fieldbook
- Pen

- 1 LAI 2000 device
- 1 Handheld radiometer device

Normalised Difference Vegetation Index (NDVI)

NDVI measurements will focus on the 150m x 150m high resolution grid. A measurement will be taken at each of the 16 vegetation biomass and water content sample points on the high resolution grid. Upon completion of these 16 measurements over the high resolution grid, time permitting, NDVI measurements will then be taken on two transects of the 62.5m farm scale grid.

One of the ground crew personnel (Jose Fenollar) will be specifically dedicated to the NDVI and LAI measurements. He will rotate through the teams spending one day with each team on regional sampling days (Mondays), this way covering the LAI/NDVI requirements once per each farm during the campaign.

Leaf Area Index (LAI)

LAI measurements will also focus on the 150m x 150m high resolution grid and be made at the same locations as for NDVI measurements.

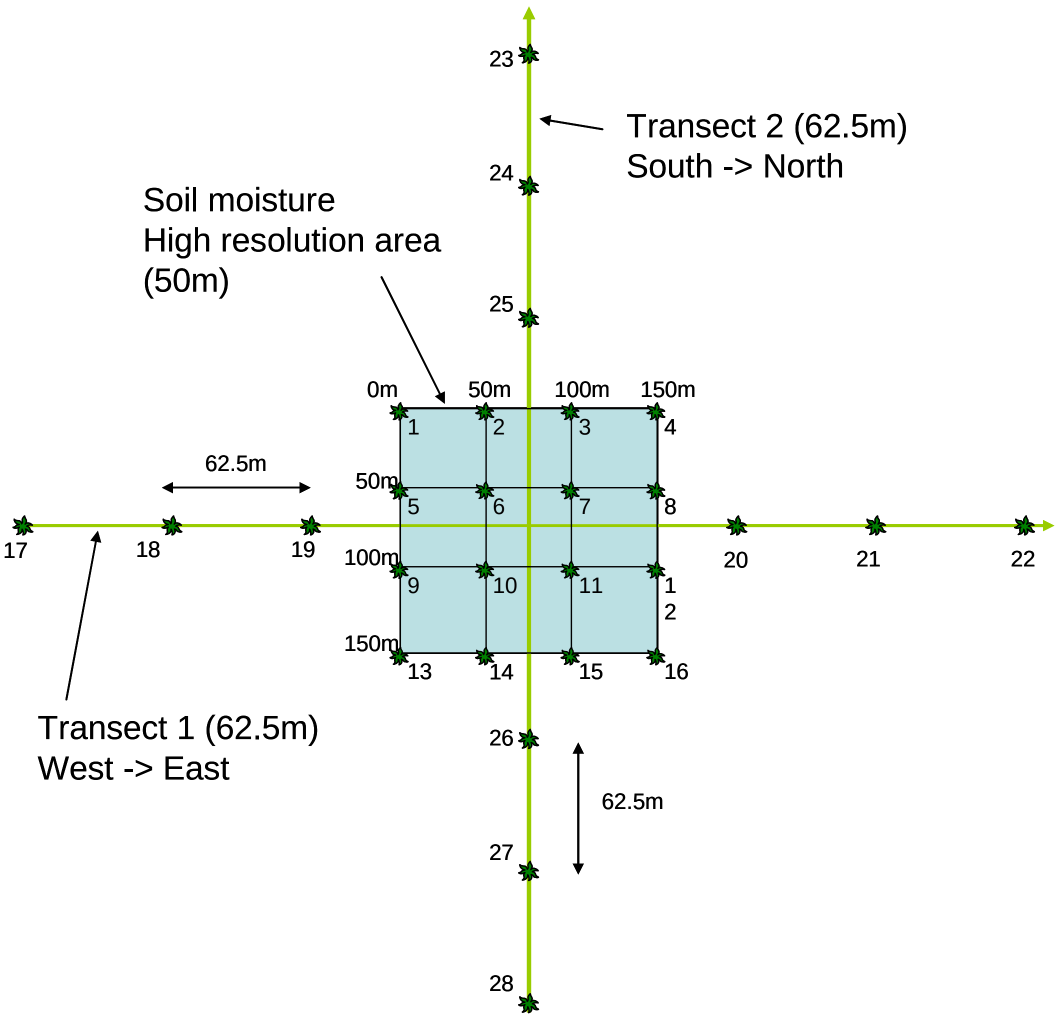

Figure 40. Vegetation sampling scheme for regional days

7.5 Sampling protocols

7.5.1 iPAQ procedures

Each person will be operating one of the iPAQs, for use with the Stevens water Hydra Probe®, both during regional and farm scale days. Every person will be responsible for their own iPAQ throughout the entire campaign. All iPAQs and accessories will be labelled with numbers, the same number indicating the accessories belonging to the same individual set. Basic items for the daily use of the iPAQ are the following:

Morning

- Check that the battery is at 100% recharge (Fig.41)

Start of sampling

- Take the iAPQ and GPS device out of the container. Install the iPAQ on the mount (see section 7.5.2)
- Ensure the gel cell battery, iPAQ, GPS receiver and hydra probe are all properly connected.
- Turn on the iPAQ by pressing the button at the top right corner of the device (Fig.41)

- Open ArcPad by tapping the program access icon on the top left corner of the iPAQ screen (Fig.41) and select "ArcPad".
- If working with GPS:
    - Turn on the GPS receiver
    - Establish a wireless connection between GPS and iPAQ (see below)
    - Activate the GPS in ArcPad, by tapping the "GPS" icon and selecting "GPS active"

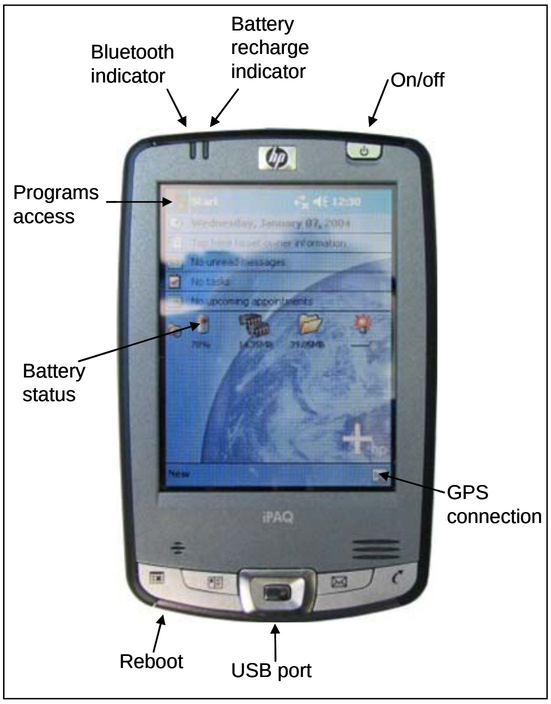

Figure 41. iPAQ basic features

During the day

- Ensure the iPAQ is constantly plugged into the gel cell battery. If so, the orange light on top of the device will be blinking (recharging) or still (fully recharged).
- Ensure the wireless connection with the GPS is active. If so the Bluetooth indicator on the iPAQ will be blinking blue.

Evening

- At the end of the sampling:
    - **Turn off** the iPAQ and the GPS device
    - Disconnect the iPAQ from the cables connected to its USB port
    - Disconnect the battery adaptor from the gel cell battery
    - Take the iPAQ off the mount and store it together with the GPS device in the iPAQ container. **DO NOT** leave the iPAQ on the mount, as it could get damaged during the car trip back to Merriwa.
- Download the data collected into the desktop computer in the right folders (see section 7.5.8 for detailed archiving procedures)
- Load into the iPAQ the blank files for the next day
- Plug the iPAQ for recharge and leave overnight

Connect the GPS to the iPAQ

A connection between iPAQ and the GPS device is required for (i) farm scale soil moisture sampling (1km, 500m, 250m or 125m resolution) (ii) high resolution area surroundings soil moisture sampling (62.5m resolution) and (iii) regional days soil moisture sampling.

The GPS device needs to be recognised by the iPAQ BEFORE activating the GPS from ArcPad, as explained in the previous section. To establish a wireless connection between iPAQ and the GPS device:

- Tap the "GPS connection" icon in the bottom right corner of the screen
- Activate Bluetooth by tapping the "Bluetooth" icon
- Select "Bluetooh Manager"

- Tap **and hold** the icon representing the GPS device you are connecting to, and select “connect”. If this is successful, two horizontal green arrows will, be added to the GPS device icon
- Exit from Bluetooth manager

iPAQ Troubleshooting

The iPAQ doesn’t respond to any input.
Perform a soft reboot of the device by GENTLY pressing the button on the bottom side of the device with the iPAQ pencil. The GPS connection will then have to be re-established and ArcPad started again. No data will be lost.

The iPAQ is dead, the battery indicator doesn’t blink despite the battery being properly connected.
The iPAQ battery is too low. Extract the battery, leave it disconnected from the device for 5 minutes, re-insert the battery and leave charging for at least 30 minutes, until the battery indicator starts blinking again.

The iPAQ doesn’t connect with the GPS device
Make sure the GPS device in turned on and charged

GPS Troubleshooting

There’s no GPS icon in the Bluetooth manager
The GPS device hasn’t been bonded with the iPAQ. Make sure the GPS device is turned on and charged. To bond the GPS device, tap “new” and select “explore a Bluetooth device”. When the GPS device is detected, tap the serial port option “SPP serial port”. When the bond is confirmed, tap “finish” and connect to the GPS device as explained above in “Connect the GPS to the iPAQ connection**”**

ArcPad Error: no fix GPS position
The GPS device is unable to determine a fix position. Stay in place and wait for a few minutes until a fix position is achieved.

ArcPad Error: too many data are received from your GPS device
Press ok and Ignore

7.5.2 HydraProbe sampling procedure

System set-up

The soil moisture measuring system will be set up as follows (see Fig. 42):

- Stevens water Hydra Probe® firmly attached at the bottom of a PVC pole
- iPAQ mounted on top of the pole. The Hydra probe cable is directly connected to the USB port at the bottom of the iPAQ (see Fig. 41), through a sequence of converters which will be firmly attached to the pole.
- The gel cell battery necessary to provide power to the iPAQ, the GPS device and the Hydra probe will be carried in a bumpack around the waist, together with the GPS device

- The gel cell battery will be connected to all the devices through a single cable running from the bumpack to the pole, firmly attached to the pole at waist height.
- Disconnection from the pole will be possible by unplugging the gel cell battery adaptor in the bumpack

The iPAQ has been programmed in order to automatically read the Hydra probe at the desired sampling location when a specific command is sent from the iPAQ, and storing the probe readings in a file together with the GPS coordinates provided by the GPS device. This is achieved with the software "ArcPad", a Geographic Information System for Handheld devices. Hereby the ArcPAd sampling procedures are described:

The ArcPad program developed for NAFE'05 to read the Hydra probe has essentially two functions:

Figure 42. Typical set up of a soil moisture measuring unit, with hydra probe communicating directly to an iPAQ and a wireless GPS receiver. Everything is powered by a battery carried by the user.

1. GPS mode: Stores the readings of the probe with the coordinates given by the GPS device. This will be used during the soil moisture sampling at farm scale and regional scale and will be active when the GPS is made active in ArcPad
2. GRID mode: Stores the readings of the probe with the coordinates of the points visited by the user on a predefined grid. This will be used for the sampling of the high resolution areas, where the predefined grid is that illustrated in section 7.3. This mode will be active when the GPS is deactivated.

In both cases, all the necessary commands will be given through the ArcPad screen, with basically no need to access any ArcPAd menu items. On the ArcPad screen there will be 4 visible layers:

- Topographic map of the area
- Grid of planned sampling locations
- Grid of effective sampling locations: this is the file that will be edited every time a soil moisture reading is taken.
- GPS position indicator

Sampling procedure

The procedure for taking a soil moisture reading with this system is:

1. Navigate to the sampling point:
    - If in GPS mode, the exact location will be indicated by the overlapping of the GPS position indicator and the sampling point on the planned sampling grid

    - If in GRID mode, point will be identified on the ground, as explained in section 7.3
2. Insert the probe vertically in the ground, until the probe head base is in intimate contact with the ground surface.
3. Take a hydra probe reading:
    - If in GPS mode: tap the question mark icon on the bottom left corner of the ArcPad menu. This will activate the program that reads the hydra probe values. To take a reading, tap ANYWHERE on the screen and wait.
    - If in GRID mode: tap the question mark icon on the bottom left corner of the ArcPad menu. To take a reading, tap on the point labelled as the point you navigated to on the ground (e.g. B17) and wait
4. The process of reading the hydra probe takes some 4-5 seconds. During this time wait and DO NOT tap anything on the iPAQ screen
5. After 4-5 seconds, a form appears in ArcPad containing several text boxes:
    - The point sequential number (for GPS mode) or the point label (for GRID mode)
    - The Hydra probe soil moisture reading (in volumetric water content fraction)
    - The Hydra probe soil temperature reading (in Celsius degrees)
    - A comment text box
    - A vegetation type text box, to be chosen from a drop down list
    - A landuse text box, to be chosen from a drop down list
    - A surface rock cover text box, to be chosen from a drop down list
    - A dew estimation text box, to be chosen from a drop down list
    - A text box for the vegetation sample sequential ID
    - A text box for the soil sample sequential ID
6. After checking on the form that all the values have been properly inserted, the user can:
    - Accept the point by tapping “ok” on the top right corner of the form. This will store the point and measurement taken.
    - Cancel the point by tapping “cancel”, next to the “ok” button. This will erase the current record permanently. You will then need to repeat the above process to retake the readings.

ArcPad troubleshooting

Error windows might appear while interrogating the probe through ArcPad. Error messages are generally vague and of the kind “error, line 89, source text unavailable”. Usually, these are associated with lack of power to the probe or disconnection of one of the many component of the iPAQ-Hydra probe system. The general rule is to press “ok” on the error window, wait a few seconds and retry the command. If the error persists, please do the following:

- Check that all the connections are firm
- Check that the battery adaptor is firmly connected to the battery
- Check that the iPAQ USB serial port is firmly connected
- Check that the iPAQ is not low in battery

If the problem persists, change the gel cell battery with the spare one.

7.5.3 Gravimetric sampling procedure

- Remove vegetation and litter.

- Lay the ring on the ground
- Put the wooden base horizontal on top of the ring and use the hammer to insert the ring in the ground, until its upper edge is levelled with the ground surface.
- Use the garden trowel to dig the side of the ring. The hole should reach the bottom of the ring (5cm) and sufficiently large to fit the spatula
- Use the spatula to cut the 0-5cm soil sample at the bottom of the ring
- Place the 0-5cm soil sample in the plastic bag and seal with the rubber band provided
- Label the external plastic bag as **farm/team/date(dd-mm-yy)/time(hh:mm)/Sample ID**

7.5.4 Gravimetric soil moisture sample processing

All gravimetric soil moisture samples are processed to obtain a wet and dry weight. It is the sampling teams responsibility to deliver the samples, fill out a sample set sheet, one sheet per day per team, and record a wet weight at the field headquarters. All gravimetric soil moisture samples taken on one day will be put to dry in the ovens at 105^{o}C in the evening and will remain in the ovens until the following evening (approximately 24 hours).

Wet Weight Procedure

1. Turn on balance.
2. Tare.
3. Obtain wet weight to two decimal places and record on sheet.
4. Process your samples in numeric order, carefully emptying contents in the trays provided.
5. Place the used bags in order. The labelled bags will be needed for permanently storing the samples after the drying procedure is finished.

Dry Weight Procedure

1. All samples should remain in the oven for a minimum of 20-22 hours at 105^{o}C.
2. Turn off oven and remove samples for a single data sheet and place on heat mat. These samples will be hot. Wear the gloves provided
3. Turn on balance.
4. Tare.
5. Obtain dry weight to two decimal places and record on sheet.
6. Process your samples in sample numeric order, returning samples to the original plastic bags and store in the assigned locations.
7. Load new samples into oven.
8. Turn oven on.

7.5.5 Vegetation sampling procedure

Vegetation biomass ("quadrant" type sample)

A 0.5m x 0.5m quadrant will be used to obtain vegetation samples. The procedure for vegetation biomass sampling is as follows:

1. Note and record type of vegetation to be sampled (e.g. crop, native grass, improved pasture)

2. Randomly place 0.5m x 0.5m quadrant on ground near area to be sampled
3. Label bag provided using a permanent marker with the following information: **farm/team/date(dd-mm-yy)/time(hh:mm)/Sample ID**
4. Take photo of area to be sampled prior to removal of vegetation
5. Record sample location with GPS and/or sample location reference number
6. Remove all aboveground biomass within the 0.5m x 0.5m quadrant using vegetation clipper and scissors provided
7. Place vegetation sample into labelled bag provided
8. Close bag with sample using rubber bands provided
9. Take photo of sample plot following removal of aboveground biomass.

Vegetation water content ("grab" type sample)

The purpose of the grab sample is to characterise the ratio between vegetation dry biomass and vegetation water content, and monitor its evolution in time. Therefore a grab type vegetation samples is taken simply cutting off the part of a reference plant that sticks out of the ground. These g/g measurements can later be scaled to g/m^2 using the reference vegetation biomass measurements from quadrants.

Vegetation dew sample

This kind of sampling is done in a very similar way to the "grab" vegetation water content. Please refer to previous sections for sampling procedures. Particular attention will have to be paid in order to make sure that all the water present on the plant is collected in the sample bag. It is suggested to cover the entire plant with the sample bag before cutting it at ground level.

LAI measurements

Measurements of Leaf Area Index will be taken with an Exotech Inc. LAI-2000® device, operated exclusively by one team member. Sampling procedures for this instrument therefore will not be included in this work plan.

NDVI measurements

Measurements of Normalised Difference Vegetation Index will be taken with an Exotech Inc. Hand Held Radiometer 100BX® device, operated exclusively by one team member. Sampling procedures for this instrument won't therefore be included in this work plan.

7.5.6 Oven drying procedure – vegetation

Vegetation samples collected will be processed either in Merriwa or at The University of Newcastle. It is the responsibility of the teams to deliver the vegetation samples to NAFE headquarters at the end of the day, weigh and store them in the appropriate place. The procedure for vegetation biomass processing will be as follows:

1. Weigh samples before drying in ovens and record green biomass
2. Weigh the plastic bag and tag and record weight and subtract from sample green biomass
3. Dry samples in oven at 40^{o}C until constant weight is reached
4. Weigh dry vegetation samples and determine dry biomass.
5. Vegetation water content will be determined by subtracting the sample dry biomass to the sample green biomass

7.5.7 Surface roughness procedure

Surface roughness measurements will be taken a using a 1 m long drop pin profiler with a pin separation of 25 mm (see Fig. 43). At each surface roughness sampling location, 2 measurements will be taken with respectively North-South and East-West orientation. The procedure for one measurement is a s follows:

1. Note on the field book the position of the roughness measurements.
2. Position the profiler making sure that all the pins touch the soil surface. The pins MUST NOT be inserted into the ground or resting on top of vegetation.
3. Note on the field book the height reached by each pin, as read on the background grid. Pins has to be read from left to right, and indicated on the field book with sequential numbers from 1 to 41.

In the evenings, all readings will then be transcribed into an appropriate excel file named “Surface roughness”, into the folder named as the farm of interest.

7.5.8 Data archiving procedures

All data collected during the day will be downloaded and backed up upon return to the NAFE headquarters on desktop PCs. There will be 2 desktop computers available for the downloading operations. It will be the responsibility of the teams to download all data collected with the iPAQs onto the appropriate folders (see “downloading” section below) and to insert into an excel worksheet all the data collected in the fieldbooks.

Figure 43. Pin profiler for surface roughness measurements

File structure

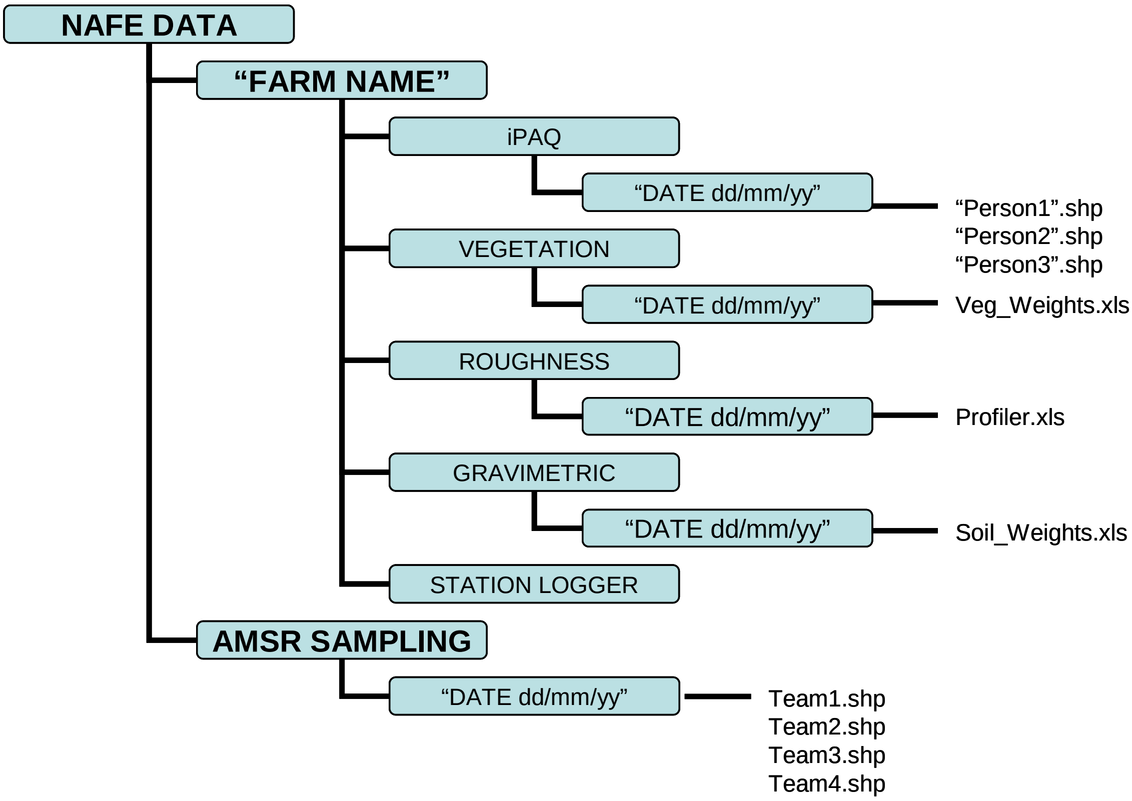

Figure 44. Tree diagram of the NAFE file structure

Downloading

- iPAQ data: Each person will download the iPAQ shapefile “hydra.shp” into the folder “Farm name”/iPAQ/”date”/.**The file hydra.shp MUST be renamed with the person name BEFORE downloading, when the file is still on the iPAQ.** Downloading will be done with the software Microsoft ActiveSync installed on the desktop computers. To download:
    - Connect the iPAQ to the desktop computer through the iPAQ USB cable
    - Start Microsoft ActiveSync
    - Establish a “Guest” partnership between the iPAQ and the desktop computer
    - Navigate to the /SD card/Goulburn folder on the iPAQ
    - Rename the file hydra.shp with your name
    - Copy the file and past it into the appropriate folder on the desktop computer (see Fig. 44)
- Vegetation data: Each team will insert into a excel worksheet named “Veg_weights.xls” contained in the folder “Farm name”/VEGETATION/”date”/ ,the samples ID of the vegetation samples taken, as a reference for the subsequent drying operations.
- Gravimetric data: Each team will insert into a excel worksheet named “Soil_weights.xls” contained in the folder “Farm name”/GRAVIMETRIC/”date”/ ,the samples ID and wet weight of the soil samples taken.
- Surface roughness data: The readings of the pin profiler will be inserted be each team into a excel worksheet named “Profiler.xls”

- AMSR sampling data: Each team will download the the iPAQ shapefile "AMSR_teamX.shp" into the folder AMSR SAMPLING/"date"/

Downloading

Daily data will be backed up on both DVD's and external hard disk drive. It will be the responsibility of the project leader to do the back up.

8 Logistics

8.1 Operation bases

Ground crew will be based in the town of Merriwa, located in the heart of the study area. The NAFE '05 headquarters will be at the local Anglican Church Hall (Fig. 45 and 46). The hall will be equipped with all the equipment needed for pre-sampling and post-sampling operations, including scales for sample weighing, ovens for soil and vegetation sample drying, computers for data downloading and processing, storage spaces for processed samples and equipment. It will be the responsibility of each team to make sure instruments and tools are stored properly overnight. The hall kitchen provides all sorts of facilities that can be used for breakfast. It is left to the individuals to arrange their own breakfast supplies, through the local bakery or supermarket (see Fig. 46).

One of the ground crew members, Rodger Young, will be based at the hall and will be dedicated to instrument repair and general technical support. Breakdowns and instrument faults must be reported to him at the end of each day.

Air crew will be based in Scone and operate both the SERA and the EMIRAD aircraft out of the Scone Airport (see Fig 47 and 48).

Figure 45. NAFE'05 headquarters

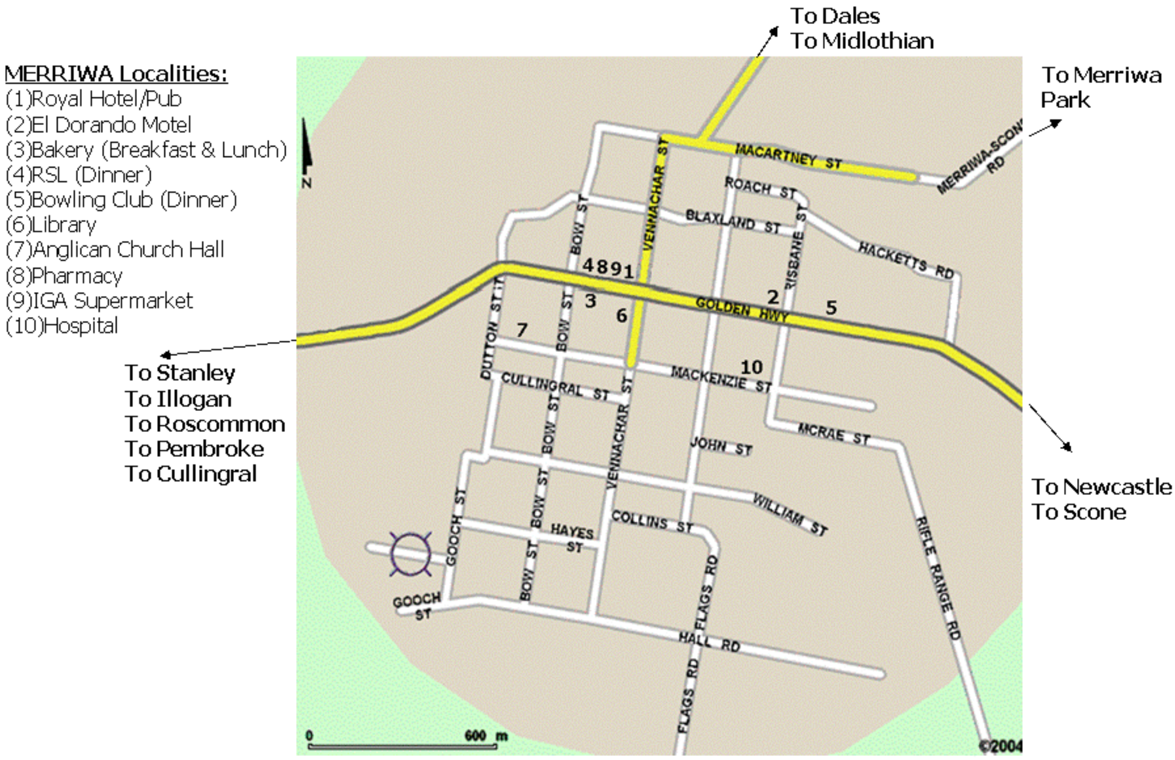

Figure 46. Map of Merriwa town centre map with NAFE ’05 logistic locations.

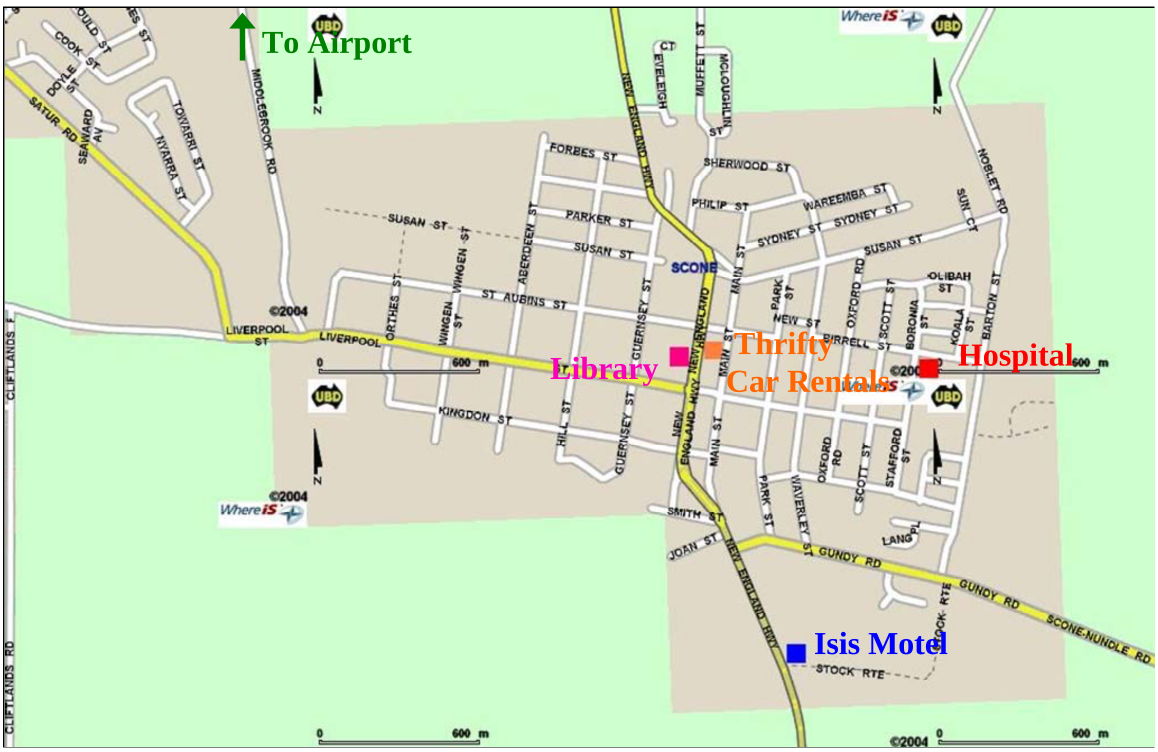

Figure 47. Map of Scone town centre

8.2 Accommodation

A block of rooms has been reserved for ground crew participants at the only motel in Merriwa, the “El Dorado” motel (see details below and Merriwa map in Fig. 46). Participants have been pre-assigned to rooms (Table 10), depending on the period of stay and the institution of origin, to facilitate check-in and check-out operations and payment. The rooms are single, double, triple or family rooms, and mostly they will be shared between participants (on a male/female basis). At your arrival, check in at the reception and make sure you provide your details. At departure, payment will be done on an individual basis. A number of the participants from Newcastle University have elected to be accommodated at one of the pubs in town, the Royal Hotel, and are responsible for their own arrangements.

The air crew will be accommodated at the Isis Motel in Scone. A block of rooms have been already booked and details are given in Table 11.

8.3 Meals

Meals arrangements are left to individuals to organise. However, following are some suggestions to facilitate organisation of the ground crew:

- Breakfast: supplies can be bought at the local supermarket (see Fig. 46) and prepared/eaten at the NAFE’05 headquarters’ kitchen;
- Lunch: can be bought at the local supermarket or at the Merriwa bakery (see Fig. 46). To facilitate this, Rodger Young will take orders for the sandwiches the day before, and collect them at the bakery every morning. Expenses will be billed to your tab.
- Dinner: apart from the supermarket (if you want to do this make sure you buy your supplies in advance, as the supermarket might be close by the time you get back from your sampling), the only options for dinner are the Royal Hotel (only on the weekends, see Fig. 46), the Returned Services League Club, and the Bowling Club, which serves some Chinese food as well as regular meals (Fig. 46).

Figure 48. PLMR hangar at Scone airport and a view of the airstrip

Table 10. Accommodation logistics for the ground crew at Merriwa "El Dorado" motel

Room N.	People	Start date	End date	N. days	Price ($/night)	Total room
5	Viviana Maggioni* Jennifer Grant	29/10/2005	26/11/2005	28	69	1932
13	Jetse Kalma**	29/10/2005	26/11/2005	28	38	1064
10	Patricia De Rosnay Gilles Boulet (Kauzer Saleh)	29/10/2005	12/11/2005	14	80	1120
10	Rob Pipunic* Chris Rüdiger* Stuart Jones*	12/11/2005	26/11/2005	14	80	1120
7	Rodger Young* Olivier Merlin*	24/10/2005	26/11/2005	33	69	2277
8	Rocco Panciera* Marco Rinaldi*	24/10/2005	2/12/2005	40	69	2760
14	Jose Fenollar Daniele Biasioni*	24/10/2005	26/11/2005	33	55	1815
15	Michael Berger	24/10/2005	5/11/2005	13	45	585

Table 11. Accommodation details for air crew at Scone "Isis" Motel

Room N.	People	Start date	End date	N. days	Price ($/night)	Total room
1	Jon Johanson	27/10/2005	26/11/2005	30	60	1560
2	Helmut Thompson	4/11/2005	26/11/2005	30	60	1200
4	Sten Schmidl Soebjaerg	4/10/2005	12/11/2005	16	60	480
6	Jorg Hacker (+Shakti)	27/10/2005	2/11/2005	6	68	408
14	Jeff Walker	27/10/2005	26/11/2005	30	60	1560
15	Ed Kim	29/10/2005	26/11/2005	28	60	1440
16	Valerio Paruscio	29/10/2005	26/11/2005	28	60	1440
17	Patrick Wurstein	28/10/2005	28/11/2005	31	60	1620
18	Jan Balling	9/11/2005	26/11/2005	17	60	900

8.4 Internet

Due to the remoteness of the area, internet service will be very limited. The only option in town is the local library (see Fig 46). As per an agreement reached with the library management, access for NAFE'05 participants will be available between 8-9pm, only on Monday, Wednesday and Thursday. There will be 10 computers available and the hourly fee will be $2.50 per user, to be paid individually.

In Scone, Internet will be available at the Upper Hunter regional library. Refer to the section 7 for contact details.

8.5 Maps and directions

8.5.1 Getting there

Airport shuttle

There will be three "Airport Shuttle" runs provided by NAFE, **Saturday 29th October**, **Saturday 12th November** and **Saturday 26th November.** Please make sure we have your arrival and departure details if you require this service.

By car

From Sydney Airport (Mascot) to Maitland (New England Highway)

1	*Start at	Elizabeth Avenue		Mascot	0 metres	0 Seconds
2		Botany Road	S	Mascot	747 metres	1:06 Minutes
3		Eastern Distributor on ramp	E	Mascot	143 metres	6 Seconds
4		Eastern Distributor	E	Botany	8.86 kms	6:37 Minutes
5		Cahill Expressway	N	Woolloomooloo	1.13 kms	57 Seconds
6		Sydney Harbour Tunnel	N	Sydney	2.45 kms	1:52 Minutes
7		Warringah Freeway	N	North Sydney	4.28 kms	3:12 Minutes
8		Gore Hill Freeway	W	Artarmon	925 metres	53 Seconds
9		Pacific Highway exit	W	Artarmon	635 metres	38 Seconds
10		Pacific Highway	NE	Lane Cove North	13.51 kms	18:12 Minutes
11		Sydney Newcastle Freeway on ramp	NE	Wahroonga	27 metres	1 Second
12		Sydney Newcastle Freeway	N	Wahroonga	126.95 kms	1:19 Hours
13		John Renshaw Drive	E	Beresfield	561 metres	1:20 Minutes
14		New England Highway on ramp	E	Beresfield	624 metres	1:29 Minutes
15		New England Highway	NW	Beresfield	13.97 kms	18:37 Minutes
16		New England Highway		Maitland	0 metres	0 Seconds
					174.90 kms	2:14 Hours

From Newcastle Airport (Williamtown) to Merriwa

Driving Directions

Driving Directions from Williamtown NSW to Merriwa NSW Reverse Route

ID		Road	Direction	Town	Distance	Time
1	*Start at	Slades Road		Williamtown	0 metres	0 Seconds
2		Unnamed	W	Williamtown	237 metres	17 Seconds
3		Williamtown Drive	SE	Williamtown	674 metres	40 Seconds
4		Unnamed	SE	Williamtown	10 metres	0 Seconds
5		Nelson Bay Road	SW	Williamtown	683 metres	30 Seconds
6		Cabbage Tree Road	W	Williamtown	6.63 kms	4:57 Minutes
7		Tomago Road	W	Tomago	8.50 kms	6:22 Minutes
8		Pacific Highway	SW	Tomago	1.41 kms	56 Seconds
9		New England Highway exit	SW	Hexham	109 metres	4 Seconds
10		New England Highway	N	Hexham	22.37 kms	28:18 Minutes
11		New England Highway	NW	Rutherford	29.78 kms	27:12 Minutes
12		Golden Highway	SW	Whittingham	25.88 kms	23:54 Minutes
13		Long Point Road	NW	Warkworth	18 metres	0 Seconds
14		Golden Highway	NW	Warkworth	13.90 kms	11:08 Minutes
15		Golden Highway		Jerrys Plains	0 metres	0 Seconds
16	S	Golden Highway		Jerrys Plains	27.59 kms	22:48 Minutes
17		Jerdan Street	SW	Denman	55 metres	5 Seconds
18		Golden Highway	W	Denman	51.20 kms	41:15 Minutes
19		Vennacher Street		Merriwa	0 metres	0 Seconds
20		Vennacher Street		Merriwa	0 metres	0 Seconds
					189.09 kms	2:48 Hours

<u>From Newcastle Airport (Williamtown) to Scone</u>

Driving Directions

Driving Directions from Williamtown NSW to Scone NSW Reverse Route

ID		Road	Direction	Town	Distance	Time
1	*Start at	Slades Road		Williamtown	0 metres	0 Seconds
2		Unnamed	W	Williamtown	237 metres	17 Seconds
3		Williamtown Drive	SE	Williamtown	674 metres	40 Seconds
4		Unnamed	SE	Williamtown	10 metres	0 Seconds
5		Nelson Bay Road	SW	Williamtown	683 metres	30 Seconds
6		Cabbage Tree Road	W	Williamtown	6.63 kms	4:57 Minutes
7		Tomago Road	W	Tomago	8.50 kms	6:22 Minutes
8		Pacific Highway	SW	Tomago	1.41 kms	56 Seconds
9		New England Highway exit	SW	Hexham	109 metres	4 Seconds
10		New England Highway	N	Hexham	22.37 kms	28:18 Minutes
11		New England Highway	NW	Rutherford	113.56 kms	1:41 Hours
12		New England Highway		Scone	0 metres	0 Seconds
					154.24 kms	2:23 Hours

8.5.2 Getting around

Krui Farms:

ILLOGAN:

- Travel approximately 28 km west along Golden Hwy
- Turn left onto Comiala Road
- Travel approximately 7km south down Comiala Road & 'Illogan' property marked on left

STANLEY:

- Travel approximately 24km west along Golden Hwy
- On right hand side of Golden Hwy

ROSSCOMMON:

- Travel approximately 20km west along Golden Hwy
- Turn left onto Redwell Road
- Travel approximately 7km south down Redwell Road (sampling site on right hand side of road);

PEMBROKE:

- Travel approximately 25km west along Golden Hwy
- Turn right onto Pembroke Road
- Travel approximately 11km north along Pembroke Road

Merriwa Farms:

MERRIWA PARK:

- Turn right off Golden Hwy onto Venacher St (Royal Pub corner)
- Turn right onto Macartney St
- Travel approximately 6km along Merriwa-Scone Road
- Turn off to left to access property

CULLINGRAL:

- Travel approximately 500m west along Golden Hwy
- Turn left onto Cullingral Road
- Travel approximately 1km south along Cullingrat Road. Cullingral homestead is marked on left

MIDLOTHIAN:

- Turn right off Golden Hwy onto Venacher St (Royal Pub corner)
- Turn right onto Macartney St
- Turn left onto Coulsons Creek Road (i.e. follow Willow Tree signage)
- Travel approximately 4.5km north along Coulsons Creek Road
- Turn left onto Mountain Station Road. The Midlothian property is on left of road (approximately 1km)

DALES:

- Turn right off Golden Hwy onto Venacher St (Royal Pub corner)
- Turn right onto Macartney St

- Turn left onto Coulsons Creek Road (i.e. follow Willow Tree signage)
- Travel approximately 19km north along Coulsons Creek Road
- Dales property on right hand side of road

8.6 Groups

The ground crew segment will be based in Merriwa and coordinated by Prof. Jetse Kalma. This group will be responsible for all the soil moisture and supporting data measurement in the Northern Goulburn study area. The sampling operations will be undertaken by 4 teams acting independently. Each team will be assigned two of the eight focus farms, one in the Merriwa sub-catchment and one in the Krui sub-catchment. Each team will sample the same two farms for the entire field campaign. Table 12 indicates the composition of each team and the focus farm assigned to each group. The air segment will operate from the Scone airport and will be coordinated by Jeff Walker (Table 13).

Table 12. NAFE '05 ground crew segment. Group leaders are indicated in red.

	Weeks 1,2	Weeks 3,4	Vehicles	Krui area	Merriwa area
Team 1	Rocco Panciera Marco Rinaldi Patricia DeRosney Gilles Boulet	Rocco Panciera Marco Rinaldi Rob Pipunic TBD	White Rodeo 4WD (STT 296) Melb Uni + 1 Quad bike	Pembroke	Midlothian
Team 2	Greg Hancock Cristina Martinez Jose' Fenollar Viviana Maggioni Mark Thyer	Greg Hancock Cristina Martinez Jose' Fenollar Viviana Maggioni	White Toyota Prado 4WD (UNI 211) Newcastle Uni	Stanley	Cullingral
Team 3	Jetse Kalma Jennifer Grant Patricia Saco Daniele Biasioni	Jetse Kalma Jennifer Grant Daniele Biasioni	Silver Toyota Prado 4WD (UNI 033) Newcastle Uni	Roscommon	Dales
Team 4	Tony Wells Olivier Merlin Kauzeer Saleh	Chris Rüdiger Olivier Merlin Stuart Jones	Newcastle Uni	Illogan	Merriwa Park

Table 13. NAFE'05 Air crew members

PLMR

Jeff Walker	27-Oct 26-Nov
Jorg Hacker + Shakti	27-Oct 2-Nov
Valerio Paruscio	29-Oct 26-Nov
Ed Kim	29-Oct 26-Nov
Garry Willgoose	29-Oct 26-Nov
Chris Dever	only day trips
Jon Johanson	27-Oct 26-Nov

EMIRAD

Helmut Thompson	4-Nov 26-Nov
Michael Berger	24-Oct 5-Nov
Patrick Wurstein	28-Oct 28-Nov
Sten Schmidl Soebjaerg	4-Nov 12-Nov
Jan Balling	9-Nov 26-Nov

Table 14. Schedule of training sessions

Time	Place	Activities	Coordinators
8.00am - 8.30am	NAFE headquarter	Presentation of NAFE'05	Jetse Kalma
8.30am - 9.30am	NAFE headquarter	Presentation of NAFE'05 sampling strategy	Rocco Panciera
9.30am - 10.30am	Example focus farm	Instrument use explanation (all together)	Rocco Panciera Cristina Martinez
10.30am - 12.30pm	Example focus farm	Instrument use practice (in teams)	Team leaders
12.30pm - 1.30pm		Lunch	
1.30pm - 6.00pm	Team farms	Study areas recognition(2 farms): *Farm scale sampling points survey *High resolution areas survey *High	Team leaders

8.7 Training sessions

Two training sections have been scheduled to ensure all the participants to NAFE are familiar with the project objectives, the sampling strategy and the use of all the instruments involved in the sampling. Training sessions will take the whole day and are scheduled for Sunday 30th October and Sunday 13th October, to match the arrival of new participants to the second two weeks of the campaign. Training session will be held at the NAFE's headquarters (morning), and at the respective farms (afternoon), with the schedule and activities indicated in table 13

Training on instrument use will include:

- iPAQ basics
- Soil moisture sampling with Stevens Hydra Probe®
- Soil moisture sampling on high resolution areas
- Gravimetric soil sampling
- Vegetation biomass sampling
- Vegetation water content sampling
- Vegetation dew sampling
- Vegetation dew estimation
- Vegetation height estimation
- Vegetation type estimation
- Surface roughness measurements
- Surface rock cover estimation

8.8 Daily activities

The Hall will be the meeting point for the morning group assembly, breakfast and sampling preparation. At the end of the day, group will report to the hall, download the data collected, put the samples in the oven for drying, control the instruments, ensure electronic devices are recharged overnight and report to the project leaders. Daily operations will proceed as per the following schedule:

- **7.00am:** Gathering of the teams at the NAFE headquarters.
  Breakfast
  Morning briefing
  Review of the activity of the day on the notice board
  Preparation of the instruments and tool for the sampling
- **7.30am:** Teams departure for the sampling locations
- **7-30am – 12.30pm:** Sampling operations
- **12.30pm – 1.30pm:** Lunch
- **1.30pm – 5.30pm**: Sampling operations
- **6.00pm:** Teams return to the hall
  Report to the project leaders
  Data downloading on the desktop/laptop computers
  Soil and vegetation samples in ovens for drying
  Recharge of electronic devices

8.9 Farm access and mobility

Farms will be accessed every day for the sampling operations. Transport from Merriwa to the farm and across the farm for sampling will be done on the team 4WD vehicle. Please note that 4WD driving on off-road areas and farm tracks can lead to injury and death and requires extreme attention and care. Sampling of the farm area will require driving along tracks and through paddocks, while walking will be necessary where driving is unfeasible, due to particular topographic or vegetation. In particular, driving through cultivated areas should be avoided at all times, due to the serious damage the transit could cause to crops.

The sampling locations have been organised so that only reasonably accessible areas will be object of the sampling. Project and team leaders have good knowledge of the areas, and in most cases they will be responsible for the farm scale sampling. The planned sampling locations will not be numbered, and no specific indication will be given as to the order to follow in covering the points. Due to logistic constraints, it will be left to the individuals to plan their own preferred sampling routes. However, following are some recommendations to make the sampling as uniform and consistent as possible between different farms and different days:

- Plan ahead: decide your sampling route and **be consistent** with it between sampling days.. This will ensure consistency between the soil moisture maps produced during the campaign.
- Sample from the big scale to the small scale: It is recommended to start from the coarse scale points, then sample the smallest scale points, then increase depending on the time left.
- Sample on a “paddock” base: we are interested in spatial patterns, so groups of points are preferred to long lines of points. If you get to a fence, make sure you sampled all the points within the paddock before getting to the next one (provided this doesn’t conflict with the previous note).

- Take the sample exactly at the location indicated on the map: exception to this rule might be the case of a sampling point falling to close to an undesirable location which might create local soil moisture condition not representative of the site (e.g. an isolated tree in a vast short grass area or creek). In the case, shift the sampling far enough to capture the average site conditions (up to 30m depending on grid resolution)
- Always sample in the same locations as the previous days to ensure consistency.

Remember that NAFE'05 activities are allowed by the property owners in the agreement that no damage will be caused to the properties. In particular:

- Be aware of the presence of stock on most of the farms during the sampling activities. Most of the animals are inoffensive cows and sheep, which will generally keep distant. However, in some cases cows could be inquisitive. A particular case is the Merriwa Park farm; Bulls are present on one of the paddocks. Although they shouldn't represent particular risk, always check the position and movement of the stock. Team members assigned to Merriwa Park will be advised properly of the conditions.
- Many farm in the area adopt the so called "intensive cell grazing" technique. This results in a dense network of interconnected single electric wires, all converging into a certain number of "nodes", where transit between paddocks is made easy through electrically isolated holds. Generally, it will be possible to crawl below or step over the wires without risk. When driving through these areas, locate the nearest node to transit into the next paddock.
- In the case of heavy rain, stop sampling and wait for better weather conditions: this is both to avoid damage to the electronic instrumentation used for the sampling and also to prevent excessive "digging" of the muddy farm tracks by the vehicle wheels.

8.10 Communications

Communications between team members and team and project leaders is important both from a logistic and safety point of view. In every team there will be at least two mobile phones and a UHF transmitter. One mobile phone will stay with the team leader, who will be sampling at farm scale, while the other will stay with the team members who will be sampling the high resolution areas. This will provide contact within the individual teams. On most farms the mobile phone coverage is extensive, while on some it is poor. On the farms with only partial coverage, team members should agree on some "check times" (<u>at least 1 every hour</u>) during the morning and the afternoon, for the farm scale sampler to report to the high resolution areas and indicate the areas he/she will be sampling next. In case a check time is missed by the farm scale sampler, actions should be taken by the team members to ensure his/her safety. In particular:

- Contact with the missing team member should be immediately attempted with the mobile phone.
- If that fails, contact should be made with the project leaders with mobile phone. The project leaders should attempt contact with UHF. The local emergency channel is **Channel 8 Duplex. To connect to this channel via the UHF receiver:**

    (1) press the DUP (i.e. duplex) button on the UHF
    (2) then dial channel 8

- If that failed, the project leader should immediately bring a vehicle to the farm and start searching in the areas indicated by the other team members

Team leaders should make themselves familiar with the use of the UHF transmitter and the emergency frequency indicated above.

8.11 Safety

There are a number of potential hazards in doing field work. The following has some good suggestions. Common sense can avoid most problems. Remember to:

- When possible, work in teams of two
- Carry a phone or UHF receiver
- Know where you are. Keep track of your position on the provided farm map.
- Do not touch or approach any unidentified objects in the field.
- Notify your NAFE supervisor after returning to the field headquarters
- Dress correctly; long pants, long sleeves, boots, hat
- Use sunscreen.
- Carry plenty of water for hydration.
- Notify your teammate and supervisors of any preexisting conditions or allergies before going into the field.

Australian Red Cross

First aid for snake bite.

Use the pressure immobilisation technique for a bite on a limb.
-apply firm pressure over the bite site
-apply broad bandage to keep pressure on bite site.
-immobilise limb
(for bites on the head or trunk do not use this technique but keep thepatient still and get medical aid asap)

Monitor the airways, breathing and circulation of the patient. Be ready to give Expired Air Resuscitation (mouth to mouth)or CPR.
Keep the patient very still and reassure.
Start transport to the nearest medical centre or call and meet an ambulance.
Do not cut the bite
Do not suck the bite.
Do not wash the bite.
Do not apply a tourniquet

* Beware of harvesting machinery. Several crops will be harvested during November. When sampling on crop, always make sure your presence is noted and watch out for the moving harvesting machines.
* Beware of Snakes. Always wear sturdy boots to avoid bites. refer to http://www.australianfauna.com/australiansnakes.php for detailed info about the most common of australian snakes species.

The temperature used for the soil drying ovens is 105 ^{o}C. Touching the metal sample cans or the inside of the oven may result in burns. Use the safety gloves provided when placing cans in or removing cans from a hot oven. Vegetation drying is conducted at lower temperatures that pose no hazard.

9 Contacts

Field work

Name	Team	Mobile
Jeffrey Walker	Air crew coordinator	0413 023 915
Panciera Rocco	Team 1	0431 688 696
Greg Hancock	Team 2	0409 328 942
Jetse Kalma	Team 3/Ground crew coordinator	0427 426 217
Tony Wells	Team 4 - weeks 1,2	n/a
Chris Rüdiger	Team 4 - weeks 3,4	0410 131 407
Rodger young	technical support	0417 504 593

Emergency

local UHF	Channel 8 Duplex	
Ambulance	12 1233	
Merriwa Hospital	6548 2006	6532 5000
Merriwa Police	6548 2203	0408 293 423
Poison information center	13 1126	
Merriwa Rescue Quad	6548 2538	

Farmers

Farm	Farmer Name	Home Phone	Mobile Phone
Illogan	Robert & Maree Goodear	(02) 63761129	n/a
Stanley	Doc & Fiona Strahan	(02) 65485154	n/a
Roscommon	Tony & Joanna O'Brien	(02) 65485161	n/a
Pembroke	Matthew & Marion Dowd	(02) 65487233	0428 233 891
Cullingral	Peter McNamara	n/a	0407 257 154
Merriwa Park	Martin Nixon	(02) 65482225	n/a
Midlothian	Mike Gilder	(02) 65482219	0429 482 219
Dales	James & Judy Bettington	(02) 65488563	n/a

Accommodation & logistics

El Dorado Motel
50 Bettington Street
Merriwa NSW 2329
Telephone: (02) 6548 2273
Facsimile: (02) 65482208
Rating: **1/2

Royal Hotel
Bettington Street
Merriwa NSW 2329
Telephone: (02) 6548 2235

NAFE headquarters
@ Anglican Church Hall
Pat Kirkby
(H): (02) 65482424
(M): 0407132436

Medical

Merriwa Community Hospital
Mackenzie Street
Merriwa NSW 2329
Telephone: (02) 6532 5000
Facsimile: (02) 6532 5005
http://www.hnehealth.nsw.gov.au/docs/transport_merriwa.pdf

Merriwa Pharmacy
106 Bettington Street
Merriwa NSW 2329
Tekephone: (02) 6548 2213

Car rentals

Off Road Rentals
1370 North Road
Huntingdale VIC 3166
Phone (03) 9543 7111
Fax (03) 9562 9205
Email: manager@offroadrentals.com.au

Scone

Isis Motel
250 New England Hwy Scone NSW 2337
ph: (02) 6545 1100

Upper Hunter Regional Library (with internet access)
214 Kelly St Scone NSW 2337
ph: (02) 6545 1451

NAFE'05

Professor Jetse Kalma
School of Engineering,
University of Newcastle,
Callaghan NSW 2308
Australia.
Phone 02 4921 5736
Fax 02 4921 6991
mailto:jetse.kalma@newcastle.edu.au

Dr. Jeffrey P. Walker
Senior Lecturer in Environmental Engineering
Room 409, Building D
Department of Civil and Environmental Engineering
The University of Melbourne
Victoria 3010
Australia.
Phone: 03 8344 5590
Fax: 03 8344 6215
Email: j.walker@unimelb.edu.au

Rocco Panciera
PhD candidate
Room 322, Block C
Department of Civil and Environmental Engineering
The University of Melbourne
Parkville,Victoria 3010,Australia
Phone: +61 03 8344 4955
Fax: +61 03 8344 6215
Email:rocco@civenv.unimelb.edu.au

10 Equipment List

The following tables list all the equipments that will be required for NAFE'05, grouped per person, team and operation base

PERSONAL EQUIPMENT		TOTAL (15 PEOPLE)
hx2110 iPaq	1	15
ipaq container box	1	15
postpack	1	15
ipaq storage card	1	15
hydra probe	1	15
sampling pole	1	15
ipaq mount	1	15
bumpack	1	15
foam (4 hydra probe)	1	15
ipaq split sync cable	1	15
ipaq power cable	1	15
ipaq AC adaptor	1	15
GPS receiver	1	15
GPS battery recharge kit	1	15
GPS power jack	1	15
coinverter CONV485	1	15
battery connector	1	15
gel cell battery	2	30
electrial isolating gloves (pair)	1	15
hat	3	45
sunscreen bottle	1	15
insect repellent	1	15

TEAM EQUIPMENT		TOTAL (4 TEAMS)
4WD vehicle	1	4
UHF receiver	1	4
rope (150m)	3	12
hi-res area pegs	8	32
rope pegs	32	128
plier	1	4
light hammer	2	8
duck tape roll	4	16
screwdriver	1	4
tool container box	1	4
hardcopy farm map	3	12
hardcopy whole area map	1	4
copy of workplan	1	4
pencil	6	24
field book	3	12
first aid kit	1	4
water jerry can	1	4
flags/colored stripes	10	40
Vegetation sampling kit	2	8
* 1 veg clipper		8
* 1 pair of scissors		8
* 1 vegetation quadrant		8
* 304 plastic bags		1216
* 304 rubber bands		1216
Soil sampling kit	2	8
* 1 soil sample ring		8
* 1 garden trowel		8
* 1 blade		8
* 1 spatula		8
* 1 wooden base		8
* 604 plastic bags		2560
* 604 rubber bands		2560
* 4 markers for bags		16

GENERAL EQUIPMENT - Merriwa	
NAFE'05 headquarters	
ovens	2
scales	2
alluminium tray	300
weight recording form	4
samples container boxes	4
desktop computer	2
field laptop	1
backup dvd	50
backup hard drive	1
color printer	1
laptop wall projector	1
cd's with data	1
multi plug base	5
gel cell battery charger	4
plug extension	5
notice board	1
board pencils	10
Monitoring stations	
TIR sensor	4
dew sensor	6
stands	4
soil temp sensor	31
starlogger	8
starlogger download cable	2
gel cell battery	22
rock temp sensor	
instruments	
pin profiler	1
hand-held temp sesnor	1
Licor LAI sensor	1
NDVI sensor	1
handheld IR radiometer	1
quad	1
quad helmet	1
theta probes	7
repairing kit	
starlogger screwdriver	2
terminal strip screwdriver	2
duck tape roll	4
wire stripper	2
wire cutter	2
solder	1
hammer	1
spare gel cell/wire multi connectors	
spare wires	
mutlimeter	

GENERAL EQUIPMENT - Scone	
UNIDATA salinity/temp sensor unit	1
gell cell battery	3
floating station	1
backup dvd	10
backup hard drive	1
field book	2
gps unit	1
handheld sal/temp sensor	1
boat	1
laptop for lake station	1

11 Appendix A: Flight Line Coordinates

Table A1. PLMR low resolution mapping flight lines and coverage reference coordinates for AMSR sampling days. The corners are counted clock-wise starting from North-West.

Line No.	Altitude AGL (ft)	Altitude ASL (ft)	Length (km)	Start Longitude (Deg)	Start Latitude (Deg.)	Stop Longitude (Deg)	Stop Latitude (Deg.)
A1	10000	11265	43	150.0568	-32.2981	150.0688	-31.9033
A2	10000	11265	43	150.1216	-31.9044	150.1098	-32.2993
A3	10000	11265	43	150.1629	-32.3004	150.1744	-31.9056
A4	10000	11265	43	150.2273	-31.9067	150.2159	-32.3016
A5	10000	11265	43	150.2684	-32.3026	150.2795	-31.9078
A6	10000	11265	43	150.3323	-31.9089	150.3214	-32.3037
A7	10000	11265	43	150.3744	-32.3048	150.3851	-31.9100
A8	10000	11265	43	150.4379	-31.9111	150.4275	-32.3058

corner	Longitude (Deg)	Latitude (Deg)
1	150.0376	-31.9141
2	150.4690	-31.9241
3	150.4580	-32.2914
4	150.0257	-32.2820

Table A2. PLMR low resolution mapping flight lines and coverage reference coordinates for farm scale sampling days.

Line No.	Altitude AGL (ft)	Altitude ASL (ft)	Length (km)	Start Longitude (Deg)	Start Latitude (Deg.)	Stop Longitude (Deg)	Stop Latitude (Deg.)
A9	10000	11265	26	150.1485	-32.1965	150.1561	-31.9574
A10	10000	11265	30	150.3715	-31.9098	150.3635	-32.1846
A11	10000	11265	30	150.4165	-32.1857	150.4243	-31.9109

Krui

	Longitude (Deg)	Latitude (Deg)
crn 1	150.1173	-32.1825
crn 2	150.1243	-31.9668
crn 3	150.1875	-31.9682
crn 4	150.1809	-32.1839

Merriwa

	Longitude (Deg)	Latitude (Deg)
crn 1	150.3325	-32.1713
crn 2	150.3397	-31.9210
crn 3	150.4560	-31.9233
crn 4	150.4490	-32.1737

Table A3. PLMR intermediate resolution mapping flight lines and coverage reference coordinates for the Krui area.

Line No.	Altitude AGL (ft)	Altitude ASL (ft)	Length (km)	Start Longitude (Deg)	Start Latitude (Deg.)	Stop Longitude (Deg)	Stop Latitude (Deg.)
B1	5000	6265	26	150.1825	-31.9580	150.1750	-32.1971
B2	5000	6265	26	150.1485	-32.1965	150.1561	-31.9574
B3	5000	6265	26	150.1297	-31.9569	150.1220	-32.1967

	Longitude (Deg)	Latitude (Deg)
crn 1	150.0376	-31.9141
crn 2	150.4690	-31.9241
crn 3	150.4580	-32.2914
crn 4	150.0257	-32.2820

Table A4. PLMR intermediate resolution mapping flight lines and coverage reference coordinates for the Merriwa area.

Line No.	Altitude AGL (ft)	Altitude ASL (ft)	Length (km)	Start Longitude (Deg)	Start Latitude (Deg.)	Stop Longitude (Deg)	Stop Latitude (Deg.)
B4	5000	6265	30	150.4507	-31.9114	150.4430	-32.1861
B5	5000	6265	30	150.4165	-32.1857	150.4243	-31.9108
B6	5000	6265	30	150.3980	-31.9097	150.3900	-32.1851
B7	5000	6265	30	150.3635	-32.1846	150.3715	-31.9098
B8	5000	6265	30	150.3448	-31.9094	150.3370	-32.1840

	Longitude (Deg)	Latitude (Deg)
crn 1	150.3276	-31.9208
crn 2	150.4658	-31.9232
crn 3	150.4591	-32.1739
crn 4	150.3205	-32.1710

Table A5. PLMR medium resolution mapping flight lines for the Krui area.

Line No.	Altitude AGL (ft)	Altitude ASL (ft)	Length (km)	Start Longitude (Deg)	Start Latitude (Deg.)	Stop Longitude (Deg)	Stop Latitude (Deg.)
C1	2500	3778	4	150.0598	-32.1683	150.0612	-32.1259
C2	2500	3778	4	150.0744	-32.1262	150.0730	-32.1686
C3	2500	3876	6	150.1221	-32.1949	150.1238	-32.1420
C4	2500	3876	6	150.1371	-32.1423	150.1354	-32.1952
C5	2500	3876	6	150.1486	-32.1954	150.1503	-32.1426
C6	2500	3855	4	150.1512	-32.1127	150.1524	-32.0742
C7	2500	3855	4	150.1392	-32.0739	150.1378	-32.1124
C8	2500	3855	4	150.1248	-32.1120	150.1260	-32.0736
C9	2500	4073	11	150.1264	-32.0614	150.1297	-31.9569
C10	2500	4073	11	150.1429	-31.9572	150.1396	-32.0617
C11	2500	4073	11	150.1526	-32.0620	150.1561	-31.9574
C12	2500	4073	11	150.1693	-31.9577	150.1660	-32.0630
C13	2500	4073	11	150.1793	-32.0633	150.1825	-31.9580

Stanley	Longitude (Deg)	Latitude (Deg)
crn 1	150.1169	-32.0855
crn 2	150.1601	-32.0865
crn 3	150.1597	-32.1005
crn 4	150.1164	-32.0996

Illogan	Longitude (Deg)	Latitude (Deg)
crn 1	150.0528	-32.1373
crn 2	150.0815	-32.1380
crn 3	150.0808	-32.1561
crn 4	150.0523	-32.1555

Roscommon	Longitude (Deg)	Latitude (Deg)
crn 1	150.1145	-32.1536
crn 2	150.1581	-32.1545
crn 3	150.1572	-32.1838
crn 4	150.1135	-32.1828

Pembroke	Longitude (Deg)	Latitude (Deg)
crn 1	150.1210	-31.9669
crn 2	150.1901	-31.9684
crn 3	150.1876	-32.0499
crn 4	150.1182	-32.0485

Table A6. PLMR medium resolution mapping flight lines and coverage reference coordinates for the Merriwa area.

Line No.	Altitude AGL (ft)	Altitude ASL (ft)	Length (km)	Start Longitude (Deg)	Start Latitude (Deg.)	Stop Longitude (Deg)	Stop Latitude (Deg.)
C14	2500	3448	4	150.3373	-32.1839	150.3386	-32.1399
C15	2500	3774	12	150.3460	-32.1049	150.3493	-31.9937
C16	2500	3774	12	150.3625	-31.9939	150.3593	-32.1052
C17	2500	3984	6	150.4292	-32.1342	150.4309	-32.0744
C18	2500	4175	9	150.4410	-31.9949	150.4433	-31.9112
C19	2500	4175	9	150.4301	-31.9109	150.4277	-31.9946

Cullingral	Longitude (Deg)	Latitude (Deg)
crn 1	150.3300	-32.1536
crn 2	150.3462	-32.1539
crn 3	150.3459	-32.1712
crn 4	150.3294	-32.1709

Midlothian	Longitude (Deg)	Latitude (Deg)
crn 1	150.3300	-32.1536
crn 2	150.3462	-32.1539
crn 3	150.3459	-32.1712
crn 4	150.3294	-32.1709

Merriwa P.	Longitude (Deg)	Latitude (Deg)
crn 1	150.4226	-32.0876
crn 2	150.4383	-32.0879
crn 3	150.4373	-32.1205
crn 4	150.4217	-32.1201

Dales	Longitude (Deg)	Latitude (Deg)
crn 1	150.4216	-31.9229
crn 2	150.4511	-31.9234
crn 3	150.4496	-31.9832
crn 4	150.4200	-31.9825

Table A7. PLMR high resolution mapping flight lines for the Krui area.

Line No.	Altitude AGL (ft)	Altitude ASL (ft)	Length (km)	Start Longitude (Deg)	Start Latitude (Deg.)	Stop Longitude (Deg)	Stop Latitude (Deg.)
D1	625	2198	11	150.1792	-31.9580	150.1760	-32.0626
D2	625	2198	11	150.1727	-32.0625	150.1759	-31.9579
D3	625	2198	11	150.1726	-31.9578	150.1694	-32.0624
D4	625	2198	11	150.1661	-32.0624	150.1693	-31.9577
D5	625	2198	11	150.1660	-31.9577	150.1627	-32.0623
D6	625	2198	11	150.1594	-32.0622	150.1627	-31.9576
D7	625	2198	11	150.1594	-31.9575	150.1561	-32.0621
D8	625	2198	11	150.1528	-32.0621	150.1561	-31.9574
D9	625	2198	11	150.1528	-31.9574	150.1495	-32.0620
D10	625	2198	11	150.1462	-32.0619	150.1495	-31.9573
D11	625	2198	11	150.1461	-31.9572	150.1429	-32.0618
D12	625	2198	11	150.1396	-32.0618	150.1428	-31.9571
D13	625	2198	11	150.1395	-31.9571	150.1363	-32.0617
D14	625	1980	4	150.1425	-32.0737	150.1413	-32.1123
D15	625	1980	4	150.1380	-32.1123	150.1392	-32.0736
D16	625	1980	4	150.1359	-32.0735	150.1347	-32.1122
D17	625	1980	4	150.1314	-32.1121	150.1326	-32.0735
D18	625	1980	4	150.1293	-32.0734	150.1281	-32.1120
D19	625	1980	4	150.1248	-32.1120	150.1260	-32.0733
D20	625	1980	4	150.1227	-32.0732	150.1214	-32.1119
D21	625	2001	6	150.1536	-32.1424	150.1520	-32.1954
D22	625	2001	6	150.1487	-32.1953	150.1504	-32.1424
D23	625	2001	6	150.1470	-32.1423	150.1454	-32.1952
D24	625	2001	6	150.1421	-32.1952	150.1437	-32.1422
D25	625	2001	6	150.1404	-32.1421	150.1387	-32.1951
D26	625	2001	6	150.1354	-32.1952	150.1371	-32.1421
D27	625	2001	6	150.1338	-32.1420	150.1321	-32.1951
D28	625	1903	4	150.0798	-32.1645	150.0809	-32.1306
D29	625	1903	4	150.0776	-32.1306	150.0765	-32.1645
D30	625	1903	4	150.0732	-32.1644	150.0743	-32.1305
D31	625	1903	4	150.0710	-32.1304	150.0699	-32.1643
D32	625	1903	4	150.0666	-32.1642	150.0676	-32.1303
D33	625	1903	4	150.0643	-32.1303	150.0632	-32.1641
D34	625	1903	4	150.0599	-32.1641	150.0610	-32.1302
D35	625	1903	4	150.0577	-32.1301	150.0566	-32.1640

Pembroke	Longitude (Deg)	Latitude (Deg)
crn 1	150.1374	-31.9671
crn 2	150.1811	-31.9681
crn 3	150.1783	-32.0499
crn 4	150.1347	-32.0489

Stanley	Longitude (Deg)	Latitude (Deg)
crn 1	150.1203	-32.0855
crn 2	150.1441	-32.0859
crn 3	150.1437	-32.1000
crn 4	150.1198	-32.0994

Roscomm	Longitude (Deg)	Latitude (Deg)
crn 1	150.1315	-32.1538
crn 2	150.1552	-32.1544
crn 3	150.1543	-32.1837
crn 4	150.1306	-32.1831

Illogan	Longitude (Deg)	Latitude (Deg)
crn 1	150.0555	-32.1374
crn 2	150.0826	-32.1380
crn 3	150.0820	-32.1561
crn 4	150.0549	-32.1555

Table A8. PLMR high resolution mapping flight lines for the Merriwa area.

Line No.	Altitude AGL (ft)	Altitude ASL (ft)	Length (km)	Start Longitude (Deg)	Start Latitude (Deg.)	Stop Longitude (Deg)	Stop Latitude (Deg.)
D36	625	2300	9	150.4444	-31.9952	150.4467	-31.9113
D37	625	2300	9	150.4434	-31.9112	150.4410	-31.9951
D38	625	2300	9	150.4377	-31.9951	150.4400	-31.9111
D39	625	2300	9	150.4367	-31.9111	150.4343	-31.9950
D40	625	2300	9	150.4310	-31.9949	150.4334	-31.9110
D41	625	2300	12	150.4301	-31.9109	150.4277	-31.9949
D42	625	1899	12	150.3691	-31.9941	150.3659	-32.1052
D43	625	1899	12	150.3626	-32.1051	150.3658	-31.9940
D44	625	1899	12	150.3625	-31.9939	150.3593	-32.1050
D45	625	1899	12	150.3560	-32.1050	150.3592	-31.9939
D46	625	1899	12	150.3559	-31.9938	150.3527	-32.1049
D47	625	1899	12	150.3494	-32.1048	150.3526	-31.9937
D48	625	1899	12	150.3493	-31.9937	150.3460	-32.1048
D49	625	1899	12	150.3427	-32.1047	150.3459	-31.9936
D50	625	1899	12	150.3426	-31.9935	150.3394	-32.1046
D51	625	1573	4	150.3320	-32.1398	150.3307	-32.1838
D52	625	1573	4	150.3340	-32.1839	150.3353	-32.1398
D53	625	1573	4	150.3386	-32.1399	150.3373	-32.1839
D54	625	1573	4	150.3406	-32.1840	150.3419	-32.1400
D55	625	1573	4	150.3452	-32.1401	150.3439	-32.1841
D56	625	2109	6	150.4226	-32.1341	150.4243	-32.0743
D57	625	2109	6	150.4276	-32.0743	150.4259	-32.1342
D58	625	2109	6	150.4292	-32.1342	150.4309	-32.0744
D59	625	2109	6	150.4342	-32.0745	150.4325	-32.1343
D60	625	2109	6	150.4358	-32.1344	150.4375	-32.0745

Cullingral	Longitude (Deg)	Latitude (Deg)
crn 1	150.3296	-32.1534
crn 2	150.3468	-32.1538
crn 3	150.3463	-32.1713
crn 4	150.3290	-32.1709

Midlothian	Longitude (Deg)	Latitude (Deg)
crn 1	150.3401	-32.0058
crn 2	150.3708	-32.0064
crn 3	150.3683	-32.0927
crn 4	150.3376	-32.0921

Cullingral	Longitude (Deg)	Latitude (Deg)
crn 1	150.3296	-32.1534
crn 2	150.3468	-32.1538
crn 3	150.3463	-32.1713
crn 4	150.3290	-32.1709

Merriwa P.	Longitude (Deg)	Latitude (Deg)
crn 1	150.4216	-32.0874
crn 2	150.4391	-32.0878
crn 3	150.4383	-32.1206
crn 4	150.4208	-32.1204

Table A9. PLMR multi-angle mapping flight lines over the Merriwa Park farm.

Line No.	Altitude AGL (ft)	Altitude ASL (ft)	Length (km)	Start Longitude (Deg)	Start Latitude (Deg.)	Stop Longitude (Deg)	Stop Latitude (Deg.)
E1	2500	3984	6	150.4226	-32.1342	150.4243	-32.0744
E2	2500	3984	6	150.4276	-32.0745	150.4259	-32.1343
E3	2500	3984	6	150.4292	-32.1344	150.4309	-32.0745
E4	2500	3984	6	150.4342	-32.0746	150.4325	-32.1344
E5	2500	3984	6	150.4358	-32.1345	150.4375	-32.0747

	Longitude (Deg)	Latitude (Deg)
crn 1	150.4226	-32.0874
crn 2	150.4385	-32.0878
crn 3	150.4375	-32.1206
crn 4	150.4216	-32.1203

Table A10. PLMR dew effect flight lines waypoints

Waypoint No.	Altitude AGL (ft)	Altitude ASL (ft)	Longitude (Deg)	Latitude (Deg.)
F1	5000	6265	150.4291	-32.1374
F2	5000	6265	150.4297	-31.9174
F3	5000	6265	150.4297	-31.9174
F4	5000	6265	150.4265	-31.9752
F5	5000	6265	150.3553	-31.9985
F6	5000	6265	150.3523	-32.1034
F7	5000	6265	150.3403	-32.1412
F8	5000	6265	150.3392	-32.1793
F9	5000	6265	150.3556	-32.1791

Table A11. Flight lines coordinates and coverage reference coordinates for NDVI observations.

Line No.	Altitude AGL (ft)	Altitude ASL (ft)	Length (km)	Start Longitude (Deg)	Start Latitude (Deg.)	Stop Longitude (Deg)	Stop Latitude (Deg.)
G1	5000	6265	4	150.0549	-32.1682	150.0563	-32.1257
G2	5000	6265	4	150.0674	-32.1260	150.0661	-32.1685
G3	5000	6265	4	150.0772	-32.1687	150.0786	-32.1262
G4	5000	6265	26	150.1093	-32.1963	150.1169	-31.9566
G5	5000	6265	26	150.1280	-31.9568	150.1208	-32.1963
G6	5000	6265	26	150.1319	-32.1966	150.1391	-31.9571
G7	5000	6265	26	150.1501	-31.9574	150.1428	-32.1972
G8	5000	6265	26	150.1539	-32.1974	150.1615	-31.9575
G9	5000	6265	26	150.1726	-31.9577	150.1654	-32.1973
G10	5000	6265	26	150.1765	-32.1976	150.1836	-31.9581
G11	5000	6265	26	150.1947	-31.9583	150.1873	-32.1982
G12	5000	6265	30	150.3256	-32.1835	150.3334	-31.9090
G13	5000	6265	30	150.3447	-31.9094	150.3368	-32.1838
G14	5000	6265	30	150.3479	-32.1840	150.3558	-31.9096
G15	5000	6265	30	150.3669	-31.9098	150.3590	-32.1842
G16	5000	6265	30	150.3702	-32.1845	150.3780	-31.9100
G17	5000	6265	30	150.3891	-31.9102	150.3813	-32.1847
G18	5000	6265	30	150.3925	-32.1849	150.4002	-31.9105
G19	5000	6265	30	150.4114	-31.9107	150.4036	-32.1852
G20	5000	6265	30	150.4148	-32.1854	150.4225	-31.9110
G21	5000	6265	30	150.4336	-31.9112	150.4259	-32.1856
G22	5000	6265	30	150.4371	-32.1858	150.4448	-31.9111
G23	5000	6265	30	150.4559	-31.9114	150.4482	-32.1861

Illogan

	Longitude (Deg)	Latitude (Deg)
crn 1	150.0492	-32.1372
crn 2	150.0849	-32.1380
crn 3	150.0843	-32.1560
crn 4	150.0485	-32.1552

Krui

	Longitude (Deg)	Latitude (Deg)
crn 1	150.1099	-31.9665
crn 2	150.2011	-31.9686
crn 3	150.1945	-32.1840
crn 4	150.1031	-32.1820

Merriwa

	Longitude (Deg)	Latitude (Deg)
crn 1	150.3266	-31.9205
crn 2	150.4622	-31.9233
crn 3	150.4553	-32.1736
crn 4	150.3193	-32.1708

12 Appendix B: Team Task Sheets

Table B1. Task sheet for Team 1. All activities to be done by all members of the team over the four week campaign unless specified otherwise. "FL","VL" stands for fixed or variable sampling locations between days.Tasks in red are for team leaders, in blue for other members.

Team Members	Rocco Panciera, Marco Rinaldi Patricia DeRosney, Gilles Boulet , Rob Pipunic
Farm Sites	Pembroke (Krui) Midlothian (Merriwa)

Farm scale sampling: Pembroke (Krui days), Cullingral (Merriwa days)

Measurement	Extent	Spacing	N. of Samples	Comments
Soil moisture (hydra probe)	High resolution grid /FL	12.5/6.25m	289	morning
Soil moisture (hydra probe)	Farm scale/FL	62.5m	Pemb: 140 Mid: 140	afternoon
Vegetation water content samples(grab type)	Farm scale/FL	-	2	End of day
Dew vegetation samples	Farm scale/FL	-	2	On dew flight days (early morning)
Soil moisture (hydra probe)	Farm scale/FL	1000/500/250/125m	Pemb: 210 Mid: 251	
Gravimetric soil samples	Farm scale/VL	-	>2	1 dry/1 wet
Vegetation type	Farm scale	1000/500/250/125m		Week 1 only
Dew visual observation	Farm scale	-		Until drying

Regional sampling: Pembroke (morning), Midlothian (afternoon), connecting roads

Measurements	Extent	Spacing	N. of Samples	Comments
Vegetation biomass samples (quadrant type)	High resolution areas/FL	50m/62.5m	16 p/farm	Week 1,4 only
Vegetation height	Farm/ FL	50m/62.5m	-	Week 1,4 only
Soil moisture (hydra probe)	Regional/FL	1 km	122	
Gravimetric soil samples	Farm/VL	-	>6 p/farm	Different soil type/wetness
Vegetation biomass samples (quadrant type)	Farm/FL	-	>6 p/farm	1 each land cover
Vegetation type	Farm	1km	-	Week 2 only
Landuse	Regional	1km	-	Week 2 only
Surface roughness	Farm		>4 p/farm	Week 2 only
Surface rock cover	Farm	1km	-	Week 2 only
LAI (Jose Fenollar)	Farm	62.5m	-	Week 1 only
NDVI (Jose Fenollar)	Farm	62.5m	-	Week 1 only

Table B2. Task sheet for Team 2. All activities to be done by all members of the team over the four week campaign unless specified otherwise. "FL","VL" stands for fixed or variable sampling locations between days. Tasks in red are for team leaders, in blue for other members

Team Members	Greg Hancock, Cristina Martinez, Jose Fenollar & Vivianna Maggioni, Mark Thyer
Farm Sites	Stanley (Krui) Cullingral (Merriwa)

Farm scale sampling: Stanley (Krui days), Cullingral (Merriwa days)

Measurement	Extent	Spacing	N. of Samples	Comments
Soil moisture (hydra probe)	High resolution grid /FL	12.5/6.25m	289	morning
Soil moisture (hydra probe)	Farm scale/FL	62.5m	Sta: 135 Cull: 197	afternoon
Vegetation water content samples(grab type)	Farm scale/FL	-	2	End of day
Dew vegetation samples	Farm scale/FL	-	2	On dew flight days (early morning)
Soil moisture (hydra probe)	Farm scale/FL	125m	Sta: 227 Cull: 89	
Gravimetric soil samples	Farm scale/VL	-	>2	1 dry/1 wet
Vegetation type	Farm scale	125m		Week 1 only
Dew visual observation	Farm scale	-		Until drying

Regional sampling: Stanley (morning), Cullingral (afternoon), connecting roads

Measurements	Extent	Spacing	N. of Samples	Comments
Vegetation biomass samples (quadrant type)	High resolution areas/FL	50m/62.5m	16 p/farm	Week 1,4 only
Vegetation height	Farm/ FL	50m/62.5m	-	Week 1,4 only
Soil moisture (hydra probe)	Regional/FL	1 km	116	
Gravimetric soil samples	Farm/VL	-	>6 p/farm	Different soil type/wetness
Vegetation biomass samples (quadrant type)	Farm/FL	-	>6 p/farm	1 each land cover
Vegetation type	Farm	1km	-	Week 2 only
Landuse	Regional	1km	-	Week 2 only
Surface roughness	Farm		>4 p/farm	Week 3 only
Surface rock cover	Farm	1km	-	Week 2only
LAI (Jose Fenollar)	Farm	62.5m	-	Week 2 only
NDVI (Jose Fenollar)	Farm	62.5m	-	Week 2 only

Table B3. Task sheet for Team 3. All activities to be done by all members of the team over the four week campaign unless specified otherwise. "FL","VL" stands for fixed or variable sampling locations between days. Tasks in red are for team leaders, in blue for other members

Team Members	Jetse Kalma, Jennifer Grant, Patricia Saco, Daniele Biasioni
Farm Sites	Roscommon (Krui) Dales (Merriwa)

Farm scale sampling: Roscommon (Krui days), Dales (Merriwa days)

Measurement	Extent	Spacing	N. of Samples	Comments
Soil moisture (hydra probe)	High resolution grid /FL	12.5/6.25m	289	morning
Soil moisture (hydra probe)	Farm scale/FL	62.5m	Ros: 140 Dales: 140	afternoon
Vegetation water content samples(grab type)	Farm scale/FL	-	2	End of day
Dew vegetation samples	Farm scale/FL	-	2	On dew flight days (early morning)
Soil moisture (hydra probe)	Farm scale/FL	500/250/125m	Ros: 223 Dales: 120	
Gravimetric soil samples	Farm scale/VL	-	>2	1 dry/1 wet
Vegetation type	Farm scale	500/250/125m		Week 1 only
Dew visual observation	Farm scale	-		Until drying

Regional sampling: Roscommon (morning), Dales (afternoon), connecting roads

Measurements	Extent	Spacing	N. of Samples	Comments
Vegetation biomass samples (quadrant type)	High resolution areas/FL	50m/62.5m	16 p/farm	Week 1,4 only
Vegetation height	Farm/ FL	50m/62.5m	-	Week 1,4 only
Soil moisture (hydra probe)	Regional/FL	1 km	130	
Gravimetric soil samples	Farm/VL	-	>6 p/farm	Different soil type/wetness
Vegetation biomass samples (quadrant type)	Farm/FL	-	>6 p/farm	1 each land cover
Vegetation type	Farm	1km	-	Week 2 only
Landuse	Regional	1km	-	Week 2 only
Surface roughness	Farm		>4 p/farm	Week 4 only
Surface rock cover	Farm	1km	-	Week 2 only
LAI (Jose Fenollar)	Farm	62.5m	-	Week 3 only
NDVI (Jose Fenollar)	Farm	62.5m	-	Week 3 only

Table B4. Task sheet for Team 4. All activities to be done by all members of the team over the four week campaign unless specified otherwise. "FL","VL" stands for fixed or variable sampling locations between days. Tasks in red are for team leaders, in blue for other members

Team Members	Tony Wells, Chris Rüdiger, Olivier Merlin, Kauzeer Saleh, Stuart Jones
Farm Sites	Illogan (Krui) Merriwa Park (Merriwa)

Farm scale sampling: Illogan (Krui days), Merriwa Park (Merriwa days)

Measurement	Extent	Spacing	N. of Samples	Comments
Soil moisture (hydra probe)	High resolution grid /FL	12.5/6.25m	289	morning
Soil moisture (hydra probe)	Farm scale/FL	62.5m	Illo: 140 Merr: 140	afternoon
Vegetation water content samples(grab type)	Farm scale/FL	-	2	End of day
Dew vegetation samples	Farm scale/FL	-	2	On dew flight days (early morning)
Soil moisture (hydra probe)	Farm scale/FL	250/125m	Illo: 228 Merr: 179	
Gravimetric soil samples	Farm scale/VL	-	>2	1 dry/1 wet
Vegetation type	Farm scale	250/125m		Week 1 only
Dew visual observation	Farm scale	-		Until drying

Regional sampling: Illogan (morning), Merriwa Park (afternoon), connecting roads

Measurements	Extent	Spacing	N. of Samples	Comments
Vegetation biomass samples (quadrant type)	High resolution areas/FL	50m/62.5m	16 p/farm	Week 1,4 only
Vegetation height	Farm/ FL	50m/62.5m	-	Week 1,4 only
Soil moisture (hydra probe)	Regional/FL	1 km	99	
Gravimetric soil samples	Farm/VL	-	>6 p/farm	Different soil type/wetness
Vegetation biomass samples (quadrant type)	Farm/FL	-	>6 p/farm	1 each land cover
Vegetation type	Farm	1km	-	Week 2 only
Landuse	Regional	1km	-	Week 2 only
Surface roughness	Farm		>4 p/farm	Week 1 only
Surface rock cover	Farm	1km	-	Week 2 only
LAI (Jose Fenollar)	Farm	62.5m	-	Week 4 only
NDVI (Jose Fenollar)	Farm	62.5m	-	Week 4 only

13 Appendix C: Flight Elevations

Table C1. Elevation statistics for the study area and the focus farm

	MIN (m)	MAX (m)	RANGE (m)	MEDIAN(m)	MEAN (m)
Norther Goulburn	180	807	627	375	384
Krui area	273	686	414	396	399
Merriwa area	220	676	456	365	372
Pembroke	346	510	204	394	399
Stanley	316	443	127	358	355
Roscommon	344	450	106	392	393
Illogan	348	420	72	381	384
Dales	330	541	211	398	404
Midlothian	259	419	159	310	312
Merriwa Park	380	483	102	413	416
Cullingral	222	319	98	233	244

Table C2. Flight altitude and ground resolution for PLMR medium resolution flights

	Flight Altitude over local maximum elevation (ft AGL)	FINAL FLIGHT ALTITUDE m(ASL)	Minimum ground pixel sixe(m)	Maximum ground pixel size (m)
Pembroke	2400	1240	240.0	293.8
Stanley	2400	1170	240.0	281.8
Roscommon	2400	1180	240.0	274.6
Illogan	2400	1150	240.0	263.5
Dales	2400	1270	240.0	309.3
Merriwa Park	2400	1210	240.0	273.6
Midlothian	2400	1150	240.0	292.3
Cullingral	2400	1050	240.0	272.1

Table C3. Flight altitude and ground resolution for PLMR high resolution flights.

	Flight Altitude over local maximum elevation (ft AGL)	FINAL FLIGHT ALTITUDE m(ASL)	Minimum ground pixel sixe(m)	Maximum ground pixel size (m)
Pembroke	525	670	52.5	106.3
Stanley	525	600	52.5	94.3
Roscommon	525	610	52.5	87.1
Illogan	525	580	52.5	76.0
Dales	525	700	52.5	121.8
Midlothian	525	580	52.5	104.8
Merriwa Park	525	640	52.5	86.1
Cullingral	525	480	52.5	84.6

Appendix A2:
The HDAS Spatial Data Acquisition System Manual

empty page

The Hydraprobe Data Acquisition System (HDAS): User Guide

Rocco Panciera, Olivier Merlin, Rodger Young and Jeffrey Walker

Department of Civil and Environmental Engineering

The University of Melbourne

Created: July 2007
Updated: October 2008

Contents

1. Introduction to the HDAS

The Hydraprobe Data Acquisition System (HDAS) is a spatially enabled soil moisture, temperature and salinity measurement platform that logs all relevant information into GIS format using ArcPad®. The HDAS was developed by the Department of Civil and Environmental Engineering at the University of Melbourne and is composed of a Stevens Water Hydraprobe®, an iPAQ® pocket PC, and a Bluetooth GPS receiver (Fig. 1). The pocket PC is used to (Fig. 2):

- display a map of the sampling area;
- communicate with the GPS receiver to get the real time position;
- display the sampling position on a background map;
- communicate with the Hydraprobe to take readings of soil moisture, temperature soil salinity, soil conductivity, real and imaginary soil dielectric constant;
- obtain metadata including sample date, time and ID;
- input any additional metadata such as vegetation type and general comments;
- store the metadata and Hydraprobe readings in a GIS shape file;

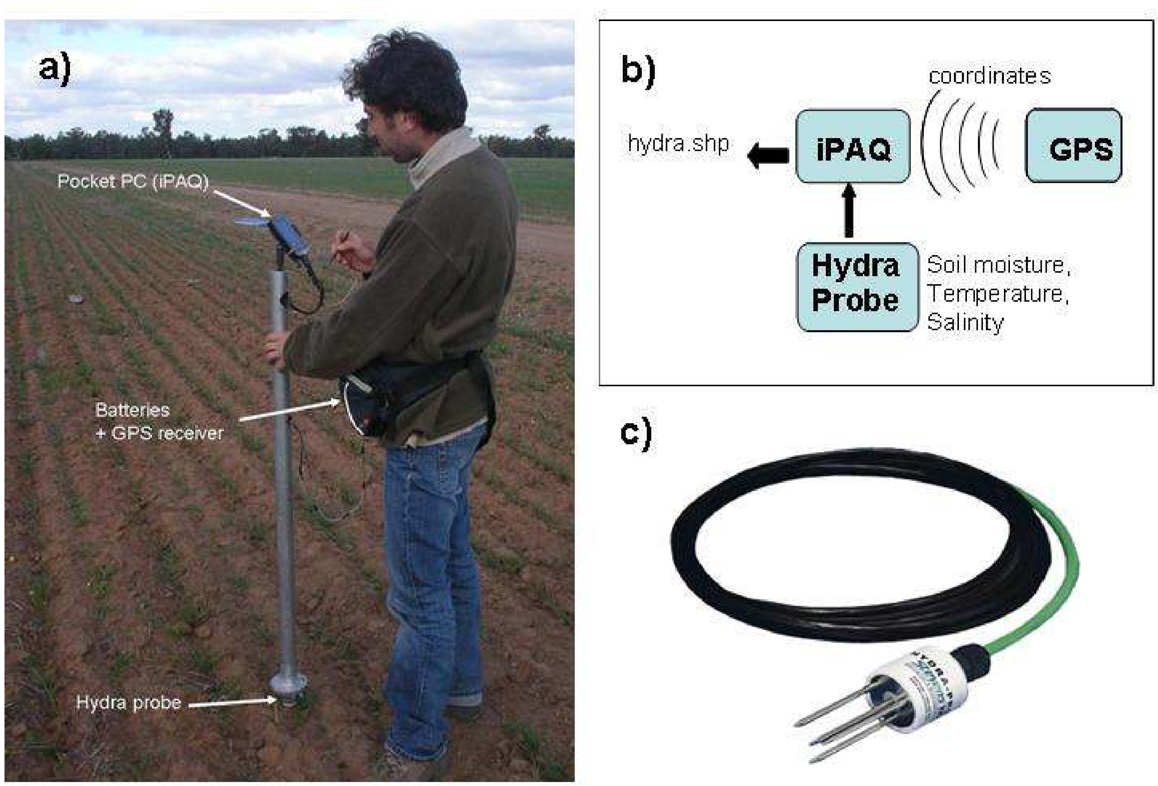

Figure 1. a) The Hydraprobe Data Acquisition System (HDAS), b) schematic of the HDAS system functionality, and c) the Stevens' Hydraprobe.

- display the location of the Hydraprobe measurements on the map.

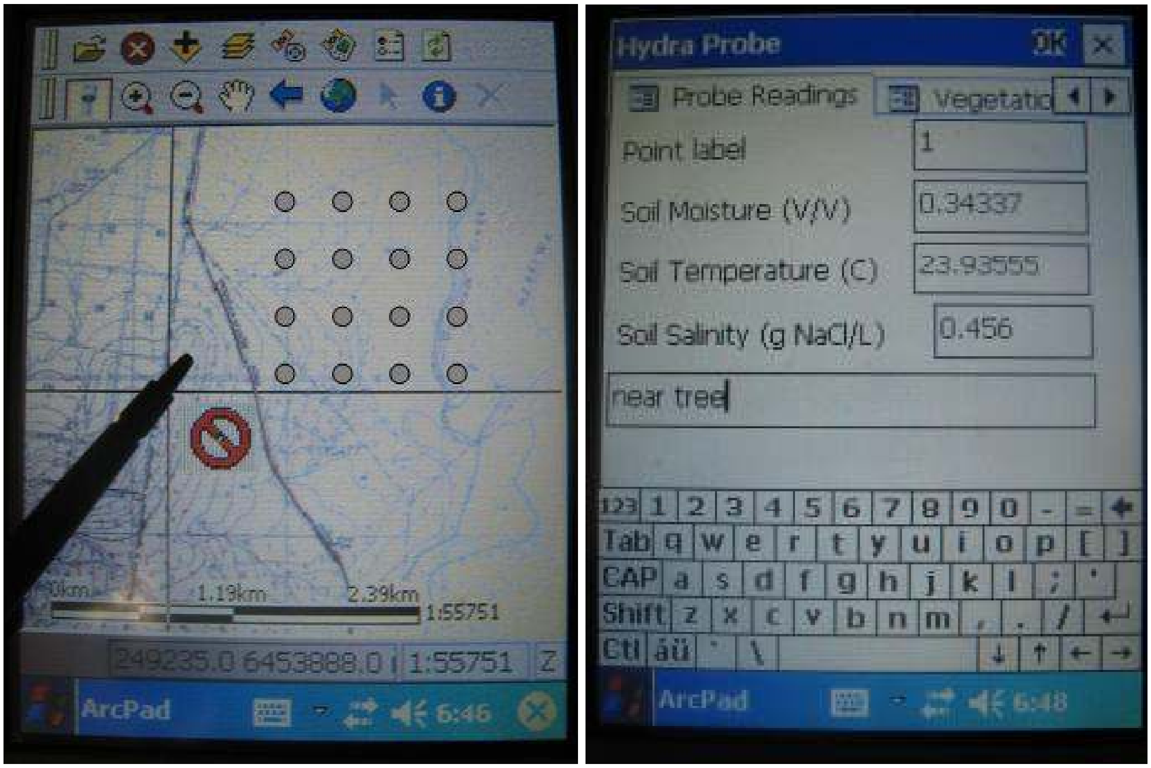

Figure 2. The HDAS interface in a) navigation and b) data entry modes.

The Stevens' Hydraprobe is a soil sensor for measuring soil moisture, temperature and salinity (for details, see Hydra Soil Moisture Probe User manual in the "Documentation" folder that accompanies this manual). The instrument determines soil moisture and salinity by making a high frequency (50 MHz) complex dielectric constant measurement. A complex dielectric constant measurement resolves simultaneously the capacitive and conductive parts of a soil's electrical response. The capacitive part of the response is most indicative of soil moisture while the conductive part reflects predominantly soil salinity. Temperature is determined from a thermistor incorporated into the probe head. As a soil is wetted, the low dielectric constant component of air is replaced by the much higher dielectric constant component of water. Thus, as a soil is wetted, the capacitive response (which depends upon the real dielectric constant) increases steadily. Through the use of appropriate models, the dielectric constant measurement can be directly related to soil moisture. The dielectric constant of moist soil has a small, but significant, dependence on the soil temperature while soil conductivity varies strongly with temperature. The soil temperature measurement that the Hydraprobe makes is used to remove temperature effects, and the raw voltages measured by the probe converted to soil moisture using some circuitry in the probe head. A soil type option can be set when programming the circuitry of each probe; Sand, Silt or Clay. In case no knowledge of the soil type is available, it is recommended by the manufacturer that the option "silt" be chosen. This affects the calculation of soil moisture output done internally by the Hydraprobe. Nevertheless, in the current version of the HDAS system described in this document, this soil type option is by-passed and a soil-specific calibration is applied to the raw Hydraprobe dielectric measurements, which are unaffected by the soil type option setting. Therefore the soil type to which the probe is initialized has no effect on the output (see section 21).

2. How to use this manual

This manual covers a variety of information, ranging from simple use of the system through to general guidance on customisation of the acquisition software for a particular application. Consequently the manual has been organised as follows:

- If you simply need to operate the HDAS system which has been already set-up for your study area: go to section 3
- If you need to set-up the physical HDAS system: go to section 4;
- If you need to set-up the HDAS system software: go to section 5;
- If you need to adapt the HDAS system software to your specific needs: go to section 6;
- If you are having trouble with using the HDAS system: go to section 7;
- For details about the HDAS soil moisture output, its calibration and expected accuracy, go to section 8.

NOTE: *The HDAS system software provided with this manual has been developed using an iPAQ hx2110 with Pocket PC operating system Windows Mobile 2003 and ArcPad version 6.03. The software provided may not work with other makes of iPAQ or versions of software.*

3. Using the HDAS system

This section assumes that the HDAS system has already been set up and all the necessary files and software have been loaded on the iPAQ. If that is not the case, refer to sections 4 and 5 before reading this section.

3.1. Navigating the iPAQ

This section gives a brief introduction to general navigation of an iPAQ (numbers reference to Fig. 3):

- To turn the iPAQ on/off: use the button at the top right corner of the device (1). NOTE that the iPAQ goes into sleep mode after a couple of minutes when on battery power. To revive it, press the on/off button again;
- To access any program (eg, ArcPad or file explorer), use the “Start” button on the top left corner (2) and select the program from the drop-down list. NOTE: Only recently used programs are available from this list; all programs are available in the folder “programs”;
- To change iPAQ settings like sleeping time, screen brightness, battery saving options etc, select “settings” from the “start” drop-down list;
- To minimise ArcPad, tap the blue cross on the bottom toolbar (14). NOTE: this does not exit the program, which can be maximised by tapping the program icon on the bottom toolbar of the main windows screen;
- To exit ArcPad, tap the red cross on the top toolbar (5).

Figure 3. a) General iPAQ commands and b) HDAS interface through the ArcPad software

Quick reference to HDAS use (refer to Fig. 3)

- *Activate the* Hydraprobe *by tapping the "Hydraprobe" command (10);*
- *Navigate to an intended sampling location (16) making use of the GPS position indicator (15) and/or a map of the area;*
- *With the "Hydraprobe" button depressed, tap anywhere on the screen to interrogate the probe;*
- *View the* Hydraprobe *readings and fill in other information in the ArcPad forms as desired (see Fig. 4);*
- *Store the measurement with the spatial coordinates by tapping "ok" at the top of the form or cancel reading by tapping the "X";*
- *The coordinates stored are those from the GPS if activated, or the position on the screen if the GPS is not activated;*
- *Move to the next sampling location and take another reading.*

3.2. Starting the HDAS system

Follow the procedure outlined below to start the HDAS system (numbers reference to Fig. 3):

1. Turn on the iPAQ by pressing the button at the top right corner of the device (1);
2. Start ArcPad by tapping the "program" access icon on the top left corner of the iPAQ (2) screen and selecting "ArcPad";
3. Load the ArcPad map file with the "load map" command (4), or individually the background map and sampling locations shape file (if you have them) together with hydra.shp and/or hydraGRID.shp with the "load layers" command (6);
4. Turn on the GPS receiver;
5. Establish a Bluetooth connection between the GPS and iPAQ (see section 3.3);
6. Activate the GPS in ArcPad by tapping the "GPS" icon (8) and tapping "ok".

3.3. Connecting the GPS to the iPAQ

The GPS device needs to be bonded with the iPAQ and a connection established BEFORE activating the GPS from ArcPad; see section 5.4 on how to bond the GPS if not already done.

To establish a Bluetooth connection between the iPAQ and the GPS device:

1. Tap the "GPS connection" icon in the bottom right corner of the screen (3);
2. Activate Bluetooth by tapping the "Bluetooth" icon (3);
3. Select "Bluetooth Manager";
4. Tap **and hold** the icon representing the GPS device you are connecting to, and select "connect". If this step is successful, two horizontal green arrows will be added to the GPS device icon. NOTE: if the GPS device is not present see section 5.4 on bonding the GPS;
5. Exit from the Bluetooth manager.

NOTE: It is not uncommon to have problems receiving a valid GPS signal from the GPS receiver (i.e. no "position fix" is available). First check that the GPS receiver has a lock on the GPS satellites as indicated by a status light; it may take several minutes for this to occur after first turning the GPS receiver switch to on. If the GPS status light is active and the problem persists, un-bond the GPS device from the iPAQ by removing the GPS device icon in the Bluetooth manager connection list, then re-bond the GPS as described in section 5.4 and repeat the connection procedure above.

3.4. Taking a Hydraprobe reading

Follow the procedure outlined below to take a Hydraprobe reading:

1. Select the "Hydraprobe" command (10) on the bottom left corner of the HDAS Toolbar menu to activate the program that reads the Hydraprobe values. NOTE: this button must be depressed in order to take a reading of the Hydraprobe – should only need to be depressed once;
2. Navigate to the sampling point by moving to the desired location in the landscape or until the GPS position indicator is overlapping with the desired sampling location on the ArcPad display;
3. Insert the Hydraprobe vertically in the ground, until the base of the Hydraprobe head is at the ground surface level. Be sure to not create air gaps when inserting the probe. Apply steady pressure to the footplate to assist with insertion in hard soils;
4. Take a Hydraprobe reading by tapping anywhere on the screen and wait for 5-9 seconds (Be patient! DO NOT tap anything on the iPAQ screen during this time);
5. After 5-9 seconds, a form appears in ArcPad containing three pages (Fig. 4), each containing several text boxes:

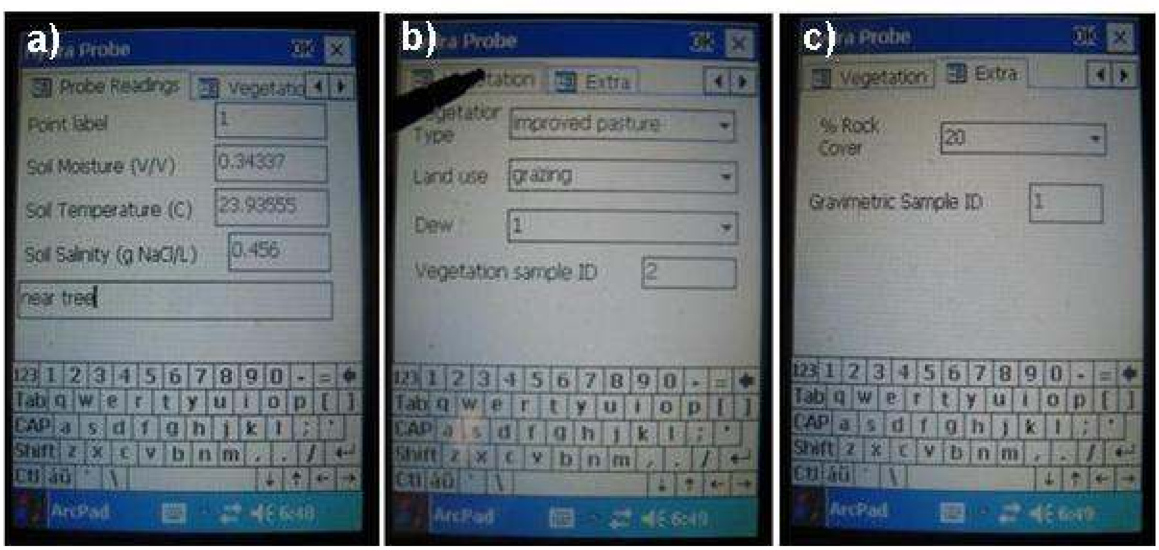

Figure 4. General layout of the pages in the HDAS form: a) Probe readings page; b) Vegetation page and c) Extra page.

***NOTE**: Before the form appears, an error message might be displayed warning that the measured soil dielectric constant is out of a specific range. This in general means that the soil volume sampled by the probe is disrupted or with significant air gaps affecting the reading. After pressing "ok" on the error window, It is suggested to cancel the current point (by tapping the "X" on the form), insert the probe carefully at a different location and repeat the reading.*

Probe readings page

- Point sequential number – AUTOMATICALLY FILLED but can be manually edited
- Hydraprobe soil moisture reading (in volumetric water content fraction) - AUTOMATICALLY FILLED
- Hydraprobe soil temperature reading (in degrees Celsius) - AUTOMATICALLY FILLED
- Hydraprobe soil salinity reading (in g of NaCl per liter) - AUTOMATICALLY FILLED
- Comment text box - MANUAL

Vegetation page

- Vegetation type text box, to be chosen from a drop down list- MANUAL;
- Landuse text box, to be chosen from a drop down list- MANUAL;
- Vegetation sample ID text box- MANUAL

Metadata page

- Soil sample sequential ID – MANUAL.

6. Navigate throughout the three pages and fill in the desired text boxes. NOTE: there is no specific order required when completing the forms in order to successfully save the points. Nevertheless, apart from the point sequential number the AUTOMATICALLY FILLED fields cannot be changed/deleted.

7. The user can:
    - Accept the point by tapping "ok" on the top right corner of the form (Fig.4). This will store the point and measurement taken.
    - Cancel the point by tapping the "X" next to the "ok" button (Fig.4). This will discard the current record permanently.

NOTE: The HDAS has been developed to save the Hydraprobe *readings together with the spatial coordinates measured by the GPS device. In case the GPS is turned off at the time of taking a reading, the reading will be saved in the shapefile "hydraGRID", with coordinates corresponding to the location tapped on the ArcPad screen by the user. Otherwise the reading is saved in the shapefile "hydra". A warning of this will be displayed upon saving the point.*

3.5. Creating and deleting points manually

To create a point in the shape file without reading the Hydraprobe:

- Make the hydra or hydraGRID shape file editable by taping on the "layer control" (7) and checking the editable box next to the shape file and taping "ok"; NOTE: this will display an "editing" toolbar which will be placed between the HDAS 1st and 2nd default toolbars (see Fig. 3b);
- Tap on the "add point" button on the new toolbar (the icon is a single blue dot to take position from screen, or blue dot with GPS to take position from the GPS) to activate the editing mode;
- Tap on the screen to create a point at the desired location and tap "ok".

To delete a point in the shape file:

- Make the hydra or hydraGRID shape file editable by taping on the "layer control" (7) and checking the editable box next to hydra.shp and taping "ok";
- Tap on the black arrow (11) to activate the selection mode;
- Select the point to be deleted by tapping on it **once**;
- Tap on the red cross (13) and click "Yes".

3.6. Review the values stored at a location

To review a point in the shape file:

- Make the hydra or hydraGRID shape file editable by taping on the "layer control" (7) and checking the editable box next to hydra.shp and taping "ok";
- Tap on the "information" button in the menu (12);
- Tap on the point to be reviewed;

3.7. Editing the values stored at a location

The values stored at a location are saved into fields of the hydra or hydraGRID shape files and can be edited manually:

- Make the shape file editable by taping on the "layer control" (7) and checking the editable box next to the shape file and taping "ok";
- Tap on the black arrow in the menu (11) to activate the selection mode;
- Select the point to be edited by tapping on it **twice**;
- Tap on a field to select it;
- Edit the selected field by using the key board (the key board appears when clicking on the icon at the bottom of the screen) and click "ok".

4. HDAS physical and electrical system setup

The components listed in Table 1 and illustrated in Fig. 5 are required to set up the HDAS system. All the electronic devices, including iPAQ, Hydraprobe and GPS receiver, are powered by a small 12V gel cell battery carried in a bumbag. This provides sufficient power for day-long sampling with the system in a field portable configuration.

The HDAS system components are to be assembled as follows:

- Connect the Hydraprobe signal cable to the "RS485" side of the CONV485 adaptor;
- Connect the "RS232" side of the CONV485 adaptor to the iPAQ Split sync (RS232/USB) cable;
- Connect the 5V iPAQ power cable to the iPAQ Split sync (RS232/USB) cable;
- Neatly thread the Hydraprobe and iPAQ cables through the pole assembly;
- Firmly attach the Hydraprobe at the bottom of the pole assembly;
- Mount the iPAQ cradle on the top of the pole assembly;
- Place the GPS receiver, power adapters, gel cell battery and any loose cable in the bumbag which is to be carried around the waist. *IMPORTANT: Make sure that the battery terminals will not be short circuited!!*
- Connect the 12V/5V power adaptor to the gel cell battery;
- Connect the Hydraprobe, iPAQ and GPS power cables to the 12V/5V power adaptor when ready to operate;
- Mount the iPAQ in the iPAQ cradle and attach the iPAQ Split sync (RS232/USB) cable when ready to operate.

Table 1. The HDAS components.

Component	Origin
Hydraprobe (12V), iPAQ (5V) and GPS (5V) power cables	Commercially available
12V gel cell battery	Commercially available
Bumbag	Commercially available
Aluminum pole	Custom made
iPAQ cradle	Commercially available
CONV485 adaptor	Commercially available
12V/5V power adaptor	Made from commercial components
Split sync (RS232/USB) cable	Modified from commercially available[1]
Stevens Water Hydraprobe®	Modified from commercially available[1]

[1] For detailed diagrams on how to modify these items refer to section 9 of this manual.

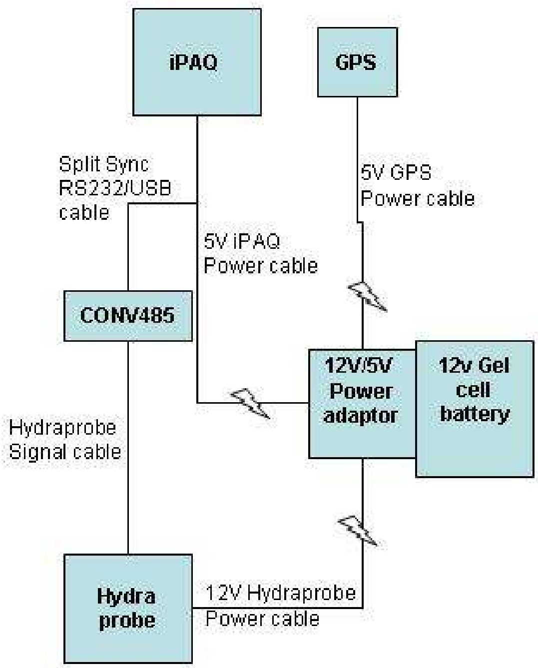

Figure 5. The HDAS electrical setup

5. HDAS software and file system setup

Use of the HDAS relies on two connections:

- Hydraprobe to iPAQ through the sync cable, and
- GPS receiver to iPAQ through Bluetooth

Setting up of the HDAS system requires connection of the iPAQ with a desktop computer and preparation of spatial database on the desktop computer. The following two sections illustrate how to achieve these tasks.

5.1. Connection with a desktop computer

- Install Microsoft ActiveSync® on the desktop computer;
- Turn on the iPAQ, connect it to the computer and establish a connection;
- Access the iPAQ file system through the "connect" command in ActiveSync®;
- To install software on the mobile device, please refer to the software manual;
- To exchange files with the iPAQ, simply copy and paste them between the iPAQ and the desktop PC folders.

5.2. Preparation of spatial data in ArcGIS

A variety of spatial data can be imported into ArcPad to serve as background information to your spatial acquisition system (eg topographic maps, road networks, predefined sampling locations, etc). The process of getting spatial data into the ArcPad environment requires the availability of ArcGIS installed on a desktop computer, and involves the following steps:

- Download and install ArcPad extension for ArcGIS from www.esri.com;
- Upload your spatial data into ArcGIS;
- Load all the layers you want to be part of your spatial acquisition system;
- Use the "Get data for ArcPad" command to create an ArcPad map file with all the desired layers. All the files will be saved into the folder "Data for ArcPad";
- Connect your iPAQ to the desktop computer using ActiveSync® (see section 5.1);
- Copy and paste the folder "Data for Arcpad" as your desired working directory on your iPAQ. Note: it is recommended your working directory be on the storage card in case of complete battery depletion.

5.3. Connection with Hydraprobe

The iPAQ communicates with the Hydraprobe through its serial port, generally called COM1 (located at the bottom of the iPAQ). The GIS software ArcPad® manages the communication with the Hydraprobe and therefore needs to be installed on the iPAQ. It is recommended that ArcPad version 6.03 be used.

The following **extension** must also be installed on the iPAQ (included in the HDAS file package in the "Utilities" folder):

1. **ArcPad menu fix extension** (for ArcPad® 6.0.3): solves some problems associated with menu items display in ArcPad on iPAQ model hx2110. To install, copy and overwrite the "ArcPad.exe" executable file into the ArcPad folder on your iPAQ (Program files/Arcpad/).

The **files** that must be uploaded on the iPAQ in order to run the HDAS system are listed below, grouped by folder **on the iPAQ** where they are to be copied (all files are included in the HDAS file package in the "Data files" and "Software" folders):

REQUIRED FILES

<u>In /Program files/Arcpad/Applets</u>

1. Visual Basic script file "**hydra_code.vbs**" and Arcpad applet file "**hydra_applet.apa**": These files contain the VB routines and forms that ArcPad uses to interrogate the Hydraprobe, and they must be the only .vbs and .apa files in this folder as ArcPad loads them automatically on start up;

2. Parameter file "**Parameters.dbf**": This table contains 5 parameters that are used in the HDAS soil moisture calculations explained in section 8. The file can be edited in order to use custom parameters.;

3. Bitmap file "**Hydra_icon**": This file is required in order to have the Hydraprobe button icon properly displayed as in Fig. 2;

<u>In Custom working directory</u>

4. Shape file "**hydra.shp**" must be uploaded into the desired working directory on the iPAQ, which can be any directory in the iPAQ file system. It is recommended that the working directory be located on your storage card in case of power depletion. This shapefile is where the measurements will be saved together with the GPS coordinates. NOTE: all the files associated with the shapefile must be loaded into the same directory;

5. The shape file "**hydraGRID.shp**" must be uploaded into the desired working directory on the iPAQ. This shapefile is where the measurements taken when the

NOTE*: The coordinate systems of all the files loaded on the iPAQ MUST be the same for ArcPad to display them. A simple trick to do this is to open the image file on a desktop version of ArcPad, then create a new file "hydra.shp" into this project and save the whole thing as a .apm map file.*

GPS is disconnected will be saved.

<u>In /Program files/Arcpad/System</u>

6. Default configuration file **“ArcPad.apx”:** This file sets the visibility of the inbuilt toolbars and the custom toolbars, and also adds the functionality to allow the coordinates (from the GPS receiver or screen) to be saved into the relevant fields of the data shapefiles (“hydra” or “hydraGRID”);

OPTIONAL FILES

<u>In Custom working directory</u>

7. A shapefile with any name, containing pre-established sampling locations can be loaded into you ArcPad working directory.

8. An **image** of the monitoring area (i.e. topographic map) can be loaded into the desired ArcPad working directory to help with navigation. It is recommended that the image be in MrSid compressed format to optimise the performance of ArcPad.

9. An ArcPad map file (*.apm) can be created and loaded into the ArcPad working directory, containing the shapefiles “**hydra.shp**” and “**hydraGRID.shp**”, together with the shape file for pre-established sampling locations and the image

Table 2. ArcPad serial port and GPS settings.

AUX tab	
Serial port	Com1
Baud rate	9600
Parity	None
Rts control	Enable
Dtr control	Enable
Data bits	8
Stop bits	1
GPS tab	
Serial port	Com8
Baud rate	4800
Parity	None
Rts control	Disable
Dtr control	Disable
Data bits	8
Stop bits	1
Infrared checkbox	Checked

file. This file simplifies the management of all the files and setting by grouping them into a single file. NOTE: An .apm file can be created using the desktop ArcPad by loading all the desired files and then choosing “save map as” from the “folder” menu.

The ArcPad **settings** regarding the serial communication with Hydraprobe – accessible through the Arcpad setting menu button (8) – must be set as indicated in Table 2.

5.4. Connection with GPS device

Virtually any GPS device can be used with the HDAS system, provided it can be connected with the particular iPAQ used and that it can be read from ArcPad. There are some known issues with the connection of ArcPAd and some brands of GPS devices (see *ESRI support website: http://support.esri.com/index.cfm?fa=homepage.homepage*). The configuration described in this section is valid for Bluetooth devices only.

The Bluetooth® software necessary to bond GPS devices must be installed on the iPAQ in order to use HDAS. This is generally part of the default Pocket PC software suite that comes with the iPAQ and does not require any particular action from the user. The ArcPad **settings** regarding GPS and serial communication – accessible through the Arcpad setting menu, button (8) – must be set as indicated in Table 2.

Before attempting any connection with the GPS device, a bond needs to be created between the device and the iPAQ. To create the bond:

1. Tap the “GPS connection” icon in the bottom right corner of the screen (3);
2. Activate Bluetooth by tapping the “Bluetooth” icon;
3. Select “Bluetooth Manager”;
4. Select “new” at the bottom right corner of the screen and scroll down until “Explore a Bluetooth device”. Tap “next” on the bottom right;
5. Wait for the GPS device to be detected and its icon displayed in the blank page. This might take a few minutes. *NOTE: in this phase, ALL Bluetooth devices that are switched on and within the range of action of Bluetooth will be shown. Make sure to identify the correct GPS device if multiple systems are in use.*
6. Tap on the GPS icon;
7. A wizard will appear with the services offered by the GPS receiver. Select the service that is available and tap “next”;
8. An information page will appear confirming that the bond has been created. Review the information and tap “finish”.

The bond between iPAQ and GPS device is temporary and can be interrupted (for example, if the GPS device battery goes flat or the GPS device stays out of range for a prolonged period). If you are having trouble getting a signal from you GPS device in ArcPad, most probably it is because the bond has been broken.

6. Customising the HDAS system

A lot of changes can be made to the HDAS system, some of which could require complex programming and different set-ups of the electronic devices involved. This section simply serves as a reference for the resources and actions that are needed in order to customise the system for some of the most simple and obvious changes.

6.1. Different data acquisition and storing

The files that control the communication and storing of data between the iPAQ, the GPS, and the Hydraprobe are:

- The ArcPad applet file "**hydra_applet.apa**": determines the structure and entries of the ArcPad forms that are displayed, and the custom toolbars. It also calls the visual basic script file for processing tasks.
- The visual basic script file "**hydra_code.vbs**": contains the VB commands to process tasks like opening the serial port, interrogating the probe etc.
- The default configuration file "**ArcPad.apx**". Determines the visibility of the inbuilt toolbars.

Both files are saved into the applets folder on your iPAQ (/Arcpad/Applets). These files can be modified within the ArcPad Application Builder Environment software (a default component of the ArcPad installation package). Most applications require none or very simple Visual Basic programming. Please refer to the ArcPad Application Builder help to learn more about customising these files.

The files where the data are stored are:

- Shapefile "hydra.shp" when the GPS is turned on
- Shapefile "hydraGRID.shp" when the GPS is turned off

The structure and content of these files can be easily changed to match the way data are stored by the .apa and .vbs files. These files must be created/changed in ArcPad, with the command "new layer".

Table 3 shows the structure of the hydra and hydraGRID shape file fields in the current HDAS system setup. The record format and whether the record value is updated automatically or is prompted by the user are also indicated.

6.2. Different iPAQ or GPS

The HDAS system was developed with HP iPAQ hx2100 series running Windows Mobile 2003 and ArcPad® version 6.0.3. Use of different iPAQ models and software versions might create problems that cannot be entirely predicted. To solve these

Table 3. Structure of the files hydra.shp and hydraGRID.shp.

FIELD NAME	DESCRIPTION	FORMAT	INPUT
DATE	Date of acquisition	MM/DD/YY	Automatic
TIME	Time of acquisition	HH.MM.SS. AM/PM	Automatic
POINT ID	Sequential number of sample	Integer	Automatic
LATITUDE	Geographic latitude	Decimal	Automatic
LONGITUDE	Geographic longitude	Decimal	Automatic
TEMP_C	Soil temperature [C]	Decimal	Automatic
CONDUCT	Soil conductivity [S/m]	Decimal	Automatic
CONDUCT_TC	Temperature corrected soil conductivity (S/m)	Decimal	Automatic
SALINITY	Soil salinity [g of NaCl/l]	Decimal	Automatic
REAL_DC	Real dielectric constant	Decimal	Automatic
REAL_DC_TC	Temperature corrected real dielectric constant	Decimal	Automatic
IMAG_DC	Imaginary dielectric constant	Decimal	Automatic
IMAG_DC_TC	Temperature corrected imaginary dielectric constant	Decimal	Automatic
CAL_MOISTU	HDAS calibrated soil moisture [%v/v]	Decimal	Automatic
COMMENT	User comment	Text	User-prompted
VEG TYPE	Vegetation type at sampling location	Text	User-prompted
LANDUSE	Landuse at sampling location	Text	User-prompted
VEG ID	Vegetation sample #	Integer	User-prompted
SOIL ID	Soil sample #	Integer	User-prompted

problems please refer to the ESRI support website: http://support.esri.com/index.cfm?fa=homepage.homepage.

Important issues to consider when testing new configurations are:

- Compatibility between ArcPad version and iPAQ operating system. In general, the latest ArcPad releases are only compatible with latest Windows Mobile versions, and commercially available iPAQs.
- Known bugs of ArcPad new releases. Check on the ESRI support website for known problems of every ArcPad release and service pack patches that fix these problems.
- Serial ports on the iPAQ. Serial ports are internally addressed by the iPAQ's OS with the code COMX. ArcPad refers to the port as named by the OS. In general, the bottom port (Hydraprobe serial cable) is addressed as COM1, and the Bluetooth port (GPS) as COM8, but that can change between iPAQs. If so, the correct port name needs to be substituted in the ArcPad AUX and GPS settings (see Table 2).

- GPS data protocol. Every GPS device has a communication protocol which has to be set in the "protocol" page of ArcPAd settings. New GPS devices with different, un-supported protocols can still be used, but some C/C++ programming is required in this case (see ArcPad Application Builder help).

7. Troubleshooting

7.1. iPAQ troubleshooting

The iPAQ doesn't respond to any input.
Perform a soft reboot of the device by pressing the button on the bottom side of the device with the iPAQ pencil. The GPS connection will then have to be re-established and ArcPad started again. No data will be lost.

The iPAQ is dead, the battery indicator doesn't blink despite the battery being properly connected.
The iPAQ battery is too low. Extract the battery, leave it disconnected from the device for 5 minutes, re-insert the battery and leave charging for at least 30 minutes, until the battery indicator starts blinking again.

The iPAQ doesn't connect to my desktop computer.
Make sure you are using the latest version of Microsoft ActiveSync. Make sure the iPAQ cable is properly connected to the desktop computer.

7.2. GPS troubleshooting

The iPAQ doesn't connect with the GPS device.
Make sure the GPS device is turned on and charged.

There is no GPS icon in the Bluetooth manager.
The GPS device hasn't been bonded with the iPAQ. Make sure the GPS device is turned on and charged. To bond the GPS device, tap "new" and select "explore a Bluetooth device". When the GPS device is detected, tap the serial port option "SPP serial port". When the bond is confirmed, tap "finish" and connect to the GPS device as explained above in "Connect the GPS to the iPAQ connection".

ArcPad Error: no fix GPS position.
The GPS device is unable to determine a fix position. Stay in place and wait for a few minutes until a fix position is achieved. Make sure the GPS status light is active and the GPS is bonded to the iPAQ.

ArcPad Error: too many data are received from your GPS device.
Press ok and Ignore.

7.3. ArcPad troubleshooting

ArcPad Error appears when I try to interrogate the probe.

Error windows might appear while interrogating the probe through ArcPad. Error messages are generally vague and of the kind “error, line 89, source text unavailable”. Usually, these are associated with lack of power to the probe or disconnection of one of the HDAS components. The general rule is to press “ok” on the error window, wait a few seconds and retry the command. If the error persists, please do the following:

- Check that all the connections are firm
- Check that the battery adaptor is firmly connected to the battery
- Check that the iPAQ USB serial port is firmly connected
- Check that the iPAQ is turned on and not low in battery
- Check that all the system components are powered properly
- Check that the GPS and AUX page of the Arcpad settings menu (accessible through the Arcpad setting menu button (8) in Figure 3b) are set as indicated in Table 2. *NOTE: these settings could have been changed during reboot or if the iPAQ battery went flat*

Repeated error at source code line 83 or “Bad reading” message box

This error has been observed in particular on new versions of iPAQ running releases of windows mobile higher then 2003. to solve it:

- Unplug and plug the iPAQ USB serial port (see figure 3a)
- Reeboot the ipaq
- Restart your HDAS session (see section 3.2)

8. HDAS soil moisture calculation

The HDAS output stored in the “hydra” and/or “hydraGRID” shapefiles includes a range of probe output quantities at each reading point. These include four voltage readings which are interpreted as soil characteristics including the real and imaginary components of the soil-water mixture dielectric constant, soil conductivity, soil temperature, soil moisture and soil salinity. All these quantities are calculated internally by the probe head and stored in the “hydra” or “hydraGRID” shapefiles as output from the probe. Note that these outputs are unaffected by the already discussed soil type option to which each probe is initialized. For details about these calculations, please refer to the Hydraprobe manual included in this package.

The accuracy of the standard Hydraprobe soil moisture output has been found by several independent field tests to be poorer than the stated manufacturer accuracy; this was observed particularly in clay soils characterised by warm temperatures. Moreover, in clayey soils, the Hydraprobe standard output showed highly reduced sensitivity to changes in soil moisture over approximately 30% v/v moisture content. Therefore, the current version of the HDAS system described in this document provides an advanced soil moisture output (CAL_MOISTU in table 3); This is calculated by the HDAS software using the calibration developed by [1]-[3]. This robust calibration is implemented in the HDAS software together with a soil temperature correction developed and tested by [4]. This soil moisture value, and NOT the Hydraprobe standard output, is also that displayed on the IPAQ screen during sampling.

This advanced soil moisture product implicitly accounts for variation in soil type through the imaginary and real parts of the dielectric constant and exhibits better accuracy over a variety of soils (+/3.5%v/v) than that from the manufacturers soil type dependent relationship. It is also more stable with respect of variations in soil temperature, particularly for clay soils. A detailed description of the calibration equations can be found in [4], a copy of which is included in this HDAS file packaged in the "documentation" folder. However, we want to draw attention to two important issues to be considered when using this advanced soil moisture product:

- The two main steps of the calibration are 1) Correction of the output real dielectric constant (REAL_DC in table 3) for soil temperature effect and 2) calculation of soil water content as a function of the corrected value of the dielectric constant. Both steps involve the use of parameters derived from experimental data. Although the soil samples used to derive these parameters cover a wide range of soil types, some error in the calculation of soil moisture might remain. Soil specific calibration of these parameters is recommended (see later in this section for details on how to apply custom parameters).
- In the case of very low values of measured real dielectric constant (less than 2.5), the resulting calibrated soil moisture value (CAL_MOISTU in table 3) might be negative. This is generally due a bad insertion of the probe tines in the soil which creates air gaps in the volume sampled, therefore reducing the value of soil dielectric constant (for air the value is ~1 and for dry soil ~2.5). In this case the soil moisture value is set automatically to zero by the HDAS software. ***It is recommended that readings with the real part of the soil dielectric constant (REAL_DC in table 3) less than 2.5 to be removed from any analysis***

8.1. Custom calibration

If independent estimation of soil water content (e.g, gravimetric soil samples) and soil temperature is available, the parameters used in the HDAS calibration and soil temperature correction equations described in [4] can be calculated for the specific soil type(s) present in the study area and updated in the file Parameters.dbf (see section 5.3). This operation will ensure the custom parameters are used to calculate the HDAS soil moisture output displayed on the IPAQ screen when sampling and saved in the output files.

These parameters include:

- Parameter DCZERO: for future use

- Slope (SLKAPPA) and offset (OFFKAPPA) of linear regression for parameter "K", in eq. (1) in [4], for soil temperature correction. Default values are respectively 0.011 and 0.0065;

- Slope (SLCONSTA) and offset (OFFCONSTA) of the calibration equation (3) in [4], for soil moisture calculation. Default values are respectively 11.0 and -18.0;

To change the default parameters, simply open the "parameters.dbf" file with Microsoft Excel, edit the values of the parameters (see Table 4) and save the file.

Table 4. Content of the parameters file

DCZERO	SLKAPPA	OFFKAPPA	SLCONSTA	OFFCONSTA
2.7000	0.0110	-0.0065	11.0	-18.0

9. Wiring diagrams

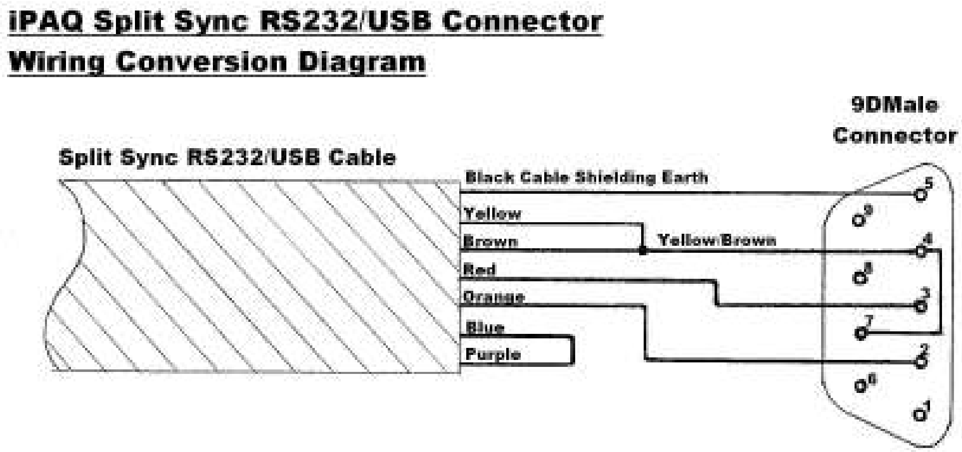

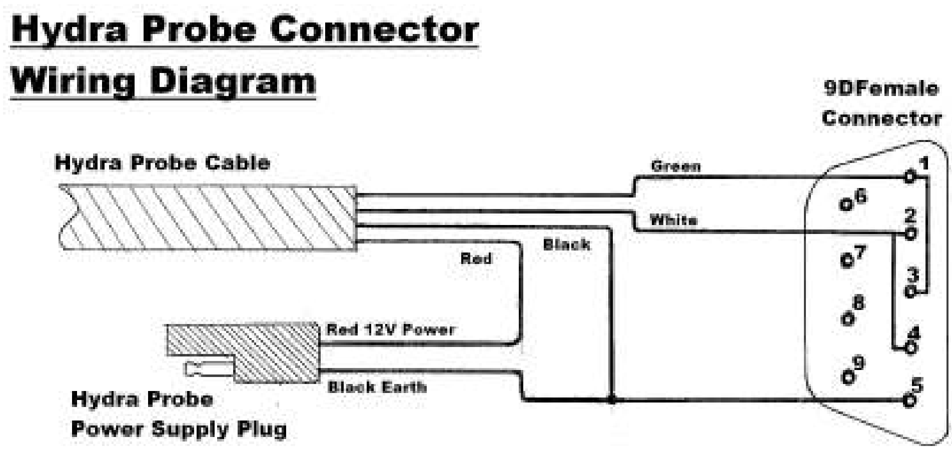

10. References

[1] Seyfried, M., and Murdock M., 2004. Measurement of soil water content with a 50-MHz soil dielectric sensor. *Soil Sci. Soc. Am. J.*, 68:394-403.

[2] Seyfried, M.S., and Murdock, M.D., 2002. Effects of soil type and temperature on soil water content measurements using a soil dielectric sensor. P1-13. In I.C. Paltineanu (ed.) First international symposium on soil water measurement using capacitance and impedance, Beltsville, MD. 6-8 Nov. 2002.

[3] Seyfried, M.S., Grant, L.E., Du, E. and Kumes, K., 2005. Dielectric loss and calibration of the Hydra Probe Soil Water Sensor *Vadose Zone J.*, 4:1070-1079.

[4] Merlin, O., Walker, J., Panciera, R., Young, R., Kalma J. and Kim, E., 2007. Soil Moisture Measurement in Heterogeneous Terrain, in *International Congress on Modelling and Simulation (MODSIM)*. 2007: Christchurch, New Zealand.

11. Contacts

Mr Rocco Panciera
PhD student
Room 322, Block C
Department of Civil and Environmental Engineering
The University of Melbourne
Victoria 3010, Australia
Phone: +61 3 8344 4955
Fax: +61 3 8344 6215
Email: rocco@civenv.unimelb.edu.au

A/Prof. Jeffrey Walker
Reader in Environmental Engineering
Room 409, Building D
Department of Civil and Environmental Engineering
The University of Melbourne
Victoria 3010, Australia
Phone: +61 3 8344 5590 Mobile: 0413 023 915
Fax: +61 3 8344 6215
Email: j.walker@unimelb.edu.au
Web: http://www.civenv.unimelb.edu.au/~jwalker

Mr Rodger Young
Field Research Engineer
Department of Civil & Environmental Engineering
The University of Melbourne
Victoria 3010, Australia
Phone +61 3 8344 7018
Fax: +61 3 8344 6215
Email: r.young@civenv.unimelb.edu.au

Appendix A3:
Calibration Accuracy of the Polarimetric L-band Microwave Radiometer (PLMR)

empty page

A3 Calibration Accuracy of the Polarimetric L-band Microwave Radiometer (PLMR)

This appendix presents an estimation of PLMR calibration accuracy based on the ground (sky and blackbody) calibration performed during NAFE'05 experiment. The estimation presented hereafter was undertaken in collaboration with Mark Goodberlet from ProSensing, which is the company responsible for the initial design and construction of PLMR.

This Appendix briefly describes: (i) The PLMR calibration procedures utilised during the NAFE'05 experiment, and (ii) the procedures used to calculate the PLMR calibration accuracy from NAFE'05 calibration data. Finally, conclusions are drawn and improvements to the PLMR calibration procedures are proposed.

It should be noted that:

- the PLMR calibration accuracy reported in this document is specific to the NAFE'05 campaign and therefore relevant only to NAFE'05 PLMR data. Aging of the instrument will change this estimation for data collected after NAFE'05; and
- it is recommended that the procedure described in this document be adopted to re-calculate the PLMR calibration accuracy each time calibration data like those collected in NAFE'05 become available.

In the following discussion, the six PLMR beams are indicated with three digits indicating the polarisation, the beam number and the side of the instrument the beam is pointing at. For example, beam 'V3L' indicates the V polarised, third beam on the left side of the instrument. Table A3.1 gives the looking angle for each beam indicated with the above convention.

A3.1 Calibration Procedures

On Seventeen dates during November 2005, pre- and post -flight calibration was performed against a blackbody target ("warm cal") and clear sky ("cold sky"). At each calibration session, PLMR was left observing the target (sky or blackbody) for 15min. In warm calibration, PLMR beams were pointing downward to the blackbody box; in cold cal, PLMR beams were pointing at ~45° above the horizon looking at clear sky (see Figure A3.1).

For each calibration session, a value of PLMR observed T_B for each beam and polarisation was calculated as the average of the 15min record, after manually removing anomalous readings (e.g., aircrafts crossing PLMR FOV during cold cal). For each warm cal, a 15min average value of blackbody T_B was calculated from the average of 15 temperature sensor data inside the blackbody box, assuming emissivity 1. The T_B of the sky was assumed to be 8K.

Table A3.1. PLMR beams nomenclature and incidence angle.

Beam	**Incidence Angle (from Nadir)**
3L	-38.5°
2L	-21.5°
1L	-7°
1R	+7°
2R	+21.5°
3R	+38.5°

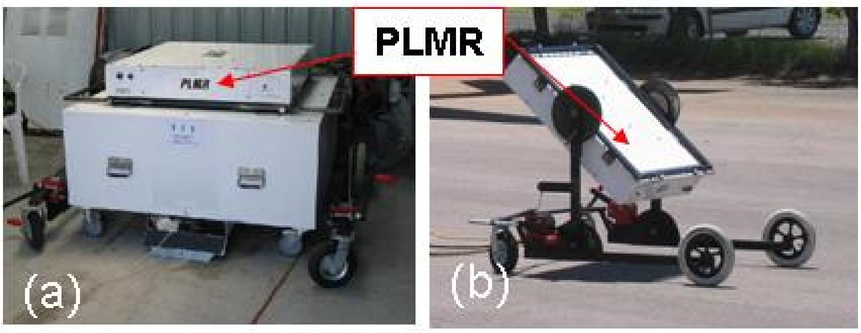

Figure A3.1. The configuration of the PLMR radiometer in (a) warm calibration and (b) cold calibration.

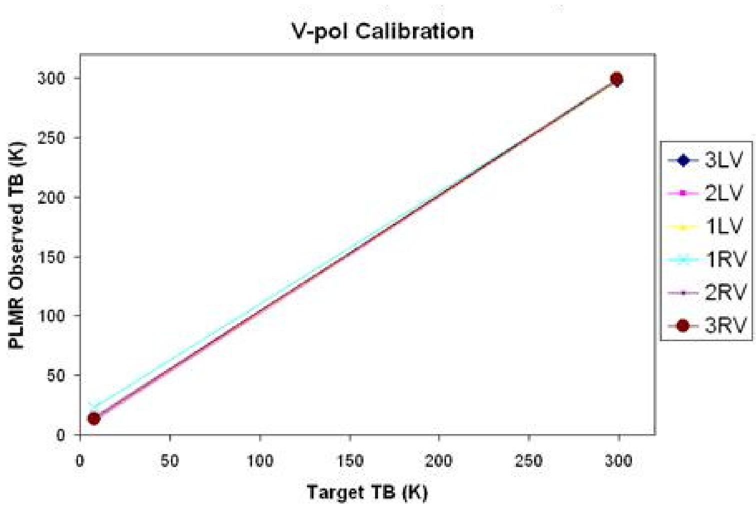

Figure A3.2. Example of post-flight calibration, for vertical polarisation, on day October 31st.

For each day, beam specific and polarisation specific calibration parameters were calculated as the average slope and offset of the pre- and post-flight calibration slope and offset between PLMR observed T_B and target T_B (see Figure A3.2). These daily parameters were then used to perform a daily adjustment of the PLMR $T_{B.}$

A3.2 Calculation of the Calibration accuracy

The following steps indicate the procedure used to calculate the PLMR calibration accuracy using all the daily calibration data from the NAFE'05 experiment:

1. the PLMR-measured T_B were plotted against the known target (sky and blackbody) T_B (see Figure A3.3) for all the calibration sessions;
2. the slope and offset of the regression between PLMR-measured and target T_B were calculated for each beam and each polarisation using the available observations;
3. the PLMR calibration accuracy (δY) was computed for each beam and each polarisation as:

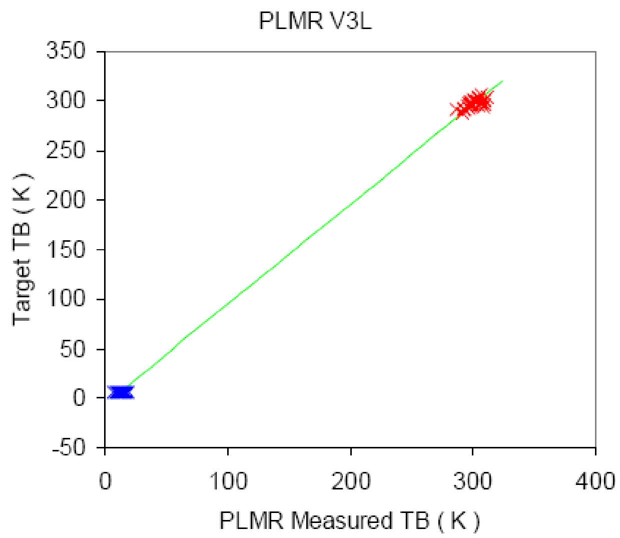

Figure A3.3. Example of plot between the PLMR-measured T_B and the target T_B. Red crosses are the warm calibration, blue crosses are the cold calibration data. The green line indicates the regression of all data.

$$\partial Y^2 = \partial Y_1^2 \cdot \left[\frac{(X - X_0)}{(X_1 - X_0)} \right]^2 + \partial Y_0^2 \cdot \left[\frac{(X_1 - X)}{(X_1 - X_0)} \right]^2, \qquad \text{(A3.1)}$$

which is the variance of a linear combination of random variables, when applied to the equation of the linear regression between the known target T_B (*Y*) and the PLMR-measured T_B (*X*):

$$Y = Y_1 \cdot \left[\frac{(X - X_0)}{(X_1 - X_0)} \right] + Y_0 \cdot \left[\frac{(X_1 - X)}{(X_1 - X_0)} \right], \qquad \text{(A3.2)}$$

where

- ∂Y_1 and ∂Y_0 are the Root Mean Square Errors (RMSE) around the regression line of, respectively, the blackbody and the sky data;
- X_0 and Y_0 are the average of *X* and *Y* for the sky calibration target; and

- X_1 and Y_1 are the average of X and Y for the blackbody calibration target;

4. using (A3.3), the calibration accuracy was calculated for each target T_B Y, using the corresponding X calculated for each Y using (A3.4): and
5. using the radiometer noise-equivalent delta-temperature (NEDT, estimated by the manufacturer to be 0.7K), the NEDT-free PLMR accuracy was calculated as:

$$\partial Y^{\text{NEDT\_FREE}} = \sqrt{(\partial Y^2 - 0.7^2)}\,. \tag{A3.5}$$

Since the NEDT quantifies the instrument radiometric uncertainty, the NEDT-free accuracy includes only the calibration error deriving from uncertainties in the sky and blackbody calibration and the instrument drift during the field campaign.

A3.3 Results and Discussion

Results of the accuracy estimation are shown in Figure A3.3 and Table A3.2 for each beam at each polarization and for target TB in the range 0-320K. The PLMR accuracy appeared the be poorer for V polarisation. Moreover, it appearsed to be poorer for outboard beams (beams 3L and 3R) as opposed to the better accuracy for inboard, nadir looking beams (beams 1L and 1R). Beam 1R at V polarisation showed an overall poor performance with respect to all the other beams

The reason for the apparent poorer accuracy at V polarisation and for outboard beams (beams 3L and 3R) was attributed by the manufacturer to the higher sidelobe levels of V-pol beams compared to H-pol beams. This made V-pol beams more sensitive to radiation coming from directions well off the beam pointing direction during calibration, being greater for the outboard beams which were more likely to be partially detecting the emission of targets at the

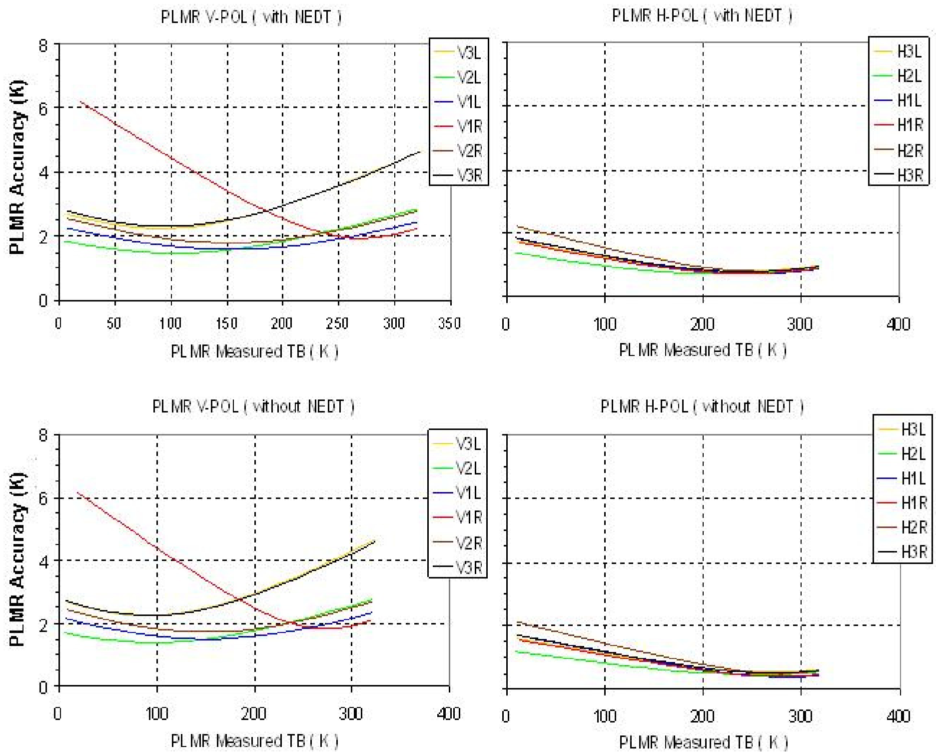

Figure A3.4. Estimated PLMR accuracy for target T_B in the range 0-320K calculated with 20K step, for each beam and each polarisation. The top panels show the accuracy when PLMR noise-equivalent delta-temperature (NEDT=0.7K) is included in the calculation. Bottom panels show the NEDT-free PLMR accuracy.

edges of the field of view during calibration. This sidelobe effect made both the sky target and the blackbody calibration error appear higher for V-pol than H-pol.

Inspection of the instrument revealed that beam 1RV had suffered a significant loss of gain with respect to the factory calibration. This was corrected in September 2008 with updated factory calibration parameters.

A3.4 Conclusions and Future Recommendations

The accuracy of PLMR in the brightness temperature range observed over water and land during the NAFE'05 campaign (150–300K) was estimated to be

Table A3.2. Estimated PLMR accuracy for target T_B in the range 0-320K calculated with 20K step, for each beam and each polarisation. The top table is the estimated PLMR accuracy including NEDT, the bottom table is the accuracy without NEDT.

Target TB (K)	PLMR Calibration Error with NEDT (K)											
	V3L	V2L	V1L	V1R	V2R	V3R	H3L	H2L	H1L	H1R	H2R	H3R
320	4.71	2.85	2.44	2.23	2.78	4.63	0.99	0.94	0.88	0.89	0.95	0.96
300	4.40	2.67	2.28	2.04	2.59	4.33	0.91	0.87	0.81	0.82	0.87	0.88
280	4.10	2.49	2.13	1.94	2.42	4.04	0.86	0.81	0.76	0.77	0.82	0.83
260	3.81	2.31	1.99	1.93	2.26	3.75	0.82	0.77	0.74	0.74	0.80	0.80
240	3.54	2.15	1.86	2.02	2.12	3.48	0.80	0.74	0.74	0.73	0.82	0.79
220	3.28	1.99	1.76	2.19	2.00	3.23	0.81	0.73	0.76	0.75	0.86	0.81
200	3.03	1.85	1.67	2.44	1.90	2.99	0.83	0.73	0.81	0.78	0.93	0.84
180	2.82	1.73	1.61	2.73	1.83	2.78	0.88	0.75	0.87	0.83	1.02	0.90
160	2.63	1.63	1.58	3.06	1.79	2.60	0.94	0.78	0.95	0.90	1.13	0.98
140	2.48	1.55	1.58	3.41	1.79	2.46	1.02	0.83	1.04	0.98	1.25	1.07
120	2.37	1.50	1.61	3.79	1.81	2.36	1.11	0.89	1.14	1.07	1.37	1.16
100	2.31	1.48	1.66	4.17	1.88	2.31	1.21	0.96	1.25	1.17	1.51	1.27
80	2.31	1.50	1.74	4.57	1.97	2.31	1.31	1.04	1.36	1.27	1.64	1.38
60	2.36	1.54	1.85	4.97	2.08	2.37	1.42	1.12	1.48	1.38	1.79	1.50
40	2.46	1.62	1.97	5.38	2.22	2.47	1.53	1.20	1.60	1.49	1.93	1.62
20	2.61	1.72	2.11	5.79	2.37	2.62	1.65	1.29	1.72	1.60	2.08	1.74
0	2.79	1.84	2.26	6.21	2.54	2.80	1.77	1.39	1.84	1.71	2.23	1.87

Target TB (K)	PLMR Calibration Error without NEDT (K)											
	V3L	V2L	V1L	V1R	V2R	V3R	H3L	H2L	H1L	H1R	H2R	H3R
320	4.64	2.75	2.32	2.10	2.67	4.57	0.63	0.55	0.44	0.47	0.57	0.58
300	4.34	2.57	2.17	1.92	2.50	4.27	0.58	0.51	0.40	0.42	0.51	0.53
280	4.05	2.40	2.02	1.82	2.33	3.98	0.55	0.48	0.38	0.40	0.50	0.51
260	3.76	2.23	1.89	1.83	2.18	3.70	0.54	0.46	0.40	0.41	0.52	0.51
240	3.49	2.07	1.77	1.93	2.04	3.44	0.56	0.46	0.45	0.45	0.58	0.54
220	3.23	1.92	1.67	2.12	1.92	3.18	0.60	0.48	0.53	0.51	0.67	0.59
200	2.99	1.78	1.59	2.38	1.83	2.95	0.65	0.51	0.61	0.58	0.77	0.66
180	2.77	1.66	1.53	2.68	1.76	2.73	0.72	0.56	0.71	0.66	0.89	0.75
160	2.58	1.55	1.50	3.02	1.72	2.55	0.80	0.61	0.81	0.75	1.01	0.84
140	2.43	1.47	1.50	3.38	1.72	2.41	0.89	0.67	0.92	0.85	1.14	0.94
120	2.31	1.41	1.52	3.75	1.74	2.30	0.99	0.73	1.02	0.94	1.27	1.05
100	2.25	1.38	1.58	4.14	1.80	2.25	1.09	0.80	1.13	1.04	1.41	1.16
80	2.24	1.39	1.65	4.53	1.89	2.24	1.19	0.88	1.25	1.14	1.55	1.27
60	2.29	1.42	1.75	4.94	2.00	2.29	1.29	0.95	1.36	1.24	1.69	1.38
40	2.38	1.49	1.87	5.34	2.13	2.39	1.40	1.03	1.47	1.35	1.83	1.49
20	2.52	1.58	2.00	5.75	2.28	2.53	1.50	1.11	1.58	1.45	1.97	1.61
0	2.70	1.69	2.14	6.17	2.44	2.71	1.61	1.18	1.70	1.56	2.11	1.72

better than 1 K at H polarization and 2.5 K for V polarization. This was calculated excluding the outboard beams (3R and 3L) and beam 1RV, for the reasons discussed in the previous section.

To avoid the problem with the higher sidelobes in the outboard beams in future application, the following improvements to the calibration procedures described in section 0 were recommended:

- **sky calibration:** sky calibration should be performed individually for the left and right side of the instrument (i.e., calibration for 3R, 2R and 1R separate from that of 1L, 2L and 3L). For each calibration, PLMR should be tilted of approximately 22º with respect to the horizontal, so that beams 2 (left or right) will be pointing vertically up; and
- **blackbody calibration:** it should be ensured that the blackbody material completely surrounds the antenna side of PLMR, so that the outboard beams are not partially detecting the radiation of non-blackbody materials.

Appendix A4:
Improved Understanding of Soil-Surface-Roughness Parameterization for L-Band Passive-Microwave Soil-Moisture Retrieval

empty page

Improved Understanding of Soil Surface Roughness Parameterization for L-Band Passive Microwave Soil Moisture Retrieval

Rocco Panciera, *Member, IEEE*, Jeffrey P. Walker, and Olivier Merlin

***Abstract*—Surface roughness parameterization plays an important role in soil moisture retrieval from passive microwave observations. This letter investigates the parameterization of surface roughness in the retrieval algorithm adopted by the Soil Moisture and Ocean Salinity mission, making use of experimental airborne and ground data from the National Airborne Field Experiment held in Australia in 2005. The surface roughness parameter is retrieved from high-resolution (60 m) airborne data in different soil moisture conditions, using the ground soil moisture as input of the model. The effect of surface roughness on the emitted signal is found to change with the soil moisture conditions with a law different from that proposed in previous studies. The magnitude of this change is found to be related to soil textural properties: in clay soils, the effect of surface roughness is higher in intermediate wetness conditions (0.2–0.3 v/v) and decreases on both the dry and wet ends. Consequently, this letter calls for a rethink of surface roughness parameterization in microwave emission modeling.**

***Index Terms*—Microwave radiometry, National Airborne Field Experiments (NAFE), soil moisture, Soil Moisture and Ocean Salinity (SMOS), surface roughness.**

I. Introduction

PASSIVE microwave remote sensing is an increasingly utilized technique to monitor surface soil moisture over large areas due to its all-weather capabilities, limited noise induced by the vegetation canopy, and high sensitivity to the dielectric properties of the soil–water medium [1]. Year 2009 will see the launch of the first soil-moisture-specific passive microwave mission, the Soil Moisture and Ocean Salinity (SMOS) mission carrying an L-band interferometric radiometer. The soil moisture retrieval algorithm adopted by SMOS requires information on the land-surface characteristics which contribute to the microwave emission of the Earth's surface. At L-band frequencies, vegetation water content (VWC) and soil surface roughness have the highest impact on the surface emission for a given soil moisture condition. Therefore, the choice of the parameters used to model the effect of surface roughness on the emission is of primary importance.

Manuscript received June 20, 2008; revised October 15, 2008 and November 16, 2008. This work was supported by the Australian Research Council under Infrastructure Grants LE0453434 and LE0560930 and Research Grant DP0557543.

The authors are with the Civil and Environmental Engineering, The University of Melbourne, Melbourne, Vic. 3010, Australia (e-mail: rocco@civenv.unimelb.edu.au; j.walker@unimelb.edu.au; omerlin@unimelb.edu.au).

Color versions of one or more of the figures in this paper are available online at http://ieeexplore.ieee.org.

Digital Object Identifier 10.1109/LGRS.2009.2013369

Surface roughness is generally parameterized with the semi-empirical model proposed by [2], which makes use of two parameters: H_R which is related to measurable geophysical characteristics of the soil surface, such as standard deviation (σ_S) and correlation length (L_C) of the surface height profiles, and a polarization mixing parameter Q_S that can be estimated from calibration to passive microwave measurements. While Q_S was found to have very low values at L-band [3], the dependence of H_R on the surface roughness characteristics is not well known. Moreover, the best geophysical parameters to describe H_R over agricultural fields were found to be the slope parameter ($m = \sigma_S/L_C$) and the surface soil moisture [3]. The dependence of H_R on soil moisture was explained by an effect of volume scattering: the spatial fluctuations of the dielectric constant within the soil volume are stronger during drying out, producing an important "dielectric" roughness effect in addition to the "physical roughness" effect linked to the soil surface height. Recent results obtained over bare and grassy surfaces at the European SMOSREX site have proposed a linear decay of H_R with increasing soil moisture between a transition soil moisture point and the field capacity, with constant values of H_R outside those limits [4], [5]. This letter extends the earlier tower-based results to scales more representative of future SMOS footprints using aircraft data at L-band, supported by detailed ground measurements of soil moisture, soil temperature, VWC, and surface roughness.

II. Data

The data used in this letter were collected during the National Airborne Field Experiment 2005 (NAFE'05). This was a large-scale airborne experiment conducted in Australia in November 2005 (full details about the experiment can be found in [6]). The four-week long campaign was conducted in the Goulburn river catchment (32° S, 150° E, Fig. 1), a semiarid area of grazing lands with native grass cover and some cropped areas (mainly wheat and barley). Heavy rainstorms delivered approximately 50 mm of cumulative rainfall during the first two weeks of the campaign, followed by a dry-down period until the end of the experiment. Aircraft L-band measurements were taken at 60-m resolution over eight experimental farms two times a week, with supporting ground monitoring of the top 5-cm soil moisture undertaken weekly at high-resolution site within each experimental farm (see Fig. 1). This letter focuses on the aircraft observations taken at the center of the high-resolution sites where ground soil moisture was monitored at 6–12-m spacing.

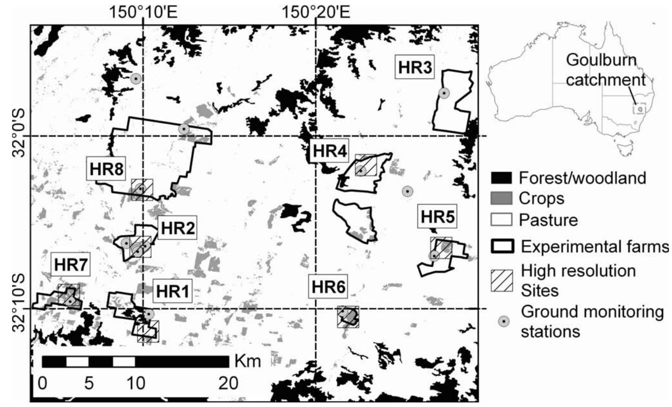

Fig. 1. NAFE'05 experiment ground-sampling layout with land-cover map. The high-resolution sites, focus of this letter, are labeled.

The high-resolution sites presented a variety of land-surface conditions and land covers. Stanley, Dales, and Roscommon were characterized by native pasture; Pembroke, Merriwa Park, Cullingral, and Illogan were cropped fields (a mix of wheat, barley, and oats); whereas Midlothian was split between a bare fallow field and a lucerne crop. Soil type was clay or clay loam for most sites, with the exception of Roscommon and Illogan (sandy loam and silt loam).

Soil moisture observations (0–5 cm) were made by means of the Hydraprobe Data Acquisition System, which integrates a GPS receiver with the Vitel HydraProbe in a portable geographic information system framework. Such observations were calibrated against gravimetric measurements (taken throughout the campaigns at different locations) and laboratory data, yielding an estimated accuracy of ± 3.5 %v/v [7]. VWC at each high-resolution site and its temporal variation were determined by means of biomass samples taken every week. Surface physical roughness was characterized with 1-m long pin profilers with two perpendicular sets of readings made at five locations within each experimental farm.

III. Surface-Roughness Retrieval

The radiative transfer model used in this letter to simulate the surface emission is the L-band Microwave Emission of the Biosphere (L-MEB) model, described in detail in [8]. The model will be the core of the soil moisture retrieval algorithm adopted for the SMOS mission. The effects of soil and vegetation on the surface brightness temperatures are described in L-MEB by the so-called "τ–ω model"

$$TB(\vartheta, P) = (1 - \omega_{\vartheta,P})(1 - \gamma_{\vartheta,P})(1 + \Gamma_{\vartheta,P}\gamma_{\vartheta,P})T_v + (1 - \Gamma_{\vartheta,P})\gamma_{\vartheta,P}T_{\text{EFF}} \quad (1)$$

where P represents the measured polarization (H or V), ϑ is the observation angle, ω and γ are, respectively, the vegetation scattering albedo and transmissivity, and the two T terms are the temperatures of the vegetation and the soil effective temperature. The vegetation transmissivity γ is calculated from the vegetation optical depth, $\tau(\gamma = \exp(\tau/\cos\vartheta)$, which can be linearly related to the VWC as $\tau = b^*\text{VWC}$ through the experimental parameter b, which depends on the plant structure and the sensor frequency and incidence angle [9]. To account for this angular effect, the expression $\tau = b^*\text{VWC}$ is used to calculate a NADIR-equivalent optical depth, which is then modulate with the incidence angle based on two polarization-dependent and vegetation-specific structure parameters, tt_h and tt_v. The reflectivity of a rough soil Γ, which is also sensitive to the observation angle and measured polarization, is derived from the smooth soil Fresnel reflectivity Γ^* as a function of the observation angle through the model soil parameters H_R and N_{RP}

$$\Gamma = \Gamma^* \exp\left[-H_R \cos(\vartheta)^{N_{RP}}\right]. \quad (2)$$

In this letter, the values for the model parameters used were those proposed for the soil moisture retrieval of the future SMOS mission for native grass and wheat crops (J.-P. Wigneron, personal communication). N_{RV} was set to -1 or 0 and N_{RH} to 0 or 1 (respectively for crop and grass). Vegetations scattering albedo was set to 0 (crops) and 0.05 (grass). VWC was determined from ground samples, whereas the effective soil temperature was determined using surface (2.5 cm) and deep (15 cm) soil temperature measurements from the local monitoring stations (see Fig. 1) at the time of the aircraft overpass using the formulation proposed in [3]. Vegetation temperature T_V was approximated with the soil temperature at 2.5 cm. Soil texture was determined from 5-cm samples taken nearby each high-resolution site.

The parameters with the highest impact on the soil moisture retrieval using the described model are b and H_R. The existing estimates of b and H_R ("SMOS default," Table I) were initially verified by using them to retrieve soil moisture and compare it with the ground soil moisture observations. "SMOS default"-retrieved soil moisture is shown in Fig. 2 against the ground soil moisture, and the mean absolute error of the retrieval (MAE) are listed for each site in Table I. It is shown that, by using "SMOS default" values for both b and H_R parameters, large retrieval errors (underestimation) are obtained, particularly for the crop sites (Pembroke, Merriwa Park, and Cullingral), whereas, for the grass sites, the errors are much smaller. Given the confounding influence of parameters H_R and b on the retrieved soil moisture, with an increase in H_R and b generally having the same effect of increasing the overall emission, these results indicate that the value of either or both parameters proposed for the SMOS retrieval are too low. It was therefore necessary to perform a site-specific calibration to separate the effect of the two parameters and to address the main objective of this letter, the surface roughness parameter.

Given the availability of five to eight daily bi-polarized aircraft observations at multiple angle for each high-resolution site, both parameters can be retrieved by taking advantage of the multi-angular capabilities of the L-MEB model and using the ground-measured soil moisture as input of the model. Two different calibration approaches were used. First, it was assumed that the "SMOS default" values for b were correct, and H_R was calibrated for each individual site. Second, b and H_R were alternatively calibrated at each site and each day through a sequence of iterations; at each step, the value of b used as input to calibrate H_R was the average of the values calibrated across all days in the previous step, whereas b was calibrated

TABLE I

VALUES OF PARAMETER b AND H_R AND MEAN ABSOLUTE ERRORS (MAE, [%v/v]) OF SOIL MOISTURE RETRIEVAL FOR SMOS DEFAULT AND THE TWO SITE-SPECIFIC CALIBRATION APPROACHES DISCUSSED IN THE TEXT. MEAN AND ± STANDARD DEVIATION IN TIME OF CALIBRATED PARAMETERS IS SHOWN. * = NATIVE GRASS; ** = MIX FALLOW/LUCERNE; *** = CROP

Site name	Range of angles	SMOS default			Calibration of only Hr b fixed to SMOS default		Iterative calibration of b and H_R		
		b	H_R	MAE	H_R	MAE	b	H_R	MAE
Roscommon*	17º	0.12	0.5	2.8	0.5+/-0.1	2.6	0.09+/-0.01	0.43+/-0.2	2.4
Stanley*	17º	0.12	0.5	13.4	0.9+/-0.1	3.5	0.36+/-0.01	0.79+/-0.1	2.7
Dales*	17º	0.12	0.5	16.0	1.1+/-0.2	5.6	0.73+/-0	0.52+/-0.4	14.9
Midlothian**	33º	0.12	0.5	24.6	1.2+/-0.3	5.2	1.2+/-0.05	0.87+/-0.3	4.5
Pembroke***	18º	0.08	0.2	32.4	1.0+/-0.1	2.7	0.14+/- 0	0.70+/-0.2	2.9
Illogan***	20º	0.08	0.2	7.5	0.4+/-0.1	6.1	0.11+/-0.01	0.38+/-0.1	6.4
MerriwaP.***	11º	0.08	0.2	19.2	0.9+/-0.2	7.4	0.1+/-0.01	0.79+/-0.2	8.1
Cullingral***	6º	0.08	0.2	24.7	1.3+/-0.2	4.6	0.59 +/-0.03	0.85+/-0.3	5.2

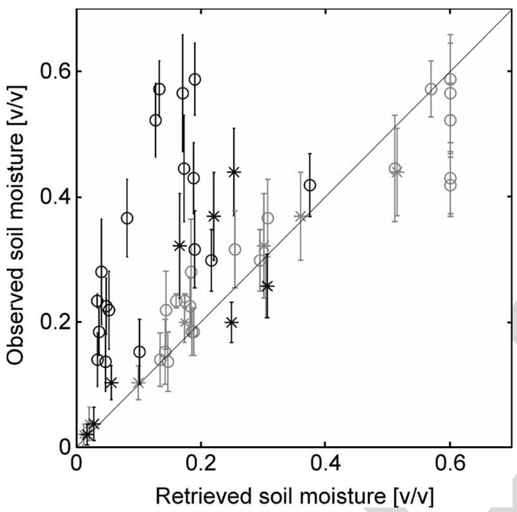

Fig. 2. Retrieved versus ground-observed soil moisture using (black symbols) SMOS default parameters and (gray symbols) NAFE'05 calibrated b and H_R. Asterix indicates native grass sites; circles indicate crop sites. Vertical error bars indicate ± of the standard deviation of observed soil moisture within each footprint.

using the calibrated values of H_R for each day in the previous step. The iterations were repeated until the mean values of both parameters would not change significantly between subsequent iterations. This process led to an adjustment of the values of both parameters to match the observed emission, while minimizing the temporal variation or retrieved parameters b, which is only dependent on the plant structure and is therefore not expected to change in time.

In both approaches, all the bi-polarized multi-angular observations available for each site on each observation day were used to retrieve one single value of the parameter for the site. Although the available range of incidence angles varied slightly between sites, due to differences in aircraft flight lines and attitude, on average each site was observed over a range of angles of 20°. This is indicated in the second column of Table I.

IV. RESULTS

The calibrated values of both the b and H_R parameters for the two approaches and the MAE of soil moisture retrieval are shown in Table I, together with the standard deviations of the retrieved values across the monitoring days to highlight the temporal variation of the parameters. Note that the MAE was calculated using the average values of the parameters for each site. Overall, the SMOS values of b were found to be suitable for crops in the study area, whereas the values of H_R had to be increased significantly from the SMOS default values in order to obtain an accurate soil moisture retrieval. This could be due to differences in agricultural practices between the NAFE'05 study area and the European sites typical of most SMOS studies which provided estimates of H_R. For the native grass sites, the SMOS values of H_R were found to be suitable, whereas values of b were somewhat too low.

It should be noted that the iterative calibration of b and H_R produced very high values for parameter b in some cases. In particular, the Midlothian, Dales, and Cullingral sites had unrealistically high b values (above ~0.5), which cannot be explained by the effect of the standing vegetation alone. This can be explained by very high surface roughness or some other sources of emission, like, for example, litter or rainfall intercepted on the plant, not explicitly modeled but implicitly accounted for in the high values of b. It should be noted that these sites also exhibited very high values of H_R in the first calibration approach (individual H_R calibration with b fixed), confirming the hypothesis of an actual deficit in the emission budget. The joint calibration of b and H_R at the Dales site did not improve the soil moisture retrieval. Analysis of the aircraft-observed surface emission at this site revealed very poor sensitivity to the ground-measured soil moisture, which could be explained by the presence of a litter layer that remained moist and, thus, saturated the signal. This effect has been observed also at some European sites [5]. The Dales site was therefore not considered further in this analysis.

It is interesting to note the lower values of H_R calibrated at the sites with more sandy soils (Roscommon and Illogan), which was not expected, as soil texture should not affect the physical roughness of the surface. This could be an effect of the dielectric model used by the L-MEB algorithm, the Dobson model [10], which is known to have poorer performance on sandy soils. It is also shown in Table I that similar soil moisture retrieval errors are obtained with the two calibration approaches (calibration of only H_R and calibration of both parameters). Nevertheless, the second approach guarantees that

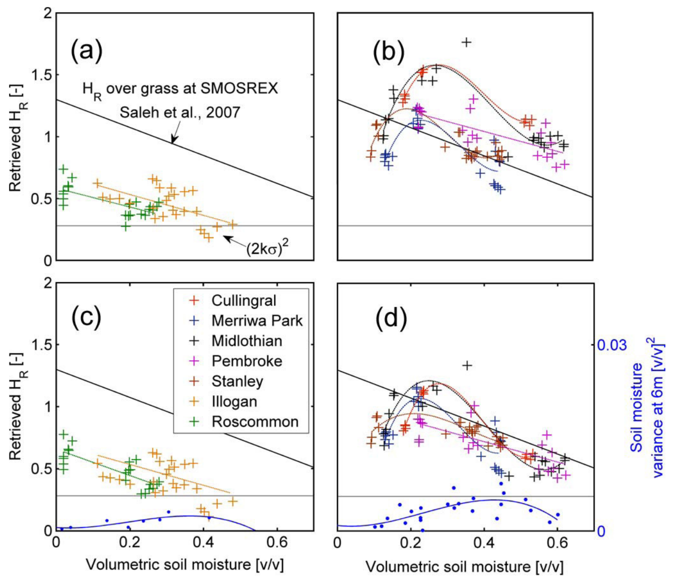

Fig. 3. Retrieved parameter H_R as a function of ground soil moisture for all the high-resolution sites; using SMOS values for parameter b for (a) sandy soils and (b) clayey soils, and using site-specific calibrated values of b for (c) sandy soils and (d) clay soils. Dashed colored lines are the best fit for each site. Solid gray lines show the value of the Choudhury parameter for physical roughness (average of all sites $= 0.25$), whereas solid black lines indicate the roughness–soil moisture relationship proposed by Saleh *et al.* [5]. (blue dots and solid lines) Soil moisture heterogeneity at 6-m spacing is also displayed for each high-resolution site and each date with cubic fit.

any vegetation effect be removed from the calibrated values of H_R, which makes it more suitable for the purpose of this letter. The soil moisture retrieved using these calibrated parameters is plotted against the ground soil moisture in Fig. 2 for comparison with SMOS default retrieval.

In order to investigate the dependence of H_R on soil moisture, H_R was retrieved for each bi-polarized observation of the high-resolution sites. This approach provides more data points at a wider range of soil moisture conditions than when using all the observations at once to retrieve on value of H_R for each day (as done thus far). The retrieved H_R as a function of the ground-observed soil moisture is shown in Fig. 3. In this plot the results obtained using both sets of values of parameter b (SMOS value and calibrated b) are presented, and the high-resolution sites are grouped by soil type, upon observing a strong soil-type dependence of retrieved values of parameter H_R in Table I.

It is observed that the values of H_R are not constant but rather change with respect to the soil moisture conditions. In the intermediate-to-wet range of soil moisture conditions (0.2 v/v to saturation), the general trend is that of a decrease of the parameter from higher value in intermediate wetness conditions to lower values in wet conditions. This is observed for all soil types and regardless of whether parameter b is calibrated or not. The trend is consistent with what were already observed in previous studies using a tower radiometer at the European SMOSREX site [4], [5]. The linear regression proposed in those studies (for natural grass) is shown in Fig. 3 for comparison. It is notable how, in the case where b is calibrated (bottom panels shown in Fig. 3), this trend is matched by the values of H_R retrieved in this letter for clay soils. On more sandy soils instead, the values of H_R are much lower, although the linear decrease with soil moisture conditions is maintained.

It is also notable in Fig. 3 that, for clay soils and when drier conditions are encountered, a negative trend between H_R and soil moisture seems to dominate, after a peak of H_R is reached at around 0.2–0.3 v/v soil moisture conditions. This is not visible for the Pembroke site, which nevertheless did not experience conditions drier then 0.2 v/v. The observed decrease of H_R on dry conditions is in contrast with previous studies which reported constant values of H_R in this range, as well as above the field capacity [4], [5]. This could have been due to the fact that the soil types in the sites analyzed by those studies were mainly sandy, whereas the decrease was observed here mainly for clays and clay loams.

In [4] and [5], it was suggested that the decrease of H_R with increasing soil moisture is associated with the presence of micro-scale heterogeneity in soil moisture during drying. This would add a component of dielectric roughness to the physical roughness of the soil surface which would instead dominate on wet conditions where soil moisture is more uniform at the microscale. On the same line of thought, the decrease of H_R observed in Fig. 3 in the dry end could be associated to the decrease in micro-scale dielectric heterogeneity that one would expect in drying clay soils due to lower limit imposed by the residual or wilting points. At the dry end, therefore, the physical-roughness component of H_R would become increasingly dominant, and the dielectric-roughness component would decrease.

In Fig. 3, the physical-roughness component is quantified through the classical Choudhury parameter $[11] = (2\ \mathrm{k}\sigma_S)^2$, function of the standard deviation of the surface heights and the wavenumber k. Here, the average between all the high-resolution sites (0.25) was taken as a reference, resulting from an average σ_S of 8.4 mm (2-mm standard deviation) across the eight sites. It is clear that, for clay soils and when calibrated values of b are used (lower left panels as shown in Fig. 3), the values of H_R approach the physical-roughness component toward both the dry and wet soil moisture ends. The range of H_R values between extreme and intermediate soil moisture conditions exhibited by clay soils in Fig. 3 is on the order of 0.3–0.5. On bare soil, this would correspond to an error in soil moisture retrieval of 15–20 %v/v. For many of the cases presented here, therefore, using a constant value or a simple linear decrease of H_R with soil moisture could lead to significant soil moisture retrieval errors.

The comparison between the relationship of H_R and soil moisture on sandy and clay soils shown in Fig. 3 further supports the hypothesis of dielectric roughness induced by micro-scale heterogeneity of soil moisture. One would in fact expect this heterogeneity to be higher in clay soils due to the highest water retention property of these. This was verified by analyzing the variance of the soil moisture measurement taken at 6- and 12-m spacing throughout each high-resolution site. This is shown in Fig. 3 (blue right axis in lower panels), where the soil moisture variance is plotted against the mean soil moisture for each area and each day. For clay soils, the soil moisture heterogeneity is in fact much higher (nearly double that of sandy sites) and achieves a maximum around

0.3–0.45 v/v with a rapid decrease below 0.3 v/v. For sandy soil, this heterogeneity is smaller, with corresponding lower values of H_R. The implicit assumption is made here that the soil moisture dependence of the heterogeneity at the 6-m scale is a good approximation of that of the micro-scale heterogeneity which would be observed on very small soil samples and which is expected to determine the dielectric roughness. The goodness of this assumption is difficult to verify, and therefore, the measure of heterogeneity adopted here is to be thought of only as an indication of the relative magnitude of soil moisture heterogeneity between soil types and its variation with wetness conditions. Further investigation is needed in order to understand what is the scale at which the soil moisture heterogeneity mostly affects the relationship between soil moisture and microwave emission and how this effect can be parameterized through H_R as a function of soil type or accounted for in a soil dielectric model. Moreover, it should be better understood whether the smaller value of H_R are not an artifact of the poor performance of the Dobson model on sandy soils.

V. Conclusion

Effective parameterization of surface roughness is important for passive microwave remote sensing of soil moisture. In this letter, the dependence of surface roughness on soil moisture microscale heterogeneity was investigated using aircraft and ground soil moisture observations. The surface roughness parameter was found to be not constant but rather variable, depending on soil moisture conditions and soil type. On clay soils, it exhibited a maximum at intermediate soil moisture conditions ($\sim$0.25 v/v) and a decrease toward both dry and wet conditions, whereas on sandy soils, it exhibited lower values and a monotonic decrease going from dry to wet conditions. In the intermediate wet soil moisture range (0.25 v/v to saturation), a soil moisture dependent linear relationship similar to that proposed by previous studies [4], [5] was found to apply well to the crops and native grasses on clay soils. However, the values of roughness approached the contribution of the surface physical roughness ($\sim$0.28) on both the wet and dry ends. This was explained as the effect of a dielectric component in the microwave roughness which is related to soil moisture microscale heterogeneity. It was shown that this effect might be higher in clay soils and maximum at intermediate soil moisture conditions when the water retention properties of clay determine high spatial variability. These results indicate the need to model the dielectric component of the surface roughness effect on the soil emission as a function of the soil textural properties and soil moisture. This letter also suggested that the values of H_R proposed for SMOS might be too low to provide accurate soil moisture estimates over crop sites, whereas they are suitable for native grass-covered sites.

Acknowledgment

The authors would like to thank the NAFE'05 participants.

References

[1] E. G. Njoku and D. Entekhabi, "Passive microwave remote sensing of soil moisture," *J. Hydrol.*, vol. 184, no. 1/2, pp. 101–129, Jan. 1996.

[2] J. R. Wang and B. J. Choudhury, "Remote sensing of soil moisture content over bare field at 1.4 GHz frequency," *J. Geophys. Res.*, vol. 86, no. C6, pp. 5277–5282, Jun. 1981.

[3] J. P. Wigneron, L. Laguerre, and Y. H. Kerr, "A simple parameterization of the L-band microwave emission from rough agricultural soils," *IEEE Trans. Geosci. Remote Sens.*, vol. 39, no. 8, pp. 1697–1707, Aug. 2001.

[4] M. J. Escorihuela, Y. H. Kerr, P. de Rosnay, J. P. Wigneron, J. C. Calvet, and F. Lemaitre, "A simple model of the bare soil microwave emission at L-band," *IEEE Trans. Geosci. Remote Sens.*, vol. 45, no. 7, pp. 1978–1987, Jul. 2007.

[5] K. Saleh, J. P. Wigneron, P. Waldteufel, P. de Rosnay, M. Schwank, J. C. Calvet, and Y. H. Kerr, "Estimates of surface soil moisture under grass covers using L-band radiometry," *Remote Sens. Environ.*, vol. 109, no. 1, pp. 42–53, Jul. 2007.

[6] R. Panciera, J. P. Walker, J. D. Kalma, E. J. Kim, J. Hacker, O. Merlin, M. Berger, and N. Skou, "The NAFE'05/CoSMOS data set: Towards SMOS soil moisture retrieval, downscaling and assimilation," *IEEE Trans. Geosci. Remote Sens.*, vol. 46, no. 3, pp. 736–745, Mar. 2008.

[7] O. Merlin, J. Walker, R. Panciera, R. Young, J. Kalma, and E. Kim, "Soil moisture measurement in heterogeneous terrain," in *Proc. Int. Congr. MODSIM*, Christchurch, New Zealand, 2007.

[8] J. P. Wigneron, Y. Kerr, P. Waldteufel, K. Saleh, M. J. Escorihuela, P. Richaume, P. Ferrazzoli, P. de Rosnay, R. Gurney, J. C. Calvet, J. P. Grant, M. Guglielmetti, B. Hornbuckle, C. Matzler, T. Pellarin, and M. Schwank, "L-band microwave emission of the biosphere (L-MEB) model: Description and calibration against experimental data sets over crop fields," *Remote Sens. Environ.*, vol. 107, no. 4, pp. 639–655, Apr. 2007.

[9] T. J. Jackson, T. J. Schmugge, and J. R. Wang, "Passive microwave sensing of soil-moisture under vegetation canopies," *Water Resour. Res.*, vol. 18, no. 4, pp. 1137–1142, 1982.

[10] M. C. Dobson, F. T. Ulaby, M. T. Hallikainen, and M. A. El-Rayes, "Microwave dielectric behavior of wet soil—Part II: Dielectric mixing models," *IEEE Trans. Geosci. Remote Sens.*, vol. GRS-23, no. 1, pp. 35–46, Jan. 1985.

[11] B. J. Choudhury, T. J. Schmugge, A. Chang, and R. W. Newton, "Effect of surface roughness on the microwave emission from soils," *J. Geophys. Res.—Oceans Atmosph.*, vol. 84, no. C9, pp. 5699–5706, Sep. 1979.

Appendix A5:
Application of the 3P-S Approach

empty page

A5 The 3P-S Approach

The second alternative approach tested in this thesis consists of performing a three-parameters retrieval: the retrieved parameters are (i) the soil moisture of the moderate vegetation fraction, (ii) the optical depth of the moderate vegetation fraction and (iii) the soil moisture of the forest fraction. The optical depth of the forest fraction is imposed *a priori* as in 2P-S. This approach relaxes the assumption of uniform soil moisture between the two fractions on which the previous approaches are based.

Since the retrieval of three parameters is attempted, it is necessary to have a minimum of three concurrent observations. These can be obtained, for example, using bi-polarised observations at two different incidence angles. As explained in Chapter 5. However, the regional airborne data were collected with the radiometer in "pushbroom" configuration in order to allow monitoring of a large area within one day, implying that only two observations for every ground location were available (single-angle, V and H-pol). While one option was to create observations of each ground location at multiple angles by applying an incidence angle normalisation procedures like that described in section 5.3.2.1, this is somewhat artificial and requires a strong assumption to be made on the angular dependence of the microwave emission over different land surface conditions.

Before attempting the 3P-S approach using the NAFE'05 airborne data, a proof-of-concept was performed using a simple synthetic scenario in order to assess the potential of the approach to reduce the error with respect to the 2P-S approach, as well as to check for algorithm convergence when retrieving three parameters with a limited number of independent observations.

A5.1 Application of 3P-S to a Synthetic Scenario

The synthetic scenario consisted of a mixed pixel composed by two fractions, one of forest the other one of a moderate vegetated land over type (grassland), having different soil moisture contents. Three heterogeneous soil moisture scenarios were simulated (dry, intermediate and wet), all characterised by a fixed soil moisture difference between the grass and forest fraction (20%v/v). In line with that observed with ground data in Chapter 6, the forest fraction was always considered to be drier than the grass fraction. Therefore the soil moisture of the forest was set to 5, 20 and 35%v/v and that of grass was 25, 40 and 55%v/v respectively in the "dry", "intermediate" and "wet" scenarios. The average pixel soil moisture was then calculated by mixing those values weighted by the respective fraction of the pixel. In order to simulate T_B observations for the mixed pixel, the optical depth of the grassland was set to 0.05 and that of the forest to 0.57, while for the other L-MEB parameters, the values specifically evaluated in the NAFE'05 conditions and used throughout this thesis were adopted (see Table 5.2). Moreover, the pixel was assumed to have a uniform surface temperature of 300K and a uniform soil texture with 21% sand and 36% clay content. Dual-polarised T_B observations of the mixed pixel were then simulated for each scenario, by running the L-MEB model in forward mode separately for the two fractions and aggregating the resulting T_B's at each polarisation and angle using their respective pixel fractions. This was done for a variety of incidence angles.

In order to check for convergence of the retrieval algorithm and to provide a statistically significant data set, the simulated T_B observations were perturbed with an assumed measurement error of 2K standard deviation before performing the retrieval. This involved adding a Gaussian noise, fully correlated between polarisation and incidence angles, with a standard deviation of 2K. This created for each observation a set of 100 independent observations. An average soil moisture retrieval error was than calculated for each scenario as the average of the 100 simulations, and the model convergence assessed using the error variance.

The mean and variance (in square root) of the error using the 3P-S approach is compared with that using the 2P-S approach in Figure A5.1 in the case of a pixel of group B (50% of pixel occupied by forest and 50% by grass), as a function of the range of incidence angles used. In this first case, for each range of angles two dual-polarised observations were simulated and used for retrieval, the two incidence angles obtained by summing and subtracting half the range to the center angle 38º. The 3P-S approach improved the 2P-S approach in intermediate and wet conditions. However, in dry conditions 3P-S had greater error than 2P-S. It can be seen in the right panel that this is associated with a strong variance of the error due to the T_B noise, indicating that the 3P-S has poorer convergence in dry conditions, causing the greater soil moisture retrieval error. This is likely due to the fact that in dry conditions the increased soil emissivity decreases the impact of the different land cover types on the “above canopy” emissivity of each pixel fraction (see Figure 8.3), therefore creating a larger amount of soil moisture distribution within the fraction which satisfy the optimisation criteria. In intermediate and wet conditions the error obtained with 3P-S had a variance comparable to that of 2P-S. This variance was approximately 2%v/v, which is the amount expected for a 2K noise in T_B.

It is also notable that increasing the range of incidence angle (always using only two observations) did not improve the performance of 2P-S. Rather, both the error and the variance of 3P-S decreased with increasing range of incidence angles. The improvement was more evident on intermediate soil moisture conditions, whereas in dry conditions the wider the range of incidence angles the greater the retrieval error and poorer the convergence (resulting in a greater variance of the error). The increased accuracy in intermediate and wet conditions is expected, since observations at different angles yield more information on the angular variation of the soil-vegetation microwave emission

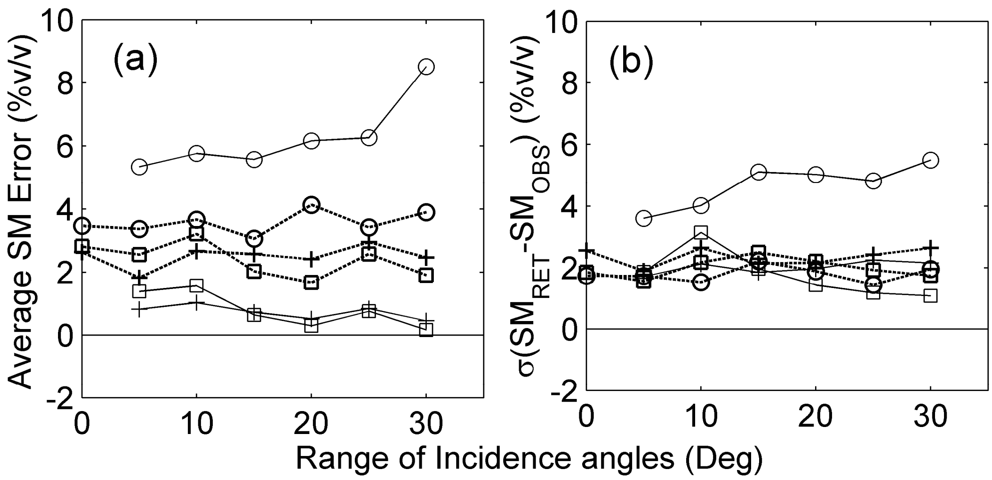

Figure A5.1. Comparison between the 3P-S (solid lines) and 2P-S (dashed lines) soil moisture retrieval from two dual-polarised observations with increasing incidence angle difference. The (a) average error in soil moisture retrieval and (b) the square root of the variance of the error due to a 2K noise in the observations are shown for three average soil moisture conditions of the pixel: 15%v/v (○), 30%v/v (□) and 45%v/v (+).

characteristics as opposed to observations with similar angle. The degradation of the retrieval for dry conditions and wider ranges of angles is attributed to poor algorithm convergence as shown in the right panel of Figure A5.1.

In Table A5.1 the comparison between 3P-S and 2P-S shown in Figure A5.1 is extended to the case of a pixel of group A (80% of pixel occupied by forest and 20% by grass) and one of group C (20% of pixel occupied by forest and 80% by grass). For simplicity, only results for the case with 30° incidence angle range are shown in this table. For the 3P-S approach the error in the retrieved values of the individual fractions is shown together with the error in pixel average soil moisture. It can be seen that the algorithm tended to smooth out the soil moisture gradient by overestimating the soil moisture of forest and underestimating that of grass. The error was greater for the land cover type with the smaller fraction (i.e., the forest fraction in group A pixels and the grass fraction in group C pixels). However when forest and grass had the same fraction (group B pixels) the error was greater over forest. This was more

Table A5.1. Comparison between the performance of 2P-S and 3P-S approaches for three synthetic scenarios and for land cover categories.

Group	Pixel Soil Moisture (%v/v)	Soil Moisture Error (%v/v) 2P-S Mixed Pixel	3P-S Mixed Pixel	3P-S Grass fraction	3P-S Forest Fraction
A.	21	1.6	1.1	-1.8	12.8
Forest<40%	36	1.3	0.4	-0.9	5.7
	51	1.3	0.3	-0.5	3.2
B.	15	3.2	6.0	-11.8	23.9
Forest =40-60%	30	2.7	0.6	-2.2	3.5
	45	2.6	0.3	-0.9	1.5
C.	9	2.4	3.3	-23.2	9.9
Forest >60%	24	2.0	1.3	-5.6	3.0
	39	2.0	1.1	-5.2	2.7

pronounced in the dry case, in which the algorithm was found to exhibit higher instability earlier on. This indicates that the error of the 3P-S approach in retrieving soil moisture estimates of the sub-pixel fractions are due to poor sensitivity of the pixel average T_B to changes in soil moisture over the land cover type having the smallest fraction, with the soil moisture of the forest fraction presenting the greatest error when the fractions are the same. However, at the pixel level, these partial errors generally cancelled each other out. Consequently, the 3P-S approach improved the 2PS in all cases, except for the case of significant forest fraction (group B and C) and in dry conditions. It should be noted that when going towards wetter conditions, the errors tended to decrease.

In Figure A5.2 the results of a second synthetic test are shown. In this case the 3P-S approach was applied using ten incidence angles rather than only two as in the previous test. This was done by dividing each range of incidence angle in nine equal intervals. This test was performed since only a limited number of independent observations can be simulated at multiple angles using the single-angle airborne data, without introducing significant assumptions. Therefore this test had the objective to understand whether the performance of the 3P-S

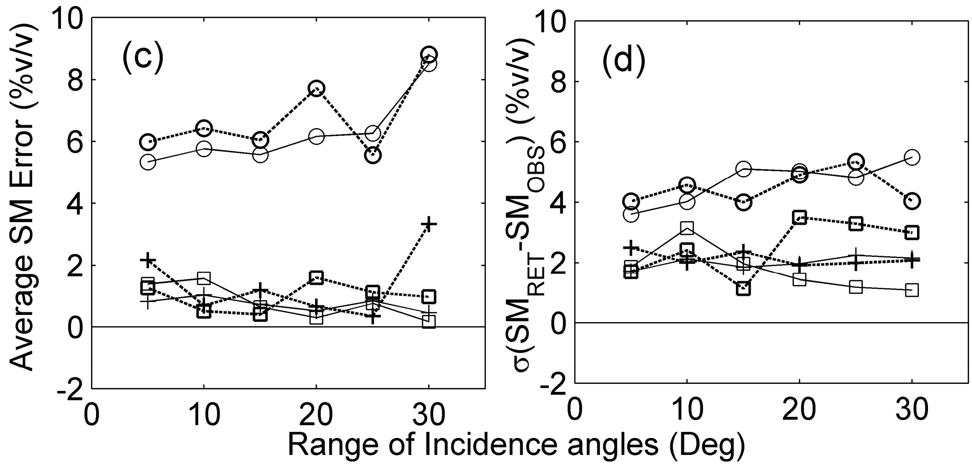

Figure A5.2. Soil moisture retrieval using the 3P-S approach with 10 dual-polarised observations (dashed lines) or 2 dual-polarised observations (solid lines) covering the same range of incidence angles. In (a) the average error in soil moisture retrieval and in (b) the square root of the variance of the error due to a 2K noise in the observations are shown for three average soil moisture conditions of the pixel: 15%v/v (○), 30%v/v (□) and 45%v/v (+).

approach improved when increasing the number of independent observations available, and therefore whether testing the 3P-S with airborne data at only a few incidence angles would be relevant.

The results show that the accuracy of 3P-S did not improve when using 10 dual-polarised observations in comparison to only 2. Rather, the accuracy of the 3P-S was largely unchanged, and in dry conditions the results were even slightly worse. Panel b of Figure A5.2 also shows that using 10 observations did not improve the convergence of the algorithm, which was also degraded in many cases.

These results are in agreement with those of [Davenport, 2008 #54], the only other study which analysed the effect of sub-pixel heterogeneity in a multi-angle, SMOS type synthetic scenario. In that study it was found that multi-angular retrievals are more affected by the sub-pixel heterogeneity of soil moisture than single angle retrievals. This was attributed to the difficulty encountered by the algorithm in finding values of the retrieved parameters that matched the variety of non linear soil moisture-microwave emission curve, which vary with the incidence angle. This implies that, even though multi-angular observations might allow more accurate soil moisture retrieval on homogeneous scenes, this might not be an advantage on scenes that are characterised by highly heterogeneous land surface conditions.

This synthetic test showed that the 3P-S approach could improve the soil moisture retrieval accuracy of the 2P-S approach, but only when the forest fraction is less than 40% (group A pixels) and the pixel is relatively moist, due to poor algorithm convergence. It was also shown that only a slight improvement in retrieval accuracy derived from increasing the range of incidence angles of the available observations, and that increasing the number of incidence angle observations for a given incidence angle range did not improve the retrieval. In the following section, 3P-S approach is tested with the NAFE'05 airborne data.

A5.2 Application of 3P-S with Airborne Data

The 3P-S approach was applied to the NAFE'05 airborne data and compared to the performance of the 2P-S approach presented in section 8.3.1. To this end, SMOS observations were simulated at 7° incidence angle in addition to the 38.5° observations used thus far for 2P-U and 2P-S approaches. This allowed the 3 parameters to be retrieved by 3P-S (soil moisture of the forest fraction, soil moisture of the moderately vegetated fraction, and optical depth of the moderately vegetated fraction) by using 4 observations for each SMOS pixel (V and H-pol at 7° and 38.5° incidence angle). The choice of these two incidence angles, having a range of 31.5°, was motivated by the fact that these are the centre angles of the PLMR radiometer outer (±38.5°) and inner (±7°) beams, and by the synthetic results that showed the maximum angular range correspond to a maximum improvement of the 3P-S approach in most scenarios tested.

Table A5.2. Comparison of the mean and standard deviation of the 1km regional brightness temperature observations normalised at 38.5° and 7°, used to obtain the dual-polarised, bi-angular coarse-resolution observations for the testing of the 3P-S approach with real data.

Date	**T_B (H) 38.5°**	**T_B (V) 38.5°**	**T_B (H) 7°**	**T_B (V) 7°**
31/10	237.7 ±11.9	255.3 ±10.0	241.4 ±11.9	243.3 ±9.8
7/11	241.4 ±10.1	261.3 ±7.5	246.7 ±10.3	249.8 ±7.6
14/11	264.7 ±6.5	277.8 ±5.1	270.1 ±6.6	272.6 ±5.2
21/11	270.9 ±4.0	282.2 ±2.9	276.8 ±4.1	279.2 ±3.1

The additional 7° observations were obtained from the 1km regional T_B in the same way as the 38.5° observations, by using the incidence angle normalisation procedure described in section 5.3.2.1 and aggregating the normalised 1km T_B to 5, 10, 20, 30 and 40km. Table A5.2 shows the average and standard deviation of the 1km T_B normalised at the two different angles. It is shown that while the averages for all data sets increase according to the drying conditions, the 38.5° observations have a larger difference between average V and H-pol.

Making use of the dual-polarised observations at 7° and 38.5°, two soil moisture values and one optical depth were retrieved for each coarse-resolution pixel. The soil moisture values are those of the forest fraction and that of the moderately vegetated fraction of the pixel, whereas the optical depth value is that of the moderately vegetated fraction of the pixel. Note that this includes both the grassland and crop fraction, meaning that although the L-MEB is run in forward mode separately (and with specific parameters) for the three fractions (forest, crop and grassland), the soil moisture is assumed to be the same between the crop and the grassland fraction. This is consistent with the SMOS L2 algorithm. Moreover, the analysis conducted thus far has shown no correlation between the retrieval error and the crop fraction. Conversely, the error was highly correlated with the ratio between forest fraction and the moderately vegetated fraction (crop and grass). A value of pixel average soil moisture was then calculated as the average of the 2 soil moisture values, weighted by the respective pixel fraction. This was done since the soil moisture retrieved by the algorithm for each fraction is essentially a soil moisture measurement with a support proportional to the area covered by the land cover type.

In Table A5.3 the performance of the 3P-S approach is compared to the 2P-S approach. For direct comparison with the 2P-S, the 3P-S approach was run here after relaxing the 20%v/v constraint on the retrieved soil moisture, since in the previous section this was found to give the best results when using 2P-S. The soil moisture retrieval using the 3P-S approach was found to be overall less accurate than the 2P-S approach. In particular, on the first two days (October 31st and November 7th, generally wet conditions) the 3P-S approach resulted in a significant wet bias which significantly impacted the overall soil moisture retrieval error. However, on dry days the two approaches yielded a similar accuracy.

In the synthetic analysis in the previous section it was shown that the burden of 3 parameters to be retrieved caused a difficulty with convergence of the optimisation algorithm. To check whether the errors observed in Table A5.3 were a result of that problem, the 3P-S retrieval was repeated by simulating a 2K measurement error (same to what was done in the synthetic case). A set of 100 perturbed observations was thus created for each pixel. Soil moisture of the

Table A5.3. Errors in retrieved soil moisture (SM) and optical depth (TAU) at 5km resolution obtained using the 2P-S and 3P-S approaches. All RMSE and biases are relative to the pixel average values, apart from (+) which is relative to the optical depth of the moderately vegetated fraction.

		2P-S			**3P-S**		
Group	**Date**	**SM RMSE (%v/v)**	**SM Bias (%v/v)**	**TAU RMSE (+)**	**SM RMSE (%v/v)**	**SM Bias (%v/v)**	**TAU RMSE (+)**
A. Forest <40%	31/10	3.6	1.8	0.02	4.4	3.1	0.02
	7/11	2.0	-0.8	0.02	3.7	3.2	0.02
	14/11	2.1	-1.3	0.02	1.6	-0.8	0.05
	21/11	2.2	-1.5	0.02	2.8	-2.4	0.10
B. Forest >40% <60%	31/10	4.6	2.6	0.04	6.4	5.4	0.06
	7/11	2.6	-1.5	0.05	5.1	4.8	0.05
	14/11	1.1	-1.0	0.08	0.7	0.0	0.03
	21/11	1.5	-1.2	0.07	1.7	-1.6	0.14
C. Forest >60%	31/10	3.3	2.4	0.09	6.7	6.1	0.23
	7/11	0.9	0.1	0.05	9.8	5.7	0.19
	14/11	0.8	-0.6	0.08	0.5	-0.3	0.16
	21/11	0.6	-0.5	0.12	0.9	-0.8	0.17
Total		2.5	-0.3	0.04	3.9	1.2	0.08

forest and moderately vegetated fraction were then retrieved and the variance of the error calculated for each fraction individually. The error in soil moisture retrieved over both fractions and the error variance are shown in Figure A5.3 as a function of both the amount of forest fraction of the pixel and the observed pixel average soil moisture.

It can be seen that, as observed in the synthetic analysis, the retrieval was very inaccurate for the forest fraction (blue dots, panel “a”). Here, very high soil moisture values were retrieved for the forest when the observed conditions were actually dry and low soil moisture values were retrieved when the soil was actually wet (panel “b”). These errors only occurred when the forest fraction was small (panel “b”). Conversely, the soil moisture of the moderately

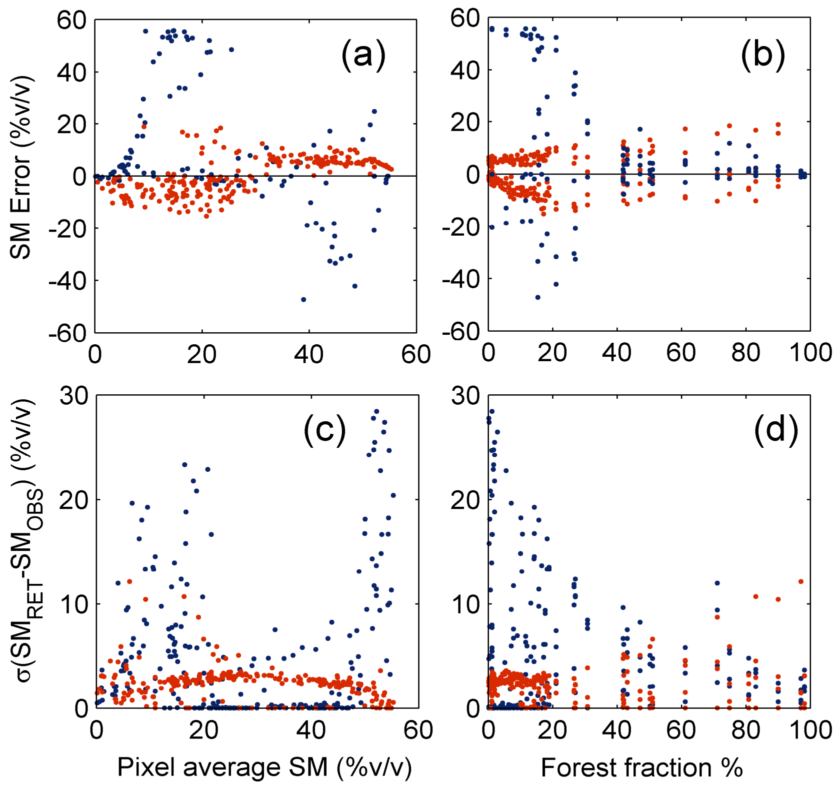

Figure A5.3. 3P-S average soil moisture (SM) error (top panels) and variance of the error (bottom panel) after a 2K noise was added to the each 5km resolution observation. Blue dots indicate the error of the soil moisture retrieved for the forest fraction, red dots the error for the moderately vegetated fraction. Both quantities are displayed as a function of the pixel average soil moisture (left panels) and the forest fraction within the pixel (right panels).

vegetated fraction (red dots) was underestimated in dry conditions and overestimated in wet conditions (above 30%v/v pixel average soil moisture), and tended also to increase when this fraction was smaller (i.e., toward higher forest fraction in panel "b"). It should be noted that, despite the magnitude of the errors in the retrieved soil moisture of the forest shown in the figure, the

error in pixel average soil moisture shown in Table A5.3 are of much smaller magnitude. This is because the pixel average soil moisture was calculated from the value retrieved in the individual fractions using the respective pixel fractions as weights.

In the lower panels of Figure A5.3, it can be appreciated that the highest soil moisture retrieval errors were associated with a strong increase in the variance of the error due to the added measurement noise. For most pixels, the variance of the error was equal or less than 2.5%v/v, with a maximum at intermediate soil moisture conditions. This is equal to the variance obtained with the synthetic example, and indicates that the algorithm had overall a good convergence. However, as observed in the synthetic analysis, the error variance increased in dry conditions for both the forest and moderately vegetated fraction (panel “c”), and increased for each land cover types when the respective pixel fraction gets small (panel “d”). Moreover the variance was generally higher for the forest fraction. This is expected due to the greater optical depth of forest with respect to that of a moderate vegetation surface, meaning the overall emissivity is less sensitive to soil moisture changes in the forest fraction. Additionally, this effect will be even smaller when the fraction occupied by forest decreases. Note that a strong increase in the error variance of the forest soil moisture was also observed for very wet soil moisture conditions of the mixed pixel, above 50%v/v. This was not observed in the synthetic case, where the soil moisture conditions analysed were not greater than 45%v/v. it should be noted that such wet conditions, although observed within relatively small areas (5km), are less likely to happen at the SMOS resolution of 40km.

These results are fairly consistent with those indicated by the synthetic test, where the algorithm was found to overestimate the soil moisture of the forest fraction and underestimate that of the moderately vegetated fraction. However, it can be seen in Figure A5.3 that at around 30%v/v the error over both fractions changed sign. In the synthetic test this “inversion” was not observed, although it was noticed that both errors were more severe when the pixel was in dry conditions (15%v/v), whereas they both decrease in intermediate and wet conditions (30%v/v and 45%v/v), matching the decrease of errors from dry to intermediate conditions observed with real data. It is likely that the “inversion”

Table A5.4. Soil moisture error obtained with the 3P-S approach depending on the a priori information on the soil moisture of forest. The soil moisture retrieval RMSE, and bias calculated for the monitoring period are shown for each group of pixel. *=without *a priori* information on the soil moisture of forest; **=with *a priori* information on the soil moisture of forest.

Retrieval Approach	Group A Forest<40%		Group B Forest=40-60%		Group C Forest>60%	
	RMSE	**Bias**	**RMSE**	**Bias**	**RMSE**	**Bias**
2P-S	2.8	-0.3	2.8	-0.3	1.8	0.4
3P-S*	2.8	1.3	4.2	2.2	4.2	2.4
3P-S**	3.2	0.9	3.4	1.9	1.9	1.0

was not observed in the synthetic test due to the soil moisture difference imposed between the two fractions, which was fixed to 20% for all cases (dry to wet) and therefore non entirely representative of all the cases encountered when using real data.

As a result of the poor sensitivity of the mixed pixel retrieval to the soil moisture of the sub-pixel fractions, the 3P-S resulted in larger errors than the 2P-S approach as seen in Table A5.3. Although in a synthetic scenario the partial soil moisture errors in the sub-pixel fractions cancelled each other out, this did not happen when using real data. A possible way to avoid this problem in an operational scenario would be to constrain the soil moisture of forest to an a priori value in order to increase the convergence of the algorithm. In order to check whether this would improve the overall retrieval of the 3P-S, the value of soil moisture of the forest fraction was set to that of the ground observations and retrieving only the soil moisture and optical depth of the moderately vegetated fraction of the pixel. This simulated the optimal scenario in which a perfect estimation of the soil moisture of the forest fraction was available from another source.

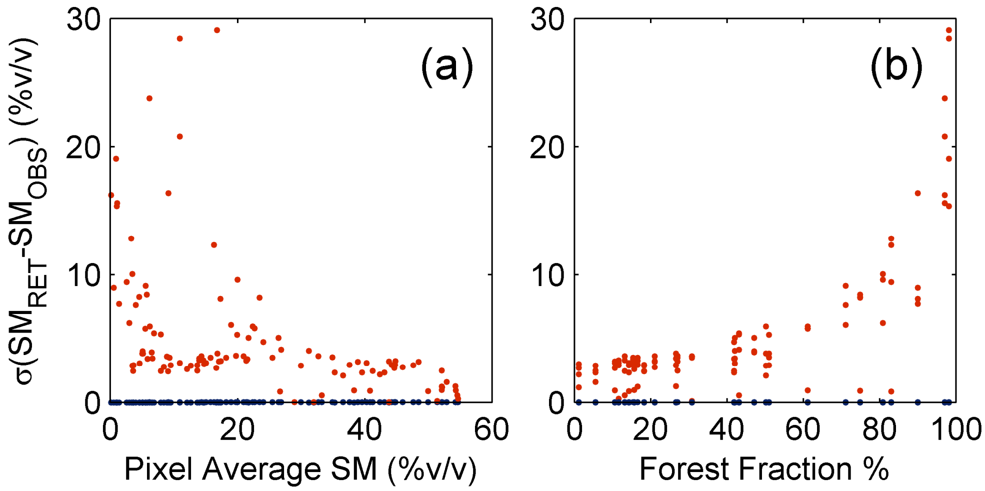

Figure A5.4. Variance of the 3P-S soil moisture retrieval error when using *a priori* information on the soil moisture of forest plotted as a function of (a) the pixel average soil moisture and the (b) forest fraction within the pixel (right panels). Blue dots are the data for the forest fraction, red dots are for the moderately vegetated fraction.

The performance of the 3P-S approach with and without the *a priori* information on the soil moisture of the forest fraction are shown in Table A5.4, where a global RMSE and bias is given for each group of pixels. The variance of the retrieval error is shown for both fractions in Figure A5.4. Imposing the a priori information on the soil moisture of the forest fraction did not improve the retrieval on group A pixel, whereas it slightly improved the retrieval in group B pixels and strongly improved in group C pixels. Figure A5.4 shows that the variance of the error of the moderately vegetated fraction was still high in dry conditions, and increased significantly with respect to the case when no a priori information on the soil moisture of forest was used (see Figure A5.4, bottom panels). Moreover, as the fraction of the pixel occupied by the moderately vegetated fraction decreased the error variance increased significantly. This is the reason why in group C pixel the 3P-S still showed residual error despite the soil moisture of the forest being imposed as the correct one. Similarly, on group B pixels the accuracy was improved when using a priori information on the soil moisture of forest, but the poor sensitivity of the pixel emissivity to the soil moisture value of the moderately vegetated fraction keeps the error above that obtained with the 2P-S approach.

A5.3 Conclusions on the Applicability of the 3P-S Approach

In summary, there was no case where the 3P-S yielded more accurate results than for the 2P-S approach. Since in this test the most accurate estimate of the forest fraction was used (that retrieved at 1km resolution using L-MEB parameters and optical depth specifically calibrated for the forest of the study area), it is not expected that the accuracy of 3P-S could be improved further. The algorithm convergence might be improved when a larger number of observations at multiple incidence angles are available. However, this could not be tested here due to the limited amount of incidence angles at which observations were available. Moreover, the synthetic test suggested that the use of multiple observations is not necessarily an advantage in the presence of strong land surface heterogeneity, since no improvement in soil moisture accuracy or algorithm convergence was observed when moving from two to ten observations within the same range of incidence angles.